NATIONAL LIBRARY
OTTAWA

CANADA

BIBLIOTHÈQUE NATIONALE
OTTAWA

NAME OF AUTHOR ..... RAY-SHING WU .....

TITLE OF THESIS ..... Convective Instability in Horizontal Fluid Flows and Horizontal Layer .....

UNIVERSITY ..... of Alberta .....

DEGREE FOR WHICH THESIS WAS PRESENTED ..... Ph.D. .....

YEAR THIS DEGREE GRANTED ..... 1976 .....

Permission is hereby granted to THE NATIONAL LIBRARY OF CANADA to microfilm this thesis and to lend or sell copies of the film.

The author reserves other publication rights, and neither the thesis nor extensive extracts from it may be printed or otherwise reproduced without the author's written permission.

(Signed) ..... Ray-Shing Wu .....

PERMANENT ADDRESS:

10977-73 Ave.
Edmonton, Alberta
T6G 0C3

DATED ..... April 22 1976

NL-91 (10-68)

INFORMATION TO USERS

THIS DISSERTATION HAS BEEN MICROFILMED EXACTLY AS RECEIVED

This copy was produced from a microfiche copy of the original document. The quality of the copy is heavily dependent upon the quality of the original thesis submitted for microfilming. Every effort has been made to ensure the highest quality of reproduction possible.

PLEASE NOTE: Some pages may have indistinct print. Filmed as received.

Canadian Theses Division
Cataloguing Branch
National Library of Canada
Ottawa, Canada K1A 0N4

AVIS AUX USAGERS

LA THESE A ETE MICROFILMEE TELLE QUE NOUS L'AVONS RECUE

Cette copie a été faite à partir d'une microfiche du document original. La qualité de la copie dépend grandement de la qualité de la thèse soumise pour le microfimage. Nous avons tout fait pour assurer une qualité supérieure de reproduction.

NOTA BENE: La qualité d'impression de certaines pages peut laisser à désirer. Microfilmée telle que nous l'avons reçue.

Division des thèses canadiennes
Direction du catalogage
Bibliothèque nationale du Canada
Ottawa, Canada K1A 0N4

THE UNIVERSITY OF ALBERTA

CONVECTIVE INSTABILITY IN HORIZONTAL FLUID FLOWS AND HORIZONTAL LIQUID LAYERS

by

RAY-SHING WU ©

A THESIS

SUBMITTED TO THE FACULTY OF GRADUATE STUDIES AND RESEARCH IN PARTIAL FULFILMENT OF THE REQUIREMENTS FOR THE DEGREE OF DOCTOR OF PHILOSOPHY

DEPARTMENT OF MECHANICAL ENGINEERING

EDMONTON, ALBERTA

SPRING, 1976

THE UNIVERSITY OF ALBERTA

FACULTY OF GRADUATE STUDIES AND RESEARCH

The undersigned certify that they have read, and recommend to the Faculty of Graduate Studies and Research, for acceptance, a thesis entitled "CONVECTIVE INSTABILITY IN HORIZONTAL FLUID FLOWS AND HORIZONTAL LIQUID LAYERS" submitted by RAY-SHING WU in partial fulfilment of the requirements for the degree of Doctor of Philosophy.

K. C. Cheng
Supervisor

....

J. P. Vandell (?)

C. M. Rodkiewicz

....

....
External Examiner

Date April 20, 1976

ABSTRACT

The linear stability problems for the onset of secondary flow driven by buoyancy force in a class of horizontal laminar fluid flows including plane Poiseuille, Hartmann and Blasius flows are investigated by a numerical method. The low Peclet number thermal entrance region problem in parallel-plate channels with unequal constant wall temperatures considers axial heat conduction effect and allows heat penetration through the thermal entrance. The solution is obtained by the eigenfunction expansion method employing Gram-Schmidt orthonormalization procedure. The axial conduction effects on convective instability of a horizontal plane Poiseuille flow in the thermal entrance region with respect to both longitudinal and transverse vortex disturbances are studied. It is found that the transverse vortex disturbances are the preferred mode over that of longitudinal disturbances for $Pe \leq 1$ and $Pr \geq 1$ (low Re) in the developing regions upstream and downstream of the thermal entrance. For other conditions, the longitudinal rolls have priority of occurrence. The maximum density effects on convective instability of water in the temperature range 0 ~ 30°C are also studied by using the same basic state temperature solution. The effects of viscous dissipation on the onset of instability for longitudinal vortices in the thermal entrance region of

a horizontal parallel-plate channel heated from below are also studied.

The basic flow solution of Hartmann flow considers axial conduction, viscous dissipation and Joulean heating effects but neglects axial heat penetration through the thermal entrance. The convective instability analysis of horizontal Hartmann flow in the thermal entrance region considers the effects of Prandtl, Peclet, Brinkman and Hartmann numbers.

The maximum density effects on thermal instability in a thin horizontal water layer induced by combined buoyancy and surface tension gradients are studied by a numerical method. The instability results provide further physical insight into the problem considered by Nield in 1964.

The convective instability analysis of Blasius flow along a horizontal semi-infinite plate with uniform wall temperature complements the hydrodynamic instability analysis of laminar boundary layers reported in the literature. The instability analysis is further extended to include the maximum density effect.

The heat transfer results for thermal entrance region problems of plane Poiseuille flows are also obtained using the basic flow solutions.

ACKNOWLEDGEMENTS

The author wishes to express his sincere appreciation to the following persons and organizations:

Dr. K.C. Cheng, thesis adviser, for his guidance and assistance in all stages of this investigation and in the preparation of this thesis,

The Department of Mechanical Engineering and the National Research Council of Canada for providing financial assistance in the form of assistantship and scholarship,

My wife, Helen Fu-mei, for her constant encouragement and patience throughout the course of his graduate studies,

Miss Susan Schultz for her excellent typing of the thesis,

Fellow Graduate Students in Mechanical Engineering for their helpful discussions on various aspects of the thesis work.

TABLE OF CONTENTS

			Page
CHAPTER I		INTRODUCTION	1
CHAPTER II		LOW PECLET NUMBER HEAT TRANSFER IN THE THERMAL ENTRANCE REGION OF PARALLEL-PLATE CHANNELS WITH UNEQUAL WALL TEMPERATURES	8
	2.1	Introduction	11
	2.2	Theoretical Analysis	12
	2.3	Results and Discussion	20
	2.4	Concluding Remarks	24
CHAPTER III		AXIAL HEAT CONDUCTION EFFECTS ON THERMAL INSTABILITY OF HORIZONTAL PLANE POISEUILLE FLOWS HEATED FROM BELOW	48
	3.1	Introduction	52
	3.2	Temperature Solutions for Basic Flow	54
	3.3	Perturbation Equations	56
	3.4	Method of Solution	61
	3.5	Results and Discussion	63
	3.6	Concluding Remarks	69

Page

CHAPTER IV: MAXIMUM DENSITY EFFECTS ON CONVECTIVE INSTABILITY OF HORIZONTAL PLANE POISEUILLE FLOWS IN THE THERMAL ENTRANCE REGION 91

4.1 Introduction 95

4.2 Upstream and Downstream Temperature Solutions for Basic Flow 96

4.3 Perturbation Equations 98

4.4 Numerical Results and Discussion 102

4.5 Concluding Remarks 106

CHAPTER V VISCOUS DISSIPATION EFFECTS ON CONVECTIVE INSTABILITY AND HEAT TRANSFER IN PLANE POISEUILLE FLOW HEATED FROM BELOW 125

5.1 Introduction 129

5.2 Graetz Problem with Viscous Dissipation Effects and Basic Solution 130

5.3 Perturbation Equations for Thermal Instability Problem 134

5.4 Results and Discussion 136

5.5 Concluding Remarks 140

Page

CHAPTER VI		THERMAL ENTRANCE REGION HEAT TRANSFER FOR MHD LAMINAR FLOW IN PARALLEL-PLATE CHANNELS WITH UNEQUAL WALL TEMPERATURES	161
	6.1	Introduction	165
	6.2	Governing Equations	166
	6.3	Solution of the Energy Equation	169
	6.4	Numerical Results and Discussion	174
	6.5	Concluding Remarks	178
CHAPTER VII		THERMAL INSTABILITY OF HARTMANN FLOW IN THE THERMAL ENTRANCE REGION OF HORIZONTAL PARALLEL-PLATE CHANNELS HEATED FROM BELOW	199
	7.1	Introduction	204
	7.2	Formulation of the Thermal Instability Problem	205
	7.3	Numerical Solution	215
	7.4	Results and Discussion	217
	7.5	Concluding Remarks	220
CHAPTER VIII		MAXIMUM DENSITY EFFECTS ON THERMAL INSTABILITY INDUCED BY COMBINED BUOYANCY AND SURFACE TENSION	250
	8.1	Introduction	254

			Page
	8.2	Formulation of the Thermal Instability Problem	255
	8.3	Numerical Results and Discussion	260
	8.4	Concluding Remarks	264
CHAPTER IX		THERMAL INSTABILITY OF BLASIUS FLOW ALONG HORIZONTAL PLATE	284
	9.1	Introduction	287
	9.2	The Basic Flow	288
	9.3	The Thermal Instability Problem	289
	9.4	Method of Solution	294
	9.5	The Neutral Stability Results and Discussion	297
	9.6	Concluding Remarks	300
CHAPTER X		MAXIMUM DENSITY EFFECTS ON THERMAL INSTABILITY OF HORIZONTAL LAMINAR BOUNDARY LAYERS	314
	10.1	Introduction	318
	10.2	Formulation of the Thermal Instability Problem	319
	10.3	Method of Solution	326
	10.4	Results and Discussion	329
	10.5	Concluding Remarks	331
CHAPTER XI		CONCLUSIONS	343
	11.1	Scope of Results	343

		Page
11.2	Conclusions and Significance	[illegible]
11.3	Recommendations	347
APPENDIX 1	DERIVATION OF HIGH ORDER FINITE-DIFFERENCE APPROXIMATIONS	349
APPENDIX 2	ALGORITHMS FOR PENTADIAGONAL AND TRIDIAGONAL MATRICES	357
APPENDIX 3	METHOD OF REGRESSION FOR TEMPERATURE EFFECT ON DENSITY OF WATER BETWEEN 0°C AND 30°C	361
APPENDIX 4	PROOF FOR $e_x^+ = e_y^+ = e_z^+ = b_x^+ = 0$	365
APPENDIX 5	DERIVATION OF STREAM FUNCTION FOR HEXAGONAL CELLS	369
APPENDIX 6	COMPUTER PROGRAMS	378

LIST OF TABLES

Table		Page
CHAPTER II		
1	Eigenvalues for Pe = 1 and 5	28
2	Eigenvalues for Pe = 10 and 50	29
3	Series Coefficients for Pe = 1, 5	30
4	Series Coefficients for Pe = 10, 50	31
5	Constants for Pe = 1, 5	32
6	Constants for Pe = 10, 50	33
7	Bulk Mean Temperature	34
8	Nusselt Numbers	35
CHAPTER III		
1	Instability Results for Pe = 1	75
2	Instability Results for Pe = 5	77
3	Instability Results for Pe = 10	78
4	Instability Results for Pe = 50	79
5	Instability Results for Transverse Rolls at Pe = 1, 5	80
CHAPTER IV		
1	Instability Results $\lambda_1 = -0.5$, $\lambda_2 = 0$ and Pe = 1, $\lambda_2 = -2$	112
2	Instability Results for Pe = 1, $\lambda_3 = -0.5$	113
3	Instability Results for Pe = 1, $\lambda_1 = -1.0$	114

Table		Page
4	Instability Results for Pe = 10, $\lambda_1 = -0.5$	115
5	Instability Results for Pe = 50, $\lambda_1 = -0.5$	117
CHAPTER V		
1	Values of Eigenvalues β_n, γ_n and Coefficients C_n, D_n, K_n for $\theta_0 = 1$	144
2	Nusselt Numbers for $\theta_0 = 1$ and Br = 0, -1, -2.5, -10, -20, -50, -100	145
3	Instability Results for Pr = 0.7 and 10	147
4	Instability Results for Pr = 100	148
CHAPTER VI		
1	Values of Eigenvalues β_n, γ_n and Coefficients C_n, D_n for Ha = 0, $\theta_0 = 1$, K = 1	183
2	Values of Eigenvalues β_n, γ_n and Coefficients C_n, D_n for Ha = 2, $\theta_0 = 1$, K = 1	184
3	Values of Eigenvalues β_n, γ_n and Coefficients C_n, D_n for Ha = 6, $\theta_0 = 1$, K = 1	185
4	Values of Eigenvalues β_n, γ_n and Coefficients C_n, D_n for Ha = 10, $\theta_0 = 1$, K = 1	186

Table		Page
5	Nusselt Numbers for $\theta_0 = 1$, $K = 1$, and $Pe = 10$	187
6	Nusselt Numbers for $\theta_0 = 1$, $K = 1$, and $Pe = 100$	189
CHAPTER VII		
1	Instability Results for $\theta_0 = 1$, $K = 1$, $Pe = 10$	225
2	Instability Results for $\theta_0 = 1$, $K = 1$, $Pe = 100$	227
3	Instability Results for $\theta_0 = 1$, $K = 1$, $Pe = \infty$	229
CHAPTER VIII		
1	Instability Results for $\lambda_1 = -1.5$ and $\lambda_2 = -0.2$	270
2	Instability Results for $\lambda_1 = -2.0$ and $\lambda_2 = 0.4$	271
CHAPTER IX		
1	Numerical Data for Δy, M, and η_1	305
2	Numerical Results for Gr_L^*	305
CHAPTER X		
1	Critical Grashof Numbers for $Pr = 10$	336

Table Page

APPENDIX

A1 Comparison of Water Density with [6]* 375

* Square brackets indicate reference at end of each Chapter.

LIST OF FIGURES

Figure		Page
CHAPTER I		
1	Schematic diagram for thermal instability problems considered in this thesis	7
CHAPTER II		
1	Coordinate system for thermal entrance region problem	36
2	Even eigenfunctions Y_n for Pe = 1	37
3	Even eigenfunctions R_n for Pe = 1	38
4	Odd eigenfunctions Z_n for Pe = 1	39
5	Odd eigenfunctions F_n for Pe = 1	40
6	Developing temperature profiles for Pe = 1	41
7	Developing temperature profiles for Pe = 5	42
8	Developing temperature profiles for Pe = 10	43
9	Developing temperature profiles for Pe = 50	44
10	Matching of temperature distributions, $\phi_{\theta 1}$ and $\phi_{\theta 2}$, at x = 0 for Pe = 1, 5, 10, 50	45

Figure		Page
11	Peclet number effect on axial bulk temperature distribution	46
12	Local Nusselt number results for $Pe = 1, 5, 10, 50, \infty$	47
CHAPTER III		
1	Coordinate system and transverse and longitudinal vortex disturbances for plane Poiseuille flow	81
2	Prandtl number effect on critical Rayleigh number versus $\bar{x}$ for $\theta_0 = 1$ and Pe = 1	82
3	Prandtl number effect on Ra* versus $\bar{x}$ for $\theta_0 = 1$ and Pe = 5	83
4	Prandtl number effect on Ra* versus $\bar{x}$ for $\theta_0 = 1$ and Pe = 10	84
5	Comparison of instability results between present work and [1] for $\theta_0 = 1$ and Pe = 50	85
6	Comparison of instability results between present work and [1] for $\theta_0 = 1$ and Pe = 5	86
7	Peclet number effect on Ra* versus $\bar{x}$ for $\theta_0 = 1$ and Pr = 0.7	87

Figure		Page
8	Peclet number effect on Ra* versus x for θ_0 = 1 and Pr = 10	88
9	Instability results for longitudinal and transverse vortex rolls at θ_0 = 1, Pe = 1 and Pr = 1, 100	89
10	Streamline pattern of transverse vortex disturbance for fully developed flow at θ_0 = 1, Pe = 1, Pr = 100, Ra* = 1717 and a* = 3.117	90
CHAPTER IV		
1	Physical model and coordinate system	118
2	Peclet number effect on relation between critical Rayleigh number and $\bar{x}$ for λ_1 = -0.5 and λ_2 = 0	119
3	Ra* versus $\bar{x}$ with λ_2 as parameter for Pe = 1, λ_1 = -0.5, -1	120
4	Ra* versus $\bar{x}$ with λ_1 as parameter for Pe = 1, λ_2 = 1.4	121
5	Disturbance profiles for u*, w* with Pe = 1, λ_1 = -0.5, λ_2 = -1	122
6	Developing basic temperature profile ϕ_θ and disturbance θ* for Pe = 1, λ_1 = -0.5, λ_2 = -1	123

Figure		Page
7	Disturbance profiles for u^* and θ^* at $\overline{x} = 5$ with Pe = 1, $\lambda_1 = -0.5$ and $\lambda_2 = 0.8, -1.0$	124
CHAPTER V		
1	Coordinate system and developing temperature profiles for Br = 0	149
2	Developing temperature profiles for Br = -2.5	150
3	Brinkman number effect on temperature profiles at x = 0.06	151
4	Brinkman number effect on temperature profiles at x = 0.2	152
5	Brinkman number effect on fully developed temperature profiles (x = 2)	153
6	Brinkman number effect on axial bulk temperature distribution	154
7	Brinkman number effect on local Nusselt number results	155
8	Viscous dissipation effect on critical Rayleigh numbers for Pr = 0.1, 0.7 and 10	156
9	Viscous dissipation effect on critical Rayleigh numbers for Pr = 100	157

Figure		Page
10.	Prandtl number effect on Ra* at Br = -1	158
11	Critical Rayleigh numbers for fully developed flow and instability results from [3]	159
12	Viscous dissipation effect on neutral stability curves for Pr = 100 and x = 5	160
CHAPTER VI		
1	Coordinate system for MHD channel flow and developing temperature profiles for Pe = 10, Ha = 0 and Br = 0	191
2	Developing temperature profiles for Pe = 10, Ha = 0 and Br = -1	192
3	Developing temperature profiles for Pe = 10, Ha = 2 and Br = 0	193
4	Developing temperature profiles for Pe = 10, Ha = 2 and Br = -1	194
5	Developing temperature profiles for Pe = 10 and Br = 0, -1 with Hartmann number as parameter	195
6	Axial bulk temperature distributions for Pe = 100 and Br = 0, -1 with Hartmann number as parameter	196

Figure		Page
7	Hartmann number effect on local Nusselt number results for Pe = 10, 10^2 and Br = 0	197
8	Hartmann number effect on local Nusselt number results for Pe = 10, 10^2 and Br = -1	198
CHAPTER VII		
1	Disturbance profiles for perturbation amplitudes w^* and θ^* at Ha = 0, 10 for Pr = 0.7, Pe = 10, Br = 0, -1 and $\bar{x}$ = 10	231
2	Disturbance profiles for perturbation amplitudes u^* at Ha = 0, 2, 6, 10 for Pr = 0.7, Pe = 10, Br = 0, -1 and $\bar{x}$ = 10	232,
3	Streamline pattern at onset of instability for Pr = 0.7, Pe = 10, Ha = 10, $\bar{x}$ = 10, Br = 0 and -1	233
4	Neutral stability curves for Pr = 0.01, Br = 0, -1 and Ha = 0, 2, 6, 10	234
5	Neutral stability curves for Pr = 0.7, Br = 0, -1 and Ha = 0, 2, 6, 10	235

Figure		Page
6	Critical Rayleigh number Ra* in thermal entrance region for Pr = 0.01, 0.7 and Pe = 10, 100, ∞ with Ha = 0, Br = 0, -1	236
7	Critical Rayleigh number Ra* in thermal entrance region for Pr = 0.01, 0.7 and Pe = 10, 100, ∞ with Ha = 2, Br = 0 and -1	237
8	Critical Rayleigh number Ra* in thermal entrance region for Pr = 0.01, 0.7 and Pe = 10, 100, ∞ with Ha = 6, Br = 0 and -1	238
9	Critical Rayleigh number Ra* in thermal entrance region for Pr = 0.01, 0.7 and Pe = 10, 100, ∞ with Ha = 10, Br = 0 and -1	239
10	Hartmann number effect on critical Ra* in thermal entrance region for Pe = 10, Br = 0 and Pr = 0.01, 0.7	240
11	Hartmann number effect on critical Ra* in thermal entrance regoin for Pe = 10, Br = -1 and Pr = 0.01, 0.7	241

Figure		Page
12	Hartmann number effect on critical Ra* in thermal entrance region for Pe = 100, Br = 0 and Pr = 0.01, 0.7	242
13	Hartmann number effect on critical Ra* in thermal entrance region for Pe = 100, Br = -1 and Pr = 0.01, 0.7	243
14	Hartmann number effect on critical Ra* in thermal entrance region for Pr = 0.01, Pe = 10 and Br = 0, -1	244
15	Hartmann number effect on critical Ra* in thermal entrance region for Pr = 0.7, Pe = 10 and Br = 0, -1	245
16	Hartmann number effect on critical Ra* in thermal entrance region for Pr = 0.01, Pe = 100 and Br = 0, -1	246
17	Hartmann number effect on critical Ra* in thermal entrance region for Pr = 0.7, Pe = 100 and Br = 0, -1	247
18	Hartmann number effect on critical a* in thermal entrance region for Pr = 0.01, Pe = 10 and Br = 0, -1	248
19	Hartmann number effect on critical a* in thermal entrance region for Pr = 0.7, Pe = 10 and Br = 0, -1	249

Figure | | Page

CHAPTER VIII

1 Neutral stability curves for $\lambda_1 = -1.0$, $\lambda_2 = -0.3$, Bi = 0, and $\lambda_1 = -1.5$, $\lambda_2 = -0.2$, Bi = 10 272

2 Neutral stability curves for $\lambda_1 = -0.75$, $\lambda_2 = 0$, Ma = 10^2 and $\lambda_1 = -2.5$, $\lambda_2 = 0.4$ and Ra = 10^3 273

3 Coordinate system and disturbance profiles for w^+/w^+_{max} and θ^+/θ^+_{max} for $\lambda_1 = -1.5$, $\lambda_2 = -0.2$, Ma = 10 with Bi as parameter 274

4 Disturbance profiles for w^+/w^+_{max} and θ^+/θ^+_{max} for $\lambda_1 = -2.0$, $\lambda_2 = 0.4$, Bi = 100 with Ma as parameter 275

5 Relation between critical Marangoni number and Rayleigh number with Bi as parameter for $\lambda_1 = -1.5$ and $\lambda_2 = -0.2$ 276

6 Relation between critical Rayleigh number and Marangoni number with Bi as parameter for $\lambda_1 = -1.25$ and $\lambda_2 = 0$ 277

Figure Page

7 Relation between critical Rayleigh number and Biot number with Ma as parameter for $\lambda_1 = -1.5$ and $\lambda_2 = -0.2$ 278

8 Relation between critical Rayleigh number and Biot number with Ma as parameter for $\lambda_1 = -2.0$ and $\lambda_2 = 0.4$ 279

9 Variation of normalized Marangoni number Ma/Ma_c with normalized Rayleigh number Ra/Ra_c with Bi as parameter for $\lambda_1 = -1.5$ and $\lambda_2 = -0.2$ 280

10 Variation of dimensionless wavenumber a with normalized Rayleigh number Ra/Ra_c with Bi as parameter for $\lambda_1 = -1.5$ and $\lambda_2 = -0.2$ 281

11 Streamlines for $\lambda_1 = -1.5$, $\lambda_2 = -0.2$, $Ma = 10$, $Bi = 10^2$,
(a) through the center and a vertex of the hexagon, 282
(b) through the center of the hexagon and the mid-point of a side 283

CHAPTER IX

1 Coordinate system and distributions of basic quantities f', F, τ and perturbation amplitudes u^*, v^*, θ^* for $Pr = 0.7$ 306

Figure		Page
2	Distributions of basic quantities f', F, τ and perturbation amplitudes u^*, v^*, θ^* for Pr = 10	307
3	Profiles for perturbation amplitudes u^*, v^*, and θ^* for Pr = 0.7 and 10	308
4	Streamline pattern of vortex disturbance for Pr = 0.7	309
5	Streamline pattern of vortex disturbance for Pr = 10	310
6	Neutral stability curves, Gr_L versus a, for Pr = 0.7 and 10	311
7	Relationship between critical Grashof number Gr_L^* and Prandtl number	312
8	Critical Grashof number (Gr_L^*) - Reynolds number (Re_x) relation and 5 percent buoyancy effect on local heat transfer from [2]	313
CHAPTER X		
1	Coordinate system and streamline pattern of vortex disturbance for $\lambda_1 = -0.5$, $\lambda_2 = -0.4$	337
2	Streamline pattern of vortex disturbance for $\lambda_1 = -0.5$ and $\lambda_2 = 0.8$	338

Figure		Page
3	Distributions of basic quantities f', F, τ and perturbation amplitudes u^*, v^* θ^* for $\lambda_1 = -0.5$ and $\lambda_2 = -0.4$	339
4	Profiles for perturbation amplitudes u^*, v^* and θ^*	340
5	Relation between critical Grashof number Gr_L^* and λ_2 with λ_1 as parameter	341
6	Neutral stability curves for $(\lambda_1, \lambda_2) = (-1.0, 0.4)$ and $(-1.0, 0.8)$	342

CHAPTER I.

INTRODUCTION

The Benard problem and the related thermal instability problem for horizontal fluid layers have been investigated extensively in recent years. The literature on thermal instability is very extensive. An excellent account of the hydrodynamic and hydromagnetic stability was given by Chandrasekhar [1] in 1961. Since then several review articles [2-7] have also appeared in the literature.

The thermal instability for the onset of stationary longitudinal vortex rolls in a horizontal plane Poiseuille flow was investigated theoretically by Nakayama, Hwang and Cheng [8] and experimentally by Akiyama, Hwang and Cheng [9]. The problem was further extended to the thermal entrance region considering axial conduction term in the energy equation for the basic flow by Hwang and Cheng [10]. The experimental investigations on convective instability in a horizontal plane Poiseuille flow heated from below were reported by Ostrach and Kamotani [11,12]. In the low Peclet number flow regime, the assumption of uniform fluid temperature at the thermal entrance is apparently unreasonable because of the upstream heat penetration through the thermal entrance. In low Peclet number flow regime, the question regarding the onset of transverse vortex rolls [2] also arises.

Consideration is next given to the Hartmann flow in a horizontal parallel-plate channel heated from below. Physically, when an adverse temperature gradient exists in the direction opposite to the gravitational force, then the basic flow system is potentially unstable because of the top-heavy situation. Apparently, the onset of secondary flow in the form of stationary longitudinal vortices in the thermal entrance region of Hartmann flow is of practical interest.

Similarly, the thermal boundary layers in Blasius flow heated from below is also potentially unstable. For the laminar forced convection problems involving melting of ice or solidification of water, the maximum density effect on thermal instability is also of practical interest since one may wish to find the condition at which free convection starts to affect the flow. Apparently, the thermal instability of the Blasius flow has not been studied in the past.

In this thesis, the convective instabilities in plane Poiseuille, Hartmann and Blasius flows are studied by the method of small disturbances where a linearization about the basic flow is made. For the cases of plane Poiseuille and Blasius flows, the effects of maximum density on convective instability are also investigated. In the linear instability analysis for fully developed Hartmann flow in the thermal entrance region of a horizontal parallel-plate channel, the effects of axial conduction, viscous and Joulean dissipations are included. In connection with the plane Poiseuille flow, the effects of viscous dissipation on thermal instability in the thermal entrance region of a horizontal parallel-plate channel heated from below are also studied. Finally, Nield's linear stability [13] for a horizontal liquid layer considering surface tension and buoyancy effects is extended to the case of water with maximum density effect for the temperature range 0 ~ 30°C.

In order to show clearly the physical problems considered in this thesis, the classification of the problems is given below (see Fig. 1):

1. Plane Poiseuille Flow
   - (a) Thermal Entrance Region Problem for Low Peclet Number Flow Regime (Basic Flow Solution), $T_1 \neq T_2$, $T = T_0$ at $X = -\infty$ (Chapter II).
   - (b) Axial Conduction Effects on Convective Instability, $T_1 > T_2$, $T = T_0$ at $X = -\infty$ (Chapter III).
   - (c) Maximum Density Effects on Convective Instability, $T_1 \gtrless T_2$, $T = T_0$ at $X = -\infty$ (Chapter IV).
   - (d) Viscous Dissipation Effects on Convective Instability, $T_1 > T_2$, $T = T_0$ at $X = 0$ (Chapter V).
2. Hartmann Flow
   - (a) Basic Flow Solution with Axial Conduction, Joule Heating and Viscous Dissipation Effects, $T_1 \neq T_2$, $T = T_0$ at $X = 0$ (Chapter VI).

(b) Magnetic Field Effects on Convective Instability, $T_1 > T_2$, $T = T_0$ at $X = 0$ (Chapter VII).

3. Horizontal Liquid Layer with Free Surface

(a) Maximum Density Effects on Thermal Instability Induced by Buoyancy and Surface Tension, $T_1 \gtrless T_{max} \gtrless T_2$ (Chapter VIII).

4. Blasius Flow

(a) Convective Instability of Blasius Flow, $T_w > T_\infty$ (Chapter IX).

(b) Maximum Density Effects on Convective Instability of Blasius Flow, $T_w \gtrless T_{max} \gtrless T_\infty$ (Chapter X).

A remark regarding the structure and the method of presentation for the present dissertation is now in order. After careful considerations, it is decided that each chapter will be treated independently. The independent presentation of each chapter affords one to discuss clearly the scope of each investigation and the results obtained therein. Thus the conclusions and significance for each problem may be assessed readily.

References

1. Chandrasekhar, S., "Hydrodynamic and Hydromagnetic Stability", Oxford University Press, 1961.
2. Ostrach, S., "Laminar Flows with Body Forces", Theory of Laminar Flows, Edited by F.K. Moore, Princeton University Press, Princeton, New Jersey, 1964, pp. 616-627.
3. Berg, J.C., Acrivos, A. and Boudart, M., "Evaporative Convection", Advances in Chemical Engineering, Vol. 6, 1966, pp. 61-123.
4. Brindley, J., "Thermal Convection in Horizontal Fluid Layers", J. Inst. Maths. Applics., Vol. 3, 1967, pp. 313-343.
5. Spiegel, E.A., "Convection in Stars, I. Basic Boussinesq Convection", Annual Review of Astronomy and Astrophysics, Vol. 9, 1971, pp. 323-352.
6. Spiegel, E.A., "Convection in Stars, II. Special Effects", Annual Review of Astronomy and Astrophysics, Vol. 10, 1972, pp. 261-304.
7. Schechter, R.S., Velarde, M.G. and Platten, J.K., "The Two-Component Benard Problem", Advances in Chemical Physics, Vol. 16, 1974, pp. 265-301.

8. Nakayama, W., Hwang, G.J. and Cheng, K.C., "Thermal Instability in Plane Poiseuille Flow, Journal of Heat Transfer, Trans. ASME, Series C, Vol. 92, 1970, pp. 61-68.

9. Akiyama, M., Hwang, G.J. and Cheng, K.C., "Experiments on the Onset of Longitudinal Vortices in Laminar Forced Convection Between Horizontal Plates", Journal of Heat Transfer, Trans. ASME, Series C, Vol. 93, 1971, pp. 335-341.

10. Hwang, G.J. and Cheng, K.C., "Convective Instability in the Thermal Entrance Region of a Horizontal Parallel-Plate Channel Heated from Below", Journal of Heat Transfer, Trans. ASME, Series C, Vol. 95, 1973, pp. 72-77.

11. Ostrach, S. and Kamotani, Y., "Heat Transfer Augmentation in Laminar Fully Developed Channel Flow by Means of Heating from Below", Journal of Heat Transfer, Trans. ASME, Series C, Vol. 97, 1975, pp. 220-225.

12. Kamotani, Y. and Ostrach, S., "Effects of Thermal Instability on Thermally-Developing Laminar Channel Flow", Journal of Heat Transfer, Trans. ASME, Series C, Vol. 98, 1976.

13. Nield, D.A., "Surface Tension and Buoyancy Effects in Cellular Convection", J. Fluid Mech., Vol. 19, 1964, pp. 341-352.

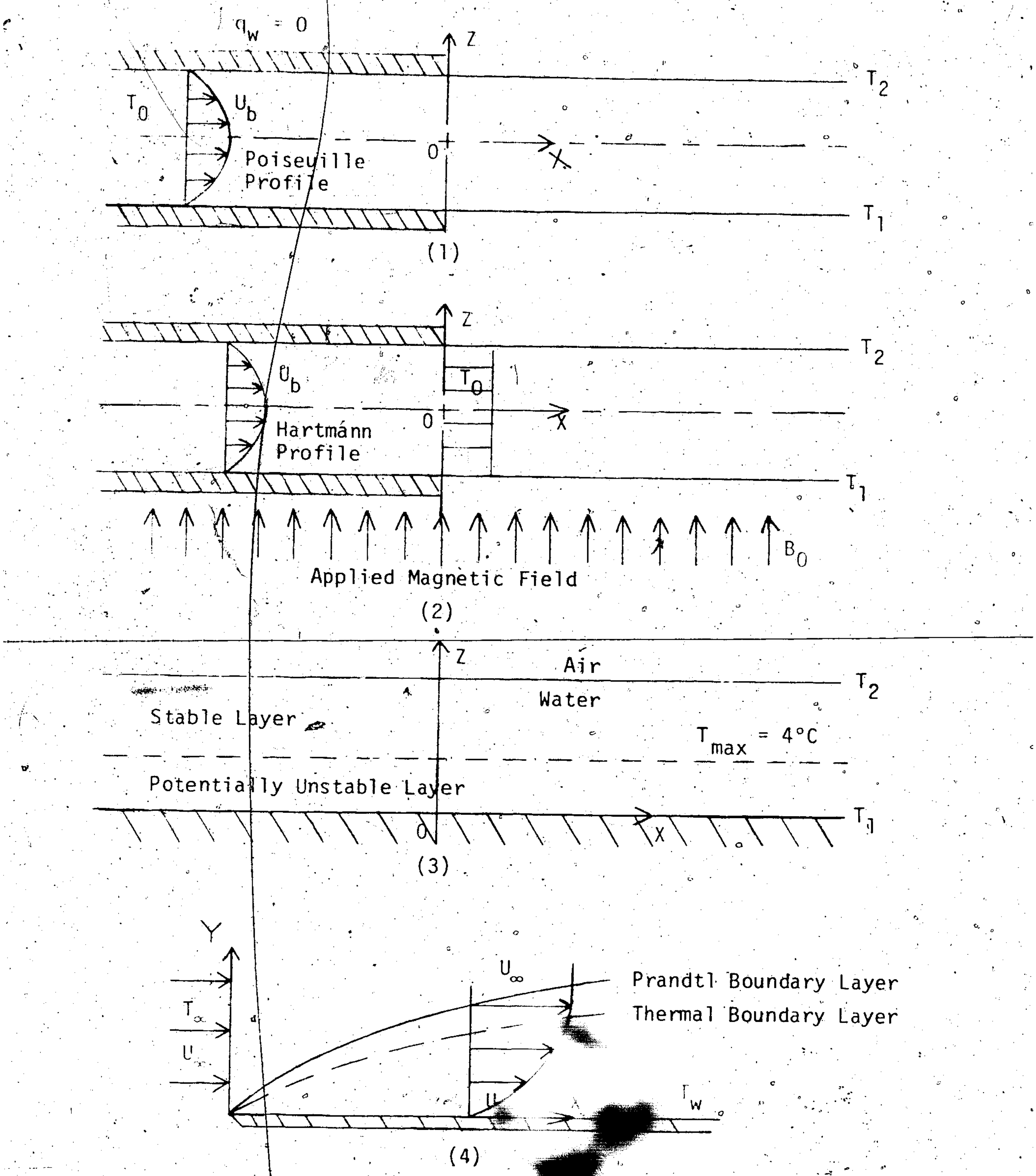

Fig. 1 Schematic Diagram for Thermal Instability Problems Considered in this Thesis

CHAPTER II

LOW PECLET NUMBER HEAT TRANSFER IN THE THERMAL ENTRANCE REGION OF PARALLEL-PLATE CHANNELS WITH UNEQUAL WALL TEMPERATURES

The problem of low-Peclet-number thermal entry heat transfer for plane Poiseuille flow in parallel-plate channels with uniform but unequal wall temperatures is approached by the eigenfunction expansion method utilizing the Gram-Schmidt orthonormalization procedure. The formulation considers axial heat conduction and allows upstream heat penetration through the thermal entrance. Numerical results are obtained for the case with entrance condition parameter $\theta_0 = 1$ and Peclet number Pe = 1, 5, 10 and 50. The effect of Peclet number on temperature distributions in both upstream and downstream regions is studied. At Pe = 50, the concept of thermal boundary layer is applicable and the present series solution does not yield physically reasonable temperature distribution locally near the upper plate at the thermal entrance. The difficulty may be attributed to the nature of thermal boundary conditions at the thermal entrance and the transition from elliptic problem to parabolic problem with the increase of Peclet number.

Nomenclature

A_n, B_n, C_n, D_n	=	coefficients of series expansion in equations (5) and (6)
$a_n^j, b_n^j, c_n^j, d_n^j$	=	coefficients in equation (13)
f_j, s_j	=	orthonormal functions
h_1, h_2	=	local heat transfer coefficients at lower and upper plates
k	=	thermal conductivity
L, ℓ	=	height of channel and $L/2$
Nu_1, Nu_2	=	local Nusselt numbers, $h_1\ell/k$ and $h_2\ell/k$
Pe	=	Peclet number, $4\, U_m \ell/\alpha$
$p_j^n, q_j^n, r_j^n, t_j^n$	=	coefficients in equation (14)
q_1, q_2	=	rates of heat transfer per unit area at lower and upper plates
T, T_0, T_1, T_2	=	fluid temperature, uniform entrance temperature, uniform but different lower and upper plate temperatures, respectively
T_b, T_m	=	bulk temperature and $(T_1 + T_2)/2$
U, U_m, u	=	axial and mean velocities, and U/U_m
X, Z	=	axial and transverse coordinates
x, z	=	dimensionless coordinates, $X/(3Pe\ell/8)$ and Z/ℓ

Y_n, R_n, F_n, Z_n	=	eigenfunctions
$\bar{z}$	=	transformed coordinate, $(z + 1)/2$

Greek Letters

α	=	thermal diffusivity
$\alpha_n, \beta_n, \lambda_n, \gamma_n$	=	eigenvalues
δ_{ij}	=	Kronecker delta
θ, θ_0	=	dimensionless temperature and uniform entrance temperature, $(T-T_m)/(T_2-T_m)$ and $(T_0-T_m)/(T_2-T_m)$
$\theta_1, \theta_2, \theta_b$	=	temperature distributions in the upstream and downstream regions and bulk temperature
ν	=	kinematic viscosity
ϕ_θ	=	dimensionless temperature profile, $(1 - \theta)/2$
ϕ_j, ψ_j	=	orthonormal functions

2.1 Introduction

When the axial heat conduction effect is important for the thermal entrance region problem in tubes or channels, the assumption of uniform entrance temperature at $X = 0$ used in the classical Graetz formulation [1] becomes physically unrealistic because of the upstream heat penetration. The elliptic energy equation with the axial conduction term has been solved by several investigators [2-6] considering the region extending from $X = -\infty$ to $X = \infty$ for fully developed laminar flow in tubes or channels using different theoretical solution methods. The thermal boundary conditions considered so far are either uniform wall temperature or uniform wall heat flux for the downstream region ($X \geq 0$) with the upstream region ($X < 0$) perfectly insulated. In addition, the fluid temperature is taken to be uniform at $X = -\infty$.

Considering the case of plane Poiseuille flow in horizontal parallel-plate channels, the thermal boundary conditions at the upper and lower plates may be different in practical applications. The interesting case of uniform but unequal wall temperatures [7] for Graetz problem does not appear to have been investigated in the past using the exact formulation [4] considering the axial heat conduction effect.

The purpose of this study is to present heat transfer results in the thermal entrance region of plane Poiseuille flow between two horizontal parallel plates maintained at unequal but constant wall temperatures. The analysis is based on a rigorous formulation [4] and the main concern here is the heat transfer characteristics in the low Peclet number flow regime. The present analysis is motivated by the thermal instability analysis (Chapter III) for the onset of longitudinal and transverse rolls in parallel-plate channels heated from below and serves as a basic flow solution. As compared with the earlier works [2-6], the present problem involves two distinct sets of eigenvalues related to even and odd sets of eigenfunctions [7] whereas the published and analytical solutions are concerned only with even eigenvalues and eigenfunctions.

2.2 Theoretical Analysis

2.2.1 Governing Equations

Neglecting the viscous dissipation effects, the energy equation and the boundary conditions in dimensionless form for the thermal entrance region problem (see Fig. 1) with axial heat conduction can be written as [4]

$$\frac{2}{3} u \frac{\partial \theta}{\partial x} = \frac{\partial^2 \theta}{\partial z^2} + \left(\frac{8}{3Pe}\right)^2 \frac{\partial^2 \theta}{\partial x^2} \tag{1}$$

$$\theta_I(-\infty, z) = \theta_0, \quad \partial\theta_I(x,1)/\partial z = -\partial\theta_I(x,-1)/\partial z = 0$$

$$\text{for } -\infty < x \le 0 \tag{2}$$

$$\theta_2(\infty,z) = \theta_f,\ \theta_2(x,1) = 1,\ \theta_2(x,-1) = -1 \quad \text{for } 0 \le x < \infty \tag{3}$$

$$\theta_1(0,z) = \theta_2(0,z),\ \partial\theta_1(0,z)/\partial x = \partial\theta_2(0,z)/\partial x \quad \text{at } x = 0 \tag{4}$$

where the dimensionless variables are defined in Nomenclature and $u = (3/2)(1 - z^2)$ for plane Poiseuille flow. As $Pe \to \infty$, one recovers the case of negligible axial conduction [1].

2.2.2 Solution

The temperature distributions in the adiabatic and the thermal entrance regions satisfying the conditions at $x = \pm\infty$ are sought in the following form [4,7]:

$$\theta_1(x,z) = \theta_0 + \sum_{n=1}^{\infty} B_n Y_n(z) \exp(\alpha_n^2 x)$$

$$+ \sum_{n=1}^{\infty} A_n F_n(z) \exp(\varepsilon_n^2 x), \quad -\infty < x \le 0 \tag{5}$$

$$\theta_2(x,z) = z + \sum_{n=1}^{\infty} C_n R_n(z) \exp(-\beta_n^2 x)$$

$$+ \sum_{n=1}^{\infty} D_n Z_n(z) \exp(-\gamma_n^2 x), \quad 0 \le x < \infty \tag{6}$$

where α_n, ε_n; and Y_n, F_n are the even and odd eigenvalues and eigenfunctions, respectively, for the adiabatic region.

Similarly, β_n, Y_n; and R_n, Z_n are the even and odd eigenvalues and eigenfunctions, respectively, for the thermal entrance region. The associated characteristic equations and boundary conditions are:

$$\frac{d^2Y_n}{dz^2} + \alpha_n^2 \left[\left(\frac{8\alpha_n}{3Pe}\right)^2 - (1 - z^2)\right]Y_n = 0, \quad dY_n(\pm 1)/dz = 0 \tag{7}$$

$$\frac{d^2F_n}{dz^2} + \varepsilon_n^2 \left[\left(\frac{8\varepsilon_n}{3Pe}\right)^2 - (1 - z^2)\right]F_n = 0, \quad dF_n(\pm 1)/dz = 0 \tag{8}$$

$$\frac{d^2R_n}{dz^2} + \beta_n^2 \left[\left(\frac{8\beta_n}{3Pe}\right)^2 + (1 - z^2)\right]R_n = 0, \quad R_n(\pm 1) = 0 \tag{9}$$

$$\frac{d^2Z_n}{dz^2} + \gamma_n^2 \left[\left(\frac{8\gamma_n}{3Pe}\right)^2 + (1 - z^2)\right]Z_n = 0, \quad Z_n(\pm 1) = 0 \tag{10}$$

It is noted that as $Pe \to \infty$, the set of equations (9) and (10) reduces to the type of the Graetz problem [1]. In this study, equations (7) to (10) are solved numerically by using a fourth-order Runge-Kutta method [9]. Two hundred equal steps are employed and the boundary conditions at $z = 0$ are used as the starting point. The eigenvalues are improved by using the variable secant method [9] which requires assuming two trial values with a difference of say 0.005 at the start. The even eigenvalues β_n are listed in reference [4] for Pe = 1, 5, 10, 50 and can be used as the initial values in this study. The number of iterations required to have a tolerance of $dY_n(1)/dz$, $dF_n(1)/dz$, $R_n(1)$, or $Z_n(1) < 10^{-8}$ depends on the initial guess for each eigenvalue but it usually takes 3 to 7 iterations. The spectrum of the eigenvalues is checked by plotting α_n, ε_n, β_n or γ_n versus n. The eigenvalues for Pe = 1, 5, 10, 50 are listed in Tables 1 and 2. The even eigenvalues α_n, β_n are found to agree with those reported in reference [4].

The series expansion coefficients A_n, B_n, C_n, D_n are determined by applying the matching conditions at x = 0, equation (4), for the two regions. Substituting equations (5) and (6) into (4) yields:

$$\sum_{n=1}^{\infty} C_n R_n(z) - \sum_{n=1}^{\infty} B_n Y_n(z) = \theta_0, \quad \sum_{n=1}^{\infty} C_n \beta_n^2 R_n(z) + \sum_{n=1}^{\infty} B_n \alpha_n^2 Y_n(z) = 0 \tag{11}$$

$$\sum_{n=1}^{\infty} D_n Z_n(z) - \sum_{n=1}^{\infty} A_n F_n(z) = -z, \quad \sum_{n=1}^{\infty} D_n \gamma_n^2 Z_n(z) + \sum_{n=1}^{\infty} A_n \varepsilon_n^2 F_n(z) = 0 \tag{12}$$

Since the axial conduction term is retained, the eigenfunctions lack the orthogonality property and the eigenfunction expansion technique commonly used for the Sturm-Liouville system cannot be used here in evaluating the series expansion coefficients. Following the procedure described in reference [4], the four complete sets of trial orthonormal functions in terms of Y_n, F_n, R_n, and Z_n, respectively, can be constructed by a linear combination in the following form:

$$\phi_j = \sum_{n=1}^{j} b_n^j Y_n(z), \quad f_j = \sum_{n=1}^{j} d_n^j F_n(z),$$

$$\psi_j = \sum_{n=1}^{j} a_n^j R_n(z), \quad s_j = \sum_{n=1}^{j} c_n^j Z_n(z) \tag{13}$$

where $\int_0^1 \phi_i \phi_j dz = \delta_{ij}$, $j = 1, 2, \ldots$ and a similar relationship holds for f_j, ψ_j and s_j. The Gramm-Schmidt orthonormalization procedure can now be applied step by step as described in references [4,10]. By the following linear transformations [4], the eigenfunctions can be expressed conversely in terms of the orthonormal functions as

$$Y_n(z) = \sum_{j=1}^{n} q_j^n \phi_j(z), \quad F_n(z) = \sum_{j=1}^{n} r_j^n f_j(z)$$

$$R_n(z) = \sum_{j=1}^{n} p_j^n \psi_j(z), \quad Z_n(z) = \sum_{j=1}^{n} t_j^n s_j(z) \tag{14}$$

The coefficients q_j^n, r_j^n, p_j^n and t_j^n can be obtained from the matrix equations $[q] = [b]^{-1}$, $[r] = [d]^{-1}$, $[p] = [a]^{-1}$ and $[t] = [c]^{-1}$. Substituting equation (14) into equations (11) and (12), one obtains

$$\sum_{n=1}^{\infty} C_n\Big(\sum_{j=1}^{n} p_j^n\psi_j\Big) - \sum_{n=1}^{\infty} B_n\Big(\sum_{j=1}^{n} q_j^n\phi_j\Big) = \theta_0$$

$$\sum_{n=1}^{\infty} C_n\beta_n^2\Big(\sum_{j=1}^{n} p_j^n\psi_j\Big) + \sum_{n=1}^{\infty} B_n\alpha_n^2\Big(\sum_{j=1}^{n} q_j^n\phi_j\Big) = 0 \qquad (15)$$

$$\sum_{n=1}^{\infty} D_n\Big(\sum_{j=1}^{n} r_j^n s_j\Big) - \sum_{n=1}^{\infty} A_n\Big(\sum_{j=1}^{n} t_j^n f_j\Big) = -z$$

$$\sum_{n=1}^{\infty} D_n\gamma_n^2\Big(\sum_{j=1}^{n} r_j^n s_j\Big) + \sum_{n=1}^{\infty} A_n\varepsilon_n^2\Big(\sum_{j=1}^{n} t_j^n f_j\Big) = 0 \qquad (16)$$

By noting the orthonormal properties for ψ_j, ϕ_j, s_j and f_j, one obtains the following sets of equations after truncating the infinite series at $n = N$.

$$\sum_{n=1}^{N} C_n\Big(\sum_{j=1}^{n} p_j^n\delta_{ij}\Big) - \sum_{n=1}^{N} B_n\Big(\sum_{j=1}^{n} q_j^n \int_0^1 \phi_j\psi_i\,dz\Big) = \int_0^1 \theta_0\psi_i\,dz$$

$$\sum_{r=1}^{N} C_n\beta_n^2\Big(\sum_{j=1}^{n} p_j^n \int_0^1 \psi_j\phi_i\,dz\Big) + \sum_{n=1}^{N} B_n\alpha_n^2\Big(\sum_{j=1}^{n} q_j^n\delta_{ij}\Big) = 0 \qquad (17)$$

$$\sum_{n=1}^{N} D_n\left(\sum_{j=1}^{n} r_j^n \delta_{ij}\right) - \sum_{n=1}^{N} A_n\left(\sum_{j=1}^{n} t_j^n \int_0^1 f_j s_i dz\right) = -\int_0^1 z s_i dz$$

$$\sum_{n=1}^{N} D_n \gamma_n^2\left(\sum_{j=1}^{n} r_j^n \int_0^1 s_j f_i dz\right) + \sum_{n=1}^{N} A_n \varepsilon_n^2\left(\sum_{j=1}^{n} t_j^n \delta_{ij}\right) = 0 \qquad (18)$$

In this study, N is taken to be 20 for Pe = 1, 5, 10 and 50.

The two systems of simultaneous equations for the coefficient B_n, C_n and A_n, D_n are solved by using the Gaussian elimination method (IBM-SSP-DGELG) on IBM-360/67 with a relative tolerance of 10^{-8}. The results and the related constants are listed in Tables 3-6. The series expansion coefficients with N = 20 are also obtained by using a method for nonorthogonal series described by Kantorovich and Krylov [11] but it yields negligible improvement in the accuracy of the series expansion coefficients. After obtaining the coefficients, the matching conditions at x = 0 given by equation (4) are checked. The first matching condition $\theta_1 = \theta_2$ is satisfied very well and three significant figures agree excluding the points near the upper and lower plates. The second matching condition $\partial\theta_1/\partial x = \partial\theta_2/\partial x$ is met satisfactorily but the agreement is one order lower. It is expected that the matching conditions at $z = \pm 1$ will not be satisfied in view of the discontinuity of the boundary conditions at x = 0. It is also found that four significant figures agree for bulk temperatures at x = 0.

2.2.3 Local Nusselt Numbers

The local Nusselt numbers Nu_1 and Nu_2 at the lower and upper plates defined by the following equations for the case of heating from below ($T_1 > T_2$) are of practical interest in this study.

$$Nu_1 = \frac{h_1(4\ell)}{k} = \frac{(4\ell)}{k}\frac{q_1}{(T_1 - T_b)} = \frac{4}{1+\theta_b}\left(\frac{\partial\theta_2}{\partial z}\right)_{z=-1} \tag{19}$$

$$Nu_2 = \frac{h_2(4\ell)}{k} = \frac{(4\ell)}{k}\frac{q_2}{(T_b - T_2)} = \frac{4}{1-\theta_b}\left(\frac{\partial\theta_2}{\partial z}\right)_{z=1} \tag{20}$$

where the bulk temperature θ_b is

$$\theta_b = \int_{-1}^{1} \theta u dz / \int_{-1}^{1} u dz \tag{21}$$

Substituting equation (6) into equations (19) to (21) yields,

$$Nu_{2,1} = \frac{4 \pm 4[\sum_{n=1}^{\infty} C_n (dR_n(1)/dz)\exp(-\beta_n^2 x) \pm \sum_{n=1}^{\infty} D_n (dZ_n(1)/dz)\exp(-\gamma_n^2 x)]}{1 \pm (3/2)\sum_{n=1}^{\infty} C_n \exp(-\beta_n^2 x)[(dR_n(1)/dz)/\beta_n^2 + (8\beta_n/3Pe)^2 \int_0^1 R_n(z)dz]} \tag{22}$$

$$\theta_{2b} = -\frac{3}{2}\sum_{n=1}^{\infty} C_n \exp(-\beta_n^2 x)\left[\frac{dR_n(1)dz}{\beta_n^2} + \left(\frac{8\beta_n}{3Pe}\right)^2 \int_0^1 R_n(z)dz\right] \tag{23}$$

The bulk temperature in the adiabatic section is

$$\theta_{1b} = \theta_0 + \frac{3}{2}\left(\frac{8}{3Pe}\right)^2 \sum_{n=1}^{\infty} B_n\alpha_n^2 \exp(\alpha_n^2 x) \int_0^1 Y_n(z)dz \qquad (24)$$

One may note that the case $Pe \to \infty$ corresponds to that of no axial conduction.

2.3 Results and Discussion

The profiles of the first eight eigenfunctions only for Y_n, R_n, Z_n and F_n are shown in Figs. 2 to 5 for Pe = 1. The developing temperature profiles, $\phi_\theta = \frac{1}{2}(1 - \theta)$, versus the transformed coordinate $\bar{z} = (z + 1)/2$ in both upstream and downstream regions are presented in Figs. 6 to 8 for Pe = 1, 5 and 10, respectively, with $\theta_0 = 1$. In Fig. 6 (Pe = 1), the temperature profile is seen to be flat upstream of x = -4 (ϕ_θ = 0.27). At x = -30, one obtains ϕ_θ = 0.027. This suggests that at Pe $\doteq$ 1 the axial heat conduction effect is felt throughout a rather extensive upstream region. For the upstream region $x \leq -4$, the effect of the lower plate $x \geq 0$ at temperature T_1 disappears completely and the transverse conduction term $\partial^2\theta/\partial z^2$ in energy equation (1) can be neglected entirely. Thus, at Pe = 1 the region $-30 \leq x \leq -4$ can be regarded to be a pure axial conduction region. The fully developed temperature profile is seen to be attained at $x \approx 6$. In the region $-0.1 \leq x \leq 0.1$, the change of the temperature profile is rather gradual. In

Fig. 6, the axial distributions of the wall temperatures in the adiabatic region are also of interest.

The effect of the axial heat conduction on developing temperature profiles in both adiabatic and heated regions persists for Pe = 5 and 10 as shown in Figs. 7 and 8, respectively. It is also seen that the uniform entrance fluid temperature $\phi_\theta = 0$ is practically reached at $\bar{x} = -2$ and -1 for Pe = 5 and 10, respectively. At Pe = 50 shown in Fig. 9, the axial heat conduction effect is confined to a rather small region $0 \leq z \leq 0.3$, $-0.05 \leq x \leq 0$. The upstream heat penetration in the region near the upper plate $0.6 \leq z \leq 1.0$, $-10^{-3} \leq x \leq 10^{-3}$, is apparently not a physical solution and the temperature field is $\phi_\theta = 0$ there. The imposition of the discontinuous boundary conditions $\partial\phi_{\theta 1}(0,1)/\partial z = 0$ and $\phi_{\theta 2}(0,1) = 0$ coupled with the uniform entrance temperature condition $\phi_{\theta 1} = 0$ at $x = -\infty$ for $0.6 \leq z \leq 1.0$ is apparently the source of difficulty. The mathematical conditions mentioned are incompatible with the physical situation and one thus concludes that the mathematical solution fails for the small region $0.6 \leq z \leq 1.0$, $-10^{-3} \leq x \leq 10^{-3}$. From practical viewpoint, it is seen that the axial heat conduction is not significant at Pe > 50. It should be pointed out that the above difficulty arises only when the boundary conditions at lower and upper plates are different. This also serves to emphasize the difference between the present problem and that of published work [4].

For the present problem, the matching of the temperatures and axial temperature gradients at $x = 0$ is critical and the results for ϕ_θ at $x = 0$ are shown in Fig. 10 for Pe = 1, 5, 10 and 50. The matching is satisfied very well for Pe = 1, 5 and 10 but the numerical result for Pe = 50 near the upper plate is not a physical solution. Physically, one knows that the upstream and downstream temperatures, $\phi_{\theta 1}$ and $\phi_{\theta 2}$, should be continuous at $x = 0$ including upper and lower plates. Fig. 10 shows that at the lower plate $z = 0$, the temperature discontinuity for ϕ_θ increases with the increase of Peclet number. On the other hand, at the upper plate $z = 1$, the agreement for $\phi_{\theta 1}$ and $\phi_{\theta 2}$ is better for Pe = 10 than for Pe = 1. At Pe = 50, the discontinuity for ϕ_θ at $z = 1$ is clearly the source of difficulty since the series solution for ϕ_θ must be continuous and $\phi_\theta = 0$ for $0.2 \leq z \leq 1.0$. The mathematical difficulty near the upper plate at $x = 0$ for Pe = 50 can also be explained from the energy equation (1). When the Peclet number is large, the concept of thermal boundary layer is applicable and $\partial\theta/\partial x$ and $\partial^2\theta/\partial x^2$ are zero in the neighbourhood of the upper plate near $x = 0$. As a result, one obtains $\partial^2\theta/\partial z^2 = 0$ only and the transverse conduction term cannot be balanced by the convective term. One notes that the above situation does not occur near the lower plate where one has thermal boundary layer. The above explanation represents another source of difficulty besides the thermal boundary conditions at $x = 0$. Further increase of the number of series coefficients to $n = 24$ does not improve the numerical results for Pe = 1, 5, 10 and 50 near $x = 0$. It is found that with $n = 26$, the Gram determinant [4] $\Delta_n \rightarrow 0$ for the odd eigenfunctions Z_n and the series coefficients cannot be obtained. It is also found that with $n = 26$, the eigenfunction Z_n is of the order 10^{-3} (see also Fig. 4). It is thus seen that as n increases Z_n decreases.

The effect of Peclet number on the axial distribution of the bulk temperature is shown in Fig. 11 and the numerical results are listed in Table 7. At Pe = 1, the axial heat conduction effect is quite appreciable but at Pe = 50 the effect may be practically negligible. The upstream and downstream development lengths for attaining the asymptotic values $\theta_b = 1$ and 0, respectively, depend on Peclet number.

The local Nusselt number results at the lower and upper plates are shown in Fig. 12 for Pe = 1, 5, 10, 50 and ∞ with $\theta_0 = 1$ and the numerical results are listed in Table 8. The behavior of the local Nusselt number at lower plate Nu_1 is generally similar to that reported in references [4,10]. Near $x = 0$, both Nu_1 and Nu_2 become quite uniform with the decrease of Peclet number. When the axial heat conduction is negligible ($Pe \rightarrow \infty$), $Nu_1 \rightarrow \infty$ as $x \rightarrow 0$ and Nu_2 is zero throughout some thermal-entry region near $x = 0$. The case of $Pe = \infty$ is also discussed in reference [7]. It is seen that both Nu_1 and Nu_2 for various Peclet numbers approach the same fully developed value 4.0 and the thermal entrance length increases with the decrease of

Peclet number.

2.4 Concluding Remarks

1. For $\theta_0 = 1$, the present physical model is not applicable when $Pe > 50$ and the classical Graetz formulation neglecting axial heat conduction should be used. It appears that the mathematical difficulty arises as the physical problem changes from elliptical problem to parabolic problem. When $Pe < 50$, the axial heat conduction effect on bulk temperature and local Nusselt numbers is appreciable. The numerical results for $\theta_0 \neq 1$ can also be obtained without difficulty.

2. The even eigenvalues α_n, β_n check very well with those reported in reference [4] and can also be used in ascertaining the eigenvalue spectrum. The characteristic equations (7) and (9) suggest that for $Pe \lesssim 1$, the approximate eigenvalues for α_n and β_n can be obtained by the following relations.

$$\alpha_n^2 = \frac{8Pe}{3}(n - 1)\pi, \quad n = 2, 3, \ldots,$$

$$\beta_n^2 = \frac{8Pe}{3}(n - \tfrac{1}{2})\pi, \quad n = 1, 2, 3, \ldots$$

Generally, the above approximations improve with the increase of n. It is found that the above approximations can still be used for Pe = 5 but the accuracy decreases by one order of magnitude as compared with the case of Pe = 1. It is also found that $\varepsilon_n = (\alpha_n + \alpha_{n+1})/2$ and $\gamma_n = (\beta_n + \beta_{n+1})/2$ for any Pe. For Pe = ∞, the eigenvalues β_n, γ_n from reference [7] are used.

3. The present numerical results as shown in Fig. 10 clearly bring out the nature of the analytical solution for the present elliptic problem with Pe = 50. The local mathematical difficulty for Pe = 50 near the upper plate at x = 0 is noteworthy and the phenomenon does not appear to have been pointed out in the past. At Pe = 50, the difficulty is confined to the local region near x = 0 and z = 1 but the bulk temperature appears to be reasonable as shown in Fig. 11.

4. For low Peclet number flow regime, the axial heat conduction can cause a considerable increase in thermal development lengths for both upstream and downstream regions.

5. For low Peclet number flow (Pe < 50), one can clearly identify three different regimes, namely pure axial heat conduction, developing and fully developed regions, for the thermal entrance region problem. When heating is from below ($T_1 > T_2$), thermal instability problem concerned with the onset of secondary flow in the form of longitudinal vortices or transverse rolls arises at a certain $\Delta T = T_1 - T_2$. The instability problem is studied in Chapter III, and the present solution serves as a basic flow solution.

References

1. Graetz, L., "Wärmeletiungsfähigk v. Flüssigk", Ann. Phys. 25, 1885, pp. 337-357.
2. Agrawal, H.C., "Heat Transfer in Laminar Flow Between Parallel Plates of Small Peclet Numbers", App. Sci. Res. A9, 1960, pp. 177-189.
3. Hennecke, D.K., "Heat Transfer by Hagen-Poiseuille Flow in the Thermal Development Region with Axial Conduction", Wärme-und Stoffübertragung, Vol. 1, 1968, pp. 177-184.
4. Hsu, C.J., "An Exact Analysis of Low Peclet Number Thermal Entry Region Heat Transfer in Transversely Non-Uniform Velocity Fields", A.I.C.H.E. Journal, Vol. 7, 1971, pp. 732-740.
5. Pirkle, J.C. and Sigillito, V.G., "A Variational Approach to Low Peclet Number Heat Transfer in Laminar Flow", J. Comp. Phys. 9, 1972, pp. 207-221.
6. Deavours, C.A., "An Exact Solution for the Temperature Distribution in Parallel Plate Poiseuille Flow", J. Heat Transfer, 96C, 1974, pp. 489-495.
7. Hatton, A.P. and Turton, J.S., "Heat Transfer in the Thermal Entry Length with Laminar Flow Between Parallel Walls at Unequal Temperatures", Int. J. of Heat Mass Transfer, Vol. 5, 1962, pp. 673-679.

8. Collatz, L., "The Numerical Treatment of Differential Equations", 3rd Ed., Springer-Verlag, Berlin, 1960, p. 69.

9. Froberg, C.E., "Introduction to Numerical Analysis", 2nd Ed., Addison-Wesley, Reading, Massachusetts, 1969, p. 22.

10. Hsu, C.J., "Theoretical Solution for Low-Peclet-Number Thermal Entry Region Heat Transfer in Laminar Flow Through Concentric Annuli", Int. J. Heat Mass Transfer, Vol. 13, 1970, pp. 1907-1924.

11. Kantorovich, L.V. and Krylov, V.I., "Approximate Methods of Higher Analysis", Interscience Publishers, 1958, pp. 54-56.

Table 1. Eigenvalues for Pe = 1 and 5

Pe = 1

n	[illegible]$_n$	[illegible]$_n$	[illegible]$_n$	[illegible]$_n$
1	0.3060040E+00	0.7287309E+00	0.7889385E+00	0.1062382E+01
2	0.1105802E+01	0.1311250E+01	0.1346581E+01	0.1519527E+01
3	0.1550091E+01	0.1702419E+01	0.1729745E+01	0.1867454E+01
4	0.1892395E+01	0.2019032E+01	0.2042120E+01	0.2159992E+01
5	0.2181588E+01	0.2292299E+01	0.2312659E+01	0.2417373E+01
6	0.2436688E+01	0.2536286E+01	0.2554701E+01	0.2649867E+01
7	0.2667499E+01	0.2758776E+01	0.2775716E+01	0.2863546E+01
8	0.2879869E+01	0.2964615E+01	0.2980385E+01	0.3062351E+01
9	0.3077620E+01	0.3157062E+01	0.3171876E+01	0.3249014E+01
10	0.3263410E+01	0.3338434E+01	0.3352446E+01	0.3425521E+01
11	0.3439178E+01	0.3510448E+01	0.3523776E+01	0.3593369E+01
12	0.3606391E+01	0.3674419E+01	0.3687155E+01	0.3753720E+01
13	0.3766187E+01	0.3831380E+01	0.3843595E+01	0.3907498E+01
14	0.3919475E+01	0.3982160E+01	0.3993914E+01	0.4055449E+01
15	0.4066991E+01	0.4127437E+01	0.4138779E+01	0.4198191E+01
16	0.4209342E+01	0.4267773E+01	0.4278743E+01	0.4336239E+01
17	0.4347036E+01	0.4403641E+01	0.4414273E+01	0.4470028E+01
18	0.4480502E+01	0.4535443E+01	0.4545767E+01	0.4599929E+01
19	0.4610108E+01	0.4663524E+01	0.4673564E+01	0.4726264E+01
20	0.4736172E+01	0.4788183E+01	0.4797963E+01	0.4849312E+01

Pe = 5

n	[illegible]$_n$	[illegible]$_n$	[illegible]$_n$	[illegible]$_n$
1	0.1508323E+01	0.1337162E+01	0.1960584E+01	0.2180762E+01
2	0.2678328E+01	0.2776457E+01	0.3174373E+01	0.3263730E+01
3	0.3606607E+01	0.3686892E+01	0.3992958E+01	0.4066260E+01
4	0.4345400E+01	0.4413191E+01	0.4671500E+01	0.4734824E+01
5	0.4976383E+01	0.5036002E+01	0.5263707E+01	0.5320192E+01
6	0.5536189E+01	0.5589979E+01	0.5795909E+01	0.5847354E+01
7	0.6044507E+01	0.6093884E+01	0.6283296E+01	0.6330835E+01
8	0.6513352E+01	0.6559242E+01	0.6735567E+01	0.6779968E+01
9	0.6950691E+01	0.6993738E+01	0.7159362E+01	0.7201172E+01
10	0.7362127E+01	0.7402800E+01	0.7559461E+01	0.7599085E+01
11	0.7751778E+01	0.7790430E+01	0.7939442E+01	0.7977189E+01
12	0.8122776E+01	0.8159679E+01	0.8302064E+01	0.8338178E+01
13	0.8477565E+01	0.8512937E+01	0.8649508E+01	0.8684183E+01
14	0.8818101E+01	0.8852119E+01	0.8983533E+01	0.9016930E+01
15	0.9145976E+01	0.9178783E+01	0.9305585E+01	0.9337834E+01
16	0.9462505E+01	0.9494223E+01	0.9616866E+01	0.9648079E+01
17	0.9768790E+01	0.9799522E+01	0.9918389E+01	0.9948661E+01
18	0.1006577E+02	0.1009560E+02	0.1021102E+02	0.1024043E+02
19	0.1035424E+02	0.1038325E+02	0.1049550E+02	0.1052412E+02
20	0.1063490E+02	0.1066314E+02	0.1077249E+02	0.1080038E+02

Table 2. Eigenvalues for Pe = 10 and 50

Pe = 10

n	α_n	β_n	ε_n	γ_n
1	0.2891829E+01	0.1539808E+01	0.3111802E+01	0.2781286E+01
2	0.4236301E+01	0.3672146E+01	0.4804503E+01	0.4392325E+01
3	0.6355316E+01	0.5012257E+01	0.5879756E+01	0.5564796E+01
4	0.5365803E+01	0.6068040E+01	0.6799235E+01	0.6533184E+01
5	0.7216787E+01	0.6967729E+01	0.7612023E+01	0.7376995E+01
6	0.7988097E+01	0.7764921E+01	0.8347501E+01	0.8134519E+01
7	0.8692241E+01	0.8488154E+01	0.9023958E+01	0.8827723E+01
8	0.9344010E+01	0.9154776E+01	0.9653538E+01	0.9470599E+01
9	0.9953508E+01	0.9776270E+01	0.1024475E+02	0.1007271E+02
10	0.1052798E+02	0.1036070E+02	0.1080382E+02	0.1064093E+02
11	0.1107282E+02	0.1091398E+02	0.1133547E+02	0.1118039E+02
12	0.1159218E+02	0.1144061E+02	0.1184335E+02	0.1169506E+02
13	0.1208932E+02	0.1194411E+02	0.1233039E+02	0.1218807E+02
14	0.1256686E+02	0.1242726E+02	0.1279896E+02	0.1266194E+02
15	0.1302694E+02	0.1289236E+02	0.1325101E+02	0.1311873E+02
16	0.1347136E+02	0.1334128E+02	0.1368817E+02	0.1356018E+02
17	0.1390160E+02	0.1377560E+02	0.1411182E+02	0.1398772E+02
18	0.1431895E+02	0.1419667E+02	0.1452313E+02	0.1440260E+02
19	0.1472449E+02	0.1460563E+02	0.1492314E+02	0.1480588E+02
20	0.1511919E+02	0.1500346E+02	0.1531273E+02	0.1519848E+02

Pe = 50

n	α_n	β_n	ε_n	γ_n
1	0.1051927E+02	0.1673994E+01	0.1584219E+02	0.3585381E+01
2	0.1584147E+02	0.5363987E+01	0.1790440E+02	0.6981863E+01
3	0.1786702E+02	0.8447450E+01	0.1922040E+02	0.9781692E+01
4	0.1885437E+02	0.1100647E+02	0.2042735E+02	0.1214060E+02
5	0.1982894E+02	0.1319919E+02	0.2165960E+02	0.1419411E+02
6	0.2104313E+02	0.1513470E+02	0.2287736E+02	0.1602834E+02
7	0.2227199E+02	0.1688098E+02	0.2406138E+02	0.1769745E+02
8	0.2347410E+02	0.1848175E+02	0.2520634E+02	0.1923720E+02
9	0.2463882E+02	0.1996661E+02	0.2631205E+02	0.2067237E+02
10	0.2576402E+02	0.2135656E+02	0.2738022E+02	0.2202094E+02
11	0.2685069E+02	0.2266708E+02	0.2841323E+02	0.2329636E+02
12	0.2790096E+02	0.2390997E+02	0.2941357E+02	0.2450899E+02
13	0.2891733E+02	0.2509439E+02	0.3038369E+02	0.2566703E+02
14	0.2990226E+02	0.2622769E+02	0.3132582E+02	0.2677706E+02
15	0.3085812E+02	0.2731579E+02	0.3224204E+02	0.2784445E+02
16	0.3178705E+02	0.2836358E+02	0.3313419E+02	0.2887367E+02
17	0.3269101E+02	0.2937515E+02	0.3400397E+02	0.2986845E+02
18	0.3357178E+02	0.3035395E+02	0.3485289E+02	0.3083200E+02
19	0.3443095E+02	0.3130292E+02	0.3568231E+02	0.3176702E+02
20	0.3526995E+02	0.3222458E+02	0.3649346E+02	0.3267588E+02

Table 3. Series Coefficients for Pe = 1, 5

Pe = 1

n	C_n	D_n	B_n	A_n
1	0.1556876E+00	-0.5631040E+00	-0.8892877E+00	0.9426643E+00
2	-0.2588527E-01	0.4289643E+00	0.3507104E-01	-0.4586241E+00
3	0.1218683E-01	-0.3693818E+00	-0.1235074E-01	0.3306520E+00
4	-0.7565136E-02	0.3345909E+00	0.6460406E-02	-0.2613842E+00
5	0.5355651E-02	-0.3116688E+00	-0.3970785E-02	0.2150673E+00
6	-0.4094527E-02	0.2954951E+00	0.2658857E-02	-0.1804733E+00
7	0.3292452E-02	-0.2835961E+00	-0.1872166E-02	0.1527655E+00
8	-0.2743783E-02	0.2746250E+00	0.1357959E-02	-0.1294506E+00
9	0.2348418E-02	-0.2677920E+00	-0.1000113E-02	0.1090760E+00
10	-0.2052343E-02	0.2626141E+00	0.7386351E-03	-0.9071079E-01
11	0.1824151E-02	-0.2587976E+00	-0.5397002E-03	0.7370476E-01
12	-0.1644527E-02	0.2561781E+00	0.3828671E-03	-0.5756203E-01
13	0.1501153E-02	-0.2546995E+00	-0.2550020E-03	0.4186291E-01
14	-0.1386052E-02	0.2544149E+00	0.1471409E-03	-0.2620781E-01
15	0.1294273E-02	-0.2555294E+00	-0.5268308E-04	0.1015734E-01
16	-0.1223370E-02	0.2585012E+00	-0.3378587E-04	0.6846355E-02
17	0.1173967E-02	-0.2643434E+00	0.1175729E-03	-0.2563501E-01
18	-0.1152708E-02	0.2755413E+00	-0.2054187E-03	0.4766345E-01
19	0.1187520E-02	-0.3003373E+00	0.3094696E-03	-0.7608606E-01
20	-0.1579937E-02	0.4215498E+00	-0.4635203E-03	0.1203376E+00

Pe = 5

n	C_n	D_n	B_n	A_n
1	0.6128442E+00	-0.7335528E+00	-0.5424658E+00	0.79[illegible]E+00
2	-0.9205655E-01	0.5115382E+00	0.1197280E+00	-0.4[illegible]E+00
3	0.4335907E-01	-0.4297348E+00	-0.4348329E-01	0.330[illegible]E+00
4	-0.2698757E-01	0.3845846E+00	0.2282867E-01	-0.2680021E+00
5	0.1913828E-01	-0.3556318E+00	-0.1404017E-01	0.2232743E+00
6	-0.1464728E-01	0.3355172E+00	0.9392467E-02	-0.1885051E+00
7	0.1178582E-01	-0.3208508E+00	-0.6599310E-02	0.1599247E+00
8	-0.9825556E-02	0.3098381E+00	0.4770626E-02	-0.1354222E+00
9	0.8411164E-02	-0.3014440E+00	-0.3496144E-02	0.1136966E+00
10	-0.7350581E-02	0.2950394E+00	0.2563402E-02	-0.9387669E-01
11	0.6531930E-02	-0.2902380E+00	-0.1852358E-02	0.7532799E-01
12	-0.5886257E-02	0.2868122E+00	0.1290290E-02	-0.5754604E-01
13	0.5369433E-02	-0.2846605E+00	-0.8302921E-03	0.4008290E-01
14	-0.4952638E-02	0.2837972E+00	0.4401113E-03	-0.2248921E-01
15	0.4617556E-02	-0.2843871E+00	-0.9562855E-04	0.4243016E-02
16	-0.4354154E-02	0.2868250E+00	-0.2235444E-03	0.1535399E-01
17	0.4161626E-02	-0.2919822E+00	0.5384772E-03	-0.3739409E-01
18	-0.4054604E-02	0.3018652E+00	-0.8778419E-03	0.6387234E-01
19	0.4056730E-02	-0.3194410E+00	0.1296098E-02	-0.9922852E-01
20	-0.5833665E-02	0.4848251E+00	-0.1934437E-02	0.1557675E+00

Table 4. Series Coefficients for Pe = 10, 50

Pe = 10

n	C_n	D_n	B_n	A_n
1	0.8919186E+00	-0.9464541E+00	-0.2892040E+00	0.5903097E+00
2	-0.1335596E+00	0.6168914E+00	0.1251294E+00	-0.3653355E+00
3	0.6208682E-01	-0.5065044E+00	0.3088496E-01	0.3207773E+00
4	-0.3855233E-01	0.4481160E+00	-0.5772156E-01	-0.2708927E+00
5	0.2731553E-01	-0.4114227E+00	-0.1912460E-01	0.2296907E+00
6	-0.2089380E-01	0.3862228E+00	0.1281574E-01	-0.1955116E+00
7	0.1680396E-01	-0.3679679E+00	-0.8991931E-02	0.1663082E+00
8	-0.1400247E-01	0.3542948E+00	0.6473763E-02	-0.1406017E+00
9	0.1198076E-01	-0.3438547E+00	-0.4710562E-02	0.1173516E+00
10	-0.1046403E-01	0.3358301E+00	0.3414628E-02	-0.9579600E-01
11	0.9292193E-02	-0.3297140E+00	-0.2422258E-02	0.7533773E-01
12	-0.8366492E-02	0.3251958E+00	0.1633614E-02	-0.5546776E-01
13	0.7623542E-02	-0.3221125E+00	-0.9837339E-03	0.3570048E-01
14	-0.7021615E-02	0.3204253E+00	0.4273208E-03	-0.1551238E-01
15	0.6533578E-02	-0.3202435E+00	0.7039815E-04	-0.5747644E-02
16	-0.6143181E-02	0.3218769E+00	-0.5402192E-03	0.2900392E-01
17	0.5844978E-02	-0.3260194E+00	0.1016211E-02	-0.5577022E-01
18	-0.5653665E-02	0.3344835E+00	-0.1547689E-02	0.8887634E-01
19	0.5360702E-02	-0.3352307E+00	0.2226568E-02	-0.1343555E+00
20	-0.8493420E-02	0.5608646E+00	-0.3233073E-02	0.2050235E+00

Pe = 50

n	C_n	D_n	B_n	A_n
1	0.1173517E+01	-0.2064599E+01	-0.1683876E-02	-0.2711125E-01
2	-0.2472103E+00	0.2202653E+01	0.1633638E-02	0.9177557E-01
3	0.1134188E+00	-0.2289122E+01	-0.8145717E-02	-0.1855223E+00
4	-0.6870827E-01	0.2230526E+01	0.1656898E-01	0.2363296E+00
5	0.4802351E-01	-0.2089294E+01	-0.1642383E-01	-0.2295194E+00
6	-0.3643923E-01	0.1929673E+01	0.1125556E-01	0.1943915E+00
7	0.2913547E-01	-0.1784788E+01	-0.7667694E-02	-0.1452574E+00
8	-0.2415691E-01	0.1664559E+01	0.5073201E-02	0.8765537E-01
9	0.2057170E-01	-0.1568214E+01	-0.3105984E-02	-0.2359406E-01
10	-0.1788212E-01	0.1491690E+01	0.1549791E-02	-0.4673073E-01
11	0.1579968E-01	-0.1430730E+01	-0.2640038E-03	0.1243541E+00
12	-0.1414644E-01	0.1381813E+01	-0.8498411E-03	-0.2114489E+00
13	0.1280749E-01	-0.1342290E+01	0.1867187E-02	0.3114783E+00
14	-0.1170593E-01	0.1310243E+01	-0.2852022E-02	-0.4293466E+00
15	0.1078596E-01	-0.1284369E+01	0.3862825E-02	0.5707804E+00
16	-0.1004443E-01	0.1263963E+01	-0.4947740E-02	-0.7385106E+00
17	0.9201800E-02	-0.1248134E+01	0.6111480E-02	0.9189002E+00
18	-0.9612815E-02	0.1245012E+01	-0.7210623E-02	-0.1048759E+01
19	0.6512986E-02	-0.1215001E+01	0.7726018E-02	0.9714917E+00
20	-0.1063265E-01	0.1389790E+01	-0.6545026E-02	-0.5091460E+00

Table 5. Constants for Pe = 1, 5

Pe = 1

n	$R_n'(1)$	$\int_0^1 R_n(z)dz$	$Z_n'(1)$	$\int_0^1 Y_n(z)dz$
1	-0.1542929E+01	0.6332777E+00	-0.9718497E+00	0.1003655E+01
2	0.4680637E+01	-0.2205305E+00	0.9853798E+00	0.2487996E 01
3	-0.7822316E+01	0.1307080E+00	-0.9901758E+00	-0.2858931E-02
4	0.1096401E+02	-0.9271975E-01	0.9926067E+00	0.8573151E 03
5	-0.1410566E+02	0.7181920E-01	-0.9940740E+00	-0.3650107E-03
6	0.1724730E+02	-0.5860316E-01	0.9950554E+00	-0.1880612E 03
7	-0.2038893E+02	0.4949364E-01	-0.9957577E+00	-0.1093154E-03
8	0.2353055E+02	-0.4283458E-01	0.9962848E+00	0.6906848E 04
9	-0.2667217E+02	0.3775464E-01	-0.9966944E+00	-0.4638502E-04
10	0.2981376E+02	-0.3375170E-01	0.9970210E+00	0.3264904E 04
11	-0.3295533E+02	0.3051613E-01	-0.9972865E+00	-0.2383416E-04
12	0.3609685E+02	-0.2784653E-01	0.9975048E+00	0.1794583E 04
13	-0.3923827E+02	0.2560637E-01	-0.9976855E+00	-0.1382625E-04
14	0.4237954E+02	-0.2369965E-01	0.9978345E+00	0.10914[illegible]7E 04
15	-0.4552058E+02	0.2205714E-01	-0.9979558E+00	-0.8722032E 05
16	0.4866127E+02	-0.2062729E-01	0.9980515E+00	0.7149447E-05
17	-0.5180146E+02	0.1937144E-01	-0.9981224E+00	-0.5850648E 05
18	0.5494094E+02	-0.1825934E-01	0.9981680E+00	0.4968200E 05
19	-0.5807947E+02	0.1726787E-01	-0.9981870E+00	-0.4113237E-05
20	0.6121670E+02	-0.1637793E-01	0.9981769E+00	0.3635954E 05

Pe = 5

n	$R_n'(1)$	$\int_0^1 R_n(z)dz$	$Z_n'(1)$	$\int_0^1 Y_n(z)dz$
1	-0.1479343E+01	0.6255824E+00	-0.8870738E+00	0.1097040E+01
2	0.4550386E+01	-0.2471675E+00	0.9325373E+00	0.1355337E+00
3	-0.7689307E+01	0.1437979E+00	-0.9532163E+00	-0.1030541E 01
4	0.1083[illegible]21E+02	-0.9984576E-01	0.9643213E+00	0.3537791E-02
5	-0.1397501E+02	0.7620965E-01	-0.9711887E+00	-0.1578519E 02
6	0.1711752E+02	-0.6155989E-01	0.9758450E+00	0.8364927E-03
7	-0.2025980E+02	0.5161474E-01	-0.9792074E+00	-0.4955463E 03
8	0.2340192E+02	-0.4442847E-01	0.9817483E+00	0.3174060E-03
9	-0.2654393E+02	0.3899535E-01	-0.9837352E+00	-0.2153866E-03
10	0.2968585E+02	-0.3474455E-01	0.9853305E+00	0.1528110E-03
11	-0.3282768E+02	0.3132847E-01	-0.9866385E+00	-0.1123004E 03
12	0.3596941E+02	-0.2852338E-01	0.9877287E+00	0.8495129E-04
13	-0.3911102E+02	0.2617897E-01	-0.9886493E+00	-0.6578752E 04
14	0.4225245E+02	-0.2419033E-01	0.9894341E+00	0.5201762E-04
15	-0.4539363E+02	0.2248227E-01	-0.9901077E+00	-0.4179376E 04
16	0.4853444E+02	-0.2099917E-01	0.9906876E+00	0.3415154E-04
17	-0.5167474E+02	0.1969948E-01	-0.9911865E+00	-0.2818365E 04
18	0.5481432E+02	-0.1855084E-01	0.9916132E+00	0.2364698E-04
19	-0.5795293E+02	0.1752861E-01	-0.9919736E+00	-0.198[illegible]602E 04
20	0.6109024E+02	-0.1661252E-01	0.9922713E+00	0.170[illegible]833E-04

Table 6. Constants for Pe = 10, 50

n	$R_n'(1)$	$\int_0^1 R_n(z)dz$	$Z_n'(1)$	$\int_0^1 Y_n(z)dz$
1	-0.1450941E+01	0.6221126E+00	-0.8234686E+00	0.1454703E+01
2	0.4399766E+01	-0.2694375E+00	0.8777721E+00	0.2782054E+00
3	-0.7516604E+01	0.1586751E+00	-0.9118169E+00	0.5467240E-02
4	0.1065870E+02	-0.1086674E+00	0.9316426E+00	-0.7086805E-02
5	-0.1380338E+02	0.8178058E-01	-0.9443031E+00	-0.2605437E-02
6	0.1694780E+02	-0.6533740E-01	0.9530353E+00	0.1437739E-02
7	-0.2009168E+02	0.5432789E-01	-0.9594095E+00	-0.8741264E-03
8	0.2323511E+02	-0.4646587E-01	0.9642633E+00	0.5701851E-03
9	-0.2637818E+02	0.4057929E-01	-0.9680807E+00	-0.3921973E-03
10	0.2952097E+02	-0.3601030E-01	0.9711605E+00	0.2811812E-03
11	-0.3266353E+02	0.3236270E-01	-0.9736962E+00	-0.2083805E-03
12	0.3580589E+02	-0.2938405E-01	0.9758186E+00	0.1587004E-03
13	-0.3894803E+02	0.2690626E-01	-0.9776190E+00	-0.1236121E-03
14	0.4208992E+02	-0.2481292E-01	0.9791628E+00	0.9818372E-04
15	-0.4523149E+02	0.2302122E-01	-0.9804977E+00	-0.7923377E-04
16	0.4837266E+02	-0.2147024E-01	0.9816589E+00	0.6492889E-04
17	-0.5151327E+02	0.2011470E-01	-0.9826729E+00	-0.5379070E-04
18	0.5465314E+02	-0.1891957E-01	0.9835593E+00	0.4517595E-04
19	-0.5779200E+02	0.1785823E-01	-0.9843324E+00	-0.3817156E-04
20	0.6092954E+02	-0.1690892E-01	0.9850026E+00	0.3272955E-04

Pe = 50

n	$R_n'(1)$	$\int_0^1 R_n(z)dz$	$Z_n'(1)$	$\int_0^1 Y_n(z)dz$
1	-0.1430361E+01	0.6195853E+00	-0.7255992E+00	0.8922377E+02
2	0.3921668E+01	-0.3136271E+00	0.6941612E+00	0.1145040E+02
3	-0.6526332E+01	0.2180790E+00	-0.7173347E+00	0.1063733E+01
4	0.9381547E+01	-0.1606071E+00	0.7513932E+00	0.2469817E+00
5	-0.1240030E+02	0.1219932E+00	-0.7827980E+00	0.4233084E-01
6	0.1549773E+02	-0.9553246E-01	0.8088148E+00	0.5624168E-02
7	-0.1862880E+02	0.7710212E-01	-0.8298795E+00	-0.1271895E-02
8	0.2177358E+02	-0.6394882E-01	0.8470042E+00	0.1147005E-02
9	-0.2492367E+02	0.5428896E-01	-0.8610975E+00	-0.8870667E-03
10	0.2807555E+02	-0.4698805E-01	0.8728580E+00	0.6988601E-03
11	-0.3122766E+02	0.4132185E-01	-0.8828024E+00	-0.5576744E-03
12	0.3437935E+02	-0.3681980E-01	0.8913119E+00	0.4508095E-03
13	0.3753032E+02	0.3316898E-01	-0.8986704E+00	-0.3688738E-03
14	0.4068045E+02	-0.3015562E-01	0.9050922E+00	0.3052741E-03
15	-0.4382964E+02	0.2763031E-01	-0.9107411E+00	-0.2552221E-03
16	0.4697782E+02	-0.2548559E-01	0.9157441E+00	0.2154448E-03
17	-0.5012490E+02	0.2364317E-01	-0.9202006E+00	-0.1833656E-03
18	0.5327072E+02	-0.2204401E-01	0.9241892E+00	0.1573830E-03
19	-0.5641508E+02	0.2064386E-01	-0.9277723E+00	-0.1359350E-03
20	0.5955770E+02	-0.1940767E-01	0.9309997E+00	0.1183396E-03

Table 7 Bulk Mean Temperatures

x	Pe = 1	5	10	50
-6.0000	0.492	1.000	1.000	1.000
-4.0000	0.387	1.000	1.000	1.000
-2.0000	0.262	0.994	1.000	1.000
-1.0000	0.192	0.941	1.000	1.000
-0.1000	0.128	0.565	0.849	1.000
-0.0500	0.124	0.521	0.781	1.000
-0.0100	0.122	0.485	0.712	0.978
-0.0050	0.121	0.480	0.703	0.963
-0.0010	0.121	0.476	0.696	0.947
0.0001	0.121	0.475	0.694	0.942
0.0002	0.121	0.475	0.694	0.942
0.0004	0.121	0.475	0.693	0.941
0.0006	0.121	0.475	0.693	0.940
0.0008	0.121	0.475	0.692	0.939
0.0010	0.121	0.475	0.692	0.938
0.0020	0.121	0.474	0.690	0.933
0.0040	0.121	0.472	0.687	0.924
0.0060	0.121	0.470	0.683	0.916
0.0080	0.121	0.468	0.679	0.908
0.0100	0.121	0.467	0.676	0.901
0.0200	0.120	0.458	0.658	0.867
0.0400	0.119	0.441	0.626	0.809
0.0600	0.117	0.425	0.595	0.760
0.0800	0.116	0.410	0.566	0.715
0.1000	0.115	0.395	0.539	0.675
0.2000	0.109	0.329	0.423	0.508
0.4000	0.098	0.229	0.263	0.290
0.6000	0.088	0.160	0.164	0.166
0.8000	0.079	0.112	0.102	0.095
1.0000	0.071	0.078	0.063	0.054
2.0000	0.042	0.013	0.006	0.003
4.0000	0.014	0.0	0.0	0.0
6.0000	0.005	0.0	0.0	0.0
8.0000	0.002	0.0	0.0	0.0
10.0000	0.001	0.0	0.0	0.0

Table 8 Nusselt Numbers

Pe	1		5	
x	Nu_1	Nu_2	Nu_1	Nu_2
0.0001	31.141	25.298	36.543	16.664
0.0002	31.111	25.273	36.367	16.578
0.0004	31.049	25.222	36.020	16.407
0.0006	30.988	25.172	35.679	16.239
0.0008	30.927	25.122	35.343	16.074
0.0010	30.866	25.072	35.012	15.911
0.0020	30.565	24.824	33.434	15.140
0.0040	29.978	24.342	30.619	13.779
0.0060	29.409	23.874	28.198	12.625
0.0080	28.858	23.422	26.108	11.643
0.0100	28.323	22.984	24.296	10.803
0.0200	25.889	20.991	18.128	8.035
0.0400	22.001	17.821	12.671	5.734
0.0600	19.095	15.463	10.330	4.803
0.0800	16.884	13.680	9.028	4.309
0.1000	15.175	12.306	8.186	4.005
0.2000	10.554	8.630	6.270	3.427
0.4000	7.497	6.246	5.104	3.323
0.6000	6.306	5.344	4.664	3.448
0.8000	5.657	4.869	4.433	3.589
1.0000	5.248	4.582	4.294	3.705
2.0000	4.413	4.067	4.049	3.950
4.0000	4.081	3.966	4.001	3.999

Pe	10		50	
0.0001	39.166	9.489	79.130	1041.693
0.0002	38.800	9.373	75.818	983.580
0.0004	38.084	9.149	69.834	879.791
0.0006	37.390	8.933	64.601	790.343
0.0008	36.717	8.725	60.010	712.957
0.0010	36.065	8.525	55.969	645.749
0.0020	33.083	7.635	41.683	415.936
0.0040	28.294	6.287	28.177	213.529
0.0060	24.688	5.347	22.142	131.038
0.0080	21.928	4.679	18.775	89.113
0.0100	19.781	4.192	16.613	64.669
0.0200	13.919	3.026	11.790	21.396
0.0400	9.992	2.384	8.867	6.253
0.0600	8.437	2.185	7.689	2.966
0.0800	7.567	2.112	7.016	1.776
0.1000	7.001	2.095	6.567	1.261
0.2000	5.697	2.288	5.506	1.246
0.4000	[illegible].876	2.884	4.824	2.601
0.6000	[illegible].537	3.325	4.506	3.299
0.8000	4.341	3.596	4.306	3.630
1.0000	4.218	3.756	4.182	3.798
2.0000	4.021	3.978	4.012	3.988
4.0000	4.000	4.000	4.000	4.000

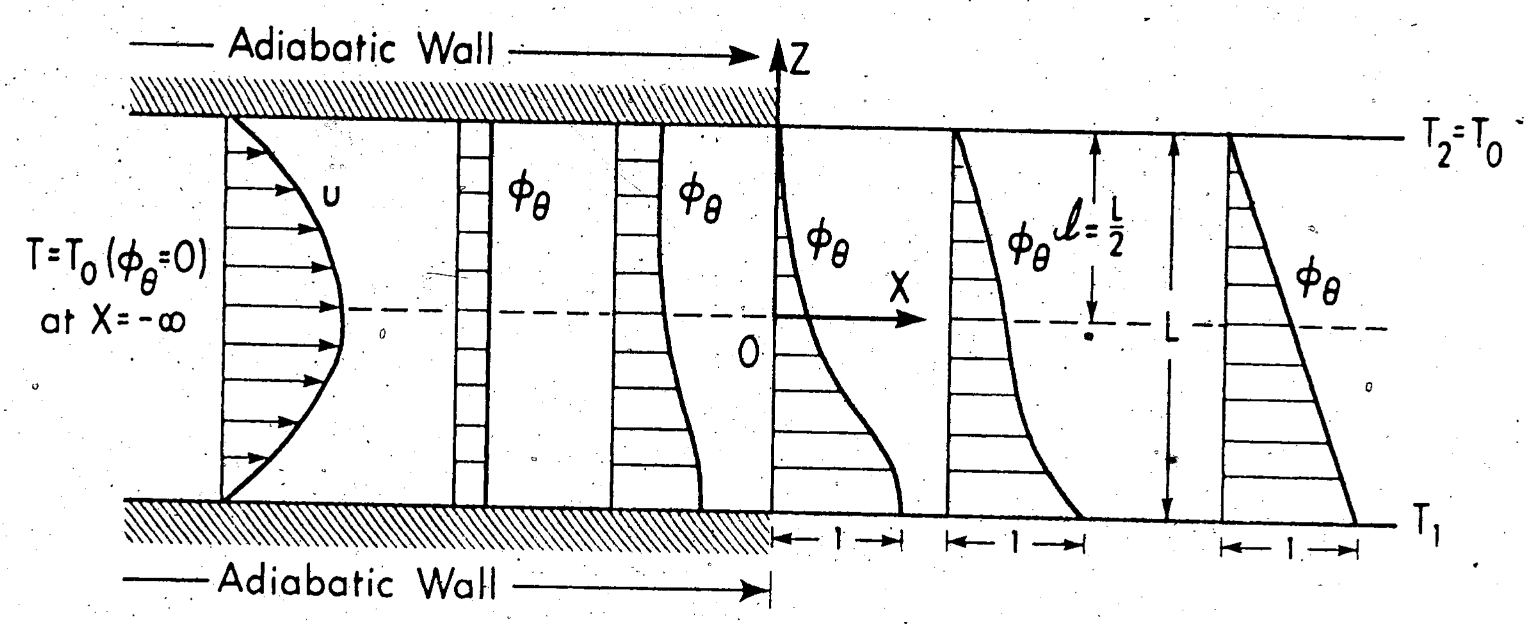

Fig. 1 Coordinate system for thermal entrance region problem.

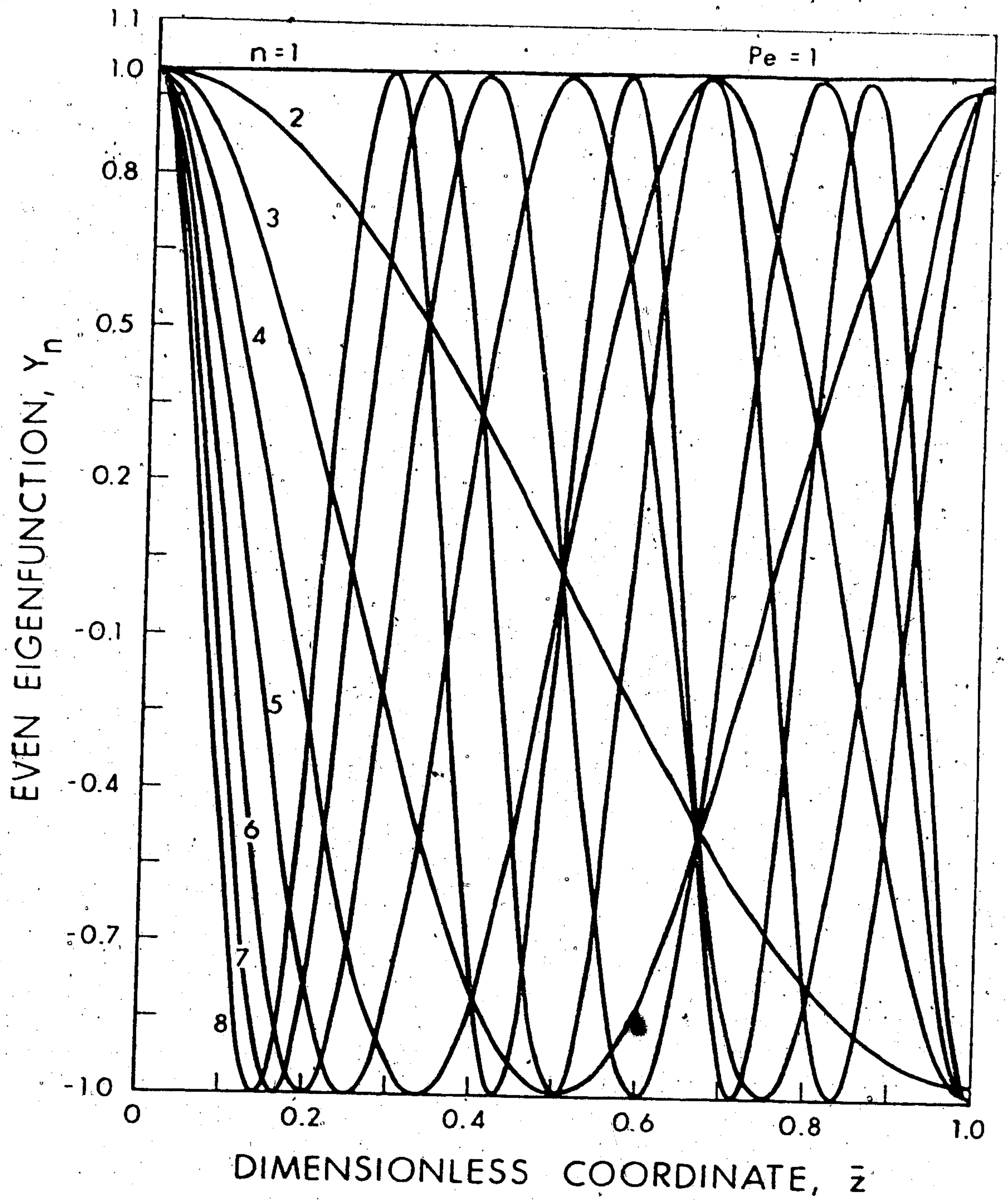

Fig. 2 Even Eigenfunctions Y_n for Pe = 1.

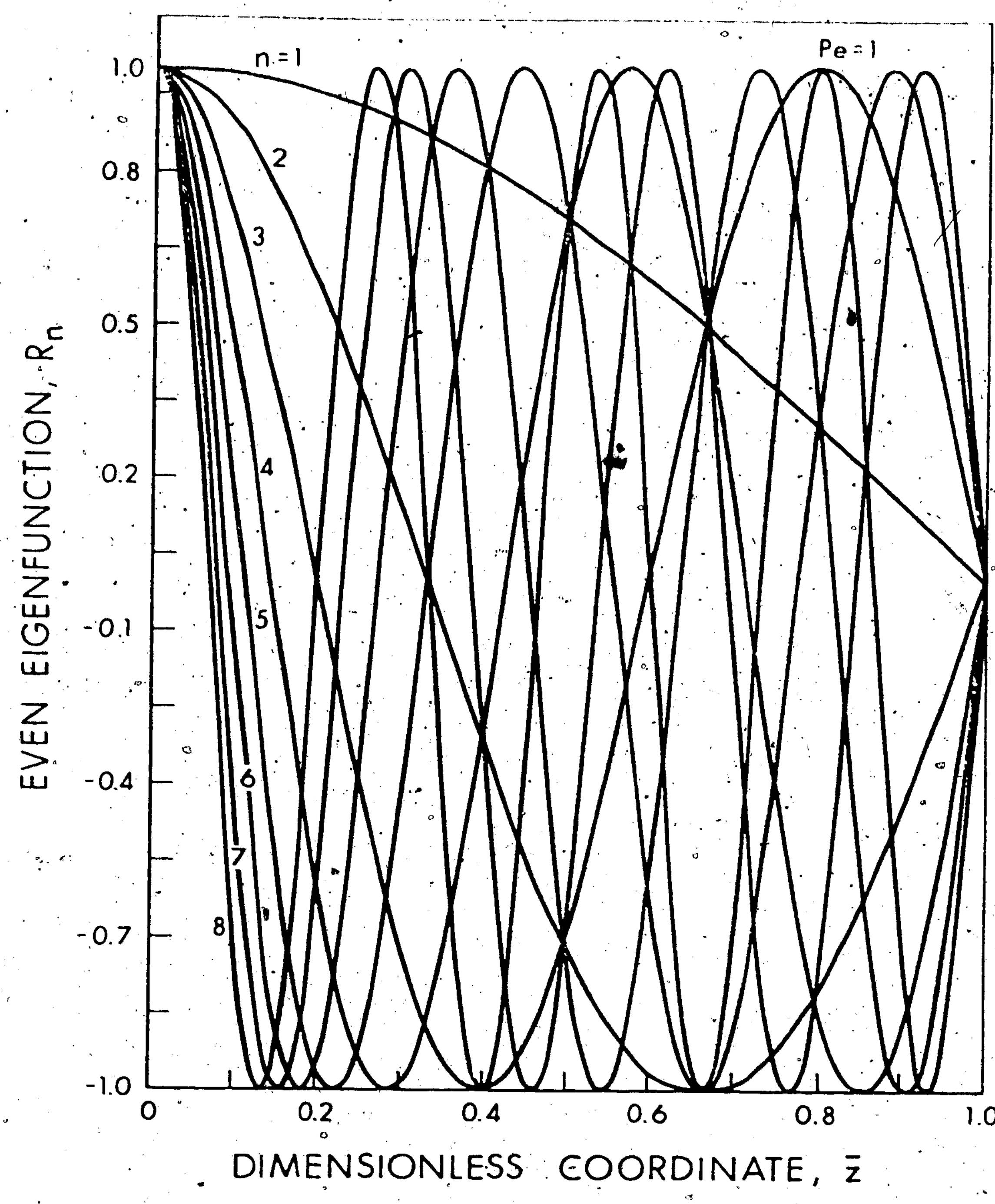

Fig. 3 Even Eigenfunctions R_n for Pe = 1.

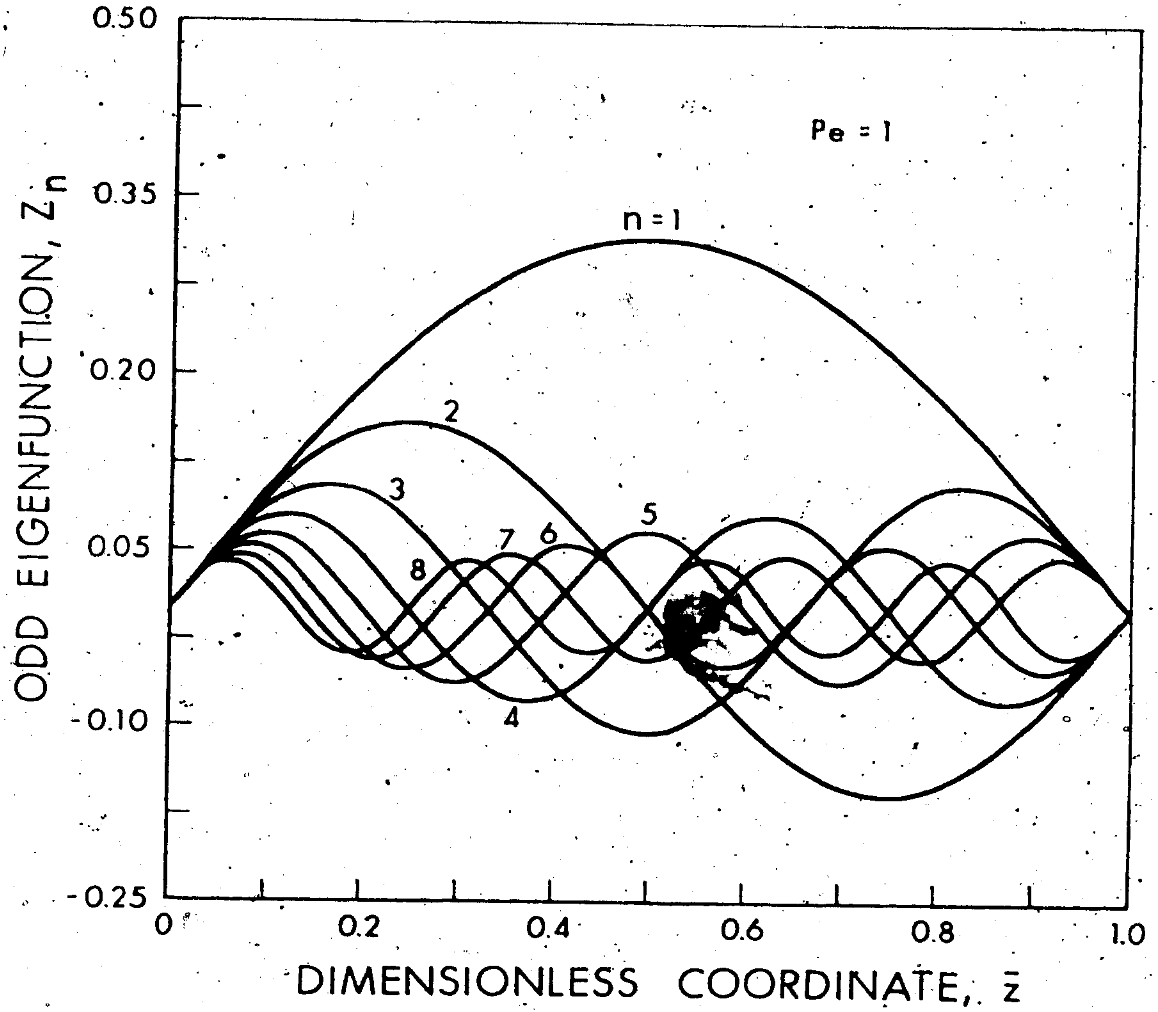

Fig. 4 Odd Eigenfunctions Z_n for Pe = 1.

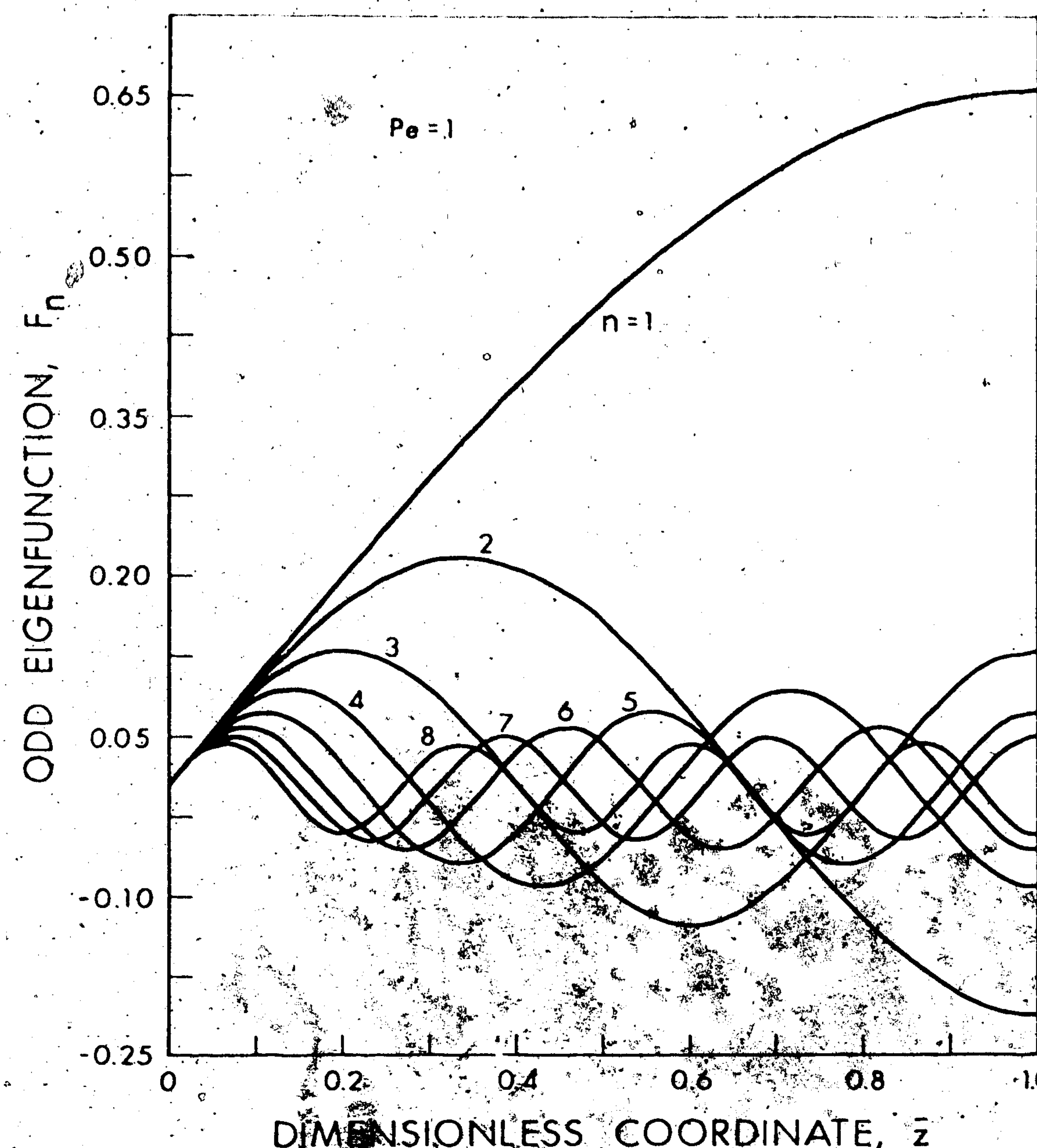

Fig. 5 Odd Eigenfunctions F_n for Pe = 1.

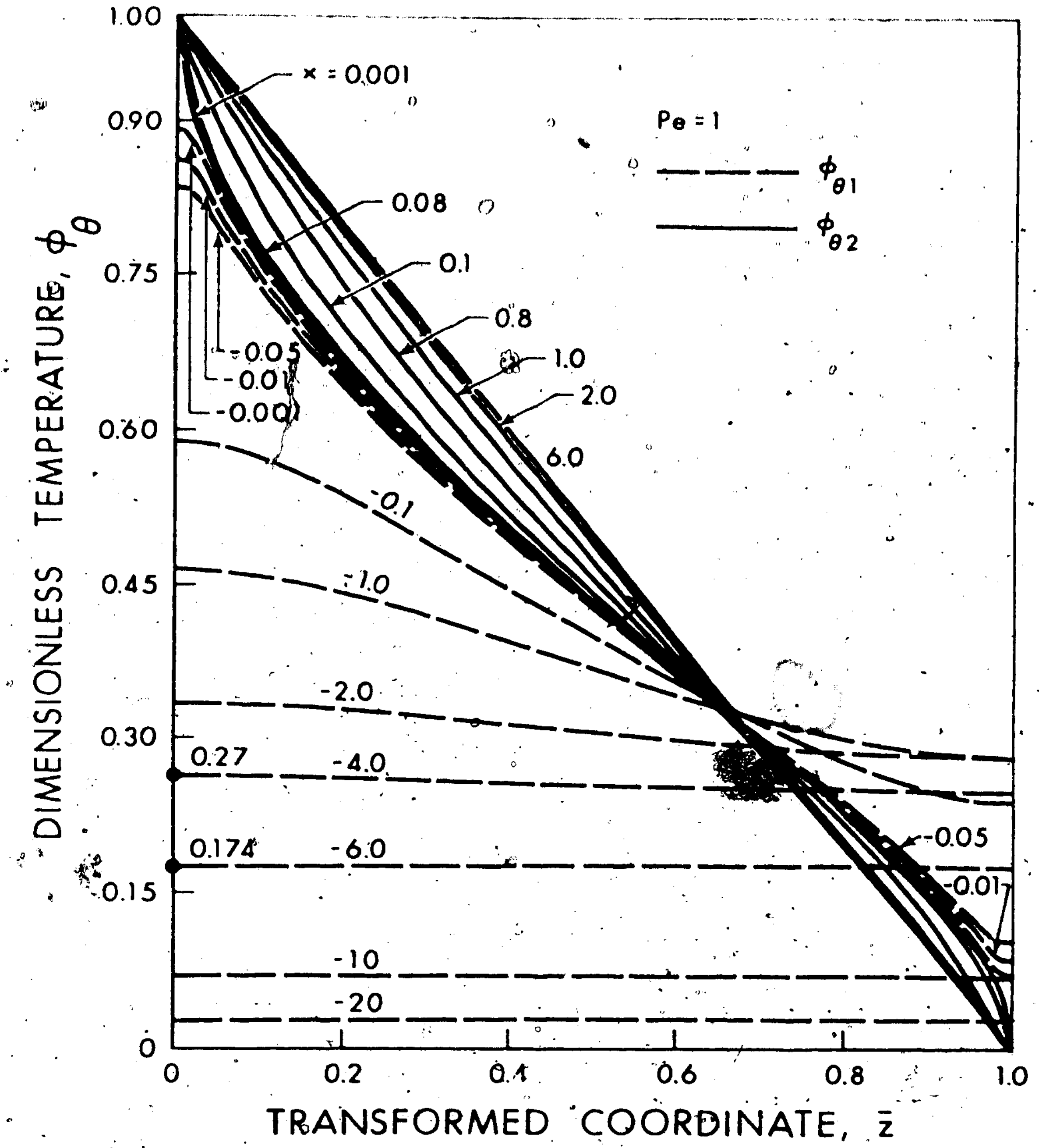

Fig. 6 Developing temperature profiles for Pe = 1.

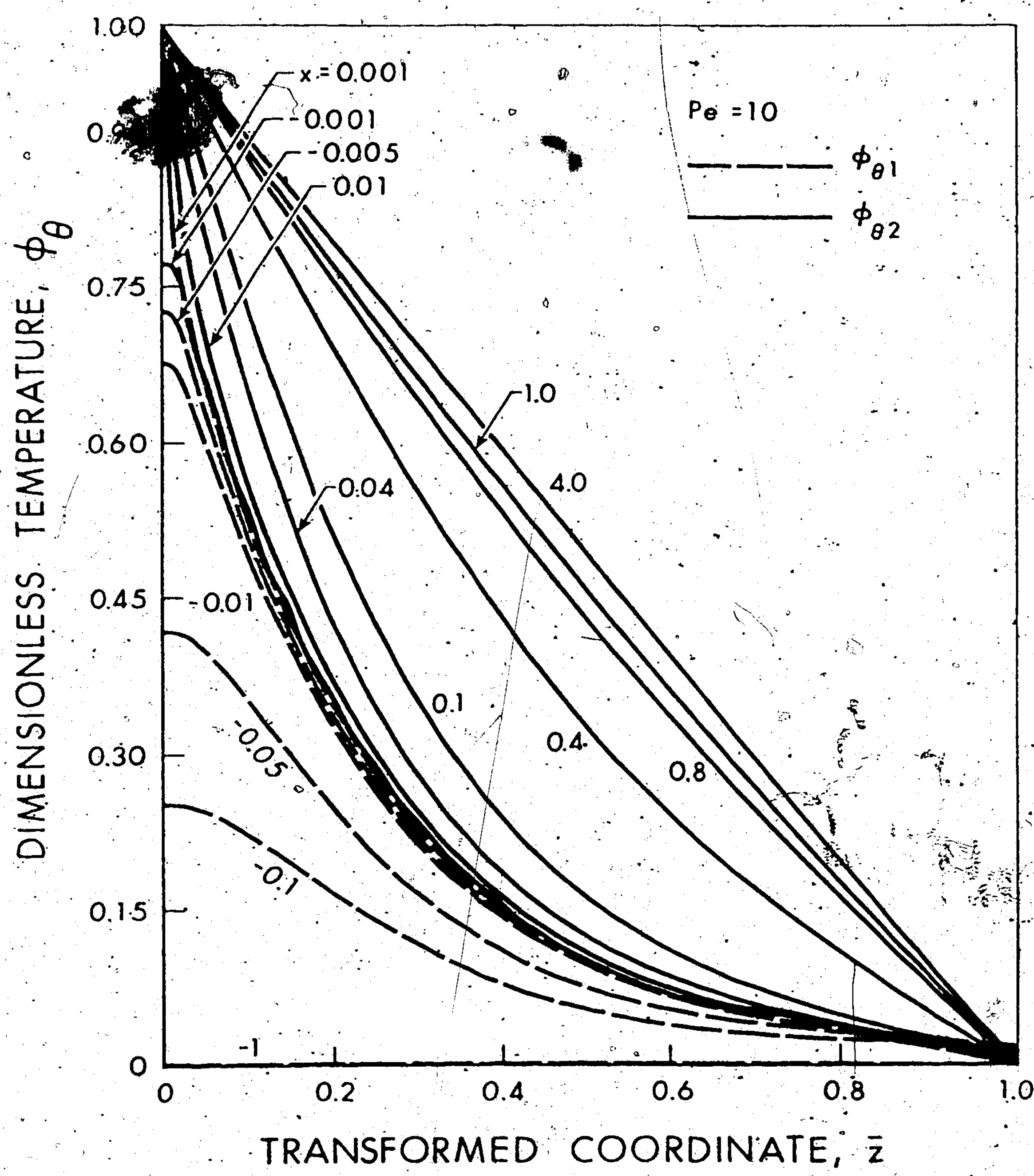

Fig. 8 Developing temperature profiles for Pe = 10.

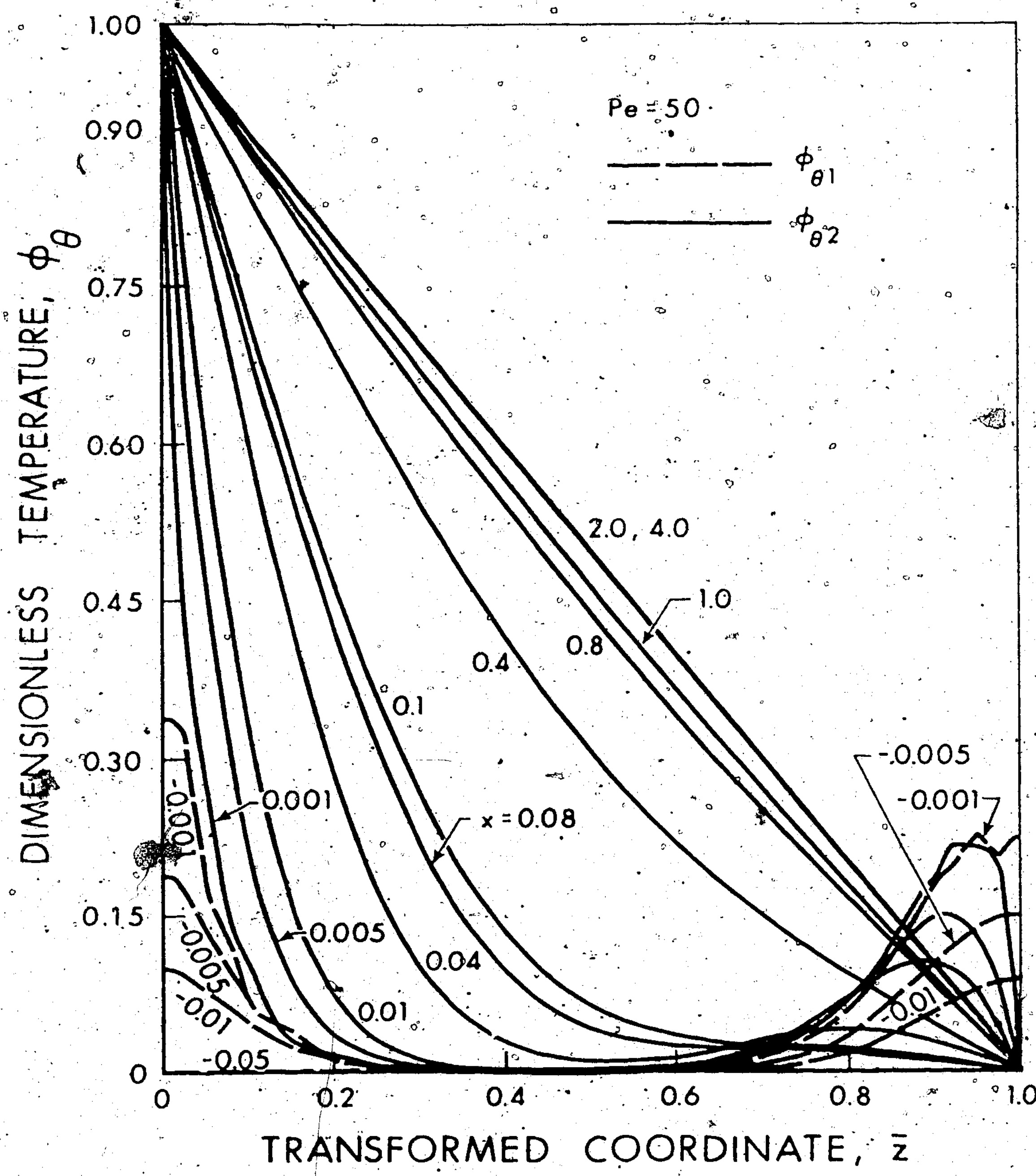

Fig. 9 Developing temperature profiles for Pe = 50.

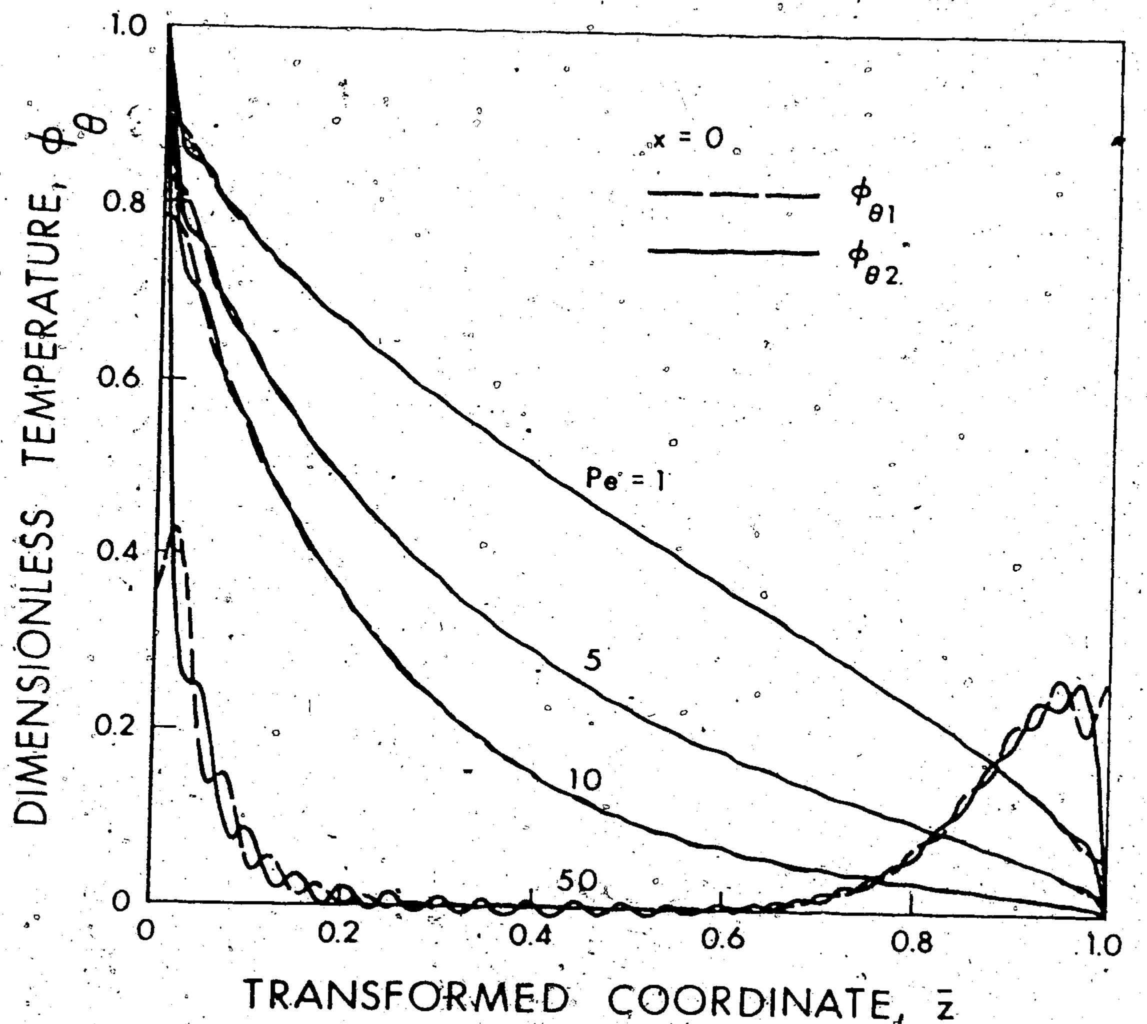

Fig. 10 Matching of temperature distributions, $\phi_{\theta 1}$ and $\phi_{\theta 2}$, at x = 0 for Pe = 1, 5, 10, 50.

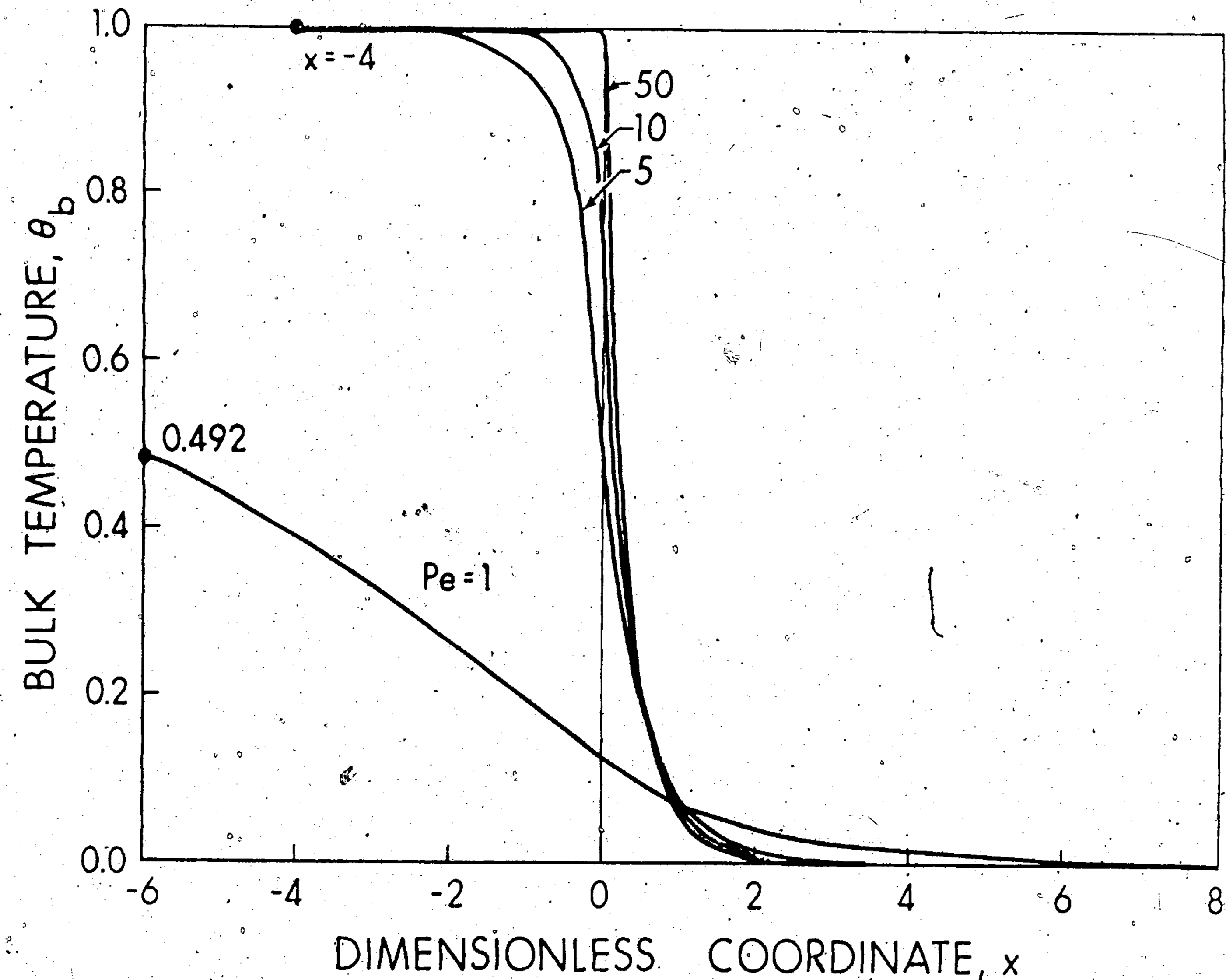

Fig. 11 Peclet number effect on axial bulk temperature distribution.

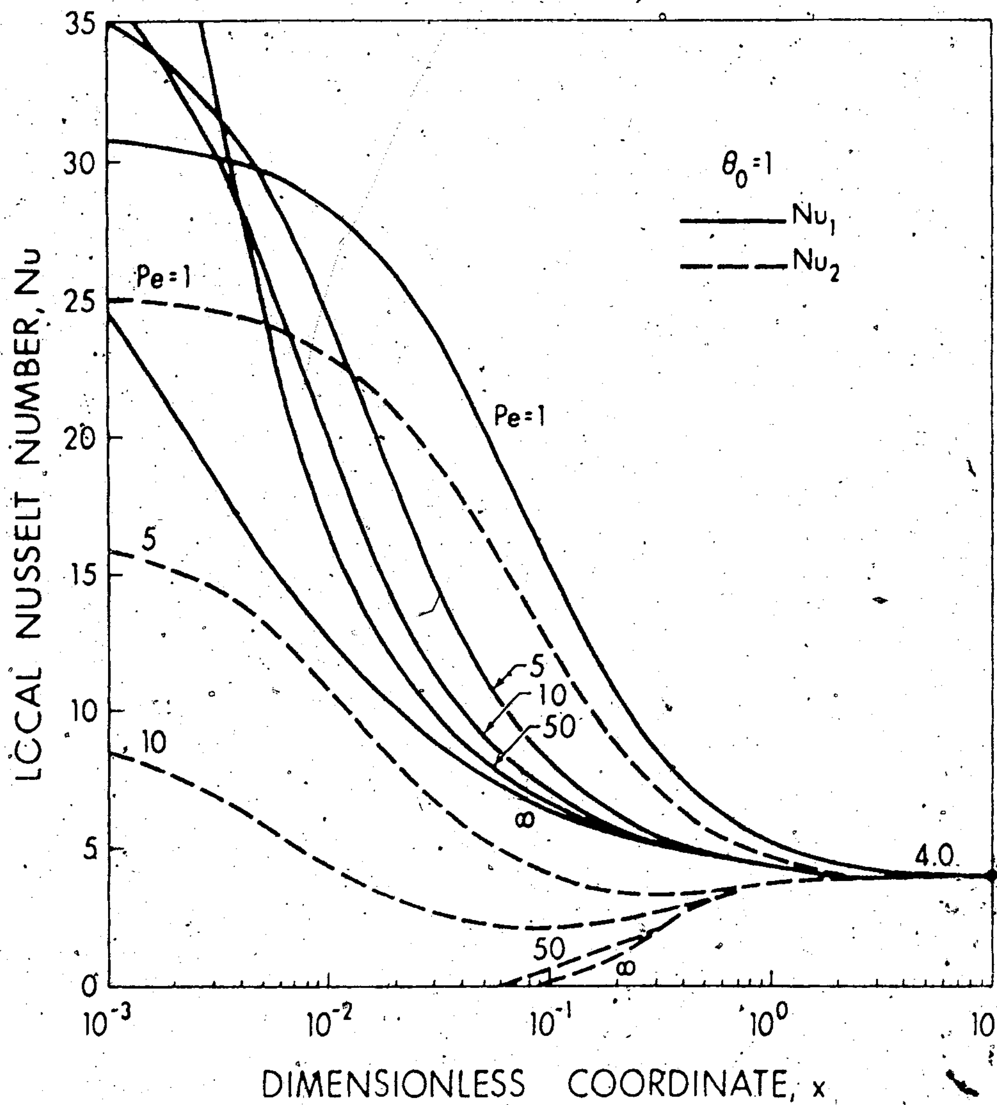

Fig. 12 Local Nusselt number results for Pe = 1, 5, 10, 50, ∞.

CHAPTER III

AXIAL HEAT CONDUCTION EFFECTS ON THERMAL INSTABILITY OF HORIZONTAL PLANE POISEUILLE FLOWS HEATED FROM BELOW

A linear stability analysis is used to study the effect of axial heat conduction on the onset of instability for longitudinal and transverse vortex disturbances for plane Poiseuille flow in the thermal entrance region of a horizontal parallel-plate channel heated from below with a constant temperature difference between two plates. The basic flow solution for temperature (Graetz problem) incorporates axial heat conduction effect and the fluid temperature is taken to be uniform at far upstream location $\bar{x} = -\infty$ to allow for the upstream heat penetration through thermal entrance $\bar{x} = 0$. Numerical results for critical Rayleigh numbers are obtained for entrance temperature parameter $\theta_0 = 1$ and Peclet numbers 1, 5, 10, 50. It is found that the transverse vortex disturbances are preferred over the longitudinal vortex disturbances for $Pe \leq 1$ and $Pr \geq 1$ (low Re) in the developing regions upstream and downstream of the thermal entrance. For other conditions, the longitudinal rolls have priority of occurrence. The Prandtl number effect on the onset of the longitudinal vortices is clarified.

Nomenclature

A_n, B_n, C_n, D_n	=	coefficients of infinite series in eqs. (5) and (6)
a_1, a_2, a	=	wave numbers in x and y directions and $(a_1^2 + a_2^2)^{1/2}$
c	=	amplification or damping factor, c = 0 at onset of instability
D	=	d/dz
Gr	=	Grashof number, $g\beta(\Delta T)L^3/\nu^2$
g	=	gravitational acceleration
i	=	$(-1)^{1/2}$
L, ℓ	=	height of channel and L/2
P, P_b	=	fluid pressure $(P_b + P')$ and basic flow pressure
Pe	=	Peclet number, $4 U_m \ell/\alpha$ = RePr
Pr	=	Prandtl number, ν/α
P	=	dimensionless perturbation pressure, $P'/(\rho\nu^2/L^2)$
Ra	=	Rayleigh number, PrGr
Re	=	Reynolds number, $4 U_m \ell/\nu$
T, T_b, T_m, T_0	=	fluid temperature $(T_b + \theta')$, basic flow temperature, $(T_1 + T_2)/2$ and uniform upstream temperature

T_1, T_2	=	constant lower and upper plate temperatures
U_b, U_m, u_b	=	axial and mean velocities and (U_b/U_m) of basic flow
U', V', W'	=	disturbance velocity components
u, v, w	=	dimensionless perturbation velocity components, $(U', V', W')/\nu/L$
X, Y, Z	=	Cartesian coordinates with origin at lower plate
X', Z'	=	coordinates with origin at center of channel
x, y, z	=	$(X, Y, Z)/L$
x', z'	=	$(X'/(3/8)\ell Pe,\ Z'/\ell)$
$\bar{x}, \bar{z}$	=	transformed coordinates, $(x/(3Pe/16), z)$
Y_n, R_n, F_n, Z_n	=	eigenfunctions
α	=	thermal diffusivity
$\alpha_n, \beta_n, \varepsilon_n, \gamma_n$	=	eigenvalues
β	=	coefficient of thermal expansion
θ	=	dimensionless disturbance temperature, $\theta'/\Delta T$
θ_b, θ_0	=	dimensionless temperature and uniform entrance temperature, $(T_b - T_m)/(T_2 - T_m)$ and $(T_0 - T_m)/(T_2 - T_m)$
ν	=	kinematic viscosity

ρ = density

ϕ_u, ϕ_θ = dimensionless basic velocity and temperature profiles, $(1/2)u_b = 3(z - z^2)$, $(1 - \theta_b)/2$

ΔT = $(T_1 - T_2)$

Superscripts and Subscripts

' = perturbation quantity

+ = amplitude of disturbance quantity

★ = transformed perturbation variable or critical value

b = basic flow quantity in unperturbed state

1,2 = upstream and downstream regions

3.1 Introduction

Thermal instability of a plane Poiseuille flow concerned with the onset of a secondary flow in the form of longitudinal vortex rolls in the thermal entrance region of horizontal parallel-plate channels heated from below was studied theoretically by Hwang and Cheng [1] considering the axial heat conduction term in the energy equation for basic flow. Recent studies by Hennecke [2] and Hsu [3] on Graetz problem with axial heat conduction effects show clearly that the usual thermal condition of uniform entrance fluid temperature at $X = 0$ used in the classical Graetz problem is unrealistic for low Peclet number flow regime ($Pe \lesssim 50$) because of the upstream heat penetration through thermal entrance $X = 0$ and the fluid temperature must be taken to be uniform far upstream at $X = -\infty$. In view of the predominance of the axial heat conduction effects near the thermal entrance $X = 0$ for very low Peclet number flows, the instability analysis [1] based on uniform entrance temperature at $X = 0$ for basic flow solution must be regarded as an approximate one when Peclet number is very small.

A deductive analysis of the Graetz problem by Ostrach [4] clarifies the importance of the axial heat conduction term in the energy equation. However, for very low Peclet number flow regime, the problem is of elliptic type and the concept of the thermal boundary layer is not applicable. Consequently, the thermal boundary-layer thickness cannot be used as a characteristic length in normalizing the equation. An explicit criterion for the neglect of viscous dissipation is also clearly given in [4]. When the Reynolds number is very small, a question on the priority of the occurrence of transverse rolls [5,6,7] over longitudinal rolls arises. Recently, Kamotani and Ostrach [8] determined experimentally the critical Rayleigh numbers for thermally-developing laminar channel flow and compared the experimental results with the results from linear stability theory [1]. A difference as large as an order of magnitude between the two results is observed but apparently this is somewhat similar to the discrepancy between the experimental [9] and theoretical [10-13] results for longitudinal vortex instability of natural convection flow on inclined surfaces. The difference can be attributed to the infinitesimal disturbances in theory and the measurable disturbances in experiment.

The purpose of this investigation is to study the effects of axial heat conduction on thermal instability of a plane Poiseuille flow between two horizontal flat plates where the lower plate is maintained at a higher constant temperature T_1 $(X \geq 0)$ and the upper plate at T_2 which is identical with the uniform entrance fluid temperature T_0 at far upstream ($X = -\infty$). The mathematical formulation for the basic flow in the thermal entrance region of the parallel-plate channel heated from below is similar to that used by Hennecke [2] and Hsu [3] which is considered to be the most rigorous analysis of the Graetz problem.

The onset of convective instability for both longitudinal and transverse vortex rolls in the low Peclet number flow regime is studied by using linear stability theory.

3.2 Temperature Solutions for Basic Flow

Neglecting the viscous dissipation effects, the governing equations in dimensionless form for the thermal entrance region problem (see Fig. 1) with axial heat conduction are [3]

$$\frac{2}{3} u_b \frac{\partial \theta_b}{\partial x'} = \frac{\partial^2 \theta_b}{\partial z'^2} + \left(\frac{8}{3Pe}\right)^2 \frac{\partial^2 \theta_b}{\partial x'^2} \tag{1}$$

$$\theta_{b1}(-\infty, z') = \theta_0,\ \partial\theta_{b1}(x',1)/\partial z' = \partial\theta_{b1}(x',-1)/\partial z' = 0$$

$$\text{for } -\infty < x' \leq 0 \tag{2}$$

$$\theta_{b2}(\infty, z') = \theta_f,\ \theta_{b2}(x',1) = 1,\ \theta_{b2}(x',-1) = -1$$

$$\text{for } 0 \leq x' < \infty \tag{3}$$

$$\theta_{b1}(0,z') = \theta_{b2}(0,z'),\ \partial\theta_{b1}(0,z')/\partial x' = \partial\theta_{b2}(0,z')/\partial x'$$

$$\text{at } x' = 0 \tag{4}$$

where the dimensionless variables are defined in Nomenclature and $u_b = (3/2)(1 - z'^2)$ for a plane Poiseuille flow.

Following the procedures outlined in [3,14], the temperature solutions θ_{b1} and θ_{b2} in the adiabatic and heated regions, respectively, satisfying the conditions at $x' = \pm\infty$ can be written as

$$\theta_{b1}(x',z') = \theta_0 + \sum_{n=1}^{\infty} B_n Y_n(z')\exp(\alpha_n^2 x')$$

$$+ \sum_{n=1}^{\infty} A_n F_n(z')\exp(\varepsilon_n^2 x'), \quad -\infty < x' < 0 \qquad (5)$$

$$\theta_{b2}(x',z') = z' + \sum_{n=1}^{\infty} C_n R_n(z')\exp(-\beta_n^2 x')$$

$$+ \sum_{n=1}^{\infty} D_n Z_n(z')\exp(-\gamma_n^2 x'), \quad 0 \le x' < \infty \qquad (6)$$

where α_n, ε_n and Y_n, F_n are the even and odd eigenvalues and eigenfunctions, respectively, for the adiabatic region. Similarly, β_n, γ_n and R_n, Z_n are the even and odd eigenvalues and eigenfunctions, respectively, for the heated region. The details of the solution method and the computed eigenvalues and eigenfunctions as well as the series expansion coefficients for the case $\theta_0 = 1$ are given in Chapter II. A fourth-order Runge-Kutta method [15] using two hundred equal steps is employed to obtain the eigenvalues and eigenfunctions from the numerical solution of the characteristic equations and their boundary conditions. The series coefficients are calculated by matching both the temperatures and the axial temperature gradients at $x = 0$ after constructing orthonormal functions from the nonorthogonal eigenfunctions [3]. In this study, the infinite series are truncated at $n = 12$ and 8 for $Pe = 1, 5$ and $Pe = 10, 50$, respectively. For the instability problem, it is more convenient to shift the coordinate origin to the lower plate as shown in Fig. 1. The basic temperature profile now becomes $\theta_b = (1 -$ [illegible]$_b/2)$.

2.3. Perturbation Equations

The derivation of the perturbation equations is based on the method of small disturbances (a linearization about the basic flow) using the Boussinesq approximation. Introducing the sum of the basic flow and the disturbance flow as $U = U_b(Z) + U'$, $V = V'$, $W = W'$, $T = T_b + \theta'$ and $P = P_b + P'$, subtracting out the basic flow equations from the conservation equations for mass, momentum and energy, one obtains the following disturbance equations after neglecting nonlinear terms.

$$\frac{\partial U'}{\partial X} + \frac{\partial V'}{\partial Y} + \frac{\partial W'}{\partial Z} = 0 \tag{7}$$

$$U_b \frac{\partial U'}{\partial X} + W' \frac{\partial U_b}{\partial X} = -\frac{1}{\rho} \frac{\partial P'}{\partial X} + \nu \nabla^2 U' \tag{8}$$

$$U_b \frac{\partial V'}{\partial X} = -\frac{1}{\rho}\frac{\partial P'}{\partial Y} + \nu\nabla^2 V' \tag{9}$$

$$U_b \frac{\partial W'}{\partial X} = -\frac{1}{\rho}\frac{\partial P'}{\partial Z} + \nu\nabla^2 W' + g\beta\theta' \tag{10}$$

$$U_b \frac{\partial \theta'}{\partial X} + U'\frac{\partial T_b}{\partial X} + W'\frac{\partial T_b}{\partial Z} = \alpha\nabla^2\theta' \tag{11}$$

where $\nabla^2 = \partial^2/\partial X^2 + \partial^2/\partial Y^2 + \partial^2/\partial Z^2$ and the disturbances are taken to be independent of time [1,8,10].

After introducing the dimensionless variables, $(x,y,z) = (X,Y,Z)/L$, $(u,v,w) = (U',V',W')/(\nu/L)$, $p = P'/(\rho\nu^2/L^2)$, $\theta = \theta'/(\Delta T)$ and the parameter $Gr = g\beta(\Delta T)L^3/\nu^2$, the disturbance equations become

$$\frac{\partial u}{\partial x} + \frac{\partial v}{\partial y} + \frac{\partial w}{\partial z} = 0 \tag{12}$$

$$Re\,\phi_u \frac{\partial u}{\partial x} + Re\,\frac{d\phi_u}{dz}\,w = -\frac{\partial p}{\partial x} + \nabla^2 u \tag{13}$$

$$Re\,\phi_u \frac{\partial v}{\partial x} = -\frac{\partial p}{\partial y} + \nabla^2 v \tag{14}$$

$$Re\,\phi_u \frac{\partial w}{\partial x} = -\frac{\partial p}{\partial z} + \nabla^2 w + Gr\,\theta \tag{15}$$

$$Re\,\phi_u \frac{\partial \theta}{\partial x} + u\frac{\partial \phi_\theta}{\partial x} + w\frac{\partial \phi_\theta}{\partial z} = \frac{1}{Pr}\nabla^2\theta \tag{16}$$

where $\phi_u = 3z(1 - z)$, $\phi_m = (T_b - T_2)/\Delta T = (1 - \theta_b)/2$ and the operator is understood to be $\nabla^2 = \partial^2/\partial x^2 + \partial^2/\partial y^2 + \partial^2/\partial z^2$. The dependent variables u, v and p can be eliminated from the continuity and three momentum equations and one obtains a single equation as

$$Re\phi_u \frac{\partial}{\partial x}(\nabla^2 w) - Re \frac{d^2\phi_u}{dz^2}\frac{\partial w}{\partial x} = \nabla^2\nabla^2 w + Gr\,\nabla_1^2\theta \qquad (17)$$

where $\nabla_1^2 = \partial^2/\partial x^2 + \partial^2/\partial y^2$ and $\nabla^2 = \nabla_1^2 + \partial^2/\partial z^2$.

A separable solution for w and θ may be sought in the following form [1].

$$f(x,y,z) = f^+(z)\,\exp\,[cx + i(a_1 x + a_2 y)] \qquad (18)$$

where c is the amplification factor and the wave numbers a_1 and a_2 are real. Confining attention to neutral stability, one has $c = 0$. After substituting equation (18) for the disturbances w and θ, respectively, into equations (17) and (16), one obtains

$$(D^2 - a^2)^2 w^+ - ia_1 Re\phi_u(D^2 - a^2)w^+ + ia_1 Re(d^2\phi_u/dz^2)w^+$$
$$= Gr\,a^2\theta^+ \qquad (19)$$

$$(D^2 - a^2)\theta^+ - ia_1 Pe\phi_u \theta^+ = Pr\ [u^+ \partial\phi_\theta/\partial x + w^+ \partial\phi_\theta/\partial z] \tag{20}$$

where $a^2 = a_1^2 + a_2^2$ and $D = d/dz$. The above two disturbance equations involve three unknowns and u remains to be specified. The following two cases [6] are of interest in this study:

1. For longitudinal rolls ($a_1 = 0$), the x-momentum equation (13) gives

$$(D^2 - a^2)u^+ = Re(d\phi_u/dz)w^+ \tag{21}$$

It is noted that at neutral stability the x-dependence for the disturbance quantities can be neglected and one has $\partial p/\partial x = 0$.

2. For transverse rolls ($a_2 = 0$), the continuity equation (12) gives [6]

$$u^+ = i\ Dw^+/a_2 \tag{22}$$

At this point, it is more convenient to introduce the transformations, $x = (3Pe/16)\overline{x}$, $z = \overline{z}$, $u^+ = Re\ u^*$, $w^+ = w^*$, $\theta^+ = Pr\theta^*$, $u^+ = Re\ u^*$, $Ra = GrPr$ and one obtains:

1. Longitudinal rolls

$$(D^2 - a_2^2)^2 w^* = Ra\ a_2^2 \theta^* \tag{23}$$

$$(D^2 - a_2^2)u^* = (d\phi_u/d\bar{z})w^* \tag{24}$$

$$(D^2 - a_2^2)\theta^* = (16/3Pr)u^*\,\partial\phi_\theta/\partial\bar{x} + w^*\partial\phi_\theta/\partial\bar{z} \tag{25}$$

2. Transverse rolls

$$(D^2 - a_1^2)^2 w^* - ia_1 Re\phi_u(D^2 - a_1^2)w^* + ia_1 Re(d^2\phi_u/d\bar{z})^2 w^*$$

$$= Ra\, a_1^2\theta^* \tag{26}$$

$$u^* = (i/a_1 Re)\ Dw^* \tag{27}$$

$$(D^2 - a_1^2)\theta^* - ia_1 Pe\phi_u\theta^* = (16/3Pr)u^*\partial\phi_\theta/\partial\bar{x} + w^*\partial\phi_\theta/\partial\bar{z} \tag{28}$$

The boundary conditions at the rigid and highly conductive walls applicable to the above two types of disturbances are

$$w^* = Dw^* = u^* = \theta^* = 0 \quad \text{at } \bar{z} = 0 \text{ and } 1 \tag{29}$$

In this study, the oblique modes ($a_1 \neq 0$, $a_2 \neq 0$) are not considered [6] since the above two modes are observed experimentally. For transverse rolls, the disturbance u^* may be eliminated by substituting equation (27) into equation (28) and only the real part of the disturbance equations is considered to have physical significance. It is seen that equation (26) is the Orr-Sommerfeld type equation and is coupled with the energy equation (28).

3.4 Method of Solution

Considering the expressions for the basic temperature profiles θ_{b1} and θ_{b2}, it is obvious that an analytical solution of the present characteristic value problem is not practical. An iterative technique using the higher order finite difference scheme [16] is used for the simultaneous solution of the coupled disturbance equations [1]. The details of the numerical solution method are in Appendix I and only an outline of the iterative procedure is presented here. Given the basic profiles ϕ_u and ϕ_θ for the specified values of Pe and θ_0, the iterative procedure for the case of the longitudinal rolls consists of the following main steps:

1. At a given axial position $\bar{x}$, a value of the wave number $a_2 = 2.5$ (say) is selected and an eigenvalue Ra is assumed. The disturbance velocity w_k^* is taken in the form of $w_k^* = 2(1 - k/M)$, $k = 2,3,\ldots,M$ and Ra = 1708 is used in this study.

2. The finite-difference solution of equation (24) gives u_k^*.

3. After knowing w_k^* and u_k^*, the energy equation (25) can be solved to obtain θ_k^*.

4. New values for w_k^* can be found from the finite-

difference solution of equation (23).

5. An improved eigenvalue $(Ra)_{new}$ can be computed by using the following equation [17].

$$(Ra)_{new} = (Ra)_{old}\left[\sum_k (w_k^*)^2_{old}\right]^{1/2} / \left[\sum_k (w_k^*)^2_{new}\right]^{1/2} \tag{30}$$

The magnitude of w_k^* is readjusted by the following equation in order to return to the original order of magnitude for computation.

$$w_k^* = (w_k^*)_{new}\ (Ra)_{new}/(Ra)_{old} \tag{31}$$

6. The steps (2) to (4) are repeated until the following preassigned convergence criterion is satisfied.

$$\varepsilon = \sum_k |(w_k^*)_{new} - (w_k^*)_{old}| / \sum_k |(w_k^*)_{new}| \leq 10^{-6} \tag{32}$$

7. The minimum Rayleigh number is then searched. It is found that only 3 to 5 iterations are required to satisfy the above criterion and five significant figures are correct for critical Ra.

The numerical method of solution for the case of transverse rolls is generally similar to that discussed above with the following differences:

1. The disturbance quantities w^*, u^* and θ^* are now complex.

2. The initial values for w_k^* are taken as $w_k^* = 2(1 - k/M) + 2i(1 - k/M)$, $k = 2,3,\ldots,M$.

3. A new and improved eigenvalue can be calculated by using the following equation [18].

$$(Ra)_{new} = (Ra)_{old}[\sum_k (w_k^*)_{old}(\bar{w}_k^*)_{old}]^{1/2}/[\sum_k (w_k^*)_{new}(\bar{w}_k^*)_{new}]^{1/2} \quad (33)$$

where $(\bar{w}_k^*)$ is the conjugate of the complex disturbance (w_k^*).

4. The convergence criterion based on equation (32) is $\leq 10^{-3}$. The number of iterations required to satisfy the above condition ranges from 20 to 25 and four significant figures are found to be correct for critical Ra at the onset of transverse rolls.

3.5 Results and Discussion

The critical Rayleigh numbers at the onset of secondary motion are of primary interest in this study. The graphical results are presented in Fig. 2 to 8 and the numerical results are summarized in Tables 1 to 5 for the case $\theta_0 = 1$. The effects of Prandtl number on the onset of longitudinal vortex rolls in both the upstream and downstream regions are shown in Fig. 2 to 5 for Pe = 1, 5, 10 and 50, respectively.

For $\theta_0 = 1$ and Pe = 1, the instability results for

Pr = 0.7, 1, 10, 100 and ∞ are practically identical and the critical Rayleigh number decreases monotonically from the asymptotic value of Ra* = ∞ at $\overline{x}$ = -6 to Ra* = 1708 at $\overline{x}$ = 3.0 for a linear basic temperature profile. The independence of the critical Rayleigh number Ra* on Prandtl number for Pr $\geq$ 0.7 in the case of Pe = 1 can be explained from perturbation equation (25). It is found that when Pe = 1, the relative magnitude of the ratio R = $(\partial\phi_a/\partial\overline{x})/(\partial\phi_a/\partial\overline{z})$ is less than 10^{-3} and consequently the forcing term $(16/3Pr)(\partial\phi_a/\partial\overline{x})u^*$ on the right-hand side of equation (18) can be neglected in comparison with the term $(\partial\phi_a/\partial\overline{z})w^*$ for the range Pr = 0.7 ~ ∞. Thus, the coupled effect of the vertical basic temperature gradient $\partial\phi_a/\partial\overline{z}$ and the vertical velocity disturbance w* dominates. On the other hand, when Pe = 5 and 10, the ratio R is found to be less than 10^{-2} and 10^{-1}, respectively. It is thus seen that the instability result is independent of Prandtl number when Pr $\geq$ 10 for Pe = 5 and Pr $\geq$ 100 for Pe = 10. The above argument assumes that the axial and vertical basic temperature gradients, $\partial\phi_a/\partial x$ and $\partial\phi_a/\partial z$ are of the same order of magnitude which is verified by the numerical results of Chapter II. From the foregoing discussion, it is also clear that the role of Prandtl number becomes increasingly important as the Prandtl number decreases for a given Peclet number. When Pr is small, the term $(16/3Pr)u^*\partial\phi_a/\partial x$ also destabilizes the flow. As is seen from Fig. 2 to 4, a local minimum for Ra* exists when Prandtl number is small. This means that when Prandtl number is small, the region near the thermal entrance $\bar{x} = 0$ is more unstable than the fully developed region and the practical implications are believed to be important for liquid metals. Noting that the basic temperature profile θ_0 is a function of Peclet number only, one sees that the effect of Prandtl number appears through the disturbance equation (25) only.

The instability results for Pe = 50 are shown in Fig. 5 where the unpublished results of the earlier analysis [1] based on the assumption that the fluid temperature is uniform at the thermal entrance $\bar{x} = 0$ are also plotted for comparison. One should note that the simplified model [1] predicts $Ra^* = \infty$ at $\bar{x} = 0$ whereas the present model predicts a finite value for Ra^* at $\bar{x} = 0$. At Pe = 50, the concept of thermal boundary layer is applicable (Chapter II) and the lower Ra^* at a given $\bar{x}$ from [1] for a given Pr can be attributed to the larger unstable thermal boundary layer thickness caused by the somewhat artificial absence of the upstream heat penetration through $\bar{x} = 0$. The effect of the axial heat conduction is seen to decrease the thermal boundary layer thickness and the axial temperature gradient $\partial\theta_0/\partial\bar{x}$. One should note that at Pe = 50, the lower limit for Pr exists because of the critical Reynolds number Re = 14,170. At Pr = 0.1, the entrance region is seen to be more unstable than the fully developed region.

In order to critically examine the effect of upstream heat conduction on critical Ra^*, the instability results for Pr = 0.7, 10, 100 and Pe = 5 are compared against the unpublished results of the earlier study [1] neglecting the upstream heat penetration through $\bar{x} = 0$ in Fig. 6. At Pe = 5, the earlier model is apparently inadequate in predicting Ra*. It is noted that the trend of the Prandtl number effect on Ra* between the present and earlier analyses for Pe = 50 (see Fig. 5) and Pe = 5 is just opposite. This is caused by the fact that at Pe = 50, the problem is basically parabolic and the concept of thermal boundary layer is applicable whereas at Pe = 5, the problem is elliptic and the heat from the lower plate already penetrates to the upper plate at $\bar{x} = 0$. It is then clear that the larger unstable fluid layer near $\bar{x} = 0$ from the present physical model leads to the considerably lower Ra*.

The ef[illegible] Peclet number on Ra* for Pr = 0.7 (air) is shown in F[illegible] 7. The Peclet number effect on Ra* in the upstream region is seen to be opposite to that in the downstream region. The lower Ra* for Pe = 1 in the adiabatic region is due to the larger unstable fluid layer caused by the axial heat conduction. The developing temperature profiles shown in Chapter II clearly confirm the above statement. The instability results for Pr = 10 (water) are also shown in Fig. 8. The thermal entrance length for Pe = 1 is longer than those of Pe = 5, 10, 50 and correspondingly the asymptotic value Ra* = 1708 for a fully developed basic flow with a linear temperature profile is approached at a farther downstream location.

The case of transverse rolls is of special interest in this study and the numerical results for Pe = 1 and Pr = 1, 100 are listed in Table 5. The graphical results are presented in Fig. 9 where the instability results for the case of longitudinal vortex rolls are also plotted for comparison. It is seen that the onset of the transverse rolls has priority over that of the longitudinal rolls in the upstream region as well as part of the downstream region ($x < 1.2$). Note that the case of Pr = 100 is more unstable than that of Pr = 1 for transverse rolls but the opposite is true for longitudinal rolls. It is also found that for Pe = 1, Pr $\lesssim$ 0.1 the transverse rolls have no priority over the longitudinal rolls. Similarly, numerical results reveal that Ra* for transverse rolls is higher than that for longitudinal rolls at $\bar{x} = 0$ for Pe $\geq$ 5. It is thus concluded that the onset of the transverse rolls has priority over that of the longitudinal rolls only when Pe $\leq$ 1 and Pr $\gtrsim$ 1 (or small Re) and it occurs in the upstream and downstream regions near the thermal entrance $\bar{x} = 0$. For fully developed region, the longitudinal rolls appear to have priority but the difference in Ra* is so small that the transverse rolls may occur under certain conditions.

For a given Pe, as Pr $\rightarrow \infty$ one obtains Re $\rightarrow$ 0. The perturbation equations for transverse rolls in the fully developed region then become:

$$(D^2 - a_1^2)^2 w^* = \text{[illegible]} \qquad (34)$$

$$(D^2 - a_1^2)^2\theta^* = ia_1 Pe \phi_u \theta^* - w^* \partial\phi_0/\partial z \qquad (35)$$

where $\partial\phi_0/\partial z = -1$. The calculation for $Pe = 1$ gives $Ra^* =$ 1717.06 and $a_1^* = 3.117$. The fact that Ra^* is larger than the value of 1708 for longitudinal rolls suggests that the term involving Pe in equation [illegible] may have a stabilizing effect.

The physical reasons for the priority of the "transverse-vortex disturbances" over the "longitudinal vortex disturbances" under the conditions stated earlier are not immediately clear from the study of the disturbance equations and a consideration of the energy exchange between the main flow and the perturbation. However, it appears that when Re is large the transverse rolls tend to be washed out. In addition, one notes that the developing basic temperature profiles show negative axial temperature gradient near upper plate ($\bar{z} = 0.6 \sim 1.0$) for $x \geq -0.1$ at $Pe = 1$ (Chapter II). At $Pe = 5$, the region of negative axial temperature gradient is rather small and negligible (Chapter II). It appears that the horizontal density gradients also play some role for the onset of transverse rolls.

The streamline pattern of the transverse-roll type disturbances in a longitudinal cross section is of particular interest and the secondary flow field configuration at the onset of instability is shown in Fig. 10 for the fully developed condition with $Pe = 1$, $Pr = 100$, $Ra^* = 1717.07$,

$a_1^* = 3.117$. The stream function is defined by $u = -\partial\psi/\partial\bar{z}$ and $w = \partial\psi/\partial\bar{x}$. From the normal modes of disturbances, one has $w = w^+(\bar{z})e^{ia_1\bar{x}}$ and $\psi = \psi^+(\bar{z})^{ia_1\bar{x}}$. Noting that $w^+ = w^*$, one obtains $\psi = (w^*/ia_1)e^{ia_1\bar{x}}$ where only the real part is considered to have physical meaning. The contour lines are based on $|\psi_{max}| = 1$ and the dimensionless wavelength $\lambda = 2\pi/a_1 = 2.0156$. The streamline pattern is quite similar to that of the longitudinal rolls and the eyes of the vortices are seen to be located at the center of the channel.

3.6 Concluding Remarks

1. The effects of axial heat conduction on the thermal instability of horizontal plane Poiseuille flow heated from below are studied for both longitudinal and transverse vortex disturbances. It is found that the transverse rolls with axes normal to the main flow are the preferred mode of disturbances for very low Peclet number regime (say $Pe \le 1$) with $Pr > 1$ (or low Re) in the developing regions upstream and downstream of the thermal entrance. For other conditions, the longitudinal rolls with axes parallel to the basic velocity are the preferred mode of disturbances. The observed Peclet number effect on disturbance modes is consistent with experimental results for combined free and forced convection in porous media [19].

2. For given entrance temperature parameter θ_0 and Peclet number, the instability mechanism relating to the Prandtl number effect on the onset of longitudinal vortex

rolls in the thermal entrance region is clarified by studying the relative order of magnitude of the forcing terms involving axial and transverse basic temperature gradients in the energy disturbance equation (25).

3. For low Peclet number regime (say Pe < 50), the assumption of uniform entrance fluid temperature at the thermal entrance $\bar{x} = 0$ for basic temperature solution is not valid because of upstream heat penetration through $\bar{x} = 0$ into the upstream adiabatic region. At Pe = 5 and $\epsilon_0 = 1$, the predictions of critical Rayleigh number for longitudinal vortex rolls show considerable discrepancy between the two models with and without upstream heat penetration. The discrepancy increases with the decrease of Peclet number.

4. The present instability results can be used in predicting the onset of free convection effect on laminar heat transfer in horizontal wide rectangular channels [8]. For Ra > Ra*, one has finite amplitude thermal convection problem and the classical Graetz formulation for thermal entrance region problem in a parallel-plate channel is not applicable. It should also be noted that the existence of stationary longitudinal vortex roll is confirmed in experiment [8]. However, the case of transverse vortex rolls remains to be confirmed by experiment.

5. The numerical experiments using 20 eigenvalues are also carried out to confirm the accuracy of the present numerical results. For $\bar{x} \geq 0.1$, the accuracy of Ra* is

within one percent for Pe = 1, 5, 10, 50 and at $\bar{x} = 0^+$, the error of Ra* is about one percent for Pe = 1, 5 and two percent for Pe = 10. The convergence of the numerical solution is thus confirmed.

6. Physically, as a low velocity main flow is imposed on Benard cells the "transverse-vortex disturbances" appear first. With further increase of steady main flow velocity, the "longitudinal vortex disturbances" appear. The effect of superposed steady flow on unstable fluid layers described in [5,20] is consistent with the present theoretical results.

7. The viscous dissipation effects are neglected within the scope of present work but should be studied in future. Apparently, the thermal radiation effect and other thermal boundary conditions such as convective boundary condition are also of practical interest.

References

1. Hwang, G.J. and Cheng, K.C., "Convective Instability in the Thermal Entrance Region of a Horizontal Parallel-Plate Channel Heated from Below", Journal of Heat Transfer, Trans. ASME, Series C, Vol. 95, 1973, pp. 72-77.
2. Hennecke, D.K., "Heat Transfer by Hagen-Poiseuille Flow in the Thermal Development Region with Axial Conduction", Wärme-und Stoffübertragung, Vol. 1, 1968, pp. 177-184.
3. Hsu, C.J., "An Exact Analysis of Low Peclet Number Thermal Entry Region Heat Transfer in Transversely Non-Uniform Velocity Fields", AIChE Journal, Vol. 17, 1971, pp. 732-740.
4. Ostrach, S., "Role of Analysis in the Solution of Complex Physical Problems", Proceedings of the Third International Heat Transfer Conference, AIChE, Vol. 6, 1966, pp. 31-43.
5. Ostrach, S., "Laminar Flows with Body Forces", Theory of Laminar Flows, Edited by F.K. Moore, Princeton University Press, Princeton, New Jersey, 1964, pp. 624-627.
6. Hart, J.E., "Stability of the Flow in a Differentially Heated Inclined Box", J. Fluid Mech., Vol. 47, 1971, pp. 547-576.

7. Weber, J.E., "On Thermal Convection Between Non-Uniformly Heated Planes", International Journal of Heat and Mass Transfer, Vol. 16, 1973, pp. 961-970.

8. Kamotani, Y. and Ostrach, S., "Effect of Thermal Instability on Thermally-Developing Laminar Channel Flow", Journal of Heat Transfer, Trans. ASME, Series C, Vol. 98, 1976.

9. Lloyd, J.E. and Sparrow, E.M., "On the Instability of Natural Convection Flow on Inclined Plate", J. Fluid Mech., Vol. 42, 1970, pp. 465-470.

10. Haaland, S.E. and Sparrow, E.M., "Vortex Instability of Natural Convection Flow on Inclined Surfaces", International Journal of Heat and Mass Transfer, Vol. 16, 1973, pp. 2355-2367.

11. Hwang, G.J. and Cheng, K.C., "Thermal Instability of Laminar Natural Convection Flow on Inclined Isothermal Plates", Canadian Journal of Chemical Engineering, Vol. 51, 1973, pp. 659-666.

12. Lee, J.B. and Lock, G.S.H., "Instability in Boundary-Layer Free Convection Along an Inclined Plate", Trans. Canadian Society for Mechanical Engineering, Vol. 1, 1972, pp. 197-203.

13. Kahawita, R.A. and Meroney, R.N., "The Vortex Mode of Instability in Natural Convection Flow Along Inclined Plates", International Journal of Heat and Mass Transfer, Vol. 17, 1974, pp. 541-548.

14. Hatton, A.P. and Turton, J.S., "Heat Transfer in the Thermal Entry Length with Laminar Flow Between Parallel Walls at Unequal Temperatures", International Journal of the Heat and Mass Transfer, Vol. 5, 1962, pp. 673-679.

15. Collatz, L., The Numerical Treatment of Differential Equations, 3rd Ed., Springer-Verlag, Berlin, 1960, p. 69.

16. Thomas, L.H., "The Stability of Plane Poiseuille Flow", Physical Review, Vol. 91, 1953, pp. 780-783.

17. Forsythe, G.E. and Wasow, W.R., Finite-Difference Methods for Partial Differential Equations, John Wiley & Sons, New York, 1960, Sec. 24.8.

18. Fröberg, C.E., Introduction to Numerical Analysis, 2nd Ed., Addison-Wesley, Reading, Massachusetts, 1969, p. 117.

19. Combarnous, M.A. and Bia, P., "Combined Free and Forced Convection in Porous Media", Society for Petroleum Engineers Journal, Vol. 11, 1971, pp. 399-405.

20. Chandra, K., "Instability of Fluids Heated from Below", Proceedings, Royal Society, London, Series A, Vol. 164, 1938, pp. 231-242.

Table 1 Instability Results for Pe = 1

Pr	0.001		0.010		0.100		0.700	
$\bar{x}$	a*	Ra*	a*	Ra*	a*	Ra*	a*	Ra*
-2.000	2.895	486.7	2.951	3205.2	3.078	6559.9	3.110	7169.6
-1.750	2.886	440.2	2.948	2827.1	3.079	5653.7	3.111	6167.7
-1.500	2.877	397.9	2.946	2494.2	3.080	4881.9	3.111	5315.3
-1.250	2.869	360.6	2.945	2205.6	3.079	4226.9	3.111	4591.8
-1.000	2.862	328.8	2.946	1960.0	3.082	3673.9	3.111	3980.1
-0.800	2.858	307.8	2.949	1794.0	3.083	3296.7	3.112	3561.6
-0.600	2.854	291.5	2.953	1655.0	3.084	2971.8	3.113	3199.6
-0.400	2.852	280.8	2.960	1544.2	3.087	2695.2	3.114	2889.3
-0.200	2.852	277.6	2.964	1464.1	3.090	2464.6	3.114	2627.2
-0.100	2.852	279.9	2.966	1437.4	3.091	2366.1	3.114	2513.6
-0.060	2.852	281.8	2.969	1429.5	3.092	2329.9	3.114	2471.4
-0.010	2.852	285.1	2.969	1422.2	3.092	2287.3	3.114	2421.3
-0.006	2.853	285.5	2.969	1421.8	3.092	2284.0	3.114	2417.4
0.0	2.853	285.9	2.970	1421.1	3.093	2279.1	3.115	2411.6
0.006	2.853	286.5	2.970	1420.7	3.093	2274.5	3.115	2406.0
0.060	2.855	292.9	2.974	1419.6	3.095	2233.5	3.116	2356.5
0.100	2.856	298.3	2.978	1420.4	3.096	2205.3	3.117	2322.2
0.200	2.859	314.4	2.986	1426.9	3.098	2142.0	3.117	2244.7
0.400	2.868	355.0	3.003	1451.0	3.102	2040.9	3.117	2119.8
0.600	2.878	405.1	3.019	1481.2	3.105	1965.5	3.117	2026.2
0.800	2.889	463.8	3.034	1512.5	3.108	1909.4	3.117	1955.4
1.000	2.900	530.3	3.047	1542.2	3.110	1864.8	3.117	1901.3
1.250	2.919	623.0	3.062	1575.3	3.111	1824.0	3.117	1850.8
1.500	2.938	724.2	3.073	1603.3	3.113	1794.2	3.117	1814.0
1.750	2.957	830.8	3.083	1626.3	3.114	1772.2	3.117	1787.0
2.000	2.976	939.5	3.091	1644.7	3.115	1756.0	3.117	1767.0
2.250	2.955	1046.4	3.097	1659.3	3.116	1743.9	3.117	1752.1
2.500	3.013	1148.1	3.102	1670.6	3.116	1734.9	3.117	1741.1
3.000	3.046	1325.9	3.109	1686.2	3.114	1723.1	3.117	1726.6
4.000	3.088	1554.9	3.114	1700.6	3.117	1712.7	3.117	1713.8

Table 1 Continued

Pr	1.000		10.000		100.000		∞	
$\bar{x}$	a*	Ra*	a*	Ra*	a*	Ra*	a*	Ra*
-2.000	3.112	7202.0	3.116	7270.4	3.117	7277.3	3.117	7278.1
-1.750	3.112	6195.1	3.116	6253.2	3.117	6259.1	3.117	6259.7
-1.500	3.113	5338.4	3.116	5387.6	3.117	5392.6	3.117	5393.1
-1.250	3.113	4611.3	3.117	4652.8	3.117	4658.0	3.117	4657.5
-1.000	3.113	3996.5	3.117	4031.4	3.117	4034.9	3.117	4035.3
-0.800	3.113	3575.8	3.117	3605.9	3.117	3609.0	3.117	3609.3
-0.600	3.114	3211.8	3.117	3237.6	3.117	3240.3	3.117	3240.5
-0.400	3.114	2899.6	3.117	2921.5	3.118	2923.7	3.118	2924.0
-0.200	3.115	2635.8	3.117	2654.1	3.118	2655.9	3.118	2656.1
-0.100	3.116	2521.4	3.117	2537.9	3.119	2539.5	3.119	2539.7
-0.060	3.115	2478.9	3.118	2494.7	3.119	2496.3	3.119	2496.4
-0.010	3.116	2428.3	3.119	2443.3	3.119	2444.8	3.119	2444.9
-0.006	3.116	2424.4	3.119	2439.3	3.119	2440.8	3.119	2440.9
0.0	3.117	2418.6	3.119	2433.4	3.119	2434.8	3.119	2435.0
0.006	3.117	2413.0	3.119	2427.7	3.119	2431.1	3.119	2429.3
0.060	3.117	2363.0	3.119	2376.7	3.119	2378.0	3.119	2396.7
0.100	3.117	2328.4	3.119	2341.3	3.119	2342.6	3.119	2342.8
0.200	3.117	2250.0	3.119	2261.4	3.119	2262.5	3.119	2262.6
0.400	3.117	2123.9	3.119	2132.5	3.119	2133.4	3.119	2133.4
0.600	3.117	2029.3	3.118	2035.9	3.119	2036.5	3.119	2036.6
0.800	3.117	1957.8	3.118	1962.8	3.119	1963.3	3.119	1963.4
1.000	3.117	1901.7	3.118	1907.1	3.119	1907.5	3.119	1907.5
1.250	3.117	1852.2	3.118	1855.1	3.119	1855.3	3.119	1855.4
1.500	3.117	1815.0	3.118	1817.1	3.118	1817.4	3.118	1817.4
1.750	3.117	1787.7	3.118	1789.3	3.118	1789.5	3.118	1789.5
2.000	3.117	1767.6	3.118	1768.7	3.118	1768.8	3.118	1768.9
2.250	3.117	1752.6	3.118	1753.4	3.118	1753.5	3.118	1753.5
2.500	3.117	1741.4	3.117	1742.0	3.118	1742.1	3.118	1742.1
3.000	3.117	1726.8	3.117	1727.1	3.117	1727.1	3.117	1727.2
4.000	3.117	1713.9	3.117	1714.0	3.117	1714.0	3.117	1714.0

Table 2 Instability Results for Pe = 5

Pr	1.0		0.7		1	
$\bar{x}$	a*	Ra*	a*	Ra*	a*	Ra*
-0.600	3.026	10249.30	3.108	20092.30	3.115	20916.80
-0.400	3.016	5387.25	3.101	9622.75	3.109	9955.20
-0.200	3.013	2863.11	3.102	4700.06	3.109	4838.21
-0.100	3.019	2171.63	3.102	3384.01	3.113	3472.09
-0.060	3.024	1980.93	3.109	3003.92	3.116	3076.62
-0.010	3.034	1812.39	3.113	2630.41	3.119	2686.70
-0.006	3.034	1802.53	3.114	2635.24	3.119	2659.86
0.0	3.036	1788.83	3.114	2568.79	3.120	2621.54
0.006	3.030	1777.77	3.114	2534.56	3.121	2585.38
0.060	3.038	1716.93	3.119	2288.45	3.124	2324.28
0.100	[illegible]	1695.94	3.121	2161.46	3.124	2189.29
0.200	[illegible]	1678.20	3.122	1962.62	3.124	1978.09
0.400	[illegible]	1683.57	[illegible]	[illegible]6.04	3.121	1801.50
0.600	3.106	1693.58	[illegible]	[illegible]739.83	3.119	1741.94
0.800	3.114	1700.01	3.118	1719.52	3.118	1720.38
1.000	3.117	1703.75	3.118	1712.05	3.118	1712.41
1.250	3.117	1706.03	3.115	1708.95	3.118	1709.07
1.500	3.117	1707.02	3.117	1708.07	3.117	1708.12
1.750	3.117	1707.45	3.117	1707.84	3.117	1707.85
2.000	3.117	1707.63	3.117	1707.78	3.117	1707.78
2.250	3.117	1707.71	3.117	1707.76	3.117	1707.77
2.500	3.117	1707.74	3.117	1707.76	3.117	1707.76

Pr	10		100		∞	
-0.600	3.132	22716.00	3.133	22918.00	3.133	22897.80
-0.400	3.127	10687.80	3.129	10771.60	3.129	10763.20
-0.200	3.127	5145.76	3.129	5180.67	3.129	5177.11
-0.100	3.130	3667.48	3.132	3690.06	3.132	3687.79
-0.060	3.131	3237.46	3.132	3256.02	3.132	3254.15
-0.010	3.133	2809.19	3.134	2823.31	3.134	2821.99
-0.006	3.133	2779.90	3.134	2793.69	3.134	2792.31
0.0	3.133	2737.34	3.134	2750.63	3.134	2749.30
0.006	3.133	2696.80	3.135	2709.57	3.135	2708.29
0.060	3.133	2401.95	3.134	2507.40	3.134	2409.90
0.100	3.132	2249.17	3.133	2255.93	3.133	2255.25
0.200	3.129	2010.88	3.129	2014.54	3.129	2014.18
0.400	3.123	1812.89	3.123	1814.15	3.123	1814.02
0.600	3.120	1746.31	3.120	1746.79	3.120	1746.74
0.800	3.119	1722.14	3.119	1722.33	3.119	1722.31
1.000	3.118	1713.13	3.118	1713.21	3.118	1713.20
1.250	3.118	1709.32	3.118	1709.34	3.118	1709.34
1.500	3.117	1708.20	3.117	1708.21	3.117	1708.21
1.750	3.117	1707.88	3.117	1707.89	3.117	1707.89
2.000	3.117	1707.79	3.117	1707.80	3.117	1707.80
2.250	3.117	1707.77	3.117	1707.77	3.117	1707.77
2.500	3.117	1707.76	3.117	1707.76	3.117	1707.76

Table 3 Instability Results for Pe = 10

Pr	0.1		0.7		1	
$\bar{x}$	a*	Ra*	a*	Ra*	a*	Ra*
-0.200	2.985	5647.97	3.095	14642.00	3.126	15805.90
-0.100	2.983	2434.50	3.098	5922.55	3.111	6346.[illegible]
-0.060	2.986	1817.37	3.014	4237.54	3.116	4518.98
-0.010	2.997	1386.76	3.116	2950.03	3.127	3115.29
-0.006	2.998	1367.77	3.117	2878.66	3.130	3036.58
0.0	3.000	1344.03	3.118	2779.71	3.132	2926.97
0.006	3.001	1346.43	3.121	2695.58	3.133	2836.12
0.060	3.03[illegible]	1340.26	3.133	2218.95	3.140	2291.[illegible]7
0.100	3.056	1378.78	3.134	2041.75	3.141	2089.00
0.200	3.092	1486.00	3.131	1834.43	3.140	1853.[illegible]
0.400	3.117	1620.46	3.124	1726.49	3.133	1731.06
0.600	3.119	1674.76	3.120	1709.18	3.124	1710.48
0.800	3.119	1695.29	3.118	1707.08	3.120	1707.49
1.000	3.118	1703.02	3.118	1707.26	3.118	1707.37
1.250	3.118	1706.33	3.118	1707.40	3.118	1707.59
1.500	3.117	1707.33	3.117	1707.62	3.117	1707.70
1.750	3.117	1707.63	3.117	1707.74	3.117	1707.74
2.000	3.117	1707.72	3.117	1707.76	3.117	1707.76
2.250	3.117	1707.75	3.117	1707.76	3.117	1707.76
2.500	3.117	1707.76	3.117	1707.76	3.117	1707.76

Pr	10		100		∞	
-0.200	3.152	18801.90	3.158	19147.90	3.158	19186.90
-0.100	3.154	7423.62	3.159	7547.22	3.159	7561.15
-0.060	3.152	5226.81	3.160	5307.46	3.160	5316.54
-0.010	3.164	3519.22	3.167	3564.38	3.167	3569.46
-0.006	3.164	3421.27	3.164	3464.18	3.164	3469.00
0.0	3.165	3283.79	3.169	3323.44	3.169	3327.89
0.006	3.160	3161.08	3.169	3197.03	3.169	3210.07
0.060	3.152	2451.40	3.162	2468.39	3.162	247[illegible].56
0.100	3.138	2191.78	3.154	2202.44	3.154	2205.41
0.200	3.124	1894.69	3.138	1898.79	3.138	1901.00
0.400	3.120	1740.35	3.124	1741.26	3.124	1742.95
0.600	3.118	1713.06	3.120	1713.31	3.120	1712.56
0.800	3.116	1708.29	3.118	1708.37	3.118	1708.99
1.000	3.118	1707.65	3.118	1707.67	3.118	1707.80
1.250	3.118	1707.66	3.118	1707.68	3.118	1707.70
1.500	3.117	1707.72	3.117	1707.73	3.117	1707.72
1.750	3.117	1707.76	3.117	1707.75	3.117	1707.76
2.000	3.117	1707.76	3.117	1707.76	3.117	1707.76
2.250	3.117	1707.76	3.117	1707.76	3.117	1707.76
2.500	3.117	1707.76	3.117	1707.76	3.117	1707.76

Table 4 Instability Results for Pe = 50

Pr	0.700		1.000		10.000		100.000	
$\bar{x}$	a*	Ra*	a*	Ra*	a*	Ra*	a*	Ra*
0.001	3.058	5163.4	3.118	7005.8	3.802	24575.[illegible]	4.104	30547.5
0.002	3.065	4849.1	3.128	6501.3	3.802	20625.9	4.102	25337.7
0.004	3.078	4384.4	3.144	5755.5	3.802	15643.4	4.002	18435.6
0.006	3.089	4053.5	3.156	5225.0	3.745	12650.5	3.942	14511.5
0.008	3.098	3803.0	3.166	4824.2	3.694	10663.6	3.854	12000.3
0.010	3.107	3604.7	3.173	4508.1	3.644	9253.4	3.774	10263.[illegible]
0.020	3.133	2999.7	3.191	3558.1	3.475	5786.2	3.532	6161.4
0.040	3.149	2461.7	3.189	2751.1	3.324	3644.8	3.344	3766.0
0.060	3.152	2197.9	3.179	2376.6	3.256	2862.0	3.265	292[illegible].4
0.080	3.152	2039.9	3.170	2160.2	3.218	2462.7	3.223	2497.8
0.100	3.150	1936.4	3.163	2021.9	3.194	2225.9	3.197	2248.4
0.200	3.140	1734.9	3.143	1758.1	3.148	1807.2	3.148	1812.1
0.400	3.127	1650.0	3.127	1698.9	3.126	1706.6	3.126	1707.3
0.600	3.121	1701.9	3.121	1702.9	3.120	1704.9	3.120	1705.1
0.800	3.118	1705.7	3.118	1706.0	3.118	1706.6	3.118	1706.7
1.000	3.118	1707.1	3.118	1707.2	3.118	1707.4	3.118	1707.4
1.250	3.117	1707.6	3.117	1707.6	3.117	1707.7	3.117	1707.7
1.500	3.117	1707.7	3.117	1707.7	3.117	1707.7	3.117	1707.7

Pe = ∞

0.001	2.972	3984.2	2.988	5550.9	3.334	31395.9	4.023	55779.9
0.002	2.995	3802.5	3.021	5197.2	3.448	22157.5	3.871	31983.9
0.004	3.029	3544.6	3.097	4347.4	3.506	14549.7	3.749	18150.5
0.006	3.052	3359.0	3.118	4077.0	3.504	11159.1	3.662	13120.1
0.008	3.069	3213.2	3.133	3859.1	3.489	9208.3	3.611	10474.5
0.010	3.083	3093.1	3.170	3171.9	3.470	7928.6	3.565	8827.6
0.020	3.122	2694.0	3.182	2546.0	3.387	5021.2	3.429	5326.0
0.040	3.142	2259.4	3.176	2243.3	3.292	3296.3	3.308	3395.4
0.060	3.153	2087.2	3.169	2065.6	3.242	2657.8	3.250	2707.4
0.080	3.153	1959.7	3.163	1951.5	3.211	2327.5	3.215	2357.1
0.100	3.152	1875.7	3.144	1736.7	3.190	2130.0	3.193	2149.4
0.200	3.142	1715.7	3.127	1696.4	3.147	1780.9	3.148	1785.4
0.400	3.127	1692.6	3.121	1702.6	3.126	1703.6	3.126	1703.3
0.600	3.121	1701.6	3.120	1706.0	3.121	1704.6	3.120	1704.8
0.800	3.118	1705.7	3.118	1707.2	3.118	1706.6	3.118	1706.7
1.000	3.118	1707.1	3.118	1707.6	3.118	1707.4	3.118	1707.4
1.250	3.117	1707.6	3.117	1707.7	3.117	1707.7	3.117	1707.7
1.500	3.117	1707.7	3.117	1707.8	3.117	1707.7	3.117	1707.7

Table 5 Instability Results for Transverse Rolls at Pe 1, 5

Pe	1				5			
Pr	1		100		1		100	
$\bar{x}$	a*	Ra*	a*	Ra*	a*	Ra*	a*	Ra*
-2.000	2.771	6007.0	2.773	5999.4				
-1.500	2.769	4504.6	2.779	4499.8				
-1.000	2.787	3425.8	2.783	3422.8	2.772	67928.5	2.832	66329.9
-0.600	2.813	2808.4	2.815	2806.2	2.785	19110.4	2.846	18606.6
-0.100	2.903	2299.6	2.905	2297.8	2.678	3402.7	2.739	3348.1
-0.060	2.913	2269.7	2.916	2268.2	2.720	3064.7	2.772	3016.4
-0.010	2.927	2233.6	2.929	2232.0	2.801	2764.2	2.856	2716.1
-0.0	2.930	2226.4	2.932	2224.7	2.830	2718.0	2.886	2666.6
0.0	2.927	2236.7	2.928	2235.4	2.810	2711.9	2.846	2665.8
0.060	2.929	2233.4	2.948	2204.0	2.915	2532.2	2.967	2486.9
0.100	2.946	2205.4	2.961	2184.7	2.967	2437.4	3.019	2392.0
0.600	3.065	1999.1	3.067	1997.4	3.065	2000.7	3.114	1965.7
1.000	3.096	1900.3	3.097	1898.6	3.065	1965.6	3.114	1941.0
1.250	3.104	1856.2	3.106	1854.6	3.065	1961.8	3.114	1931.9
1.500	3.109	1822.5	3.111	1821.0	3.065	1960.7	3.113	1928.2
1.750	3.112	1797.0	3.114	1795.5	3.065	1960.4	3.113	1927.1
2.000	3.113	1777.7	3.116	1761.7	3.065	1960.3	3.113	1926.9
2.500	3.114	1752.1	3.117	1750.7	3.065	1960.3	3.113	1926.8
3.000	3.115	1737.5	3.117	1736.2	3.065	1960.3	3.113	1928.8
4.000	3.115	1724.5	3.117	1719.1	3.065	1960.3	3.113	1926.8
5.000	3.115	1720.3	3.117	1717.7	3.065	1960.3	3.113	1926.8
6.000	3.115	1718.9	3.117	1717.1	3.065	1960.3	3.113	1926.8

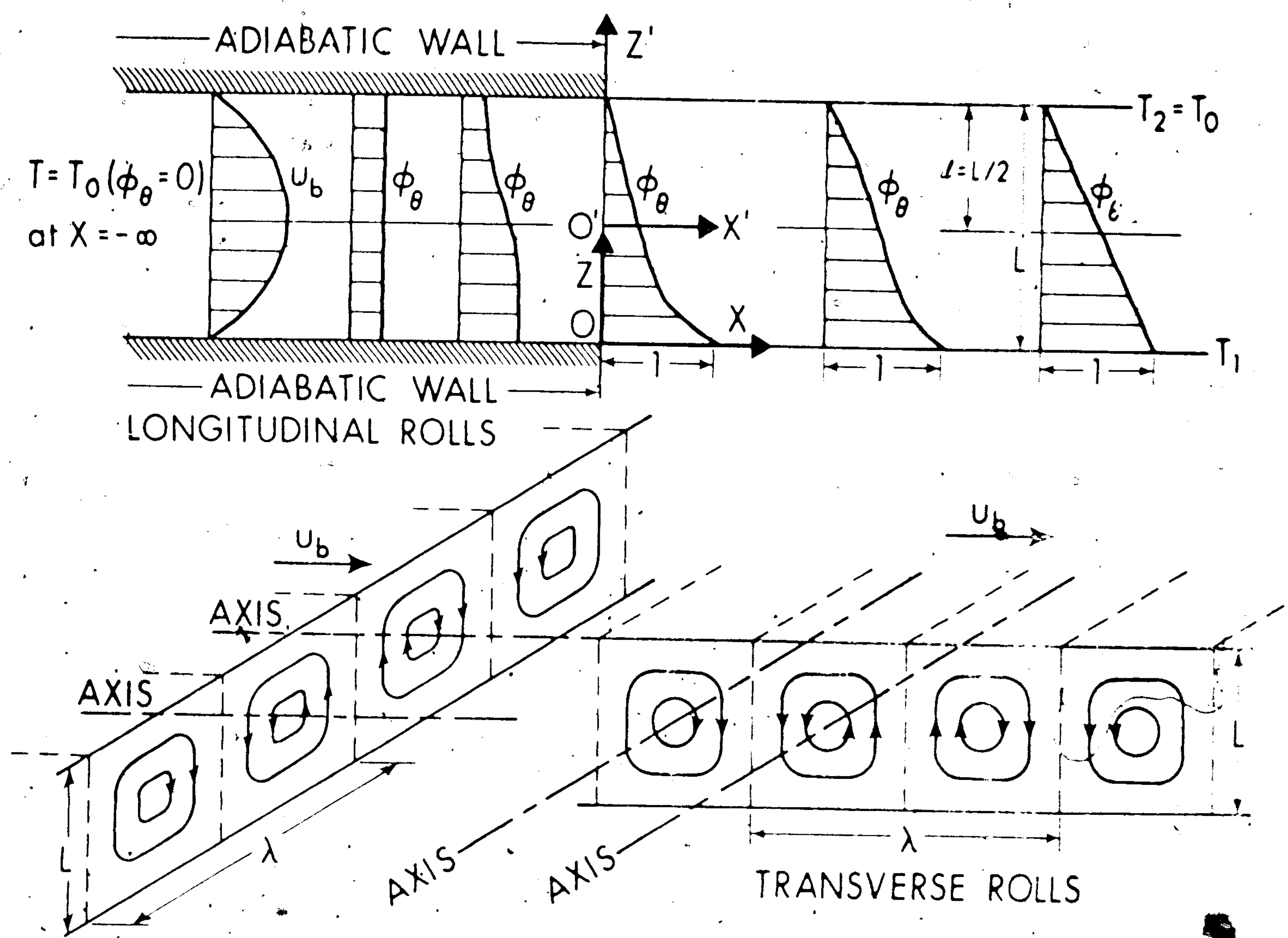

Fig. 1 Coordinate system and transverse and longitudinal vortex disturbances for plane Poiseuille flow

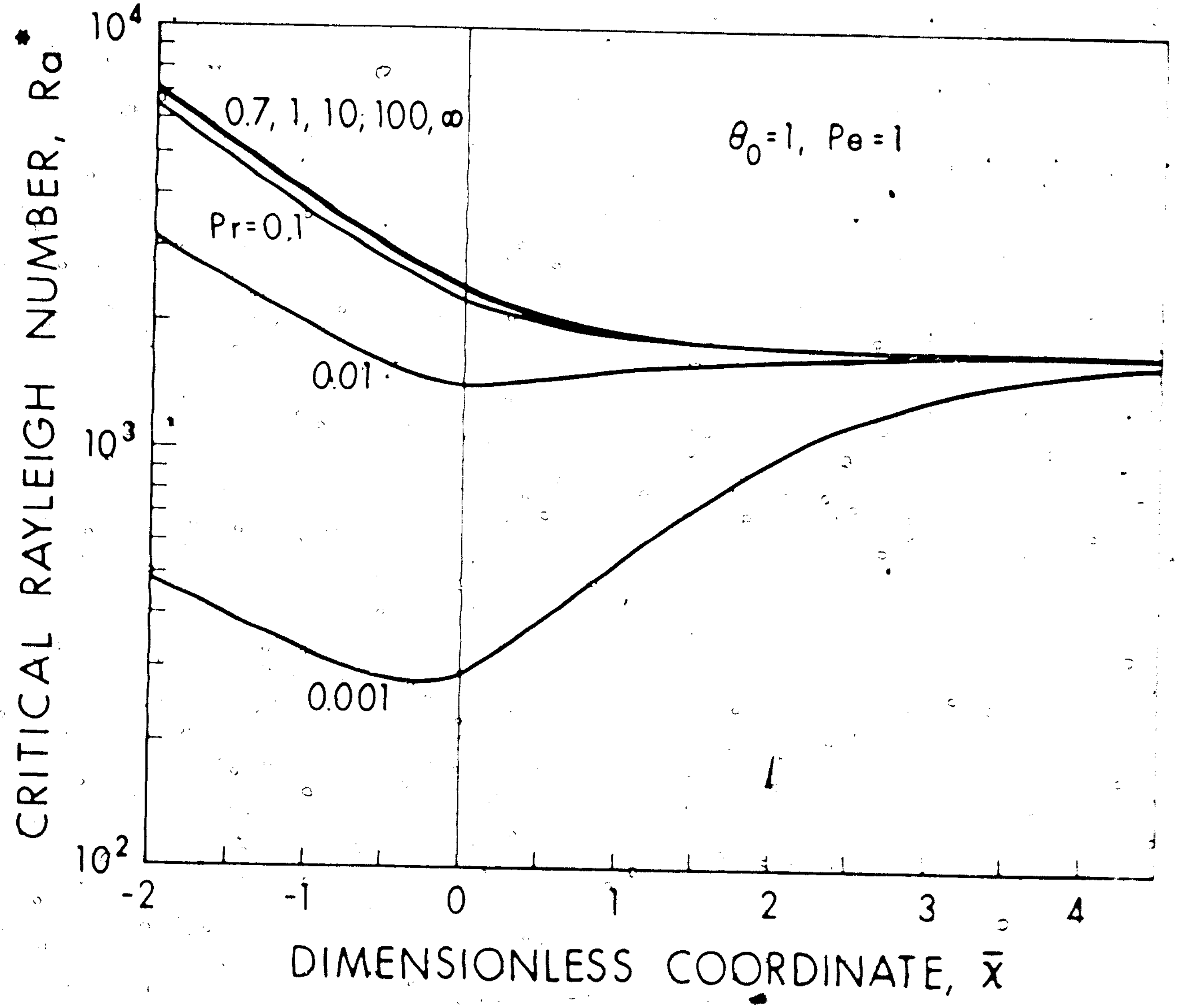

Fig. 2 Prandtl number effect on critical Rayleigh number versus $\bar{x}$ for θ_0 = 1 and Pe = 1.

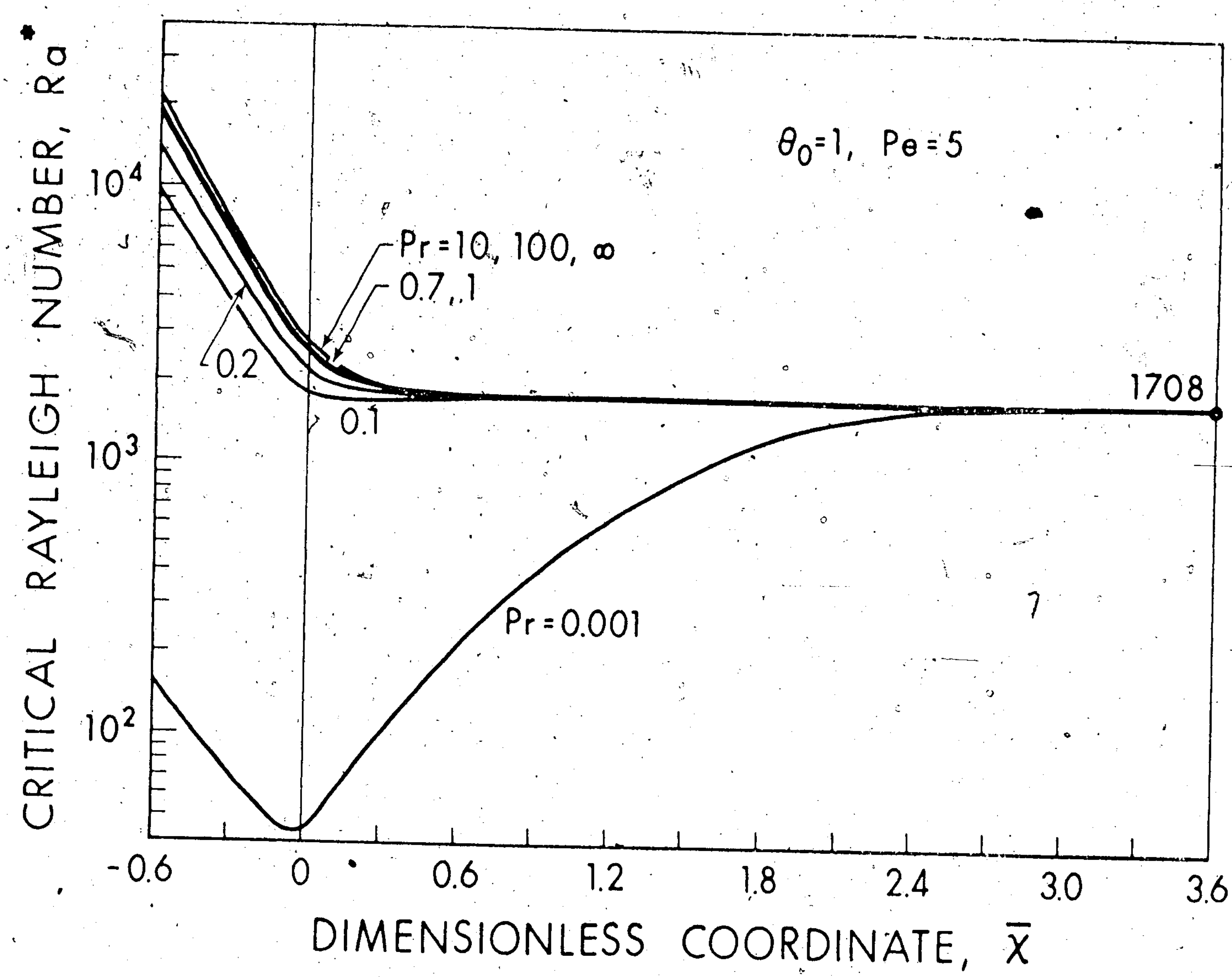

Fig. 3 Prandtl number effect on Ra* versus $\overline{x}$ for θ_0 = 1 and Pe = 5

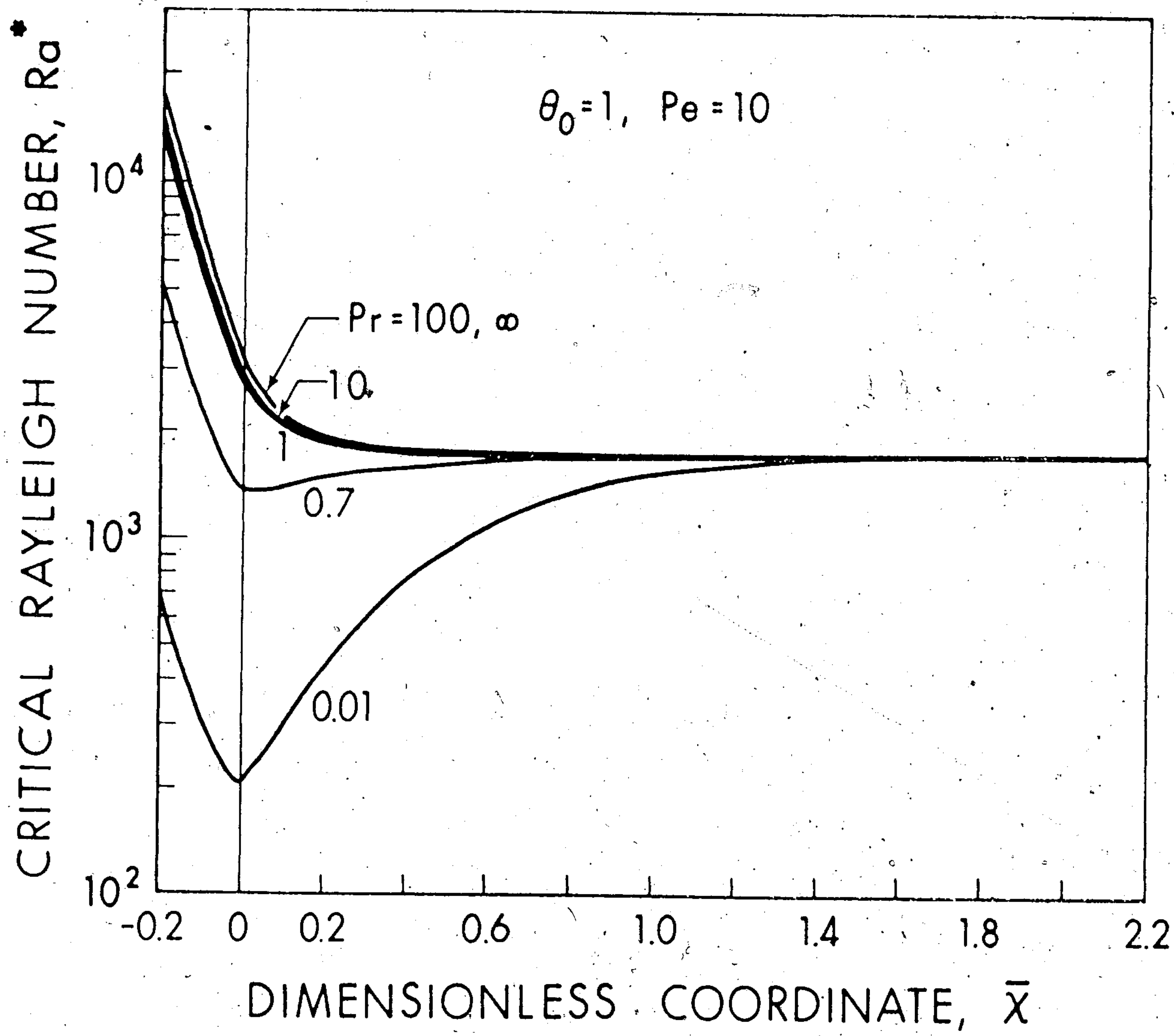

Fig. 4 Prandtl number effect on Ra* versus $\bar{x}$ for $\theta_0 = 1$ and Pe = 10

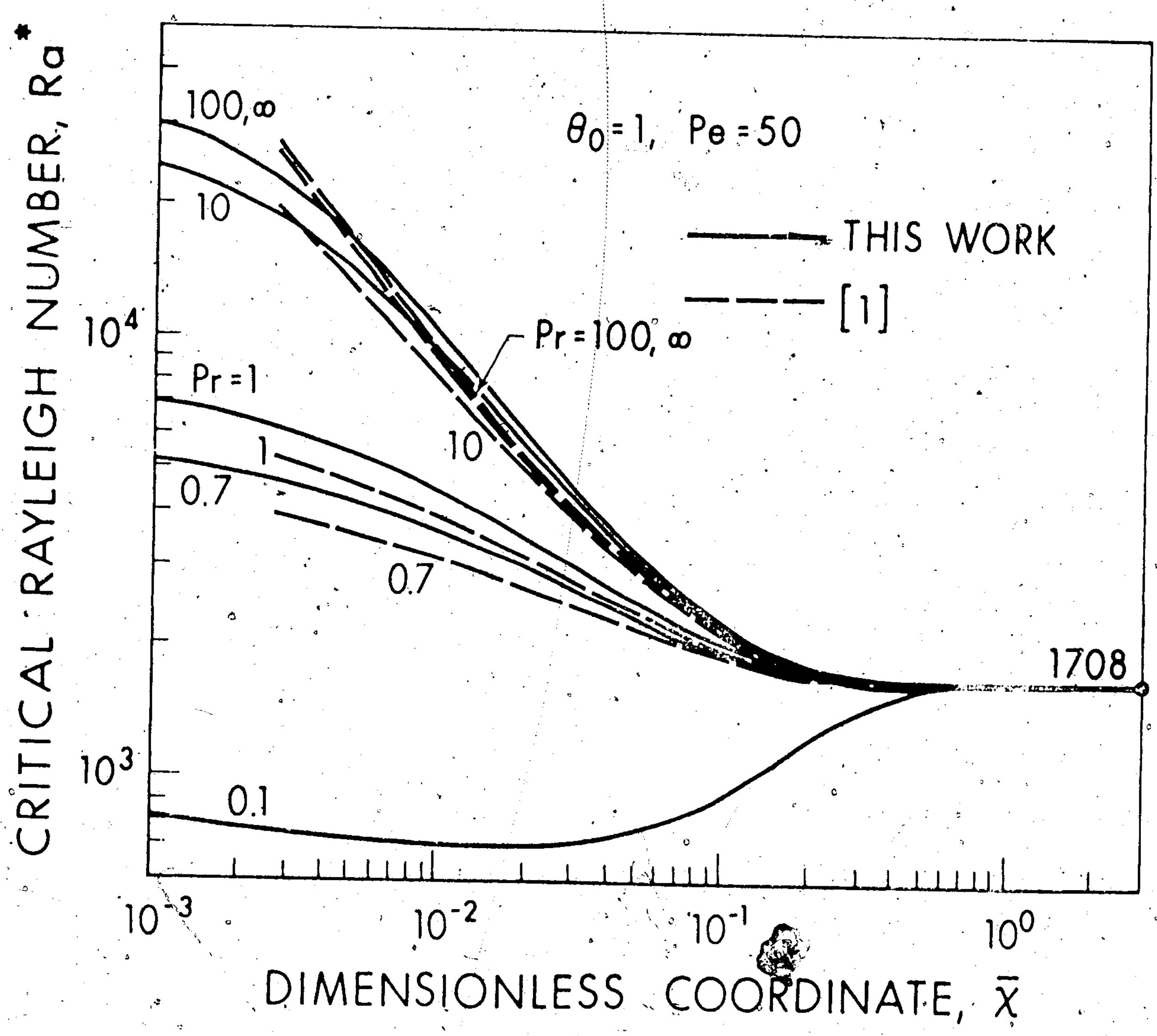

Fig. 5 Comparison of instability results between present work and [1] for $\theta_0 = 1$ and Pe = 50.

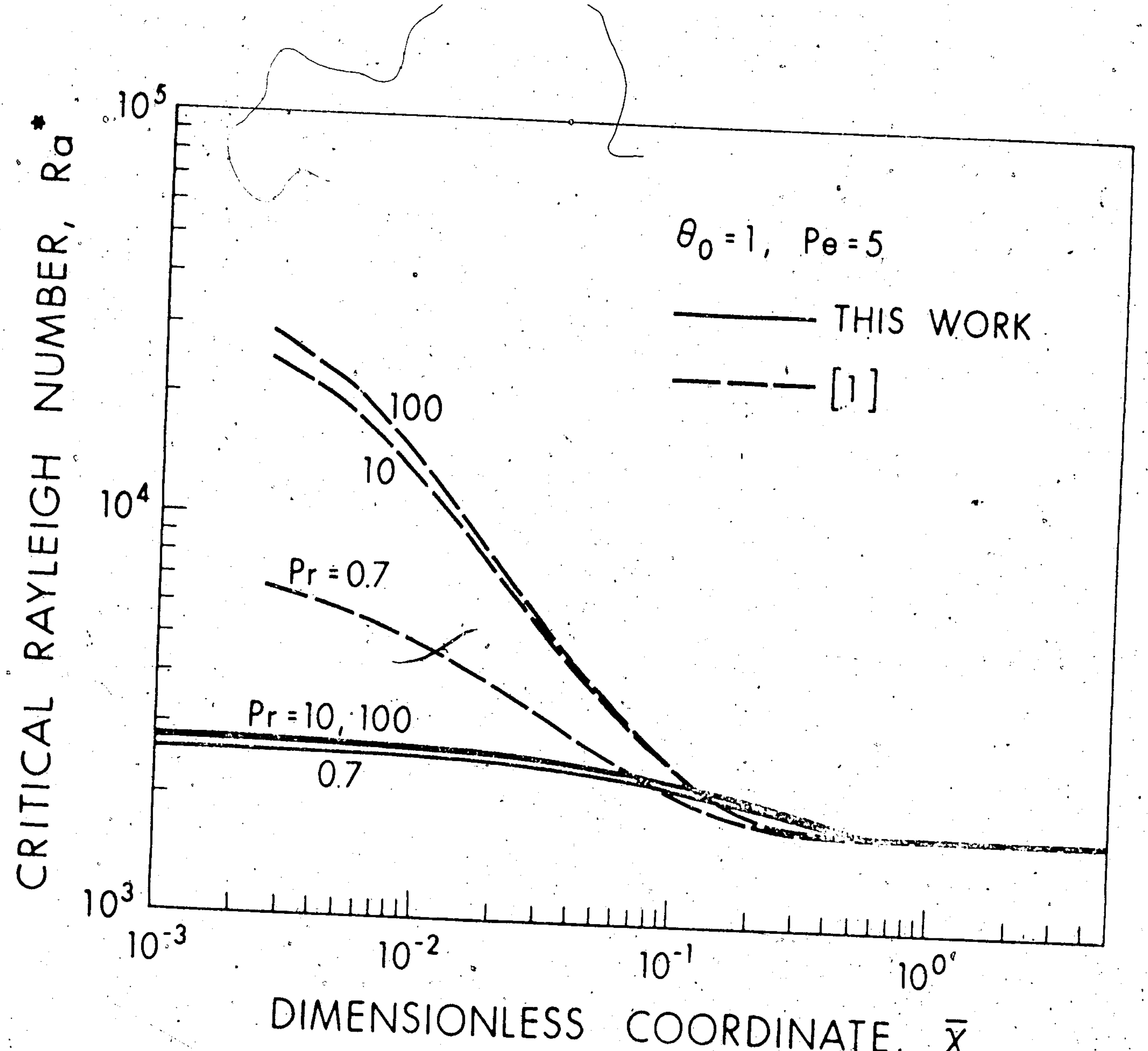

Fig. 6 Comparison of instability results between present work and [1] for $\theta_0 = 1$ and Pe = 1.5

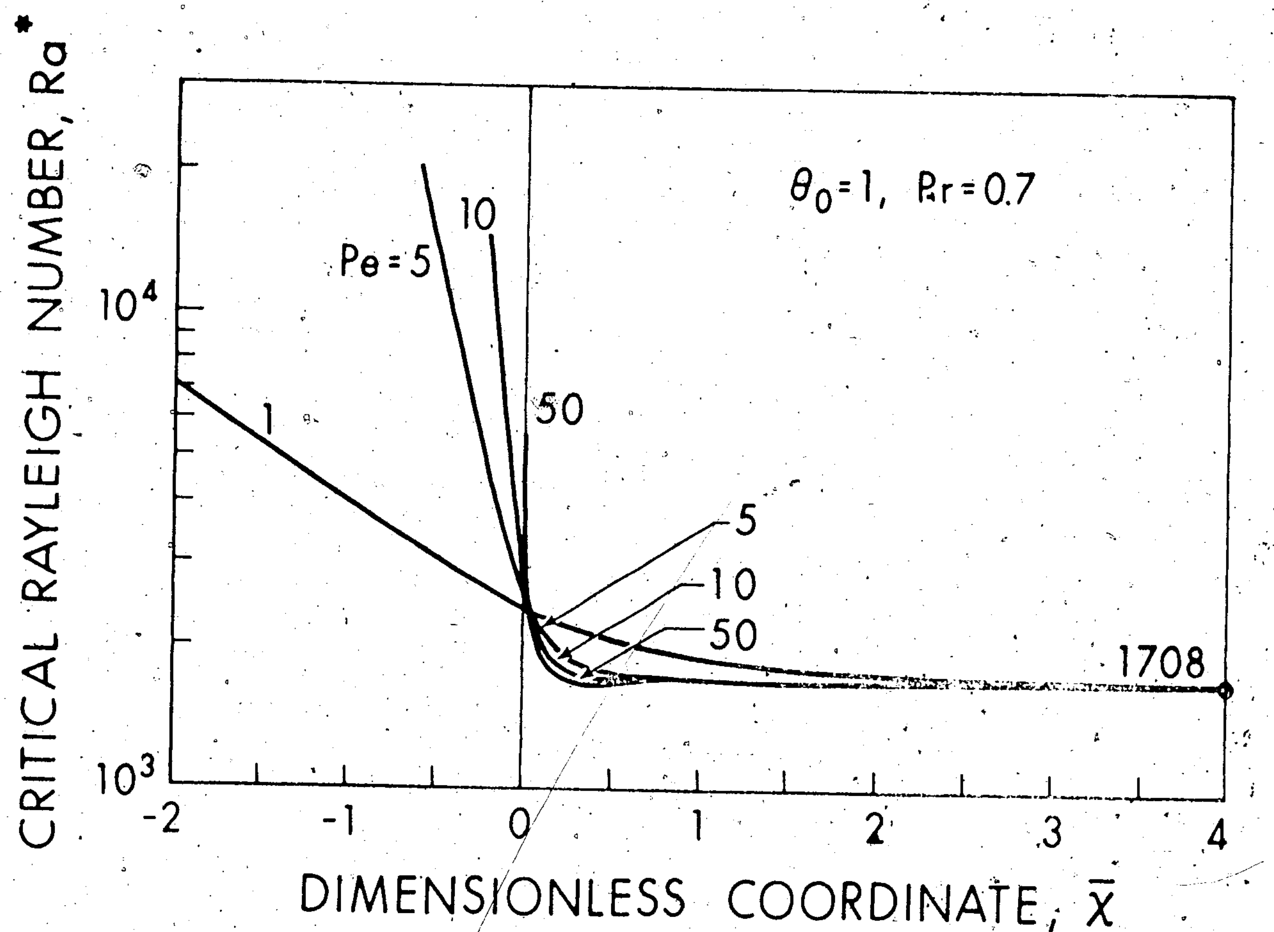

Fig. 7 Peclet number effect on Ra* versus $\bar{x}$ for $\theta_0 = 1$ and $Pr = 0.7$

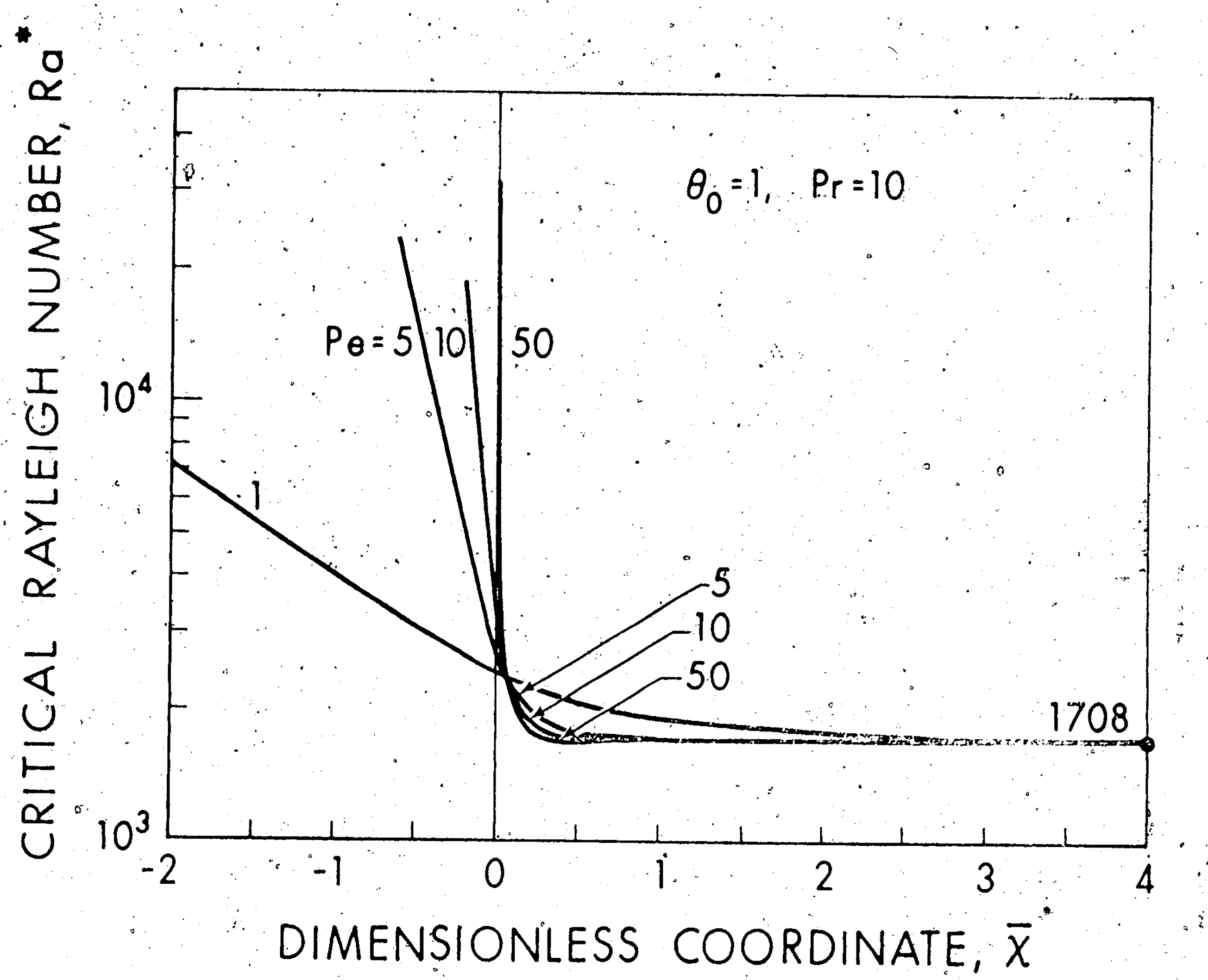

Fig. 8 Peclet number effect on Ra* versus $\overline{x}$ for $\theta_0 = 1$ and Pr = 10

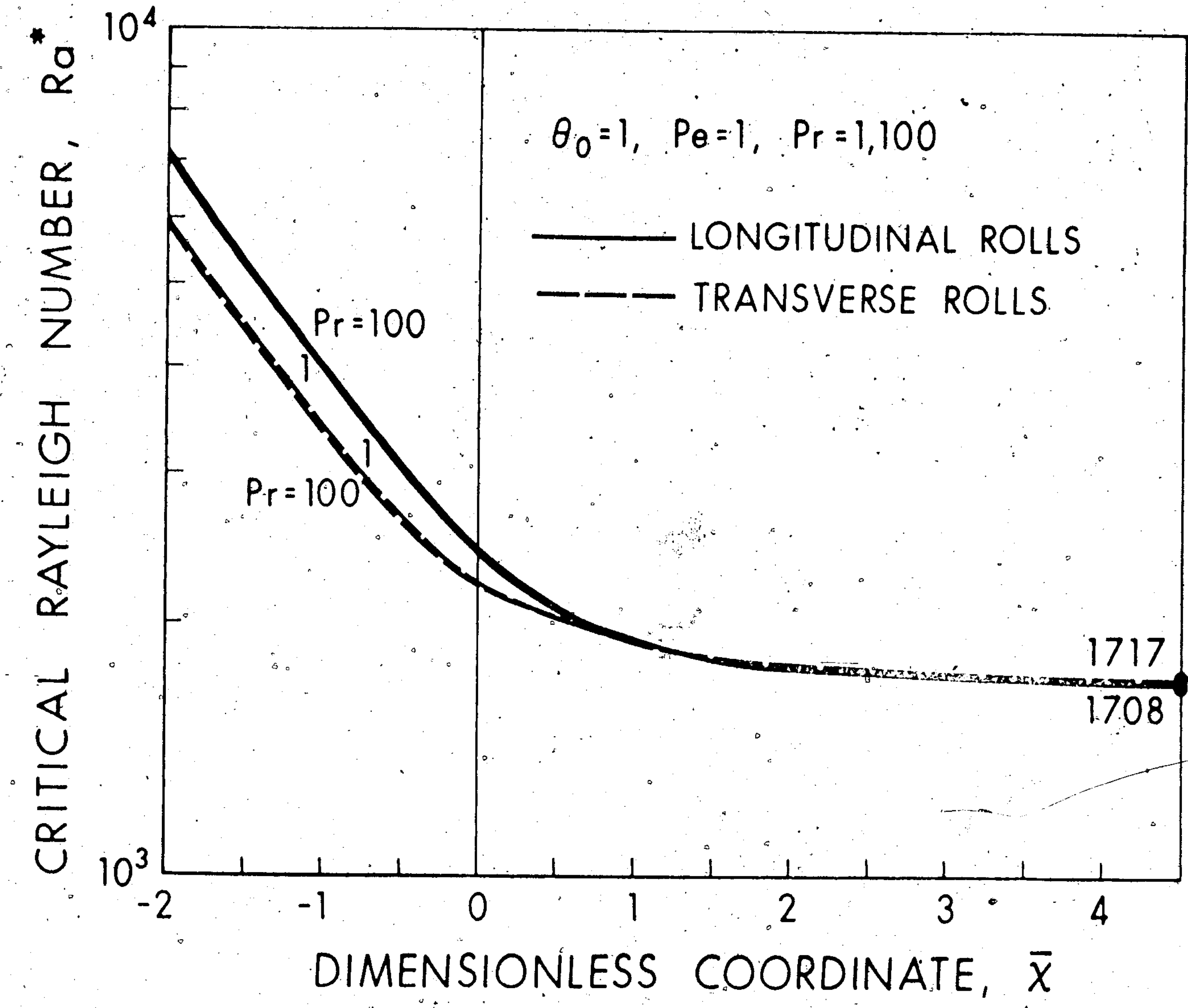

Fig. 9 Instability results for longitudinal and transverse vortex rolls at $\theta_0 = 1$, Pe = 1 and Pr = 1, 100.

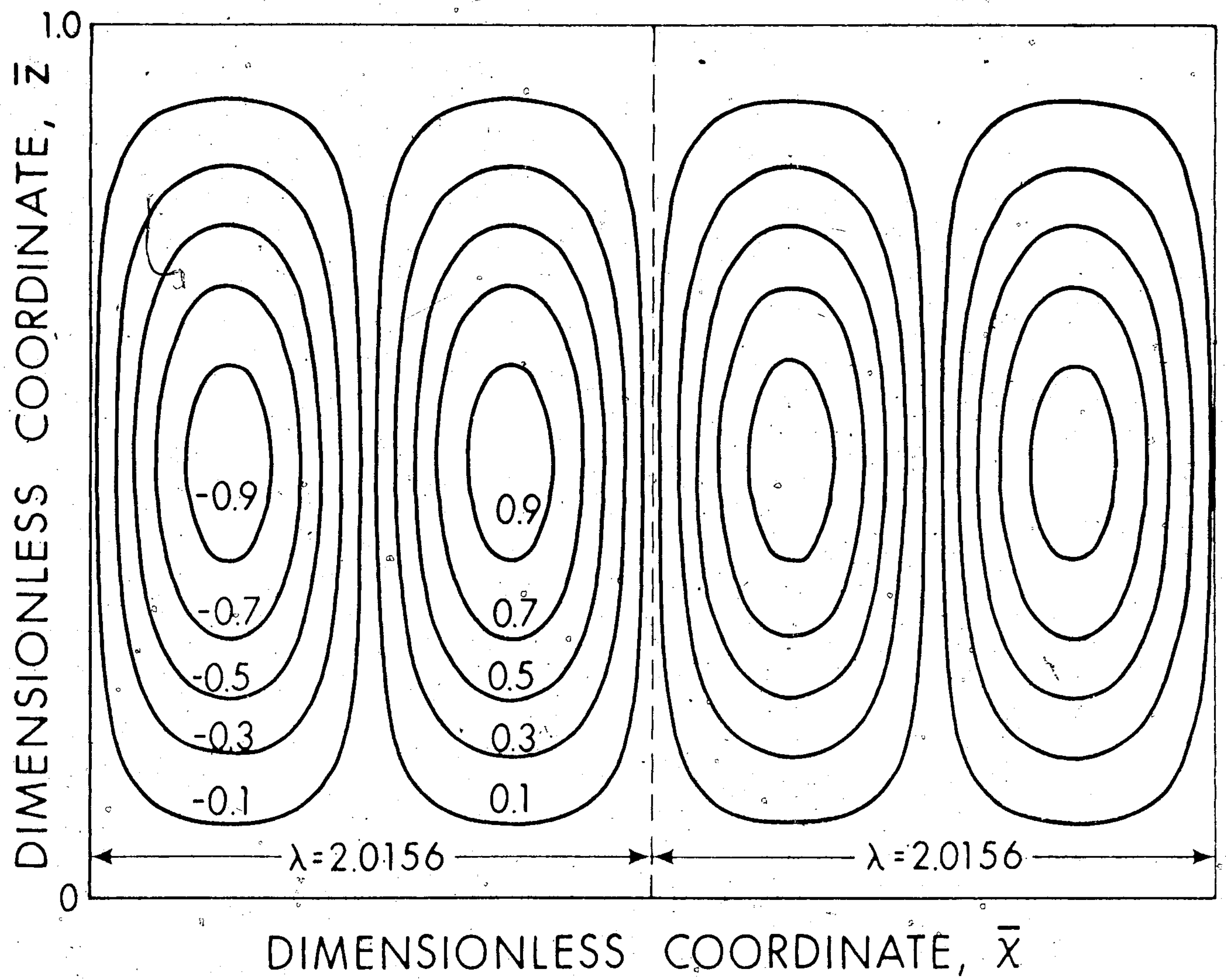

Fig. 10 Streamline pattern of transverse vortex disturbance for fully developed flow at $\theta_0 = 1$, Pe = 1, Pr = 100; Ra* = 1717 and a* = 3.117

CHAPTER IV

MAXIMUM DENSITY EFFECTS ON CONVECTIVE INSTABILITY OF HORIZONTAL PLANE POISEUILLE FLOWS IN THE THERMAL ENTRANCE REGION

A linear stability analysis is used to study the conditions marking the onset of secondary flow in the form of longitudinal vortices for plane Poiseuille flow of water in the thermal entrance region of a horizontal parallel-plate channel by a numerical method. The water temperature range under consideration is 0 ~ 30°C and the maximum density effect at 4°C is of primary interest. The basic flow solution for temperature includes axial heat conduction effect and the entrance temperature is taken to be uniform at far upstream location $\bar{x} \to -\infty$ to allow for the upstream heat penetration through thermal entrance $\bar{x} = 0$. Numerical results for critical Rayleigh number are obtained for Peclet numbers 1, 10, 50 and thermal condition parameters (λ_1, λ_2) in the range of $-2.0 \le \lambda_1 \le -0.5$ and $-1.0 \le \lambda_2 \le 1.4$. The analysis is motivated by a desire to determine the free convection effect on freezing or thawing in channel flow of water.

Nomenclature

A	= temperature difference ratio, $(T_1 - T_{max})/\Delta T$
A_n, B_n, C_n, D_n	= coefficients of infinite series defined by eqs. (5) and (6)
a	= dimensionless wave number
D	= operator, d/dz
f	= $(1 - \lambda_1 \xi + \lambda_2 \xi^2)$
Gr	= Grashof number defined below eq. (14)
g	= gravitational acceleration
L, ℓ	= height of channel and $L/2$
P, P_b	= Liquid pressure $(P_b + P')$ and basic flow pressure
Pe	= Peclet number, $4\ U_m \ell/\alpha$ = Re Pr
Pr	= Prandtl number, ν/α
p	= dimensionless perturbation pressure, $P'/(\rho\nu^2/L^2)$
Ra	= Rayleigh number, Pr Gr
Re	= Reynolds number, $4\ U_m \ell/\nu$
T, T_b, T_m, T_0	= water temperature $(T_b + \theta')$, basic flow temperature, $(T_1 + T_2)/2$ and uniform upstream temperature

T_1, T_2, T_{max}	=	constant lower and upper plate temperatures, and maximum density temperature (4°C)
U_b, U_m, u_b	=	axial and mean velocities and (U_b/U_m) of basic flow
u, v, w	=	dimensionless perturbation velocity components, $(U', V', W')/(\nu/L)$
$X, Y, Z,$	=	Cartesian coordinates with origin at lower plate
$x, y, z,$	=	$(X, Y, Z)/L$
x', z'	=	$(X'/(3/8)Pe\ell, Z'/\ell)$
$\bar{x}, \bar{z}$	=	transformed coordinates, $(x/(3Pe/16), z)$
Y_n, R_n, F_n, Z_n	=	eigenfunctions
Z'	=	transverse coordinate with origin at center of channel
α	=	thermal diffusivity
$\alpha_n, \beta_n, \varepsilon_n, \gamma_n$	=	eigenvalues
γ_1, γ_2	=	temperature coefficients for density-temperature relationship
θ	=	dimensionless temperature disturbance, $\theta'/\Delta T$
θ_b, θ_0	=	dimensionless temperature and uniform entrance temperature, $(T_b - T_m)/(T_2 - T_m)$ and $(T_0 - T_m)/(T_2 - T_m)$

θ_1, θ_2 = thermal condition parameters defined below eq. (13)

ν = kinematic viscosity

ρ, ρ_{max} = density and maximum density at 4°C

$\phi, \phi_u, \phi_\theta$ = $(\phi_\theta - 1)$, dimensionless basic velocity and temperature profiles, $(1/2)u_b$ = $3(z - z^2)$, $(1 - \theta_b)/2$

ΔT = $(T_1 - T_2)$

Superscripts and Subscripts

' = perturbation quantity

+ = amplitude of disturbance quantity

* = transformed perturbation variable or critical value

b = basic flow quantity in unperturbed state

1,2 = upstream and downstream regions

f = fully developed value

4.1 Introduction

Thermal instability analysis for horizontal liquid layers with a density maximum was made by Veronis [1], Debler [2], Tien [3] using a parabolic temperature-density relationship valid for the temperature range 0-8 C and recently by Sun, Tien and Yen [4] using a third degree polynomial expansion for the temperature-density relationship applicable to the temperature 0 to 30 °C. The onset of convection in a horizontal porous medium containing liquid with a density maximum was also studied by Sun, Tien and Yen [5]. It is noted that these thermal instability analyses are concerned with a horizontal liquid layer without main flow and represent an extension of the classical Benard problem to the case with maximum density effect.

The objective of this investigation is to study the effects of maximum density on the onset of longitudinal vortex rolls in the thermal entrance region of a horizontal plane Poiseuille flow where the lower and upper plate temperatures are maintained at T_1 and T_2, respectively, with $T_1 > T_2$ or $T_1 < T_2$. Recent theoretical analysis [6] based on Boussinesq approximation and experimental investigation [7] show that the instability sets in as steady longitudinal vortices in the thermal entrance region of a horizontal parallel-plate channel heated from below when a critical temperature difference is exceeded. For basic flow in the low Peclet number regime, the upstream heat penetration through the thermal entrance X = 0 becomes significant and the boundary condition of uniform entrance fluid temperature must be shifted from $X = 0$ to the far upstream location at $X = -\infty$ [8] to allow for the upstream heat conduction. The present work is motivated by the interest in determining the effect of free convection on ice formation or thawing in horizontal parallel-plate channels since water possesses maximum density at 4°C. The water temperatures under consideration range from 0 to 30°C and the temperature regime is also of interest in studying the decay and growth of ice in northern lakes or rivers.

4.2 Upstream and Downstream Temperature Solutions for Basic Flow

If one neglects the viscous dissipation effects, the energy equation and the boundary conditions in dimensionless form for the thermal entrance region problem (see Fig. 1) with axial heat conduction can be written as

$$\frac{2}{3} u_b \frac{\partial \theta_b}{\partial x'} = \frac{\partial^2 \theta_b}{\partial z'^2} + \left(\frac{8}{3Pe}\right)^2 \frac{\partial^2 \theta_b}{\partial x'^2} \tag{1}$$

$$\theta_{b1}(-\infty, z') = \theta_0, \quad \partial\theta_{b1}(x',1)/\partial z' = \partial\theta_{b1}(x',-1)/\partial z' = 0$$

$$\text{for } -\infty < x' \leq 0 \tag{2}$$

$$\theta_{b2}(\infty, z') = \theta_f, \quad \theta_{b2}(x',1) = 1, \quad \theta_{b2}(x',-1) = -1 \quad \text{for } 0 \leq x' < \infty \tag{3}$$

$$\theta_{b1}(0^-,z') = \theta_{b2}(0^+,z'), \; \partial\theta_{b1}(0^-,z')/\partial x' = \partial\theta_{b2}(0^+,z')/\partial x'$$

$$\text{at } x' = 0 \tag{4}$$

where the dimensionless variables are defined in Nomenclature and $u_b = (3/2)(1 - z'^2)$ for a plane Poiseuille flow.

The solution methods described in [8,9] may be adapted to the present problem and the temperature solutions θ_{b1} and θ_{b2} in the adiabatic and heated regions, respectively, can be written as (Chapter II).

$$\theta_{b1}(x',z') = \theta_0 + \sum_{n=1}^{\infty} B_n Y_n(z') \exp(\alpha_n^2 x')$$

$$+ \sum_{n=1}^{\infty} A_n F_n(z') \exp(\varepsilon_n^2 x'), \quad -\infty < x' \leq 0 \tag{5}$$

$$\theta_{b2}(x',z') = z' + \sum_{n=1}^{\infty} C_n R_n(z') \exp(-\beta_n^2 x')$$

$$+ \sum_{n=1}^{\infty} D_n Z_n(z') \exp(-\gamma_n^2 x'), \quad 0 \leq x' < \infty \tag{6}$$

where α_n, ε_n and Y_n, F_n are the even and odd eigenvalues and eigenfunctions, respectively, for the adiabatic (upstream) region. Similarly, β_n, γ_n and R_n, Z_n are the even and odd eigenvalues and eigenfunctions, respectively, for the heated (downstream) region. The details of the solution method, the computed eigenvalues and the series expansion coefficients for the case $\theta_0 = 1$ are given in Chapter II. A fourth-order Runge-Kutta method [10] using two hundred equal steps is employed to obtain the eigenvalues and eigenfunctions from the numerical solution of the characteristic equations and the related boundary conditions. The series coefficients are calculated by using the matching conditions at $x = 0$ for both the temperature and temperature gradients after constructing orthonormal functions from the nonorthogonal eigenfunctions [8]. In this study, the infinite series are truncated at $n = 12$ and 8 for Pe = 1 and Pe = 10, 50, respectively. For the instability analysis, it is more convenient to shift the coordinate origin to the lower plate as shown in Fig. 1. As a result, the basic temperature profile now becomes $\phi_\theta = (1 - \theta_b)/2$.

4.3 Perturbation Equations

If the basic flow field is perturbed, one obtains $U = U_b + U'$, $V = V'$, $W = W'$, $T = T_b + \theta'$, $P = P_b + P'$ and $\rho = \rho_b + \delta\rho$. Introducing the dimensionless variables, $(x,y,z) = (X,Y,Z)/L$, $(u,v,w) = (U',V',W')/(\nu/L)$, $p = P'/(\rho\nu^2/L^2)$, $\theta = \theta'/(\Delta T)$ and applying the linear stability analysis [5,6] using Boussinesq approximation, the perturbation equations in dimensionless form become

$$\frac{\partial u}{\partial x} + \frac{\partial v}{\partial y} + \frac{\partial w}{\partial z} = 0 \tag{7}$$

$$Re[\phi_u \frac{\partial u}{\partial x} + w \frac{d\phi_u}{dz}] = - \frac{\partial p}{\partial x} + \nabla^2 u \tag{8}$$

$$Re\phi_u \frac{\partial v}{\partial x} = - \frac{\partial p}{\partial y} + \nabla^2 v \tag{9}$$

$$Re\phi_u \frac{\partial w}{\partial x} = - \frac{\partial p}{\partial z} + \nabla^2 w - \frac{L^2}{\nu^2} \frac{\delta\rho}{\rho} g \tag{10}$$

$$Re\phi_u \frac{\partial \theta}{\partial x} + u \frac{\partial \phi_\theta}{\partial x} + w \frac{\partial \phi_\theta}{\partial z} = \frac{1}{Pr} \nabla^2 \theta \tag{11}$$

where $\phi_u = 3z(1 - z)$, $\phi_\theta = (T_b - T_2)/\Delta T = (1 - \theta_b)/2$ and $\nabla^2 = \partial^2/\partial x^2 + \partial^2/\partial y^2 + \partial^2/\partial z^2$.

The density-temperature relationship for water in the temperature range 0 to 30°C is given as [5]

$$\rho = \rho_{max} [1 - \gamma_1(T - T_{max})^2 - \gamma_2(T - T_{max})^3] \tag{12}$$

Here the temperature at maximum density T_{max} is assumed to lie between the lower and upper plate temperatures T_1 and T_2. Considering the change in the density, $\delta\rho = \rho(T_b + \theta') - \rho(T_b)$, caused by the temperature perturbation θ', one obtains the following expression after neglecting the terms involving $(\theta')^2$ and $(\theta')^3$.

$$\delta\rho = -\rho_{max}[2\gamma_1(A\Delta T)\theta'(1 + (3\gamma_2/2\gamma_1)A\Delta T)][1 - \lambda_1\phi + \lambda_2\phi^2] \tag{13}$$

where $\lambda_1 = (-1/A)[1 + (3\gamma_2/\gamma_1)(A\Delta T)]/[1 + (3\gamma_2/2\gamma_1)(A\Delta T)]$, $\lambda_2 = (1/A^2)[(3\gamma_2/2\gamma_1)A\Delta T]/[1 + (3\gamma_2/2\gamma_1)(A\Delta T)]$, $\phi_0 = (T_b - T_2)/\Delta T$, $\phi = \phi_0 - 1$, $\Delta T = T_1 - T_2$ and $A = (T_1 - T_{max})/\Delta T$. The thermal parameters λ_1 and λ_2 were first introduced by Sun, Tien and Yen [4,5].

The dependent variables u, v and p can be eliminated from the three momentum equations by using continuity equation. Noting that $\rho = \rho_{max}$ from Boussinesq approximation, one then obtains

$$Re\phi_u \frac{\partial}{\partial x}(\nabla^2 w) - Re\frac{d^2\phi_u}{dz^2}\frac{\partial w}{\partial x} = \nabla^2\nabla^2 w$$

$$+ Gr\nabla_1^2[(1 - \lambda_1\phi + \lambda_2\phi^2)\theta] \qquad (14)$$

where $Gr = g(2\gamma_1 A\Delta T)(\Delta T)L^3[1 + (3\gamma_2/2\gamma_1)(A\Delta T)]/\nu^2$ and $\nabla_1^2 = \partial^2/\partial x^2 + \partial^2/\partial y^2$. Since the disturbance variable u appears also in energy equation (11), equations (8), (14) and (11) now become the set of governing perturbation equations. It is seen that because of the presence of $(\Delta T)^2$ in the expression for Gr, the onset of secondary flow is possible for heating from below as well as above.

At the onset of instability in the form of steady longitudinal vortices (the type of Taylor-Görtler vortices), one may assume the perturbation form of $f = f^+(z)e^{iay}$ for the disturbance quantities w, u and θ [6]. Furthermore, for vortex-type instability $\partial p/\partial x = 0$ and the set of perturbation equations becomes:

$$(D^2 - a^2)^2 w^+ = Gr[a^2 f - \frac{\partial^2 f}{\partial x^2}]\theta^+ \qquad (15)$$

$$(D^2 - a^2)u^+ = Re\ w^+ \frac{d\phi_u}{dz} \qquad (16)$$

$$(D^2 - a^2)\theta^+ = Pr[u^+ \frac{\partial\phi_\theta}{\partial x} + w^+ \frac{\partial\phi_\theta}{\partial z}] \qquad (17)$$

where $f = 1 - \lambda_1\phi + \lambda_2\phi^2$ and $D = d/dz$.

In order to use the parameters Pr, Pe and Ra instead of Pr, Re and Gr which appear in the above set of equations, one may further introduce the transformations, $x = (3Pe/16)\bar{x}$, $z = \bar{z}$, $u^+ = Re\ u^*$, $w^+ = w^*$, and $\theta^+ = Pr\ \theta^*$. One thus obtains

$$(D^2 - a^2)^2 w^* = Ra[a^2(1 - \lambda_1\phi + \lambda_2\phi^2)$$

$$+ \{(-\lambda_1 + 2\lambda_2\phi) \frac{\partial^2\phi}{\partial\bar{x}^2} + 2\lambda_2(\frac{\partial\phi}{\partial\bar{x}})^2\}(\frac{16}{3Pe})^2]\theta^* \qquad (18)$$

$$(D^2 - a^2)u^* = w^* \frac{d\phi_u}{d\bar{z}} \qquad (19)$$

$$(D^2 - a^2)\theta^* = (\frac{16}{3Pr})\ u^* \frac{\partial\phi_\theta}{\partial\bar{x}} + w^* \frac{\partial\phi_\theta}{\partial\bar{z}} \qquad (20)$$

The boundary conditions for the disturbances at the walls are

$$w^* = Dw^* = u^* = \theta^* = 0 \text{ at } \bar{z} = 0 \text{ and } 1$$

For given values of θ_0, Pr, Pe and $\bar{x}$, one is interested in determining the minimum critical Rayleigh number and the corresponding wave number through the solution of the coupled equations (18) to (21). The numerical method of solution [6] employing the higher order finite-difference scheme developed by Thomas [11] may be applied to the present eigenvalue problem. The details are given in Chapter III.

4.4 Numerical Results and Discussion

The Prandtl number of water varies from 13.6 at 0°C to 7.02 at 20°C and is taken to be 10 in this study. The temperature coefficients for water [12] are $\gamma_1 = 7.7319 \times 10^{-6} (\frac{1}{°C})^2$ and $\gamma_2 = -5.1821 \times 10^{-8} (\frac{1}{°C})^3$ with a standard deviation of 0.4×10^{-5}. The details of the determination of the coefficients γ_1 and γ_2 using the method of regression are given in Appendix III. One notes that the parameter $A = (T_1 - T_{max})/\Delta T$ is always positive and λ_1 is always negative for the temperature range 0-30°C under consideration. The expression for λ_2 reveals that the value λ_2 is negative when $T_1 > T_{max}$ (heating from below) and positive when $0°C \leq T_1 < T_{max}$ (heating from above). For $T_1 > 4°C$, the potentially unstable layer is confined to the region $T_1 > T > 4°C$ near the lower plate. Similarly, when $0 \leq T_1 < 4°C$ the potentially unstable layer with temperature ranging from T_1 to 4°C is also located near the lower plate. It is noted that without maximum density effects, the case of heating from above is always stable. As $T_2 \to T_{max}$, $A \to 1$ and the whole channel becomes potentially unstable whether $T_1 \leq 4°C$ or $T_1 \geq 4°C$. This is in contrast to the classical Benard problem where the horizontal fluid layer is unstable only when heating is from below. Also as $T_1 \to T_{max}$, $A \to 0$ and the whole layer becomes potentially stable.

The typical numerical results for critical Rayleigh number and wave number are listed in Tables 1 to 5 for Pe = 1, 10, 50 and the ranges of parameters $-2.0 \leq \lambda_1 \leq -0.5$, $-1.0 \leq \gamma_2 \leq 1.4$. The special case of $\lambda_2 = 0$ corresponds to the parabolic density-temperature relationship ($\lambda_2 = 0$) for the temperature range 0-8°C and the parameter λ_1 becomes simply $\lambda_1 = (-1/A)$. The effect of Peclet number on the axial distribution of the critical Rayleigh number is shown in Fig. 2 for $\lambda_1 = -0.5$ (or $A = 2$) and $\lambda_2 = 0$ (or $\gamma_2 = 0$). The axial heat conduction is clearly seen to have a destabilizing effect near the thermal entrance ($\bar{x} = 0$) and the trend reverses before approaching the asymptotic value of $Ra^* = 2275$ corresponding to a linear basic temperature profile. The upstream temperature profile ϕ_θ, becomes practically uniform at $\bar{x} = -2$, -1 and -0.05 for Pe = 1, 10 and 50, respectively (Chapter II), and it is concluded that $Ra^* \to \infty$ there.

The instability results for Pe = 1 and λ_1 = -0.5, -1 are presented graphically in Fig. 3 for various values of λ_2. Since the upstream temperature profile is uniform at $\bar{x}$ = -2, the asymptotic value for Ra* in the upstream region is infinity. The downstream asymptotic results agree exactly with those reported in [4] and the parametric effect of λ_2 is also similar to that of Fig. 4 in [4]. The two special cases of T_2 = 0°C and T_1 = 0°C [4] are of considerable practical interest since they correspond to the cases of melting from below (heating from below) and melting from above (heating from above), respectively. The physical interpretation of the numerical results can best be provided by considering a specific example. From Table 5 of [4] for the case of melting from below (T_2 = 0) for a horizontal liquid layer, one finds that at λ_1 = -1.014 and λ_2 = -0.301 ($T_1 \approx$ 18°C), the theoretical and experimental values of Ra* are 4,021 and 4,663, respectively. The thermal instability of a horizontal liquid layer considered in [4] corresponds to the fully developed case with a linear basic temperature profile (independent of Peclet number) in the present problem. A simple linear interpolation of the asymptotic results for λ_2 = 0 and -0.5 with λ_1 = -1.0 in Table 3 gives Ra* = 4,10 -1.0 and λ_2 = -0.3. Fig. 3 also shows that th sult agrees with Ra* = 4,021 for λ_1 = - -0.301 given in [4]. Noting the parametric efi f λ_1 for a given value of λ_2 shown in Fig. 3, one sees that the trend of the present asymptotic results also agrees with the experimental and theoretical results given in Table 4 of [4] for the case of melting from above ($T_1 = 0$, heating from above). The above qualitative comparison suggests that the present instability analysis may be used in predicting the onset of longitudinal vortex rolls in a horizontal parallel-plate channel with main flow involving melting from below or above. This information is of particular interest in assessing the free convection effect on ice formation or thawing in horizontal channels.

Further instability results for Pe = 1 and $\lambda_2 = 1.4$ are shown in Fig. 4 with λ_1 as parameter. As noted earlier, positive λ_2 signifies heating from above with $0°C \leq T_1 < 4°C$. The vertical distributions of the disturbances u^*, w^* and θ^* together with the basic profiles ϕ_u and ϕ_θ are illustrated in Fig. 5 and 6 for Pe = 1, $\lambda_1 = -0.5$ and $\lambda_2 = -1.0$ at various axial positions. In the plotting, the maximum amplitude of each disturbance is taken to be 0.1.

The profiles for u^* and θ^* at $\bar{x} = 5$ are further illustrated in Fig. 7 for Pe = 1, $\lambda_1 = -0.5$ and $\lambda_2 = 0.8$, -1.0. It is seen that u^* is negative near the lower plate and positive near the upper plate. The relatively weaker disturbance u^* near the upper plate for $\lambda_2 = -1.0$ as compared with u^* for $\lambda_2 = 0.8$ is apparently related to the smaller unstable layer thickness near the lower plate which is indicated by the higher critical Rayleigh number. In contrast to the reversal of sign for u^*, the profile θ^* for

$\lambda_2 = -1.0$ is quite similar to that of $\lambda_2 = 0.8$ except that the position of maximum θ^* is located nearer to the lower plate. The information on the location of maximum θ^* is useful in the experimental determination of critical Rayleigh number by measurement of spanwise temperature distribution [7].

4.5 Concluding Remarks

1. The accuracy and convergence of the numerical solution are checked by an excellent agreement between the present downstream asymptotic results and the theoretical results for liquid layer reported in [4]. The latter theoretical results in turn are confirmed by the experimental investigation as indicated by the comparison shown in Fig. 7 of [4]. The matching of the critical Rayleigh numbers for the upstream and downstream regions at $\bar{x} = 0$ also provides a severe test for the convergence of the numerical solution and the critical Rayleigh numbers for the upstream and downstream regions are found to agree within three significant digits at $\bar{x} = 0$. The numerical results can be seen in Tables 1 to 5. Furthermore, it is found that the increase of the number of eigenvalues and series coefficients to 20 for the basic temperature solution improves only slightly the degree of the matching at $\bar{x} = 0$.

2. The results of the present thermal instability analysis show that the effect of axial heat conduction on the onset of longitudinal vortex rolls in horizontal plane

Poiseuille flow is important when Re < 5 or Pe < 50. For water with $T_1 \lessgtr T_{max} \lessgtr T_2$, the density inversion effect must be considered in thermal instability analysis [4]. The present analysis may be used in assessing the importance of free convection effect on melting and ice formation problems in horizontal parallel-plate channels by considering the case with $T_1 = 0°C$ or $T_2 = 0°C$. The free convection effect involving the density inversion is also of interest in studying the melting of ice formation problems for northern lakes or rivers.

3. Since the entrance temperature parameter θ_0, two thermal condition parameters (λ_1, λ_2) and Peclet number are involved, only sample numerical results with $\theta_0 = 1$, are presented. The numerical method is confirmed to be applicable to the ranges of parameters, $-2.0 \leq \lambda_1 \leq -0.5$ and $-1.0 \leq \lambda_2 \leq 1.4$. Outside these ranges, the unstable layer with temperature distribution in the range $T_1 < T < T_{max}$ near the lower plate becomes so thin that the buoyancy effect tends to be washed out by the forced main flow. In other words, as A decreases or the relative magnitude of $(T_1 - T_{max})$ decreases with respect to $\Delta T = T_1 - T_2$, then correspondingly the unstable layer thickness also decreases. It is also noteworthy that the parametric ranges for λ_1 and λ_2 in this study are narrower than those indicated in [4].

4. When one assumes the entrance temperature at $\bar{x} = 0$ to be uniform as in the case of classical Graetz problem [6], then the thermal boundary layer develops starting

at $\bar{x} = 0$. For the basic flow solution for temperature considered in this study, the fluid temperature is taken to be uniform at $\bar{x} = -\infty$ in order to accommodate the effect of upstream conduction and consequently the thermal boundary layer thickness is not zero at $\bar{x} = 0$. As a matter of fact, the basic temperature profiles at $\bar{x} = 0$ for Pe = 1 and 10 [10,11] show that the heat already penetrates to the upper plate and the whole cross section is potentially unstable (see Fig. 1). It is then seen that for Pe = 1 and 10, the concept of thermal boundary layer is no longer applicable. The foregoing fact accounts for the decrease of critical Rayleigh number near $\bar{x} = 0$ with the decrease of Peclet number as shown in Fig. 2. When Pe > 100 or ~~Pe → ∞, the critical Ra* becomes infinity at $\bar{x} = 0$.~~

5. The experimental instability data in the thermally developing region of a horizontal channel flow of water in the temperature range 0 ~ 30°C do not appear to be available in the literature. In view of the importance of environmental heat transfer problem (freezing or thawing) involving 4°C for water, the experimental investigation is apparently in order.

6. The potentially unstable layer with temperature ranging from T_1 to T_{max} near the lower plate may be seen more clearly by considering the fully developed region where the basic temperature profile is linear. The upper limit of the unstable layer is then given by $z = 1 - (T_{max} - T_2)/(T_1 - T_2)$. By keeping T_2 constant, one finds

that $(\partial z/\partial T_1)_{T_2} > 0$ for the case $T_{max} > T_2$ (heating from below). This means that as T_1 increases the unstable layer thickness also increases. On the other hand, by keeping T_1 constant one obtains $(\partial z/\partial T_2)_{T_1} < 0$ indicating that as T_2 increases the unstable layer z decreases when $T_1 < T_{max}$ (heating from above). Physically, positive or negative value of λ_2 signifies heating either from above or below whereas the larger value of $|\lambda_1|$ indicates the smaller unstable layer with the corresponding higher critical Rayleigh number. The above observation is useful in physical interpretation of λ_1 and λ_2 and agrees with the results shown in Tables 3, 4 and 5 of [4].

References

1. Veronis, G., "Penetrative Convection", Astrophysical J. 137, 1963, pp. 641-663.

2. Debler, W.R., "On the Analogy Between Thermal and Rotational Hydrodynamic Stability", J. Fluid Mechanics 24, 1966, pp. 165-176.

3. Tien, C., "Thermal Instability of a Horizontal Layer of Water Near 4°C", A.U.Ch.E. J. 14, 1968, pp. 652-653.

4. Sun, Z.S. and Yen, Y.C., "Thermal Instability of a Horizontal Layer of Liquid with Maximum Density", A.I.Ch.E. J. 15, 1969, pp. 910-915.

5. Sun, Z.S. and Yen, Y.C., "Onset of Convection in a Porous Medium Containing Liquid with a Density Maximum", Heat Transfer, 1970, Vol. 4, NC2-11, Elsevier Publishing Co., Amsterdam.

6. Hwang, G.J. and Cheng, K.C., "Convective Instability in the Thermal Entrance Region of a Horizontal Parallel-Plate Channel Heated from Below", J. Heat Transfer 95C, 1973, pp. 72-77.

7. Kamotani, Y. and Ostrach, S., "Effect of Thermal Instability on Thermally-Developing Laminar Channel Flow", J. Heat Transfer 97C, 1975.

8. Hsu, C.J., "An Exact Analysis of Low Peclet Number Thermal Entry Region Heat Transfer in Transversely Non-Uniform Velocity Fields", A.I.Ch.E. J. 17, 1971, pp. 732-740.

9. Hatton, A.P. and Turton, J.S., "Heat Transfer in the Thermal Entry Length with Laminar Flow Between Parallel Walls at Unequal Temperatures", Int. J. Heat Mass Transfer 5, 1962, pp. 675-679.

10. Collatiz, L., "The Numerical Treatment of Differential Equations", 3rd Ed., Springer-Verlag, 1960, p. 69.

11. Thomas, L.H., "The Stability of Plane Poiseuille Flow", Physical Review 91, 1953, pp. 780-783.

12. Dorsey, N.E., "Properties of Ordinary Water Substance", Hafner Publishing Co., New York, 1968, p. 200.

TABLE 1. Instability Results $\lambda_1 = -0.5$, $\lambda_2 = 0$ and Pe = 1, $\lambda_1 = -2$

$\lambda_1 = -0.5$, $\lambda_2 = 0$

Pe	1		10		50	
$\bar{x}$	a*	Ra*	a*	Ra*	a*	Ra*
0.001	3.081	3311.4	3.205	5575.8	5.001	77289.7
0.005	3.081	3305.3	3.200	5401.9	3.932	26780.7
0.010	3.081	3297.8	3.190	5195.9	3.702	16909.3
0.020	3.080	3283.0	3.172	4829.8	3.505	10334.8
0.040	3.080	3254.1	3.14[illegible]	4269.3	3.358	6402.5
0.060	3.078	3226.0	3.12[illegible]	3876.9	3.291	4952.7
0.080	3.078	3189.9	3.108	3592.7	3.253	4199.8
0.100	3.077	3172.5	3.101	3379.4	3.229	3743.1
0.200	3.074	3053.0	3.092	2819.8	3.172	2862.2
0.400	3.072	28[illegible].4	3.098	2482.9	3.139	2501.4
0.600	3.073	2726.3	3.106	2380.9	3.128	2395.9
0.800	3.075	2623.5	3.111	2336.2	3.122	2343.2
1.000	3.077	2546.0	3.113	2312.2	3.121	2313.8
1.250	3.082	2474.4	3.115	2295.4	3.120	2294.3
1.500	3.086	2422.7	3.116	2286.3	3.118	2284.6
1.750	3.088	2384.9	3.117	2281.2	3.118	2279.8
2.000	3.092	2357.1	3.116	2278.5	3.119	2277.4
5.000	3.112	2277.9	3.118	2275.1	3.118	2275.1

Pe = 1, $\lambda_1 = -2$

λ_2	1.4		0.8		0.2	
$\bar{x}$	a*	Ra*	a*	Ra*	a*	Ra*
-0.70	3.319	11791.0	3.436	34244.0		
-0.50	3.301	10353.0	3.336	26781.0		
-0.10	3.174	7749.1	2.960	15566.0		
-0.05	3.148	7451.1	2.892	14476.0		
-0.00	3.126	7183.1	2.829	13605.0		
+0.00	3.211	7129.1	2.996	14977.0		
0.05	3.124	6995.3	2.798	12774.0		
0.10	3.057	6621.7				
0.50	2.930	5376.1				
0.70	2.923	5079.6				
1.00	2.937	4810.3				
2.00	3.022	4496.3	2.902	7425.6		
5.00	3.111	4401.9	3.146	7343.5	3.614	15153.0
7.00	3.121	4399.0	3.175	7336.8	3.666	15060.0
10.00	3.124	4398.4	3.187	7334.2	3.685	15015.0

TABLE 2. Instability Results for Pr = 1, $\lambda_1 = -0.5$

λ_2	1.4		0.8		0.2	
$\bar{x}$	a*	Ra*	a*	Ra*	a*	Ra*
-2.00	3.132	5891.5	3.130	7290.8	3.128	9562.0
-1.00	3.172	3433.9	3.155	4147.8	3.128	5235.0
-0.70	3.187	2953.1	3.163	3538.4	3.126	4410.3
-0.50	3.194	2680.1	3.166	3195.0	3.123	3950.5
-0.10	3.191	2227.9	3.158	2635.8	3.109	3219.3
-0.05	3.188	2180.0	3.156	2577.2	3.107	3144.7
-0.00	3.186	2145.0	3.154	2522.8	3.105	3074.4
+0.00	3.230	2188.6	3.189	2566.6	3.115	3091.3
0.05	3.190	2098.4	3.155	2476.0	3.103	3010.3
0.10	3.175	2046.1	3.144	2417.7	3.098	2945.2
0.50	3.149	1805.3	3.124	2131.3	3.088	2592.2
0.70	3.144	1732.3	3.121	2043.4	3.088	2482.7
1.00	3.140	1656.6	3.120	1951.6	3.090	2367.6
2.00	3.137	1546.2	3.120	1815.8	3.100	2194.7
5.00	3.125	1502.3	3.120	1760.6	3.115	2122.8
7.00	3.120	1501.0	3.117	1759.0	3.116	2120.6
10.00	3.120	1500.9	3.117	1758.8	3.116	2120.4

λ_2	0.0		-0.5		-1.0	
$\bar{x}$	a*	Ra*	a*	Ra*	a*	Ra*
-2.00	3.126	10670.0	3.121	15020.0	3.111	25359.0
-1.00	3.116	5735.6	3.070	7532.5	2.978	10940.0
-0.70	3.109	4803.7	3.048	6175.3	2.928	8601.1
-0.50	3.103	4286.9	3.032	5436.4	2.897	7376.8
-0.10	3.087	3472.8	3.007	4307.8	2.858	5508.7
-0.05	3.084	3390.6	3.005	4197.1	2.856	5231.1
-0.00	3.081	3312.7	3.000	4090.3	2.850	5065.1
+0.00	3.081	3312.9	2.957	4012.1	2.720	4986.1
0.05	3.079	3239.9	2.993	3983.0	2.831	5084.0
0.10	3.077	3172.5	3.001	3911.1	2.861	5014.7
0.50	3.073	2790.1	3.014	3429.6	2.910	4376.2
0.70	3.073	2671.2	3.022	3280.3	2.933	4184.9
1.00	3.077	2546.0	3.034	3123.2	2.964	3985.9
2.00	3.092	2357.1	3.066	2883.3	3.033	3679.3
5.00	3.112	2277.9	3.110	2780.3	3.117	3542.8
7.00	3.112	2275.4	3.118	2777.0	3.113	3537.9
10.00	3.118	2275.2	3.123	2776.5	3.140	3537.1

TABLE 3. Instability Results for $Pe = 1$, $\lambda_1 = -1.0$

λ_2	1.4		0.8		0.2	
x	a*	Ra*	a*	Ra*	a*	Ra*
-1.00	3.189	4597.0	3.170	5973.9	3.135	8523.5
-0.70	3.202	3937.9	3.173	5052.4	3.121	7036.7
-0.50	3.207	3560.6	3.171	4529.6	3.107	6208.0
-0.10	3.188	2923.8	3.142	3664.6	3.060	4878.2
-0.05	3.182	2854.6	3.155	3573.0	3.052	4740.8
-0.00	3.178	2791.1	3.131	3487.4	3.045	4611.3
+0.00	3.247	2883.6	3.182	3572.6	3.063	4650.4
0.05	3.181	2740.7	3.131	3416.0	3.039	4494.4
0.10	3.160	2662.9	3.114	3321.6	3.029	4374.9
0.50	3.122	2325.5	3.081	2888.0	3.007	3772.8
0.70	3.116	2226.6	3.077	2760.7	3.010	3598.9
1.00	3.114	2125.7	3.079	2630.6	3.021	3422.5
2.00	3.120	1982.6	3.096	2444.5	3.061	3165.2
5.00	3.122	1927.5	3.115	2371.3	3.111	3067.6
7.00	3.120	1925.9	3.114	2369.1	3.119	3064.3
10.00	3.119	1925.8	3.118	2368.8	3.122	3063.9

λ_2	0.0		-0.5		-1.0	
$\bar{x}$	a*	Ra*	a*	Ra*	a*	Ra*
-2.00	3.155	20036.0	3.178	43921.0		
-1.00	3.115	9933.8	3.018	16887.0		
-0.70	3.092	8090.6	2.956	12848.0		
-0.50	3.072	7074.6	2.910	10757.0		
-0.10	3.016	5467.4	2.814	7681.0		
-0.05	3.007	5303.5	2.800	7383.8		
-0.00	2.998	5147.8	2.784	7096.1		
+0.00	2.998	5147.7	2.790	7105.2		
0.05	2.990	5003.1	2.760	6805.6		
0.10	2.983	4872.2	2.772	6637.7		
0.50	2.969	4183.9	2.789	5612.4		
0.70	2.976	3988.3	2.829	5347.5		
1.00	2.992	3791.1	2.877	5091.3		
2.00	3.046	3508.5	2.997	4731.4	2.941	6905.6
5.00	3.112	3394.3	3.127	4580.3	3.214	6739.6
7.00	3.122	3390.5	3.148	4574.2	3.252	6724.5
10.00	3.126	3390.0	3.156	4572.9	3.267	6719.0

TABLE 4. Instability Results for Pe = 10, λ_1 = -0.5

λ_2	1.4		0.8		0.2	
$\bar{x}$	a*	Ra*	a*	Ra*	a*	Ra*
-0.10	2.927	3877.5	3.013	5718.5	3.212	10788.0
-0.05	2.999	2713.8	3.073	3917.0	3.241	6993.4
-0.00	3.292	2165.7	3.205	2958.0	3.224	4652.9
+0.00	3.360	2273.1	3.331	3166.3	3.260	4722.5
0.05	3.253	1809.2	3.227	2373.9	3.168	3455.1
0.10	3.258	1620.2	3.222	2091.1	3.147	2933.6
0.50	3.161	1419.0	3.142	1726.8	3.114	2200.5
0.70	3.141	1444.3	3.130	1733.0	3.113	2161.9
1.00	3.128	1472.1	3.122	1745.3	3.115	2139.4
2.00	3.120	1498.2	3.118	1757.5	3.117	2122.1
5.00	3.119	1500.9	3.118	1758.8	3.118	2120.3
7.00	3.119	1500.9	3.118	1758.8	3.118	2120.3

λ_2	0.0		-0.5		-1.0	
$\bar{x}$	a*	Ra*	a*	Ra*	a*	Ra*
+0.00	3.207	5620.1	3.000	9938.3		
0.05	3.130	4056.4	2.833	6906.5		
0.10	3.101	3379.4	2.804	5298.0		
0.50	3.103	2420.0	3.060	3210.0	2.991	4680.1
0.70	3.180	2354.8	3.090	3020.6	3.074	4161.7
1.00	3.113	2312.2	3.109	2889.3	3.116	3816.2
2.00	3.116	2278.5	3.123	2786.6	3.139	3561.3
5.00	3.118	2275.1	3.124	2776.5	3.141	3537.0
7.00	3.118	2275.1	3.124	2776.5	3.141	3537.0

λ_2	1.4		0.8		0.2	
$\bar{x}$	a*	Ra*	a*	Ra*	a*	Ra*
+0.00	3.449	3383.2	3.460	5269.8	3.467	11529.0
0.05	3.271	2472.2	3.240	3671.2	3.119	6957.7
0.10	3.262	2196.8	3.218	3158.4	3.052	5498.4
0.50	3.157	1866.3	3.131	2434.5	3.087	3477.3
0.70	3.137	1883.0	3.122	2402.2	3.100	3298.8
1.00	3.125	1904.1	3.118	2384.3	3.111	3173.4
2.00	3.119	1923.8	3.116	2370.3	3.122	3073.8
5.00	3.119	1925.8	3.118	2368.8	3.123	3063.9
7.00	3.119	1925.8	3.118	2368.8	3.123	3063.8

Page 2, TABLE 4
Instability Results for Pe = 10, λ_1 = -0.5

λ_2	0.0		-0.5		-1.0	
x	a*	Ra*	a*	Ra*	a*	Ra*
+0.00	3.392	17890.0				
0.05	2.942	9601.9				
0.10	2.865	7137.1				
0.50	3.065	4042.2	2.989	6596.4	3.312	13310.1
0.70	3.092	3757.7	3.085	5650.9	3.288	9952.5
1.00	3.111	3559.4	3.130	5045.0	3.276	8037.1
2.00	3.126	3405.0	3.156	4613.1	3.271	6824.2
5.00	3.128	3389.9	3.158	4572.1	3.270	6717.7
7.00	3.128	3389.9	3.158	4572.7	3.270	6717.7

TABLE 5. Instability Results for Pe = 50, λ_1 = -0.5

λ_2	1.4		0.8		0.2	
x	a*	Ra*	a*	Ra*	a*	Ra*
+0.00						
0.05	3.255	1961.7	3.267	2714.5	3.297	4399.5
0.10	3.161	1433.4	3.174	1950.4	3.206	3045.9
0.50	3.113	1365.8	3.118	1684.8	3.127	2194.2
0.70	3.115	1425.6	3.117	1719.9	3.122	2163.7
1.00	3.117	1469.5	3.117	1743.6	3.119	2139.8
2.00	3.119	1499.1	3.118	1757.9	3.118	2121.6
5.00	3.119	1500.9	3.118	1758.8	3.118	2120.3

λ_2	0.0		-0.5		-1.0	
x	a*	Ra*	a*	Ra*	a*	Ra*
+0.00						
0.05	3.320	5542.1	3.650	15211.0		
0.10	3.229	3743.1	3.458	8498.5		
0.50	3.133	2438.2	3.162	3360.2	3.263	5259.9
0.70	3.125	2365.6	3.142	3074.8	3.192	4329.6
1.00	3.121	2313.8	3.131	2896.3	3.159	3834.9
2.00	3.119	2277.4	3.124	2783.4	3.142	3553.5
5.00	3.118	2275.1	3.124	2776.5	3.141	3537.0

λ_2	1.4		0.8		0.2	
x	a*	Ra*	a*	Ra*	a*	Ra*
+0.00						
0.05	3.260	2664.7	3.282	4273.9	3.399	10687.0
0.10	3.165	1942.2	3.189	3029.4	3.297	6805.0
0.50	3.116	1803.7	3.125	2402.3	3.151	3571.8
0.70	3.112	1862.4	3.121	2395.6	3.137	3338.4
1.00	3.117	1901.2	3.119	2383.4	3.128	3178.4
2.00	3.118	1924.4	3.116	2369.8	3.123	3070.6
5.00	3.119	1925.8	3.118	2368.8	3.123	3063.8

λ_2	0.0		-0.5		-1.0	
x	a*	Ra*	a*	Ra*	a*	Ra*
+0.00						
0.05	3.722	20578.0				
0.10	3.489	11324.0				
0.50	3.173	4246.1	3.360	7621.5		
0.70	3.150	3831.4	3.237	5929.0	3.648	10725.0
1.00	3.136	3568.1	3.185	5072.3	3.383	8087.6
2.00	3.128	3400.3	3.160	4600.1	3.276	6788.8
5.00	3.128	3389.9	3.158	4572.7	3.270	6717.7

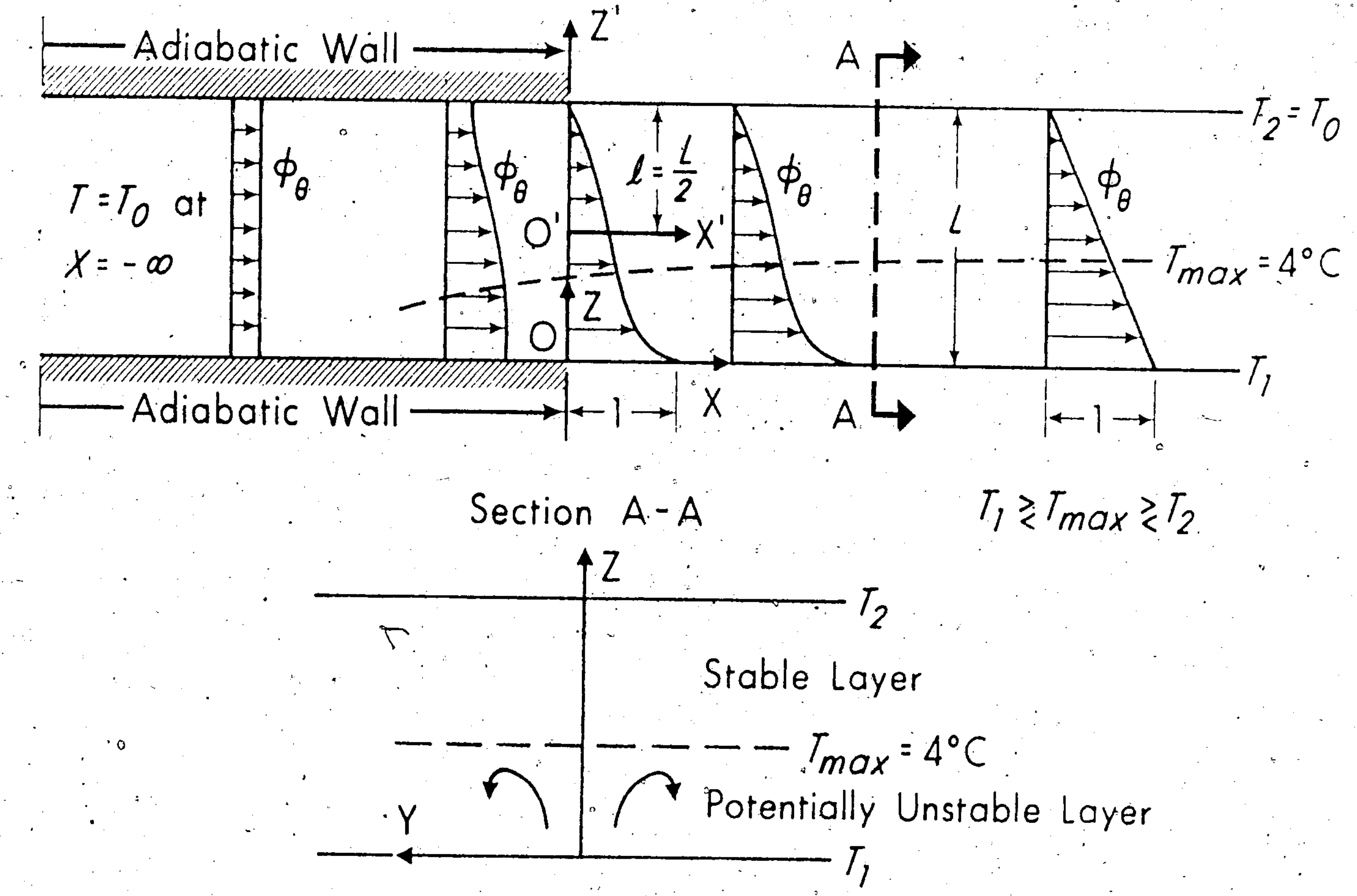

Fig. 1. Physical model and coordinate system.

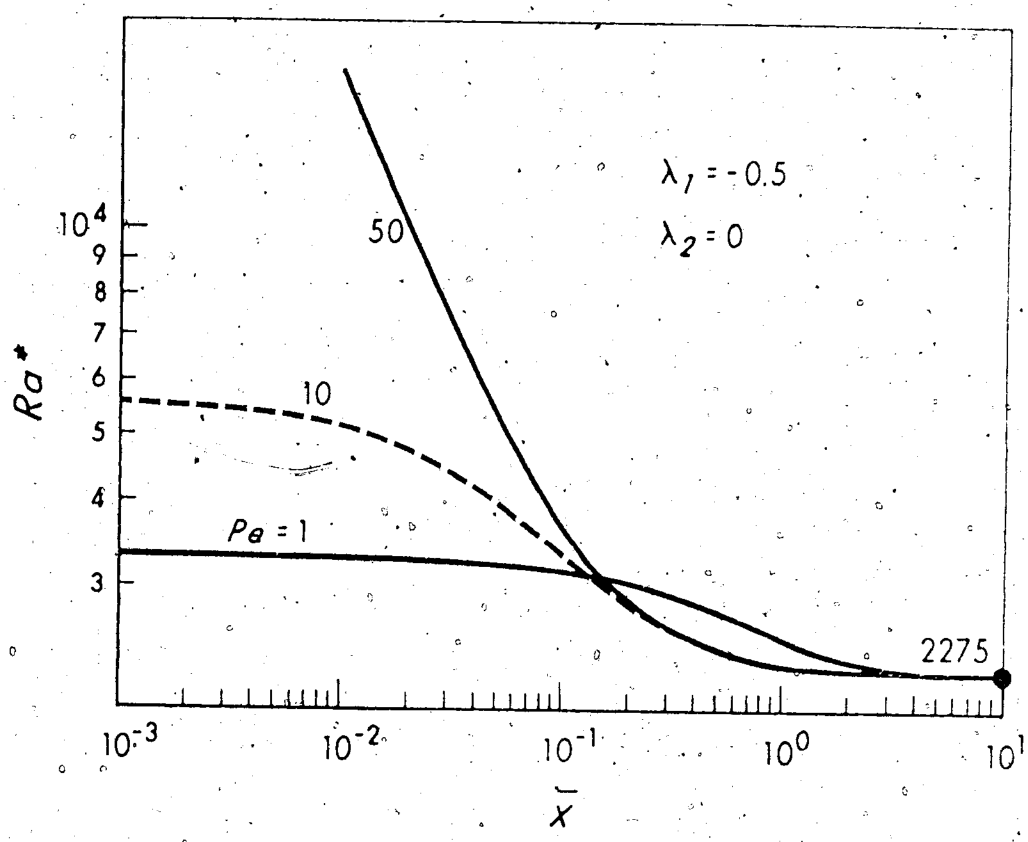

Fig. 2. Peclet number effect on relation between critical Rayleigh number and $\bar{x}$ for $\lambda_1 = -0.5$ and $\lambda_2 = 0$.

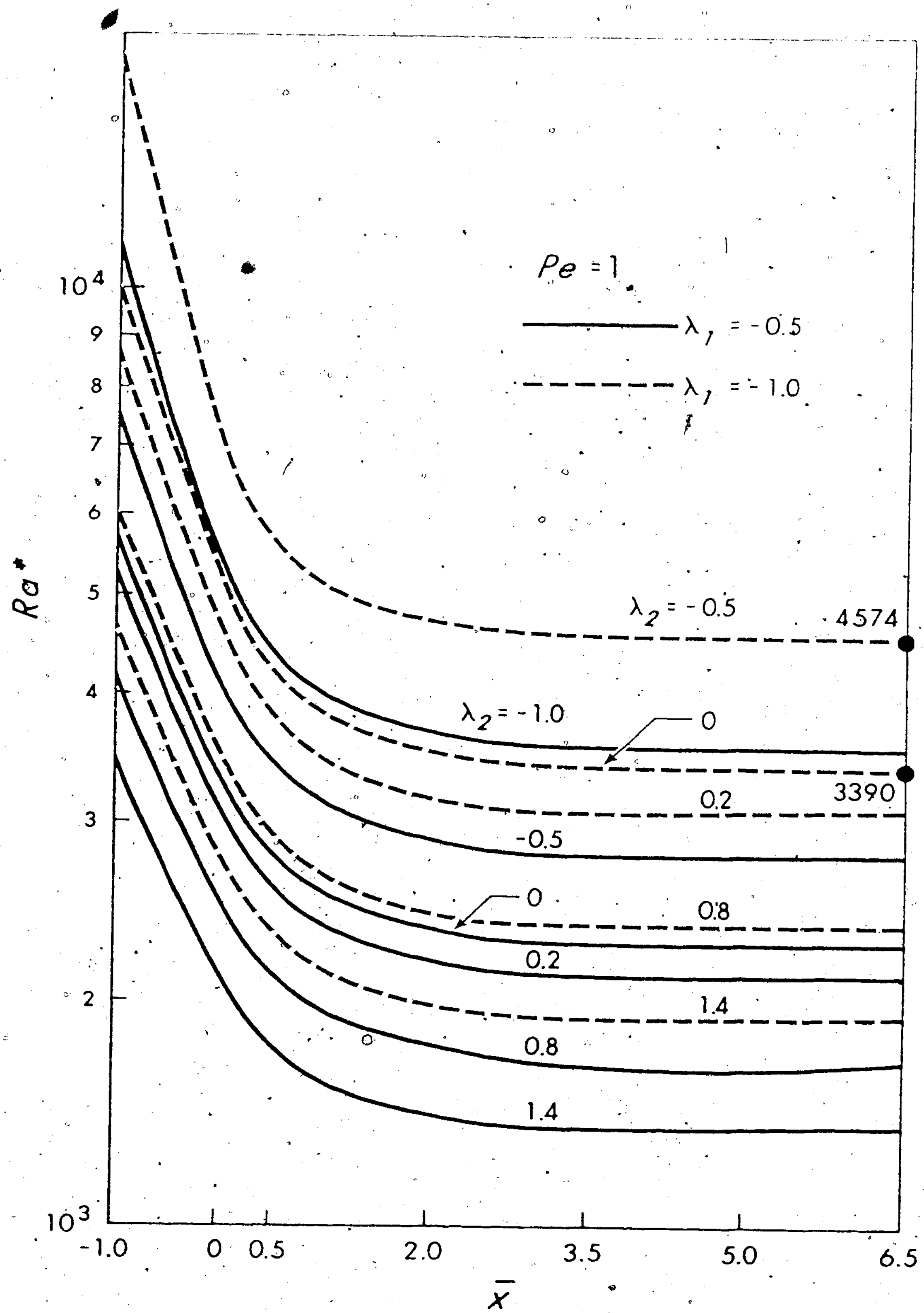

Fig. 3. Ra* vs. $\bar{x}$ with λ_2 as parameter for Pe = 1, λ_1 = -0.5, -1.

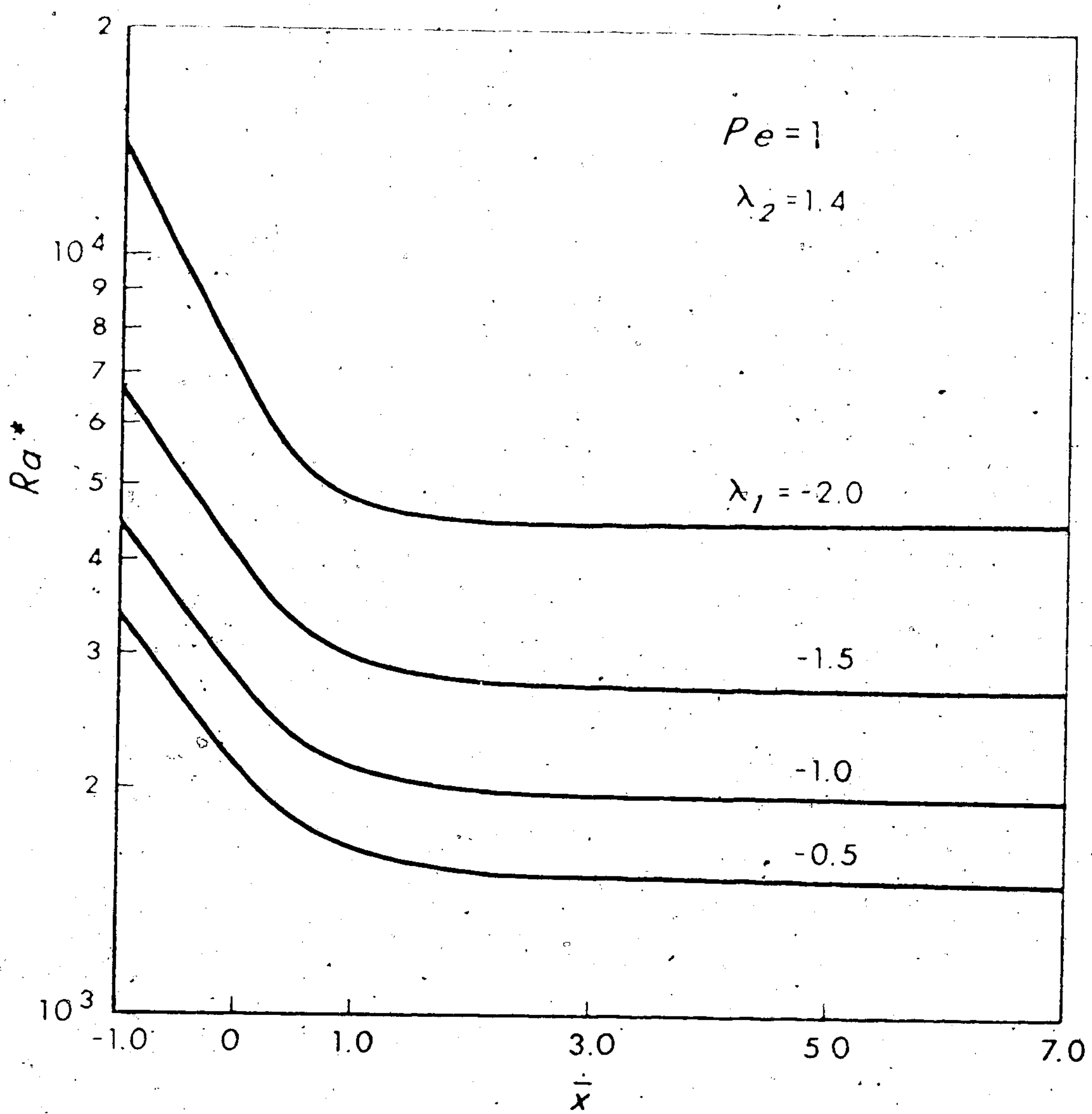

Fig. 4. Ra^* vs. $\bar{x}$ with λ_1 as parameter for $Pe = 1$, $\lambda_2 = 1.4$.

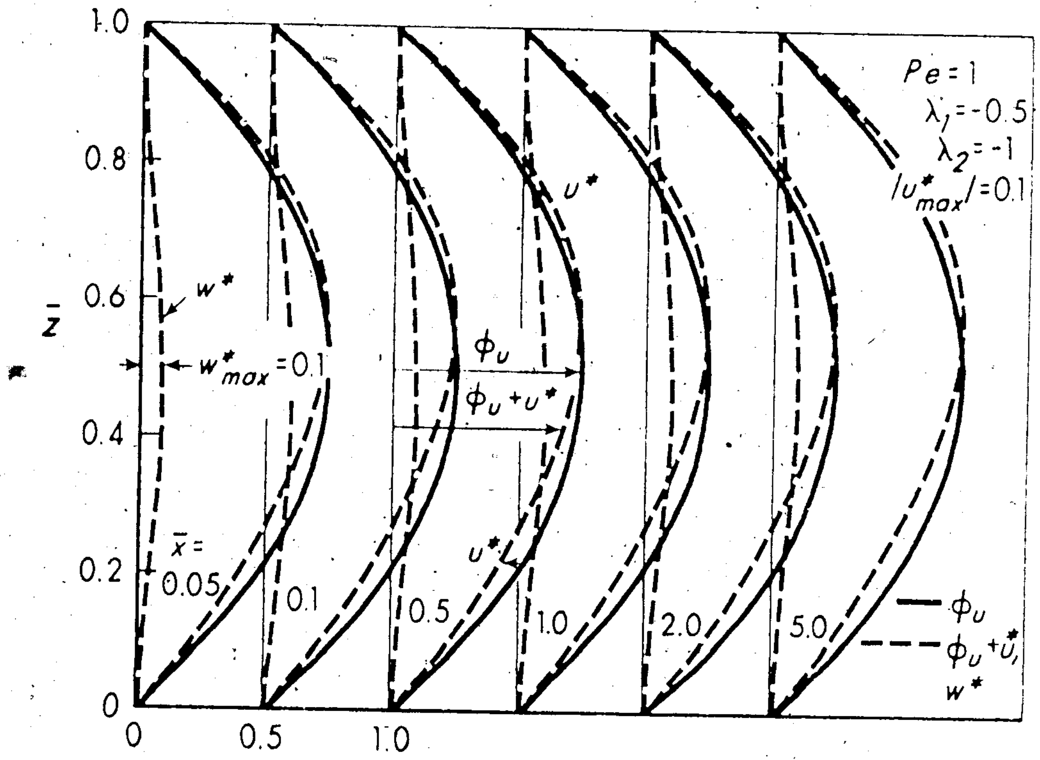

Fig. 5. Disturbance profiles for u*,w* with Pe = 1, λ_1 = -0.5, λ_2 = -1.

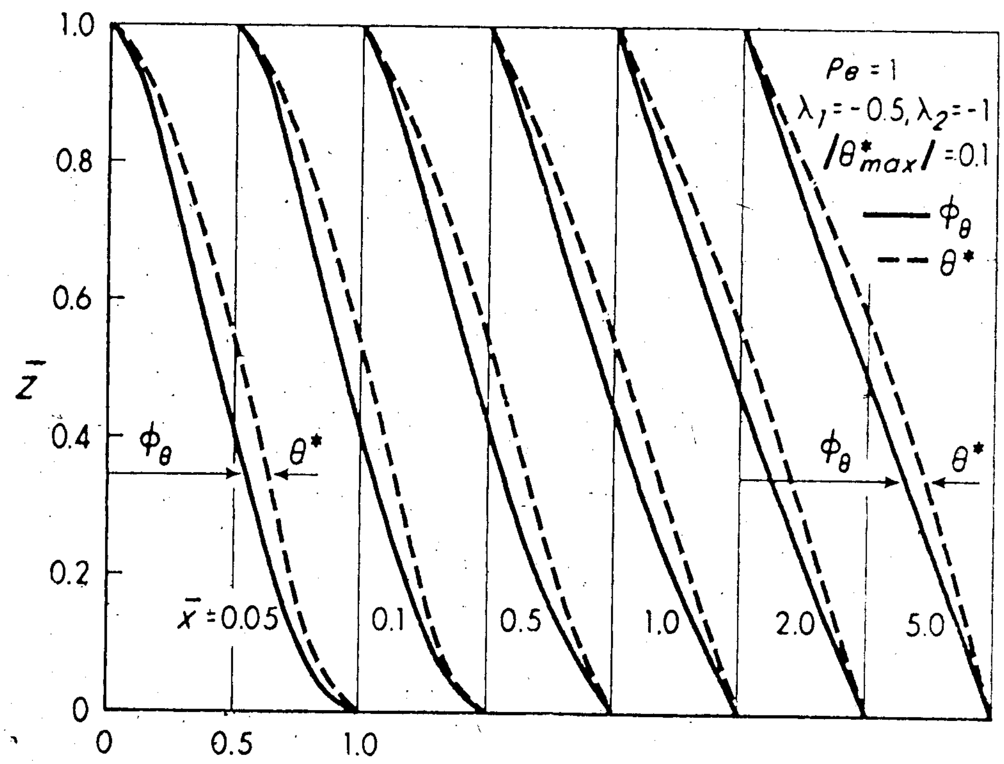

Fig. 6. Developing basic temperature profile ϕ_θ and disturbance θ^* for $Pe = 1$, $\lambda_1 = -0.5$, $\lambda_2 = -1$.

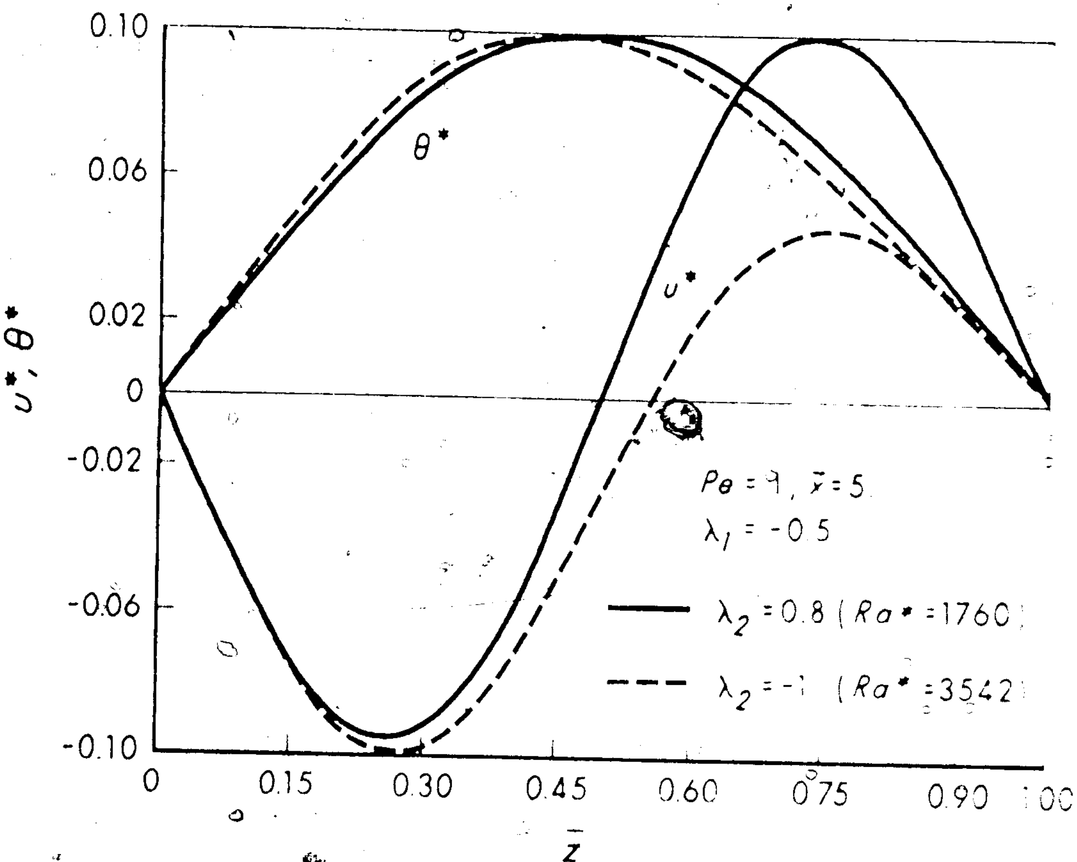

Fig. 7. Disturbance profiles for u^* and θ^* at $\bar{x} = 5$ with $P_e = 9$, $\lambda_1 = -0.5$ and $\lambda_2 = 0.8, -1.0$

CHAPTER V

VISCOUS DISSIPATION EFFECTS ON CONVECTIVE INSTABILITY AND HEAT TRANSFER IN PLANE POISEUILLE FLOW HEATED FROM BELOW

The effects of viscous dissipation on the onset of instability for longitudinal vortices in the thermal entrance region of a horizontal parallel-plate channel are studied by a numerical method for the case when the lower plate is heated isothermally and the upper one is cooled isothermally. Numerical results are obtained for Pr = 0.1, 0.7, 10 and 100. It is found that viscous heating has a destabilizing influence. The effect is significant for large Prandtl number fluid (Pr $\geq$ 10) but is insignificant for small Prandtl number fluid (Pr $\leq$ 0.7). The viscous dissipation effects on thermal entrance region heat transfer for basic flow (without secondary flow) are also studied.

Nomenclature

a	=	dimensionless wave number
Br	=	Brinkman number, $\mu U_m^2/(k\theta_c)$
C_n, D_n	=	coefficients in the series expansion of θ_e
C_n', K_n	=	coefficients defined by eq. (10)
c_p	=	specific heat at constant pressure
D	=	d/dz
Gr	=	Grashof number, $g\beta(\Delta T)L^3/\nu^2$
g	=	gravitational acceleration
h_1, h_2	=	local heat transfer coefficients at lower and upper plates
k	=	thermal conductivity
L, ℓ	=	a distance between two horizontal flat plates and $L/2$
Nu_1, Nu_2	=	local Nusselt numbers, $h_1(4\ell)/k$, $h_2(4\ell)/k$
P, P_b	=	fluid pressure $(P_b + P')$ and pressure for basic flow
Pe	=	Peclet number, $4\,U_m\ell/\alpha$ = RePr
Pr	=	Prandtl number, ν/α
p	=	dimensionless perturbation pressure, $P'/(\rho\nu^2/L^2)$

q_1, q_2 = rate of heat transfer per unit area, $-k(\partial T/\partial Z')_{Z=-\ell}$, $-k(\partial T/\partial Z')_{Z=\ell}$

Ra = Rayleigh number, $g\beta\Delta TL^3/\nu\alpha$ = PrGr

Re = Reynolds number, $4\,U_m\ell/\nu$

R_n, S_n = even and odd eigenfunctions

T, T_b, T_{bm}, T_0 = fluid temperature $(T_b + \theta')$, fluid temperature of basic flow, bulk temperature and uniform entrance temperature

T_1, T_2, T_m = constant lower and upper plate temperatures, and $(T_1 + T_2)/2$

U_b, U_m, u_b = axial and mean velocities and (U_n/U_m) of basic flow

u, v, w = dimensionless perturbation veloci[illegible]ponents, $(U', V', W')/(\nu/L)$

X, Y, Z = Cartesian coordinates with origi[illegible] lower plate

x = $x'/(3/16)Pe = \bar{x}$

x', y, z = dimensionless coordinates, $(X, Y, Z)/L$

$\bar{x}, \bar{z}$ = dimensionless coordinates with origin at center of channel, $(X/(3/8)Pe\ell, Z'/\ell = 2z - 1)$

Z' = transverse coordinate with origin at center of channel

α = thermal diffusivity

β = coefficient of thermal expansion

β_n, γ_n = even and odd eigenvalues

$\theta, \theta_b, \theta_0$ = dimensionless perturbation, basic flow and entrance temperatures, $\theta'/\Delta T$, $(T_b - T_m)/(T_2 - T_m)$, $(T_0 - T_m)/(T_2 - T_m)$

$\theta_c, \theta_e, \theta_f$ = characteristic temperature difference $(T_2 - T_m) = (T_2 - T_1)/2$, and dimensionless fluid temperatures defined by eq. (3)

θ', θ_{bm} = perturbation and dimensionless bulk temperatures

μ = fluid viscosity

ν = kinematic viscosity

ρ = fluid density

Φ_u, Φ_θ = dimensionless basic velocity and temperature profiles $(1/2)u_b = 3(z - z^2)$, $(1 - \theta_b)/2$

ΔT = $(T_1 - T_2) = -2\theta_c$

Superscripts and Subscripts

' = perturbation quantity

+ = amplitude of disturbance quantity

* = transformed perturbation variable or critical value

b = basic flow quantity in unperturbed state

f = fully developed value

α = coefficient of thermal expansion

β_n, γ_n = even and odd eigenvalues

$\theta, \theta_b, \theta_0$ = dimensionless perturbation, basic flow and entrance temperatures, $\theta'/\Delta T$, $(T_b - T_m)/(T_2 - T_m)$, $(T_0 - T_m)/(T_2 - T_m)$

$\theta_c, \theta_e, \theta_f$ = characteristic temperature difference $(T_2 - T_m) = (T_2 - T_1)/2$, and dimensionless fluid temperatures defined by eq. (3)

θ', θ_{bm} = perturbation and dimensionless bulk temperatures

μ = fluid viscosity

ν = kinematic viscosity

ρ = fluid density

ϕ_u, ϕ_θ = dimensionless basic velocity and temperature profiles $(1/2)u_b = 3(z - z^2)$, $(1 - \theta_b)/2$

ΔT = $(T_1 - T_2) = -2\theta_c$

Superscripts and Subscripts

$'$ = perturbation quantity

$+$ = amplitude of disturbance quantity

$*$ = transformed perturbation variable or critical value

b = basic flow quantity in unperturbed state

f = fully developed value

5.1 Introduction

Thermal instability of a plane Poiseuille flow in the thermal entrance region of a horizontal parallel-plate channel heated from below has been studied theoretically by Hwang and Cheng [1] and experimentally by Kamotani and Ostrach [2]. For Graetz problem (thermal entrance region problem) in pipes or channels, the effect of viscous dissipation on convective heat transfer is represented by the frictional heating parameter, Eckert or Brinkman number. When the value of the parameter is not small (say $Br > 0.01$), it is expected that the viscous dissipation will have an effect on the onset of longitudinal vortex rolls in the parallel-plate channel and on heat transfer in the subsequent post-critical regime.

Thermal instability in a horizontal fluid layer with a non-linear basic temperature profile caused by a uniform internal heat generation was studied by Sparrow, Goldstein and Jonsson [3]. It is noted that the role of the viscous dissipation term in the energy equation is qualitatively similar to that of internal heat generation term. The influence of viscous dissipation on Benard finite amplitude convection was studied by Turcotte et al. [4]. The viscous dissipation effect on Benard problem arises only if the main flow exists and apparently the problem has not been considered in the past.

The purpose of this investigation is to study the role of the viscous dissipation in thermal instability of the plane Poiseuille flow between two horizontal flat plates where the lower plate is maintained at higher temperature T_1 and the upper plate T_2 with uniform entrance temperature $T_0 = T_2$. It is known that the instability sets in as steady longitudinal vortices in the thermal entrance region when a critical temperature difference is exceeded [1,2]. Since the basic temperature profile is required in the present thermal instability analysis, the Graetz problem with viscous dissipation effects will be considered first and the heat transfer results will also be presented.

5.2 Graetz Problem with Viscous Dissipation Effects and Basic Solution

For Graetz problem (as shown in Fig. 1) with viscous heating, the energy equation and the associated boundary conditions in dimensionless form can be written as

$$\frac{2}{3} u_b \frac{\partial \theta_b}{\partial \bar{x}} = \frac{\partial^2 \theta_b}{\partial \bar{x}^2} + Br \left(\frac{du_b}{d\bar{z}}\right)^2 \qquad (1)$$

$$\theta_b(0,\bar{z}) = \theta_0, \ \theta_b(\bar{x},1) = 1, \ \theta_b(\bar{x},-1) = -1 \qquad (2)$$

where the dimensionless variables and parameters are defined Nomenclature and $u_b = (3/2)(1 - \bar{z}^2)$ for plane Poiseuille v.

Taking cognizance of the fully developed condition, the solution of eq. (1) can be written in the following form:

$$\theta_b = \theta_f(\bar{z}) + \theta_e(\bar{x},\bar{z}) \tag{3}$$

where θ_f (fully developed solution) and θ_e (difference temperature) satisfy the following two sets of equations:

$$\frac{d^2\theta_f}{d\bar{z}^2} + 9\ \mathrm{Br}\ \bar{z}^2 = 0,\quad \theta_f(1) = 1,\quad \theta_f(-1) = -1 \tag{4}$$

$$(1 - \bar{z}^2)\ \frac{\partial\theta_e}{\partial\bar{x}} = \frac{\partial^2\theta_e}{\partial\bar{z}^2}\ ,\quad \theta_e(0,\bar{z}) = \theta_0$$

$$\theta_e(\bar{x},1) = \theta_e(\bar{x},-1) = 0 \tag{5}$$

The solution for θ_f is

$$\theta_f = \bar{z} + \frac{3}{4}\ \mathrm{Br}(1 - \bar{z}^4) = \bar{z} + \mathrm{Brf}(\bar{z}) \tag{6}$$

where $f(\bar{z}) = (3/4)(1 - \bar{z}^4)$. The general solution of eq. (5) can be constructed in the form of infinite series [5] as

$$\theta_e = \sum_{n=1}^{\infty} C_n R_n(\bar{z}) \exp(-\beta_n^2 \bar{x}) + \sum_{n=1}^{\infty} D_n S_n(\bar{z}) \exp(-\gamma_n^2 \bar{x}) \tag{7}$$

where β_n, γ_n and R_n, S_n are the even and odd eigenvalues and eigenfunction, respectively, of the following Sturm-Liouville problems.

$$\frac{d^2 R_n}{d\bar{z}^2} + \beta_n^2 (1 - \bar{z}^2) R_n = 0, \quad R_n(\pm 1) = 0 \tag{8}$$

$$\frac{d^2 S_n}{d\bar{z}^2} + \gamma_n^2 (1 - \bar{z}^2) S_n = 0, \quad S_n(\pm 1) = 0 \tag{9}$$

The eigenvalues and eigenfunctions are obtained by applying the fourth-order Runge-Kutta method [6] employing two hundred equal steps. Applying the boundary condition at the channel entrance $\bar{x} = 0$ and using the orthogonality property of the Sturm-Liouville system, one obtains the following expressions for C_n and D_n.

$$C_n = C_n' + BrK_n \tag{10}$$

where $C_n' = [\theta_0 \int_0^1 (1 - \bar{z}^2) R_n(\bar{z}) d\bar{z}]/[\int_0^1 (1 - \bar{z}^2) R_n(\bar{z}) d\bar{z}]$

and $K_n = -[\int_0^1 f(\bar{z})(1 - \bar{z}^2) R_n(\bar{z}) d\bar{z}]/[\int_0^1 (1 - \bar{z}^2) R_n^2(\bar{z}) d\bar{z}]$

$$D_n = -[\int_0^1 \bar{z}(1 - \bar{z}^2) S_n(\bar{z}) d\bar{z}]/[\int_0^1 (1 - \bar{z}^2) S_n^2(\bar{z}) d\bar{z}] \tag{11}$$

Here Simpson's rule (IBM-SSP) is used for numerical integration. It is noted that when $\theta_0 = 1$, the first coefficient C_n' is identical to that of the Graetz problem and the second coefficient K_n corresponds to the viscous dissipation effect. The first eight values for C_n', K_n, D_n as well as β_n, γ_n are listed in Table 1.

Although the basic solution to be used for the thermal instability problem is of primary interest here, the local Nusselt numbers Nu_1 and Nu_2 at the lower and upper plates defined by the following equations for the case of heating from below ($T_1 > T_2$) are also of practical interest.

$$Nu_1 = \frac{h_1(4\ell)}{k} = \frac{(4\ell)}{k}\frac{q_1}{(T_1 - T_{bm})} = \frac{4}{1 + \theta_{bm}}\left(\frac{\partial\theta_b}{\partial\bar{z}}\right)_{\bar{z}=-1} \quad (12)$$

$$Nu_2 = \frac{h_2(4\ell)}{k} = \frac{(4\ell)}{k}\frac{q_2}{(T_{bm} - T_2)} = \frac{4}{1 - \theta_{bm}}\left(\frac{\partial\theta_b}{\partial\bar{z}}\right)_{\bar{z}=1} \quad (13)$$

where the bulk temperature θ_{bm} is

$$\theta_{bm} = (T_{bm} - T_m)/(T_2 - T_m) = \int_{-1}^{1} \theta_b u_b d\bar{z} / \int_{-1}^{1} u_b d\bar{z}$$

$$= (24/35)Br + (3/2)\sum_{n=1}^{\infty} C_n' \exp(-\beta_n^2\bar{x}) \int_0^1 (1-\bar{z}^2) R_n(\bar{z}) d\bar{z} \quad (14)$$

Of particular practical interest here are the following asymptotic results ($\bar{x} \to \infty$) valid far downstream from the thermal entrance. $Nu_{1f} = 4(1 + 3Br)/(1 + 24Br/35)$, $Nu_{2f} = 4(1 - 3Br)/(1 - 24Br/35)$.

$$\theta_f = \bar{z} + (3/4)Br\ (1 - \bar{z}^4), \quad \theta_{bf} = (24/35)Br \tag{15}$$

5.3 Perturbation Equations for Thermal Instability Problem

Within the thermal boundary layer, a top-heavy situation prevails and the layer occupying only partial region of the channel is potentially unstable. It is readily seen that the thermal boundary layer is more stable than the fully-developed region where the whole region is subjected to an adverse temperature gradient. At this point, it is convenient to shift the coordinate origin to the lower plate as shown in Fig. 1 for thermal instability problem. Applying the method of small disturbances (a linearization about the basic flow) and using the Boussinesq approximation, the perturbation equations in dimensionless form can be written as [1]:

$$Re(\phi_u \frac{\partial}{\partial x'} \nabla^2 w - \frac{d^2\phi_u}{dz^2} \frac{\partial w}{\partial x'}) = \nabla^2\nabla^2 w + Gr\ \nabla_1^2 \theta \tag{16}$$

$$Re(\phi_u \frac{\partial u}{\partial x'} + w \frac{d\phi_u}{dz}) = -\frac{\partial p}{\partial x'} + \nabla^2 u \tag{17}$$

$$Re\,\phi_u \frac{\partial \theta}{\partial x'} + u \frac{\partial \phi_\theta}{\partial x'} + w \frac{\partial \phi_\theta}{\partial z} = \frac{1}{Pr} \nabla^2 \theta - \frac{4Br}{Pe} \frac{d\phi_u}{dz} (\frac{\partial u}{\partial z} + \frac{\partial w}{\partial x'}) \tag{18}$$

where the dimensionless quantities and parameters are defined in Nomenclature, $\phi_u = (1/2)u_b = 3(z - z^2)$, $\phi_\theta = (1 - \theta_b)/2$, $\nabla_1^2 = \partial^2/\partial x'^2 + \partial^2/\partial y^2$, and $\nabla^2 = \partial^2/\partial x'^2 + \partial^2/\partial y^2 + \partial^2/\partial z^2$. It is noted that the terms involving Br on the right-hand side of perturbation eq. (18) represent the viscous dissipation effect.

At the state of neutral stability, one may assume that the perturbations θ, w, and u have the form, $f = f^+(z)e^{iaj}$, for instability in the form of longitudinal vortices (the type of Taylor-Görtler vortices) [1]. The set of perturbation equations then becomes:

$$(D^2 - a^2)^2 W^+ = a^2 Gr\theta^+ \tag{19}$$

$$(D^2 - a^2)u^+ = Re \frac{d\phi_u}{dz} w^+ \tag{20}$$

$$(D^2 - a^2)\theta^+ = Pr(u^+ \frac{\partial\phi_\theta}{\partial x'} + w^+ \frac{\partial\phi_\theta}{\partial z}) + \frac{4Br}{Re} \frac{d\phi_u}{dz} Du^+ \tag{21}$$

where $D = d/dz$. In view of the dimensionless basic flow variables, it is convenient to introduce the transformations, $w^+ = w^*$, $\theta^+ = Pr\theta^*$, $u^+ = Reu^*$, $x' = (3/16)Pex$ and one finally obtains,

$$(D^2 - a^2)^2 w^* = a^2 Ra\theta^*$$

$$(D^2 - a^2)u^* = \frac{du}{dz} w^* \tag{23}$$

$$(D^2 - a^2)\theta^* = \frac{3}{16Pr} \frac{\partial \theta_u}{\partial x} u^* + \frac{\partial \theta_u}{\partial z} w^* + \frac{4Br}{Pr} \frac{du}{dz} Du^* \tag{24}$$

$$w^* = Dw^* = u^* = \theta^* = 0 \quad \text{at } z = 0 \text{ and } 1 \tag{25}$$

For given values of Br and Pr, one is interested in determining the critical Rayleigh number and the corresponding wave number for the onset of instability through the solution of the set of eq. (22) to (25). The method of solution for the eigenvalue problem used in [1] may be applied to the present problem and the details of the numerical solution will be omitted.

5.4 Results and Discussion

5.4.1 Heat Transfer Results for Graetz Problem

The numerical results are obtained for $\theta_0 = 1$ corresponding to the ease with the entrance temperature T_0 being equal to the upper plate temperature T_2. The developing temperature profiles are shown in Fig. 1 and 2 for Br = 0 and -2.5, respectively. The Brinkman number effect or temperature profiles at x = 0.06, 0.2 and 2 is shown in Fig. 3 to 5 where the local bulging of the profile near the upper and lower plates is apparently caused by viscous heating. At x = 2, the temperature profiles become fully established. In interpreting the result, it is well to note that in practice the Eckert number ($Ec = Br/Pr$) can be of order one. Consequently, $Br = 100$, for example, is practicable only if Prandtl number is of order 10^2. An inspection of the developing temperature profiles readily identifies the region of the channel cross-section where the top-heavy situation exists. The axial distributions of the bulk mean temperature θ_{bm} and the local Nusselt numbers Nu_1, Nu_2 are shown in Fig. 6 and 7, respectively. Fig. 7 shows that as the magnitude of Br increases, the value of Nu_1 decreases and that of Nu_2 increases. The change of sign for Nu_1 is related to the reversal of heat transfer direction. Equation (12) shows that as $\theta_{bm} \to -1$, $Nu_1 \to \pm\infty$ depending on the sign of $(\partial\theta_b/\partial z)_{z=-1}$. Apparently, the singularity for Nu_1 has no particular physical significance. In Fig. 7, the effects of Brinkman number on the asymptotic results are of special interest.

5.4.2 Instability Results

The influence of viscous dissipation on the onset of longitudinal vortices in the thermal entrance region of plane Poiseuille flow between two horizontal plates with heating from below is of principal interest in this study. The instability results are shown in Fig. 8 and 9 for $Pr = 0.1$, 0.7, 10 and 10^2, respectively. As noted in [1], with $Pr = 0.1$ the flow is more unstable in the thermal entrance region than in the fully-developed region. The viscous heating is clearly seen to be a destabilizing effect but it depends also on Prandtl number. With $Pr = 0.1$, $Br = -0.1$ and $Pr = 0.7$, $Br = -1$, the viscous heating effect on critical Rayleigh numbers in the thermal boundary layer appears to be negligible practically. For $Pr = 10$ and 10^2, a local maximum for Ra* appears at $x \approx 0.4$ before approaching the asymptotic value when the magnitude of Br exceeds a certain value. Since this phenomenon does not occur for the case without viscous dissipation effects [1], one may attribute the cause to the combined effect of the forcing terms on the right-hand side of the disturbance eq. (24). In this connection, one should note that the developing basic temperature profiles θ_0 depend on Br only. The reason for the local stabilization near $x = 0.4$ is not immediately clear and remains to be clarified.

At $Br = -1$, the effect of Prandtl number on Ra* in the entry region is shown in Fig. 10 where the critical Rayleigh number is seen to be a monotonically decreasing function of x. One also observes that Prandtl number has a stabilizing effect but the effect diminishes as fully-developed condition is approached. It is found that for fully-developed flow the ratio of the term $(\partial\theta_0/\partial z)w^*$ over the term $4(d\theta_u/\partial z)Du^*$ on the right-hand side of eq. (24) is of order 10^2 for $Br = -1$. Thus, the critical Rayleigh numbers for $Pr = 0.7$ and 100 differ very little at $Br = -1$ as $x \to \infty$.

For thermally fully-developed Poiseuille flow, a qualitative comparison between the present thermal instability problem and that of a horizontal fluid layer with uniform heat sources [3] is possible. For fully developed flow, one obtains $\partial\phi_0/\partial x = 0$. Furthermore, without viscous dissipation ($Br = 0$) the perturbation eq. (23) is not required and the resulting set of equations becomes:

$$(D^2 - a^2)^2 w^* = a^2 Ra\,\theta^*, \quad (D^2 - a^2)\theta^* = (\partial\phi_0/\partial z) w^* \qquad (26)$$

The above set of perturbation equations is apparently equivalent to that of [3] or the classical Benard problem and the critical Rayleigh number is known to be 1708. For a horizontal fluid layer with uniform heat sources, the basic temperature profile can be written as [3]

$$\phi_0 = (T - T_2)/(T_1 - T_2) = (1 - z) + N_s(z - z^2) \qquad (27)$$

where the heat source parameter N_s is defined in [3]. On the other hand, the fully-developed temperature profile ϕ_0 for the present problem is given by

$$\phi_0 = (1 - \theta_f)/2 = (1 - z) + (-3Br)(z - 3z^2 + 4z^3 - 2z^4) \qquad (28)$$

Based on eq. (27) and (28) for basic temperature profiles, one may conclude that the heat source parameter N_s [3] is equivalent to the viscous dissipation parameter (-3Br). It is noted that the basic temperature profiles shown in Fig. 5 are somewhat similar to those shown in Fig. 2 of [3]. The instability results for the fully-developed flow are shown in Fig. 11 where the curve for $T_1 > T_2$, $N_s > 0$ shown in Fig. 3 of [3] is also displayed for comparison. In Fig. 11, one sees that with viscous dissipation effect, the fully-developed critical Rayleigh number depends on Prandtl number. For a given Pr, one can clearly identify the range of (-3Br) where Ra* is practically equal to that of the linear temperature case (Ra* = 1708). As (-3Br) increases, Ra* decreases, at first slowly and later rather rapidly. In this respect, the present instability results are qualitatively similar to the critical Rayleigh number behavior for a horizontal fluid layer with heat sources [3]. Fig. 11 also shows the difference between the two instability problems.

The viscous dissipation effects on fully developed neutral stability curves are shown in Fig. 12 for Pr = 100 and x = 5. The viscous heating is clearly seen to be a destabilizing influence. Within the range of present investigation, the fully-developed instability results for Pr = 0.7 and 10 do not differ appreciably from that of Pr = 100.

5.5 Concluding Remarks

1. The viscous dissipative heating is an inherent

irreversible process and it is desirable to establish the range of parametric values for Brinkman number or Eckert number where the viscous heating is significant in forced convective flows. In this investigation, the viscous dissipation effects on Graetz problem [5] and on thermal instability problem [1] in the thermal entrance region of plane Poiseuille flow between two horizontal flat plates with heating from below are studied.

2. It is found that the destabilizing effect of viscous dissipation is significant for large Prandtl number fluid (say $Pr \geq 10$) but the effect is insignificant for small Prandtl number fluid (say $Pr \leq 0.7$).

3. The present instability results for the limiting case of $Br = 0$ agree with those of [1] for $Pe \to \infty$. For fully-developed flow, the destabilizing effect of viscous heating is found to be similar to that of internal heat generation in a horizontal fluid layer discussed in [3].

4. It is observed that the combined effect of Prandtl and Brinkman numbers in the perturbation eq. (24) may lead to a locally stabilizing effect resulting in a local maximum for Ra^* before reaching the fully-developed region.

5. In this study, the viscous dissipation effect in the perturbation eq. (24) is represented by the Eckert number ($Ec = Br/Pr$). In this connection, it may be of some interest to point out the relationship between the Eckert number and the viscous dissipation parameter, $Di = g\beta L/c_p$, appearing in Benard finite amplitude convection problem [4].

Interpreting $g\beta(T_1 - T_2)L$ as (characteristic velocity)^2 and the characteristic temperature difference as $(T_1 - T_2)$, it is seen that the parameter $Di = g\beta L/c_p$ in [4] is equivalent to the Eckert number for the present problem.

6. The present analysis is based on constant physical property assumption and the variable property effect is not considered. The complete numerical results are listed in Table 2 to 4.

7. With viscous dissipation effects, the entrance condition of uniform fluid temperature at $x = 0$ must be regarded as an approximate one.

References

1. Hwang, G.J. and Cheng, K.C., "Convective Instability in the Thermal Entrance Region of a Horizontal Parallel-Plate Channel Heated from Below", J. Heat Transfer, Vol. 95C, 1973, pp. 72-77.

2. Kamotani, Y. and Ostrach, J., "Effect of Thermal Instability on Thermally-Developing Laminar Channel Flow", J. Heat Transfer, Vol. 97C, 1975.

3. Sparrow, E.M., Goldstein, R.J. and Jonsson, V.K., "Thermal Instability in a Horizontal Fluid Layer: Effect of Boundary Conditions and Non-Linear Temperature Profile", J. Fluid Mechanics 18, 1964, pp. 513-528.

4. Turcotte, D.L., Hsui, A.T., Torrance, K.E. and Schubert, G., "Influence of Viscous Dissipation on Bernard Convection", J. Fluid Mechanics 64, 1974, pp. 369-374.

5. Hatton, A.P. and Turton, J.S., "Heat Transfer in the Thermal Entry Length with Laminar Flow Between Parallel Walls at Unequal Temperatures", Int. J. Heat Mass Transfer, Vol. 5, pp. 673-679.

6. Collatz, L., "The Numerical Treatment of Differential Equations", 3rd Ed., Springer-Verlag, Berlin, 1960, p. 69.

TABLE [illegible]. Values of eigenvalues [illegible], [illegible] and coefficients C_n', D_n, K_n for [illegible]$_0$ = 1

[illegible]$_n$:	1.6816948	5.6698570	9.6682425	13.6676617	
	17.6673737	21.6672058	25.6670990	29.6670227	(n=8)
[illegible]$_n$:	3.6722898	7.6688089	11.6679001	15.6674995	
	19.6672974	23.6671753	27.6671143	31.6670990	(n=8)
C_n':	1.2008305	-0.2991608	0.1608264	-0.1074367	
	0.0796462	-0.0627759	0.0515197	-0.0435115	(n=8)
D_n:	-1.8453674	1.6217909	-1.5101128	1.4369555	
	-1.3831587	1.3409348	-1.3063698	1.2772303	(n=8)
K_n:	-0.8623510	0.1431560	-0.0436764	0.0195555	
	-0.0106126	0.0065595	-0.0043674	0.0030796	(n=8)

Table 2 Nusselt Numbers for [illegible]$_0$ = 1.

Br	0		-1	
x	Nu_0	Nu_1	Nu_0	Nu_1
0.001	0.0[illegible]	24.5[illegible]56	166.4780	23.1753
0.002	0.0[illegible]	20.9088	111.5080	19.2906
0.004	0.[illegible]	16.9627	78.7729	15.0178
0.006	0.[illegible]	14.8723	65.2821	12.7020
0.008	0.[illegible]	13.5434	57.1376	11.1994
0.010	0.0	12.6002	51.4688	10.1134
0.020	0.0000	10.1089	35.9094	7.1280
0.040	0.0001	8.1860	26.1340	4.6123
0.060	0.0019	7.2854	21.2291	3.2935
0.080	0.0194	6.7368	18.2909	2.3947
0.100	0.0753	6.3603	16.3196	1.6981
0.200	2.9293	5.4457	12.0999	-0.7764
0.400	2.5612	4.8224	10.3455	-5.0919
0.600	3.2928	4.5077	9.8925	-9.7117
0.800	3.6294	4.3067	9.7002	-14.1926
1.000	3.7985	4.1809	9.6048	-17.9511
1.250	3.9034	4.0916	9.5458	-21.2721
1.500	3.9530	4.0458	9.5179	-23.2504
1.750	3.9772	4.0227	9.5044	-24.3294
2.000	3.9887	4.0112	9.4979	-24.8900

Br	-2.5		-5.	
0.001	297.1699	21.0950	420.2700	17.6013
0.002	202.5400	16.8414	281.9819	12.6997
0.004	141.2860	12.0501	192.3380	6.9649
0.006	115.0470	9.3647	154.2560	3.5731
0.008	99.3586	7.5681	131.8300	1.1876
0.010	88.5954	6.2328	116.6412	-0.6692
0.020	61.7052	2.3138	79.5096	-6.7762
0.040	42.6218	-1.5463	53.9719	-14.6832
0.060	34.2023	-4.0389	42.9520	-21.9215
0.080	29.2359	-6.1152	36.5251	-30.3302
0.100	25.9148	-8.0725	32.2496	-41.5230
0.200	18.4768	-20.1360	22.6006	693.9939
0.400	14.7014	-185.1720	17.4851	42.4115
0.600	13.5616	90.7047	15.8974	30.2077
0.800	13.0657	53.4172	15.2047	26.4461
1.000	12.8190	44.1042	14.8631	24.8171
1.250	12.6665	39.7468	14.6472	23.8788
1.500	12.5945	37.9589	14.5467	23.4527
1.750	12.5597	37.1485	14.4982	23.2505
2.000	12.5427	36.7644	14.4745	23.1529

Table [illegible] Continued

Br	-10		-[illegible]0	
x	Nu_0	Nu_1	Nu_0	Nu_1
0.001	536.4390	10.5125	624.7830	-4.0849
0.002	351.9221	4.1845	402.1240	-13.8356
0.004	234.8160	-3.7612	263.9850	-27.7416
0.006	185.9470	-8.9545	207.2350	-38.5941
0.008	157.5790	-12.9649	174.6340	-48.4949
0.010	138.5750	-16.3708	152.9560	-58.3441
0.020	92.9141	-30.3886	101.4680	-124.5270
0.040	62.2618	-62.1608	67.4417	1858.3601
0.060	49.2518	-131.5070	53.1499	165.7200
0.080	41.7279	-633.1960	44.9283	96.4625
0.100	35.7446	307.8250	39.4984	71.2200
0.200	25.4861	51.4787	27.2376	36.8338
0.400	19.4176	28.3314	20.5846	24.6231
0.600	17.5150	23.5317	18.4902	21.3449
0.800	16.6842	21.6764	17.5756	19.9873
1.000	16.2713	20.8022	17.1211	19.3287
1.250	16.0161	20.2773	16.8403	18.9271
1.500	15.8957	20.0134	16.7079	18.7392
1.750	15.8376	19.9165	16.6439	18.6484
2.000	15.8092	19.8597	16.6126	18.6043

Br	-50		-100	
0.001	694.2361	-51.5512	721.1160	-145.4910
0.002	439.9209	-77.3727	454.1741	-230.8180
0.004	285.2581	-129.2640	293.1321	-584.7881
0.006	222.5240	-195.9370	228.1340	-11048.6992
0.008	186.7650	-303.3000	191.1910	872.0259
0.010	163.1140	-530.1699	166.8060	458.6350
0.020	107.4000	351.1980	109.5350	166.7290
0.040	70.9848	114.6370	72.2500	89.1893
0.060	55.7996	76.6249	56.7426	65.6792
0.080	47.0955	60.0140	47.8651	53.6621
0.100	41.3586	50.4553	42.0185	46.2037
0.200	28.4137	31.8026	28.8296	30.4659
0.400	21.3657	22.9111	21.6413	22.4043
0.600	19.1423	20.2586	19.3722	19.9269
0.800	18.1713	19.1228	18.3814	18.8554
1.000	17.6889	18.5637	17.8891	18.3255
1.250	17.3910	18.2000	17.5851	17.9990
1.500	17.2504	18.0583	17.4416	17.8452
1.750	17.1825	17.9807	17.3724	17.7710
2.000	17.1494	17.9423	17.3386	17.7348

Table 3 Instability Results for Pr = 0.7 and 10

Pr = 0.7

Br	[illegible]		-1		0		1	
[illegible]	a*	Ra*	a*	Ra*	a*	Ra*	a*	Ra*
0.001	2.972	3984.2	3.053	4115.9	3.334	31335.9	3.460	32208.[illegible]
0.002	[illegible]	3802.5	3.078	3907.6	3.448	22157.5	3.572	2077[illegible]
0.004	3.029	3544.6	3.113	3614.2	3.506	14549.7	3.624	1336[illegible]
0.006	3.052	3359.0	3.139	3405.2	3.504	11159.1	3.619	[illegible]
0.008	3.069	3213.2	3.157	3242.7	3.489	9208.3	3.601	835[illegible].5
0.010	3.083	3093.1	3.172	3110.1	3.473	7928.6	3.582	7178.4
0.020	3.122	2694.0	3.120	2681.1	3.387	5021.2	3.495	4558.[illegible]
0.040	3.142	2295.4	3.226	2275.8	3.292	3296.3	3.385	3046.4
0.060	3.153	2087.1	3.219	2076.4	3.242	2657.8	3.318	2499.3
0.080	3.153	1959.7	3.207	1959.1	3.211	2327.5	3.272	2219.6
0.100	3.152	1875.7	3.196	1883.8	3.190	2130.0	3.239	2053.5
0.200	3.142	1715.7	3.151	1744.9	3.147	1782.9	3.162	1763.0
0.400	3.127	1692.6	3.117	1713.1	3.126	1703.6	3.124	1707.3
0.600	3.121	1701.6	3.110	1697.5	3.120	1704.6	3.118	1708.0
0.800	3.118	1705.7	3.112	1681.7	3.118	1706.6	3.117	1706.3
1.000	3.118	1707.1	3.114	1670.1	3.118	1707.4	3.118	1703.7
1.250	3.117	1707.6	3.116	1661.5	3.117	1707.7	3.120	1701.3
1.500	3.117	1707.7	3.118	1656.9	3.117	1707.7	3.121	1699.9
1.750	3.117	1707.8	3.118	1654.6	3.117	1707.8	3.123	1699.1
2.000	3.117	1707.8	3.118	1653.5	3.117	1707.8	3.123	1698.8

Pr = 10

Br	-2.[illegible]		-5.[illegible]		-10		-20	
0.001	3.864	28482.0	3.982	25763.0	4.400	21217.0	4.772	15416.0
0.002	3.786	18878.0	3.973	16222.0	4.232	12484.0	4.402	8444.7
0.004	3.769	11806.[illegible]	3.935	9786.6	4.102	7207.5	4.202	4678.9
0.006	3.752	8875.6	3.899	7250.0	4.042	5247.1	4.102	335[illegible].7
0.008	3.731	7251.7	3.868	5878.2	3.902	4218.8	4.002	2673.7
0.010	3.712	6212.9	3.844	5014.2	3.902	3577.8	4.002	2256.[illegible]
0.020	3.622	3944.8	3.758	3173.3	3.802	225[illegible].6	3.902	1439.5
0.040	3.506	2687.9	3.652	2202.6	3.792	1586.1	3.802	1035.[illegible]
0.060	3.428	2255.2	3.576	1896.2	3.732	1402.1	3.802	905.7
0.080	3.368	2043.8	3.510	1764.8	3.691	1344.8	3.802	889.7
0.100	3.321	1923.2	3.450	1702.4	3.639	1339.1	3.702	911.8
0.200	3.190	1732.0	3.249	1668.7	3.330	1520.3	3.620	12[illegible].8
0.400	3.122	1710.8	3.123	1710.9	3.135	1690.7	3.193	1583.0
0.600	3.120	1702.[illegible]	3.142	1664.6	3.227	1518.2	3.410	1179.[illegible]
0.800	3.13[illegible]	1686.3	3.177	1629.8	3.312	1382.7	3.516	990.3
1.000	3.142	1673.[illegible]	3.202	1572.1	3.361	1306.7	3.552	903.7
1.250	3.142	1663.1	3.222	1545.1	3.389	1258.0	3.582	853.0
1.500	3.15[illegible]	1657.7	3.230	1531.4	3.402	1234.6	3.592	829.9
1.750	3.152	1654.9	3.236	1524.5	3.410	1223.3	3.592	816.5
2.000	3.152	1653.5	3.238	1521.1	3.413	1217.8	3.602	8[illegible]3.5

Table 8 Instability Results for [illegible]

	[illegible]		-1		[illegible]		[illegible]	
	k^*	Ra^*	k^*	Ra^*	k^*	Ra^*	k^*	Ra^*
0.001	4.[illegible]	[illegible]798.7	4.026	50694.0	4.083	43981[illegible]	4.125	[illegible]
0.002	3.9[illegible]1	131983.9	3.942	28588.0	4.000	24487.0	4.048	19621.[illegible]
0.004	3.749	18152.5	3.833	16127.0	3.902	13694.0	3.966	10853.0
0.006	3.6[illegible]2	13120.1	3.761	11641.0	3.844	9854.3	3.914	7775.8
0.008	3.611	10474.5	3.708	9295.0	3.792	7862.0	3.872	6191.7
0.010	3.565	[illegible]927.6	3.666	7842.5	3.762	6634.3	3.842	5221.5
0.020	3.429	5326.0	3.533	4778.9	3.644	4074.4	3.750	3223.[illegible]
0.040	3.30[illegible]	3395.4	3.401	3117.3	3.516	2723.6	3.644	2205.3
0.060	3.252	2707.4	3.326	2534.4	3.433	2269.4	3.566	1889.6
0.080	3.215	2357.1	3.277	2239.8	3.370	2049.3	3.500	1752.4
0.100	3.193	2149.5	3.242	2066.0	3.321	1924.2	3.442	1687.5
0.200	3.148	1785.4	3.163	1764.6	3.190	1726.8	3.245	1653.7
0.400	3.126	1703.3	3.124	1706.4	3.123	1708.6	3.123	1709.5
0.600	3.12[illegible]	1704.8	3.118	1707.9	3.120	1704.9	3.141	1680.1
0.800	3.118	1706.7	3.118	1706.8	3.130	1692.4	3.177	1633.7
1.000	3.119	1707.7	3.120	1704.8	3.138	1681.3	3.203	1599.6
1.250	3.117	1707.7	3.121	1702.7	3.146	1672.4	3.222	1574.6
1.500	3.117	1707.7	3.122	1701.6	3.149	1667.6	3.233	1561.7
1.750	3.117	1707.8	3.123	1701.0	3.151	1665.1	3.237	1555.[illegible]
2.000	3.117	1707.8	3.123	1700.6	3.152	1663.9	3.240	1552.[illegible]

[illegible]	-10		-20		-50		-100	
0.001	4.[illegible]	[illegible]5900.0	4.102	16576.0	4.200	7888.7	4.102	4239.5
0.002	4.[illegible]2	13944.0	4.002	8784.6	4.102	4119.3	4.002	2204.8
0.004	3.[illegible]	76[illegible]9.2	3.902	4748.8	4.002	2218.6	4.002	1174.7
0.006	3.[illegible]	5426.7	3.902	3365.9	3.900	1569.1	3.902	829.6
0.008	3.[illegible]	43[illegible]4.6	3.902	2665.3	3.902	1239.7	3.902	654.9
0.010	3.8[illegible]2	3632.2	3.902	2241.2	3.902	1041.2	3.902	549.7
0.020	3.[illegible]	2249.4	3.802	1386.9	3.902	644.3	3.902	34[illegible].1
0.040	3.[illegible]	1568.5	3.802	982.7	3.802	461.2	3.90[illegible]	244.[illegible]
0.060	3.7[illegible]2	1374.4	3.722	883.4	3.822	420.3	3.802	224.[illegible]
0.080	3.[illegible]2	1319.3	3.702	864.5	3.802	419.2	3.802	225.1
0.100	3.[illegible]	13[illegible]0.5	3.702	881.3	3.802	436.6	3.802	236.4
0.200	3.3[illegible]	1478.5	3.550	1168.6	3.702	670.8	3.802	390.4
0.400	3.[illegible]3	1701.2	3.190	1647.0	3.565	1320.5	4.197	854.3
0.600	3.229	1572.0	3.461	1276.4	3.702	719.7	3.902	400.8
0.800	3.32[illegible]	1442.0	3.587	1066.7	3.822	551.7	3.902	300.[illegible]
1.000	3.382	1365.4	3.632	969.7	3.802	486.6	3.902	282.2
1.250	3.414	[illegible]	3.662	913.0	3.802	450.9	3.902	241.8
1.500	3.432	1291.1	3.672	887.1	3.802	435.1	3.902	232.8
1.750	3.437	1279.3	3.672	874.5	3.802	427.7	3.902	228.6
2.000	3.441	1233.5	3.682	868.9	3.802	424.2	3.902	226.6

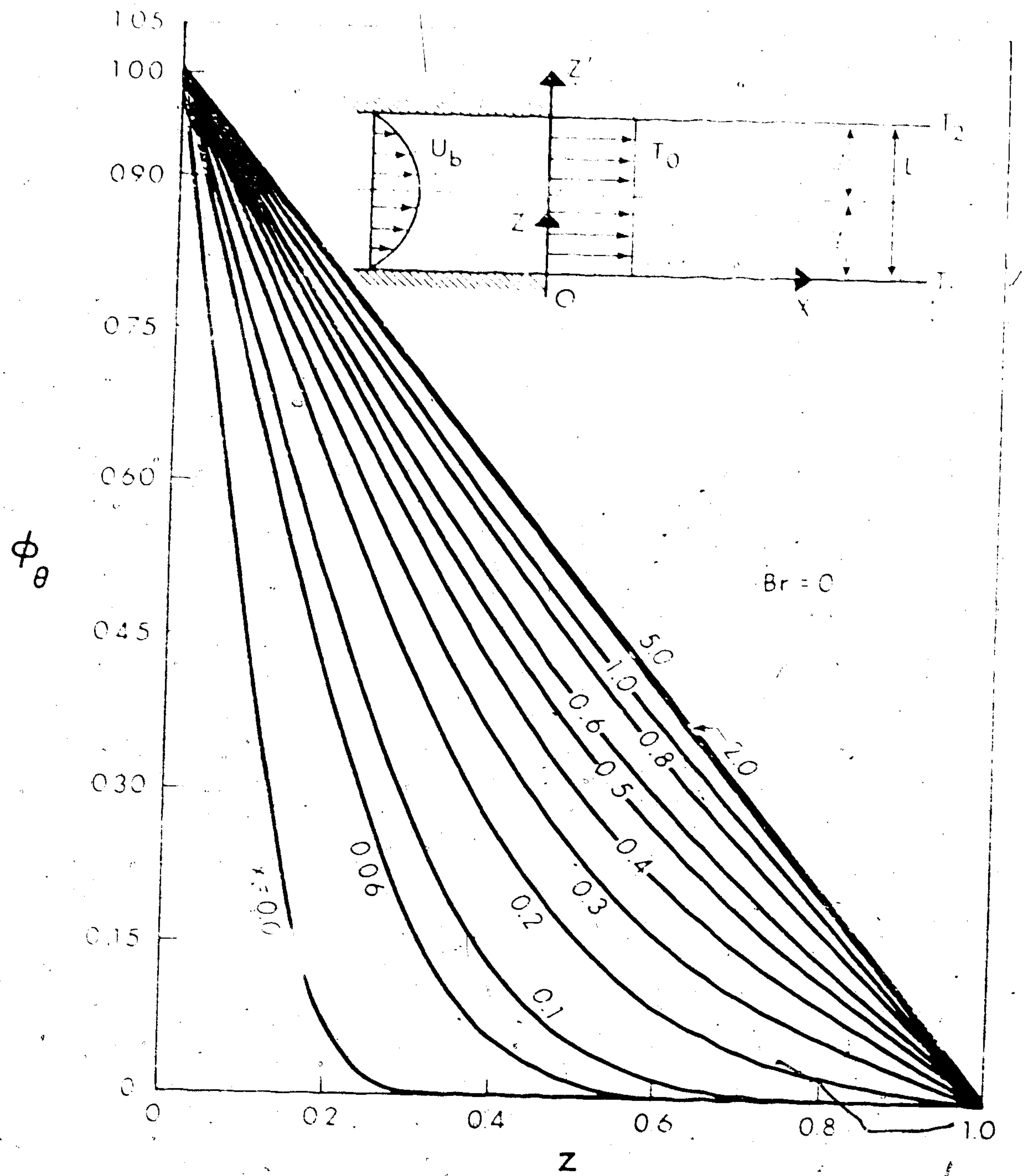

... ster and developing temperature profiles for Br = 0.

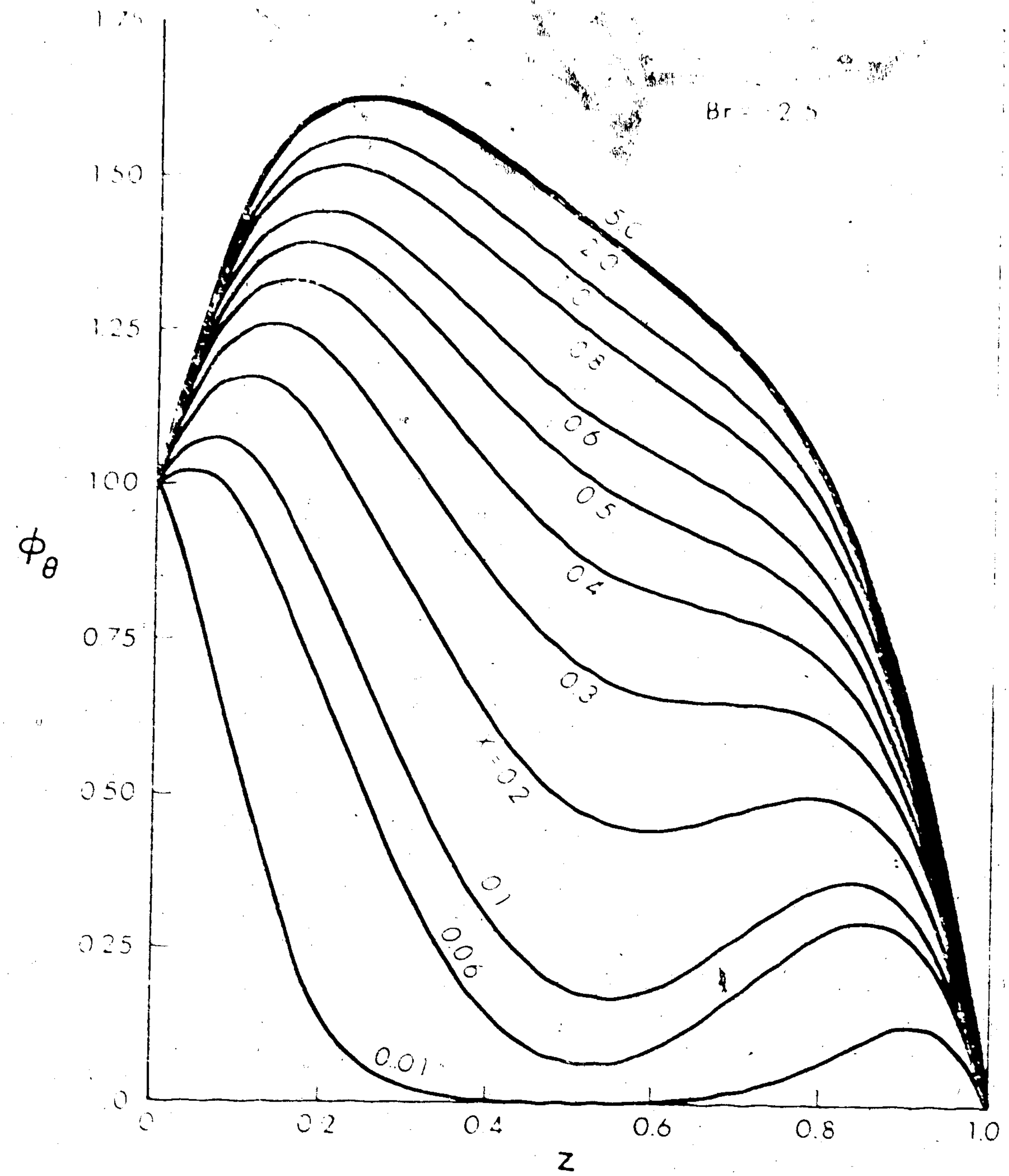

[illegible] temperature profiles for Br = -2.5.

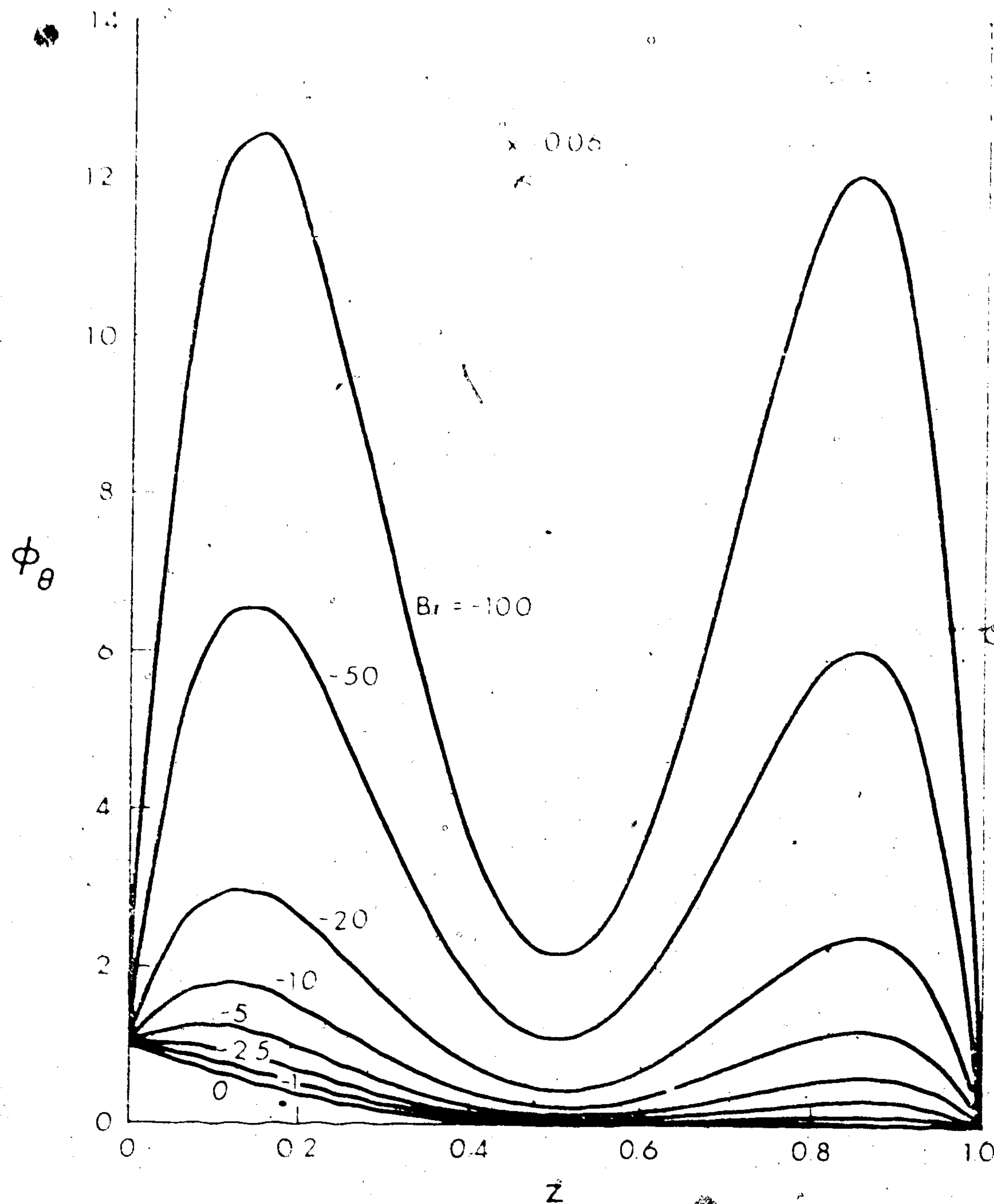

Fig. 32 Brinkman number effect on temperature profiles at x = 0.06.

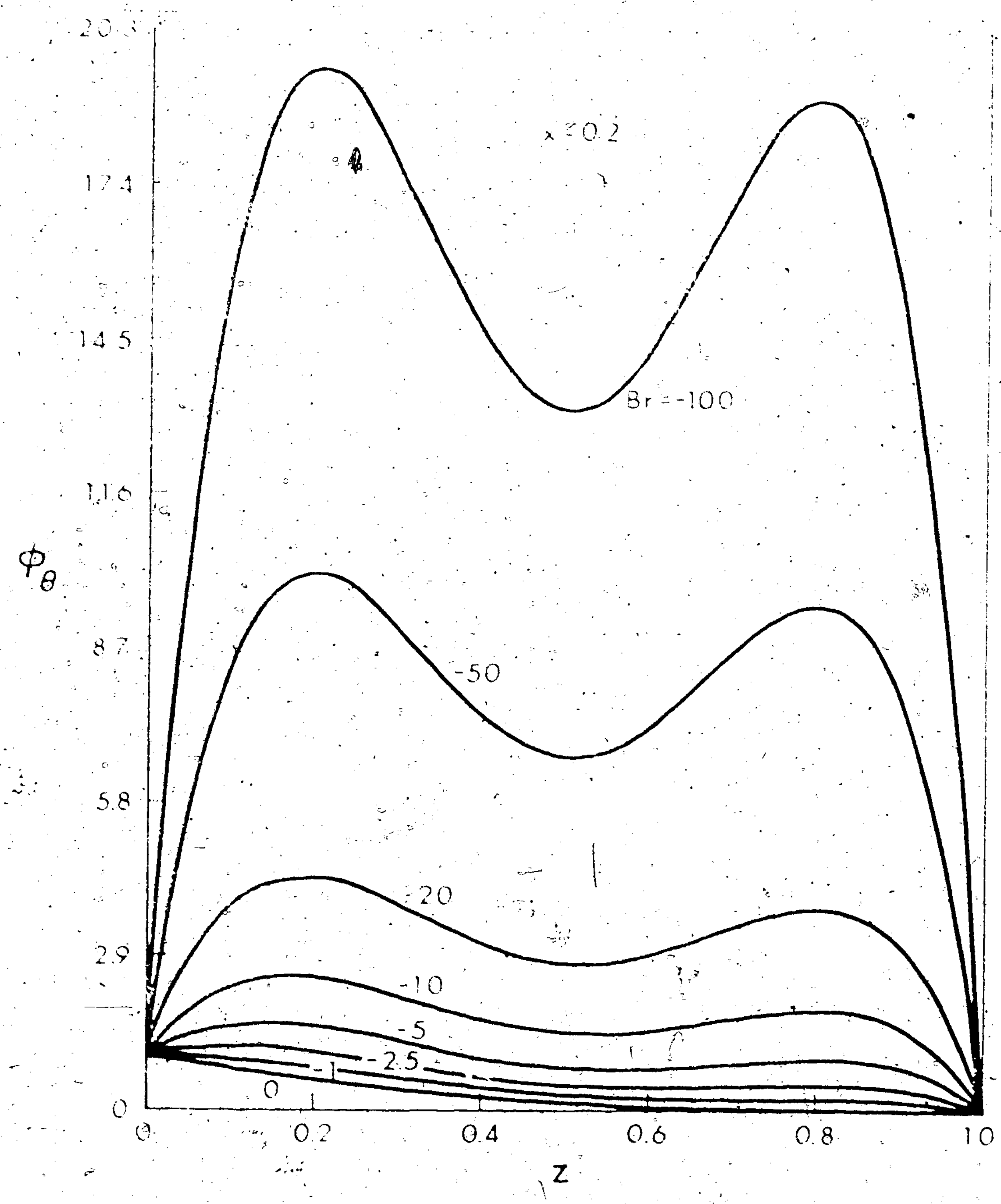

Fig. 4. Brinkman number effect on temperature profiles at x = 0.2

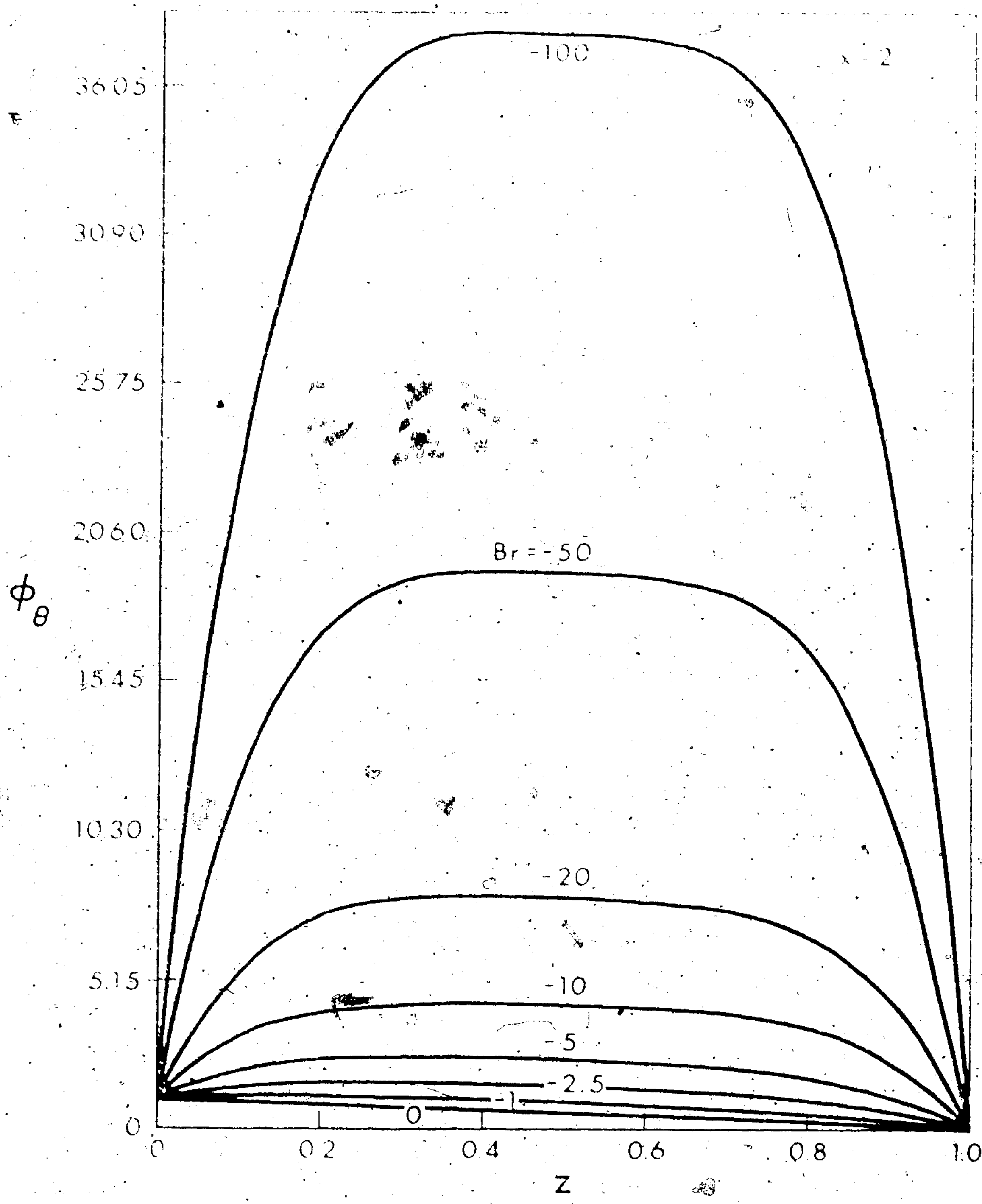

Fig. 5 Brinkman number effect on fully developed temperature profiles (x = 2)

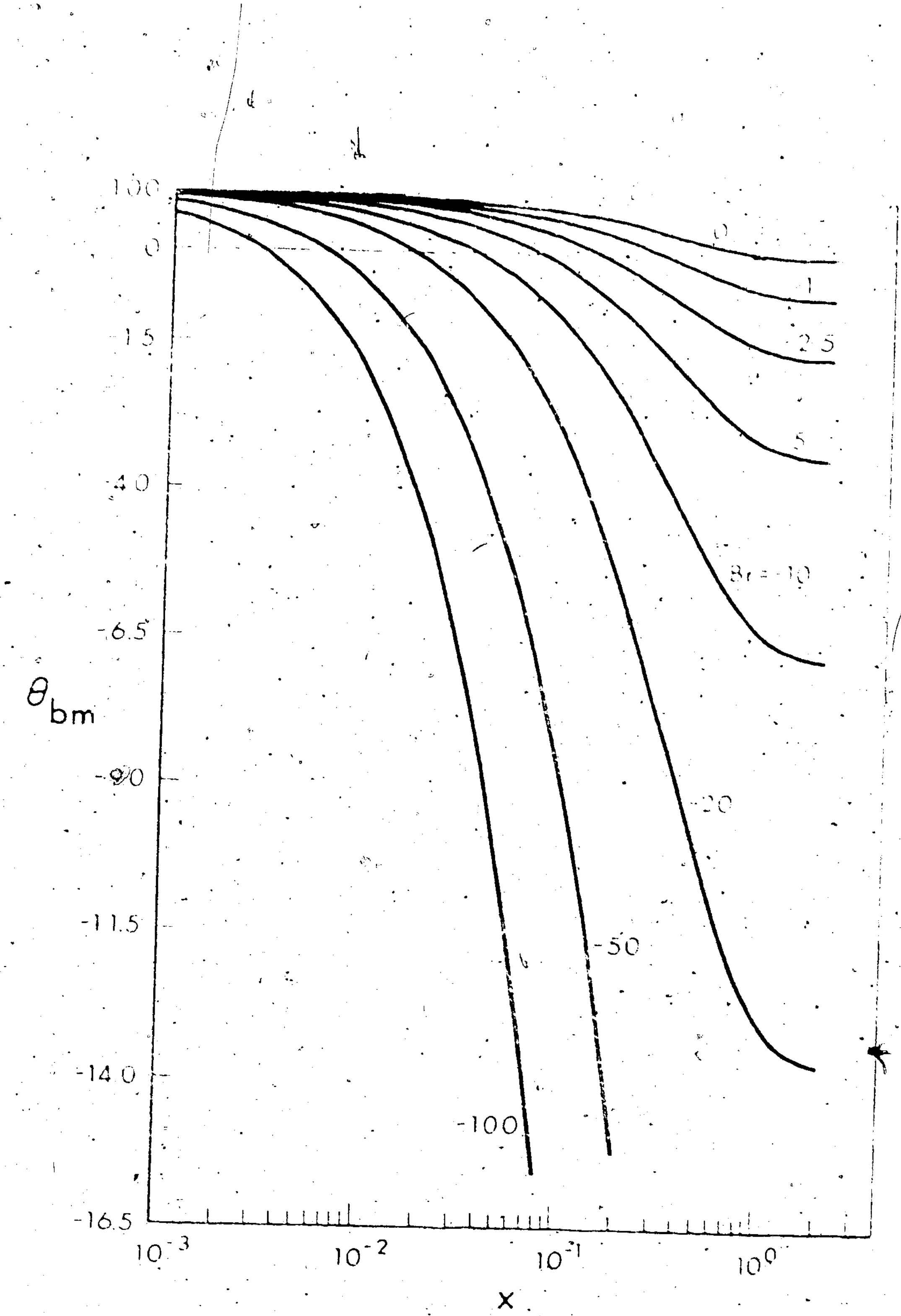

Fig. 6 Brinkman number effect on axial bulk temperature distribution.

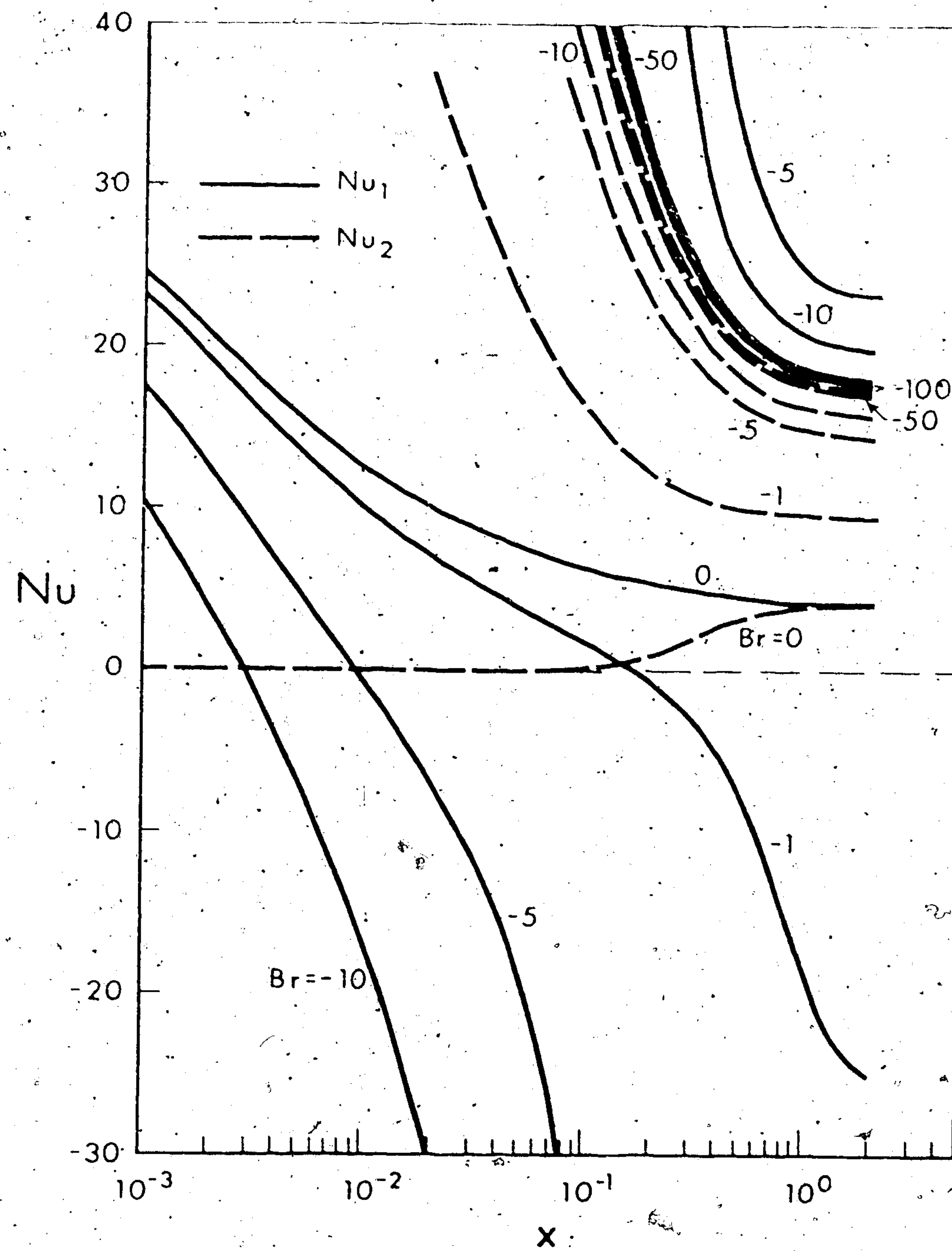

Fig. 7 Brinkman number effect on local Nusselt number results.

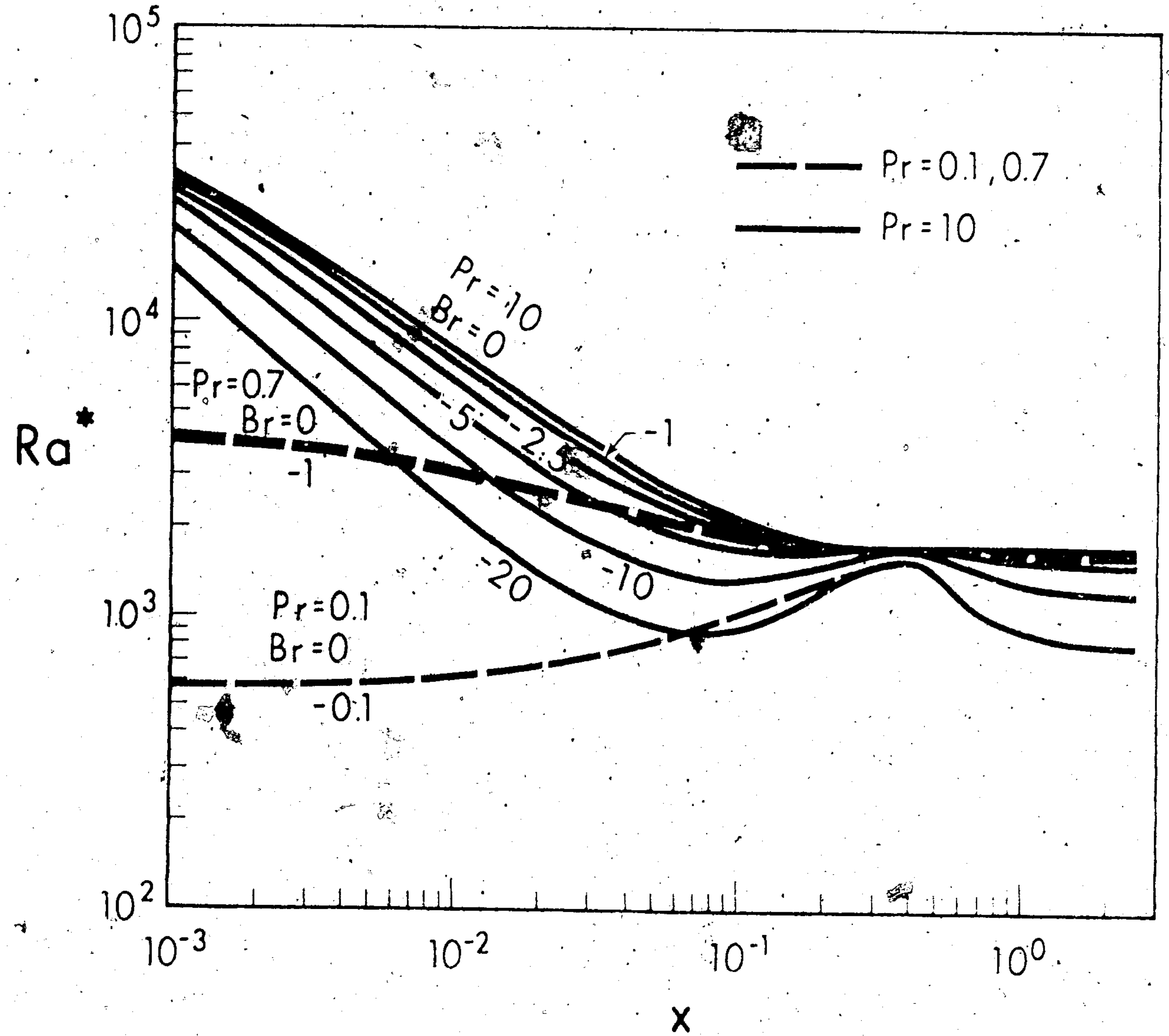

Fig. 8 Viscous dissipation effect on critical Rayleigh numbers for Pr = 0.1, 0.7 and 10.

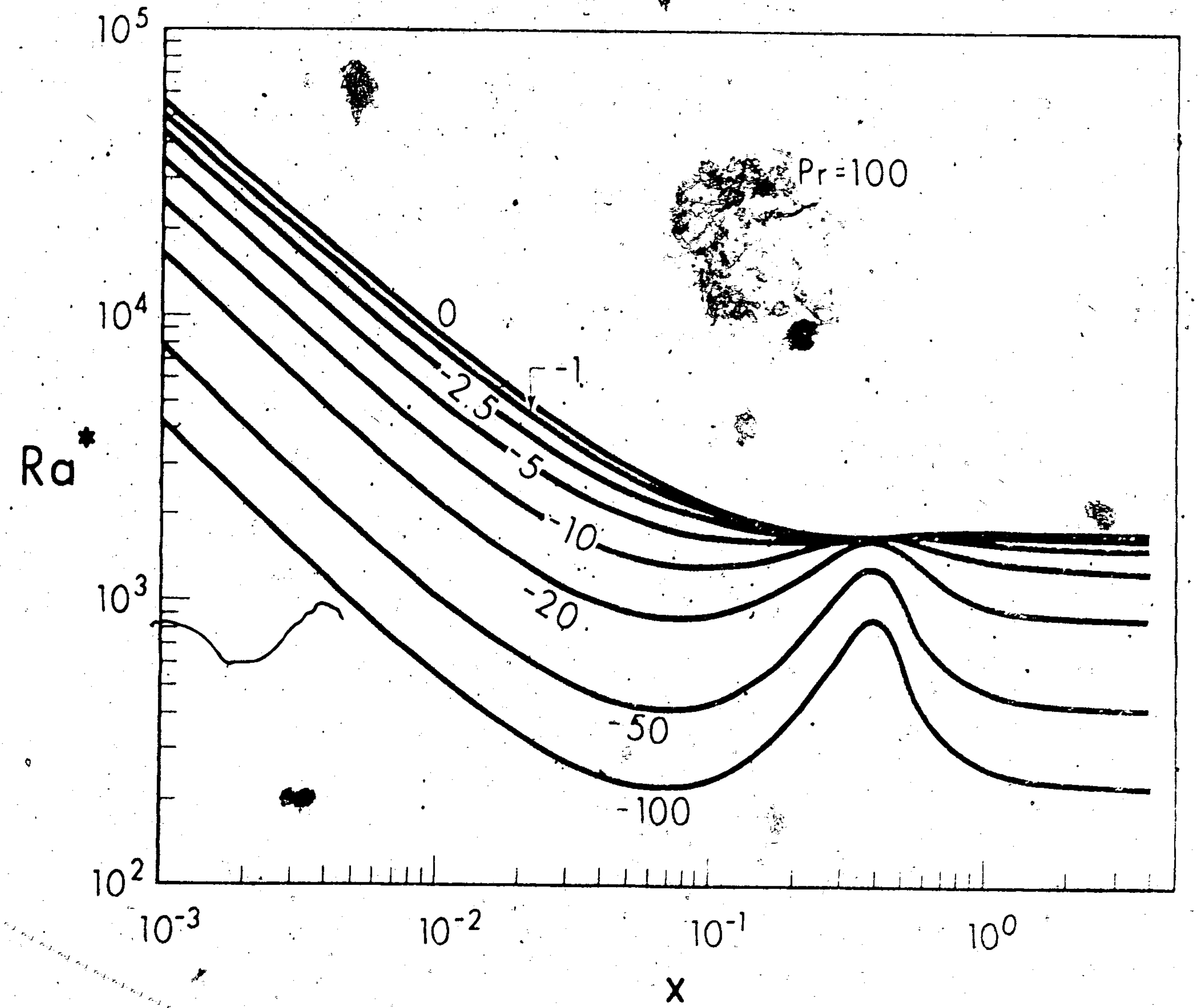

Fig. 9 · Viscous dissipation effect on critical Rayleigh numbers for Pr = 100.

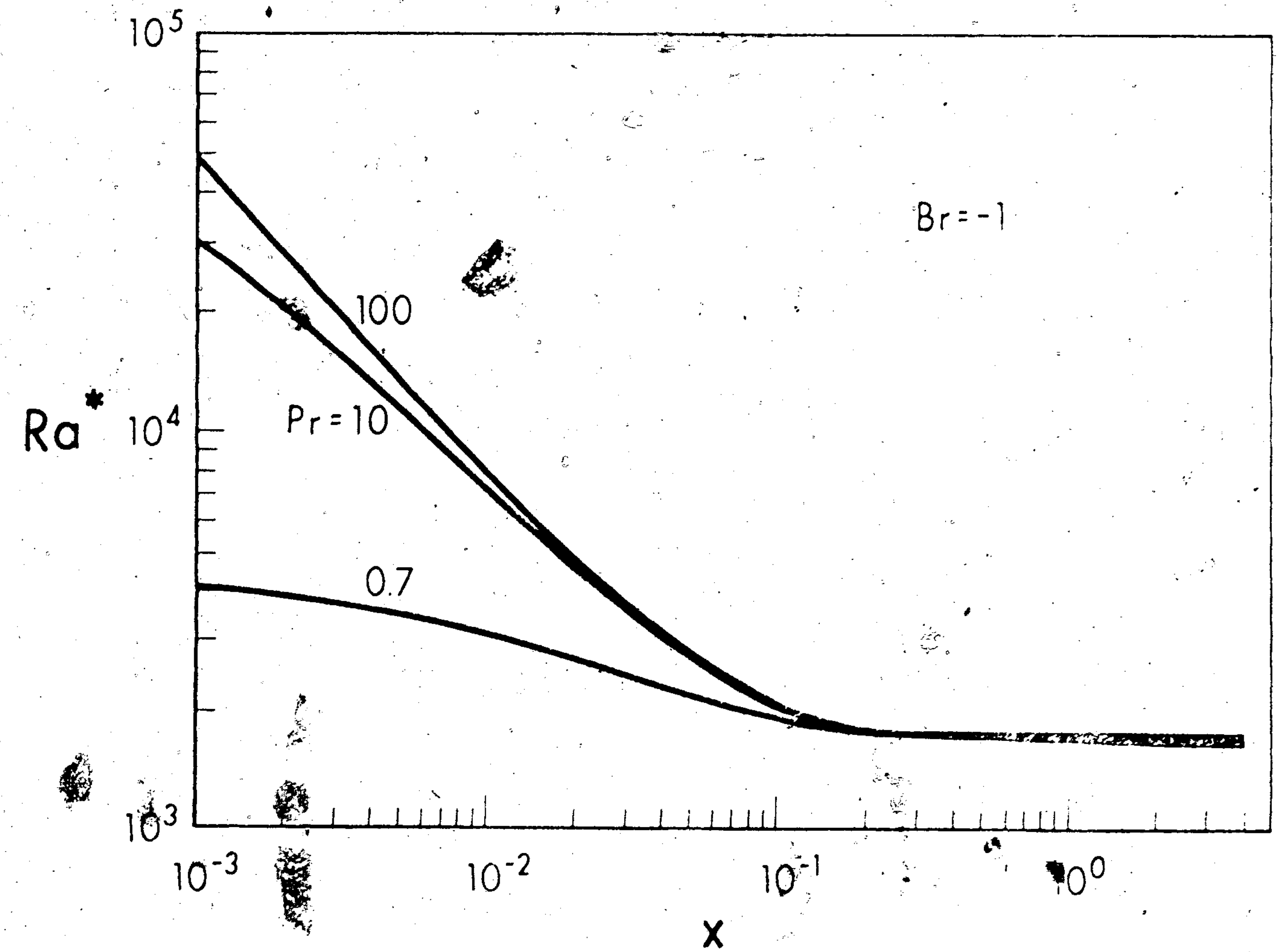

Fig. 10 Prandtl number effect on Ra* at Br = -1.

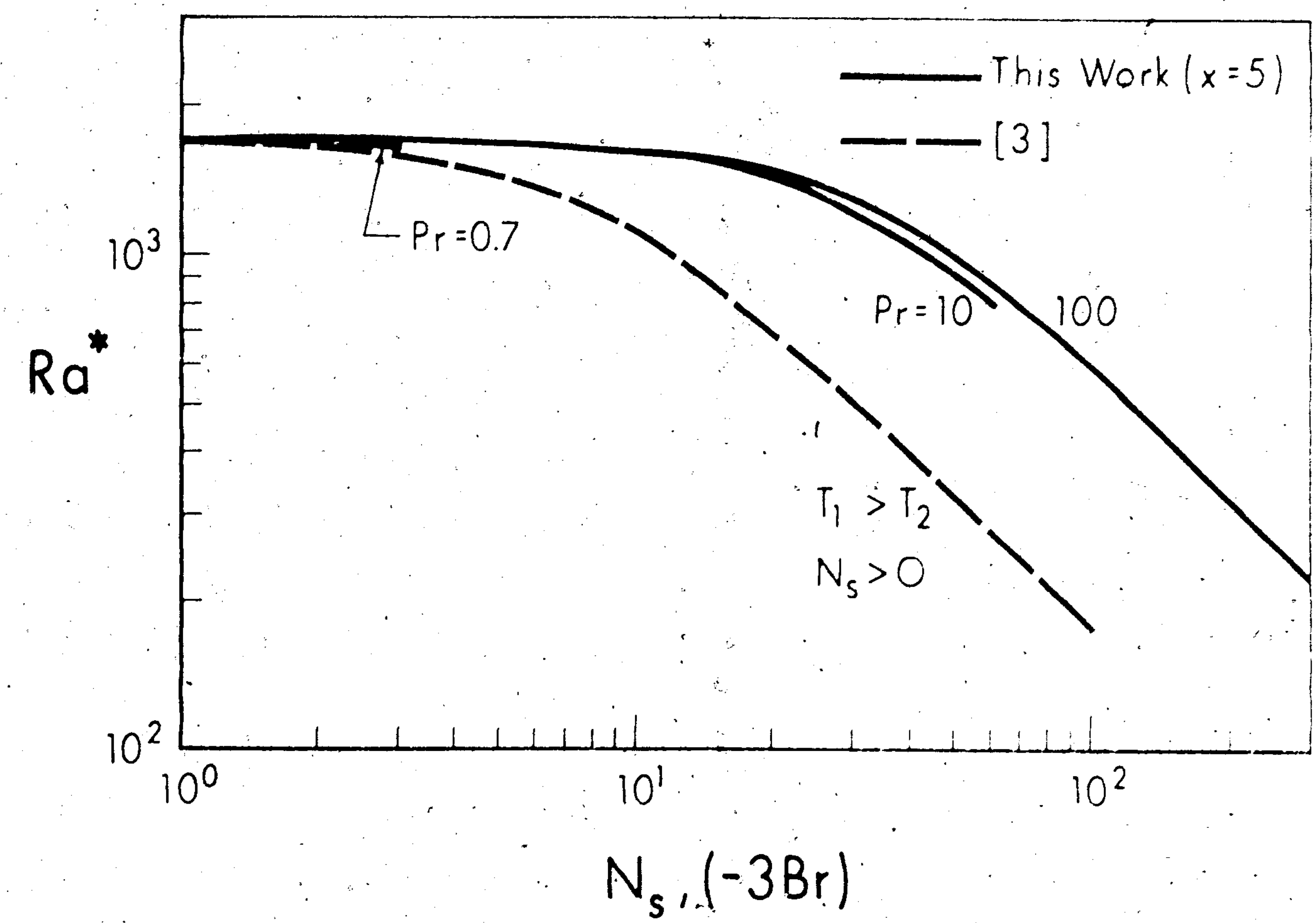

Fig. 11 Critical Rayleigh numbers for fully developed flow and instability results from [3].

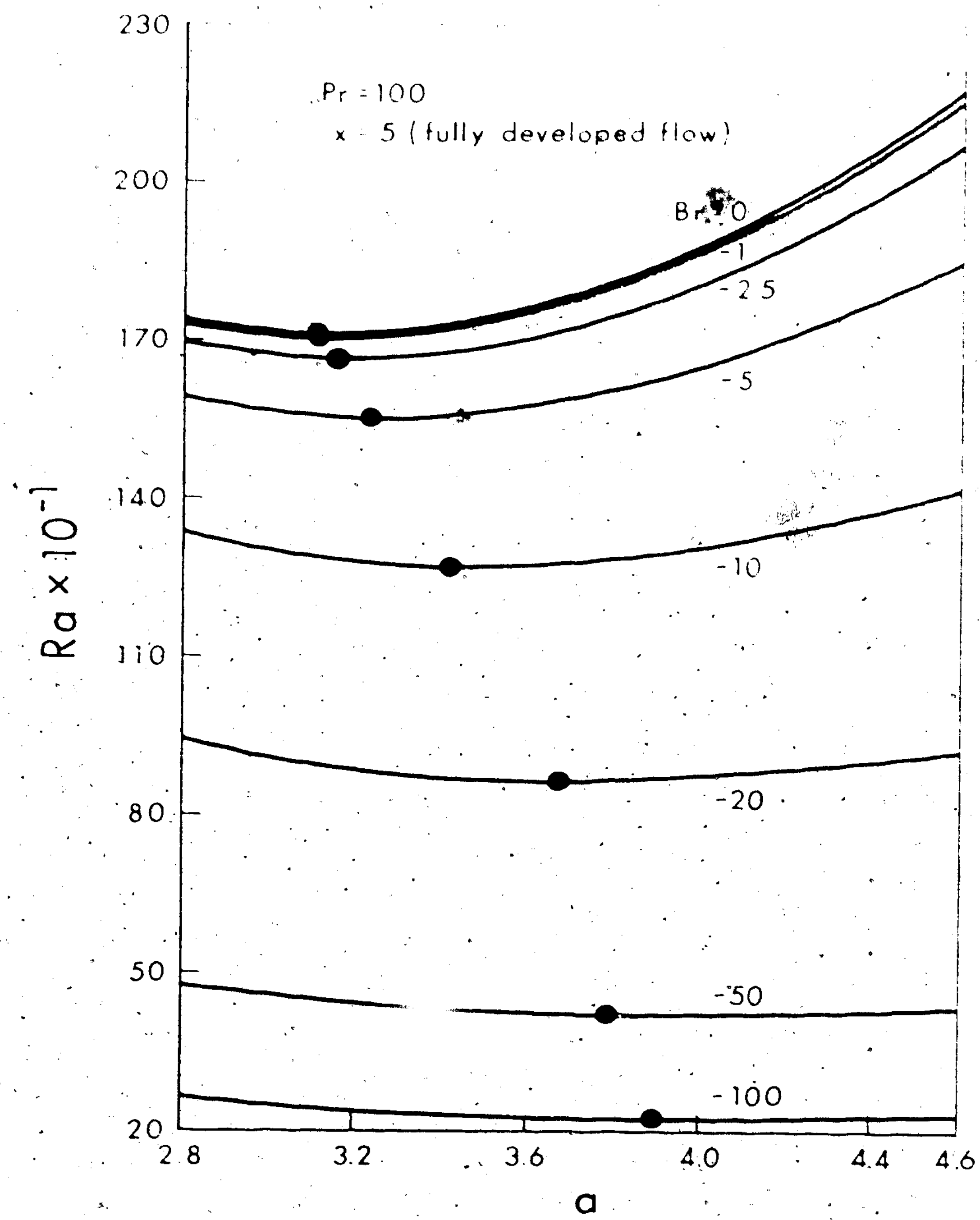

Fig. 12 Viscous dissipation effect on neutral stability curves for Pr = 100 and x = 5.

CHAPTER VI

THERMAL ENTRANCE REGION HEAT TRANSFER FOR MHD LAMINAR FLOW IN PARALLEL-PLATE CHANNELS WITH UNEQUAL WALL TEMPERATURES

The problem of thermal entry heat transfer for Hartmann flow in parallel-plate channels with uniform but unequal wall temperatures considering viscous dissipation, Joule heating and axial conduction effects is approached by the eigenfunction expansion method. The series expansion coefficients for the nonorthogonal eigenfunctions are obtained by using a method for nonorthogonal series described by Kantorovich and Krylov [20]. Numerical results are obtained for the case with entrance condition parameter $\xi_0 = 1$ and open circuit condition $k = 1$. The parametric values of Ha = 0, 2, 6, 10 and Br = 0, -1 are considered for Hartmann and Brinkman numbers, respectively.

Nomenclature

a	=	one-half of channel height
B, B_0	=	magnetic field induction vector and magnitude of applied magnetic field
Br	=	Brinkman number, $\mu_f U_m^2/(k$ [illegible]$)$
C_n, D_n	=	coefficients in the series expansion of θ_e, see eq. (16)
c_p	=	specific heat at constant pressure
E, E_0	=	electric field intensity vector and component
F_n	=	even and odd eigenfunctions
Ha	=	Hartmann number, $(\sigma/\mu_f)^{1/2} B_0 a$.
h_1, h_2	=	local heat transfer coefficients at lower and upper plates
J, J_y	=	electric current density vector and component
K	=	external loading parameter, $E_0/(B_0 U_m)$
k	=	thermal conductivity
Nu_1, Nu_2	=	local Nusselt numbers, $h_1 a/k$ and $h_2 a/k$, respectively
p	=	fluid pressure
Pe	=	Peclet number, PrRe

[illegible]	=	Prandtl number, [illegible]
[illegible]	=	rates of heat transfer per unit area, $-k(\partial T/\partial Y)_{Y=-a}$, $-k(\partial T/\partial Y)_{Y=a}$, respectively
Re	=	Reynolds number, $\rho U_m a/\mu$
[illegible]	=	fluid temperature, uniform entrance temperature, uniform but different lower and upper plate temperatures, respectively
[illegible]	=	bulk temperature and $(T_1 + T_2)/2$
[illegible]	=	axial, mean and dimensionless velocities, respectively
[illegible]	=	velocity vector
[illegible]	=	axial and transverse coordinates
[illegible]	=	dimensionless coordinates
[illegible]	=	even and odd eigenvalues
[illegible]	=	dimensionless fluid, entrance and bulk temperatures, respectively
[illegible]	=	characteristic temperature difference $(T_2 - T_m)$, and dimensionless fluid temperatures, defined by eq. (10)
[illegible]	=	magnetic permeability and viscosity of fluid
[illegible]	=	fluid density
[illegible]	=	electrical conductivity

viscous dissipation function

(1 − [illegible])/2

6.1 Introduction

Magnetohydrodynamic flow in the entrance region of a parallel plate channel has been studied by many investigators in the past. The problem of laminar forced convection heat transfer for fully developed MHD flow (Hartmann flow) in the thermal entrance region of parallel-plate channels has also been studied for the cases of constant wall temperature [1-6] and constant wall heat flux [5-8]. Similarly, the forced convection heat transfer of an MHD flow in the hydrodynamic entrance region of parallel-plate channels has been investigated for both uniform wall temperature [9-12] and uniform wall heat flux [13]. Combined forced and free convection heat transfer for MHD flow in vertical parallel-plate channels has been investigated extensively in recent years for the fully developed flow case. Recently, the problem of combined forced and free convection magnetohydrodynamic flow in the entrance region of a vertical parallel-plate channel was studied for both the constant wall heat flux and constant wall temperature boundary conditions [14].

For magnetohydrodynamic flow in the thermal entrance region of a horizontal parallel-plate channel heated from below, thermal instability problem concerning the onset of longitudinal vortex rolls [15] arises. After a critical value of Rayleigh number is reached, the flow assumes a three-dimensional character and consequently the published heat transfer results for thermal entrance region may no longer be applicable. A literature survey shows that the published works on thermal entrance region heat transfer are concerned with the thermal boundary condition of either uniform wall temperature or uniform wall heat flux only at both upper and lower plates. The purpose of this study is to present the heat transfer results in the thermal entrance region of Hartmann flow between horizontal parallel plates at unequal but constant temperatures. The present problem deals with the basic flow solution required in the thermal instability analysis discussed in Chapter VII. In the analysis, the internal heat generation terms due to both Joule heating and viscous dissipation as well as axial conduction term [5] in the energy equation are retained. As noted in [16], heat transfer problem in the thermal entry region for fully developed laminar flow between parallel plates at uniform but unequal wall temperatures involves two distinct sets of eigenvalues related to odd and even sets of eigenfunctions, respectively.

6.2 Governing Equations

Consideration is given to a steady, viscous, incompressible, electrically-conducting fluid with constant physical properties flowing in a horizontal parallel-plate channel under the action of a constant transverse magnetic field B_0. The laminar velocity profile is already the fully developed Hartmann profile at a certain cross-section $x = 0$ (see Fig. 1) and the fluid temperature T_0 is constant up to $X = 0$. For $X \geq 0$, the wall temperatures at lower and upper plates are maintained at constant values T_1 and T_2, respectively. For the steady system under consideration, the basic equations are the equations of continuity, momentum and energy, Maxwell's equations and Ohm's Law. In vector notation, one obtains [17]

$$\nabla \cdot \bar{V} = 0 \tag{1}$$

$$(\bar{V} \cdot \nabla)\bar{V} = -\frac{1}{\rho}\nabla P + \nu\nabla^2\bar{V} + \frac{1}{\rho}\bar{J} \times \bar{B} \tag{2}$$

$$\rho c_p(\bar{V} \cdot \nabla)T = k\nabla^2 T + \Phi + \frac{1}{\sigma}(\bar{J} \cdot \bar{J}) \tag{3}$$

$$\nabla \cdot \bar{B} = 0, \quad \nabla \times \bar{B} = \mu_e \bar{J}, \quad \nabla \cdot \bar{E} = 0, \quad \nabla \times \bar{E} = 0 \tag{4}$$

$$\bar{J} = \sigma(\bar{E} + \bar{V} \times \bar{B}) \tag{5}$$

where $\bar{V} = (U,0,0)$, $\bar{J} = (0,J_y,0)$, $\bar{E} = (0,E_0,0)$, $\bar{B} = (0,0,B_0)$ for the present problem and Φ = viscous dissipation function. The effect of the induced magnetic field B_x is assumed to be negligible in comparison with the applied field B_0. Referring to the coordinate system shown in Fig. 1, the energy equation becomes

$$\rho c_p U \frac{\partial T}{\partial X} = k\left(\frac{\partial^2 T}{\partial X^2} + \frac{\partial^2 T}{\partial Z^2}\right) + \mu_f\left(\frac{dU}{dZ}\right)^2 + \frac{J_y^2}{\sigma} \quad (6)$$

where $J_y = \sigma(E_0 - UB_0)$ and the simplified version of the Ohm's law without Hall effect is used. Introducing the dimensionless variables and parameters,

$$(X,Z) = [a](xPe, z), \quad U = [U_m](u), \quad \theta = (T-T_m)/(T_2-T_m),$$

$$\theta_0 = (T_0-T_m)/(T_2-T_m), \quad Re = \rho U_m a/\mu_f, \quad Pe = PrRe = \rho c_p U_m a/k,$$

$$Ha = (\sigma/\mu_f)^{1/2} B_0 a, \quad K = E_0/B_0 U_m, \quad Br = \mu_f U_m^2/(k\theta_c)$$

with $U_m = \int_{-a}^{a} UdZ/(2a)$, $T_m = (T_1+T_2)/2$, $\theta_c = T_2 - T_m = (T_2-T_1)/2$, equation (6) becomes

$$u\frac{\partial\theta}{\partial x} = \frac{1}{Pe^2}\frac{\partial^2\theta}{\partial x^2} + \frac{\partial^2\theta}{\partial z^2} + Br\left[\left(\frac{du}{dz}\right)^2 + Ha^2(K-U)^2\right] \quad (7)$$

The thermal boundary conditions at the thermal entrance, the walls and thermally fully developed region are

$$\theta(0,z) = \theta_0, \quad \theta(x,1) = 1, \quad \theta(x,-1) = -1, \quad \theta(\infty,z) = \theta_f \quad (8)$$

It is seen that viscous dissipation and Joule heating represent the heat source terms in the energy equation. For magnetohydrodynamic fully developed laminar flow, the well-known Hartmann solution [17] of equation (2) is

$$u = Ha(\cosh Ha - \cosh Haz)/(Ha \cosh Ha - \sinh Ha)$$

$$= C_1(\cosh Ha - \cosh Haz) \qquad (9)$$

where $C_1 = Ha/(Ha \cosh Ha - \sinh Ha)$. It is noted that when $Ha = 0$, one obtains $u = (3/2)(1 - z^2)$.

6.3 Solution of the Energy Equation

It is convenient to seek the solution of equation (7) in the following form.

$$\theta = \theta_f(z) + \theta_e(x,z) \qquad (10)$$

where θ_f is the fully developed solution and θ_e is the excess temperature satisfying the following set of equations.

$$\frac{d^2\theta_f}{dz^2} + Br[(\frac{du}{dz})^2 + Ha^2(K-u)^2] = 0 \qquad (11)$$

with the boundary conditions,

$$\theta_f(1) = 1, \quad \theta_f(-1) = -1 \qquad (12)$$

$$u \frac{\partial \theta_e}{\partial x} = \frac{1}{Pe^2} \frac{\partial^2 \theta_e}{\partial x^2} + \frac{\partial^2 \theta_e}{\partial x^2} \tag{13}$$

with the entrance and boundary conditions,

$$\theta_e(0,z) = \theta_0, \; \theta_e(x,1) = \theta_e(x,-1) = 0 \tag{14}$$

Substituting equation (9) into equation (11) and integrating twice, using the boundary condition, one obtains the solution for θ_f in the following form:

$$\theta_f = z + Br[(C_1^2/4)(\cosh 2Ha - \cosh 2Haz) + 2C_1C_2(\cosh Ha - \cosh Haz) + (C_2^2Ha^2/2)(1 - z^2)] = z + Brf(z) \tag{15}$$

where $C_2 = K - C_1 \cosh Ha$ and $f(z)$ = terms inside square brackets. When $Ha = 0$, one obtains $\theta_f = z + (3Br/4)(1 - z^4)$. The general solution of equation (13) can be constructed in the form of infinite series as

$$\theta_e = \sum_{n=1}^{\infty} C_n E_n(z) \exp(-\beta_n x) + \sum_{n=1}^{\infty} D_n O_n(z) \exp(-\gamma_n x) \tag{16}$$

where β_n, γ_n and E_n, O_n are the even and odd eigenvalues and eigenfunctions, respectively, of the following characteristic equation and the associated boundary conditions.

$$\frac{d^2E_n}{dz^2} + (\beta_n u + \frac{\beta_n^2}{Pe^2})E_n = 0, \quad E_n(\pm 1) = 0 \tag{17}$$

$$\frac{d^2O_n}{dz^2} + (\gamma_n u + \frac{\gamma_n^2}{Pe^2})O_n = 0, \quad O_n(\pm 1) = 0 \tag{18}$$

It is noted that as $Pe \to \infty$, equations (17) and (18) reduces to the classical Sturm-Liouville systems typified by the Graetz-type problem neglecting axial conduction term. The eigenvalues and the corresponding eigenfunctions are determined in this study ~~by~~ solving equations (17) and (18) using the fourth-order Runge-Kutta method [18]. Two hundred equal steps are employed and the boundary conditions for E_n and O_n at the starting point are $E_n(0) = 1$, $dE_n(0)/dz = 0$ and $O_n(0) = 0$, $dO_n(0)/dz = 1$, respectively. The eigenvalues are improved by using variable secant method [19] which requires assuming two trial values for β_n or γ_n with the difference of say 0.1 at the start. The even eigenvalues β_n are listed in [6] for Ha = 2, 6, 10 and Pe = 1, 10, 10^2, ∞ and can be used as the initial values in this study. The number of iterations required to reach $E_n(1)$ or $O_n(1) < 10^{-8}$ depends on the initial value of β_n or γ_n but usually it takes only 5 to 7 iterations. The spectrum of eigenvalues is checked by plotting $(\beta_n)^{1/2}$ or $(\gamma_n)^{1/2}$ versus n.

The series expansion coefficients C_n and D_n remain to be determined by the application of the entrance condition. Since the axial conduction term is retained, the eigenfunctions lack the property of orthogonality and the eigenfunction expansion technique for Sturm-Liouville system no longer applies. To overcome the difficulty the method for nonorthogonal series described in [20] is used in this study. From the thermal entrance condition at $z = 0$; one obtains

$$\sum_{n=1}^{\infty} C_n E_n(z) + \sum_{n=1}^{\infty} D_n \theta_n(z) = \theta_0 - Brf(z) - z \qquad (19)$$

Here, one notes that $[\theta_0 - Brf(z)]$ is an even function and z is an odd function. After multiplying both sides of equation (19) by $E_i(z)$ and integrating it, one obtains a system of N equations by taking the first N terms of the series.

$$\sum_{n=1}^{N} C_n \int_{-1}^{1} E_n(z) E_i(z)\,dz = \int_{-1}^{1} [\theta_0 - Brf(z)] E_i(z)\,dz,$$

$$(i = 1, 2, \ldots, N) \qquad (20)$$

In practice, the lower limit of the integral may be replaced by 0 and Simpson's rule (IBM-SSP) is used for numerical integration. The system of N linear simultaneous equations with N unknown coefficients is solved by Gauss-Seidel method

(IBM-SSP). Similarly, for the odd coefficients D_n, one obtains

$$\sum_{n=1}^{N} D_n \int_0^1 \Theta_n(z)\Theta_i(z)dz = \int_0^1 (-z)\Theta_i(z)dz, \quad i=1,2,\ldots,N \tag{21}$$

Considering the case of heating from below ($T_1 > T_2$), the expressions for the local Nusselt numbers Nu_1 and Nu_2 at the lower and upper plates, respectively, are defined by

$$Nu_1 = \frac{h_1 a}{k} = \frac{a}{k}\frac{q_1}{(T_1 - T_b)} = \frac{1}{1+\theta_b}\left(\frac{\partial\theta}{\partial z}\right)_{z=-1} \tag{22}$$

$$Nu_2 = \frac{h_2 a}{k} = \frac{a}{k}\frac{q_2}{(T_b - T_2)} = \frac{1}{1-\theta_b}\left(\frac{\partial\theta}{\partial z}\right)_{z=1} \tag{23}$$

where the bulk temperature θ_b is

$$\theta_b = \int_{-1}^{1} \theta u dz / \int_{-1}^{1} \theta u dz \tag{24}$$

The following limiting expressions corresponding to the fully developed condition ($x \to \infty$) are also of interest

$$\theta_{bf} = (Br/2)[\frac{C_1^2}{2} \cosh 2Ha + \frac{C_1^3}{12} (3 + \cosh 2Ha)$$

$$+ 4 C_1^2 C_2 (1 + \frac{1}{2} \cosh 2Ha - \frac{3}{4Ha} \sinh 2Ha) + C_2^2 Ha \text{[illegible]}$$

$$- C_1 \cosh Ha (\frac{1}{2} + \frac{2}{Ha^2}) + \frac{C_1}{Ha} (1 + \frac{2}{Ha^2}) \sinh Ha] \quad (25)$$

$$Nu_{1f} = [1 - BrHa(\frac{C_1^2}{2} \sinh 2Ha + 2C_1C_2 \sinh Ha$$

$$+ C_2^2 Ha)]/(1 - \theta_{bf}) \quad (26)$$

$$Nu_{2f} = [1 + BrHa(\frac{C_1^2}{2} \sinh 2Ha + C_1C_2 \sinh Ha$$

$$+ C_2^2 Ha)]/(1 + \theta_{bf}) \quad (27)$$

6.4 Numerical Results and Discussion

The present problem involves five parameters (Pe, Ha, K, Br, θ_0) and the range of variation of each parameter which is of practical interest in this study is Pe = 10 ~ ∞, Ha = 0 ~ 10, K = 0 ~ 2, Br = 0 ~ -1, θ_0 = -∞ ~ ∞, respectively. Because of the number of parameters present, computations are made for the parametric values of Pe = 10, 10^2, ∞, Ha = 0, 2, 6, 10, K = 1 (open circuit condition), Br = 0, -1 and θ_0 = 1($T_0 = T_2$) only. These are designed to study the axial conduction, Hartmann number and viscous dissipation effects on thermal entrance region heat transfer.

The eigenvalues $_n$, $_n$ and the coefficients C_n, D_n for Pe [illegible] 10, $10^{[illegible]}$, [illegible] and Br [illegible] 0, -1 are listed in Tables 1 to 4 for the cases of Ha [illegible] 0, 2, 6 and 10, respectively, with $_0$ = 1 and K [illegible] 1. The eigenvalues $_n$ and $_n$ are independent of the values for $_0$ and K. The numerical values of C_n are a function of $_0$ and K as well as Br. The values of D_n are independent of Br and a function of $_0$ and K only as can be seen from equation (21).

The developing temperature profiles ([illegible] = $\frac{1}{2}$ (1 - [illegible]) versus z' = $\frac{1}{2}$ (z + 1)) at various axial positions in the thermal entrance region are presented in Figs. 1 to 5. With K = 1 (the lowest current or open circuit case), the Joule heating is minimum and the viscous dissipation produces more heating than the Joule heating. Fig. 1 shows that with Pe = 10, Ha = 0, Br = 0, a fully developed linear temperature profile is already attained at x = 5.0. It is found that twelve eigenvalues are not sufficient to yield convergent solution near the thermal entrance x ~ 10^{-3}. The case of Br = -1 (heating from below) represents dominent overall dissipation and Brinkman effect can be seen clearly by a comparison between Figs. 1 and 2. Fig. 2 also shows that viscous heating effect is particularly appreciable near the upper and lower walls. Similar plottings for Pe = 10 and Ha = 2 are shown in Figs. 3 and 4 for Br = 0 and -1.0, respectively. With Br = 0, Hartmann number effect can be seen by comparing Fig. 3 with Fig. 1 and one notes that thermal entrance length does not appear to be affected by magnetic field at Ha = 2. Fig. 4 shows that dissipation effects are further magnified by Joule heating at Ha = 2. The behavior of fully developed temperature profile shown in Fig. 4 can be understood by invoking the membrane analogy for equation (11). In equation (15), the term Br $f(z)$ apparently represents the dissipation effects. The Hartmann number effects on developing temperature profiles (θ) and on bulk temperature distribution (θ_b) are further illustrated in Figs. 5 (Pe = 10) and 6 (Pe = 100), respectively. One notes that the difference between the axial bulk temperature distributions for Pe = 10 and 100 can hardly be distinguished graphically.

Of particular practical interest in this study are the effects of Hartmann number on local Nusselt number variations at the lower and upper plates and the results are presented in Figs. 7 and 8 for Br = 0 and −1, respectively, and in Table 5 and 6. The effect of magnetic field on local heat transfer is clearly seen in Fig. 7 for Br = 0. At Pe = 100, the axial conduction effect is practically negligible and the local Nusselt number Nu_1 at the lower plate increases with the increase of Ha. Similar effect also exists at the upper plate but the local Nusselt number is seen to be zero up to a certain axial distance ($x \approx 8 \times 10^{-2}$). At Pe = 10, the axial conduction effect is quite pronounced and the local Nu_1 decreases as Ha increases up to $x = 9 \times 10^{-3}$ but further downstream the trend reverses and is similar to that of $Pe = 100$. At the upper plate, the difference in local Nusselt numbers (Nu_2) between $Pe = 10$ and 100 is very small but the case of $Pe = 100$ has higher value for a given Ha. It is seen clearly that the axial conduction effect disappears completely at $x = 1$.

With $Br = -1$, the local Nusselt number behavior is more complicated than that of $Br = 0$. In Fig. 8, the zero Nusselt number signifies a change in the direction of the heat transfer at the wall. At $Br = -1$, the viscous dissipation effect is dominant and the Hartmann number effect is similar for $Pe = 10$ and 100. The local Nu_1 decreases as Ha increases and the trend is opposite to that of the case $Pe = 100$, $Br = 0$. The merging of the two curves for $Pe = 10$ and 100 with the same value of Ha at a certain axial distance x indicates the vanishing axial conduction effect. The behavior of the fully developed Nusselt number Nu_{1f} can be explained from the fully developed temperature profiles at $x = 5$ shown in Fig. 5 where the fluid temperature is seen to be higher than the lower wall temperature. Because of the viscous dissipation effect, the local Nusselt number Nu_2 at the upper plate is not zero near the thermal entrance $x = 0$ and the Nusselt number Nu_2 decreases monotonically toward a fully developed value depending on Ha. The effect of Ha on fully developed Nusselt numbers Nu_2 can be explained from the corresponding temperature profiles shown in Fig. 5.

[illegible] Concluding Remarks

1. The present method of computation for the series expansion coefficients is different from that of [5]. The present computational procedure is very straightforward and leads to accurate results. The method of solution is valid for any values of $[illegible]_0$ and [illegible].

2. The odd eigenvalues listed in Tables 1 to 4 take values between those of the even eigenvalues. The even eigenvalues check well with those reported in [5]. The numerical eigenvalues of $[illegible]_n$ and $[illegible]_n$ for the case of Pe [illegible] and [illegible] also agree with the corresponding equivalent values ($[illegible]_n$ [illegible] ([illegible]) γ^2_{En}, $[illegible]_n$ [illegible] (2/3) γ^2_{0n}) listed in Table 1 of [16].

3. For the present formulation including viscous dissipation effect, the entrance condition of uniform fluid temperature at x = 0 must be regarded as an approximate one. Consequently, numerical calculation is not made for Pe < 10. In this respect, the present numerical results as well as the published results [2,5,8] must be understood under this light. In general, if one includes both viscous dissipation and axial heat conduction effects in the classical Graetz problem (thermal entrance region problem), even the entrance condition of uniform fluid temperature at x = −∞ must be regarded as an approximate one. In the physical problem, the specification of uniform entrance temperature and the inclusion of viscous dissipation effect in the problem formulation are seen to be incompatible to some extent.

4. The present solution serves as a basic flow solution for thermal instability of Hartmann flow in horizontal parallel-plate channel heated from below which will be discussed in Chapter VII.

5. Within the range of parametric values studied, thermal entrance length does not appear to be affected by magnetic field up to Ha = 10. It is noted that the heat transfer results are independent of Prandtl number. In this study, the numerical computation is limited to Ha $\leq$ 10 in order to check the even eigenvalues against those given in [5]. However, no computational difficulty is expected for Ha > 10. One notes that the influence of the flattening Hartmann velocity profile on heat transfer continues with further increase of the Hartmann number. The flat velocity distribution for Ha $\to \infty$ or slug flow is practically approached at Ha $\approx$ 20.

References

1. Nigam, S.D. and Singh, S.N., "Heat Transfer by Laminar Flow Between Parallel Plates Under the Action of Transverse Magnetic Field", Quart. J. Mech. and Appl. Math., Vol. 13, 1960, pp. 85-97.

2. Erickson, L.E., Wang, C.S., Hwang, C.L. and Fan, L.T., "Heat Transfer to Magnetohydrodynamic Flow in a Flat Duct", Z. Angew. Math. Phys., Vol. 15, 1964, pp. 408-418.

3. Jain, M.K. and Srinivasan, J., "Hydromagnetic Heat Transfer in the Thermal Entrance Region of a Channel with Electrically Conducting Walls", AIAA Jl., Vol. 2, 1964, pp. 1886-1892.

4. Michiyoshi, H. and Matsumoto, R., "Heat Transfer by Hartmann Flow in Thermal Entrance Region", Int. J. Heat Mass Transfer, Vol. 7, 1964, pp. 101-112.

5. LeCrog, R.C. and Eraslan, A.H., "The Solution of Temperature Development in the Entrance Region of an MHD Channel by the Galerkin Method", J. Heat Transfer, Vol. 91C, 1969, pp. 212-220.

6. Eraslan, A.H. and Eraslan, N.F., "Heat Transfer in Magnetohydrodynamic Channel Flow", Phys. Fluids, Vol. 12, 1969, pp. 120-128.

7. Perlmutter, M. and Siegel, R., "Heat Transfer to an Electrically Conducting Fluid Flowing in a Channel with a Transverse Magnetic Field", NASA Technical Note D-875, 1961.

8. Hwang, C.L., Knieper, P.J. and Fan, L.T., "Heat Transfer to MHD Flow in the Thermal Entrance Region of a Flat Duct", Int. J. Heat Mass Transfer, Vol. 9, 1966, pp. 773-789.

9. Shohet, J.L., Osterle, J.F. and Yong, F.J., "Velocity and Temperature Profiles for Laminar Magnetohydrodynamic Flow in the Entrance Region of a Plane Channel", Phys. Fluids, Vol. 5, 1962, pp. 545-549.

10. Shohet, J.L., "Velocity and Temperature Profiles for Laminar Magnetohydrodynamic Flow in the Entrance Region of an Annual Channel", Phys. Fluids, Vol. 5, 1962, pp. 879-884.

11. Hwang, C.L., "A Finite Difference Analysis of Magnetohydrodynamic Flow with Forced Convection Heat Transfer in the Entrance Region of a Flat Rectangular Duct", Ph.D. Thesis, Kansas State University, 1962.

12. Dhanak, A.M., "Heat Transfer in Magnetohydrodynamic Flow in an Entrance Section", J. Heat Transfer, Vol. 87C, 1965, pp. 231-236.

13. Fan, L.T., Hwang, C.L., Knieper, P.J. and Hwang, W.P., "Heat Transfer on Magnetohydrodynamic Flow in the Entrance Region of a Flat Duct", 2. Angew. Math. Phys., Vol. 18, 1967, pp. 826-844.

14. Yang, H.K. and Yu, C.P., "Entrance Flow in MHD Channel with Combined Forced and Free Convection", Developments in Theoretical and Applied Mechanics (SECTAM), Vol. 17, The Catholic University of America, 1974, pp. 61-82.

15. Hwang, G.J. and Cheng, K.C., "Convective Instability in the Thermal Entrance Region of a Horizontal Parallel-Plate Channel Heated from Below", J. Heat Transfer, Vol. 95C, 1973, pp. 72-77.

16. Hatton, A.P. and Turton, J.S., "Heat Transfer in the Thermal Entry Length with Laminar Flow Between Parallel Walls at Unequal Temperatures", Int. J. Heat Mass Transfer, Vol. 5, 1962, pp. 673-679.

17. Sutton, G.W. and Sherman, A., "Engineering Magnetohydrodynamics", McGraw-Hill, New York, 1965, Chapter 10.

18. Collatz, L., "The Numerical Treatment of Differential Equations", 3rd Ed., Springer-Verlag, Berlin, 1960, p. 69.

19. Fröberg, C.E., "Introduction to Numerical Analysis", 2nd Ed., Addison-Wesley, Reading, Massachusetts, 1969, p. 22.

20. Kantorovich, L.V. and Krylov, V.I., "Approximate Methods of Higher Analysis", Interscience Publishers, 1958, pp. 54-56.

Table 1 Values of eigenvalues [illegible]$_n$, [illegible]$_n$ and coefficient C_n, D_n for Ha=0, [illegible]$_0$=1 and K=1

Pe	n	[illegible]$_n$	[illegible]$_n$	C_n Br=0	C_n Br=1	D_n
10	1	0.185887 (1)	0.836433 (1)	0.12176 (1)	0.20347 (1)	-0.19451 (1)
	2	0.182476 (2)	0.301671 (2)	-0.34295	-0.49417	0.19448 (1)
	3	0.432620 (2)	0.570574 (2)	0.21798	0.26642	-0.20517 (1)
	4	0.712974 (2)	0.858383 (2)	-0.16688	-0.18819	0.21345 (1)
	5	0.100594 (3)	0.115510 (3)	0.13603	0.14678	-0.21786 (1)
	6	0.130549 (3)	0.145685 (3)	-0.11441	-0.12034	0.21962 (1)
	7	0.160898 (3)	0.176173 (3)	0.98342 (-1)	0.10185	-0.21998 (1)
	8	0.191501 (3)	0.206871 (3)	-0.86028 (-1)	-0.88235 (-1)	0.21972 (1)
	9	0.222278 (3)	0.237716 (3)	0.76390 (-1)	0.77851 (-1)	-0.21933 (1)
	10	0.253180 (3)	0.268666 (3)	-0.68759 (-1)	-0.69772 (-1)	0.21920 (1)
	11	0.284172 (3)	0.299696 (3)	0.62831 (-1)	0.63561 (-1)	-0.22014 (1)
	12	0.315235 (3)	0.330787 (3)	-0.59519 (-1)	-0.60076 (-1)	0.22703 (1)
100	1	0.188491 (1)	0.893327 (1)	0.12033 (1)	0.20658 (1)	-0.18610 (1)
	2	0.213379 (2)	0.390500 (2)	-0.30630	-0.44992	0.16842 (1)
	3	0.619270 (2)	0.899226 (2)	0.17282	0.21717	-0.16550 (1)
	4	0.122948 (3)	0.160894 (3)	-0.12552	-0.14601	0.17177 (1)
	5	0.203638 (3)	0.251044 (3)	0.10747	0.11951	-0.19114 (1)
	6	0.302968 (3)	0.359259 (3)	-0.11587	-0.12516	0.25310 (1)
	1	0.188518 (1)	0.899048 (1)	0.12030 (1)	0.20654 (1)	-0.18587 (1)
	2	0.214315 (2)	0.392071 (2)	-0.30538	-0.44881	0.16753 (1)
	3	0.623116 (2)	0.907599 (2)	0.17137	0.21553	-0.16365 (1)
	4	0.124537 (3)	0.163647 (3)	-0.12369	-0.14402	0.16889 (1)
	5	0.208091 (3)	0.257868 (3)	0.10548	0.11743	-0.18757 (1)
	6	0.312979 (3)	0.373423 (3)	-0.11403	-0.12338	0.24990 (1)

Note: The numbers in parentheses represent $10^{(n)}$.

Table 2 Values of eigenvalues $_n$, $_n$ and coefficients C_n, D_n for Ha=2, $_0$=1 and k=1

Pe	n	$_n$	$_n$	C_n Br=0	C_n Br=-1	D_n
	1	0.191166 (1)	0.833855 (1)	0.122510 (1)	0.215654 (1)	-0.194332 (1)
	2	0.181273 (2)	0.299776 (2)	-0.352809	-0.498455	0.193044 (1)
	3	0.430360 (2)	0.568196 (2)	0.220897	0.280144	-0.201945 (1)
	4	0.710624 (2)	0.856133 (2)	-0.167509	-0.197170	0.209563 (1)
10	5	0.100382 (3)	0.115311 (3)	0.136078	0.152484	-0.214132 (1)
	6	0.130363 (3)	0.145510 (3)	-0.114413	-0.124102	0.216383 (1)
	7	0.160733 (3)	0.176018 (3)	0.984211 (-1)	0.104456	-0.217273 (1)
	8	0.191353 (3)	0.206731 (3)	-0.861824 (-1)	-0.901222 (-1)	0.217497 (1)
	9	0.222145 (3)	0.237589 (3)	0.766031 (-1)	0.792847 (-1)	-0.217529 (1)
	10	0.253058 (3)	0.268550 (3)	-0.690253 (-1)	-0.709202 (-1)	0.217802 (1)
	1	0.194003 (1)	0.895478 (1)	0.121240 (1)	0.213977 (1)	-0.187107 (1)
	2	0.212029 (2)	0.386464 (2)	-0.320382	-0.458045	0.170463 (1)
10^2	3	0.612283 (2)	0.838748 (2)	0.181044	0.234387	-0.167443 (1)
	4	0.121496 (3)	0.158988 (3)	-0.131183	-0.158547	0.173315 (1)
	5	0.201233 (3)	0.248104 (3)	0.111463	0.128534	-0.191391 (1)
	6	0.299462 (3)	0.355163 (3)	-0.115508	-0.128892	0.243596 (1)
	1	0.194033 (1)	0.896196 (1)	0.121212 (1)	0.213941 (1)	-0.186912 (1)
	2	0.212454 (2)	0.387925 (2)	-0.319568	-0.457037	0.169706 (1)
	3	0.616035 (2)	0.896783 (2)	0.179759	0.232869	-0.165856 (1)
	4	0.123017 (3)	0.161620 (3)	-0.129550	-0.156705	0.170824 (1)
	5	0.205487 (3)	0.254618 (3)	0.109683	0.126622	-0.188273 (1)
	6	0.309013 (3)	0.368671 (3)	-0.113937	-0.127338	0.240907 (1)

Note: The numbers in parentheses represent $10^{(n)}$.

Table 3 Values of eigenvalues ϵ_n, γ_n and coefficients C_n, D_n for Ha=6, θ_0=1 and K 1

Pe	n	ϵ_n	γ_n	C_n Br=0	C_n Br=-1	D_n
10	1	0.209393 (1)	0.834994 (1)	0.124935 (1)	0.231587 (1)	-0.194704 (1)
	2	0.178949 (2)	0.295538 (2)	-0.385179	-0.542307	0.190468 (1)
	3	0.424963 (2)	0.562266 (2)	0.231335	0.317296	-0.194218 (1)
	4	0.704579 (2)	0.850217 (2)	-0.170250	-0.225077	0.199415 (1)
	5	0.998159 (2)	0.114776 (3)	0.136509	0.173224	-0.203870 (1)
	6	0.129859 (3)	0.145037 (3)	-0.114487	-0.139811	0.207291 (1)
	7	0.160289 (3)	0.175601 (3)	0.988010 (-1)	0.116707	-0.209995 (1)
	8	0.190961 (3)	0.206361 (3)	-0.871307 (-1)	-0.100099	0.212518 (1)
	9	0.221794 (3)	0.237256 (3)	0.783543 (-1)	0.879861 (-1)	-0.215610 (1)
	10	0.252741 (3)	0.268248 (3)	-0.718893 (-1)	-0.792509 (-1)	0.220194 (1)
10^2	1	0.213141 (1)	0.897547 (1)	0.124227 (1)	0.230618 (1)	-0.190674 (1)
	2	0.208549 (2)	0.377727 (2)	-0.366768	-0.517457	0.177678 (1)
	3	0.596792 (2)	0.865089 (2)	0.208415	0.287380	-0.174294 (1)
	4	0.118182 (3)	0.154607 (3)	-0.149736	-0.199853	0.178603 (1)
	5	0.195679 (3)	0.241284 (3)	0.123744	0.159284	-0.191771 (1)
	6	0.291300 (3)	0.345596 (3)	-0.114574	-0.142739	0.218127 (1)
	1	0.213180 (1)	0.898278 (1)	0.124210 (1)	0.230596 (1)	-0.190563 (1)
	2	0.208956 (2)	0.379090 (2)	-0.366275	-0.516797	0.177246 (1)
	3	0.600244 (2)	0.872420 (2)	0.207630	0.286350	-0.173383 (1)
	4	0.119526 (3)	0.156985 (3)	-0.148737	-0.198589	0.177172 (1)
	5	0.199510 (3)	0.247138 (3)	0.122670	0.157998	-0.189984 (1)
	6	0.299868 (3)	0.357701 (3)	-0.113674	-0.141767	0.216567 (1)

Note: The numbers in parentheses represent $10^{(n)}$.

Table 4 Values of eigenvalues [illegible]$_n$; [illegible]$_n$ and coefficients C_n, D_n for [illegible]

Pe	n	β_n	γ_n	C_n Br=0	C_n Br=1	D_n
10	1	0.219682 (1)	0.847124 (1)	0.126137 (1)	0.236889 (1)	-0.196235 (1)
	2	0.179137 (2)	0.294636 (2)	-0.402524	-0.581681	0.192094 (1)
	3	0.423256 (2)	0.560051 (2)	0.232657	0.336793	-0.193240 (1)
	4	0.702089 (2)	0.847617 (2)	-0.172993	-0.239637	0.196804 (1)
	5	0.995556 (2)	0.114522 (3)	0.137638	0.186200	-0.200945 (1)
	6	0.129615 (3)	0.144805 (3)	-0.115460	-0.151910	0.205151 (1)
	7	0.160070 (3)	0.175394 (3)	0.100165	0.128136	-0.209483 (1)
	8	0.1907660 (3)	0.206177 (3)	-0.890387 (-1)	-0.110897	0.214046 (1)
10^2	1	0.224018 (1)	0.912733 (1)	0.125743 (1)	0.236334 (1)	-0.193850 (1)
	2	0.208932 (2)	0.376115 (2)	-0.391823	-0.566737	0.184256 (1)
	3	0.592571 (2)	0.857707 (2)	0.224773	-0.317751	-0.180643 (1)
	4	0.117076 (3)	0.153085 (3)	-0.160316	-0.222857	0.183303 (1)
	5	0.193698 (3)	0.238806 (3)	0.129455	0.176207	-0.192136 (1)
	6	0.288292 (3)	0.342030 (3)	-0.113738	-0.151336	0.207382 (1)
	1	0.224064 (1)	0.913503 (1)	0.125733 (1)	0.236320 (1)	-0.193779 (1)
	2	0.209343 (2)	0.377464 (2)	-0.391510	-0.566302	0.183978 (1)
	3	0.595953 (2)	0.864848 (2)	0.224266	0.317056	-0.180056 (1)
	4	0.118415 (3)	0.155386 (3)	-0.159673	-0.221995	0.182384 (1)
	5	0.197397 (3)	0.244450 (3)	0.128774	0.175329	-0.191000 (1)
	6	0.296543 (3)	0.353677 (3)	-0.113159	-0.150651	0.206339 (1)

Note: The numbers in parentheses reprent $10^{(n)}$.

Table 5 Nusselt Numbers for [illegible] 1, K [illegible] 1, [illegible]

Ha [illegible] 0

x	Br 0: Nu_2	Br 0: Nu_1	(Ha = 0) -1: Nu_2	(Ha = 0) -1: Nu_1
0.001	0.0	18.7500	167.4000	18.6200
0.002	0.0	16.2000	75.6600	16.0400
0.004	0.0	12.4800	34.9600	12.2500
0.006	0.0	9.9940	23.9700	9.7080
0.008	0.0	8.2820	19.3500	7.9460
0.010	0.0	7.0700	16.8600	6.6890
0.020	0.0	4.2910	11.8900	3.7500
0.040	0.0011	2.8310	8.4230	2.1130
0.060	0.0031	2.3300	6.8200	1.5020
0.080	0.0065	2.0680	5.8550	1.1560
0.100	0.0122	1.9020	5.1980	0.9196
0.200	0.0919	1.5310	3.6420	0.2692
0.400	0.3936	1.3060	2.8160	-0.4975
0.600	0.6284	1.2130	2.5970	-1.2160
0.800	0.7683	1.1550	2.5050	-1.9710
1.000	0.8513	1.1120	2.4560	-2.7370
2.000	0.9796	1.0190	2.3840	-5.4650
5.000	0.9999	1.0000	2.3730	-6.3600
8.000	1.0000	1.0000	2.3730	-6.3640

Ha = 2

x	Nu_2	Nu_1	(Ha = 2) Nu_2	(Ha = 2) Nu_1
0.001	0.0	18.8100	185.8000	18.5800
0.002	0.0	16.2800	90.0000	15.9800
0.004	0.0	12.5700	45.8700	12.1700
0.006	0.0	10.0900	32.9900	9.6040
0.008	0.0	8.3810	27.1000	7.8240
0.010	0.0	7.1710	23.6900	6.5510
0.020	0.0	4.3870	16.2500	3.5590
0.040	0.0010	2.9100	11.0900	1.8630
0.060	0.0029	2.3960	8.8050	1.2160
0.080	0.0063	2.1230	7.4690	0.8407
0.100	0.0118	1.9500	6.5770	0.5794
0.200	0.0901	1.5590	4.5120	-0.1817
0.400	0.3914	1.3190	3.3990	-1.1830
0.600	0.6281	1.2200	3.0790	-2.1870
0.800	0.7693	1.1570	2.9390	-3.2770
1.000	0.8530	1.1130	2.8640	-4.4100
2.000	0.9808	1.0180	2.7530	-8.5790
5.000	0.9999	1.0000	2.7360	-9.9250
8.000	1.0000	1.0000	2.7360	-9.9300

Table 5 Continued

Ha 6

[illegible] 0 -1

	Nu_2	Nu_1	Nu_2	Nu_1
0.001	0.0	16.2600	329.1001	15.1400
0.002	0.0	14.5100	179.5000	13.2500
0.004	0.0	11.8000	102.1000	10.3000
0.006	0.0	9.8580	75.8100	8.1680
0.008	0.0	8.4380	62.2800	6.5900
0.010	0.0	7.2790	53.8500	5.4010
0.020	0.0	4.7300	34.9400	2.3340
0.040	0.0	3.1840	22.6900	0.3765
0.060	0.0023	2.6190	17.6200	-0.4494
0.080	0.0057	2.3110	14.7400	-0.9709
0.100	0.0111	2.1110	12.8700	-1.3640
0.200	0.0877	1.6500	8.6040	-2.7270
0.400	0.3905	1.3580	6.1940	-5.0670
0.600	0.6324	1.2380	5.4160	-7.7680
0.800	0.8615	1.1630	5.0570	-10.9100
1.000	0.9845	1.1120	4.8630	-14.3300
2.000	1.0000	1.0150	4.5900	-27.3200
5.000	1.0000	1.0000	4.5560	-31.0000
8.000	1.0000	1.0000	4.5560	-31.0000

Ha = 10

0.001	0.0	13.6000	511.7000	10.8600
0.002	0.0	12.5000	294.3999	9.5970
0.004	0.0	10.6900	169.1000	7.5120
0.006	0.0	9.3000	124.1000	5.8830
0.008	0.0	8.2100	100.0000	4.5960
0.010	0.0	7.3490	85.9600	3.5660
0.020	0.0	4.9480	54.1500	0.5918
0.040	0.0	3.3570	34.7500	-1.6120
0.060	0.0023	2.7500	26.9300	-2.6320
0.080	0.0057	2.4160	22.5400	-3.3180
0.100	0.0877	2.1980	19.6800	-3.8610
0.200	0.3905	1.6940	13.1400	-5.9370
0.400	0.6325	1.3760	9.3440	-9.9180
0.600	0.7769	1.2430	8.0690	-14.7400
0.800	0.7769	1.1640	7.4750	-20.4400
1.000	0.8615	1.1100	7.1540	-26.6800
2.000	0.9845	1.0130	6.7130	-49.6900
5.000	1.0000	1.0000	6.6630	-55.4100
8.000	1.0000	1.0000	6.6630	-55.4200

Table 6 Nusselt Numbers for [illegible]$_0$ = 1, k = 1, Pe = 100

Ha = 0

	Br = 0		Br = −1	
[illegible]	Nu_2	Nu_1	Nu_2	Nu_1
0.001	0.0	6.7620	99.8000	6.4370
0.002	0.0	6.1070	51.5600	5.7440
0.004	0.0	5.1590	28.4300	4.7330
0.006	0.0	4.5260	21.4200	4.0510
0.008	0.0	4.0850	18.0800	3.5700
0.010	0.0	3.7640	16.0600	3.2140
0.020	0.0	2.9350	11.4200	2.2690
0.040	0.0	2.3340	8.0850	1.5340
0.060	0.0	2.0590	6.5770	1.1680
0.080	0.0	1.8910	5.6680	0.9273
0.100	0.0	1.7750	5.0460	0.7484
0.200	0.0676	1.4860	3.5590	0.1942
0.400	0.3981	1.2920	2.7900	-0.5461
0.600	0.6393	1.2060	2.5870	-1.2700
0.800	0.7773	1.1500	2.5000	-2.0360
1.000	0.8579	1.1080	2.4530	-2.8100
2.000	0.9810	1.0180	2.3840	-5.5140
5.000	0.9999	1.0000	2.3730	-6.3600
8.000	1.0000	1.0000	2.3730	-6.3640

Ha = 2

0.001	0.0	7.0600	131.6000	6.5160
0.002	0.0	6.3870	71.4300	5.7920
0.004	0.0	5.4080	40.6300	4.7290
0.006	0.0	4.7480	30.6100	4.0050
0.008	0.0	4.2850	25.6200	3.4090
0.010	0.0	3.9450	22.5300	3.1080
0.020	0.0	3.0640	15.4500	2.0840
0.040	0.0	2.4200	10.5900	1.2810
0.060	0.0	2.1270	8.4660	0.8769
0.080	0.0	1.9470	7.2190	0.6073
0.100	0.0	1.8230	6.3810	0.4029
0.200	0.065[illegible]	1.5130	4.4150	-0.2637
0.400	0.394[illegible]	1.3040	3.3660	-1.2440
0.600	0.6385	1.2120	3.0650	-2.2610
0.800	0.7782	1.1520	2.9310	-3.3700
1.000	0.8596	1.1080	2.8580	-4.5190
2.000	0.9821	1.0170	2.7520	-8.6550
5.000	0.9999	1.0000	2.7360	-9.9250
8.000	1.0000	1.0000	2.7360	-9.9300

Table 6 Continued

Ha = 6

Pr	0		1	
x	Nu_2	Nu_1	Nu_2	Nu_1
0.001	0.0	8.1000	256.0001	6.3220
0.002	0.0	7.3630	153.0000	5.4790
0.004	0.0	6.2670	91.6100	4.2160
0.006	0.0	5.5130	69.2200	3.3350
0.008	0.0	4.9470	57.3700	2.6940
0.010	0.0	4.5730	49.8700	2.2100
0.020	0.0	3.5090	32.7500	0.8752
0.040	0.0	2.7210	21.6200	-0.2227
0.060	0.0	2.3580	16.9600	-0.8109
0.080	0.0	2.1370	14.3000	-1.2290
0.100	0.0	1.9840	12.5300	-1.5660
0.200	0.0603	1.6020	8.4510	-2.8430
0.400	0.2908	1.3430	6.1320	-5.1960
0.600	0.6418	1.2290	5.3830	-7.9610
0.800	0.7855	1.1570	5.0360	-11.1800
1.000	0.8679	1.1070	4.8490	-14.6700
2.000	0.9358	1.0140	4.5870	-27.5700
5.000	1.0000	1.0000	4.5560	-30.9900
8.000	1.0000	1.0000	4.5560	-31.0000

Ha = 10

0.001	0.0	8.8310	364.6001	5.4220
0.002	0.0	8.0370	230.0000	4.4810
0.004	0.0	6.8500	141.7000	3.0570
0.006	0.0	6.0260	107.6000	2.0490
0.008	0.0	5.4310	89.1500	1.3080
0.010	0.0	4.9860	77.3400	0.7414
0.020	0.0	3.7910	50.4300	-0.8600
0.040	0.0	2.8990	33.1500	-2.2410
0.060	0.0	2.4900	26.0000	-3.0240
0.080	0.0	2.2410	21.9100	-3.6060
0.100	0.0	2.0700	19.2100	-4.0940
0.200	0.0597	1.6450	12.9300	-6.0900
0.400	0.3939	1.3590	9.2500	-10.1300
0.600	0.6480	1.2350	8.0160	-15.0800
0.800	0.7923	1.1570	7.4390	-20.9500
1.000	0.8743	1.1050	7.1290	-27.3400
2.000	0.9877	1.0120	6.7090	-50.1300
5.000	1.0000	1.0000	6.6630	-55.4100
8.000	1.0000	1.0000	6.6630	-55.4200

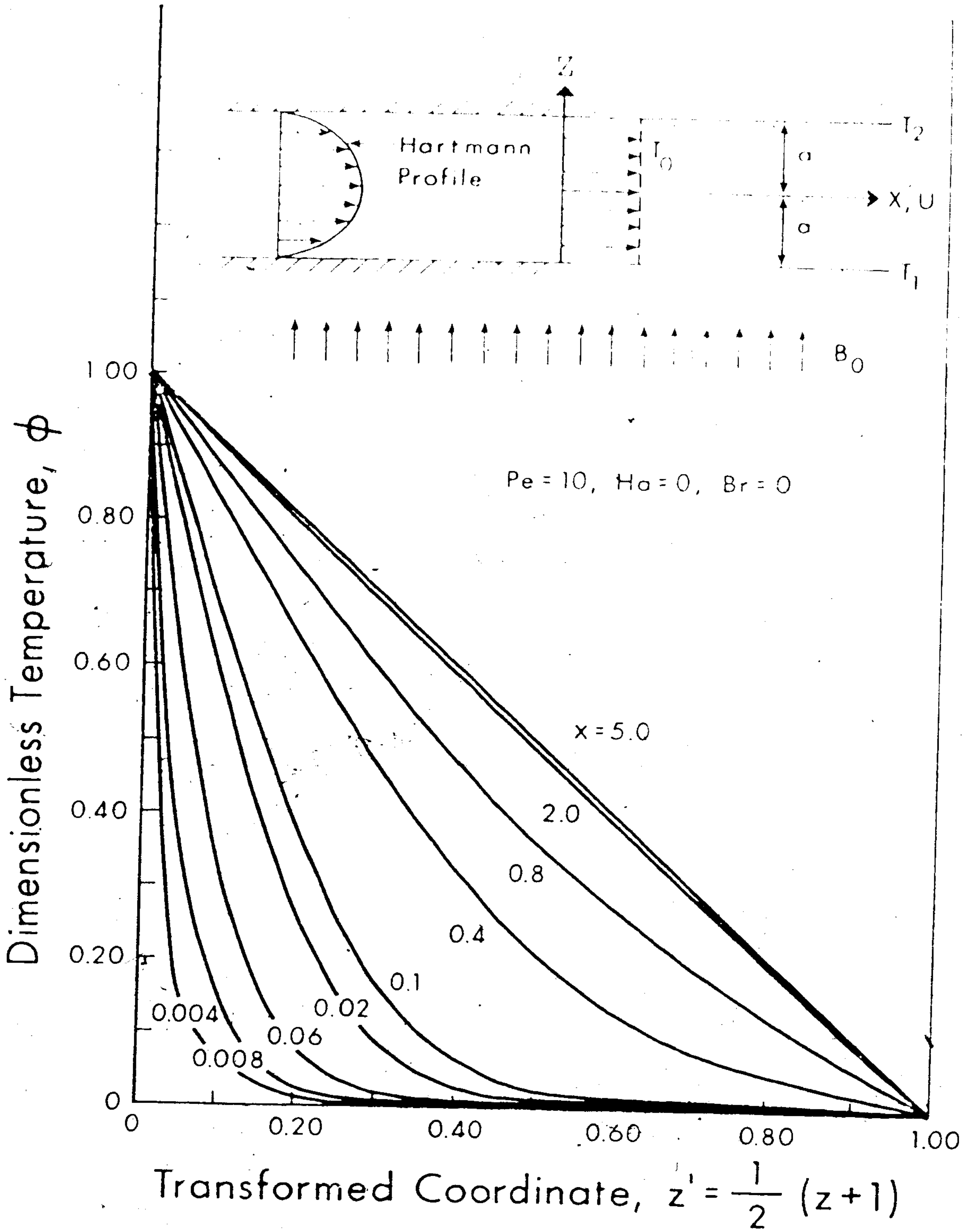

Fig. 1 Coordinate System for MHD channel flow and developing temperature profiles for Pe = 10, Ha = 0 and Br = 0

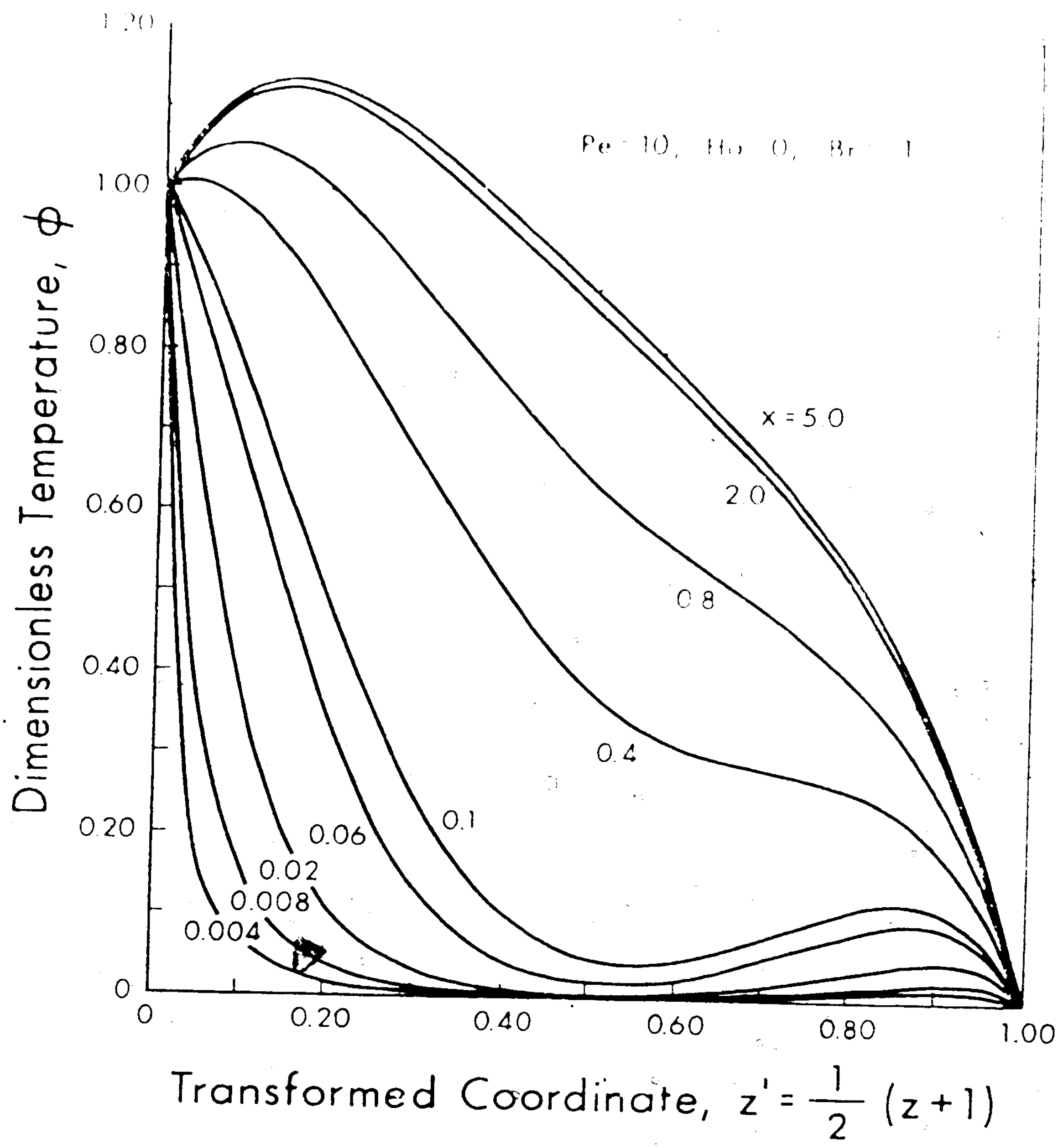

Fig. 2 Developing temperature profiles for Pe = 10, Ha = 0 and Br = - 1

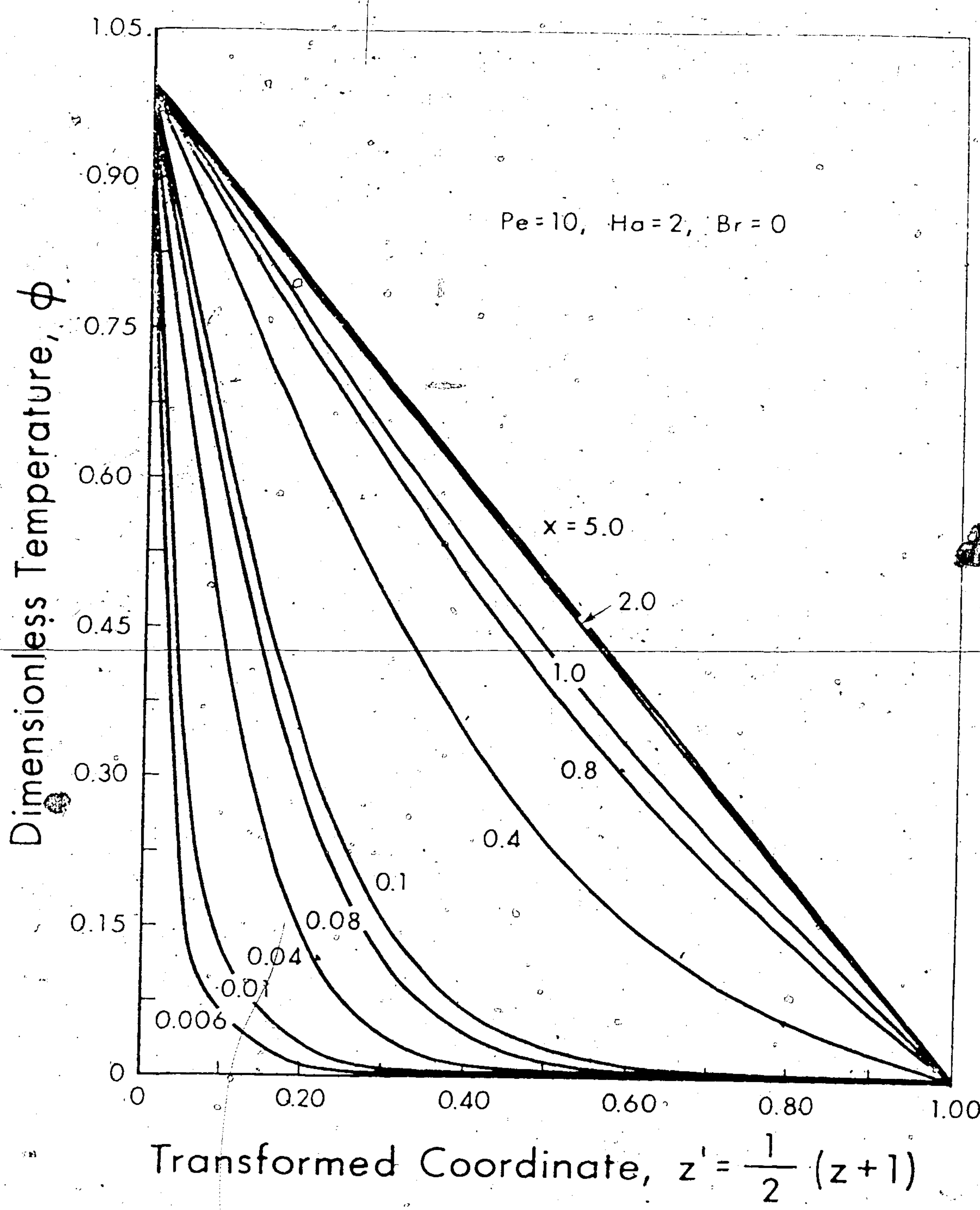

Fig. 3 Developing temperature profiles for Pe = 10, Ha = 2 and Br = 0

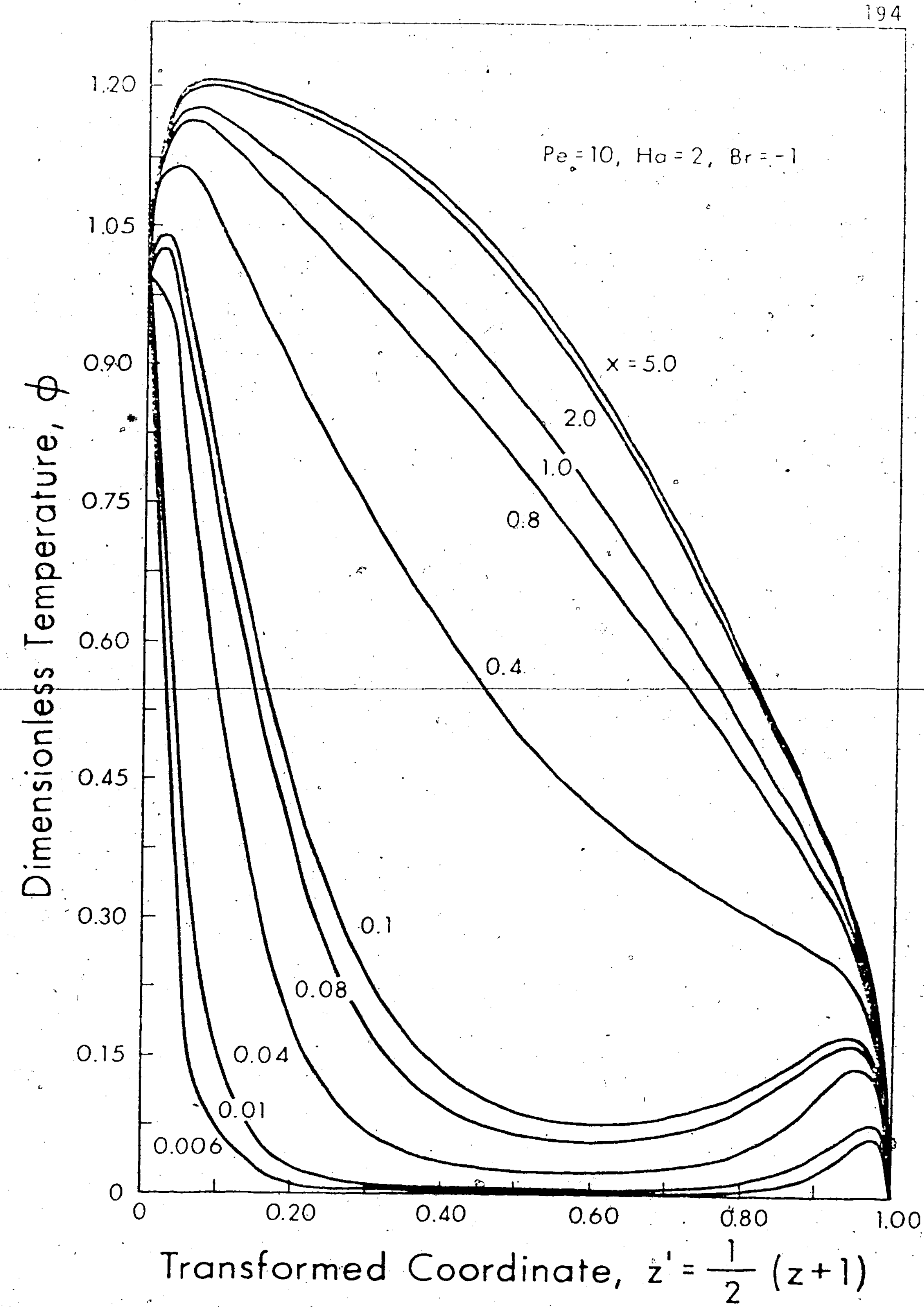

Fig. 4 Developing temperature profiles for Pe = 10, Ha = 2 and Br = - 1

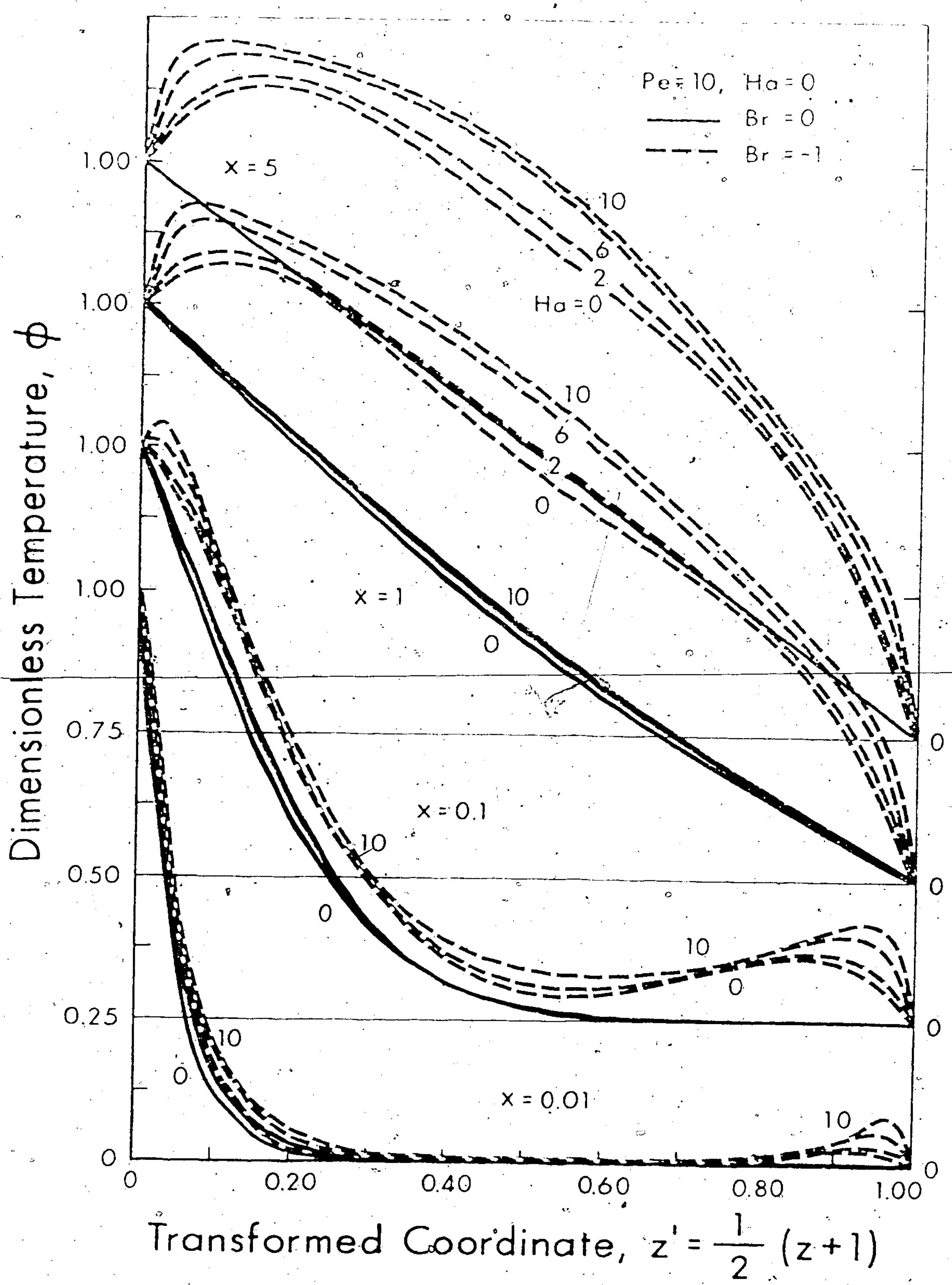

Fig. 5 Developing temperature profiles for Pe = 10 and Br = 0, -1 with Hartmann number as parameter

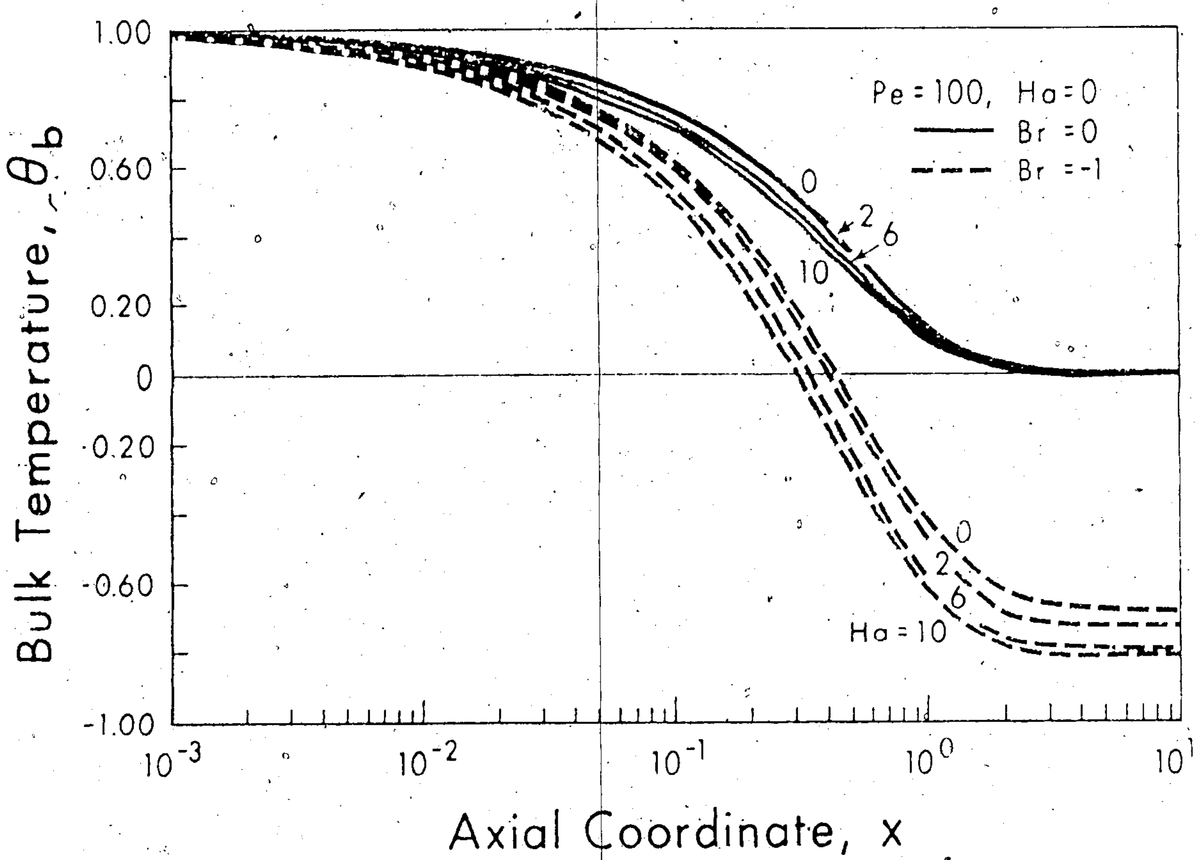

Fig. 6 Axial bulk temperature distributions for Pe = 100 and Br = 0, -1 with Hartmann number as parameter

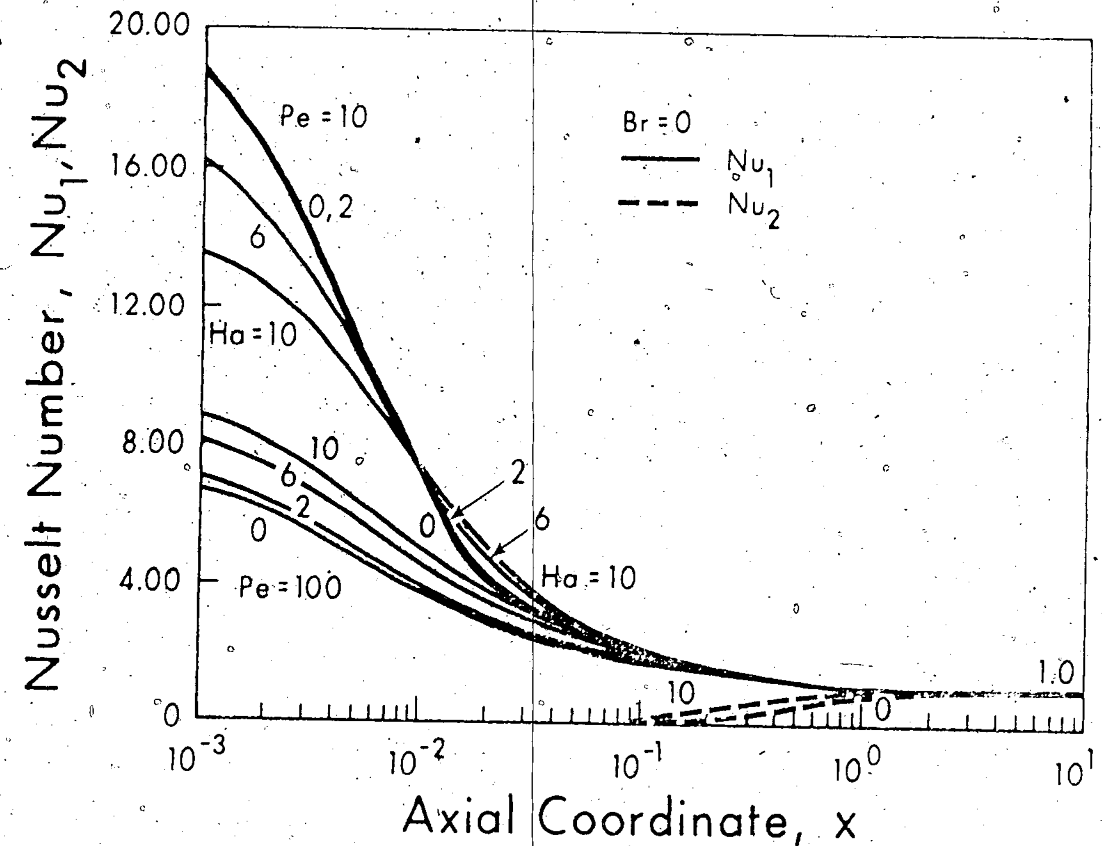

Fig. 7 Hartmann number effect on local Nusselt number results for Pe = 10, 10^2 and Br = 0

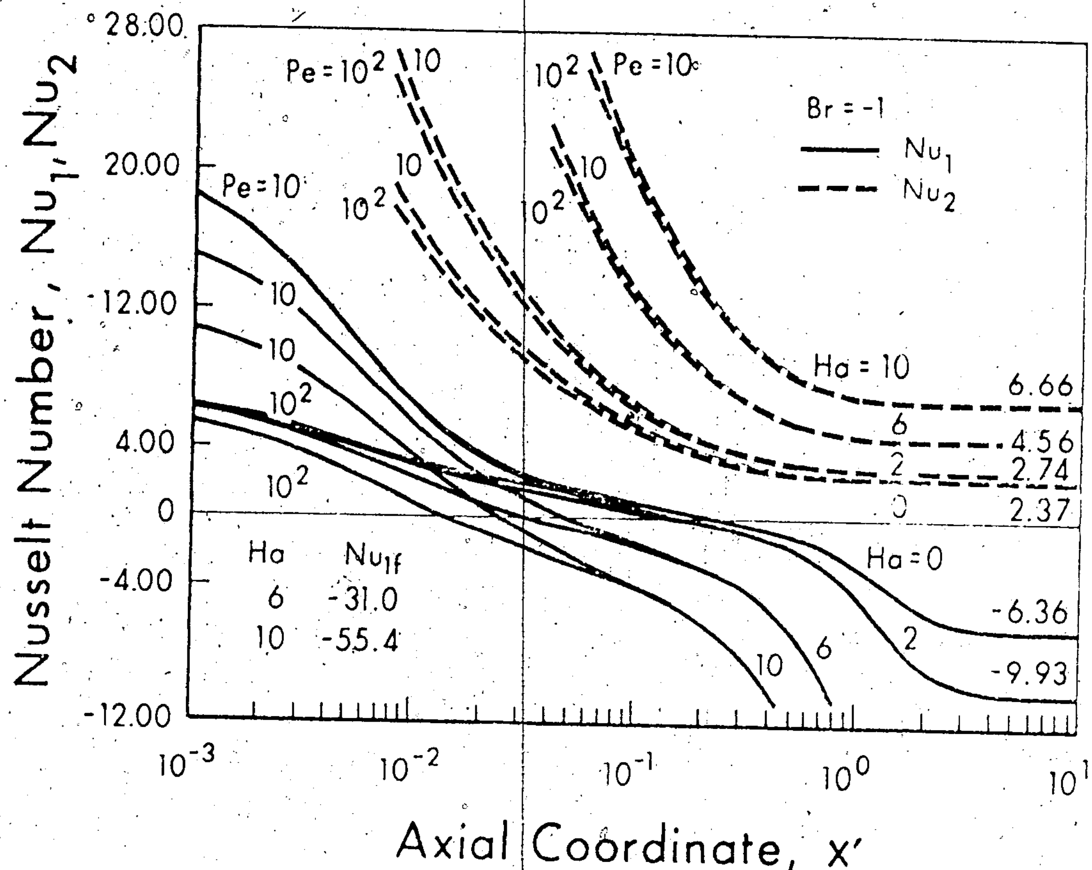

Fig. 8 Hartmann number effect on local Nusselt number results for Pe = 10, 10^2 and Br = - 1

CHAPTER VII

THERMAL INSTABILITY OF HARTMANN FLOW IN THE THERMAL ENTRANCE REGION OF HORIZONTAL PARALLEL-PLATE CHANNELS HEATED FROM BELOW

The onset of instability in the form of longitudinal vortices for fully developed Hartmann laminar flow in the thermal entrance region of horizontal parallel-plate channels is investigated by a numerical method for the case with a uniform vertical magnetic field and heating from below. Numerical results are obtained for Pr = 0.7, 0.01, Pe = 10, 100, ∞, Br = 0, -1, and Ha = 0, 2, 6, 10. The effects of Prandtl, Peclet (axial conduction), Brinkman (viscous dissipation and Joule heating) and Hartmann numbers on thermal instability of magnetohydrodynamic flow are studied.

Nomenclature

a	=	dimensionless wave number
$\overline{B}$	=	magnetic field induction vector, $(0,0,B_0)$
Br	=	Brinkman number, $\mu_f U_m^2/(k\theta_c)$
$\overline{b}$	=	dimensionless perturbation vector of impressed magnetic field, (b_x,b_y,b_z)
C_n, D_n	=	coefficients in the series expansion of θ_e
c_p	=	specific heat at constant pressure
D	=	d/dz
$\overline{E}$	=	electric field intensity vector, $(0,E_0,0)$
E_n, O_n	=	even and odd eigenfunctions
$\overline{e}$	=	dimensionless perturbation vector of electric field, (e_x,e_y,e_z)
Gr	=	Grashof number, $g\beta(\Delta T)\ell^3/\nu^2$
g	=	gravitational acceleration
Ha	=	Hartmann nu[illegible]$\mu_f)^{1/2}B_0\ell$
$\overline{J}$	=	electric cu[illegible]y vector, $(0,J_y,0)$
J_0	=	$\sigma B_0 U_m J$
$\overline{j}$	=	dimensionless perturbation vector of $\overline{J}$, (j_x,j_y,j_z)

K = external loading parameter, $E_0/(B_0U_m)$

k = thermal conductivity

L = a distance between two infinite horizontal flat plates

ℓ = $L/2$

M = number of divisions in z direction

P, P_b = fluid pressure $(P_b + P')$ and pressure for basic flow

Pe = Peclet number, $PrRe$

Pr = Prandtl number, $c_p\mu_f/k$

p = dimensionless perturbation pressure, $P'/(\rho U_m^2)$

Ra = Rayleigh number, $g\beta\Delta T\ell^3/\nu\alpha$

Re = Reynolds number, $\rho U_m\ell/\mu_f$

Rm = magnetic Reynolds number, $U_m\ell/(1/\mu_e\sigma)$

T, T_b, T_0 = fluid temperature $(T_b + \theta')$, fluid temperature of basic flow and uniform entrance temperature

T_1, T_2, T_m = uniform but different lower and upper plate temperatures, and $(T_1 + T_2)/2$

U_b, U_m, u_b = axial, mean and dimensionless velocities of basic flow

u, v, w = dimensionless perturbation velocity components

V, V_b, V'	=	velocity vector ($V_b + V'$), basic velocity vector (U_b,0,0) and perturbation velocity vector (U',V',W')
X, Y, Z	=	Cartesian coordinates with origin at lower plate
x, y, z	=	dimensionless coordinates
$\bar{x}, \bar{z}$	=	transformed coordinates, x/Pe, $\bar{z} = z$
Z', z'	=	dimensional and dimensionless transverse coordinates with origin at centre of channel
α	=	thermal diffusivity
β	=	coefficient of thermal expansion
β_n, γ_n	=	even and odd eigenvalues
$\theta, \theta_b, \theta_0$	=	dimensionless perturbation, basic flow and entrance temperatures
$\theta_c, \theta_e, \theta_f$	=	characteristic temperature difference $(T_2 - T_m) = (T_2 - T_1)/2$, and dimensionless fluid temperatures defined by eq. (7)
μ_e, μ_f	=	magnetic permeability and viscosity of fluid
ν	=	kinematic viscosity
ρ	=	fluid density
σ	=	electric conductivity
Φ	=	viscous dissipation function

ϕ_U, ϕ_θ = dimensionless basic velocity and temperature profiles, U_b/U_m and $(T_b - T_2)/\Delta T$

Ψ = dimensionless stream function

ΔT = $(T_1 - T_2) = -2\theta_c$

Superscripts and Subscripts

$'$ = perturbation quantity

$+$ = amplitude of disturbance quanity

$*$ = transformed perturbation variable or critical value

b = basic quantity in unperturbed state

k = space subscript of a grid point

7.1 Introduction

In recent years, the problem of the laminar forced convection for fully developed MHD laminar flow in the thermal entrance region of a parallel-plate channel has been studied by many investigators for the thermal boundary conditions of both uniform wall heat flux and constant wall temperature. The literature on the subject is well reviewed in [1,2] and in Chapter VI. It is known that when a horizontal fluid layer is subjected to an adverse temperature gradient, a top-heavy situation results and the system is potentially unstable due to the buoyancy forces. With a superposed fully developed laminar flow between two horizontal flat plates, heated from below, the onset of the ~~secondary flow in the form of longtiudinal vortices [3-7]~~ is characterized by a critical Rayleigh number. With the appearance of the vortex rolls, the flow takes on a three-dimensional character and the heat transfer rate is expected to increase with the Rayleigh number. Thus, it is of practical interest to determine the conditions for the onset of secondary flow.

The effects of a vertical, uniform magnetic field on the thermal instability of horizontal stationary fluid layers were studied theoretically by Thompson [8] and Chandrasekhar [9,10] and experimentally by Nakagawa [11-14]. The thermal instability of a magnetofluid in a vertical rectangular channel heated from below was investigated by Yu [15] quoting the related references. The thermal instability of a Hartmann flow in the thermal entrance region of a horizontal parallel-plate channel with heating from below does not appear to have been studied in the past. The purpose of this study is to determine the conditions marking the onset of longitudinal vortex rolls in the said passage where the two plates are maintained at uniform but different surface temperatures. The present study can be regarded as a first step toward investigating the change of heat transfer rate due to the thermal instability for a Hartmann flow and represents an extension of the thermal instability problem for a confined horizontal fluid layer studied by Thompson [8] and Chandrasekhar [9.10] to the case with a superposed fully developed laminar flow. The basic velocity and temperature fields in the thermal entrance region of the channel required for the present thermal instability analysis are reported in Chapter VI.

7.2 Formulation of the Thermal Instability Problem

7.2.1. Basic Flow and Temperature Fields

Consideration is given to a Hartmann flow between two horizontal flat plates under the action of a homogeneous transverse magnetic field B_0 and heated from below. The basic equations of motion, of Maxwell, and of energy appropriate to the thermal entrance region heat transfer problem [3] are:

$$\nabla \cdot \overline{V}_b = 0 \tag{1}$$

$$(V_b\cdot\nabla)V_b = -\frac{1}{\rho}\nabla P_b + \nu\nabla^2 V_b + \frac{1}{\rho} J \times B \qquad (2)$$

$$\nabla\cdot B = 0,\ \nabla\times B = \mu_e J,\ \nabla\cdot E = 0,\ \nabla\times E = 0,\ J = \sigma(E + V_b\times B) \qquad (3)$$

$$\rho c_p(V_b\cdot\nabla)T_b = k\nabla^2 T_b + \Phi + \frac{1}{\sigma}(J\cdot J) \qquad (4)$$

where $\vec{V}_b = (U_b,0,0)$, $\vec{J} = (0, J_y = \sigma(E_0 - UB_0), 0)$, $\vec{E} = (0,E_0,0)$, $\vec{B} = (0,0,B_0)$, $\Phi = \mu_f(dU_b/dZ')^2$ and $\nabla^2 = \partial^2/\partial X^2 + \partial^2/\partial Z'^2$ in energy equation (4) and the coordinate system is defined in Fig. 1. The boundary conditions are:

$$U_b(0,\pm\ell) = 0,\ T_b(0,Z') = T_0,\ T_b(X,-\ell) = T_1,\ T_b(X,\ell) = T_2 \qquad (5)$$

Introducing the following dimensionless variables and physical parameters, $(X,Z') = [\ell](x\,Re, z')$, $U_b = [U_m](u_b)$, $\theta_b' = (T_b - T_m)/(T_2 - T_m)$, $\theta_0 = (T_0 - T_m)/(T_2 - T_m)$, $Re = \rho U_m\ell/\mu_f$, $Pe = PrRe = \rho c_p U_m \ell/k$, $Ha = (\sigma/\mu_f)^{1/2} B_0\ell$, $K = E_0/(B_0U_m)$, $Br = \mu_f U_m^2/(k\theta_c)$, where $U_m = \int_{-\ell}^{\ell} U_b dZ'/(2\ell)$, $T_m = (T_1 + T_2)/2$, $\theta_c = T_2 - T_m = (T_2 - T_1)/2$, the well known Hartmann solution [16] for equation (2) and the solution of energy equation (4) considering both the viscous dissipation and axial conduction effects can be written as

$$u_b = Ha(\cosh Ha - \cosh Ha\, z')/(Ha \cosh Ha - \sinh Ha)$$

$$= C_1(\cosh Ha - \cosh Ha\, z') \qquad (6)$$

$$\theta_b = \theta_f(z') + \theta_e(x, z') \qquad (7)$$

where $\theta_f = z' + Br[(C_1^2/4)(\cosh 2Ha - \cosh 2Ha\, z') + 2\, C_1 C_2(\cosh Ha - \cosh Ha\, z) + (C_2^2\, Ha^2/2)(1 - z'^2)]$, $C_2 = K - C_1 \cosh Ha$, $\theta_e = \sum_{n=1}^{\infty} C_n E_n(z')\exp(-\beta_n x) + \sum_{n=1}^{\infty} D_n O_n(z') \exp(-\gamma_n x)$. The details of the infinite series solution for θ are given in Chapter VI and the expression for θ is given here for reference purpose only. At this point, it is convenient to shift the coordinate origin to the bottom plate for the instability problem and one obtains $z = \frac{1}{2}(z' + 1)$ and the developing temperature profile $\phi_0 = \frac{1}{2}(1 - \theta_b)$.

7.2.2 Perturbation Equations

In order to study the thermal instability concerned with the onset of secondary flow in the form of longitudinal vortices for the horizontal Hartmann flow heated from below, the perturbation quantities are superimposed on the basic quantities as

$$\overline{V} = \overline{V}_b + \overline{V}' = [U_b(Z) + U', V', W'],\ T = T_b + \theta',\ P = P_b + P'$$

$$\bar{E} = \bar{E}_b + \bar{e}' = (e_x', E_0 + e_y', e_z'), \quad \bar{B} = \bar{B}_b + \bar{b}'$$

$$= (b_x', b_y', B_0 + b_z') \tag{8}$$

$$\bar{J} = \bar{J}_b + \bar{j}' = (j_x', J_0 + j_y', j_z')$$

The above perturbation quantities are considered to be in the steady state and are of a function of space variables X, Y and Z only. After applying the linear stability theory and using Boussinesq approximation, the perturbation equations become:

$$\frac{\partial U'}{\partial X} + \frac{\partial V'}{\partial Y} + \frac{\partial W'}{\partial Z} = 0 \tag{9}$$

$$\rho(U_b \frac{\partial U'}{\partial X} + W' \frac{dU_b}{dZ}) = - \frac{\partial P'}{\partial X} + \mu_f \nabla^2 U' + (J_0 b_z' + B_0 j_y') \tag{10}$$

$$\rho U_b \frac{\partial V'}{\partial X} = - \frac{\partial P'}{\partial Y} + \mu_f \nabla^2 V' - B_0 j_x' \tag{11}$$

$$\rho U_b \frac{\partial W'}{\partial X} = - \frac{\partial P'}{\partial Z} + \mu_f \nabla^2 W' - J_0 b_x' + \rho g \beta \theta' \tag{12}$$

$$\rho c_p (U_b \frac{\partial \theta'}{\partial X} + U' \frac{\partial T_b}{\partial X} + W' \frac{\partial T_b}{\partial Z}) = k \nabla^2 \theta'$$

$$+ 2\mu_f (\frac{dU_b}{dZ})(\frac{\partial U'}{\partial Z}) + 2 \frac{J_0}{\sigma} j_y' \tag{13}$$

$$j_x' = \sigma(e_x' + B_0V'),\ j_y' = \sigma(e_y' - B_0U' - U_b b_z'),\ j_z' = \sigma(e_z' + U_b b_y') \tag{14}$$

$$\nabla \cdot \bar{e}' = 0,\ \nabla X \bar{e}' = 0,\ \nabla \cdot \bar{b}' = 0,\ \nabla X \bar{b}' = \mu_e \bar{j}' \tag{15}$$

where $\nabla^2 = \partial^2/\partial X^2 + \partial^2/\partial Y^2 + \partial^2/\partial Z^2$.

Introducing the following non-dimensional quantities and physical parameters,

$$(X,Y,Z) = L(x,y,z),\ (U',V',W') = U_m(u,v,w),\ \theta' = (\Delta T)\theta$$

$$P' = (\rho U_m^2)p,\ (b_x', b_y', b_z') = B_0(b_x, b_y, b_z),\ (e_x', e_y', e_z')$$

$$= E_0(e_x, e_y, e_z),\ (j_x', j_y', j_z') = \sigma B_0 U_m(j_x, j_y, j_z)$$

$$Gr = \frac{g\beta(\Delta T)\ell^3}{\nu^2},\ Rm = U_m\ell/(1/\mu_e\sigma)$$

and noting that $U_b = U_m\phi_u$, $T_b - T_2 = (\Delta T)\phi_\theta$, $J_0 = \sigma B_0 U_m J = \sigma B_0 U_m(K - \phi_u)$, $\Delta T = (T_1 - T_2) = -2\theta_c$, the perturbation equations become

$$\frac{\partial u}{\partial x} + \frac{\partial v}{\partial y} + \frac{\partial w}{\partial z} = 0 \tag{16}$$

$$\phi_u \frac{\partial u}{\partial x} + w \frac{d\phi_u}{dz} = - \frac{\partial p}{\partial z} + \frac{1}{2Re} \nabla^2 u + \frac{2Ha^2}{Re} (Jb_z + j_y) \tag{17}$$

$$\phi_u \frac{\partial v}{\partial x} = - \frac{\partial p}{\partial y} + \frac{1}{2Re} \nabla^2 v - \frac{2Ha^2}{Re} j_x \tag{18}$$

$$\phi_u \frac{\partial w}{\partial x} = - \frac{\partial p}{\partial z} + \frac{1}{2Re} \nabla^2 w - \frac{2Ha^2}{Re} Jb_x + \frac{2Gr}{Re^2} \theta \tag{19}$$

$$2Pe[\phi_u \frac{\partial \theta}{\partial x} + u \frac{\partial \phi_\theta}{\partial x} + w \frac{\partial \phi_\theta}{\partial z}] = \nabla^2 \theta - Br[\frac{d\phi_u}{dz} \frac{du}{dz} + 4Ha^2 Jj_y] \tag{20}$$

$$j_x = Ke_x + v, \; j_y = Ke_y - u - \phi_u b_z, \; j_z = Ke_z + \phi_u b_y \tag{21}$$

$$\nabla \cdot \overline{e} = 0 \; (a), \; \nabla X \overline{e} = 0 \; (b), \; \nabla \cdot \overline{b} = 0 \; (c), \; \nabla X \overline{b} = 2Rm \overline{j} \; (d) \tag{22}$$

Here it is understood that the operators ∇^2 and ∇ are dimensionless.

After eliminating u, v, p and using continuity equation, the three momentum equations can be combined into a single equation as

$$\nabla^2 \nabla^2 w - 4Ha^2 \frac{\partial^2 w}{\partial z^2} - 2Re[\phi_u \frac{\partial}{\partial x} \nabla^2 w - \frac{\partial w}{\partial x} \frac{d^2 \phi_u}{dz^2}] = - \frac{4Gr}{Re} \nabla_1^2 \theta$$

$$+ 4Ha^2 [J(\nabla_1^2 b_x + \frac{\partial^2 b_z}{\partial x \partial z}) - 2 \frac{d\phi_u}{dz} \frac{\partial b_z}{\partial x} - \phi_u \frac{\partial^2 b_z}{\partial x \partial z}] \tag{23}$$

where $\nabla_1^2 = \partial^2/\partial x^2 + \partial^2/\partial y^2$.

From equations (20), (23) and noting further that for vortex-type instability $\partial p/\partial x = 0$, one has 7 unknowns u, w, θ, b_x, b_z, j_y and e_y. Consequently, one needs additionally one momentum equation, Ohm's law, two magnetic induction equations and one electric field equation as follows.

$$\nabla^2 u - 2Re\,\phi_u \frac{\partial u}{\partial x} = 2Re\,w \frac{d\phi_u}{dz} - 4Ha[(K - \phi_u)b_z + j_y] \tag{24}$$

$$j_y = Ke_y - u - \phi_u b_z \tag{25}$$

$$\nabla^2 b_x - 2Rm\,\phi_u \frac{\partial b_x}{\partial x} = -2Rm[\frac{\partial u}{\partial z} + \frac{d\phi_u}{dz} b_z] \tag{26}$$

$$\nabla^2 b_z - 2Rm\,\phi_u \frac{\partial b_z}{\partial x} = -2Rm \frac{\partial w}{\partial z} \tag{27}$$

$$\nabla^2 e_y = 0 \tag{28}$$

The boundary conditions are

$$u = w = \frac{\partial w}{\partial z} = \theta = 0 \quad \text{at } z = 0,1 \quad \text{(rigid walls)}$$

$$j_z = 0 \quad \text{at } z = 0,1 \quad \text{(non-conducting walls)} \tag{29}$$

For the disturbances in the form of longitudinal vortices, one may assume the disturbance form [6] $f = f^+(z)e^{iay}$ for the disturbance quantities. The set of equations then becomes:

$$(D^2 - a^2)^2 w^+ - 4Ha^2 D^2 w^+ = 4Ha^2[(K - \phi_u)(-a^2)b_x{}^+] + \frac{4Gr}{Re} a^2 \theta^+ \tag{30}$$

$$(D^2 - a^2)u^+ - 4Ha^2 u^+ = 2Re \frac{d\phi_u}{dz} w^+ - 4Ha^2[(K - 2\phi_u)b_z{}^+] \tag{31}$$

$$(D^2 - a^2)\theta^+ = 2Pe[u^+ \frac{\partial\phi_\theta}{\partial x} + w^+ \frac{\partial\phi_\theta}{\partial z}] + Br[\frac{d\phi_u}{dz} Du^+ - 4Ha^2(K - \phi_u)j_y{}^+] \tag{32}$$

$$j_y{}^+ = Ke_y{}^+ - u^+ - \phi_u b_z{}^+ \tag{33}$$

$$(D^2 - a^2)b_x{}^+ = - 2Rm(Du^+ + \frac{d\phi_u}{dz} b_z{}^+) \tag{34}$$

$$(D^2 - a^2)b_z{}^+ = - 2Rm\, Dw^+ \tag{35}$$

$$(D^2 - a^2)e_y{}^+ = 0 \tag{36}$$

where $D = d/dz$, $\nabla^2 = D^2 - a^2$ and $\nabla_1^2 = -a^2$. A study of the electromagnetic boundary conditions is now in order. When the magnetic Reynolds number Rm is very small, an order of magnitude analysis reveals that the right-hand sides of equations (34) and (35) can be neglected. From Maxwell's equations and equations (34), (36) and (29) it can be shown that $e_x^+ = e_y^+ = e_z^+ = b_x^+ = 0$ for the whole domain and the details are given in Appendix IV. It is convenient to introduce the transformations $x = Pe\bar{x}$, $z = \bar{z}$, $u^+ = Reu^*$, $w^+ = w^*$, $\theta^+ = Pe\theta^*$, $j_y^+ = Rej_y^*$, $b_z^+ = Rmb_z^*$ and one obtains

$$[(D^2 - a^2)^2 - 4Ha^2D^2]w^* = 4Ra\ a^2\theta^* \tag{37}$$

$$[(D^2 - a^2) - 4Ha^2]u^* = 2\ \frac{d\phi_u}{dz}\ w^* - [4Ha^2(K - 2\phi_u)\ \frac{Rm}{Re}\ b_z^*] \tag{38}$$

$$(D^2 - a^2)\theta^* = 2[\frac{u^*}{Pr}\ \frac{\partial\phi_\theta}{\partial\bar{x}} + w^*\ \frac{\partial\phi_\theta}{\partial\bar{z}}] + \frac{Br}{Pr}\ [Re\ \frac{d\phi_u}{d\bar{z}}\ Du^*$$

$$- 4Ha^2(K - \phi_u)j_y^*] \tag{39}$$

$$j_y^* = -u^* - [\phi_u\ \frac{Rm}{Re}\ b_z^*] \tag{40}$$

Since Rm/Re is very small, the terms involving Rm/Re in equations (38) and (40) can be neglected [17] entirely in comparison with the other terms. Thus, one sees that the present eigenvalue problem can be solved independently of the boundary conditions on the magnetic field. The physical parameters are seen to be Pr, Pe, Br, Ha and Ra. The boundary conditions are

$$u^* = w^* = Dw^* = \theta^* = 0 \quad \text{at } \bar{z} = 0, 1 \tag{41}$$

It is instructive to note that the term $4a^2 Ra\theta^*$ in equation (37) represents the effect of buoyancy forces and is balanced by the viscous term $(D^2 - a^2)^2 w^*$ and the Lorentz force term $(-4Ha^2 D^2 w^*)$. In equation (38) the inertia term $w^* \, \partial\phi_u/\partial z$ is caused by the coupled effect of upward disturbance velocity w^* and the vertical gradient of basic velocity profile function and is seen to be balanced by the viscous term $(D^2 - a^2)u^*$ and the Lorentz force term $(-4Ha^2 u^*)$. Furthermore, in energy equation (39) there are two convective motions; one is the convective term caused by the coupled effect of velocity disturbance u^* and basic temperature gradient $\partial\phi_\theta/\partial x$ in the main flow direction, and the other is the convective term caused by velocity disturbance w^* and the basic temperature gradient $\partial\phi_\theta/\partial z$ in the vertical direction. It is seen that the two convective terms, a viscous dissipation term $(Br \cdot Re/Pr \cdot d\phi_u/dz \cdot Du^*)$, and a Joule heating term $[(Br/Pr) \cdot (-4Ha^2(K - \phi_u))j_y^*]$ are balanced by the conduction term $(D^2 - a^2)\theta^*$. Equation (40) shows that the current disturbance amplitude in y-direction is simply equal to the negative velocity disturbance amplitude in x-direction. One also notes that the terms involving Ha^2 are preceded by a negative sign suggesting that the transverse magnetic field has a stabilizing effect on the instability. Without the effects of magnetic field, Joule heating and viscous dissipation, the present thermal instability problem reduces to that studied in [6]. For given values of Pr, Pe, Br and Ha, one is interested in determining the minimum critical Rayleigh number and the corresponding wave number for the onset of instability as stationary longitudinal vortices through the solution of equations (37) to (41).

7.3 Numerical Solution

In view of the expressions for the basic velocity and temperature profiles, an analytical solution of the characteristic value problem is apparently not practical. A finite-difference method using an iterative technique is used for the simultaneous solution of the disturbance equations [6]. Using the higher order finite-difference scheme due to Thomas [18], equation (37) and its boundary conditions may be transformed into a quidiagonal system of matrix for a set of algebraic equations and two tridiagonal systems result from equations (38) and (39) and their boundary conditions. Noting that for given values of Pr, Pe, Br and Ha, the basic profiles ϕ_u and ϕ_θ are known, the solution of a coupled set of equations (37) to (41) can be carried out by using an iterative procedure consisting of the following main steps:

1. At a given axial position x, a value of the wave number a is selected and an eigenvalue Ra is assumed. The disturbance velocity w_k^* is taken as $w_k^* = 2(1 - k/M)$, $k = 2,3,\ldots,M$ to conform to the primary mode of disturbance.

2. The finite-difference solution of equation (38) then yields u_k^*.

3. After knowing w_k^* and u_k^*, equation (39) is solved to obtain θ_k^*.

4. Since the right-hand side of equation (37) is now known, new value for w_k^* can be found.

5. An improved eigenvalue $(Ra)_{new}$ can be computed by using the following equation[19]:

$$(Ra)_{new} = (Ra)_{old}\left[\sum_k (w_k^*)_{old}^2\right]^{1/2} / \left[\sum_k (w_k^*)_{new}^2\right]^{1/2} \qquad (42)$$

The magnitude of the quantity w_k^* is readjusted by the following equation in order to return to the original order of magnitude for computation.

$$w_k^* = (w_k^*)_{new}\,(Ra)_{new}/(Ra)_{old} \qquad (43)$$

6. The steps (2) to (4) are repeated until the following prescribed convergence criterion is satisfied.

$$\epsilon = \sum_k |(w_k^*)_{new} - (w_k^*)_{old}| / \sum_k (w_k^*)_{new} \leq 10^{-6} \qquad (44)$$

It is found that only a few iterations are required to satisfy the above condition and five significant figures are found to be correct for critical Ra.

7.4 Results and Discussion

Before presenting the numerical results, it is well to note that the basic fully-developed velocity profile ϕ_u depends on Ha only and the basic temperature profile ϕ_θ is a function of the parameters Pe, Br and Ha and is independent of Pr. The typical profiles for ϕ_θ are shown in Chapter VI. In the perturbation equations (37) to (39), only two prescribed parameters Pr and Ha appear. The numerical results will be presented in such a way to illustrate the effects of the aforementioned physical parameters on thermal instability.

The effects of the Hartmann number on disturbance profiles w^*, θ^* and u^* are shown in Figs. 1 and 2, respectively, for fully developed condition ($\bar{x} = 10$) with Pr = 0.7, Pe = 10 and Br = 0,-1. From the normal modes of the disturbances and the definition of the stream function $v = \partial\psi/\partial z$, $w = -\partial\psi/\partial y$, one obtains $\psi = (iw^+/a)e^{iay}$ and one may compute the stream function ψ by noting that physical meaning is attached only to the real part. The results are shown in Fig. 3. In Figs. 1, 2 and 3, the magnitude of the maximum disturbance quantity is taken to be one. The neutral stability curves for $Pe = 10$, $Pr = 0.01$ and 0.7 are shown in Figs. 4 and 5, respectively, where one may see the effects of Hartmann and Brinkman numbers clearly.

The effect of Peclet number on critical Rayleigh numbers Ra^* along the axial coordinate $\bar{x}$ is shown in Figs. 6 to 9 with $Pr = 0.01$, 0.7 and $Br = 0$, -1 for $Ha = 0$, 2, 6 and 10. In Fig. 6 ($Ha = 0$) with $Pr = 0.7$, the critical Ra^* is seen to decrease monotonically with $\bar{x}$ until an asymptotic value is approached. On the other hand, with $Pr = 0.01$ and $Br = -1$, a local maximum value for Ra^* exists at a certain axial location before reaching the asymptotic value. Furthermore, the region near the thermal entrance ($\bar{x} = 0$) is seen to be more unstable than the region near the fully developed region ($\bar{x} \geq 10$) for $Pr = 0.01$. It is found that the curve for $Pe = 100$ can be regarded as $Pe = \infty$ practically. The merging of the two curves for $Pe = 10$ and 100 at some axial position signifies the disappearance of the axial conduction effect. With $Ha = Br = 0$, the asymptotic value of $Ra^* = 213.47$ which is independent of Prandtl number agrees with the well-known value of 1708/8 for the Benard problem. This can be explained from the perturbation equations. For fully developed flow, $\partial\Phi_\theta/\partial x = 0$ in equation (39) and with $Ha = Br = 0$, equations (37) and (39) become identical with those of the Benard problem.

It is difficult to explain the reasons for the occurrence of the local maximum for Ra^* in the thermal entrance region as noted earlier. Considering the case with $Ha = 0$, it appears that the cause for the phenomenon is due to the combined effect of the convective term $(u^*/Pr)\partial\phi_0/\partial x$ and the term involving Br on the right-hand side of the perturbation equation (39). Noting that the basic profiles $\phi_u(z)$ and $\phi_0(x,z)$ are independent of Pr, one may conclude that the relative magnitude of Pr and Br also plays some role leading to the occurrence of the phenomenon. Figs. 7 to 9 reveal that as the value of Ha increases, the phenomenon becomes less appreciable. The effect of the Hartmann number on the asymptotic value of Ra* is of interest since for the fully developed flow, one has $\partial\phi_0/\partial\bar{x} = 0$ and the perturbation equations (37) and (39) become identical with those of Chandrasekhar [9] when Br = 0. It is found that the present asymptotic results with Br = 0 agree with those of [9]. From Fig. 6 to 9, it is seen that with the increase of Hartmann number, the effect of Brinkman number on the asymptotic value of Ra* becomes less appreciable. Figs. 10 to 13 show clearly the effects of Ha and Pr on the distribution of Ra* along the axial direction $\bar{x}$ for given values of Pe and Br. The present investigation shows that magnetic field has a stabilizing effect and the decreasing Prandtl number has a destabilizing effect in the thermal entrance region. The effects of Ha and Br on the distribution of Ra* along $\bar{x}$ are shown in Figs. 14 to 17 for given values of Pe and Pr. For reference, the distributions of the wave numbers a* corresponding to Fig. 14 and 15 are shown in Fig. 18 and 18, respectively.

7.5 Concluding Remarks

1. The analysis [9] on thermal instability of a horizontal fluid layer confined between two rigid plates subjected to a vertical uniform magnetic field is extended to the case with main flow (Hartmann flow). The present analysis includes the axial conduction, viscous dissipation and Joule heating effects.

2. The numerical Results are obtained for Pr = 0.7 (air), 0.01 (liquid metal), Pe = 10, 100, ∞, Br = 0, -1, and Ha = 0, 2, 6, 10 with K = 1 and θ_0 = 1 only. The case with K = 1 signifies the open circuit condition and θ_0 = 1 means $T_0 = T_2$ (entrance temperature is equal to upper plate temperature). At Br = -1, the viscous dissipation effect may be considered to be appreciable. It is found that the axial conduction and the magnetic field have a stabilizing effect and the effect of Brinkman number appears to be dependent upon other parameters such as Ha and Pe. It is observed that the combined effect of Prandtl and Brinkman numbers in the perturbation equation (39) may lead to a locally stabilizing effect in some region of the channel before the fully-developed region.

3. For high Prandtl number fluid, the flow is more stable in the thermal entrance region than in the fully-developed region, but the opposite is true for small Prandtl number fluid. However, the Brinkman number has a destabilizing effect in the fully-developed region. When Pr is small, the critical Rayleigh number does not change appreci-

ably throughout the whole entrance length at say Ha = 10.

4. The accuracy and convergence of the numerical solution are checked by comparing the present numerical results with those reported in the literature for the limiting cases [6,9].

5. The present instability results are useful in predicting the onset of longitudinal vortex rolls in wide horizontal rectangular channels and the complete numerical results for Ra* and a* are listed in Table 1 to 3.

6. As noted in Chapter VI, for low Peclet number flow regime with viscous dissipation effects, the entrance condition of uniform fluid temperature at $\overline{x} = 0$ must be regarded as an approximate one. Consequently, numerical calculation is not made for Pe < 10.

References

1. Hwang, C.L., Knieper, P.J. and Fan, L.T., "Heat Transfer to MHD Flow in the Thermal Entrance Region of a Flat Duct", Int. J. Heat Mass Transfer 9, 1966, pp. 773-789.
2. Fan, L.T., Hwang, C.L., Knieper, P.J. and Hwang, U.P., "Heat Transfer on Magnetohydrodynamic Flow in the Entrance Region of a Flat Duct", Z. Angew. Math. Phys. 18, 1967, pp. 826-844.
3. Mori, Y. and Uchida, Y., "Forced Convective Heat Transfer between Horizontal Flat Plates", Int. J. Heat Mass Transfer 9, 1966, pp. 803-817.
4. Nakayama, W., Hwang, G.J. and Cheng, K.C., "Thermal Instability in Plane Poiseuille Flow", J. Heat Transfer 92C, 1970, pp. 61-68.
5. Akiyama, M., Hwang, G.J. and Cheng, K.C., "Experiments on the Onset of Longitudinal Vortices in Laminar Forced Convection between Horizontal Plates", J. Heat Transfer 93C, 1971, pp. 335-341.
6. Hwang, G.J. and Cheng, K.C., "Convective Instability in the Thermal Entrance Region of a Horizontal Parallel-Plate Channel Heated from Below", J. Heat Transfer 95C, 1973, pp. 72-77.
7. Ostrach, S. and Kamotani, Y., "Heat Transfer Augmentation in Laminar Fully-Developed Channel Flow by Means of Heating from Below", J. Heat Transfer, 97C, 1975, pp. 220-227.

8. Thompson, W.B., "Thermal Convection in a Magnetic Field", Phil. Mag. 42, 1951, pp. 1417-1432.

9. Chandrasekhar, S., "On the Inhibition of Convection by a Magnetic Field", Phil. Mag. 43, 1952, pp. 501-532.

10. Chandrasekhar, S., "On the Inhibition of Convection by Magnetic Field: II", Phil. Mag. 45, 1954, pp. 1177-1191.

11. Nakagawa, Y., "An Experiment on the Inhibition of Thermal Convection by a Magnetic Field", Nature 175, 1955, pp. 417-419.

12. Nakagawa, Y., "Experiments on the Inhibition of Thermal Convection by a Magnetic Field", Proc. Roy. Soc. (London) 240A, 1957, pp. 108-113.

13. Nakagawa, Y., "Some Results on Heat Transport by Convection in the Presence of a Magnetic Fie[ld]", Rev. Mod. Phys. 32, 1960, pp. 916-918.

14. Nakagawa, Y. and Goroff, I.R., "Experiments on Heat Transport by Convection in Presence of a Magnetic Field", Physics of Fluids 4, 1961, pp. 349-354.

15. Yu, C.P., "Thermal Instability of a Magnetofluid in a Vertical Rectangular Channel", Physics of Fluids 11, 1968, pp. 756-760.

16. Sutton, G.W. and Sherman, A., "Engineering Magnetohydrodynamics", McGraw-Hill, New York, 1965, Chapter 10.

17. Chandrasekhar, S., "Hydrodynamic and Hydromagnetic Stability", Oxford University Press, 1961, p. 402.

18. Thomas, L.H., "The Stability of Plane Poiseuille Flow", Physical Review 91, 1953, pp. 780-783.

19. Forsythe, G.E. and Wasow, W.R., "Finite Difference Methods for Partial Differential Equations", John Wiley & Sons, New York, 1960, Sec. 24.8.

Table I Instability Results for θ_0 = 1, k = 1, Pe = 10

Ha = 0

Br	0				-1			
Pr	0.01		0.7		0.01		0.7	
x	a*	Ra*	a*	Ra*	a*	Ra*	a*	Ra*
0.001	2.918	11.8	2.933	805.0	2.989	13.0	3.012	306.3
0.002	2.918	11.5	2.946	756.0	2.984	12.5	3.013	299.9
0.004	2.917	10.9	2.970	681.3	2.976	11.9	3.017	288.7
0.006	2.916	10.5	2.990	626.6	2.969	11.4	3.021	279.3
0.008	2.915	10.3	3.007	584.6	2.964	11.2	3.026	271.2
0.010	2.914	10.1	3.021	551.0	2.958	11.0	3.032	264.1
0.020	2.908	9.9	3.073	448.2	2.936	10.8	3.057	238.1
0.040	2.900	10.7	3.120	358.1	2.902	12.0	3.092	208.8
0.060	2.897	12.1	3.140	314.3	2.872	13.9	3.111	191.9
0.080	2.897	13.7	3.148	287.7	2.842	16.4	3.121	180.8
0.100	2.901	15.6	3.152	269.7	2.809	19.3	3.126	172.9
0.200	2.941	27.4	3.149	229.4	2.566	40.3	3.129	154.2
0.400	3.018	55.1	3.136	213.0	2.597	47.8	3.120	145.3
0.600	3.052	82.5	3.129	211.8	2.712	37.8	3.115	143.4
0.800	3.071	110.0	3.122	212.4	2.702	32.1	3.116	142.6
1.000	3.084	137.6	3.120	212.9	2.702	29.0	3.118	141.9
2.000	3.098	168.5	3.118	213.2	2.702	26.8	3.120	141.2
5.000	3.115	209.2	3.117	213.5	2.802	24.4	3.124	140.2
8.000	3.117	213.5	3.117	213.5	2.802	23.7	3.125	139.8

Ha = 2

0.001	3.287	24.3	3.310	1617.7	3.214	30.6	3.266	2003.5
0.002	3.285	23.5	3.331	1486.9	3.216	29.3	3.315	1800.2
0.004	3.281	22.3	3.365	1292.8	3.219	27.5	3.385	1510.2
0.006	3.277	21.5	3.391	1154.7	3.213	26.3	3.432	1313.7
0.008	3.273	20.9	3.411	1050.7	3.208	25.6	3.464	1171.5
0.010	3.270	20.6	3.427	969.2	3.201	25.1	3.488	1063.6
0.020	3.253	20.2	3.468	729.0	3.165	24.5	3.544	764.0
0.040	3.231	21.8	3.481	533.4	3.101	26.7	3.554	541.1
0.060	3.221	24.4	3.470	445.2	3.054	30.4	3.535	447.2
0.080	3.219	27.7	3.457	394.3	3.024	34.6	3.512	395.2
0.100	3.223	31.4	3.443	361.1	3.009	39.0	3.489	362.2
0.200	3.286	53.9	3.401	290.4	3.059	55.9	3.412	294.1
0.400	3.400	103.8	3.368	262.2	3.189	57.7	3.355	266.8
0.600	3.430	147.6	3.355	259.1	3.201	50.5	3.342	261.8
0.800	3.421	184.6	3.348	259.4	3.201	45.5	3.342	259.5
1.000	3.399	213.9	3.345	259.8	3.201	42.5	3.346	257.6
2.000	3.373	238.3	3.340	260.1	3.201	40.3	3.352	255.7
5.000	3.346	258.9	3.343	260.3	3.201	37.9	3.361	252.8
8.000	3.343	260.3	3.343	260.3	3.201	3[illegible].2	3.365	251.8

Table 1 Continued

Ha = 6

Br	0				-1			
Pr	0.01		0.7		0.01		0.7	
x	a*	Ra*	a*	Ra*	a*	Ra*	a*	Ra*
0.001	4.995	235.0	4.995	13325.0	4.910	306.5	5.441	16261.0
0.002	4.939	228.8	5.043	10524.0	4.931	298.3	5.519	12003.0
0.004	4.908	220.6	5.077	7466.1	4.871	287.8	5.448	7889.7
0.006	4.879	215.9	5.075	5831.8	4.801	282.2	5.372	5919.7
0.008	4.852	213.6	5.059	4815.1	4.721	280.0	5.309	4770.3
0.010	4.828	212.9	5.037	4121.6	4.650	279.9	5.255	4018.2
0.020	4.727	220.3	4.915	2494.1	4.380	292.8	5.065	2351.7
0.040	4.602	250.9	4.733	1524.4	4.171	322.1	4.848	1424.5
0.060	4.530	282.7	4.618	1170.2	4.170	334.7	4.717	1099.9
0.080	4.484	311.5	4.539	986.4	4.214	337.5	4.625	935.6
0.100	4.453	327.0	4.482	874.6	4.257	336.4	4.555	837.3
0.200	4.386	426.0	4.344	656.2	4.389	320.9	4.363	650.6
0.400	4.327	509.5	4.268	575.5	4.493	289.2	4.249	582.5
0.600	4.281	543.0	4.246	566.0	4.531	266.4	4.228	571.4
0.800	4.253	557.0	4.235	566.0	4.551	252.2	4.232	566.6
1.000	4.239	563.0	4.231	566.7	4.571	243.5	4.242	562.6
2.000	4.232	566.0	4.229	567.2	4.591	237.0	4.254	558.6
5.000	4.228	567.5	4.228	567.6	4.600	229.9	4.270	553.0
8.000	4.228	567.6	4.228	567.6	4.600	228.1	4.275	551.3

Ha = 10

0.001	6.813	993.7	6.642	47793.0	8.231	985.4	7.413	45517.0
0.002	6.748	992.5	6.577	31098.0	8.101	994.7	7.061	28527.0
0.004	6.642	996.0	6.515	18330.0	7.890	1017.5	6.820	16324.0
0.006	6.554	1005.3	6.445	13121.0	7.711	1045.2	6.671	11556.0
0.008	6.480	1018.4	6.374	10305.0	7.561	1076.4	6.570	9027.2
0.010	6.416	1033.9	6.307	8540.2	7.431	1110.2	6.481	7461.6
0.020	6.171	1121.4	6.141	4825.8	6.871	1294.0	6.199	4213.7
0.040	5.859	1245.2	5.730	2858.4	5.851	1577.0	5.882	2526.9
0.060	5.655	1284.8	5.550	2180.4	5.315	1651.8	5.691	1957.2
0.080	5.512	1278.7	5.431	1836.7	5.104	1610.3	5.567	1674.2
0.100	5.410	1254.6	5.347	1630.1	5.018	1535.2	5.470	1507.4
0.200	5.171	1135.6	5.143	1232.2	4.959	1242.3	5.194	1200.3
0.400	5.045	1070.3	5.031	1089.3	5.047	1036.9	5.013	1098.8
0.600	5.004	1068.8	4.998	1074.3	5.193	957.9	4.976	1084.9
0.800	4.987	1073.2	4.984	1075.1	5.193	913.8	4.979	1077.5
1.000	4.980	1076.0	4.979	1076.9	5.232	886.6	4.992	1070.3
2.000	4.977	1077.6	4.976	1077.8	5.262	866.2	5.007	1062.7
5.000	4.975	1078.4	4.975	1078.4	5.292	844.1	5.028	1052.3
8.000	4.975	1078.4	4.975	1078.4	5.300	838.9	5.034	1049.5

Table 2 Instability Results for $\theta_0 = 1$, $k = 1$, Pe = 100

Ha = 0

Br	0				1			
Pr	0.01		0.7		0.01		0.7	
x	a*	Ra*	a*	Ra*	a*	Ra*	a*	Ra*
0.001	2.938	7.7	2.945	534.9	3.014	263.7	2.990	7.9
0.002	2.935	7.7	2.965	513.0	3.008	258.4	2.998	7.9
0.004	2.932	7.7	2.995	480.1	2.998	249.9	3.011	7.9
0.006	2.928	7.7	3.018	456.0	2.989	243.1	3.022	8.0
0.008	2.925	7.8	3.037	437.2	2.981	237.4	3.032	8.1
0.010	2.922	7.9	3.051	421.8	2.974	232.6	3.040	8.3
0.020	2.910	8.5	3.097	370.7	2.944	215.0	3.071	9.1
0.040	2.896	10.1	3.133	317.7	2.900	194.1	3.104	11.1
0.060	2.892	11.9	3.147	288.2	2.866	181.4	3.119	13.6
0.080	2.894	13.9	3.151	269.0	2.833	172.8	3.127	16.5
0.100	2.899	16.0	3.153	255.4	2.796	166.6	3.130	19.9
0.200	2.947	28.8	3.149	223.9	2.528	151.5	3.129	43.6
0.400	3.025	57.2	3.136	211.8	2.592	144.6	3.120	48.7
0.600	3.056	84.3	3.127	211.6	2.712	143.2	3.116	37.8
0.800	3.072	111.9	3.122	212.4	2.702	142.5	3.116	32.0
1.000	3.085	139.5	3.120	212.9	2.702	141.8	3.118	28.9
2.000	3.099	170.3	3.118	213.3	2.702	141.2	3.120	26.7
5.000	3.116	209.6	3.117	213.5	2.702	140.2	3.124	24.4
8.000	3.117	213.5	3.117	213.5	2.802	139.8	3.125	23.7

Ha = 2

0.001	3.342	16.6	3.357	1142.1	3.401	18.9	3.430	1285.4
0.002	3.332	16.4	3.385	1058.7	3.378	18.6	3.465	1173.7
0.004	3.316	16.2	3.425	939.9	3.344	18.5	3.513	1019.3
0.006	3.304	16.2	3.450	857.9	3.317	18.5	3.542	916.1
0.008	3.294	16.2	3.468	796.6	3.296	18.6	3.561	840.9
0.010	3.285	16.4	3.479	748.5	3.275	18.9	3.574	782.9
0.020	3.253	17.5	3.501	601.6	3.200	20.5	3.593	612.7
0.040	3.222	20.5	3.492	470.2	3.107	24.7	3.572	470.0
0.060	3.211	23.9	3.473	405.6	3.052	29.4	3.542	403.8
0.080	3.211	27.7	3.456	366.4	3.021	34.3	3.513	365.1
0.100	3.218	31.9	3.441	340.1	3.008	39.3	3.488	339.8
0.200	3.295	56.4	3.398	282.6	3.063	57.6	3.409	286.0
0.400	[illegible]11	107.3	3.367	260.4	3.190	58.3	3.354	264.8
0.600	[illegible]4	150.4	3.351	258.8	3.202	50.4	3.341	261.3
0.800	[illegible]1	186.8	3.348	259.3	3.202	42.4	3.342	259.3
1.000	3.398	215.7	3.345	259.8	3.202	37.8	3.346	257.4
2.000	3.372	239.5	3.344	260.1	3.202	37.8	3.352	255.6
5.000	3.345	259.0	3.343	260.3	3.202	37.2	3.362	252.7
8.000	3.343	260.3	3.343	260.3	3.202	37.2	3.365	251.8

Table 2 Continued

Ha = 6

Br	0				-1			
Pr	0.01		0.7		0.01		0.7	
x	a*	Ra*	a*	Ra*	a*	Ra*	a*	Ra*
0.001	5.283	155.1	5.512	9891.8	6.131	170.5	6.621	10176.0
0.002	5.194	156.3	5.487	7735.8	5.921	175.3	6.246	7771.7
0.004	5.069	159.5	5.432	5514.7	5.601	184.6	5.902	5364.9
0.006	4.983	163.4	5.367	4379.1	5.361	194.0	5.712	4183.3
0.008	4.920	167.8	5.302	3683.4	5.184	203.6	5.476	3479.0
0.010	4.870	172.5	5.241	3209.2	5.024	213.2	5.164	3008.2
0.020	4.714	196.9	5.011	2072.2	4.481	258.1	4.878	1913.1
0.040	4.572	241.6	4.761	1348.6	4.153	312.0	4.727	1246.0
0.060	4.502	279.1	4.624	1067.3	4.156	329.5	4.626	996.0
0.080	4.460	310.5	4.537	916.6	4.204	333.2	4.551	865.4
0.100	4.434	337.1	4.477	823.0	4.256	332.4	4.356	785.9
0.200	4.381	427.8	4.338	637.4	4.392	319.6	4.246	632.2
0.400	4.327	511.5	4.266	571.0	4.495	288.8	4.228	578.0
0.600	4.279	544.2	4.244	565.1	4.540	265.8	4.233	570.2
0.800	4.252	557.7	4.235	565.8	4.565	251.6	4.243	566.0
1.000	4.239	563.4	4.231	566.7	4.580	243.0	4.254	562.2
2.000	4.232	566.1	4.229	567.3	4.591	236.6	4.271	558.3
5.000	4.228	567.5	4.228	567.6	4.602	229.8	4.275	552.9
8.000	4.228	567.6	4.228	567.6	4.605	228.1	4.275	551.3

Ha = 10

0.001	7.196	617.3	9.401	30236.0	8.101	568.9	10.567	25454.0
0.002	7.033	648.5	7.971	21239.0	7.921	606.8	8.615	18223.0
0.004	6.798	706.4	7.320	13193.0	7.641	680.0	7.632	11351.0
0.006	6.635	759.6	7.029	9765.2	7.446	750.4	7.252	8392.6
0.008	6.516	808.9	6.828	7875.7	7.292	818.3	7.013	6765.4
0.010	6.424	854.5	6.672	6671.9	7.165	883.9	6.838	5731.8
0.020	6.138	1033.7	6.201	4042.3	6.671	1174.2	6.343	3488.7
0.040	5.828	1208.9	5.777	2546.1	5.791	1524.9	5.921	2232.0
0.060	5.628	1252.6	5.564	1999.5	5.291	1602.3	5.708	1784.0
0.080	5.489	1244.9	5.432	1714.1	5.100	1557.6	5.568	1556.1
0.100	5.389	1220.7	5.341	1539.4	5.017	1483.3	5.465	1420.3
0.200	5.160	1113.6	5.135	1198.6	4.959	1212.5	5.184	1168.9
0.400	5.042	1064.6	5.028	1081.3	5.050	1028.1	5.009	1091.0
0.600	5.003	1067.7	4.996	1072.7	5.137	953.8	4.976	1082.8
0.800	4.987	[illegible]	4.984	1074.9	5.197	911.0	4.980	1076.5
1.000	4.980	1076.2	4.979	1076.8	5.235	884.5	4.993	1069.5
2.000	4.976	1077.7	4.976	1077.9	5.263	864.7	5.008	1062.1
5.000	4.975	1078.4	4.975	1078.4	5.292	843.6	5.028	1052.0
8.000	4.975	1078.5	4.975	1078.5	5.299	838.9	5.340	1049.5

Table 3 Instability Results for $_{0}$ 1, k 1, Pe

Ha 0

Br	0				-1			
Pr	0.01		0.7		0.01		0.7	
x	a*	Ra*	a*	Ra*	a*	Ra*	a*	Ra*
0.001	2.938	7.5	2.945	522.0	3.013	7.7	2.989	260.8
0.002	2.936	7.5	2.965	503.0	3.007	7.8	2.997	256.1
0.004	2.932	7.6	2.996	473.6	2.997	7.8	3.011	248.2
0.006	2.928	7.6	3.019	451.4	2.989	7.9	3.022	241.9
0.008	2.925	7.7	3.037	433.8	2.981	8.1	3.032	236.5
0.010	2.922	7.9	3.052	419.1	2.974	8.2	3.041	231.8
0.020	2.909	8.5	3.097	369.5	2.944	9.1	3.071	214.6
0.040	2.896	10.1	3.134	317.2	2.900	11.1	3.104	193.9
0.060	2.892	11.9	3.137	287.9	2.866	13.6	3.120	181.3
0.080	2.894	13.9	3.152	268.7	2.832	16.5	3.127	172.7
0.100	2.899	16.0	3.153	255.2	2.795	19.9	3.130	166.5
0.200	2.947	28.9	3.149	223.9	2.527	43.7	3.129	151.5
0.400	3.025	57.2	3.136	211.8	2.592	48.7	3.120	144.6
0.600	3.056	84.4	3.127	211.6	2.712	37.8	3.116	143.2
0.800	3.072	111.9	3.122	212.4	2.702	32.0	3.116	142.5
1.000	3.085	139.6	3.120	212.9	2.702	28.9	3.118	141.8
2.000	3.099	170.4	3.118	213.3	2.702	26.7	3.120	141.2
5.000	3.116	209.6	3.117	213.5	2.802	24.4	3.124	140.2
8.000	3.117	213.5	3.117	213.5	2.802	23.7	3.125	139.8

Ha [illegible]

0.001	3.344	16.2	3.359	1119.2	3.403	18.4	3.433	1254.5
0.002	3.333	16.1	3.387	1041.2	3.380	18.3	3.467	1150.6
0.004	3.317	16.0	3.426	928.6	3.345	18.2	3.515	1005.1
0.006	3.304	16.0	3.452	849.9	3.318	18.3	3.544	906.3
0.008	3.294	16.1	3.469	790.7	3.296	18.5	3.563	833.7
0.010	3.285	16.3	3.481	743.8	3.276	18.8	3.575	777.3
0.020	3.253	17.5	3.502	599.5	3.200	20.5	3.593	610.2
0.040	3.222	20.5	3.492	469.3	3.107	24.7	3.573	469.0
0.060	3.211	23.9	3.473	405.0	3.052	29.4	3.542	403.2
0.080	3.211	27.8	3.456	366.0	3.021	34.3	3.513	364.7
0.100	3.218	31.9	3.441	339.8	3.008	39.3	3.488	339.5
0.200	3.295	56.4	3.398	282.5	3.036	57.6	3.409	285.9
0.400	3.411	107.4	3.367	260.4	3.181	58.3	3.354	264.8
0.600	3.434	150.5	3.353	258.8	3.202	50.4	3.340	261.3
0.800	3.421	186.8	3.348	259.3	3.202	42.4	3.342	259.3
1.000	3.398	215.8	3.345	259.8	3.202	40.2	3.348	257.4
2.000	3.372	239.5	3.344	260.1	3.202	37.8	3.352	255.6
5.000	3.345	259.0	3.343	260.3	3.202	37.2	3.361	252.7
8.000	3.343	260.3	3.343	260.3	3.202	37.2	3.365	251.8

Table 3 Continued

Ha = 6

Br	0				-1			
Pr	0.01		0.7		0.01		0.7	
x	a*	Ra*	a*	Ra*	a*	Ra*	a*	Ra*
0.001	5.289	153.0	5.534	9746.9	6.131	167.6	6.641	9981.0
0.002	5.198	154.6	5.503	7638.4	5.921	172.7	6.263	7650.0
0.004	5.070	158.2	5.442	5605.5	5.601	182.7	5.912	5303.1
0.006	4.984	162.4	5.373	4344.1	5.361	192.5	5.719	4145.1
0.008	4.920	167.1	5.306	3658.5	5.184	202.4	5.584	3452.7
0.010	4.869	171.9	5.244	3190.5	5.025	212.3	5.479	2988.8
0.020	4.713	196.7	5.012	2065.0	4.484	257.8	5.165	1905.9
0.040	4.571	241.6	4.761	1345.9	4.152	311.9	4.878	1243.4
0.060	4.501	279.1	4.624	1065.8	4.153	329.5	4.726	994.6
0.080	4.460	310.5	4.537	915.6	4.208	333.1	4.626	864.4
0.100	4.430	337.2	4.477	822.3	4.256	332.4	4.551	785.2
0.200	4.381	427.8	4.337	637.1	4.392	319.6	4.356	632.0
0.400	4.327	511.6	4.266	571.0	4.495	288.8	4.246	578.0
0.600	4.279	544.2	4.244	565.1	4.540	265.8	4.228	570.1
0.800	4.252	557.7	4.235	565.8	4.565	251.6	4.233	566.0
1.000	4.238	563.4	4.231	566.7	4.580	243.0	4.243	562.2
2.000	4.232	566.1	4.229	567.3	4.591	236.6	4.252	558.3
5.000	4.228	567.5	4.228	567.6	4.602	229.8	4.271	552.9
8.000	4.228	567.6	4.228	567.6	4.605	228.1	4.275	551.3

Ha = 10

x	a*	Ra*	a*	Ra*	a*	Ra*	a*	Ra*
0.001	7.204	610.1	9.491	29720.0	8.104	561.6	10.605	24999.0
0.002	7.037	642.3	8.023	20953.0	7.921	600.4	8.658	17960.0
0.004	6.798	701.9	7.343	13065.0	7.640	675.2	7.654	11235.0
0.006	6.634	756.3	7.043	9690.9	7.438	746.8	7.266	8325.9
0.008	6.514	806.4	6.838	7826.2	7.248	815.7	7.022	6721.2
0.010	6.422	852.7	6.679	6636.3	7.158	882.1	6.845	5699.9
0.020	6.236	1023.4	6.203	4029.7	6.676	1174.1	6.334	3477.3
0.040	5.827	1208.8	5.778	2541.9	5.728	1525.0	5.922	2227.9
0.060	5.628	1252.3	5.564	1997.0	5.291	1601.9	5.708	1781.7
0.080	5.488	1244.6	5.432	1712.5	5.100	1557.0	5.568	1554.6
0.100	5.388	1220.3	5.341	1538.3	5.017	1482.6	5.465	1419.2
0.200	5.160	1113.4	5.135	1198.3	4.959	1212.2	5.184	1168.6
0.400	5.041	1064.5	5.028	1081.2	5.050	1028.0	5.009	1090.9
0.600	5.003	1067.7	4.996	1072.6	5.137	953.8	4.976	1082.8
0.800	4.987	1073.2	4.984	1074.9	5.197	911.0	4.979	1076.5
1.000	4.980	1076.2	4.979	1076.8	5.236	884.5	4.993	1069.5
2.000	4.977	1077.7	4.976	1077.9	5.263	864.7	5.008	1062.1
5.000	4.975	1078.4	4.975	1078.4	5.292	843.6	5.028	1052.0
8.000	4.975	1078.5	4.975	1078.5	5.230	838.9	5.034	1049.5

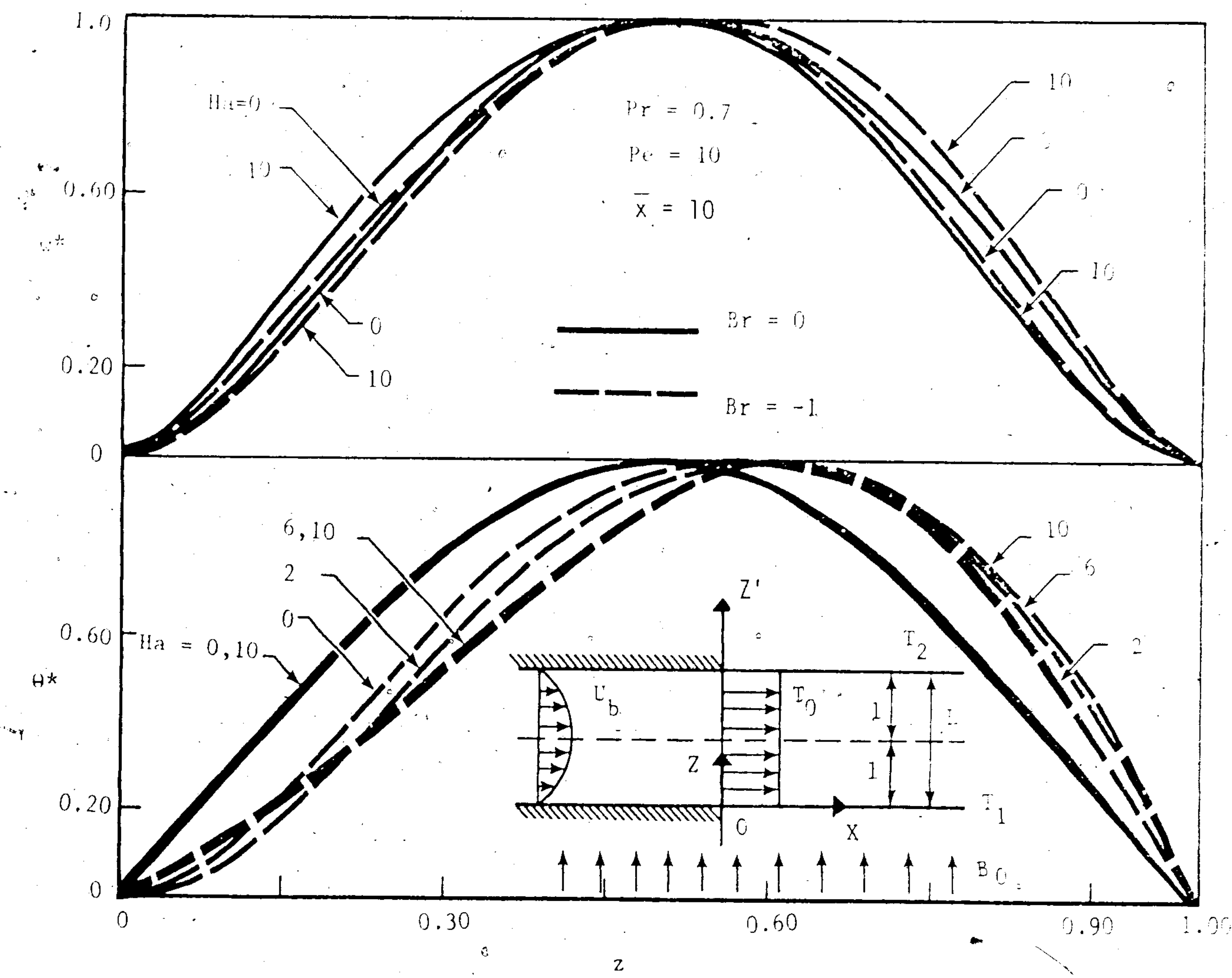

Fig. 1 Disturbance profiles for perturbation amplitudes w^* and θ^* at Ha = 0,10 for Pr = 0.7, Pe = 10, Br = 0,-1 and $\overline{x}$ = 10.

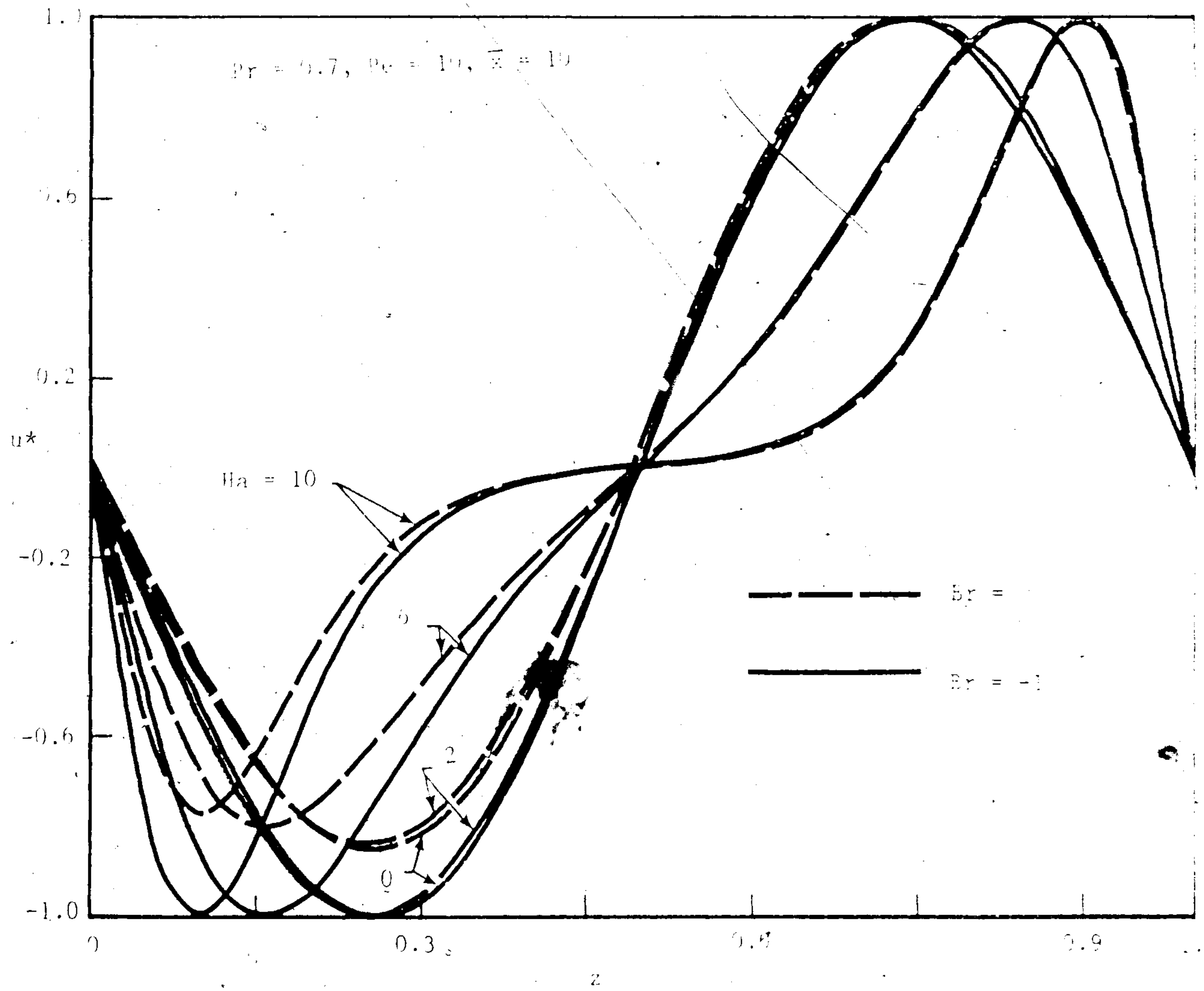

Fig. 2 Disturbance profiles for perturbation amplitudes u* at Ha = 0,2,6,10 for Pr = 0.7, Pe = 10, Br = 0,-1 and $\overline{x}$ = 10.

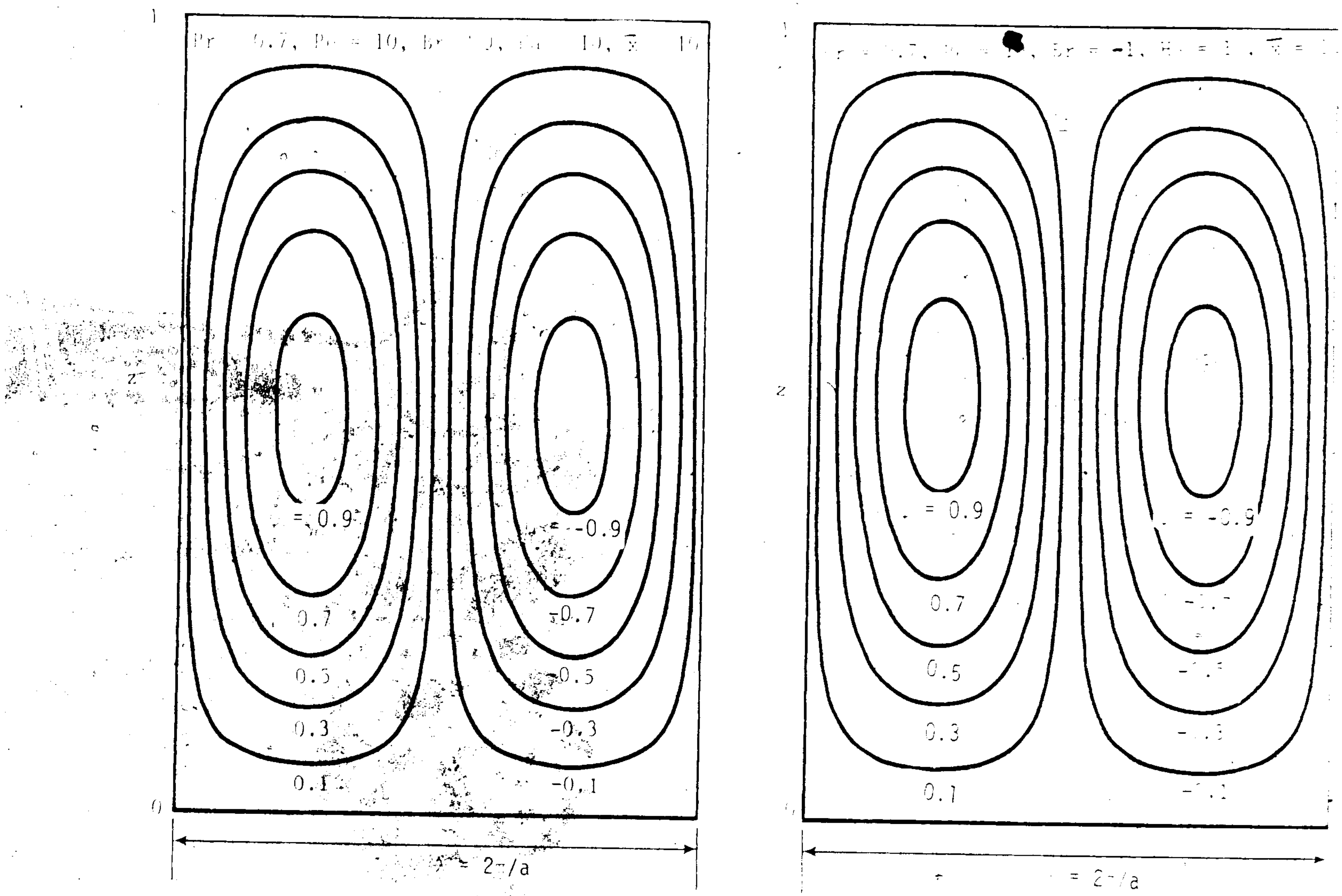

Fig. 3 Streamline pattern at onset of instability for Pr = 0.7, Pe = 10, Ha = 10, $\bar{x}$ = 10, Br = 0, and -1.

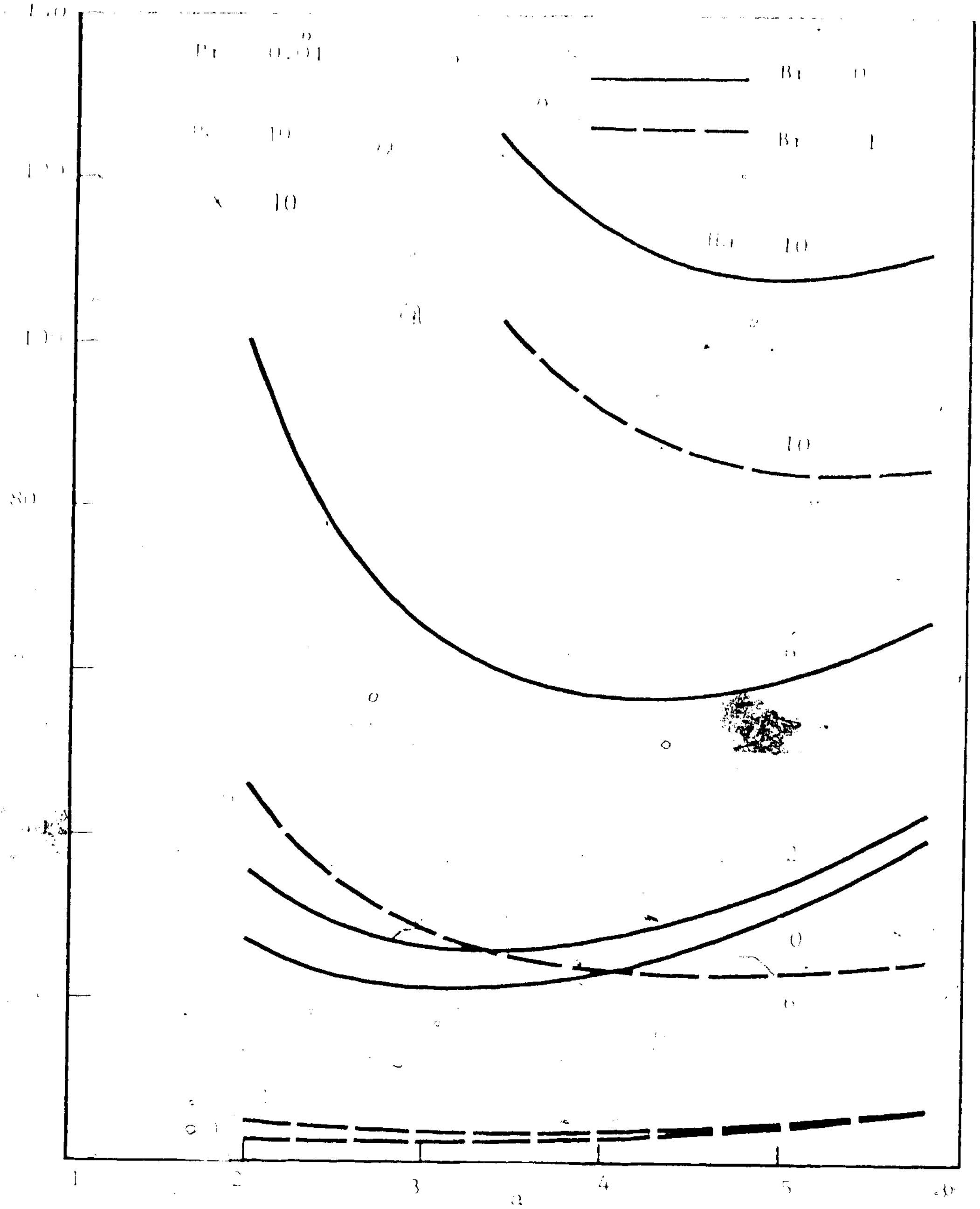

Fig. 4 Neutral stability curves for Pr = 0.01, Br = 0,-1 and Ha = 0, 2,6,10.

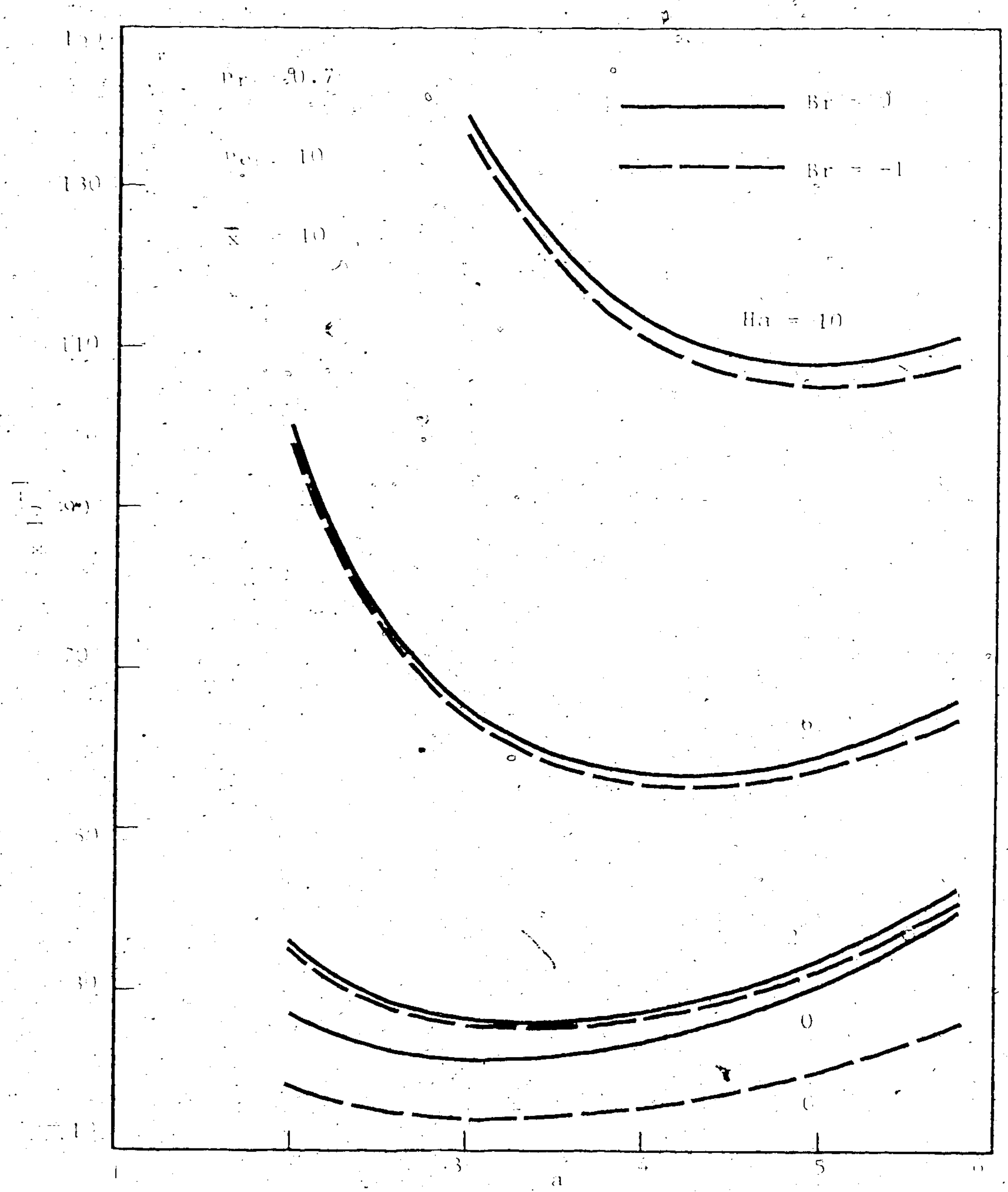

Fig. 5 Neutral stability curves for Pr = 0.7, Br = 0,-1 and Ha = 0,2,6,10.

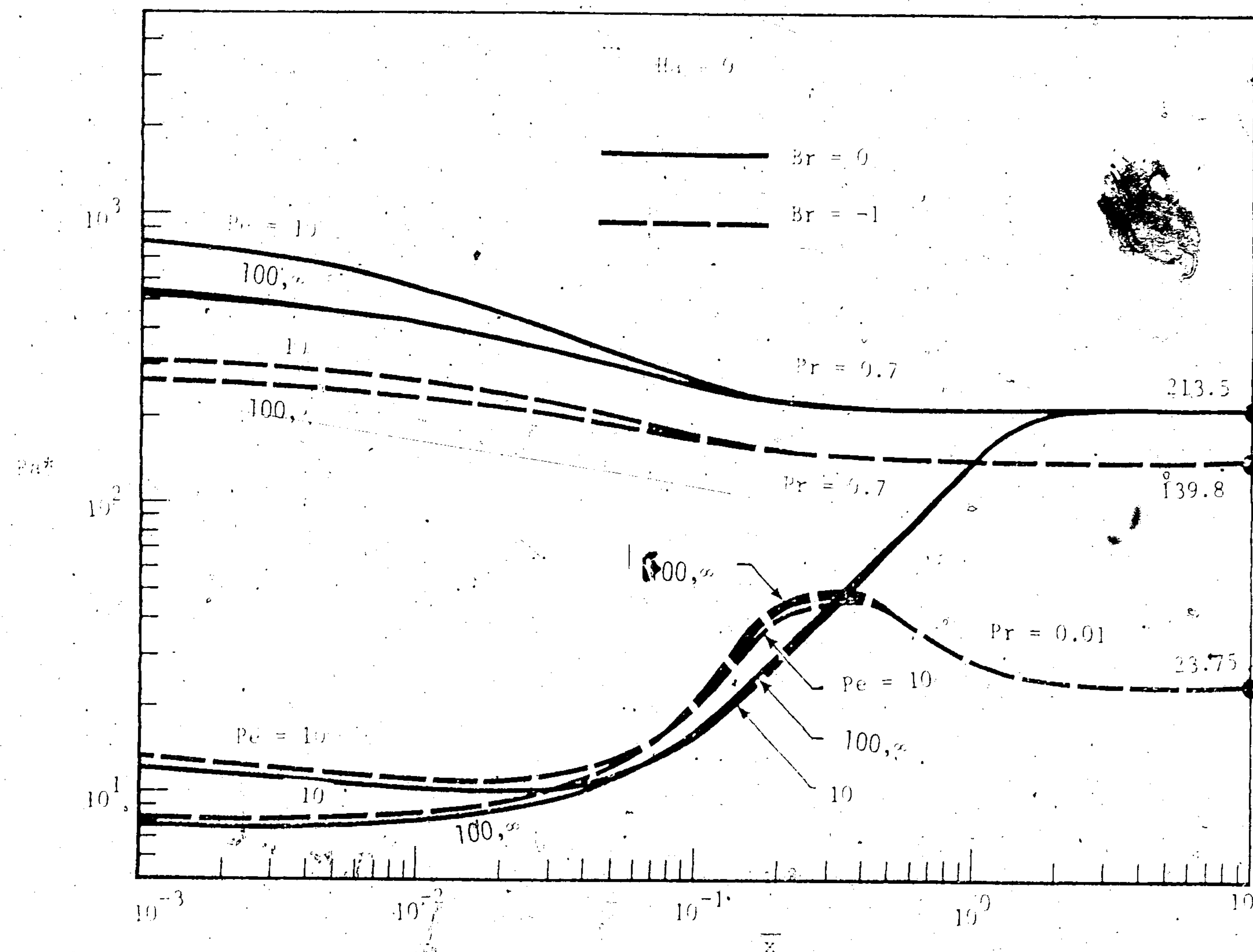

Fig. 6 Critical Rayleigh number Ra* in thermal entrance region for Pr = 0.01,0.7 and Pe = 10,100,∞ with Ha = 0, Br = 0,-1.

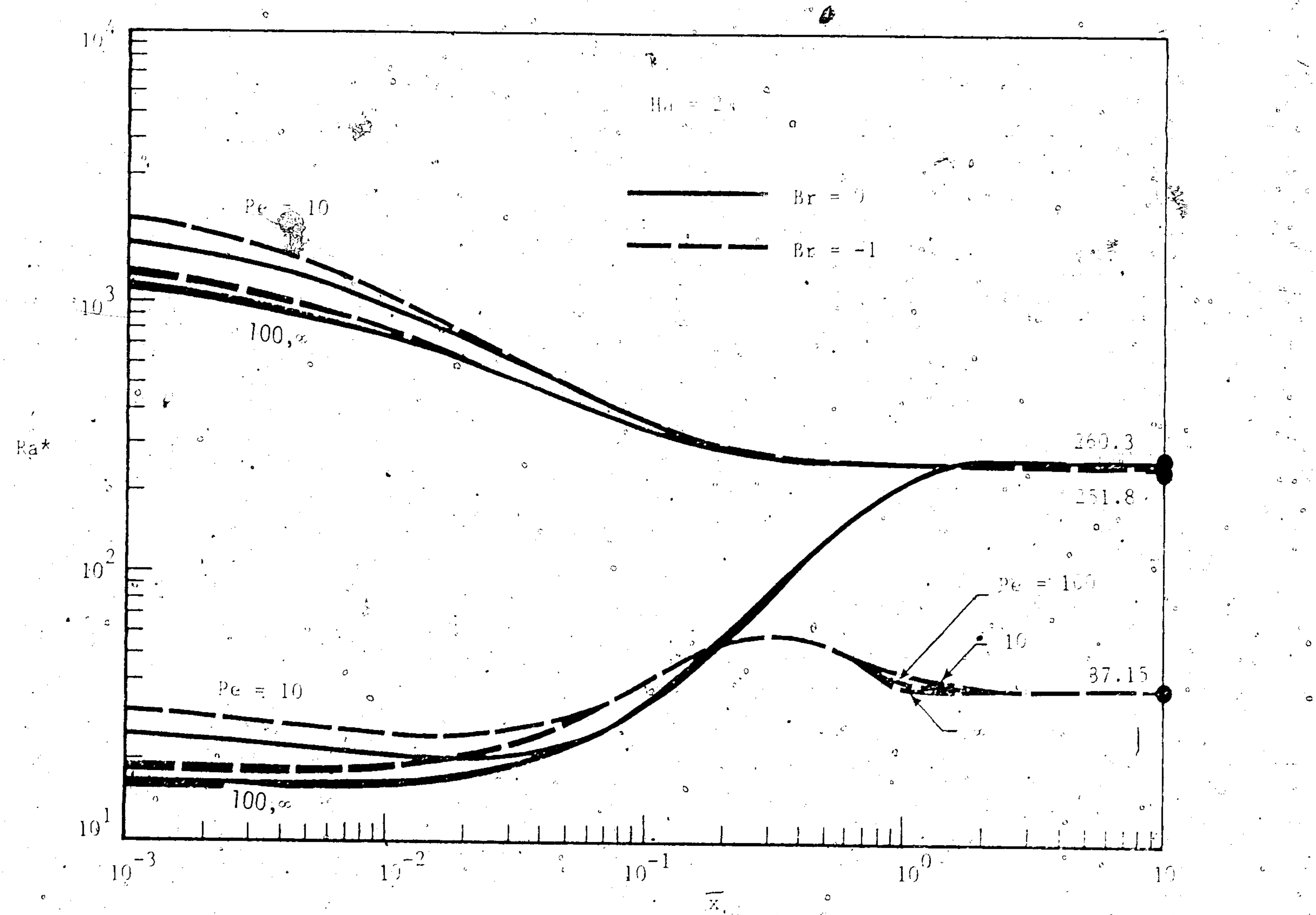

Fig. 7 Critical Rayleigh number Ra* in thermal entrance region for Pr = 0.01,0.7, and Pe = 10,100,∞ with Ha = 2, Br = 0,-1.

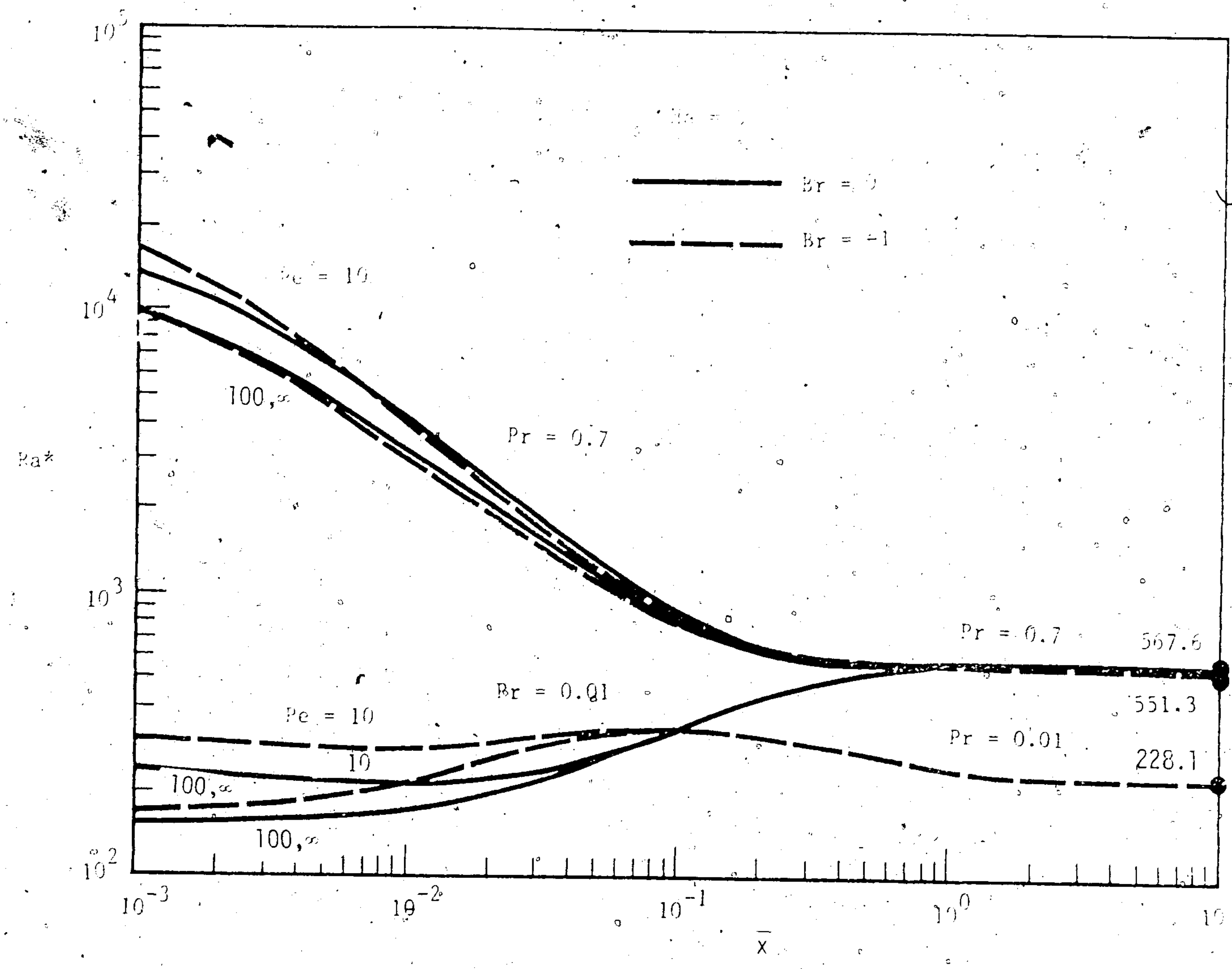

Fig. 8 Critical Rayleigh number Ra* in thermal entrance region for Pr = 0.01,0.7 and Pe = 10,100,∞ with Ha = 6, Br = 0,-1.

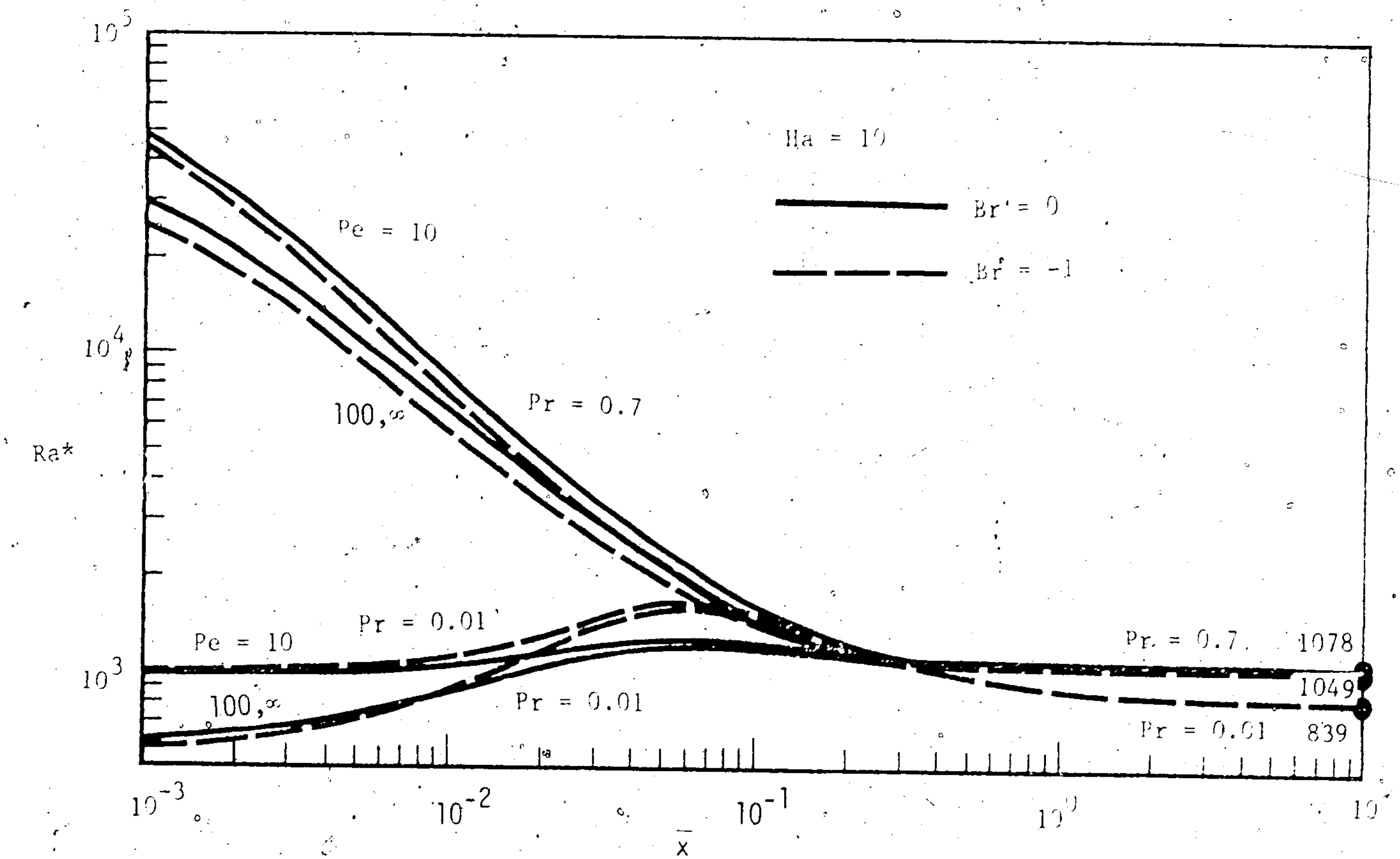

Fig. 9 Critical Rayleigh number Ra* in thermal entrance region for $Pr = 0.01, 0.7$ and $Pe = 10, 100, \infty$ with $Ha = 10$, $Br = 0, -1$.

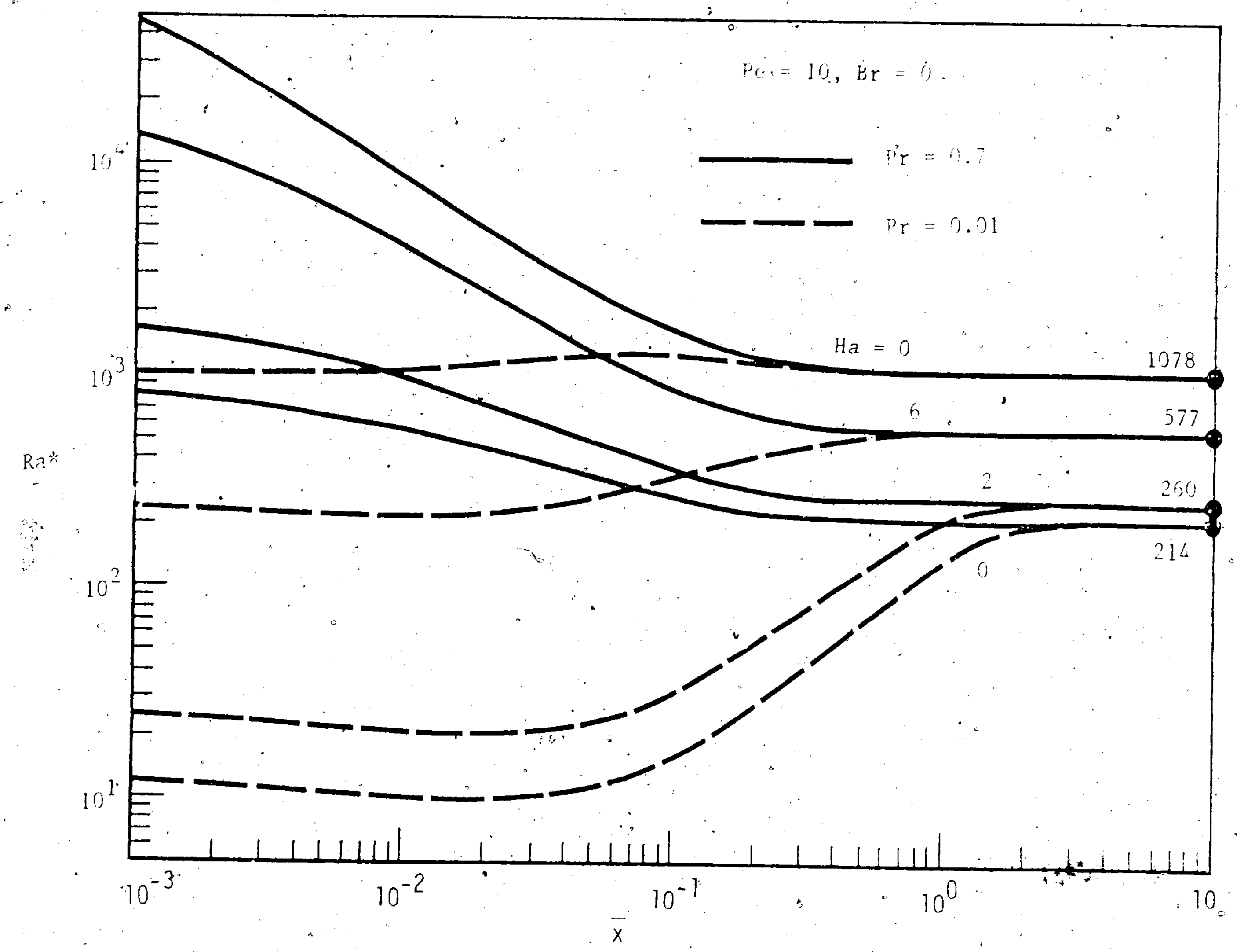

Fig. 10 Hartmann number effect on critical Ra* in thermal entrance region for Pe = 10, Br = 0 and Pr = 0.01,0.7.

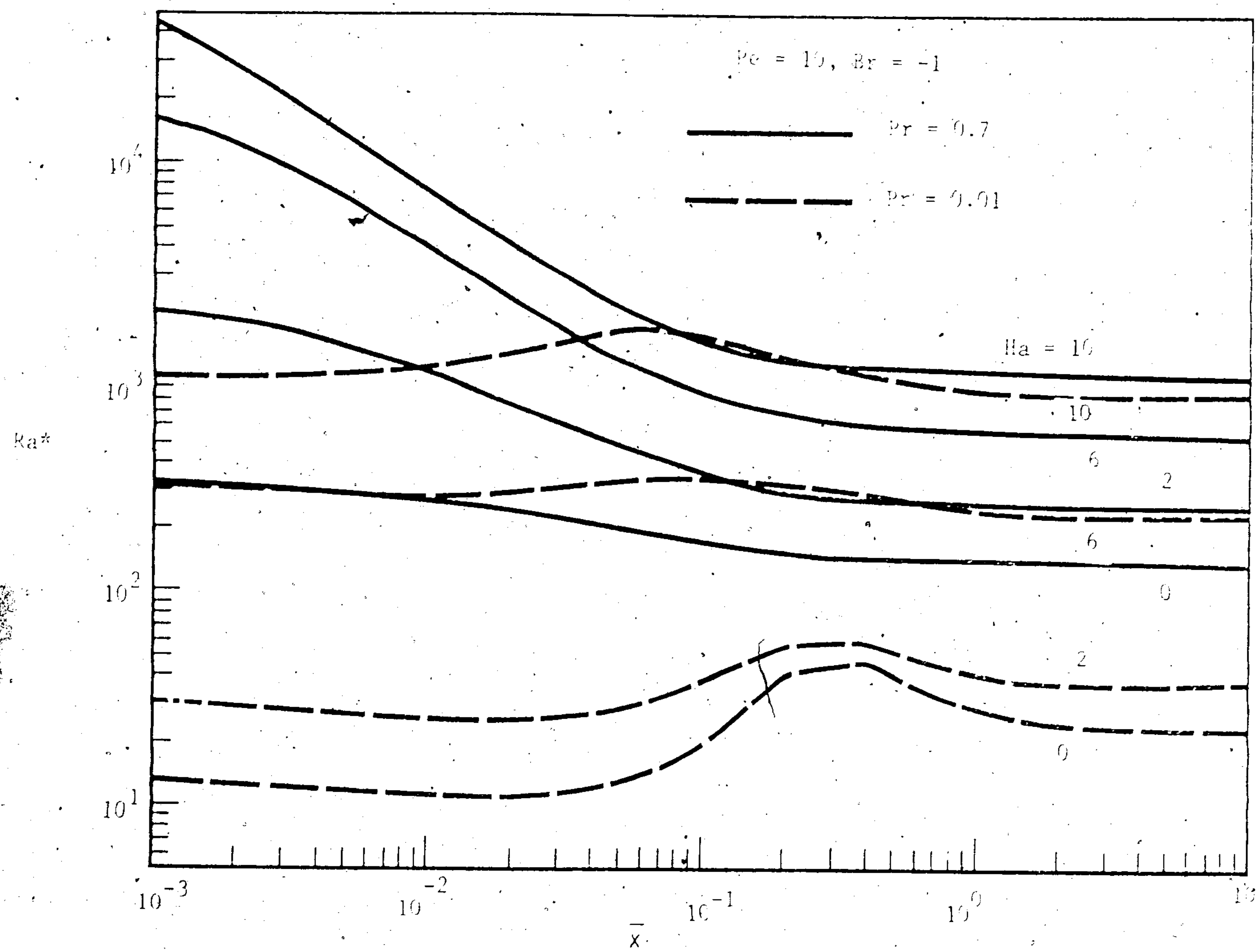

Fig. 11 Hartmann number effect on critical Ra* in thermal entrance region for Pe = 10, Br = -1 and Pr = 0.01,0.7.

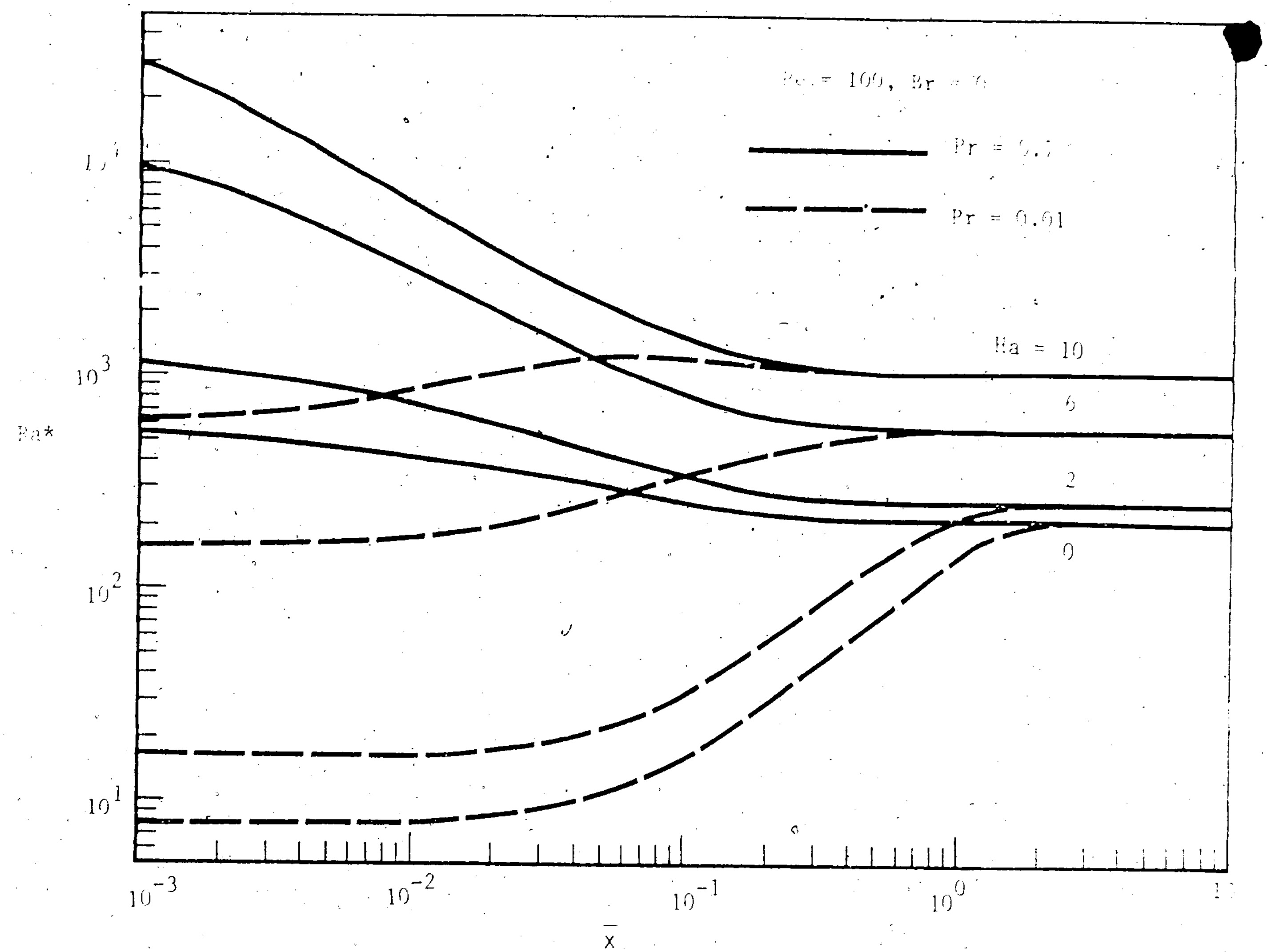

Fig. 12 Hartmann number effect on critical Ra* in thermal entrance region for Pe = 100, Br = 0 and Pr = 0.01,0.7.

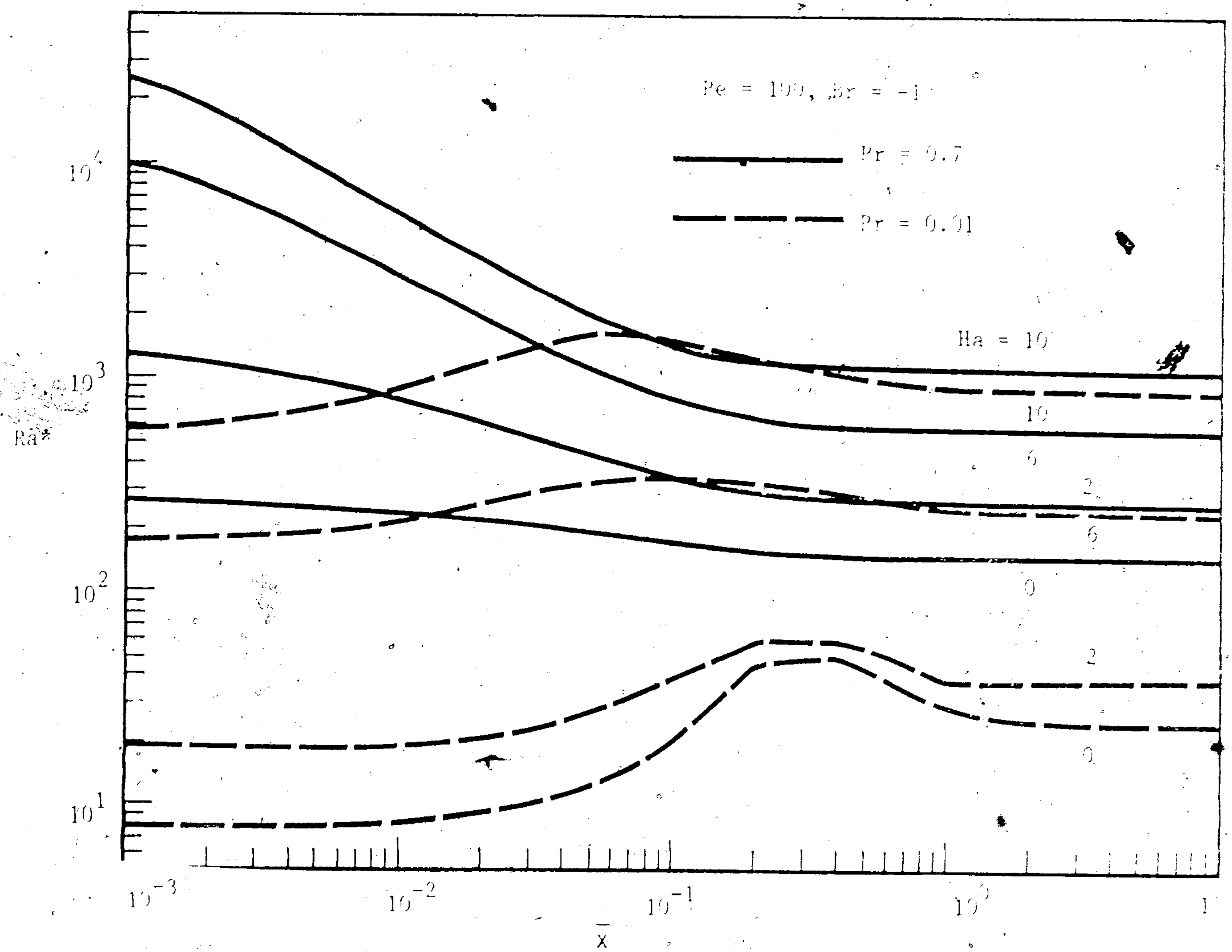

Fig. 13 Hartmann number effect on critical Ra* in thermal entrance region for Pe = 100, Br = -1 and Pr = 0.01,0.7.

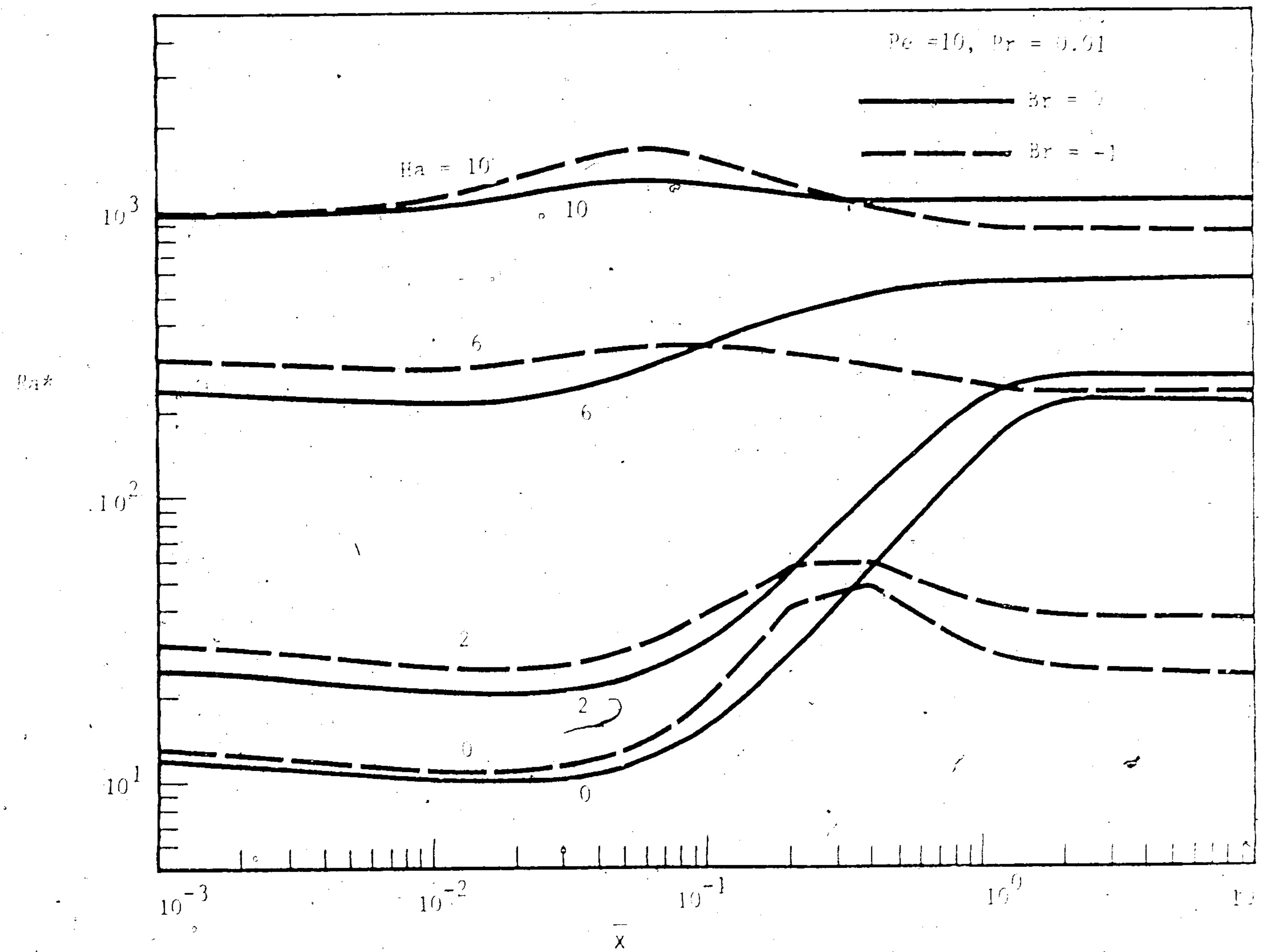

Fig. 14 Hartmann number effect on critical Ra* in thermal entrance region for Pr = 0.01, Pe = 10 and Br = 0,-1.

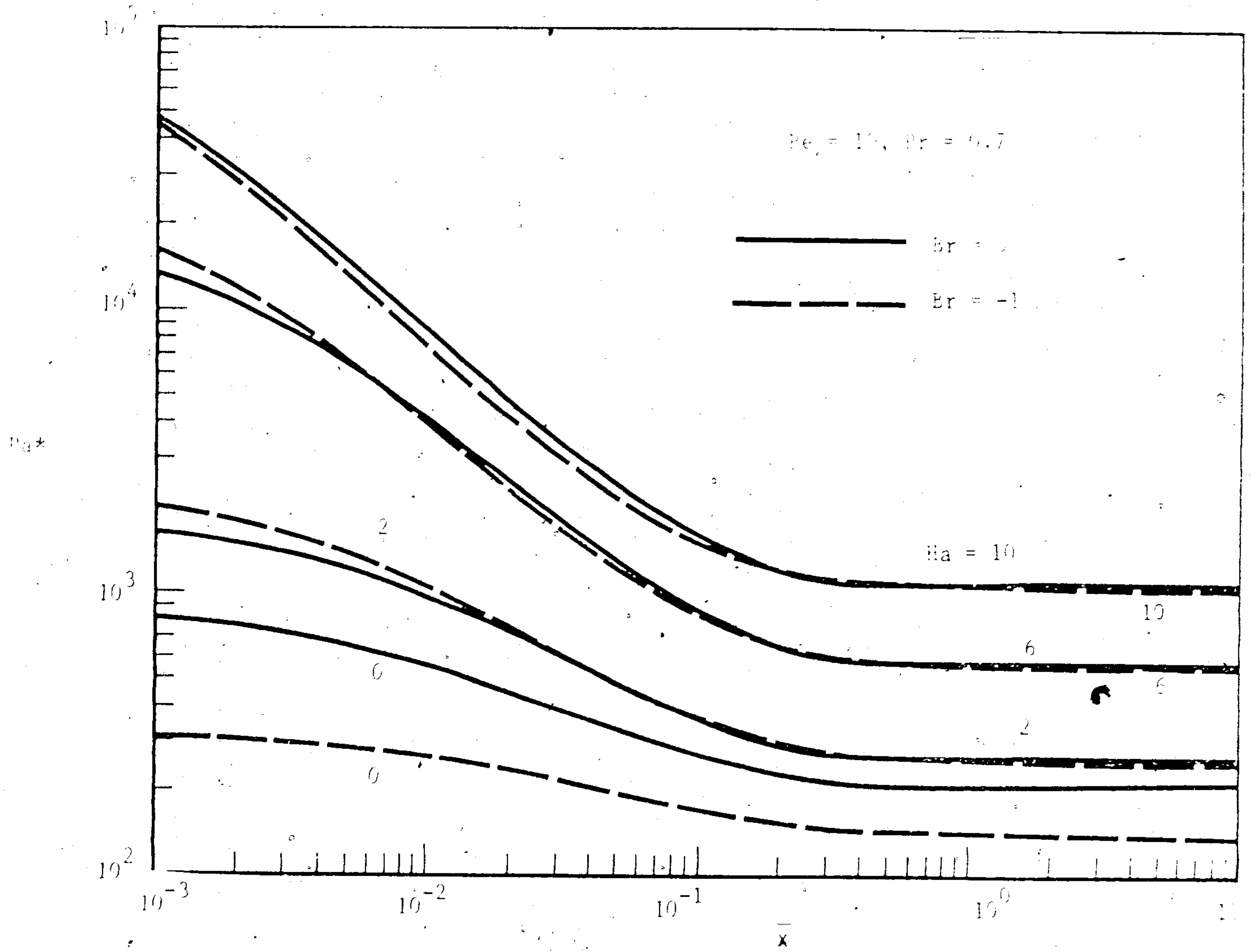

Fig. 15 Hartmann number effect on critical Ra* in thermal entrance region for Pr = 0.7, Pe = 10 and Br = 0,-1.

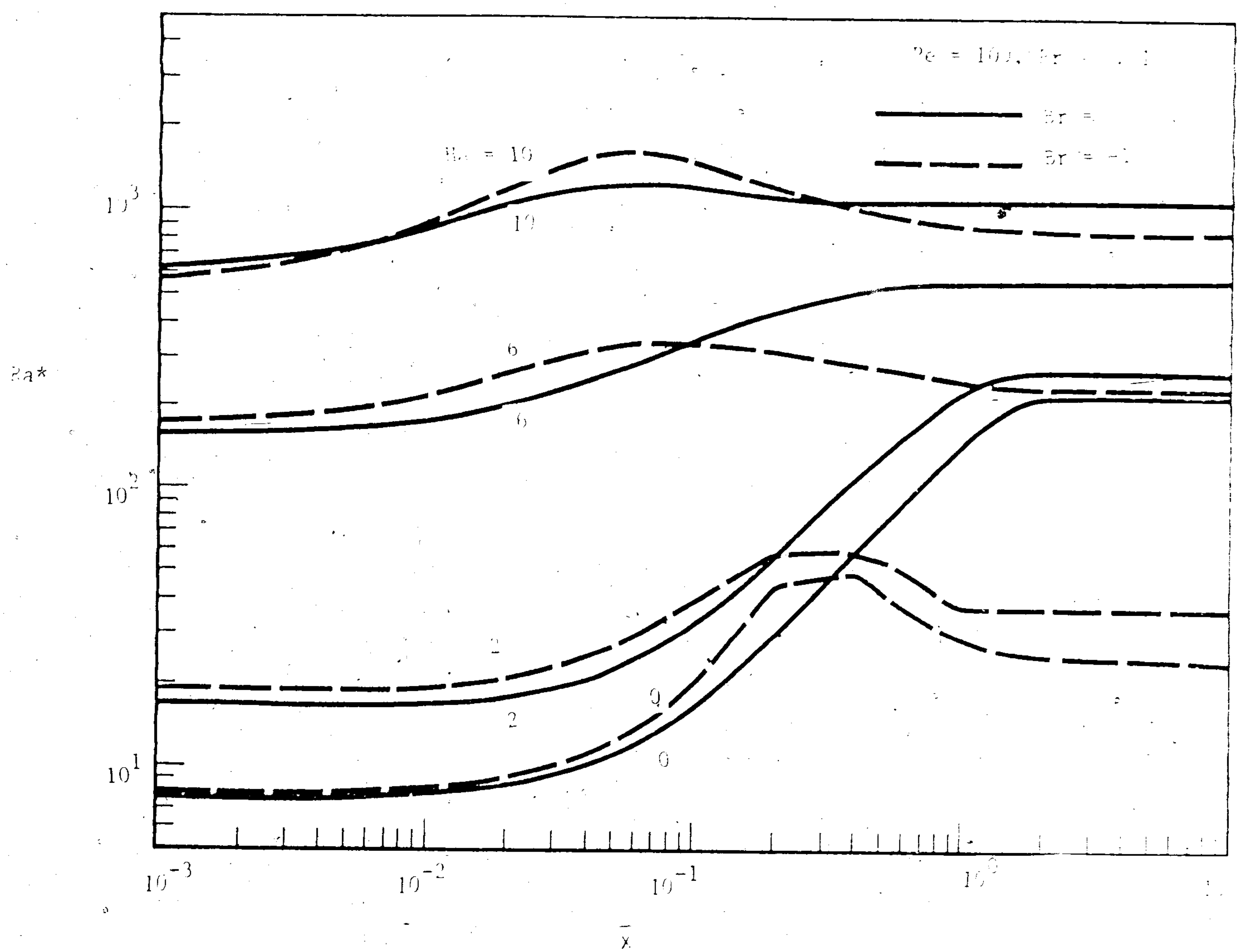

Fig. 16 Hartmann number effect on critical Ra* in thermal entrance region for Pr = 0.01, Pe = 100 and Br = 0,-1.

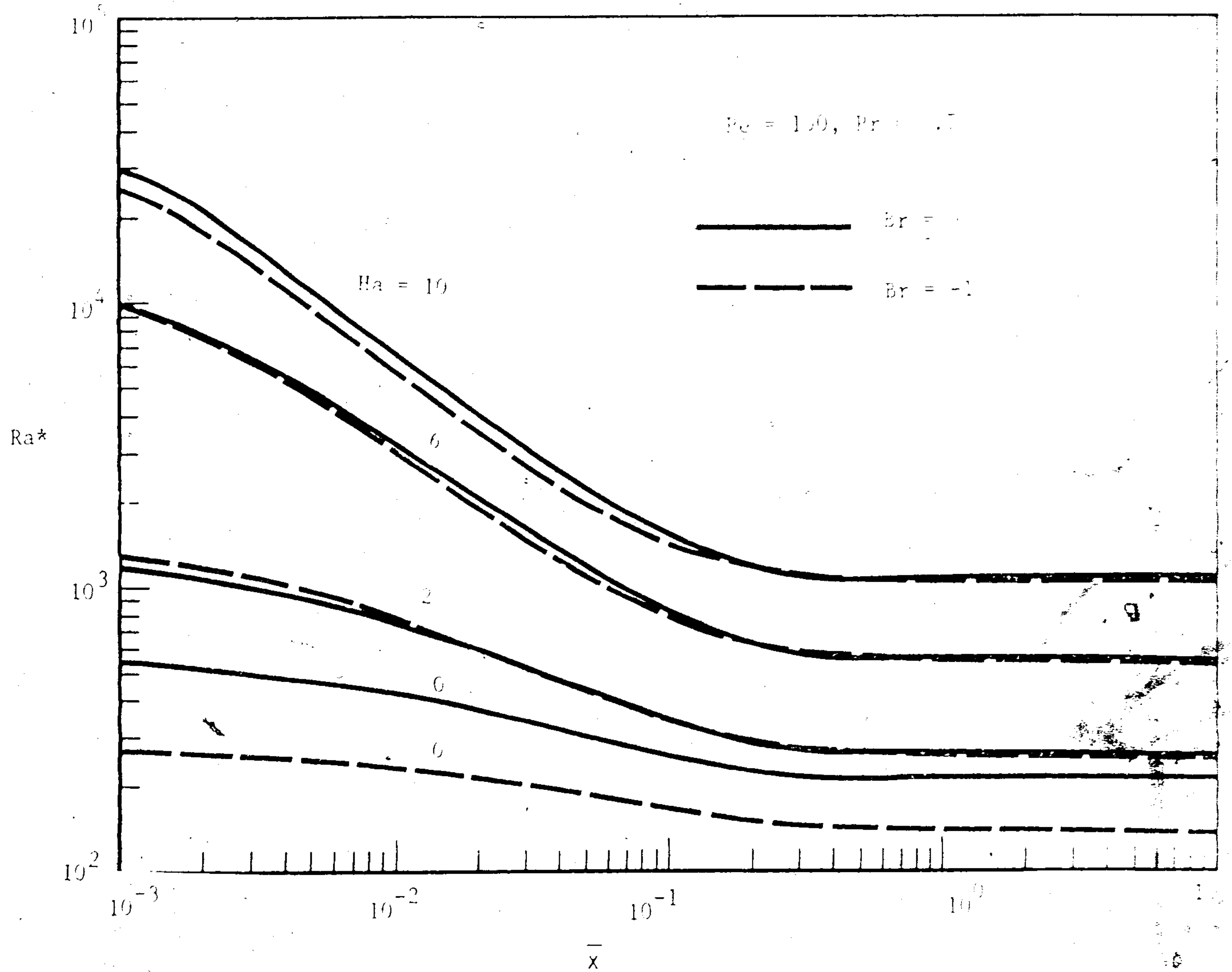

Fig. 17 Hartmann number effect on critical Ra* in thermal entrance region for Pr = 0.7, Pe = 100 and Br = 0,-1.

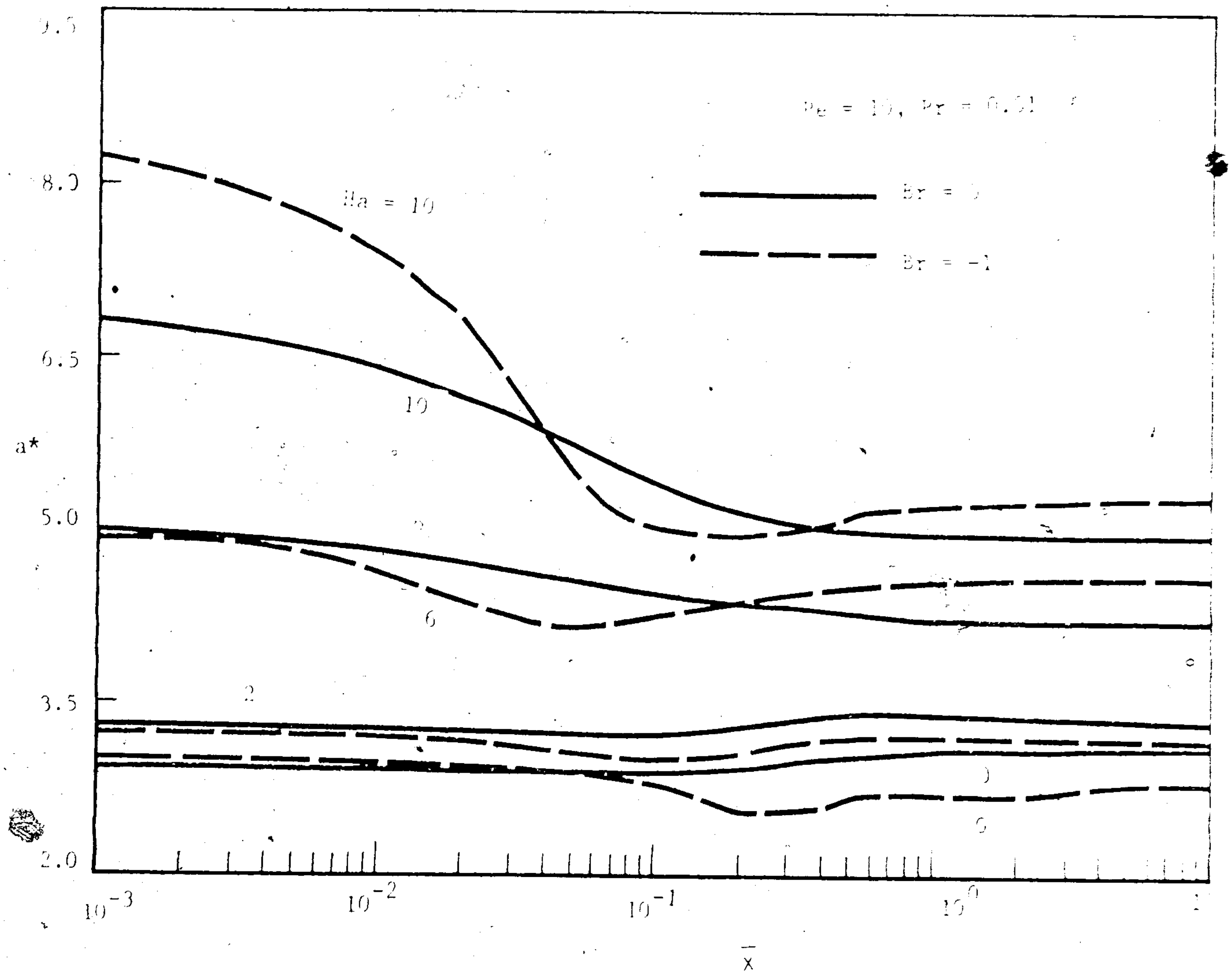

Fig. 18 Hartmann number effect on critical a* in thermal entrance region for Pr = 0.01, Pe = 10 and Br = 0,-1.

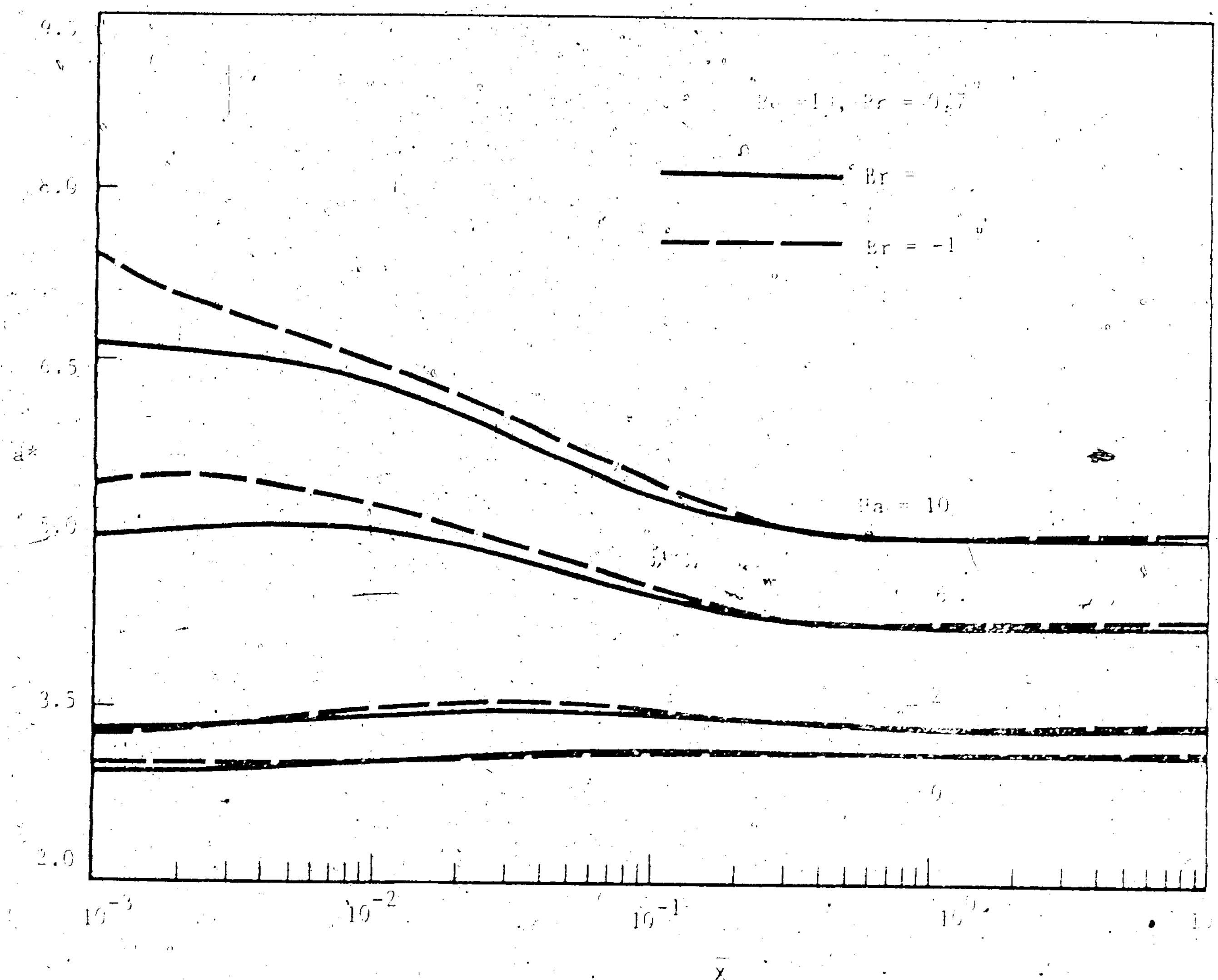

Fig. 19 Hartmann number effect on critical a* in thermal entrance region for Pr = 0.7, Pe = 10 and Br = 0,-1.

CHAPTER VIII

MAXIMUM DENSITY EFFECTS ON THERMAL INSTABILITY INDUCED BY COMBINED BUOYANCY AND SURFACE TENSION

Nield's linear stability analysis (1964) for a horizontal liquid layer considering surface tension and buoyancy effects is extended to the case of water with maximum density effect for the temperature range 0 - 30°C. Two thermal parameters (λ_1, λ_2) and three physical parameters (Bi, Ra, Ma) appear in the analysis. Typical results are presented for the cases involving heating from below and above.

Nomenclature

A	=	temperature difference ratio, $(T_1 - T_{max})/\tau d$
a	=	dimensionless wave number
Bi	=	Biot number, $q_0 d/K$
d	=	liquid layer thickness
g	=	gravitational acceleration
K	=	thermal conductivity of liquid
M	=	number of divisions for liquid layer
Ma	=	Marangoni number, $\sigma_0(\Delta T)d/(\mu\alpha)$
P	=	pressure
p	=	dimensionless perturbation pressure, $P'/(\rho_0 \alpha\nu/d^2)$
q_0	=	rate of change with temperature of the time rate of heat loss per unit area from free upper surface
Ra	=	Rayleigh number (see equation (10))
T, T_1, T_2	=	temperature, lower plate temperature, free surface temperature, respectively
t	=	time
U, V, W	=	perturbation velocity components in X, Y, Z, directions

u, v, w	=	dimensionless perturbation velocities, $(U,V,W)/(\kappa/d)$
X, Y, Z	=	rectangular coordinates
x, y, z	=	dimensionless coordinates, $(X,Y,Z)/d$
	=	thermal diffusivity
	=	coefficient of thermal expansion
γ_1, γ_2	=	temperature coefficients for density-temperature relationship
θ	=	dimensionless temperature disturbance, $\theta'/\Delta T$
μ	=	viscosity
λ_1, λ_2	=	thermal parameters defined in equation (9)
	=	kinematic viscosity
ρ, ρ_0	=	density, reference density
σ_0	=	negative of the rate of change of surface tension with temperature
	=	vertical temperature gradient, $(T_1 - T_2)/d$
ΔT	=	temperature difference, $(T_1 - T_2) = \beta d$

Superscripts and Subscripts

		prime, perturbation quantity

$+$ = dimensionless disturbance amplitude

b = quantity at unperturbed static state

max = value at a density maximum

8.1 Introduction

In recent years, experimental investigations on the onset of convection in a horizontal water layer have been reported in the literature for the thermal conditions involving both melting [1-4] and formation [1,5] of ice. In these studies, the water layer is characterized by stable upper region and potentially unstable lower region separated by an interface with maximum density at 4°C and by continuously changing layer thickness. Theoretical studies on thermal instability of a horizontal liquid layer with maximum density have also been presented for various boundary conditions corresponding to rigid and free surfaces [6-10]. Previous theoretical and experimental investigations on thermal instability with maximum density effects are confined to Rayleigh problem only where the driving force for convection is buoyancy force. For thin horizontal liquid layers with an upper free surface, it is known that the onset of convection can be induced by surface-tension gradients [11] and buoyancy forces [12,13].

The purpose of this study is to determine the stability criteria for the onset of cellular convection driven by surface tension and buoyancy force in a horizontal thin liquid layer by considering the density inversion effect for water using a cubic temperature-density relationship. The lower boundary is taken to be rigid and thermally conducting while at the upper free surface Pearson's boundary conditions [11,12] are imposed to facilitate the analysis.

With the maximum density effect, the liquid layer can be unstable regardless of whether heating is from below or above. The physical model in the present instability analysis is patterned after that of Nield [12]. The maximum density effect for water temperatures ranging from 0 to 30 °C of primary concern in this study. The temperature regime under consideration may be observed under northern climatic conditions. The results of present analysis may be used in assessing the importance of cellular convection in the growth and decay of ice in contact with a thin water layer. The incorporation of the maximum density effect in instability analysis on buoyancy and surface-tension induced cellular convection does not appear to have been considered in the past.

8.2 Formulation of the Thermal Instability Problem

Following the known procedure for linear stability analysis [10,14,15] and referring to the coordinate system shown in Fig. 3, the perturbation equations can be written as

$$\frac{\partial U}{\partial X} + \frac{\partial V}{\partial Y} + \frac{\partial W}{\partial Z} = 0 \qquad (1)$$

$$\frac{\partial U}{\partial t} = -\frac{1}{\rho_0}\frac{\partial P'}{\partial X} + \nu \nabla^2_{X,Y,Z} U \qquad (2)$$

$$\frac{\partial V}{\partial t} = -\frac{1}{\rho_0}\frac{\partial P'}{\partial Y} + \nu \nabla^2_{X,Y,Z} V \qquad (3)$$

$$\frac{\partial W}{\partial t} = -\frac{1}{\rho_0}\frac{\partial P'}{\partial Z} + \nu \nabla^2_{X,Y,Z} W - \frac{\Delta\rho}{\rho_0} g \qquad (4)$$

$$\frac{\partial \theta'}{\partial t} = \beta W + \alpha \nabla^2_{X,Y,Z} \theta' \qquad (5)$$

where $\nabla^2_{X,Y,Z} = \partial^2/\partial X^2 + \partial^2/\partial Y^2 + \partial^2/\partial Z^2$ and the perturbed quantities for temperature, pressure and density are defined by $T = T_b(Z) + \theta'(t,X,Y,Z)$, $P = P_b + P'$ and $\rho = \rho_b + \Delta\rho$, respectively. As shown in [12], the boundary conditions at the lower boundary are

$$W = 0, \quad \frac{\partial W}{\partial Z} = 0 \text{ and } \theta' = 0 \text{ at } Z = 0$$

while at the upper boundary

$$W = 0, \quad \rho\nu \frac{\partial^2 W}{\partial Z^2} = \sigma_0\left(\frac{\partial^2 \theta'}{\partial X^2} + \frac{\partial^2 \theta'}{\partial Y^2}\right) \text{ and}$$

$$-K\frac{\partial \theta'}{\partial Z} = q_0 \theta' \text{ at } Z = d \qquad (7)$$

The density-temperature relationship for water can be approximated by the following equation for the temperature range 0 to 30°C [10].

$$\rho = \rho_{max}\left[1 - \gamma_1 (T - T_{max})^2 - \gamma_2 (T - T_{max})^3\right] \qquad (8)$$

Considering the change in the density $\delta\rho$ caused by the temperature perturbation θ', one obtains the following expression after neglecting the terms containing $(\theta')^2$ or higher order.

$$\delta\rho = \rho_{max}[2\gamma_1(A\Delta T)\{1 + \frac{3\gamma_2}{2\gamma_1}(A\Delta T)\}]\theta'[1 + \lambda_1 (\frac{z}{d}) + \lambda_2 (\frac{z}{d})^2] \tag{9}$$

where $\lambda_1 = (-\frac{1}{A}) \dfrac{1 + 3\frac{\gamma_2}{\gamma_1}(A\Delta T)}{1 + \frac{3\gamma_2}{2\gamma_1}(A\Delta T)}$, $\lambda_2 = (\frac{1}{A^2}) \dfrac{\frac{3\gamma_2}{2\gamma_1}(A\Delta T)}{1 + \frac{3}{2}\frac{\gamma_2}{\gamma_1}(A\Delta T)}$,

$A = (T_1 - T_{max})/\Delta T$ and $\Delta T = T_1 - T_2 = \tau d$. The thermal parameters λ_1 and λ_2 were first introduced by Sun, Tien and Yen [10].

Introducing the dimensionless variables $(X,Y,Z) = d(x,y,z)$, $(U,V,W) = (\alpha/d)\ (u,v,w)$, $P' = (\rho_0\alpha\nu/d^2)p$, $\theta' = (\Delta T)\theta$, and eliminating u, v [illegible] y using continuity equation, one obtains the following perturbation equations by assuming the principle of exchange of stability to be valid [10,15].

$$\nabla^2\nabla^2 w = -Ra(1 + \lambda_1 z + \lambda_2 z^2)\nabla_1^2\theta \tag{10}$$

$$\nabla^2\theta = -w \tag{11}$$

where $Ra = g(2\gamma_1 A\Delta T)(\Delta T)d^3[1 + (3\gamma_2/2\gamma_1)(A\Delta T)]/(\nu\kappa)$, $\nabla^2 = \partial^2/\partial x^2 + \partial^2/\partial y^2 + \partial^2/\partial z^2$ and $\nabla_1^2 = \partial^2/\partial x^2 + \partial^2/\partial y^2$. The boundary conditions are

$$w = \frac{\partial w}{\partial z} = \theta = 0 \text{ at } z = 0 \tag{12}$$

$$w = 0, \quad \frac{\partial^2 w}{\partial z^2} = Ma\,\nabla_1^2\theta \text{ and } \frac{\partial\theta}{\partial z} = -Bi\,\theta \text{ at } z = 1 \tag{13}$$

where $Ma = \sigma_0(\Delta T)d/(\mu\kappa)$ = Marangoni number and $Bi = q_0 d/K$ = Biot number. In contrast to the classical Benard Problem, the onset of convection is possible with heating from below or above because of the presence of $(\Delta T)^2$ in the expression for Rayleigh number. Since restriction is made to the case where instability first appears in the form of cellular convection rather than oscillations associated with over-stability, the following normal modes can be assumed for the disturbance quantities.

$$[w,\theta] = [w^+(z),\theta^+(z)]\exp[i(a_1x + a_2y)] \tag{14}$$

Substituting equation (14) into equations (10) and (11), one obtains

$$(D^2 - a^2)^2 w^+ = a^2 Ra(1 + \lambda_1 z + \lambda_2 z^2)\theta^+ \tag{15}$$

$$(D^2 - a^2)\theta^+ = -w^+ \tag{16}$$

With the boundary conditions

$$w^+ = Dw^+ = \theta^+ = 0 \text{ at } z = 0 \tag{17}$$

$$w^+ = 0,\ D^2w^+ = -a^2 Ma\theta^+ \text{ and } D\theta^+ = -Bi\theta^+ \text{ at } z = 1 \tag{18}$$

where $D = d/dz$ and $a = (a_1^2 + a_2^2)^{1/2}$ is the wave number of the disturbance. For the limiting case Ma = 0 and Bi = ∞, the present eigenvalue problem reduces to that discussed by Sun, Tien a[redacted] [10]. When Ra = 0, the problem reduces to that solved [redacted]arson [11]. The limiting values Bi = 0 and ∞ correspond to constant heat flux and constant temperature and the surface is usually referred to as "insulating" and "thermally conducting" respectively. For given thermal boundary conditions (given λ_1, λ_2 and Bi) and a given Marangoni number Ma, the neutral stability relations give Ra as a function of a and the critical (minimum) Rayleigh number is sought. Conversely when Ra is known, one can determine the critical Marangoni number and the corresponding wave number. Apparently, the present problem can be solved by analytical method [10,12,15,16] as well as finite-difference method.

The finite-difference scheme used is due to Thomas

[17,18] and the iterative solution starts with equation (11) by using $w_k^+ = \sin(2\pi k/M)$, $k = 2, \ldots, M$ for the disturbance velocity w^+. The mesh size used is $M = 50$ and a new and improved eigenvalue Ra or Ma is calculated by the following equation [19].

$$(Ra, Ma)_{new} = (Ra, Ma)_{old} \left[\sum_k (w_k^+)^2_{old}\right]^{1/2} \Big/ \left[\sum_k (w_k^+)^2_{new}\right]^{1/2} \tag{19}$$

The convergence criterion is

$$\sum_k |(w_k^+)_{new} - (w_k^+)_{old}| \Big/ \sum_k |(w_k^+)_{new}| \le 10^{-6} \tag{20}$$

It is found that only a few iterations are required to satisfy the above criterion and five significant figures for critical eigenvalue are correct.

8.3 Numerical Results and Discussion

Because of the number of parameters involved, only typical numerical results can be presented here. The thermal condition parameters λ_1, λ_2 depend on A as well as $\Delta T = \iota d$. For the temperature range (0 - 30°C) under consideration, A is always positive and λ_1 is always negative. Furthermore, the temperature coefficient γ_1 (positive) is of order 10^{-5} and λ_2 (negative) is of order 10[illegible]. The expression for λ_2 reveals that λ_2 is negative for heating from below and positive for heating from above. In addition, the unstable liquid layer is always confined to the region near the bottom plate and instability occurs only when T_1 [illegible] 4°C for heating from below and when T_1 [illegible] 4°C for heating from above.

Figs. 1 and 2 show neutral stability curves for various cases and the effect of the parameter can be seen clearly. The limiting cases of Ra = 0 and Ma = 0 corresponds to Pearson problem [11] and Rayleigh problem, respectively. The distributions of eigenfunctions w^+ and θ^+ are shown in Fig. 3 for Ma = 10, λ_1 = -1.5, λ_2 = -0.2 (heating from below) with Biot number as parameter. It is seen that the curves are quite similar in the lower region up to the location z where the value is maximum. Near the upper free surface, the Biot number effect is quite appreciable particularly for θ^+. The disturbance profiles for λ_1 = -2, λ_2 = 0.4 (heating from above) and Bi = 100 are shown in Fig. 4. With Ma = 0, the disturbance quantity becomes negative. Otherwise the curves for Ma = -30 and -1000 are similar.

The relation between critical Marangoni number Ma* and Rayleigh number is shown in Fig. 5 for a range of Biot numbers with λ_1 = -1.5 and λ_2 = -0.2 (heating from below). As Bi increases, the critical Marangoni number also increases supporting the physical explanation given in [12] for the case of conducting free surface (Bi = ∞). Fig. 6 illustrates the variation of the critical Rayleigh number Ra* with the Marangoni number for a range of Biot numbers with

$\lambda_1 = -1.25$ and $\lambda_2 = 0$. The general trend is similar to that shown in Fig. 2 of [13] which corresponds to the limiting case without maximum density effect. For smaller Biot numbers, the Marangoni effect is seen to be appreciable. As explained in [12], the critical Rayleigh number for a fixed value of Ma is clearly seen to be an increasing function of Bi. The expression for the thermal parameter γ_2 reveals that $\lambda_2 = 0$ when $\gamma_2 = 0$ (parabolic density-temperature relation valid for temperature range 0 – 8°C) or $T_1 = T_{max}$. For given values of Marangoni number, the relation between critical Rayleigh number Ra* and Biot number is shown in Fig. 7 for $\lambda_1 = -1.5$ and $\lambda_2 = -0.2$ (heating from below). At $Bi = 10^4$, the asymptotic value Ra* = 7023.4 is reached. In interpreting the behavior of the curves for Ma = 100 and 1000 at the other end, it is useful to note that for a given Marangoni number a critical value of Ra* does not exist below a certain value of Bi as shown in Fig. 6. Similar plot for the case of heating from above with $\lambda_1 = -2.0$ and $\lambda_2 = 0.4$ is shown in Fig. 8. One also notes the existence of the asymptotic value for Ra* at $Bi = 10^4$. Selected numerical instability results are listed in Tables 1 and 2 for future reference. For the case when buoyancy effects are negligible (Ra = 0), the values of the critical Marangoni number and the corresponding wave number agree excellently with those listed in [12,20] for various values of Bi. On the other hand, with Ma = 0 and $Bi = 10^4$, the values of Ra* = 7023.4 and a* = 2.992 compare well with

$Ra^* = 7027.86$ and $a^* = 2.987$ listed in [21] for $Bi = \infty$. Thus, one may conclude that the present numerical results are sufficiently accurate (five significant figures are correct).

Nield [12,25] concludes for the case of linear density variation that the coupling between the buoyancy and surface-tension effects is surprisingly tight for all values of Bi and especially tight for $Bi = 0$. It is instructive to compare the present results considering maximum density effects with those shown in Figs. 1 and 2 of [12]. The comparison is shown in Figs. 9 (plot of Marangoni and Rayleigh numbers for marginal stability) and 10 (plot of wave number corresponding to marginal stability against normalized Rayleigh number). Fig. 9 shows that with maximum density effect the coupling is rather weak and the Biot number effect is characteristically different. Furthermore, Nield's result [12] shows that the form of the relationship between Ma and Ra is a rather weak function of the Biot number but this is not so for the present problem. As noted by Nield [12,25], the departure of an actual curve from the straight line, $Ra/Ra_c + Ma/Ma_c = 1$, representing perfect coupling, is a measure of the amount of uncoupling. Ra_c is the critical Rayleigh number corresponding to $Ma = 0$ and Ma_c corresponds to $Ra = 0$. In Fig. 10, one sees that when the free surface is "insulating" ($Bi = 0$), the coupling is especially tight for the case of linear density variation [12] but the dimensionless wave number for the present problem varies considerably as the value of Ra/Ra_c increases from 0 to 1. Fig. 10 also shows that larger cells or smaller wave numbers are associated with the insulating case $Bi = 0$. At this point, Fig. 3 also supports the observation that with an insulated boundary it is easier for temperature perturbations to be set up [12]. As Bi increases, the corresponding wave number increases and the size of the convection cell decreases.

Streamlines in Benard convection cells induced by surface tension and buoyancy are given by Nield [22]. The streamlines in the two vertical planes of symmetry of a hexagonal cell at the onset of convection are shown in Fig. 11 (a) and (b) for $\lambda_1 = -1.5$, $\lambda_2 = -0.2$, Ma = 10 and Bi = 100 by using equations (4) and (5) of [22]. In Fig. 11, the left-hand margin represents the cell boundary and the right-hand margin corresponds to the cell centre. In contrast to the streamline patterns shown in [22], the eyes of the streamlines are seen to be located nearer to the lower rigid plate. Fig. 3 also shows that the maximum vertical disturbance w^+ is located nearer to the bottom plate. One notes that for the present problem the unstable layer is situated near the bottom plate.

8.4 Concluding Remarks

1. The physical model [12] assumes that the free upper liquid surface remains undeformed. Nield's linear stability analysis [12] considering surface tension and buoyancy

effects has been confirmed by experiments [23,24]. The limitation of the assumption that departures of the upper surface from a horizontal plane are negligible as well as the possibility for oscillatory instability is well discussed by Nield [25]. Future analysis should include surface viscosity effect and surface deformation pointed out by Scriven and Sternling [26].

2. The case of heating from above may have direct application in surface melting involving ice layer on a lake or pond. The present analysis can be used in predicting the onset of convection for a thin liquid layer on ice driven by surface-tension gradients and buoyancy forces.

3. Within the scope of present study, a full parametric study of the problem is not practical since two thermal condition parameters (λ_1, λ_2) and three flow parameters (Bi, Ra, Ma) appear in the analysis. The graphical results presented are useful in assessing the effects of Bi, Ra and Ma on the onset of instability.

4. The Biot number effect is similar to that discussed in [12]. The detailed physical explanation given in [12] provides further insight into the role of maximum density in the present instability problem.

References

1. Boger, D.V. and Westwater, J.W., "Effect of Buoyancy on the Melting and Freezing Process", J. Heat Transfer 89C, 1967, pp. 81-89.
2. Yen, Y.C., "Onset of Convection in a Layer of Water Formed by Melting Ice from Below", Physics of Fluids 11, 1968, pp. 1263-1270.
3. Yen, Y.C. and Galea, F., "Onset of Convection in a Water Layer Formed Continuously by Melting Ice", Physics of Fluids 12, 1969, pp. 509-516.
4. Sugawara, M., Fukusako, S. and Seki, N., "Experimental Studies on the Melting of a Horizontal Ice Layer", Trans. Japan Soc. Mech. Engrs. 40, 1974, pp. 3155-3165.
5. Tankin, R.S. and Farhadieh, R., "Effects of Thermal Convection Currents on Formation of Ice", Int. J. Heat Mass Transfer 14, 1971, pp. 953-961.
6. Veronis, G., "Penetrative Convection", Astrophysical J. 137, 1963, pp. 641-663.
7. Roberts, P.H., "Characteristic Value Problems Posed by Differential Equations Arising in Hydrodynamics and Hydromagnetics", J. Math. Analysis and Appl. 1, 1960, pp. 195-214.
8. Debler, W.R., "On the Analyogy between Thermal and Rotational Hydrodynamic Stability", J. Fluid Mech. 24, 1966, pp. 165-176.

9. Tien, C., "Thermal Instability of a Horizontal Layer of Water Near 4°C", A.I.Ch.E. J. 14, 1968, pp. 652-653.

10. Sun, Z.S., Tien, C. and Yen, Y.C., "Thermal Instability of a Horizontal Layer of Liquid with Maximum Density", A.I.Ch.E. J. 15, 1969, pp. 910-915.

11. Pearson, J.R.A., "On Convection Cells Induced by Surface Tension", J. Fluid Mech. 4, 1958, pp. 489-500.

12. Nield, D.A., "Surface Tension and Buoyancy Effects in Cellular Convection", J. Fluid Mech. 19, 1964, pp. 341-352.

13. Kobayashi, R., "Instabilität einer von unten erwärmten Flüssigkeitsschicht bei gleichzeitiger Berücksichtigung von Oberflächenspannung und Auftriebskraft", 2 Angew. Math. Phys. 18, 1967, pp. 845-851.

14. Pellow, A. and Southwell, R.V., "On Maintained Convective Motion in a Fluid Heated from Below", Pro. Roy. Soc. (London) 176A, 1940, pp. 312-343.

15. Sun, Z.S., Tien, C. and Yen, Y.C., "Onset of Convection in a Porous Medium Containing Liquid with a Density Maximum", Heat Transfer, 1970, Vol. 4, NC2.11.

16. Nield, D.A., "Surface Tension and Buoyancy Effects in the Cellular Convection of an Electrically Conducting Liquid in Magnetic Field", 2 Angew. Math. Phys. 17, 1966, pp. 131-139.

17. Thomas, L.H., "The Stability of Plane Poiseuille Flow", Physical Review 91, 1953, pp. 780-783.

18. Chen, T.S., "Hydrodynamic Stability of Developing Flow in a Parallel Plate Channel", Ph.D. Thesis, University of Minnesota, 1966.

19. Forsythe, G.E. and Wasow, W.R., "Finite-Difference Methods for Partial Differential Equations", John Wiley & Sons, New York, 1960, Sec. 24.8.

20. Davis, S.H., "Buoyancy-Surface Tension Instability by the Method of Energy", J. Fluid Mech. 39, 1969, pp. 347-359.

21. Sun, Z.S., "Thermal Instability and Heat Transfer of a Horizontal Layer of Liquid with Maximum Density and Heated from Below", M.S. Thesis, Syracuse University, New York, 1968.

22. Nield, D.A., "Streamlines in Benard Convection Cells Induced by Surface Tension and Buoyancy", Z Angew Math. Phys. 17, 1966, pp. 226-232.

23. Palmer, H.J. and Berg, J.C., "Convective Instability in Liquid Pools Heated from Below", J. Fluid Mech. 47, 1971, pp. 779-787.

24. Koschmieder, E.L., "On Convection Under an Air Surface", H. Fluid Mech. 30, 1967, pp. 9-15.

25. Nield, D.A., "Convection Driven by Surface-Tension Gradients and Buoyancy Forces", Proc. 2nd Australasian Conf. Hydraulic and Fluid Mech. University of Auckland, 1965, C45-56.

26. Scriven, L.E. and Sternling, C.V., "On Cellular Convection Drivey by Surface-Tension Gradients: Effects of Mean-Surface Tension and Surface Viscosity", J. Fluid Mech. 19, 1964, pp. 321-340.

Table 1 Instability Results for $\lambda_1 = -1.5$ and $\lambda_2 = -0.2$

Ra	0		$3x10^3$		$5 x 10^3$	
Bi	a*	Ma*	a*	Ma*	a*	Ma*
0	1.993	79.687	2.054	76.107	2.282	64.023
1	2.246	116.25	2.242	104.41	2.422	82.070
10	2.742	413.92	2.592	339.32	2.652	235.25
10^2	2.975	3307.8	2.722	2642.0	2.732	1745.8
10^3	3.009	$32.21x10^3$	2.742	$25.65x10^3$	2.742	$16.84x10^3$
10^4	3.013	$32.12x10^4$				

Ma	0		10^2		10^3	
Bi	a*	Ra*	a*	Ra*	a*	Ra*
0	3.137	758[illegible]				
1	3.093	7471.0				
4	3.040	7297.4	2.693	5840.2		
10	3.013	7176.7	2.856	6482.8		
60	2.995	7056.0	2.967	6923.5	2.774	5203.[illegible]
10^2	2.994	704[illegible]	2.977	6962.8	2.831	6067.5
10^3	2.992	702[illegible]	2.990	7017.1	2.975	6941.5
10^4	2.992	702[illegible]	2.991	7022.6	2.990	7015.2

Table 2. Instability Results for $\lambda_1 = -2.0$, $\lambda_2 = 0.4$

Ma	Bi	0.1	1.0	10	10^2	10^3	∞
0	a*	4.603	4.002	3.402	3.332	3.322	3.322
	Ra*	13535	12502	11804	11539	11500	11495
-10^2	a*				3.346	3.324	3.322
	Ra*				11600	11507	11496
-10^3	a*				3.402	3.338	3.322
	Ra*				12059	11565	11496

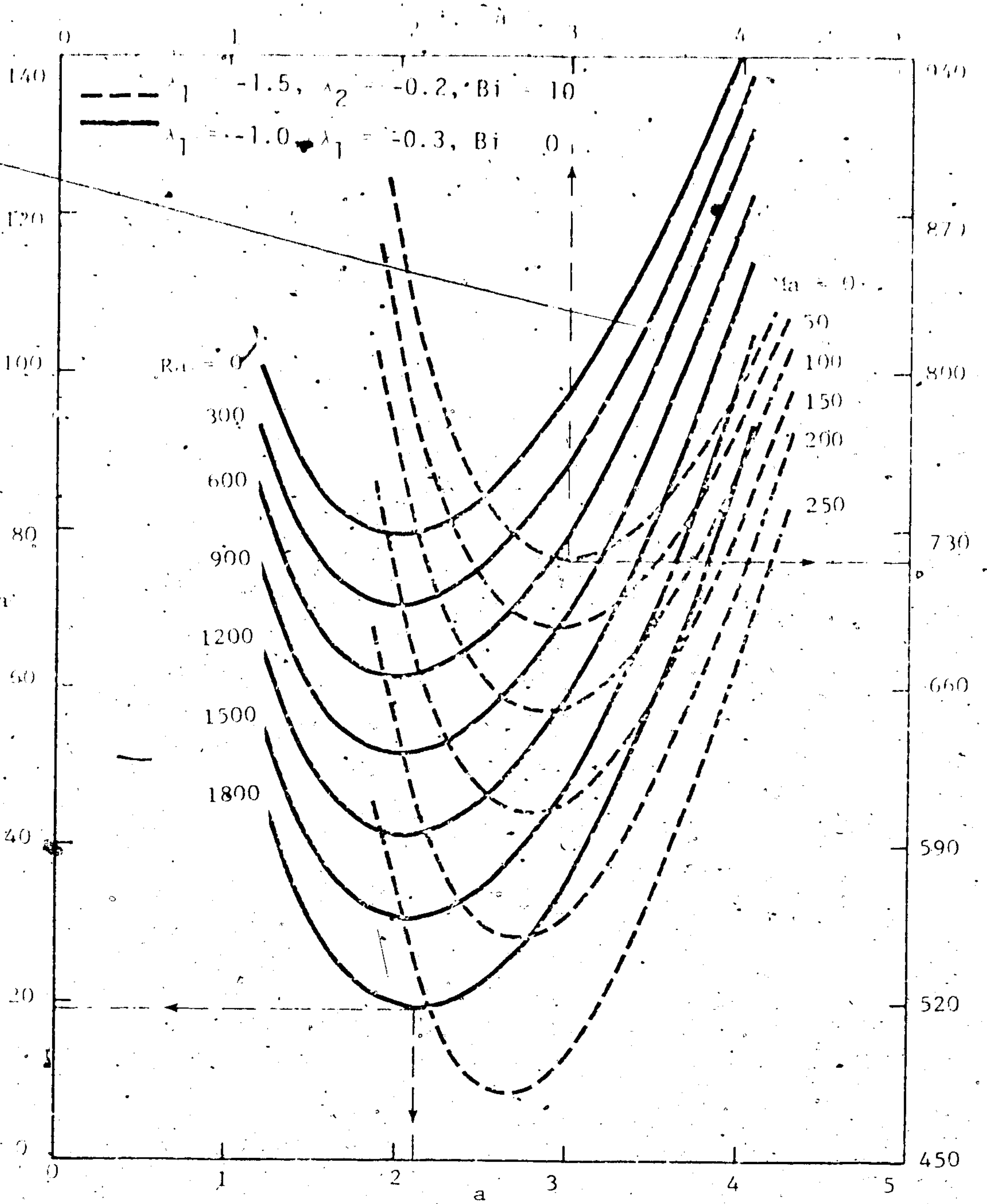

Fig. 1 Neutral Stability Curves for λ_1 = -1.0, λ_2 = -0.3, Bi = 0 and λ_1 = -1.5, λ_2 = -0.2, Bi = 10

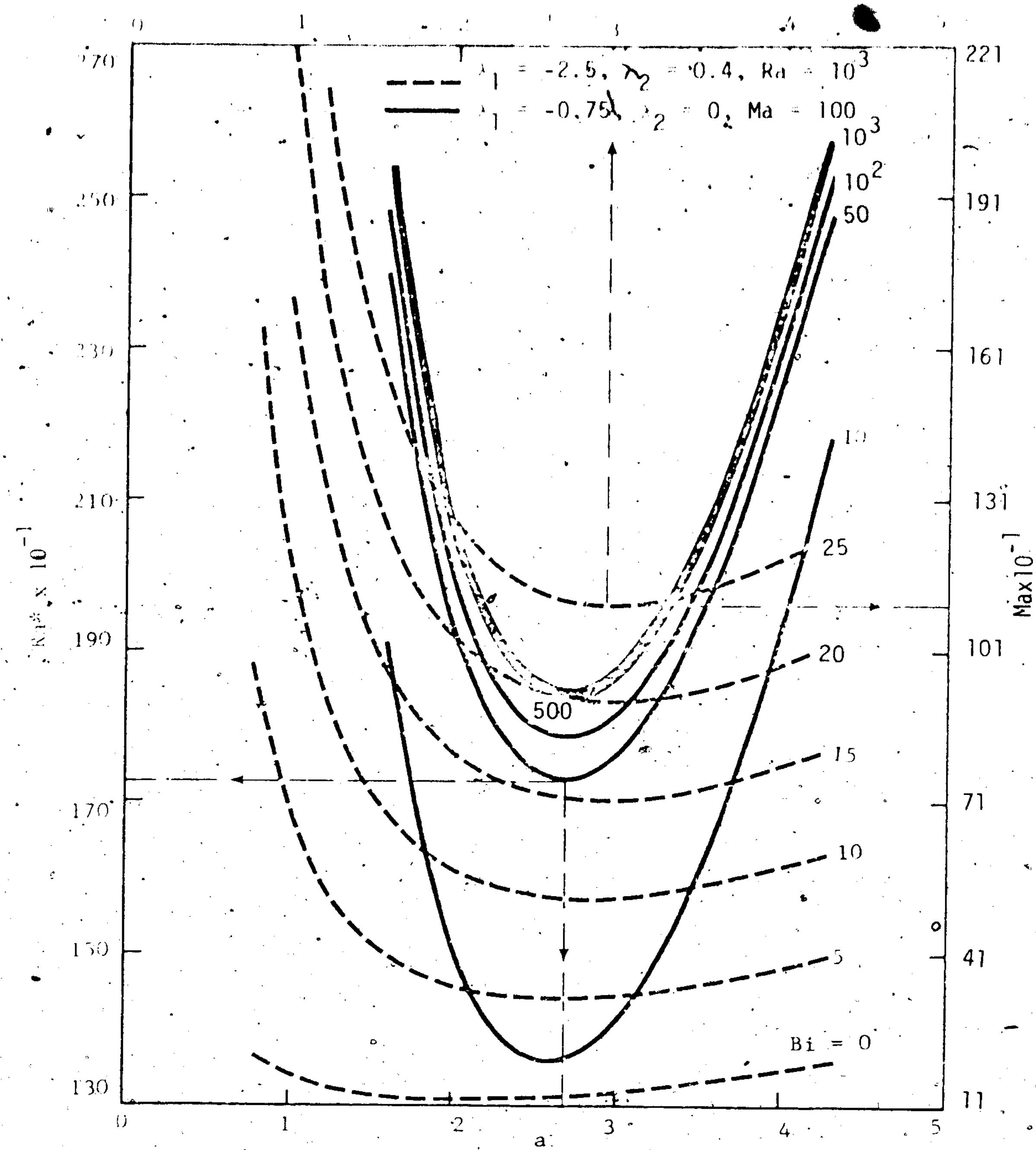

Fig. 2 Neutral stability curves for $\lambda_1 = -0.75$, $\lambda_2 = 0$, $Ma = 10^2$ and $\lambda_1 = -2.5$, $\lambda_2 = 0.4$ and $Ra = 10^3$

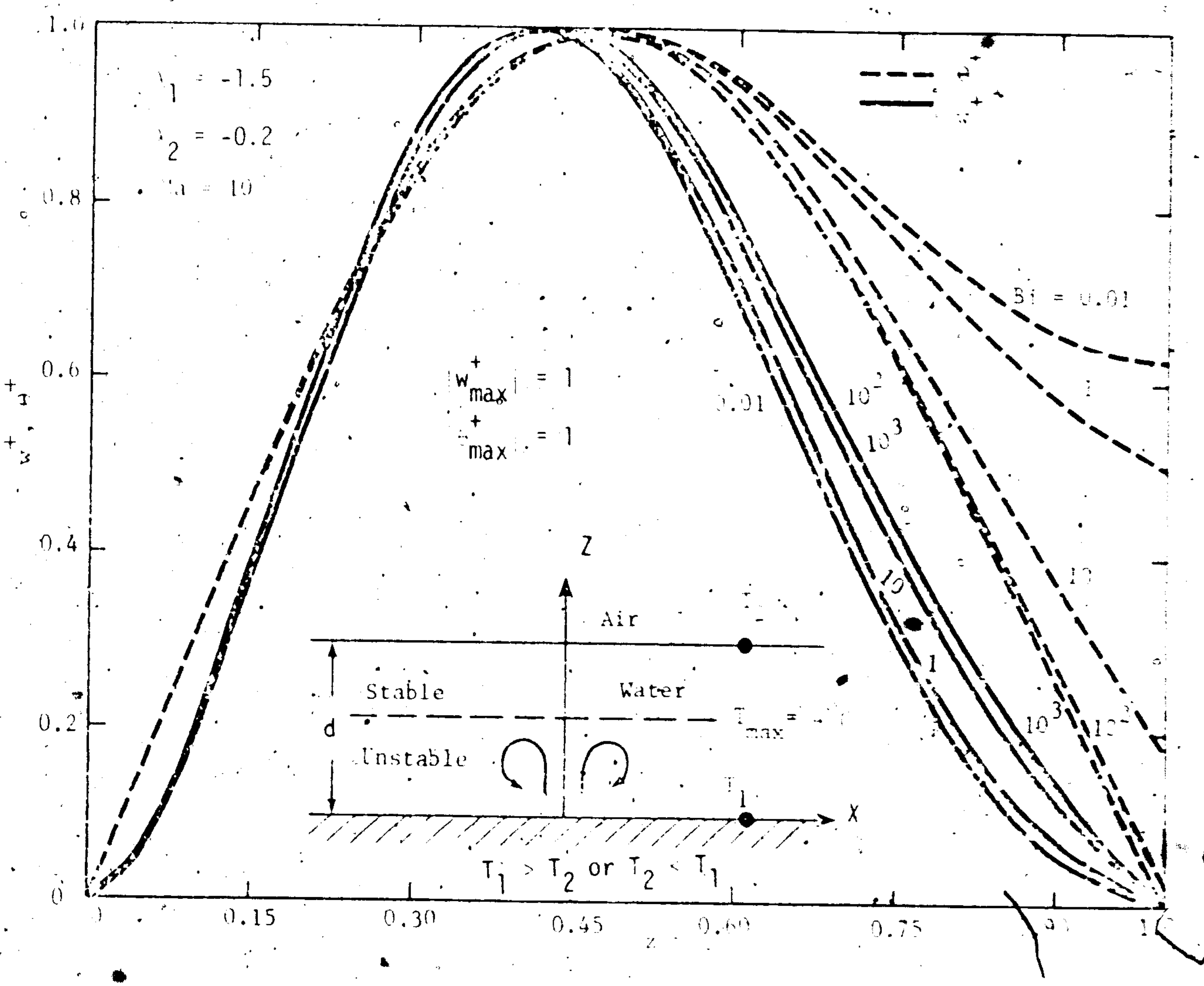

Fig. 3 Coordinate system and disturbance profiles for w^+/w^+_{max} and θ^+/θ^+_{max} for $\lambda_1 = -1.5$, $\lambda_2 = -0.2$, Ma = 10 with Bi as parameter

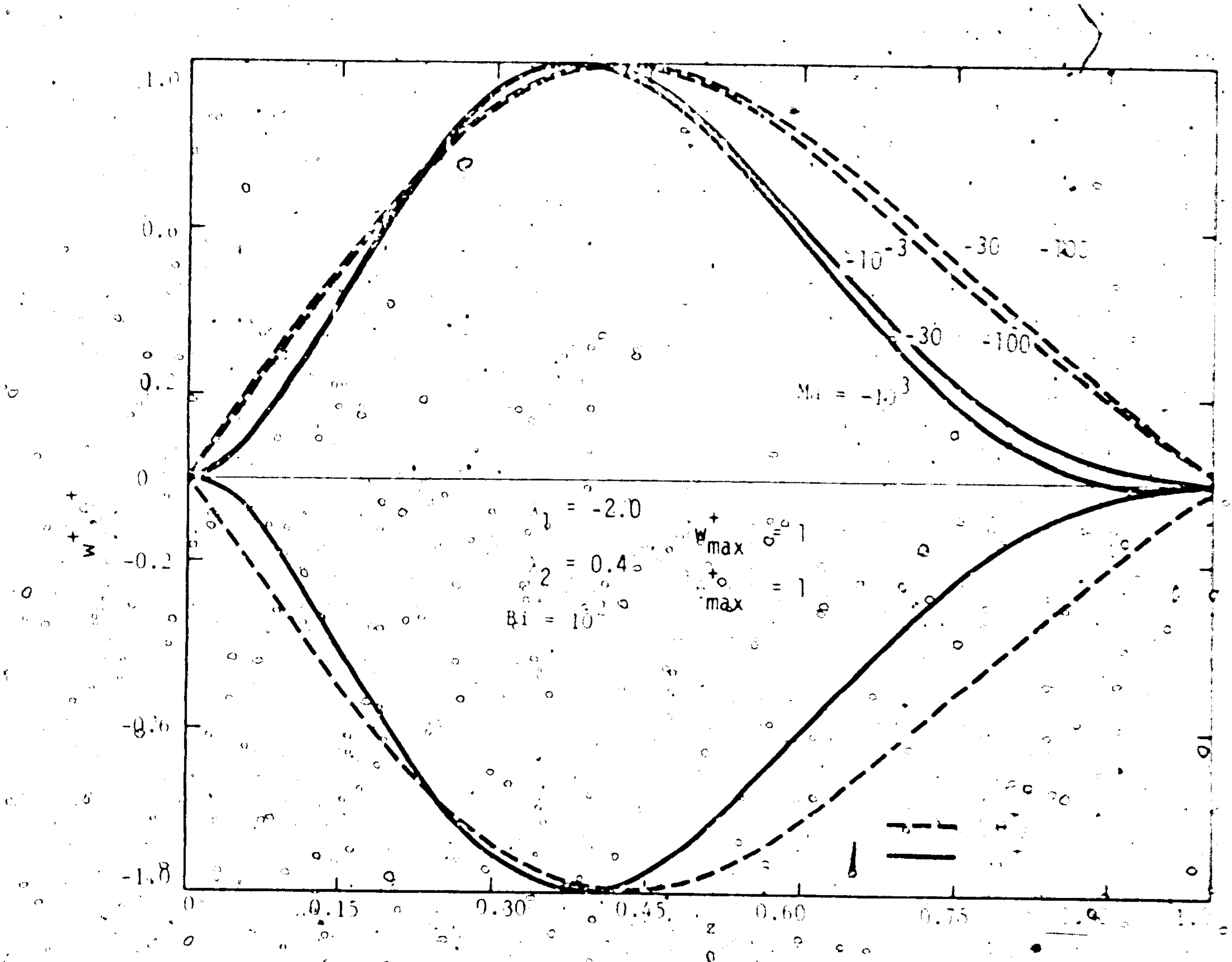

Fig. 4 Disturbance profiles for w^+/w^+_{max} and θ^+/θ^+_{max} for $\lambda_1 = -2.0$, $\lambda_2 = 0.4$, $Bi = 100$ with Ma as parameter.

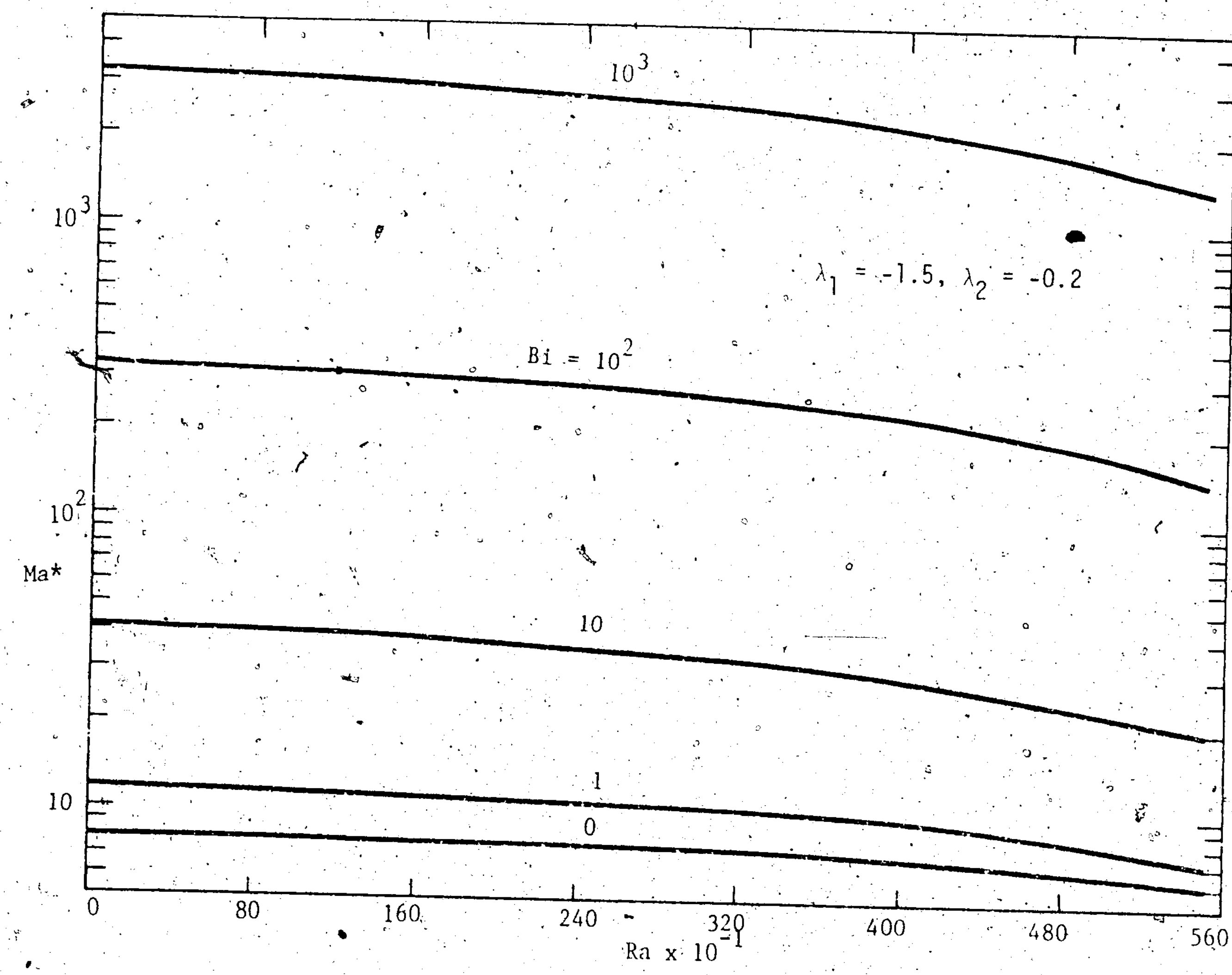

Fig. 5 Relation between critical Marangoni number and Rayleigh number with Bi as parameter for $\lambda_1 = -1.5$ and $\lambda_2 = -0.2$.

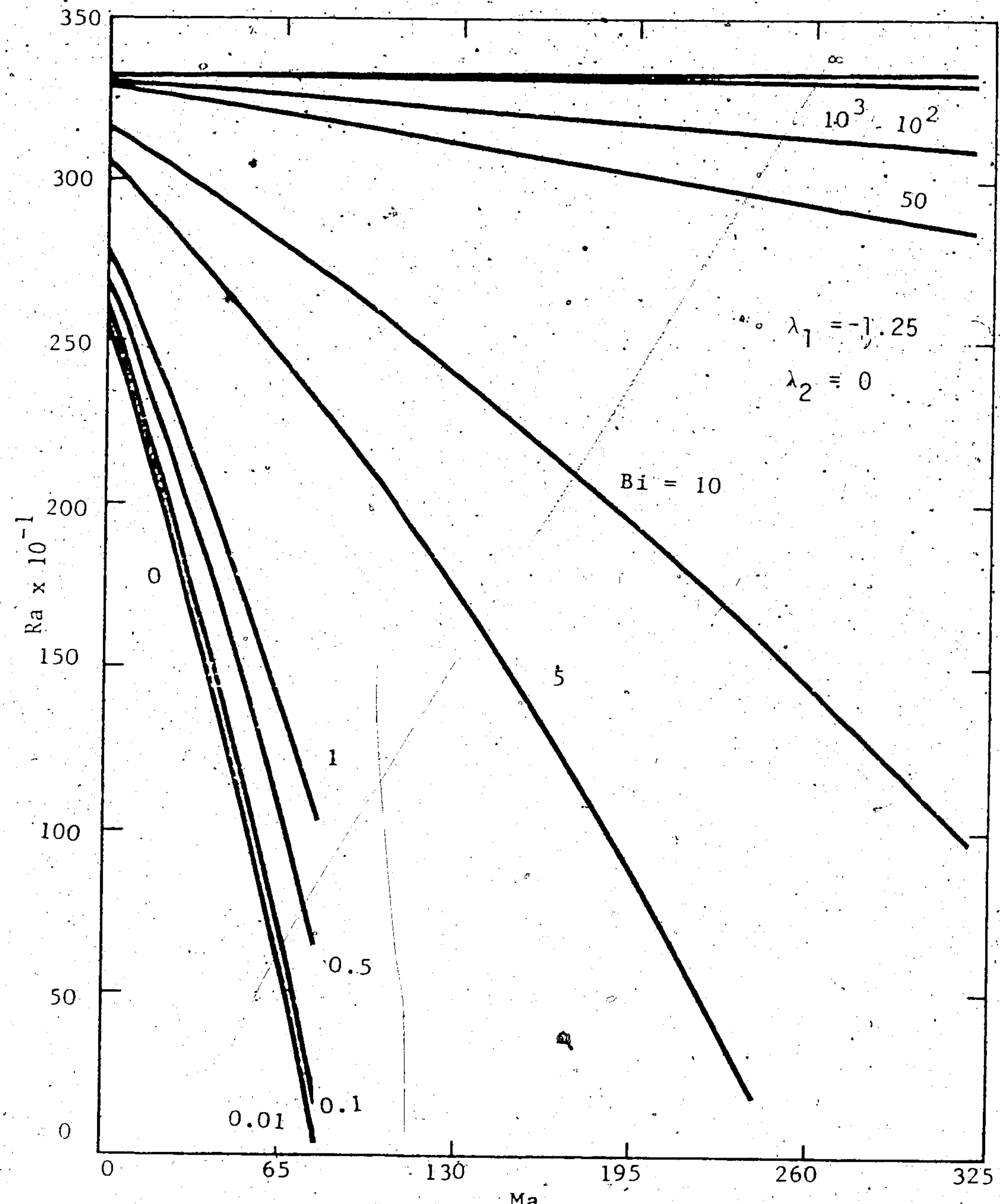

Fig. 6 Relation between critical Rayleigh number and Marangoni number with Bi as parameter for $\lambda_1 = -1.25$ and $\lambda_2 = 0.2$

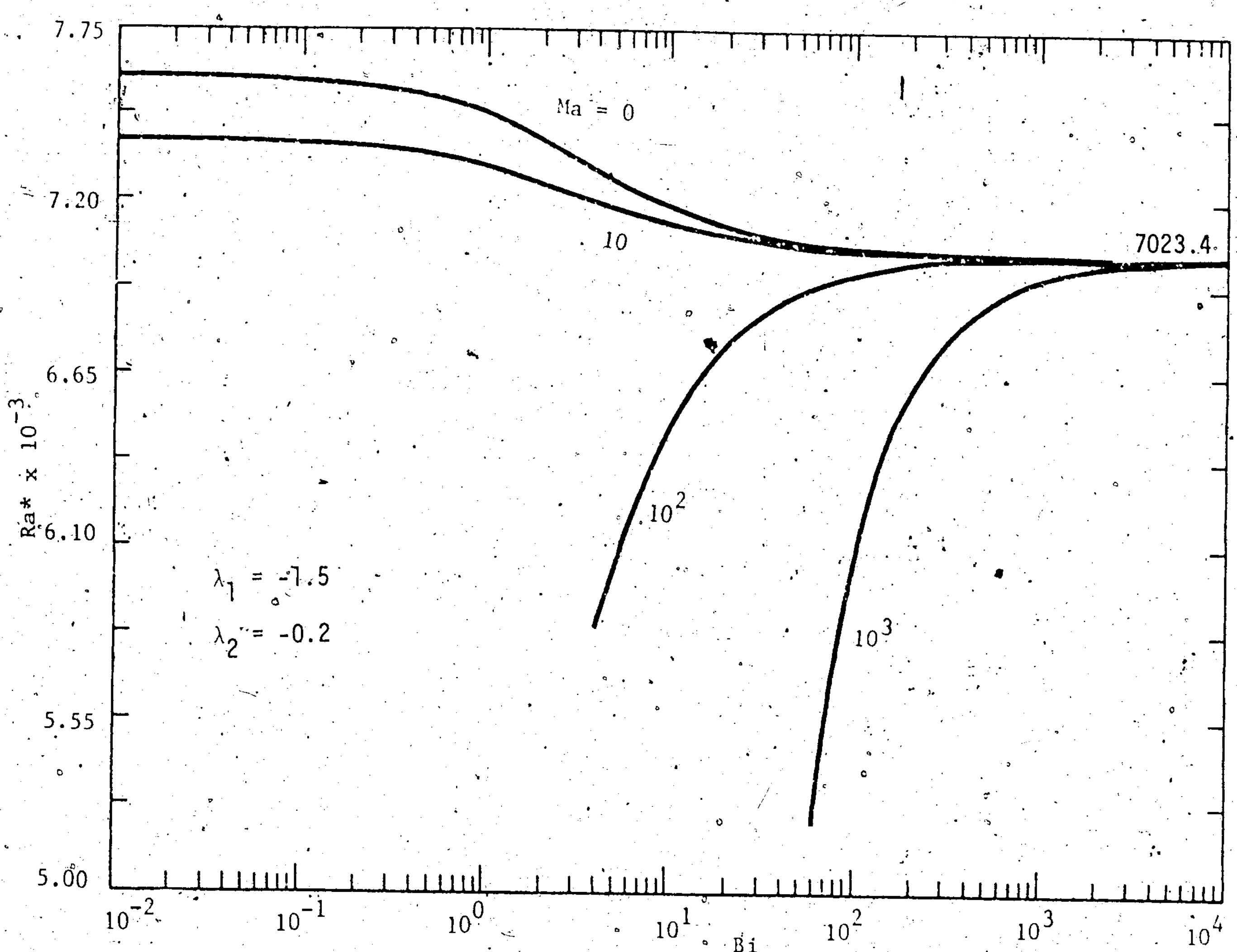

Fig. 7 Relation between critical Rayleigh number and Biot number with Ma as parameter for $\lambda_1 = -1.5$ and $\lambda_2 = 0.2$

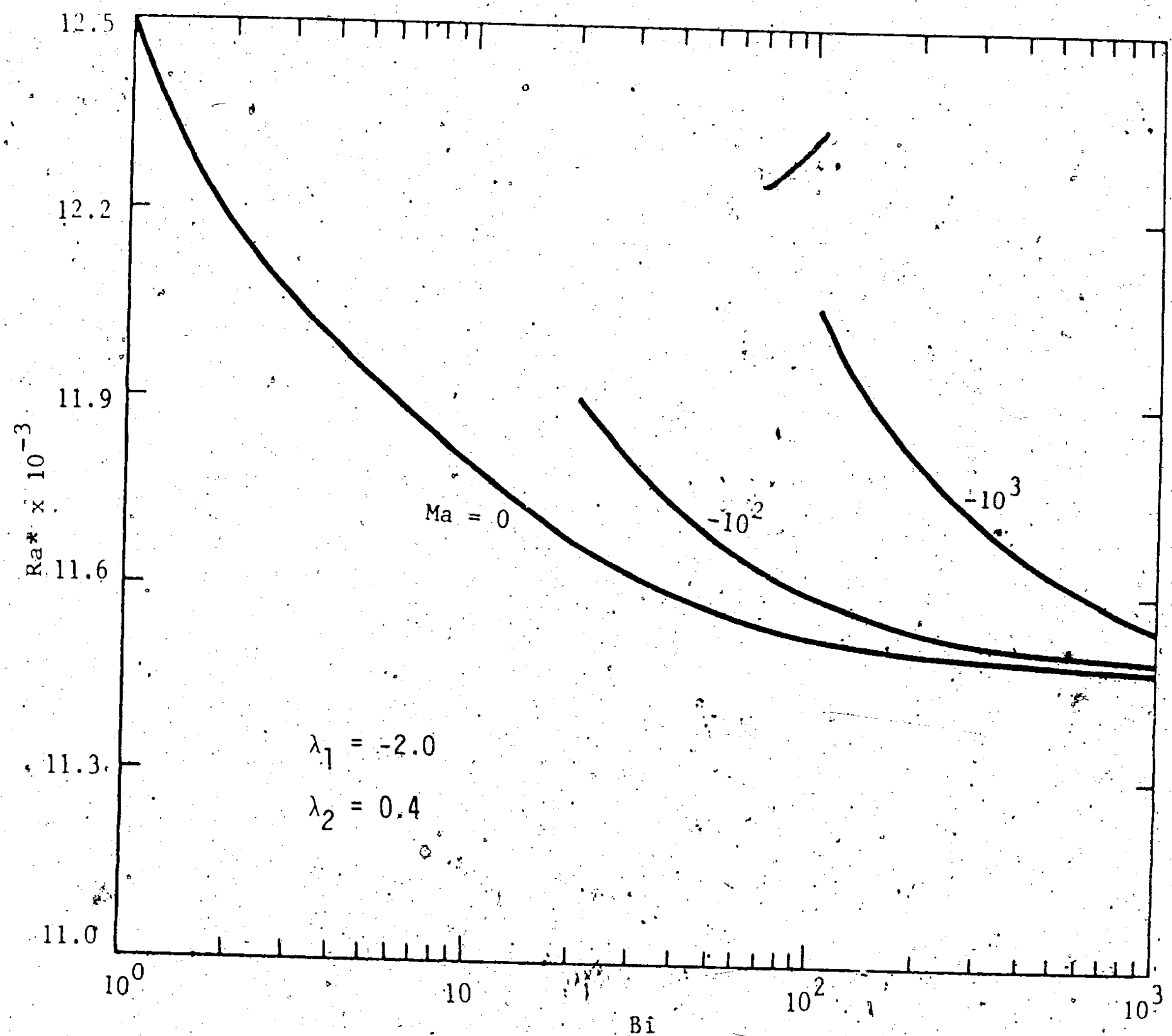

Fig. 8 Relation between critical Rayleigh number and Biot number with Ma as parameter for $\lambda_1 = -2.0$ and $\lambda_2 = 0.4$.

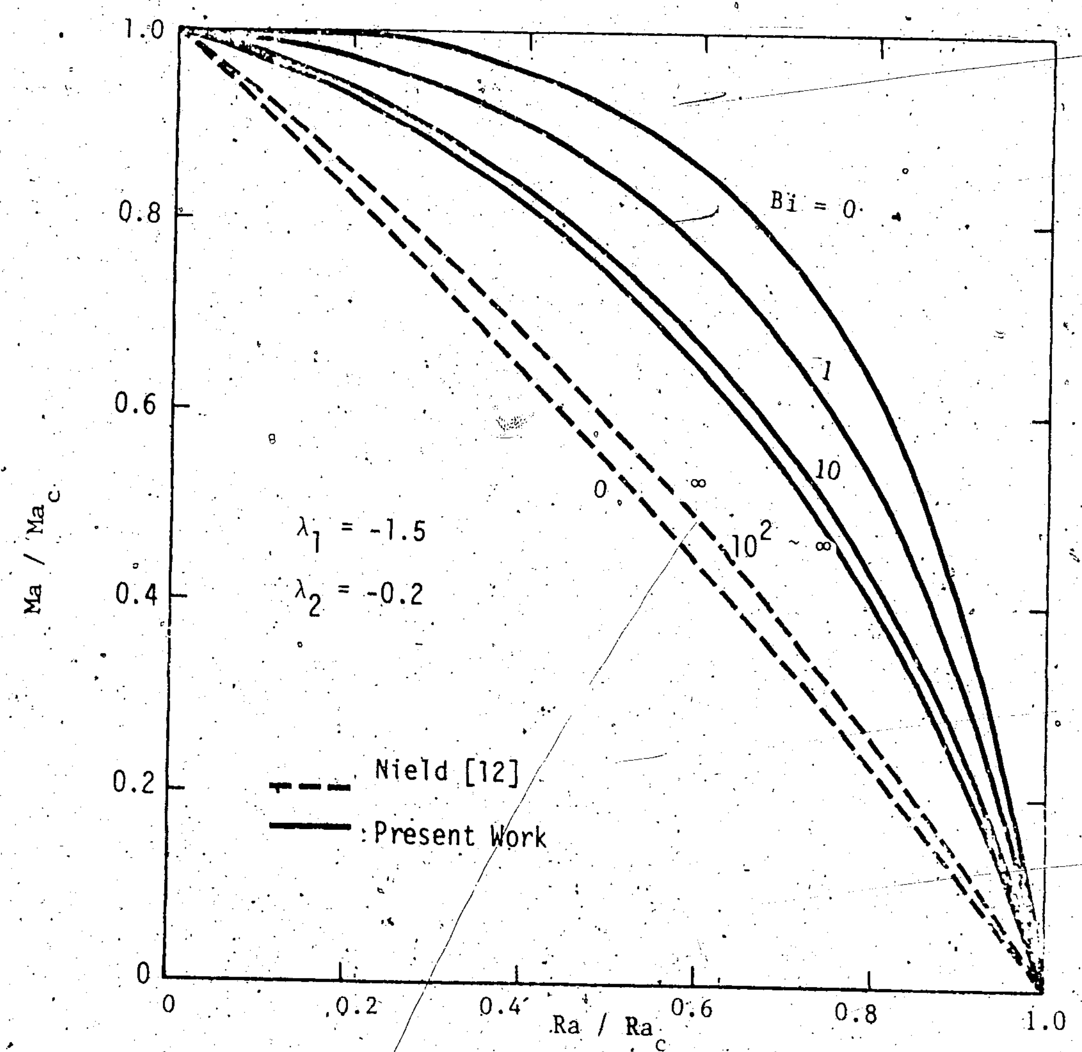

Fig. 9 Variation of normalized Marangoni number Ma/Ma_c with normalized Rayleigh number Ra/Ra_c with Bi as parameter for $\lambda_1 = -1.5$ and $\lambda_2 = -0.2$

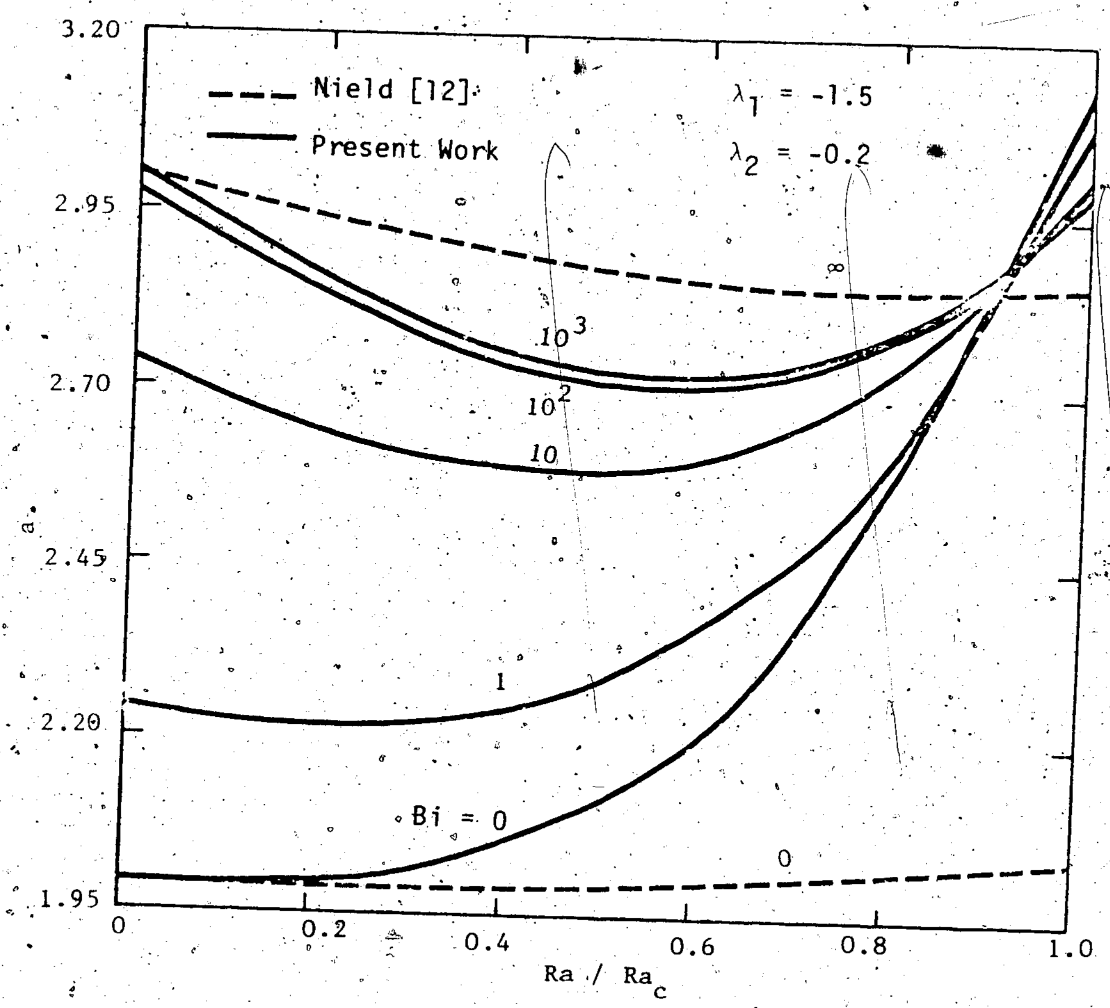

Fig. 10 Variation of dimensionless wavenumber a with normalized Rayleigh number Ra/Ra_c with Bi as parameter for $\lambda_1 = -1.5$ and $\lambda_2 = -0.2$

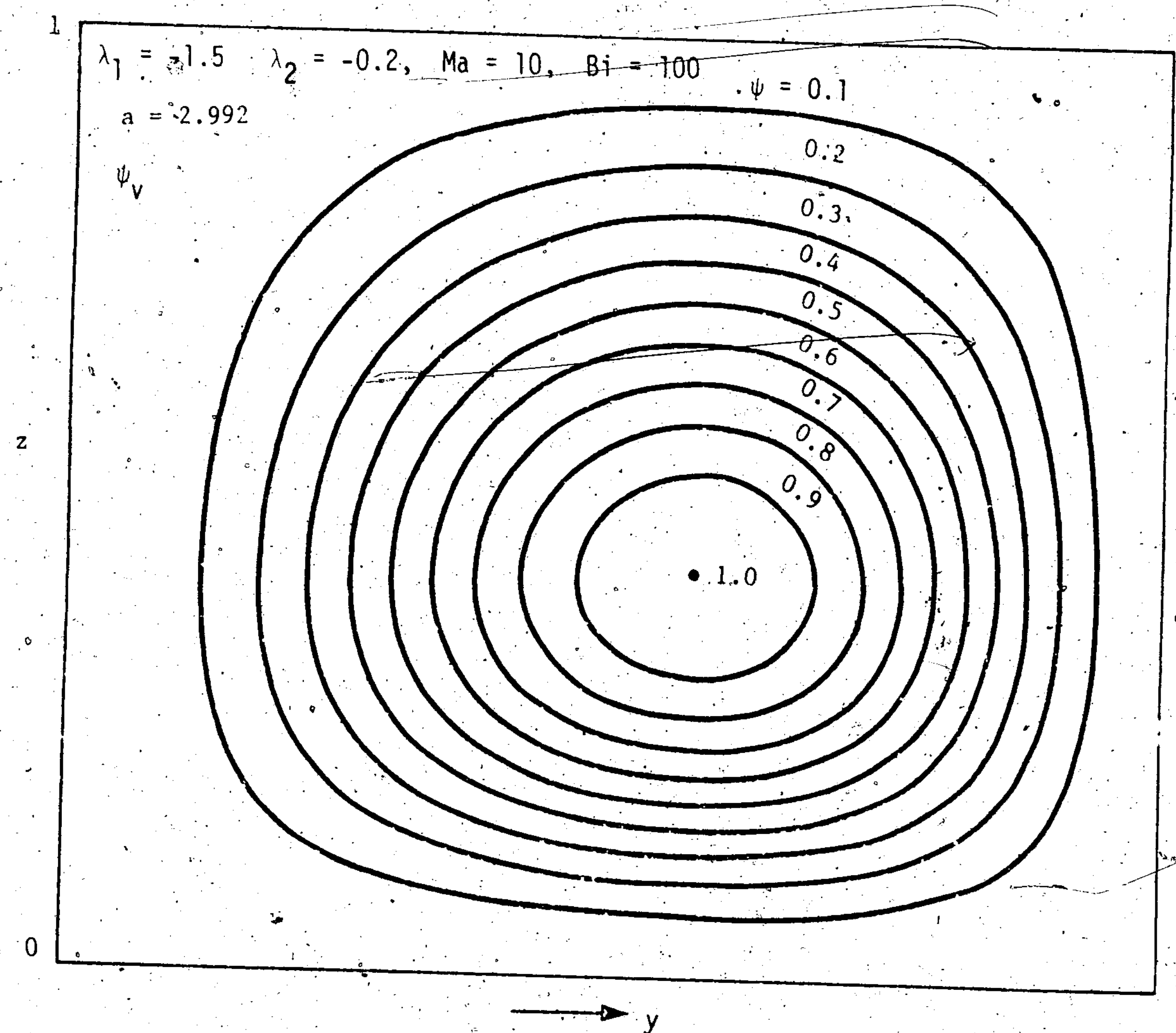

Fig. 11 Streamlines for $\lambda_1 = -1.5$, $\lambda_2 = -0.2$, Ma = 10, Bi = 10^2, (a) through the center and a vertex of the hexagon.

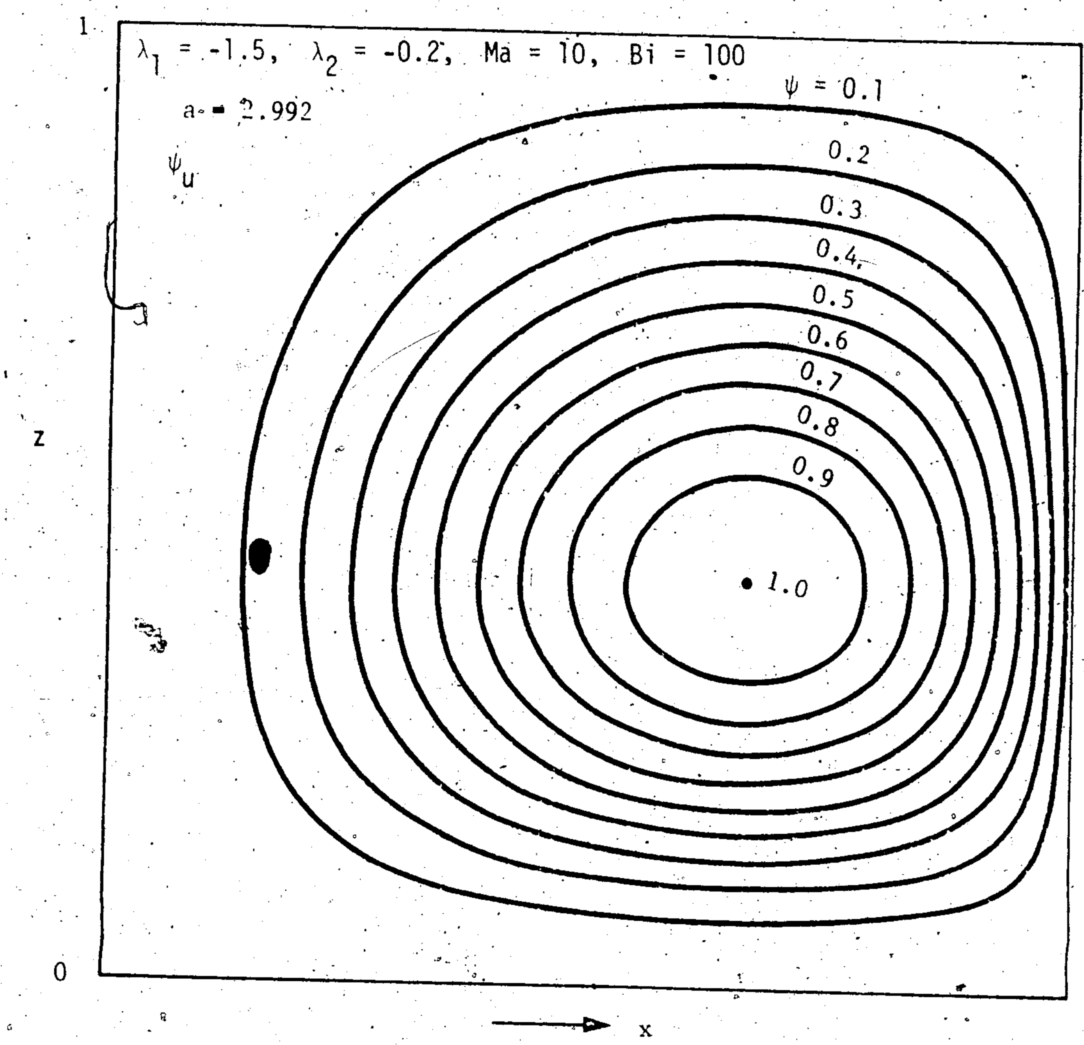

Fig.11 (b) through the center of the hexagon and the mid-point of a side.

CHAPTER IX

THERMAL INSTABILITY OF BLASIUS FLOW ALONG HORIZONTAL PLATES

The thermal instability of laminar forced convection flow along a horizontal semi-infinite flat plate heated isothermally from below or cooled isothermally from above is investigated for disturbances in the form of stationary longitudinal vortices which are periodic in the spanwise direction. The analysis uses non-parallel flow model considering the variation of the basic flow and temperature fields with the streamwise coordinate as well as the transverse velocity component in the disturbance equations. The critical values of the Grashof number $Gr_L^* = Gr_x^*/Re_x^{3/2}$ are obtained for Prandtl numbers ranging from 10^{-2} to 10^4. The Prandtl and Reynolds numbers effects on vortex-type instability for Blasius flow along horizontal plates are clarified.

Nomenclature

a	=	wave number, $2\pi/\lambda$
D	=	$d/d\eta$
F	=	$(\eta f' - f)/2$
f	=	dimensionless stream function
g	=	gravitational acceleration
G	=	eigenvalue, Gr_L/Re_L
Gr_L	=	Grashof number based on L, $g\beta(\Delta T)L^3/\nu^2$
Gr_X	=	Grashof number based on X, $g\beta(\Delta T)X^3/\nu^2$
L	=	characteristic length, $(\nu X/U_\infty)^{1/2}$
M	=	number of divisions in y direction
P	=	Pressure
Pr	=	Prandtl number, ν/α
p	=	dimensionless pressure, $P'/(\rho U_\infty^2/Re_L)$
Re_L, Re_X	=	Reynolds numbers, $(U_\infty L/\nu) = Re_X^{1/2}$ and $(U_\infty X/\nu)$, respectively.
T	=	temperature
U,V,W	=	velocity components in X,Y,Z directions
u,v,w	=	dimensionless perturbation velocities, $(U',V',W')/U_\infty$
$X,Y,Z,$	=	rectangular coordinates
x,y,z	=	dimensionless coordinates, $(X,Y,Z)/L$

α	=	thermal diffusivity
β	=	coefficient of thermal expansion
η	=	similarity variable, $Y/L = Y(U_\infty/\nu X)^{1/2} = y$
θ	=	dimensionless temperature disturbance, $\theta'/\Delta T$
λ	=	dimensionless wavelength of vortex rolls, $2\pi/a$
ν	=	kinematic viscosity
ρ	=	density
τ	=	dimensionless temperature, $(T_b - T_\infty)/\Delta T$
ΔT	=	temperature difference, $(T_w - T_\infty)$

Subscripts and Superscripts

*	=	critical value or dimensionless disturbance amplitude
'	=	prime, disturbance quantity or differentiation with respect to η
b	=	basic flow quantity
w	=	value at wall
∞	=	free stream condition

9.1 Introduction

Buoyancy effects in laminar forced convective flow over a heated horizontal semi-infinite flat plate were first studied by Mori [1] and Sparrow and Minkowycz [2] independently. These early studies apparently motivated further investigations [3-6] in recent years. When a horizontal laminar boundary layer is heated from below or cooled from above, the layer is potentially unstable because of its top-heavy situation due to the density variation of fluid with temperature. The situation is somewhat analogous to the thermal instability of plane Poiseuille flow [7-10] or the well-known Görtler instability of curved boundary layers [11]. The problem of hydrodynamic stability for the laminar boundary layer involving the solution of Orr-Sommerfeld equation has been studied rather extensively in the past. In contrast, the thermal instability problem does not appear to have been reported in the literature.

The purpose of this study is to determine theoretically the conditions marking the onset of longitudinal vortex rolls in a horizontal Blasius flow where the flat plate is heated isothermally from below or cooled isothermally from above. After the onset of vortex rolls, the flow and temperature fields assume a three-dimensional character and the existing flow and heat transfer results for laminar forced convection over a flat plate may no longer apply. It is then obvious that the present problem is of considerable practical interest.

9.2 The Basic Flow

Consideration is given to a horizontal laminar boundary-layer flow with free stream velocity U_∞ and free stream temperature T_∞ along a flat plate where the wall temperature $T_w (> T_\infty)$ is constant. The laminar forced convection flow problem is governed by the following set of equations [12].

$$f''' + \frac{1}{2} ff'' = 0 \tag{1}$$

$$\tau'' + \frac{1}{2} Pr\ f\ \tau' = 0 \tag{2}$$

with the boundary conditions

$$f(0) = f'(0) = \tau(\infty) = 0, \quad f'(\infty) = \tau(0) = 1 \tag{3}$$

where the Blasius similarity variable is $\eta = Y(U_\infty/\nu X)^{1/2} = Y/L(X)$ with $L(X) = (\nu X/U_\infty)^{1/2}$, the stream function $\psi = (\nu X U_\infty)^{1/2} f(\eta)$, the normalized temperature $\tau(\eta) = (T_b - T_\infty)/(T_w - T_\infty)$ and $Pr = \nu/\alpha$ = Prandtl number. Equation (1) is solved by the fourth order Runge-Kutta method and the temperature distribution τ is

$$\theta(\eta) = 1 - \frac{\int_0^\eta [\exp(-\frac{Pr}{2}\int_0^\eta f\, d\eta)]d\eta}{\int_0^\infty [\exp(-\frac{Pr}{2}\int_0^\eta f\, d\eta)]d\eta} \qquad (4)$$

The basic flow is a two-dimensional boundary layer flow which depends on streamwise and transverse directions.

9.3 The Thermal Instability Problem

To study the vortex instability of the basic Blasius flow heated from below (or cooled from above), the perturbation quantities are superimposed on the basic quantities as

$$U = U_b(X,Y) + U'(Y,Z),\ V = V_b(X,Y) + V'(Y,Z),\ W = W'(Y,Z)$$

$$T = T_b(X,Y) + \theta'(Y,Z),\ P = P_b - \rho_\infty g Y + P'(Y,Z)$$

As discussed in [13,14], all of the flow disturbance quantities are taken to be a function of Y and Z only for neutral stability involving Görler vortices. Further details regarding the assumed form of disturbances and some experimental fact are explained clearly in [13]. After applying the linear stability theory and using Boussinesq approximation, the perturbation equations referring to the coordinate system shown in Fig. 1 become

$$\frac{\partial V'}{\partial Y} + \frac{\partial W'}{\partial Z} = 0 \tag{6}$$

$$U' \frac{\partial U_b}{\partial X} + V_b \frac{\partial U'}{\partial Y} + V' \frac{\partial U_b}{\partial Y} = \nu \nabla_1^2 U' \tag{7}$$

$$V_b \frac{\partial V'}{\partial Y} + V' \frac{\partial U_b}{\partial X} = -\frac{1}{\rho} \frac{\partial P'}{\partial Y} + \nu \nabla_1^2 V' + g\beta\theta' \tag{8}$$

$$V_b \frac{\partial W'}{\partial Y} = -\frac{1}{\rho} \frac{\partial P'}{\partial Z} + \nu \nabla_1^2 W' \tag{9}$$

$$U' \frac{\partial T_b}{\partial X} + V' \frac{\partial T_b}{\partial Y} + V_b \frac{\partial \theta'}{\partial Y} = \alpha \nabla_1^2 \theta' \tag{10}$$

---

where $\nabla_1^2 = \partial^2/\partial Y^2 + \partial^2/\partial Z^2$ and the terms involving V_b, $\partial U_b/\partial X$ and $\partial T_b/\partial X$ are retained. The term $U'\partial V_b/\partial X$ is neglected following the boundary layer approximation $\partial V_b/\partial X \approx 0$. The non-parallelism of the basic flow is found to be important in recent investigations [13,14] dealing with the vortex instability of natural convection flow on inclined isothermal plates. The basic flow and temperature quantities can be written in the following form

$$U_b = U_\infty f'(\eta),\ V_b = (U_\infty/2Re_L)(\eta f' - f) = (U_\infty/Re_L)F,$$
$$T_b = T_\infty + \Delta T \tau(\eta) \tag{11}$$

where $Re_L = U_\infty L/\nu = (U_\infty X/\nu)^{1/2} = Re_X^{1/2}$, $F = (\eta f' - f)/2$ and $\Delta T = T_w - T_\infty$.

After introducing the following dimensionless variables, $(x, y = \eta, z) = (X, Y, Z)/L(X)$, $(u, v, w) = (U', V', W')/U_\infty$, $p = P'/(\rho U_\infty^2/Re_L)$, $\theta = \theta'/\Delta T$ the disturbance equations can be recast into the dimensionless form as

$$\frac{\partial v}{\partial y} + \frac{\partial w}{\partial x} = 0 \tag{12}$$

$$F\frac{\partial u}{\partial y} - \frac{1}{2}\eta f''u + Re_L f''v = \nabla^2 u \tag{13}$$

$$F\frac{\partial v}{\partial y} + \frac{1}{2}\eta f''v = \nabla^2 v - \frac{\partial p}{\partial y} + G\theta \tag{14}$$

$$F\frac{\partial w}{\partial y} = \nabla^2 w - \frac{\partial p}{\partial z} \tag{15}$$

$$F\frac{\partial \theta}{\partial y} - \frac{1}{2}\eta\tau' u + Re_L \tau' v = \frac{1}{Pr}\nabla^2\theta \tag{16}$$

where $G = g\beta(\Delta T)LRe_L/U_\infty^2 = Gr_L/Re_L$, $Gr_L = g\beta(\Delta T)L^3/\nu^2 = Gr_X/Re_X^{3/2}$, $Gr_X = g\beta(\Delta T)X^3/\nu^2$ and $\nabla^2 = \partial^2/\partial y^2 + \partial^2/\partial z^2$. Upon eliminating the dependent variable w and the pressure terms from equations (14) and (15) using continuity equation (12), one obtains

$$\nabla^2 u - F \frac{\partial u}{\partial y} + \frac{1}{2} \eta f'' u = Re_L f'' v \tag{17}$$

$$\nabla^2 \nabla^2 v - F \frac{\partial}{\partial y} \nabla^2 v - \frac{1}{2} \eta f'' \nabla^2 v = - G \frac{\partial^2 \theta}{\partial z^2} \tag{18}$$

$$\nabla^2 \theta - Pr\, F \frac{\partial \theta}{\partial y} = Pr \tau' (Re_L v - \frac{1}{2} \eta u) \tag{19}$$

The boundary conditions are $u = v = v' = \theta = 0$ at $y = 0$ and ∞. For the stationary longitudinal vortices which are periodic in the spanwise direction and neglecting the x-dependences [13,14] at the neutral stability, the following disturbance forms are applicable.

$$u = u^+(y) \exp(iaz), \quad v = v^+(y) \exp(iaz), \quad \theta = \theta^+(y) \exp(iaz) \tag{20}$$

The quantity a is the wave number of the disturbance. Substituting equation (20) into the perturbation equations (17) to (19), the following set of equations results.

$$[(D^2 - a^2) - FD + \frac{1}{2} \eta f'']u^+ = Re_L f'' v^+ \tag{21}$$

$$[(D^2 - a^2)^2 - F(D^3 - a^2 D) - \frac{1}{2} \eta f''(D^2 - a^2)]v^+ = a^2 G \theta^+ \tag{22}$$

$$[(D^2 - a^2) - PrFD]\theta^+ = Pr\ \tau'(Re_L v^+ - \frac{1}{2}\eta u^+) \qquad (23)$$

where $D = d/dy$. By setting $u^+ = u^*$, $Re_L v^+ = v^*$, $\theta^+ = \theta^*$ and $GRe_L = Gr_L$, the parameter Re_L does not appear explicitly and the resulting system of equations becomes

$$[(D^2 - a^2) - FD + \frac{1}{2}\eta f'']u^* = f''v^* \qquad (24)$$

$$[(D^2 - a^2)^2 - F(D^3 - a^2D) - \frac{1}{2}\eta f''(D^2 - a^2)]v^* = a^2 Gr_L \theta^* \qquad (25)$$

$$[(D^2 - a^2) - Pr\ FD]\theta^* = Pr\ \tau'(v^* - \frac{1}{2}\eta u^*) \qquad (26)$$

The boundary conditions are

$$u^* = v^* = Dv^* = \theta^* = 0 \text{ and } \eta = 0 \text{ and } \infty \qquad (27)$$

For the conventional parallel flow assumption for the basic flow, the terms involving F as well as the x-derivatives of the basic quantities are neglected. In the disturbance equations, the terms on the right-hand side may be regarded as the driving terms. Equations (24) to (27) form an eigenvalue problem and the solution will be effected by a numerical method.

9.4 Method of Solution

The fourth-order finite-difference scheme used in this study is due to Thomas [15] in his study on the stability of plane Poiseuille flow and the detailed derivations are given by Chen [16] in a study on the hydrodynamic stability of developing flow in a parallel-plate channel. In the present finite-difference solution, a finite value of η must be prescribed to satisfy the boundary condition at $\eta = \infty$ [17]. For this purpose, two cases are considered depending on the value of Prandtl number. When $Pr \geq 1$, the condition at infinity for θ^* is replaced by $\theta^* = 0$ at $\eta = \eta_1$ corresponding to $\tau \leq 10^{-8}$ since as $\tau \to 0$ one has $\tau' \to 0$. Euqation (26) reveals that the flow field is stable for the region $\eta = \eta_1 \sim \infty$. On the other hand, when $Pr < 1$ the boundary condition $u^* = 0$ is set at $\eta = \eta_2$ corresponding to $(f' - 1) \leq 10^{-8}$ and the conditions $v^* = \theta^* = 0$ are set at $\eta = \eta_1 (> \eta_2)$ corresponding to $\tau \leq 10^{-8}$. As $f' \to 1$, one has $f'' \to 0$ and equation (24) shows that $u^* = 0$ for the region $\eta = \eta_1 \sim \infty$. Noting that with $Pr < 1$ the thickness of the thermal boundary layer is larger than that of the hydrodynamic boundary layer, one obtains $v^* = \theta^* = 0$ for the region $\eta = \eta_1 \sim \infty$ from equations (25) and (26). The satisfactory values for the step size Δy, the number of divisions M and the end position η_1 for various Prandtl numbers are found by numerical experiments and the results are listed in Table 1 with η_2 fixed at $\eta_2 = 10.4$.

The finite-difference technique transforms equation

(25) and its boundary conditions into a quidiagonal system of matrix for a set of algebraic equations and similarly two diagonal systems result from equations (24) and (26) and their boundary conditions. The numerical solutions of the quidiagonal and tridiagonal systems are reported in [18] and [19], respectively, and will not be elaborated here.

The iterative procedure for the simultaneous solution of the three perturbation equations consists of the following main steps:

1. With the basic velocity and temperature given, a value of the wave number is selected for a particular Prandtl number.

2. The initial values for the eigenvalue Gr_L and the disturbance velocity v_k^* in the vertical direction are assigned. The selection of the initial value for v_k^* should correspond to the primary mode of disturbance. In this study, $v_k^* = 2(1 - k/M)$, $k = 2,3,\ldots,M$ is used. However, one may note that the initial disturbance in the form of $v_k^* = \sin[(k - 1)\pi/M]$, $k = 1,2,\ldots,M+1$, also leads to a satisfactory result. Any arbitrary form of the disturbance profile satisfying the boundary conditions may be used but the profiles mentioned above are found to yield a faster convergence.

3. The finite-difference form of equation (24) is solved to obtain u_k^*.

4. With v_k^* and u_k^* known, the finite-difference form

of equation (26) is solved to obtain θ_k^*.

5. The right-hand side of equation (25) is now known, and new values of v_k^* are obtained by the finite-difference solution of equation (25).

6. A new and improved eigenvalue can now be computed by the following equation [20].

$$(Gr_L)_{new} = (Gr_L)_{old} \frac{\left|\sum_k (v_k^*)^2_{old}\right|^{1/2}}{\left|\sum_k (v_k^*)^2_{new}\right|^{1/2}} \tag{27}$$

The magnitude of the quantity v_k^* is readjusted by the following equation in order to return to the original order of magnitude.

$$v_k^* = (v_k^*)_{new}\ (Gr_L)_{new}/(Gr_L)_{old} \tag{28}$$

It is well to note that the absolute value for v_k^* cannot be determined from the linearized theory and the correct profile satisfying the governing equation is sought.

7. The steps (3) to (6) are repeated until the following convergence criteria are satisfied.

$$\varepsilon_1 = \sum_k \left|(v_k^*)_{new} - (v_k^*)_{old}\right| / \sum_k (v_k^*)_{new}\Big| \leq 10^{-6} \tag{29}$$

$$\varepsilon_2 = |(Gr_L)_{new} - (Gr_L)_{old}|/(Gr_L)_{new} \leq 10^{-8} \qquad (30)$$

Numerical experiments show that only a few iterations are required to satisfy the above conditions.

By varying the wave number a and carrying out the above iterative procedure, a minimum eigenvalue Gr_L^*, which permits a solution of the set of the disturbance equations, can be found. The minimum eigenvalue and the corresponding wave number are the critical values which correspond to the onset of instability.

9.5 The Neutral Stability Results and Discussion

9.5.1 Perturbed Velocity and Temperature Fields

Although the primary objective of this investigation is to obtain the critical value of the eigenvalue for the onset of stationary longitudinal rolls which are periodic in the spanwise direction, a study of the perturbed velocity and temperature fields may provide some insight into the physical mechanism of thermal instability. Figs. 1 and 2 show the distributions of the basic profiles for f', F and τ with the disturbance amplitudes u*, v* and θ* superimposed for the cases of Pr = 0.7 and [illegible] respectively. Since the magnitudes of the disturbance quantities cannot be determined by using the linear stability theory, the magnitude of the maximum disturbance quantity is taken to be 0.1 in the plotting. In order to study the decay of the disturbance quantity in the vertical direction, the distributions of the disturbances are also shown in Fig. 3 for Pr = 0.7 and 10 where the largest magnitude of the disturbances u^*, v^* and θ^* is again taken to be 0.1. It is noted that the horizontal disturbance velocity u^* is negative suggesting that the secondary flow also derives its energy from the main flow through mutual interactions as represented by the second and third terms on the left-hand side of equation (25). The profiles for u^* and θ^* are seen to be qualitatively similar.

The secondary flow pattern at the onset of instability is of considerable interest. For this purpose one may define a stream function ψ with $v = \partial\psi/\partial z$ and $w = -\partial\psi/\partial y$ satisfying the continuity equation $\partial v/\partial y + \partial w/\partial z = 0$. From the normal modes of the disturbances, one has $v = v^+(y)e^{iaz}$ and $\psi = \psi^+(y)e^{iaz}$. Using $v = \partial\psi/\partial z$ and $v^* = Re_L v^*$, one obtains $\psi = -[iv^*(y)/a]e^{iaz}$. The physical meaning is attached only to the real part of the stream function and the contour lines are shown in Figs. 4 and 5 for Pr = 0.7 and 10, respectively. It is noted that the dimensionless wavelength is $\lambda = 2\pi/a$ and ψ_{max} is taken to be one. One immediately notices the striking resemblance between the streamline pattern of vortex disturbance for flow over concave wall [11] and the present secondary streamline pattern caused by buoyancy forces as illustrated in Figs. 4 and 5.

9.5.2 The Neutral Stability Results

The neutral stability curves for Prandtl numbers 0.7 and 10 are presented in Fig. 6 where the eigenvalue Gr_L is plotted against the wave number a. The numerical results for the critical (minimum) values of the Grashof number Gr_L^* and the corresponding wave number a* are listed in Table 2 for various Prandtl numbers for future reference and the effect of Prandtl number on the critical Grashof number Gr_L^* is shown in Fig. 7.

Taking cognizance of the relationship $Gr_L \doteq Gr_X/Re_X^{3/2}$, the effect of Reynolds number on the critical Grashof number Gr_X^* can be studied readily and the results are presented in Fig. 8 using logarithmic coordinates. It is of particular interest to compare the present result with Sparrow and Minkowycz's result [2] for five percent increase in local heat transfer rate due to buoyancy effect based on pure forced convection flow. For this purpose, the curves on Fig. 1 of [2] are also plotted in Fig. 8. To study the implication of the present result, consider the case of Prandtl number 10. The intersection of the two curves for Pr = 10 indicates that at $Re_X = 4.8 \times 10^2$, the longitudinal vortices may set in at $Gr_X = 7.9 \times 10^5$. The present results clearly suggest the possible upper limit of the applicability of the published results [1-6]. Fig. 8 also shows that for the lower Reynolds number flow, the critical Grashof number Gr_X^* is lower for a given Prandtl number.

9.6 Concluding Remarks

1. The thermal instability of the horizontal Blasius flow heated from below or cooled from above is studied by using linear stability theory based on non-parallel flow model whereby the variations of the basic flow quantities, U_b and T_b, with X as well as the transverse velocity component V_b are retained in the perturbation equations. Some similarity exists between the present problem and the Görtler problem.

2. The result shown in Fig. 7 reveals that the minimum critical value of Gr_L^* is lower for higher Prandtl number. The Prandtl number effect can be explained from the definition of Gr_L. For the pure laminar forced convection problem the ratio of the thermal boundary-layer thickness over the velocity boundary-layer thickness is known to be $\delta_T/\delta = Pr^{-1/3}$ approximately with $\delta = 5.83(\nu X/U_\infty)^{1/2} = 5.83\ L$. Noting the above expression and considering the same $T = T_w - T_\infty$ and Re_X for two different Prandtl numbers, the ratio of the critical Grashof number Gr_L^* can be readily shown to be $(Gr_L^*)/(Gr_L^*)_2 = (g\beta/\nu^2)_1/(g\beta/\nu^2)_2$. For example, with $(Pr)_1 = 0.73$ and $(Pr)_2 = 1170$, one finds the ratio $(Gr_L^*)_1/(Gr_L^*)_2 = (4.2 \times 10^6)/(1.17 \times 10^4)$ and the order of magnitude checks with the results from the present analysis. It is also noted that the temperature gradient $(\Delta T/\delta_T)$ for large Prandtl number fluid is much larger than that of small Prandtl number fluid. In other words, the unstable region for large Prandtl number fluid is confined to a small region inside

the velocity boundary layer. On the other hand, for small Prandtl number fluid, the unstable region extends over a region outside the velocity boundary layer.

3. The basic flow solution for pure forced convection used in this analysis is not valid when Re_X is small (say $< O[10^2]$). For small Re_X, the terms $\partial^2 U_b/\partial X^2$ and $\partial^2 T_b/\partial X^2$ must be included. When $Re_X = 0$, the eigenvalue problem does not exist and a free convection on a heated horizontal semi-finite flat plate arises. On the other hand, the approximate limit of boundary layer theory is $Re_X < 5 \times 10^5$. In interpreting the present results, it must be pointed out that buoyancy effects are considered only in the perturbation equations. An exact analysis would have to consider combined free and forced convection for basic flow. This together with the variable property effect remains to be investigated in future.

4. The experimental data do not appear to be available for comparison with the present results. It remains for future experiments to obtain the vortex instability data.

References

1. Mori, Y., "Buoyancy Effects in Forced Laminar Convection Flow Over a Horizontal Flat Plate", J. Heat Transfer 83C, 1961, pp. 479-482.
2. Sparrow, E.M. and Minkowycz, W.J., "Buoyancy Effects on Horizontal Layer Flow and Heat Transfer", Int. J. Heat Mass Transfer 5, 1962, pp. 501-511.
3. Hauptmann, E.G., "Laminar Boundary-Layer Flows with Small Buoyancy Effects", Int. J. Heat Mass Transfer 8, 1965, pp. 289-295.
4. Tsuruno, S. and Nagai, S., "Buoyancy Effects in Laminar Boundary Layer on a Horizontal Flat Plate", Memoirs of Defense Academy, Japan 9, 1969, pp. 213-219.
5. Redekopp, L.G. and Charwat, A.F., "Role of Buoyancy and the Boussinesq Approximation in Horizontal Boundary Layers", J. Hydronautics 5, 1972, pp. 34-39.
6. Leal, L.G., "Combined Forced and Free Convection Heat Transfer from a Horizontal Flat Plate", J. Applied Mathematics and Physics (ZAMP) 24, 1973, pp. 20-42.
7. Mori, Y. and Uchida, Y., "Forced Convective Heat Transfer Between Horizontal Flat Plates", Int. J. Heat Mass Transfer 9, 1966, pp. 803-817.
8. Nakayama, W., Hwang, G.J. and Cheng, K.C., "Thermal Instability in Plane Poiseuille Flow", J. Heat Transfer 92C, 1970, pp. 61-68.

9. Akiyama, M., Hwang, G.J. and Cheng, K.C., "Experiments on the Onset of Longitudinal Vortices in Laminar Forced Convection Between Horizontal Plates", J. Heat Transfer 93C, 1971, pp. 335-341.

10. Hwang, G.J. and Cheng, K.C., "Convective Instability in the Thermal Entrance Region of a Parallel-Plate Channel Heated from Below", J. Heat Transfer 95C, 1973, pp. 72-77.

11. Görtler, H., "Über eine dreidimensionale Instabilität laminar Grenzschichten an Konkaven Wänden", Nachr. Ges. Wiss, Göttingen, Fachgr. I (N.F.) 2, 1940, pp. 1-26.

12. Schlichting, H., "Boundary-Layer Theory", 6th ed., Chapter 12, McGraw-Hill, New York, 1968.

13. Haaland, S.E. and Sparrow, E.M., "Vortex Instability of Natural Convection Flow on Inclined Surfaces", Int. J. Heat Mass Transfer 16, 1973, pp. 2355-2367.

14. Hwang, G.J. and Cheng, K.C., "Thermal Instability of Laminar Natural Convection Flow on Inclined Isothermal Plates", Canadian J. of Chemical Engineering 51, 1973, pp. 659-666.

15. Thomas, L.H., "The Stability of Plane Poiseuille Flow", Physical Review 91, 1953, pp. 780-783.

16. Chen, T.S., "Hydrodynamic Stability of Developing Flow in a Parallel-Plate Channel", Ph.D. Thesis, University of Minnesota, 1966.

17. Collatz, L., "The Numerical Treatment of Differential Equations", 3rd Ed., Springer-Verlag, Berlin, 1960, pp. 150-151.

18. Conte, S.D. and Dames, R.T., "An Alternating Direction Method for Solving the Biharmonic Equation", Math. Tables and Other Aids to Computation 12, 1958, pp. 198-205.

19. Wachspress, E.L., "Iterative Solution of Elliptical Systems and Applications to the Neutron Diffusion Equations of Reactor Physics", Sec. 1.5, Prentice-Hall, New Jersey, 1966.

20. Forsythe, G.E. and Wasow, W.R., "Finite-Difference Methods for Partial Differential Equations", Sec. 24.8, John Wiley & Sons, New York, 1960.

Table 1 Numerical data for Δy M and η_1

Pr	0.01	0.1	0.7	1.0	10	10^2	10^3
Δy	0.04	0.04	0.04	0.04	0.02	0.01	0.01
M	1600	650	275	260	250	200	105
η_1	64	24	11	10.4	5.0	2.0	1.05

Table 2 Numerical Result for Gr_L^*

Pr	0.01	0.04	0.06	0.1	0.7	1.0	10	10^2	10^3	10^4
a*	0.040	0.050	0.050	0.060	0.11	0.14	1.72	2.95	3.90	7.20
Gr_L^*	2472	475.9	360.3	303.9	292.5	270	75.48	13.46	2.406	1.816

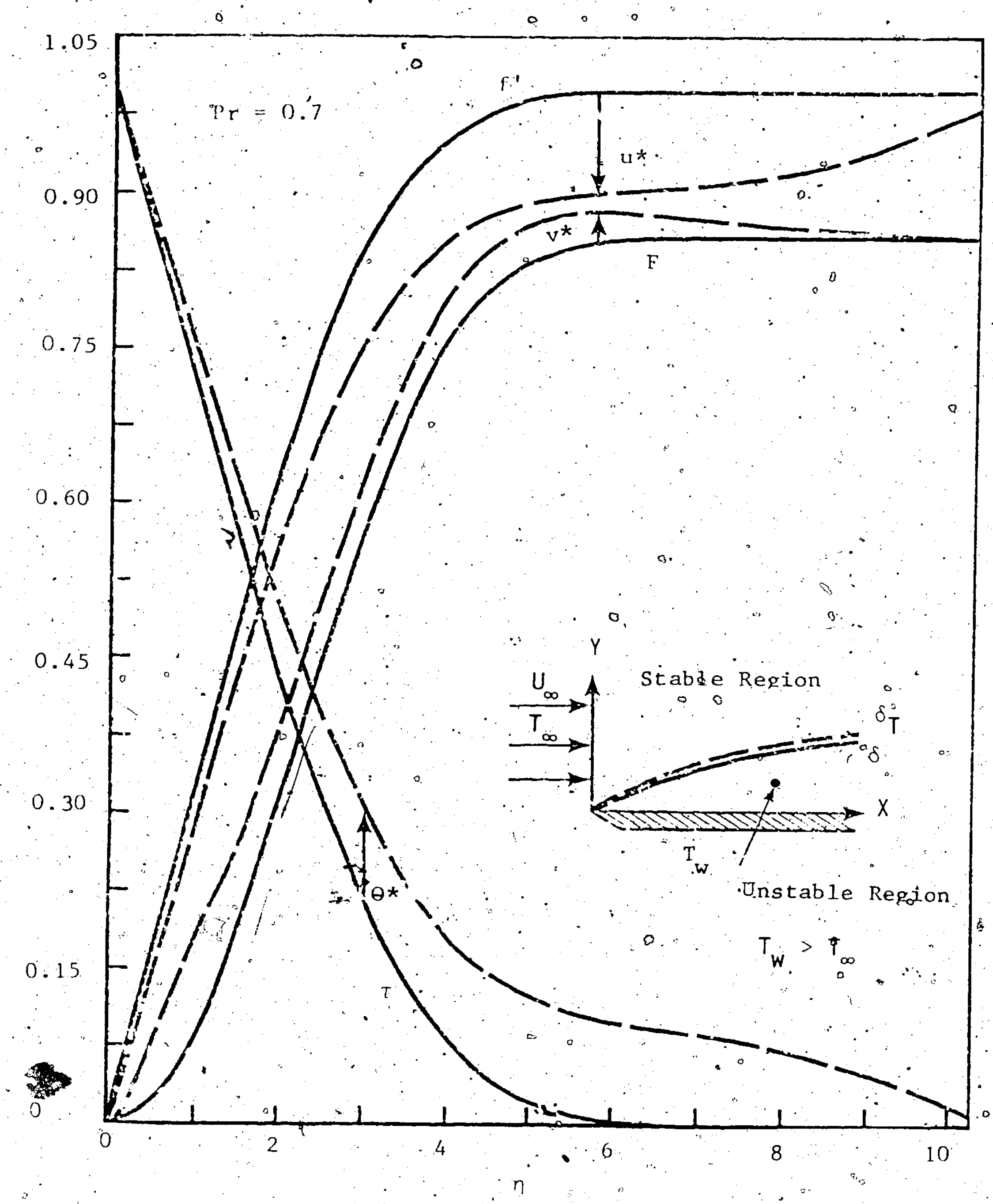

Fig. 1 Coordinate system and distributions of basic quantities f', F, τ and perturbation amplitudes u^*, v^*, θ^* for $Pr = 0.7$

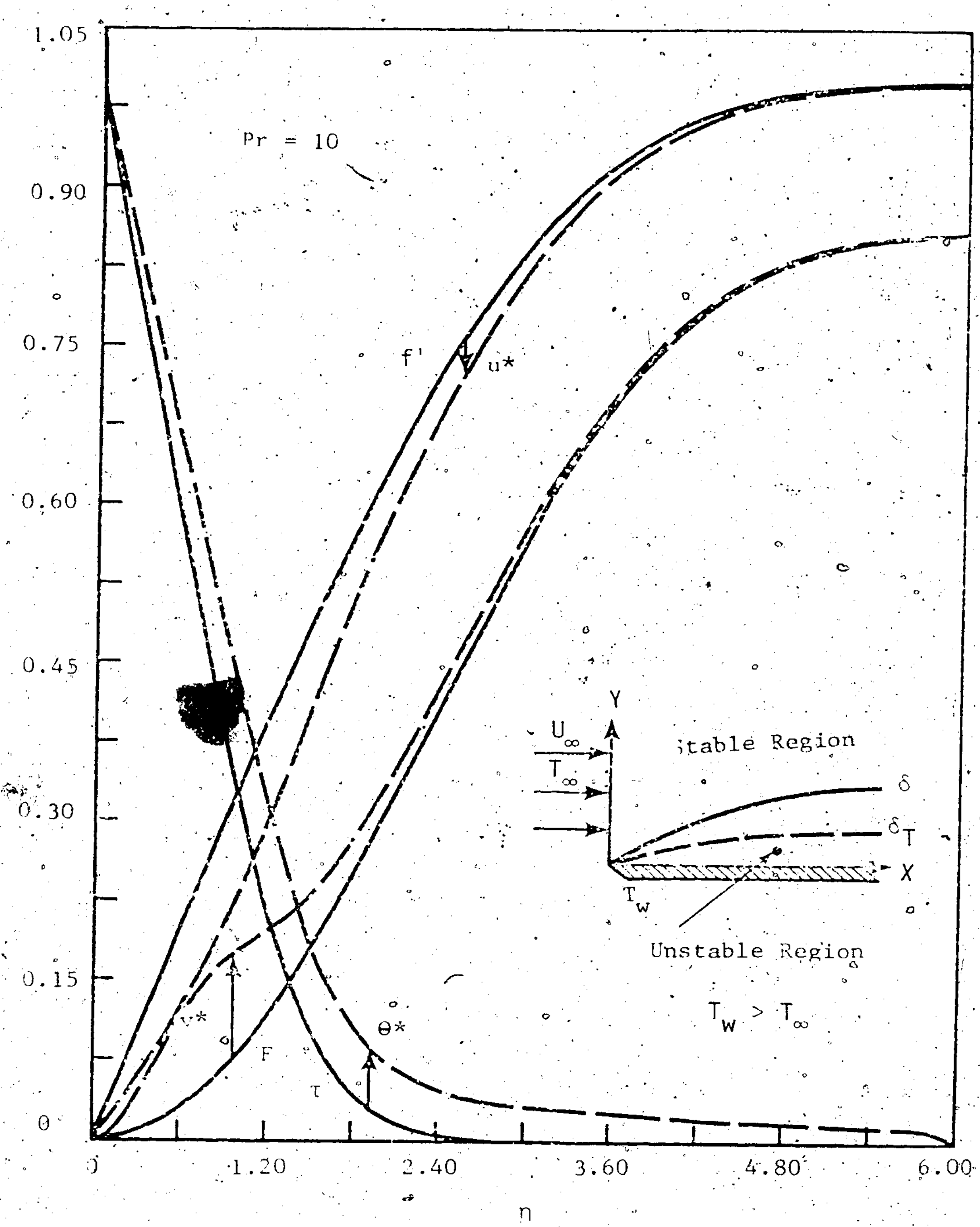

Fig. 2 Distributions of basic quantities f', F, τ and perturbation amplitudes u*, v*, θ* for Pr = 10

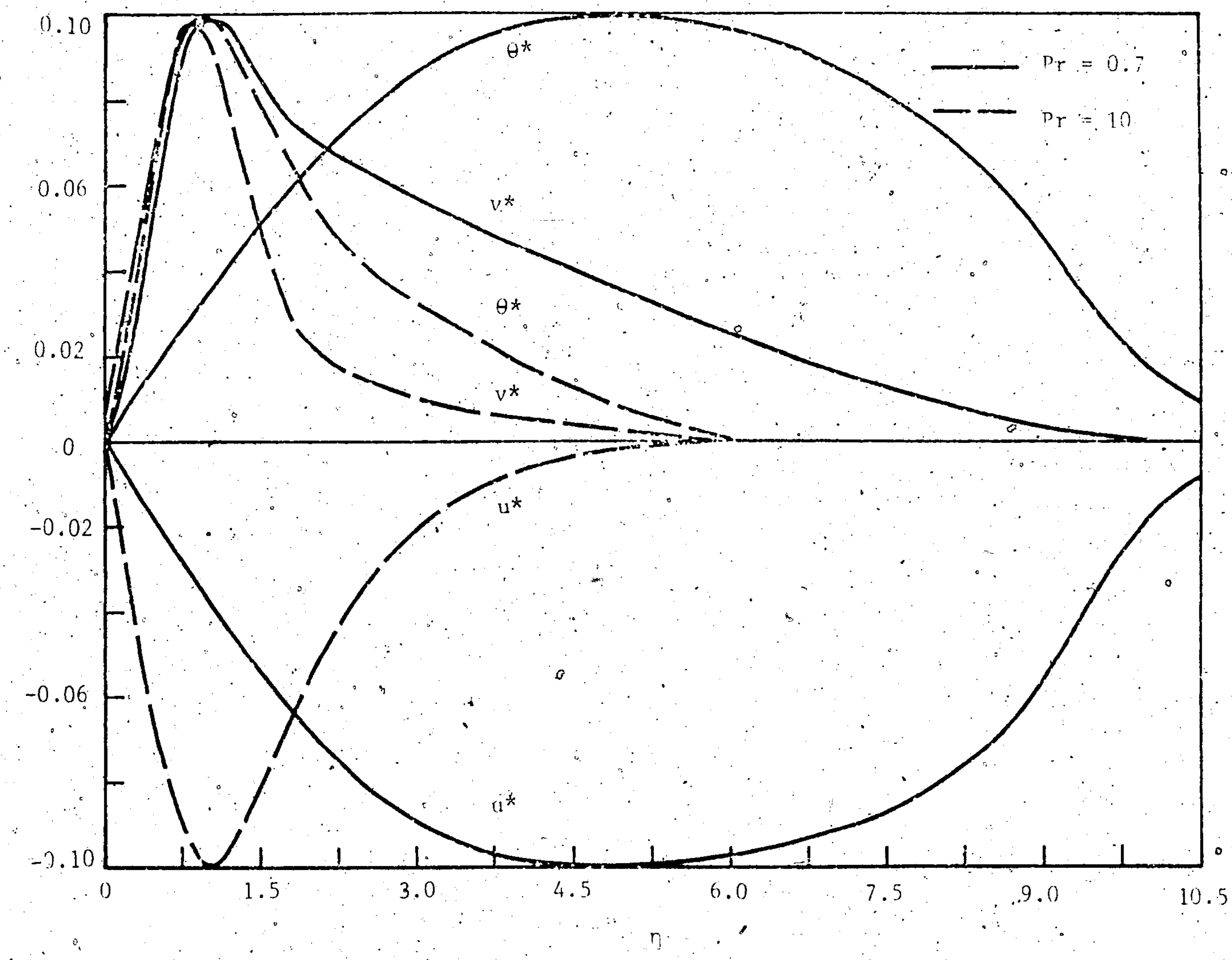

Fig. 3 Profiles for perturbation amplitudes u^*, v^*, and θ^* for $Pr = 0.7$ and 10

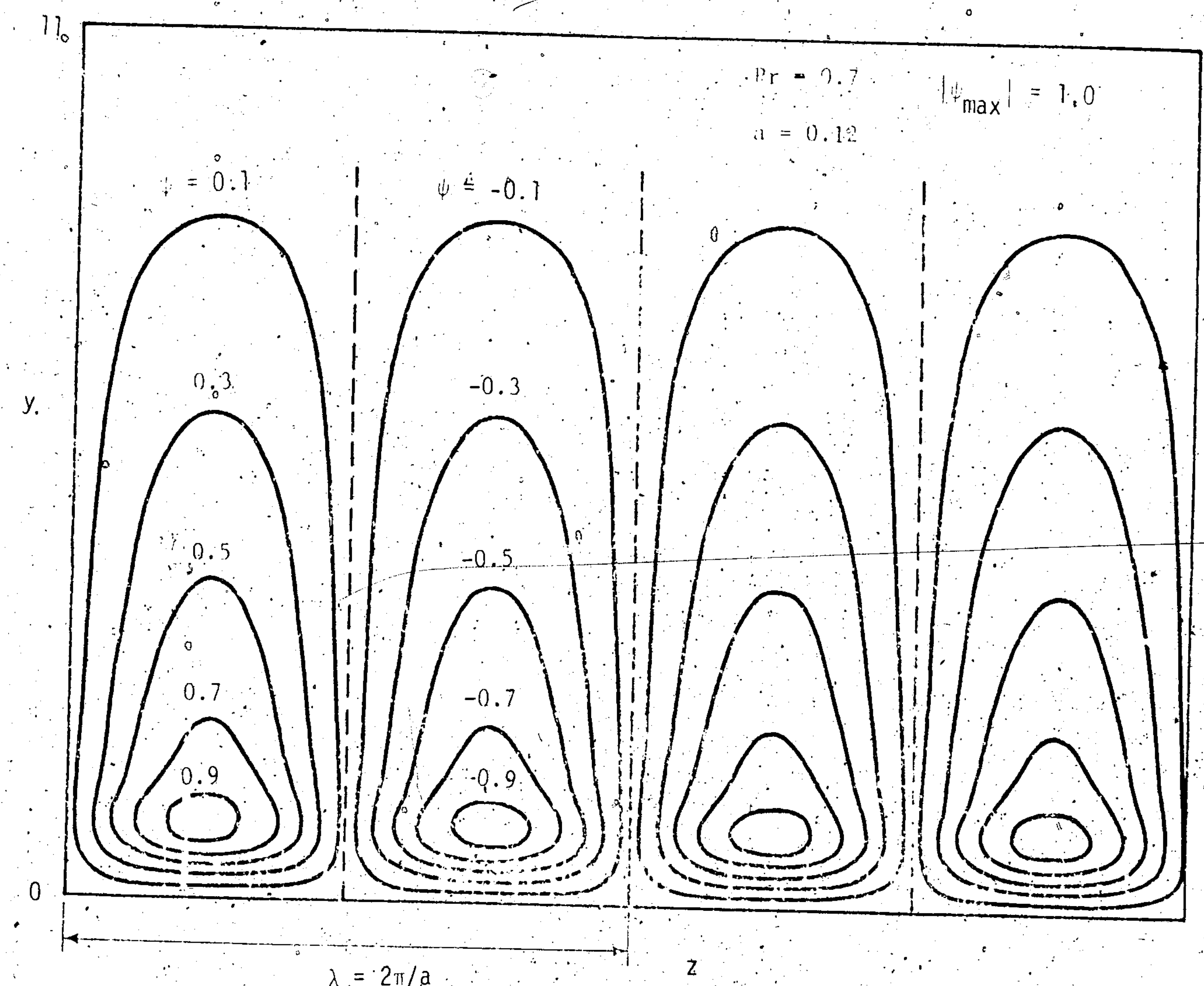

Fig. 4 Streamline pattern of vortex disturbance for Pr = 0.7

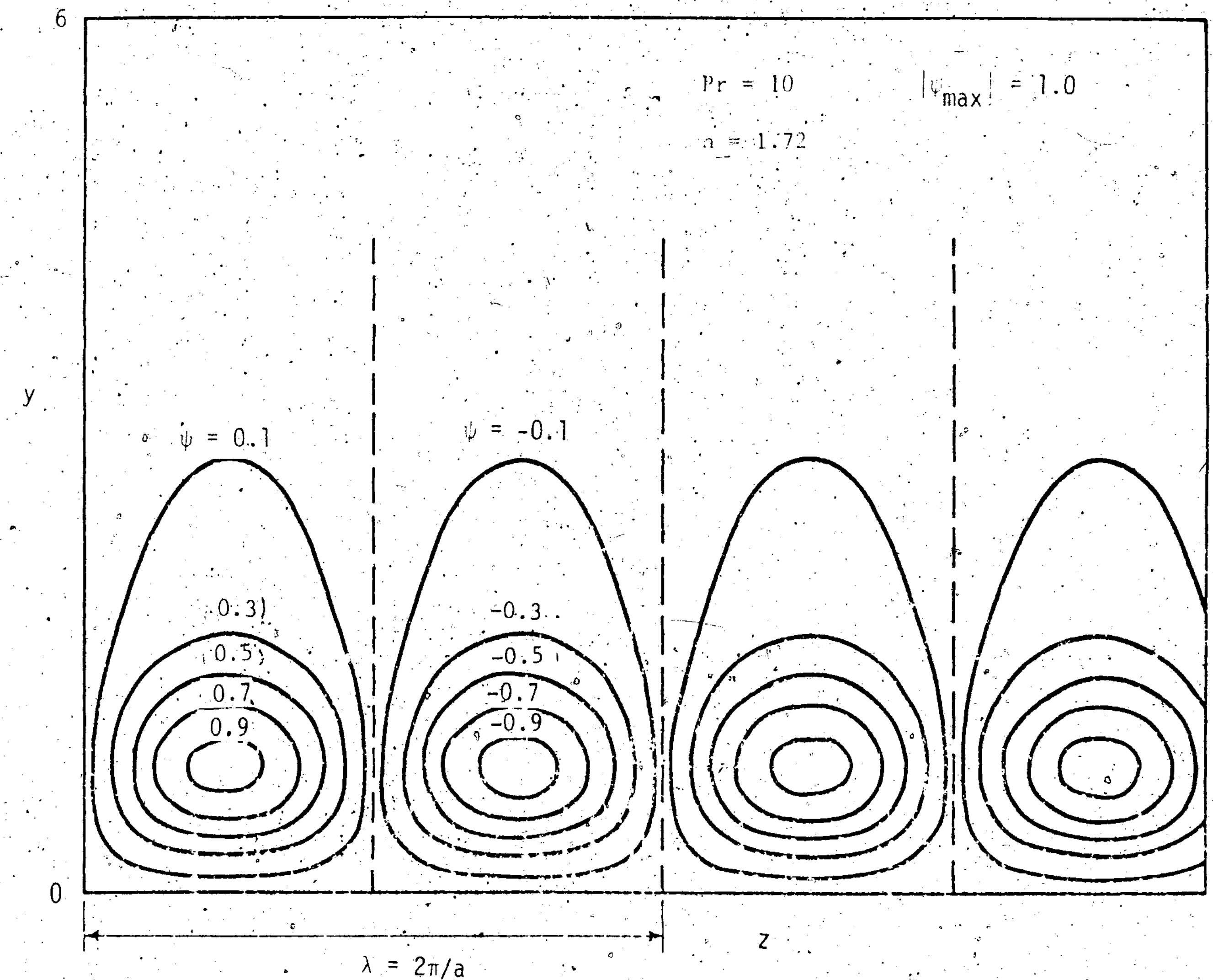

Fig. 5 Streamline pattern of vortex disturbance for Pr = 10

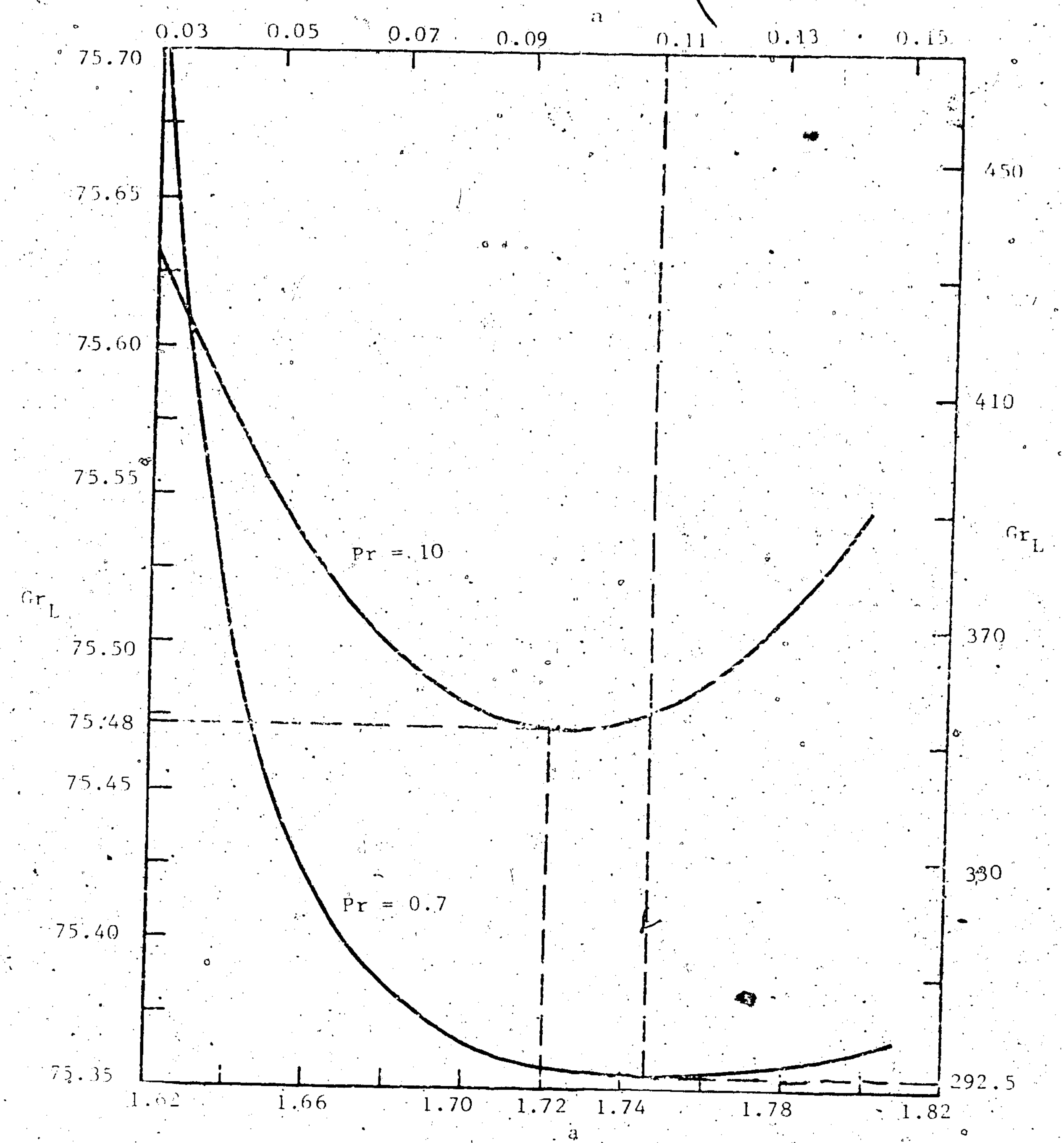

Fig. 6 Neutral stability curves, Gr_L vs. a, for Pr = 0.7 and 10

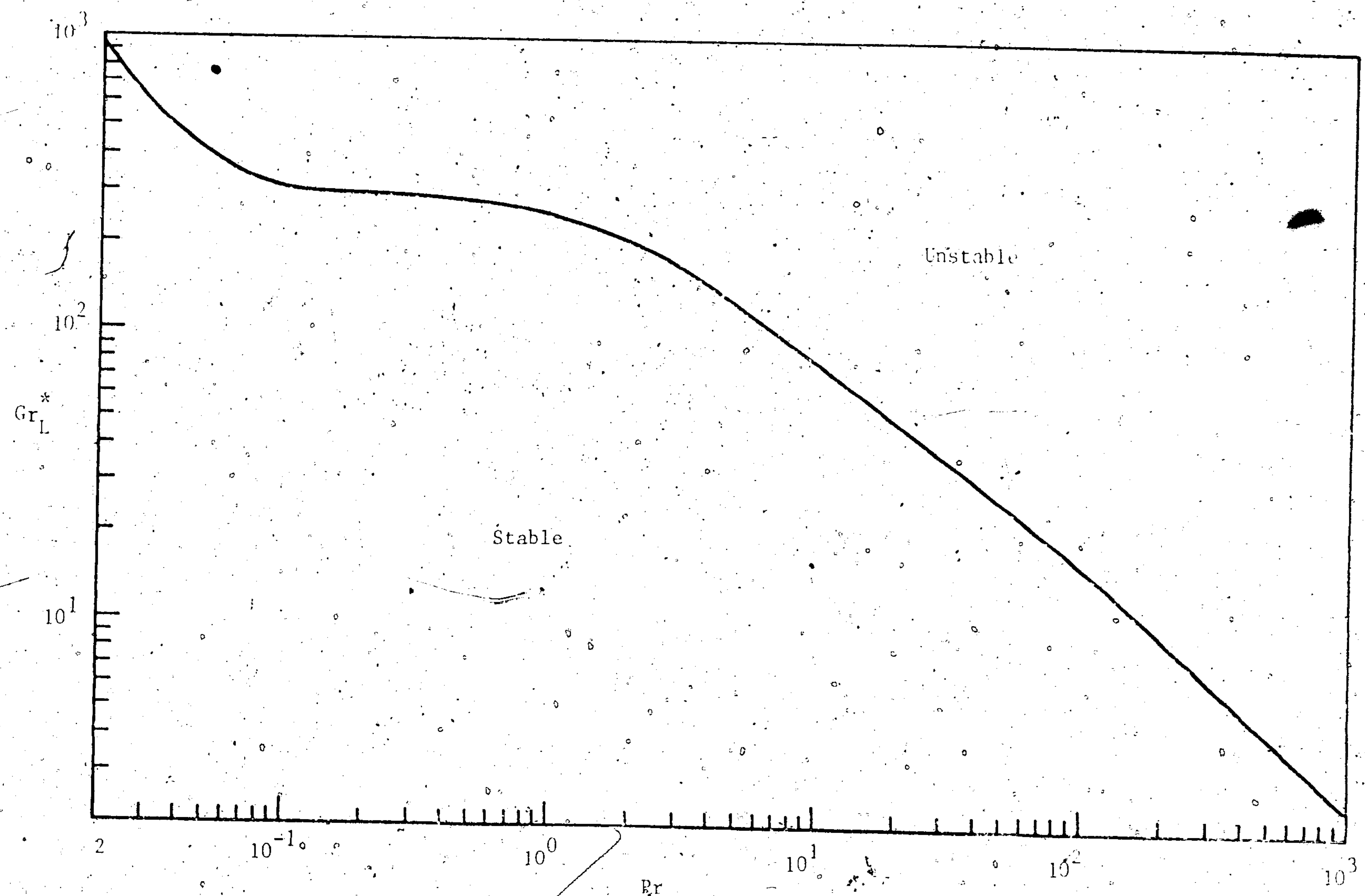

Fig. 7 Relationship between critical Grashof number Gr_L^* and Prandtl number

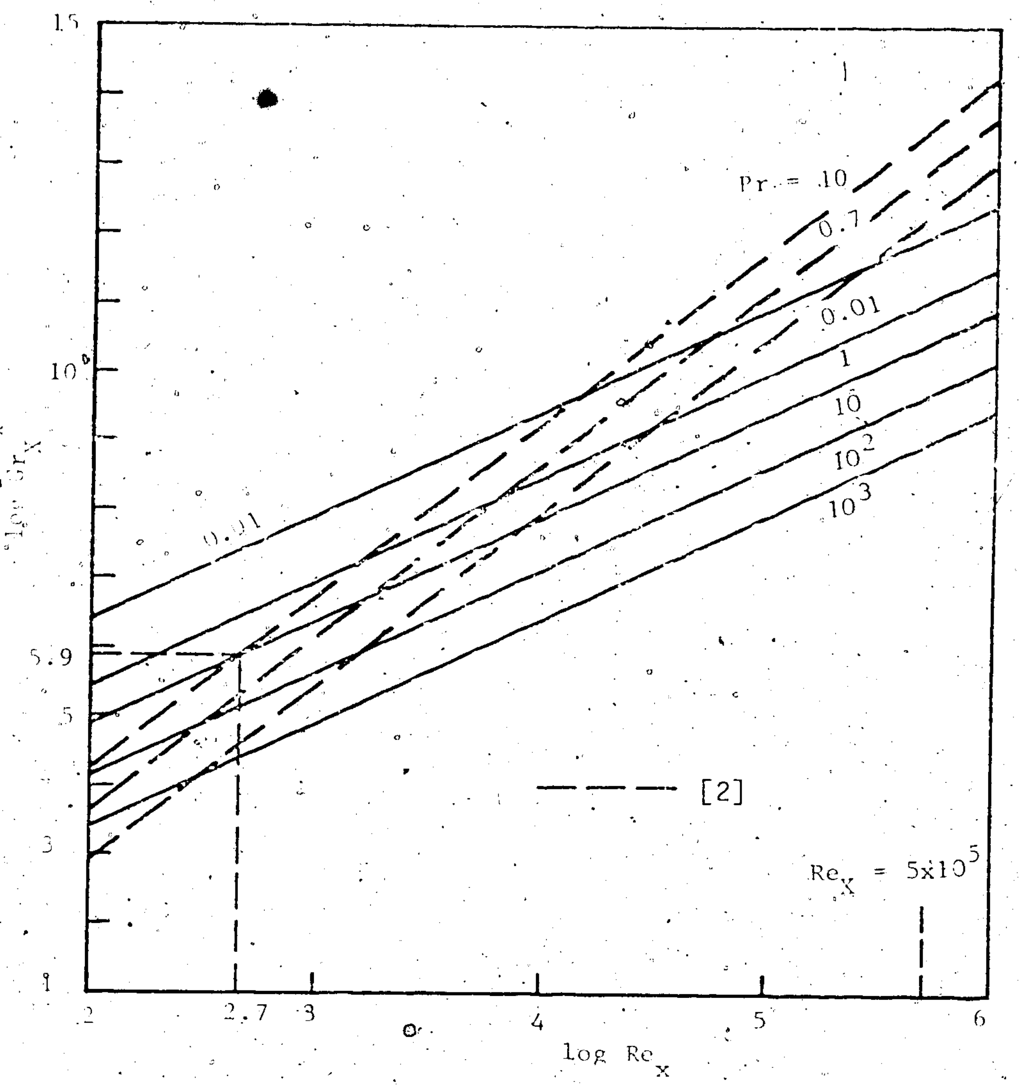

Fig. 8 Critical Grashof number (Gr_x^*) - Reynolds number (Re_x) relation and 5 percent buoyancy effect on local heat transfer from [2]

CHAPTER X

MAXIMUM DENSITY EFFECTS ON THERMAL INSTABILITY OF HORIZONTAL LAMINAR BOUNDARY LAYERS

Linear stability theory is used to investigate the onset of longitudinal vortices in laminar boundary layers along horizontal semi-infinite flat plates heated or cooled isothermally from below by considering the density inversion effect for water using a cubic temperature-density relationship. The analysis employs non-parallel flow model incorporating the variation of the basic flow and temperature fields with the streamwise coordinate as well as the transverse velocity component in the disturbance equations. Numerical results for the critical Grashof number $Gr_L^* = Gr_X^*/Re_X^{3/2}$ are presented for thermal conditions corresponding to $-0.5 \le \lambda_1 \le -2.0$ and $-0.8 \le \lambda_2 \le 1.2$.

Nomenclature

a	=	wave number, $2\pi/\lambda$
D	=	operator, $d/d\eta$
F	=	$(\eta f' - f)/2$
f	=	dimensionless stream function
g	=	gravitational acceleration
G	=	eigenvalue, Gr_L/Re_L
Gr_L	=	Grashof number based on L
Gr_X	=	Grashof number based on X
L	=	characteristic length, $(\nu X/U_\infty)^{1/2}$
M	=	number of divisions in y direction
P	=	pressure
Pr	=	Prandtl number, ν/α
p	=	dimensionless pressure, $P'/(\rho U_\infty^2/Re_L)$
Re_L, Re_X	=	Reynolds numbers, $(U_\infty L/\nu) = Re_X^{1/2}$ and $(U_\infty X/\nu)$, respectively
T	=	temperature
U,V,W	=	velocity components in X,Y,Z, directions
u,v,w	=	dimensionless perturbation velocities, $(U',V',W')/U_\infty$
X,Y,Z	=	rectangular coordinates

x, y, z	=	dimensionless coordinates, $(X, Y, Z)/L$
α	=	thermal diffusivity
β	=	coefficient of thermal expansion
γ_1, γ_2	=	temperature coefficients for density-temperature relationship
η	=	similarity variable, $Y/L = y$
θ	=	dimensionless temperature disturbance, $\theta'/\Delta T$
λ	=	dimensionless wavelength of vortex rolls, $2\pi/a$
λ_1, λ_2	=	thermal parameters defined by equation (12)
ν	=	kinematic viscosity
ρ	=	density
τ	=	dimensionless basic temperature, $(T_b - T_\infty)/\Delta T$
ϕ	=	$\tau - 1$
ΔT	=	temperature difference, $(T_w - T_\infty)$

Superscripts and Subscripts

$*$	=	critical value or dimensionless disturbance amplitude
$'$	=	prime, disturbance quantity or differentiation with respect to η

b	=	basic flow quantity
max	=	value at a density maximum
w	=	value at wall
[illegible]	=	free stream condition

10.1 Introduction

Thermal instability problems involving a horizontal layer of water with maximum density effect have been studied by various investigators [1-6] in recent years. Experimental investigations utilizing a melting [7-10] or freezing [11] horizontal ice layer were also reported recently. The maximum density effect is known to be important for free convection phenomenon in water exposed to near freezing temperatures. A literature survey shows that the published thermal instability results with maximum density effect are mainly concerned with the initially stationary liquid layer. On the other hand, one notes that little attention has been focussed so far to the related thermal instability problems with main flow.

When a body of water with temperatures ranging from 0°C to say 30°C flows in a horizontal direction, there exists a possibility for the onset of secondary motion regardless of whether the liquid layer is heated (or cooled) from below or above. This is obvious since part of the flowing liquid layer is potentially unstable with density inversion due to a top-heavy situation. The temperature regime mentioned may be found in natural phenomena such as flowing water near the ice cover in northern rivers or lakes.

The physical model chosen for study here is a Blasius flow (laminar boundary-layer flow) along a horizontal flat semi-infinite plate with a constant wall temperature T_w. The free stream temperature is T_∞ and the liquid possesses a maximum density over the temperature range between T_w and T_∞. The purpose of this study is to determine the conditions marking the onset of stationary longitudinal vortices in a horizontal laminar boundary-layer with maximum density effect. After the onset of longitudinal vortex rolls, the flow resumes a three-dimensional character and the conventional heat transfer results based on steady two-dimensional flow model may no longer apply. The results of present investigation may also provide some insight into the growth and decay of ice layer in contact with flowing water under certain conditions.

10.2 Formulation of the Thermal Instability Problem

The basic flow solutions for velocity and temperature in the steady laminar boundary-layer flow past a horizontal flat plate are well known [12]. Referring to the coordinate system shown in Fig. 1 and introducing the following variables, $\psi = (\nu X U_\infty)^{1/2} f(\eta)$, $\eta = Y(U_\infty/\nu X)^{1/2} = Y/L$, $L = (\nu X/U_\infty)^{1/2}$ and $\tau(\eta) = (T_b - T_\infty)/(T_w - T_\infty)$, the governing equations and the boundary conditions become [12]

$$f''' + \frac{1}{2} ff'' = 0, \quad \tau'' + \frac{1}{2} Prf\tau' = 0 \tag{1}$$

$$f(0) = f'(0) = \tau(\infty) = 0, \quad f'(\infty) = \tau(0) = 1 \tag{2}$$

The Blasius problem is solved by the fourth order Runge-Kutta method and the temperature distribution becomes

$$\tau(\eta) = 1 - \frac{\int_0^{\eta} [\exp(-\frac{Pr}{2} \int_0^{\eta} f d\eta)] d\eta}{\int_0^{\infty} [\exp(-\frac{Pr}{2} \int_0^{\eta} f d\eta)] d\eta} \tag{3}$$

As the temperature difference $|T_w - T_\infty|$ increases, the vortex rolls will appear eventually in the laminar boundary layer. To study the vortex-type instability of the Blasius flow with a maximum density value at T_{max} between T_w and T_∞, the perturbation quantities are superimposed on the basic quantities as

$$U = U_b(X,Y) + U'(Y,Z), \quad V = V_b(X,Y) + V'(Y,Z), \quad W = W'$$

$$T = T_b(X,Y) + \theta'(Y,Z), \quad P = P_b - \rho_\infty gY + P'(Y,Z) \tag{4}$$

The assumed disturbance forms for the longitudinal vortices which are periodic in the spanwise direction are similar to those given in [13]. Specifically, the secondary flow vortices (Görtler vortices) are assumed to be unchanging with time and non-oscillatory in the streamwise direction. The amplified disturbances are assumed to grow in the main flow direction but since the neutral stability is of interest here, the first derivatives of all disturbance quantities with respect to X are zero. Furthermore, the second-order derivatives $\partial^2/\partial X^2$ of the disturbances are neglected in conformity with the boundary layer approximation [13,14]. Based on the foregoing discussion, the disturbance quantities are taken to be a function of Y and Z only.

Applying the linear stability theory and using the Boussinesq approximation, the governing equations for the disturbed flow can be written as

$$\frac{\partial V'}{\partial Y} + \frac{\partial W'}{\partial Z} = 0 \tag{5}$$

$$U' \frac{\partial U_b}{\partial X} + V_b \frac{\partial U'}{\partial Y} + V' \frac{\partial U_b}{\partial Y} = \nu \nabla_1^2 U' \tag{6}$$

$$V_b \frac{\partial V'}{\partial Y} + V' \frac{\partial V_b}{\partial Y} = -\frac{1}{\rho}\frac{\partial P'}{\partial Y} + \nu \nabla_1^2 V' + \frac{\delta\rho}{\rho_0} g \tag{7}$$

$$V_b \frac{\partial W'}{\partial Y} = -\frac{1}{\rho}\frac{\partial P'}{\partial Z} + \nu \nabla_1^2 W' \tag{8}$$

$$U' \frac{\partial T_b}{\partial X} + V' \frac{\partial T_b}{\partial Y} + V_b \frac{\partial \theta'}{\partial Y} = \alpha \nabla_1^2 \theta' \tag{9}$$

where $\nabla_1^2 = \partial^2/\partial Y^2 + \partial^2 Z^2$. It is noted that non-parallel flow model is employed by retaining the terms involving V_b, $\partial U_b/\partial X$ and $\partial T_b/\partial X$. The term $U'\partial V_b/\partial X$ is neglected since $\partial V_b/\partial X \approx 0$ according to the boundary layer approximation. Recent investigations [13,14] on vortex instability of natural convection flow on inclined surfaces show that the conventional parallel flow assumption is inapplicable for the prediction of the onset of steady longitudinal vortices in boundary layer flow.

The density inversion effect is of primary interest here and the equation of state for water can be approximated by the following equation for the temperature range 0 to 30°C [5].

$$\rho - \rho_{max} = -\rho_{max}[\gamma_1(T - T_{max})^2 + \gamma_2(T - T_{max})^3] \tag{10}$$

For the perturbed flow, the temperature difference $(T - T_{max})$ becomes

$$T - T_{max} = T_b + \theta' - T_{max} = (T_b - T_w) + (T_w - T_{max})$$

$$+ \theta' = (\Delta T)(\phi + A + \theta) \tag{11}$$

where $\phi = (T_b - T_w)/\Delta T = \tau - 1$, $A = (T_w - T_{max})/(T_w - T_\infty)$,

$\theta = \theta'/\Delta T$ and $\Delta T = T_w - T_\infty$. Considering the change in the density $\delta\rho$ caused by the perturbation θ' in the temperature, one obtains the following expression for $-\delta\rho/\rho$ after neglecting the terms involving θ^2 and θ^3.

$$-\frac{\delta\rho}{\rho} = 2\gamma_1(A\Delta T)\theta(\Delta T)[1 + \frac{3}{2}\frac{\gamma_2}{\gamma_1}(A\Delta T)](1 - \lambda_1\phi + \lambda_2\phi^2) \qquad (12)$$

where $\lambda_1 = (-\frac{1}{A})\left[\dfrac{1 + 3\dfrac{\gamma_2}{\gamma_1}A\Delta T}{1 + \dfrac{3}{2}\dfrac{\gamma_2}{\gamma_1}A\Delta T}\right]$ and $\lambda_2 = (\frac{1}{A^2})\left[\dfrac{\dfrac{3}{2}\dfrac{\gamma_2}{\gamma_1}A\Delta T}{1 + \dfrac{3}{2}\dfrac{\gamma_2}{\gamma_1}A\Delta T}\right]$.

The thermal parameters λ_1 and λ_2 were first introduced by Sun, Tien and Yen [5]. The temperature coefficient γ_1 (positive) is or order 10^{-5} and γ_2 (negative) is of order 10^{-7}. It is noted that A is always positive and λ_1 is always negative for the temperature range (0-30°C) under consideration. The expression for λ_2 reveals that the value λ_2 is negative for heating ($T_w > T_\infty$) and positive for cooling ($T_w < T_\infty$). In addition, the unstable layer is always confined to the region near the plate and instability occurs only when $T_w \geq 4°C$ for heating from below ($T_w > T_\infty$) and when $T_w < 4°C$ for cooling from below ($T_w < T_\infty$).

Noting the basic flow quantities in the following form

$$U_b = U_\infty f'(\eta), \quad V_b = (U_\infty/2Re_L)(\eta f' - f) = (U_\infty/Re_L)F \qquad (13)$$

where $Re_L = U_\infty L/\nu = (U_\infty X/\nu)^{1/2} = Re_X^{1/2}$, $F = (\eta f' - f)/2$ and introducing the following dimensionless variables, $(x, y = \eta, z) = (X, Y, Z)/L$, $(u, v, w) = (U', V', W')/U_\infty$, $p = P'/(\rho U_\infty^2/Re_L)$, $\theta = \theta'/\Delta T$ the disturbance equations in linearized dimensionless form become

$$\frac{\partial v}{\partial y} + \frac{\partial w}{\partial z} = 0 \qquad (14)$$

$$\nabla^2 u - F\frac{\partial u}{\partial y} + \frac{1}{2}\eta f''u = Re_L f''v \qquad (15)$$

$$\nabla^2 v - F\frac{\partial v}{\partial y} - \frac{1}{2}\eta f''v = \frac{\partial p}{\partial y} - G(1 - \lambda_1\phi + \lambda_2\phi^2)\theta \qquad (16)$$

$$\nabla^2 w - F\frac{\partial w}{\partial y} = \frac{\partial p}{\partial z} \qquad (17)$$

$$\nabla^2\theta - Pr\,F\frac{\partial\theta}{\partial y} = Pr\,\tau'(Re_L v - \frac{1}{2}\eta u) \qquad (18)$$

where $G = (\nu/U_\infty L)(gL^3/\nu^2)(\Delta T)[2\gamma_1(A\Delta T)\{1 + (3\gamma_2/2\gamma_1)(A\Delta T)\}]$

$= Gr_L/Re_L$, $Gr_L = (gL^3/\nu^2)(\Delta T)[2\gamma_1(A\Delta T)\{1 + (3\gamma_2/2\gamma_1)(A\Delta T)\}]$

where $\nabla^2 = \partial^2/\partial y^2 + \partial^2/\partial z^2$. In the expression for Gr_L, one can readily recognize the quantity inside the square brackets as the equivalent coefficient of thermal expansion. Furthermore, the instability is possible with heating or cooling from below because of the presence of $(\Delta T)^2$. Upon eliminating p and w from equations (16) and (17) using continuity equation (14), one obtains

$$\nabla^2\nabla^2 v - F \frac{\partial}{\partial y} \nabla^2 v - \frac{1}{2} \eta f''\nabla^2 v = - G(1 - \lambda_1\phi + \lambda_2\phi^2) \frac{\partial^2\theta}{\partial z^2} \quad (19)$$

The boundary conditions are $u = v = v' = \theta = 0$ at $y = 0$ and ∞.

For the stationary longitudinal vortices, the following disturbance forms are applicable for the present neutral stability analysis [13,14].

$$[u, v, \theta] = [u^+(y),\ v^+(y),\ \theta^+(y)] \exp(iaz) \quad (20)$$

Substituting equation (20) into equations (15), (19) and (18) and further resetting $u^+ = Re_L u^*$, $v^+ = v^*$, $\theta^+ = Re_L \theta^*$, one obtains

$$[(D^2 - a^2) - FD + \frac{1}{2} \eta f'']u^* = f''v^* \quad (21)$$

$$[(D^2 - a^2)^2 - F(D^2 - a^2)D - \frac{1}{2}\eta f''(D^2 - a^2)]v^*$$

$$= a^2 Gr_L(1 - \lambda_1\phi + \lambda_2\phi^2)\theta^* \qquad (22)$$

$$[(D^2 - a^2) - Pr\ FD]\theta^* = Pr\ \tau'(v^* - \frac{1}{2}\eta u^*) \qquad (23)$$

where $D = d/dy$. The boundary conditions are

$$u^* = v^* = Dv^* = \theta^* = 0 \text{ at } y = 0 \text{ and } \infty. \qquad (24)$$

It is seen that the present eighth order eigenvalue problem is independent of Reynolds number Re_L. For given Pr, λ_1 and λ_2, there exists the functional dependence of Gr_L on a and the minimum critical value of Gr_L corresponding to the onset of longitudinal rolls with axes in the direction of the steady flow is sought. With the existence of laminar main flow, the analytical solution does not appear to be practical and a numerical method of solution is employed.

10.3 Method of Solution

The high order finite-difference scheme due to Thomas [15] is used in the present study. The detailed derivation is also given by Chen [16]. In carrying out the numerical solution, it is necessary to assign a finite value of η to satisfy the boundary conditions at $\eta = \infty$ [17]. With Pr = 10, the thermal boundary layer is inside the hydrodynamic boundary layer. After numerical experiments, the conditions at infinity for Q^* and v^* are replaced by those at $\eta = 5.0$ corresponding to $\tau \leq 10^{-8}$ since as $\tau \to 0$, one has $\tau' \to 0$. An examination of equations (22) and (23) reveals that the flow field is stable for the region $\eta = 5.0 \sim \infty$. On the other hand, the condition for u^* at $\eta = \infty$ is also set at $\eta = 5.0$ since v^* vanishes for $\eta \geq 5.0$ in equation (21). It is of interest to note that at $\eta = 10.4$ one has $(f' - 1) \leq 10^{-8}$ and $f'' \to 0$ for the region $\eta = 10.4 \sim \infty$. In addition, the step size $\Delta y = 0.02$ and the number of divisions M = 250 are found to be satisfactory.

The finite difference transformation of equation (22) and its boundary conditions leads to a quidiagonal system [18] of matrix for a set of algebraic equations and similarly two tridiagonal systems [19] result from equations (21) and (23) with their boundary conditions. Since the dependent variables are all coupled through a set of equations (21) to (23), an iterative procedure with the following main steps is used for the numerical solution. It is noted that the basic velocity and temperature distributions are known and Pr = 10.

1. The initial values for wave number a and eigenvalue Gr_L are assumed. The disturbance velocity v_k^* is taken as $v_k^* = 2(1 - k/M)$, $k = 2,3,\ldots,M$.

2. The finite-difference solution of equation (21)

yields u_k^*.

3. After knowing v_k^* and u_k^*, equation (23) is solved to obtain θ_k^*.

4. The right-hand side of equation (22) is now known and new values for v_k^* can be found.

5. A new and improved eigenvalue can be computed by using the following equation [20].

$$(Gr_L)_{new} = (Gr_L)_{old} \frac{[\sum_k (v_k^*)^2_{old}]^{1/2}}{[\sum_k (v_k^*)^2_{new}]^{1/2}} \qquad (25)$$

The magnitude of the quantity v_k^* is readjusted by the following equation in order to return to the original order for computation.

$$v_k^* = (v_k^*)_{new} \, (Gr_L)_{new}/(Gr_L)_{old} \qquad (26)$$

6. The steps (2) to (4) are repeated until the following convergence criterion is satisfied.

$$\sum_k |(v_k^*)_{new} - (v_k^*)_{old}| / \sum_k |(v_k^*)_{new}| \leq 10^{-6} \qquad (27)$$

Numerical experiments show that only a few iterations are required to satisfy the above condition and five significant figures for critical Gr_L are found to be correct.

10.4 Results and Discussion

The present numerical solution also yields results for secondary flow pattern and disturbance profiles for u^*, v^* and θ^* in addition to neutral stability results. The results are presented in Figs. 1 to 4 for some typical cases. The stream function ψ defined by $v = \partial\psi/\partial z$ and $w = -\partial\psi/\partial y$ can be obtained by considering the normal modes of the disturbances, $v = v^+(y)e^{iaz}$ and $\psi = \psi^+(y)e^{iaz}$, as

$$= -[i\,v^*(y)/a]e^{iaz} \qquad (28)$$

The contour lines shown in Figs. 1 and 2 for heating and cooling from below, respectively, are obtained by noting that physical meaning is attached only to the real part of the stream function. In Fig. 3, the magnitude of the maximum disturbance quantity is taken to be 0.1 and the disturbance amplitudes are superimposed on basic quantities. The horizontal disturbance velocity amplitude u^* is seen to be negative suggesting that the secondary flow also derives its energy from the main flow.

The neutral results for the critical values of the Grashof number Gr_L^* and the corresponding a^* are listed in Table 1 and also plotted in Fig. 5. The marginal stability curves are shown in Fig. 6 for illustration.

In interpreting the numerical results, one notes that the parameters λ_1 and λ_2 depend on A as well as ΔT $(T_w - T_\infty)$. When ΔT and $(T_w - T_{max})$ are known, λ_1 and λ_2 can be computed. Because of the rather complicated expressions for λ_1 and λ_2, one cannot readily understand the physical situation corresponding to a particular combination of λ_1 and λ_2. In Fig. 5, the effect of λ_1 on Gr_L^* may be understood by considering the case of $\lambda_2 = 0$ representing a parabolic density-temperature relationship. For this case, one obtains $\lambda_1 = -A^{-1} = -(T_w - T_\infty)/(T_w - T_{max})$ and it is seen that for a given $(T_w - T_\infty) = \Delta T$, the magnitude of λ_1 increases as the temperature difference $(T_w - T_{max})$ decreases. When $(T_w - T_{max})$ is small, the unstable liquid layer near the plate is small and consequently it is more stable as represented by higher Gr_L^*. In Table 1, the numerical solution does not converge for higher Gr_L^* than those listed. This is presumably due to the rather thin unstable layer requiring a yet larger number of divisions M. For a given λ_1, the liquid layer becomes more stable as λ_2 decreases.

The theoretical results for the critical Rayleigh numbers reported in [5] for the stationary horizontal liquid layers with both rigid-rigid and rigid-free surface conditions agree excellently with the experimental results. With the exception of the characteristic length, the present definition of the Grashof number is comparable to that used in [5,21]. Although the present instability problem with steady laminar main flow (Blasius flow) is different from that of a horizontal liquid layer without main flow, the trend of the instability results regarding λ_1 and λ_2 effects shown in Table 1 agrees with those listed in [21]. It is of some interest to compare the present instability results with those of the rigid-rigid case reported in [5,21] since the boundary conditions for the disturbance quantities are comparable. For given A, ΔT or λ_1, λ_2, the ratio of the critical Gr_L^* from this study over that of [5,21] simply becomes $Gr_L^*/(Gr_d)_{cr} = (L/d)^3$ where d = liquid layer thickness [5]. At this point, it appears to be more reasonable to use the thermal boundary layer thickness δ_T instead of the characteristic length L for the comparison. From the boundary layer theory [12], it is known that $\delta_T/\delta = Pr^{-1/3}$ approximately with $\delta = 5.83(\nu X/U_\infty)^{1/2} = 5.83L$. It is then found that $L = 0.370\ \delta_T$ and the ratio becomes $Gr_L^*/(Gr_d)_{cr} = 0.051$ after setting $\delta_T = d$. On the other hand, the ratio $Gr_L^*/(Gr_d)_{cr}$ based on numerical results from this study and Table 2 of [21] gives the value which is approximately one order higher than the value of 0.051. This suggests immediately that the above rather simple intuitive comparison is not correct. However, the above simple discussion serves to emphasize the essential difference between the present instability problem and the classical Benard problem with maximum density effect [5,21].

10.5 Concluding Remarks

1. In contrast to the classical Benard problem, the

present thermal instability problem for the Blasius flow is characterized by the existence of the stable upper liquid layer above the unstable lower layer near the plate. With $Pr = 10$, it is known that $\delta_T/\delta = 0.464$ and the thermal boundary layer is inside the hydrodynamic boundary layer. The basic temperature profile for the present instability problem is non-linear.

2. By using the characteristic length L, the eigenvalue Gr_L^* is shown to be independent of Re_L. To study the Reynolds number effect based on the familiar definition $Re_X = (U_\infty X/\nu)$, one must use the relationship $Gr_L = Gr_X/Re_L^3 = Gr_X/Re_X^{3/2}$ where $Gr_X = (gX^3/\nu^2)(\Delta T)[2\gamma_1(A\Delta T)\{1 + (3\gamma_2/2\gamma_1(A\Delta T)\}]$.

3. In applying the present instability results, it is useful to recall that the approximate limits of the laminar boundary layer theory are $O[10^2] < Re_X \lesssim 5 \times 10^5$. The experimental data do not seem to be available for comparison with the present theoretical results.

References

1. Ver[illegible], G., "Penetrative Convection", Astrophysics J. [illegible] 137, 1963, pp. 64[illegible]-663.
2. Roberts, P.H., "Characteristic Value Problems Posed by Differential Equations Arising in Hydrodynamics and Hydromagnetics", J. Math. Analysis and Appl. 1, 1960, pp. 195-214.
3. Debler, W.R., "On the Analogy Between Thermal and Rotational Hydrodynamic Stability", J. Fluid Mech. 24, 1966, pp. 165-176.
4. Tien, C., "Thermal Instability of a Horizontal Layer of Water Near 4°C", A.I.Ch.E. J. 14, 1968, pp. 652-653.
5. Sun, Z.S., Tien, C. and Yen, Y.C., "Thermal Instability of a Horizontal Layer of Liquid with Maximum Density", A.I.Ch.E. J. 15, 1969, pp. 910-915.
6. Sun, Z.S., Tien, C. and Yen, Y.C., "Onset of Convection in a Porous Medium Containing Liquid with a Density Maximum", Heat Transfer, Vol. 4, 1970, NC 2.11.
7. Townsend, A.A., "Natural Convection in Water Over an Ice Surface", Quat. J. Roy. Soc. 90, 1964, pp. 248-259.
8. Yen, Y.C., "Onset of Convection in a Layer of Water Formed by Melting Ice from Below", Physics of Fluids 11, 1968, pp. 1263-1270.

9. Yen, Y.C. and Galea, F., "Onset of Convection in a Water Layer Formed Continuously by Melting Ice", Physics of Fluids 12, 1969, pp. 509-516.

10. Sugawara, M., Fukusako, F. and Seki, N., "Experimental Studies on the Melting of a Horizontal Ice Layer", Trans. Japan Soc. Mech. Engrs. 40, 1974, pp. 3155-3165.

11. Tankin, R.S. and Farhadieh, R., "Effects of Thermal Convection Currents on Formation of Ice", Int. J. Heat Mass Transfer 14, 1971, pp. 953-961.

12. Schlichting, H., "Boundary-Layer Theory", 6th Ed., McGraw-Hill, New York, 1968, Chapter 12.

13. Haaland, S.E. and Sparrow, E.M., "Vortex Instability of Natural Convection Flow on Inclined Surface", Int. J. Heat Mass Transfer 16, 1973, pp. 2355-2367.

14. Hwang, G.J. and Cheng, K.C., "Thermal Instability of Laminar Natural Convection Flow on Inclined Isothermal Plates", Canadian J. of Chemical Engineering 51, 1973, pp. 659-666.

15. Thomas, L.H., "The Stability of Plane Poiseuille Flow", Physical Review 91, 1953, pp. 780-783.

16. Chen, T.S., "Hydrodynamic Stability of Developing Flow in a Parallel-Plate Channel", Ph.D. Thesis, University of Minnesota, 1966.

17. Collatz, L., "The Numerical Treatment of Differential Equations", 3rd Ed., Springer-Verlag, Berlin, 1966, pp. 150-151.

18. Conte, S.D. and Dames, R.T., "An Alternating Direction Method for Solving the Biharmonic Equation", Mathematical Tables and Other Aids to Computation 12, 1958, pp. 198-205.

19. Wachspress, E.L., "Iterative Solution of Elliptic Systems and Applications to the Neutron Diffusion Equations of Reactor Physics", Sec. 1.5, Prentice-Hall, New Jersey, 1966.

20. Forsythe, G.E. and Wasow, W.R., "Finite-Difference Methods for Partial Differential Equations", John-Wiley & Sons, New York, 1960.

21. Sun, Z.S., "Thermal Instability and Heat Transfer of a Horizontal Layer of Liquid with Maximum Density and Heated from Below", M.S. Thesis, Syracuse University, New York, 1968.

TABLE 1. Critical Grashof Numbers for Pr = 10

λ_1	-0.5		-1.0		-1.5		-2.0	
λ_2	a^*	Gr^*_L	a^*	Gr^*_L	a^*	Gr^*_L	a^*	Gr^*_L
1.2	1.40	55.21	1.50	76.24	1.58	123.35	2.18	292.99
0.8	1.54	67.43	1.60	101.56	2.00	195.22	3.00	491.18
0.4	1.60	86.29	2.00	145.51	2.78	304.70		
0	1.98	115.88	2.60	210.72	3.02	435.32		
-0.4	2.40	158.13	2.94	292.30				
-0.8	2.80	211.36	3.14	387.00				

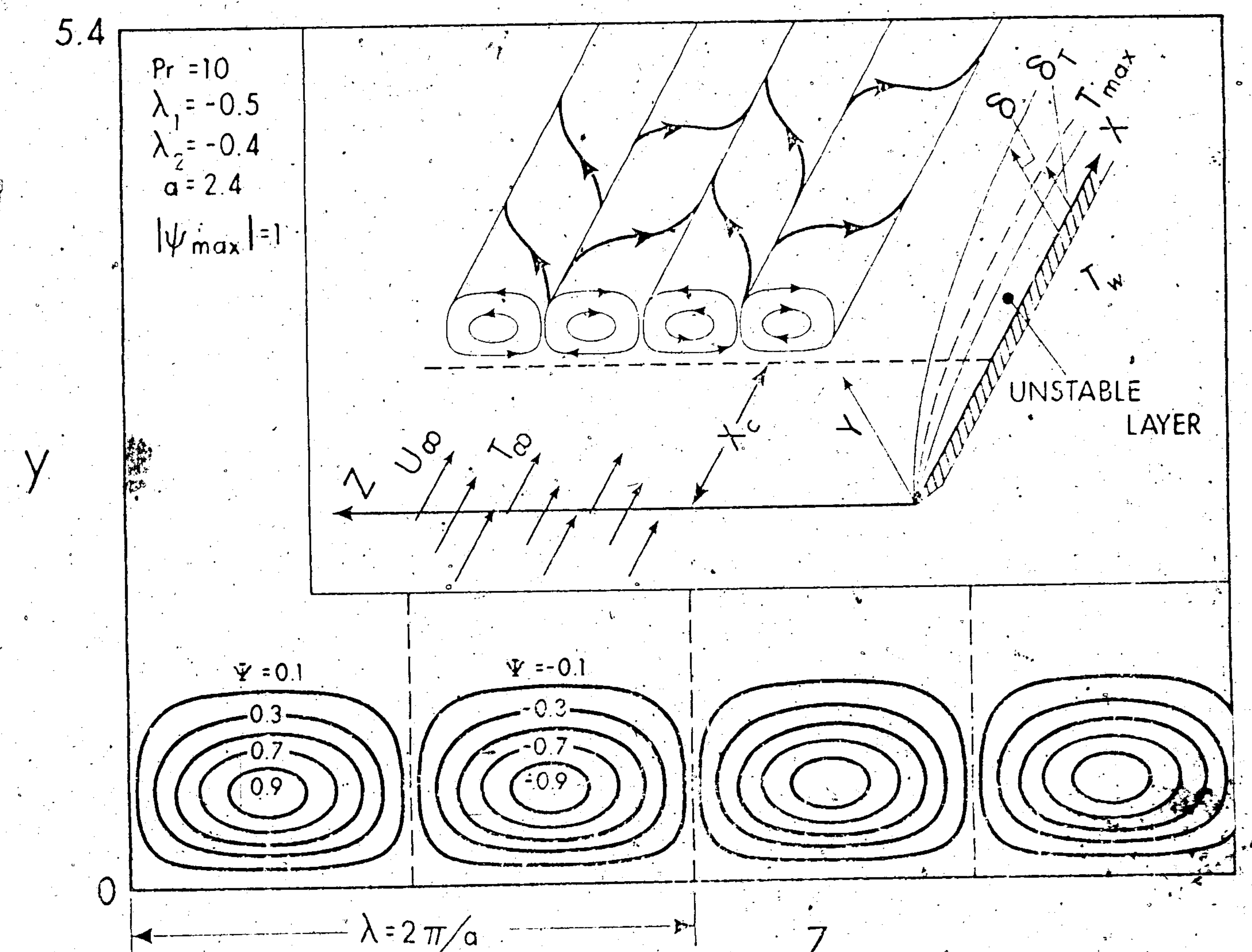

Fig. 1 Coordinate system and streamline pattern of vortex disturbance for $\lambda_1 = -0.5$, $\lambda_2 = -0.4$.

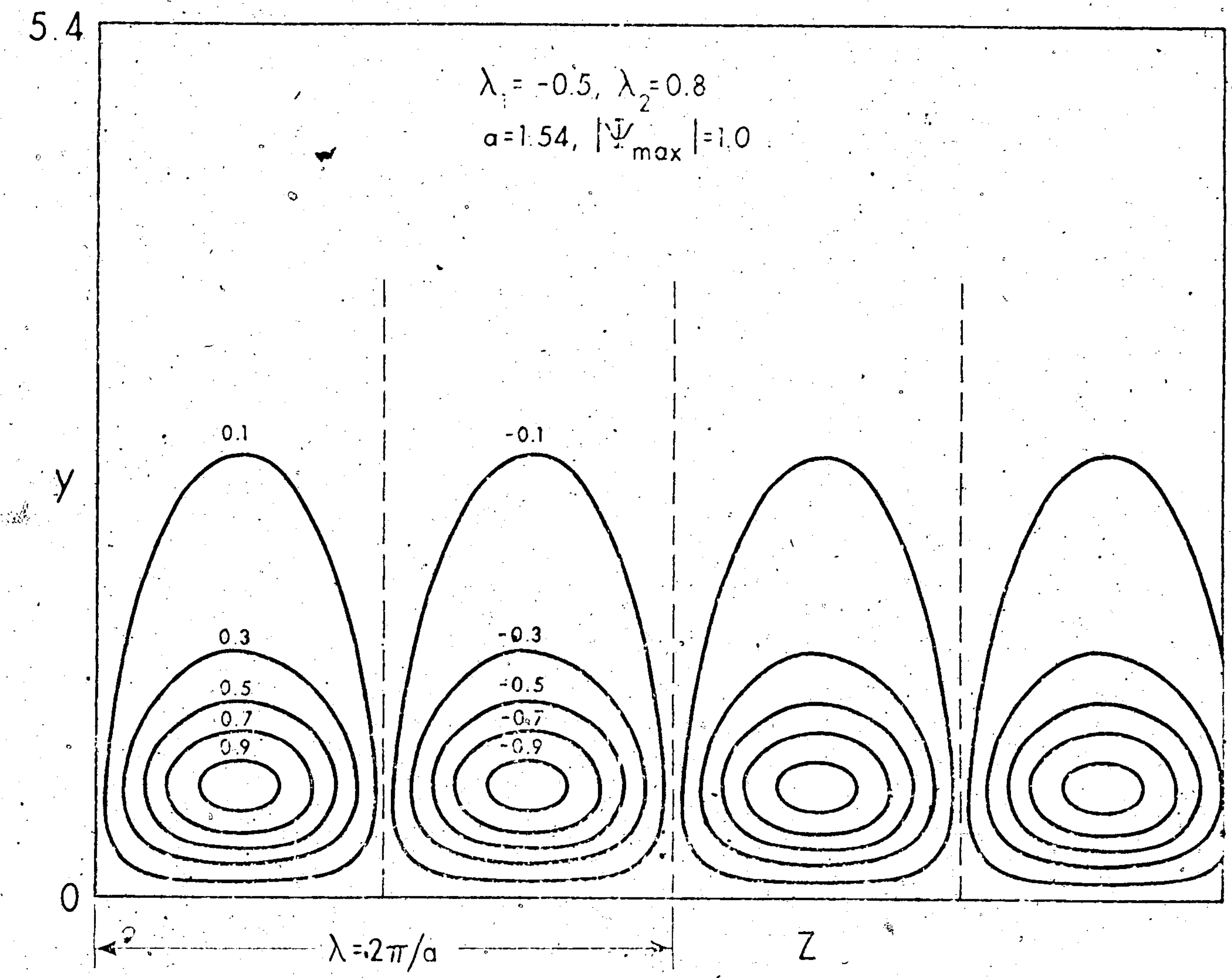

Fig. 2 Streamline pattern of vortex disturbance for $\lambda_1 = -0.5$ and $\lambda_2 = 0.8$.

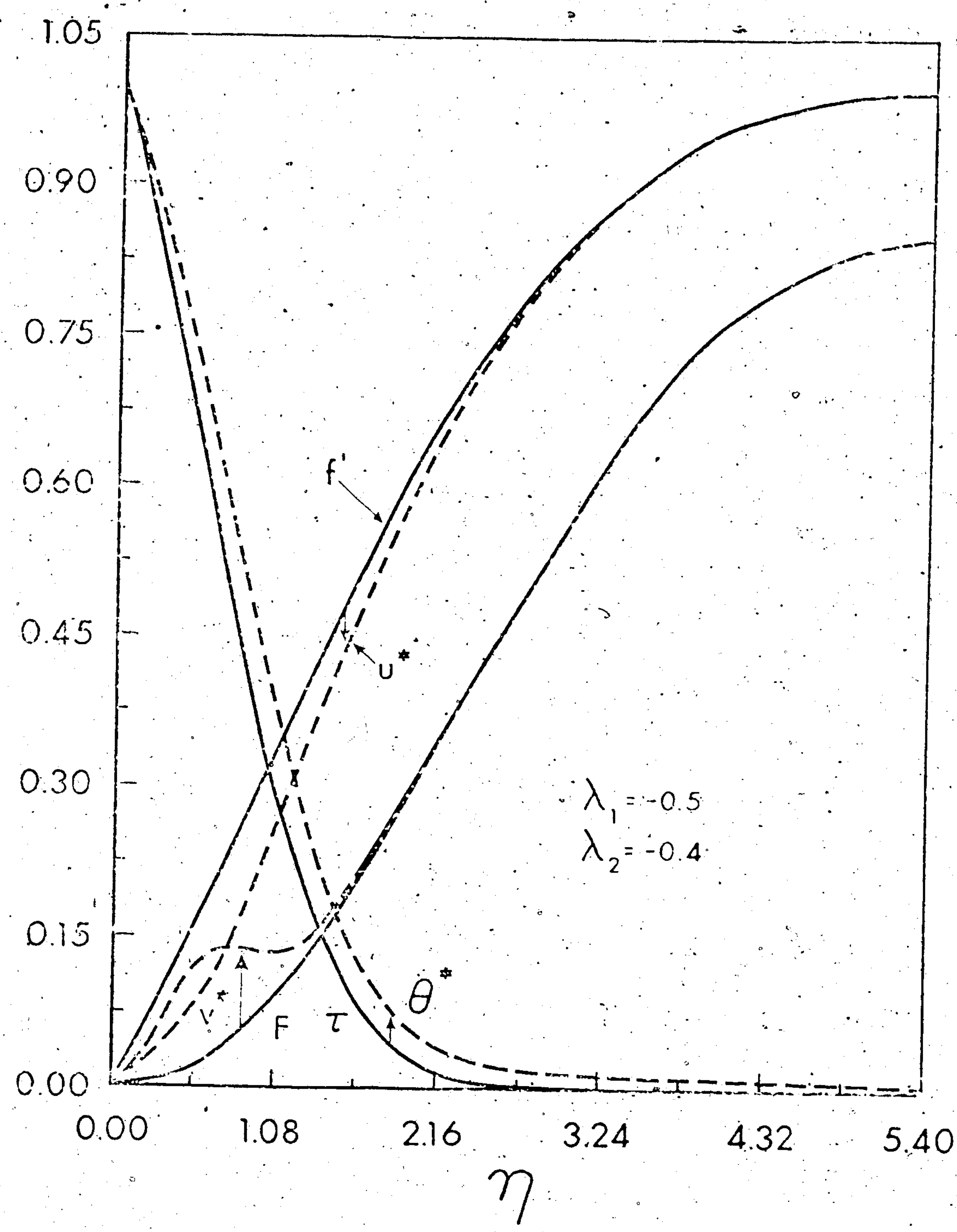

Fig. 3 Distributions of basic quantities f', F, τ and perturbation amplitudes u^*, v^* and θ^* for $\lambda_1 = -0.5$ and $\lambda_2 = -0.4$.

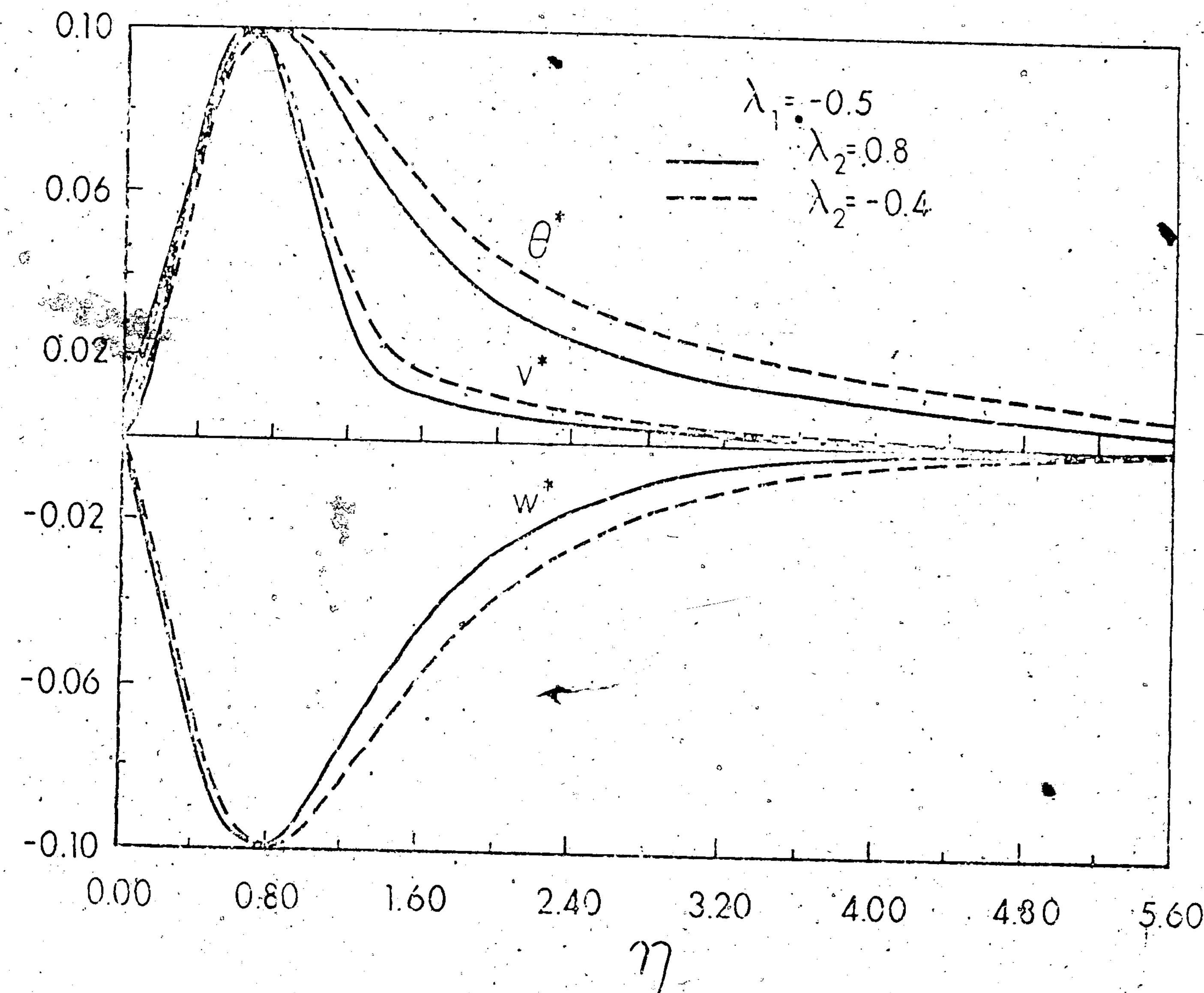

Fig. 4 Profiles for perturbation amplitudes u^*, v^* and θ^*.

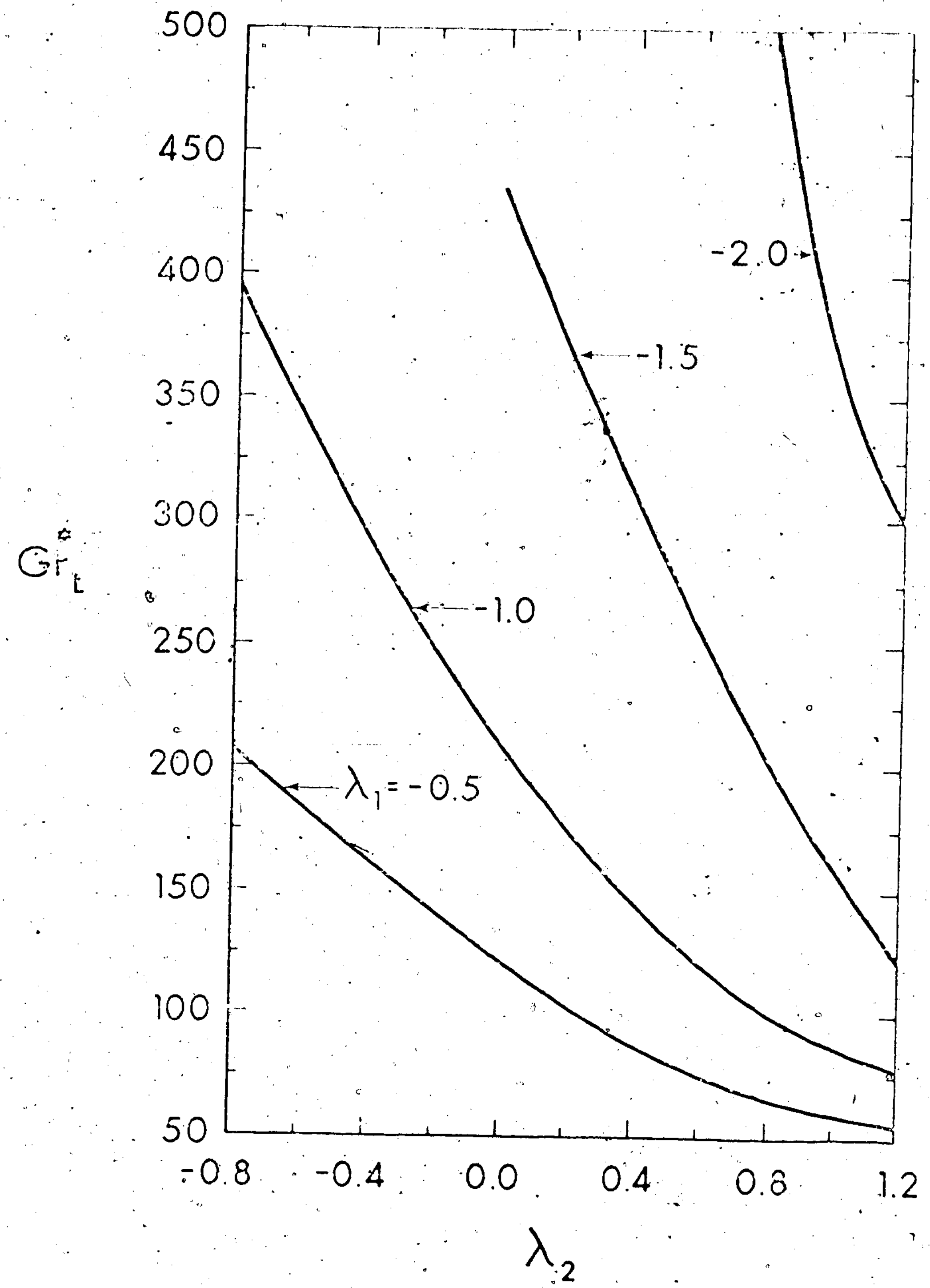

Fig. 5 Relation between critical Grashof number Gr_L^* and λ_2 with λ_1 as parameter.

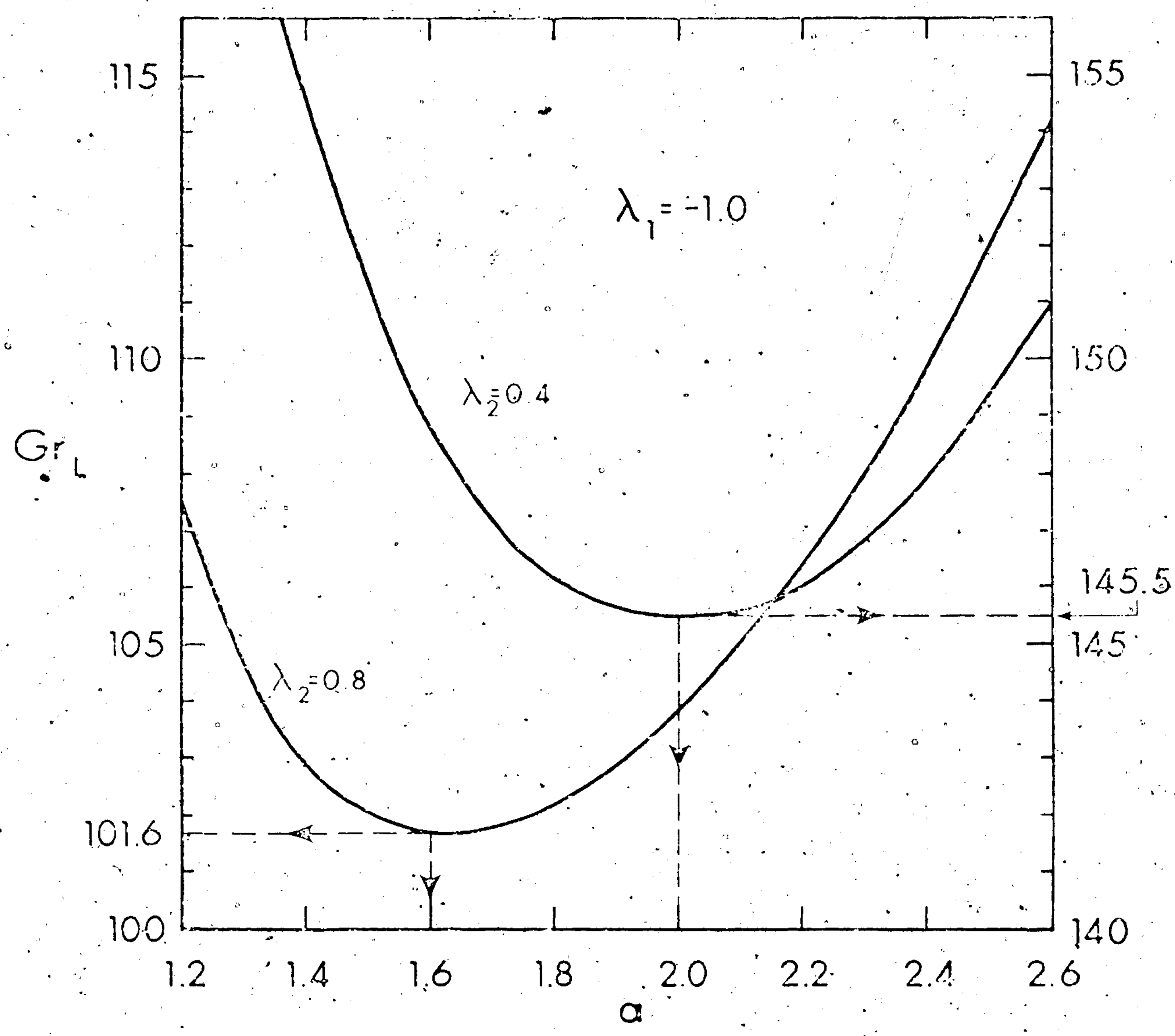

Fig. 6 Neutral stability curves for $(\lambda_1, \lambda_2) = (-1.0, 0.4)$ and $(-1.0, 0.8)$.

CHAPTER XI

CONCLUSIONS

11.1 Scope of Results

This thesis investigates a class of thermal instability problems involving plane Poiseuille, Hartmann and Blasius flows. The onset of secondary flow driven by buoyancy force for the above mentioned fully developed laminar flow is of considerable practical interest since after the onset of instability the flow takes on a three-dimensional character and the heat transfer rate is expected to increase with Rayleigh number. The flow configurations under consideration occur in many industrial operations and processes and the critical Rayleigh numbers marking the onset of instability are required in design. For the case of plane Poiseuille flow in the thermal entrance region of a horizontal parallel-plate channel heated from below, both the longitudinal and transverse vortex disturbances are considered. For each linear instability analysis, typical numerical instability results are obtained to clarify the various physical effects. Among the various physical effects considered, the maximum density effects on convective instability of water layer with main flow is noteworthy since the instability results are applicable to the melting of ice or ice formation involving main flow. It should be pointed out that the basic flow and temperature fields upon which the instability problem is considered neglects the free convection effect and the basic velocity profile remains to be plane Poiseuille, Hartmann or Blasius flow. Thus, the problem is to find the condition at which the free convection starts to affect the main flow. Furthermore, it is assumed that the instability sets in as stationary convection since the stationary longitudinal vortices are observed in experiments. The assumption is also consistent with previous investigations.

Besides the convective instability in horizontal fluid flows, the maximum density effects on thermal instability in a thin horizontal water layer driven by combined buoyancy and surface tension gradients are investigated. The problem represents an extension of Nield's linear stability analysis in 1964 to water in the temperature range 0 ~ 30°C.

The coupled perturbation equations for each instability problem are solved by a higher order finite-difference method using an iterative procedure. It is found that the iterative numerical solution is very efficient and powerful for the present instability problems. Apparently, the numerical technique has a wide applicability for the related instability problems.

11.2 Conclusions and Significance

The low Peclet number convective heat transfer problem in the thermal entrance region of a parallel-plate channel with unequal constant wall temperatures is approached by the eigenfunction expansion method employing the Gram-Schmidt orthonormalization procedure. When Pe $\leq$ 10, the axial heat conduction effect on heat transfer is considerable but when Pe $\gtrsim$ 50, the axial heat conduction may be negligible. The critical Rayleigh numbers versus the channel distance are determined for both upstream and downstream regions of the channel with Pe = 1, 5, 10. For Pe = 50, instability results are obtained for downstream region only. It is established that the transverse vortex disturbances are the preferred mode over the longitudinal vortex disturbances for Pe $\leq$ 1 and Pr $\gtrsim$ 1 (or low Reynolds number flow), in the regions upstream and downstream of the thermal entrance. For other conditions, the longitudinal vortex rolls have priority of occurrence. It is noted that generally the axial heat conduction has a destabilizing effect in the upstream region and a stabilizing effect in the downstream region. The theoretical instability results considering maximum density effects for water in the temperature 0 ~ 30°C are useful in assessing the free convection effect on freezing or thawing in channel flow of water. The viscous dissipation effect on convective instability is qualitatively similar to that of internal heat generation in a horizontal fluid layer and represents a destabilizing influence. It is found that the viscous dissipation effect is significant for Pr $\gtrsim$ 10 but is insignificant for Pr $\leq$ 0.7.

The basic flow solution for Hartmann flow considers the effects of axial conduction, viscous dissipation and Joulean heating but neglects the axial heat penetration through the thermal entrance. The magnetic Reynolds number is assumed to be small and the Hall effect is neglected. When the magnetic Reynolds number is very small compared to unity, the magnetic field is not distorted by the flow. In engineering problems, it is difficult to obtain the magnetic Reynolds number greater than unity because of the low electrical conductivity of the useful fluids. The Hall effect can be neglected when the fluid has a scalar electrical conductivity. The convective instability analysis of horizontal Hartmann flow in the thermal entrance region of a parallel-plate channel considers the effects of Prandtl, Peclet, Brinkman and Hartmann numbers. It is found that the magnetic field has a stabilizing effect and a decrease in Prandtl number has a destabilizing effect in the thermal entrance region.

The maximum density effects on thermal instability driven by combined buoyancy and surface tension provide further physical insight into the thermal instability problem discussed by Nield in 1964. The instability results may have direct applications in predicting the onset of convection in surface melting involving ice layer on a northern lake or pond. Similarly, one is also interested in predicting the onset of convection in a thin freezing water layer.

The convective instability analysis of laminar forced convection along a horizontal semi-infinite flat plate with uniform wall temperature is believed to be one of the basic problems and complements the hydrodynamic instability analysis of laminar boundary layers reported in the literature. The maximum density effects on convective instability of horizontal laminar boundary layer are studied in order to predict the onset of free convection effect in laminar boundary layers along ice surface where melting or solidification occurs.

11.3 Recommendations

This theoretical investigation demonstrates the applicability of the numerical method in predicting the critical Rayleigh number for various thermal instability problems. It is believed that the numerical method used is a powerful one and can be applied to many linear instability analyses which remain to be explored in future.

Experimental verification is required to substantiate the theoretical results reported in this thesis. The experimental investigations on the increase of heat transfer rate with the increase of Rayleigh number after the onset of instability may pave the way for theoretical investigations on finite amplitude convection problems.

Future investigations on convective instability of MHD channel flows may include the influence of Hall effect and iron slip in addition to the viscous dissipation, Joule heating and axial heat conduction effects. In the present analysis of thermal instability for Blasius flows along a horizontal plate, the free convection effects are not considered in the basic flow solution. Because of practical interest in the prediction of the onset of thermal instability in flow over a horizontal flat plate, the thermal instability of combined forced and free laminar convection along a horizontal flat plate with respect to stationary longitudinal vortex disturbances should be investigated in future. Finally, one notes that the thermal radiation effects on convective instability of various horizontal fluid flows may prove to be fruitful and important research topics for future theoretical investigations.

APPENDIX 1

DERIVATION OF HIGH ORDER FINITE-DIFFERENCE APPROXIMATION

The high order finite-difference approximation due to Thomas [1], who used it in a study on the stability of Plane Poiseuille flow, is employed in this thesis for the numerical solution of the thermal instability problems. The detailed derivation of the approximation is given by Chen [2] in a study on the hydrodynamic stability of developping flow in a parallel-plate channel. For convenience, the derivation is summarized here.

The various orders of derivatives of a function g(z) can be expressed in finite-difference form as:

$$Dg = \frac{1}{h}\{u\delta - \frac{1}{6}u\delta^3 + \frac{1}{30}u\delta^5 - \frac{1}{140}u\delta^7 + \frac{1}{630}u\delta^8 \ldots\}g \qquad (1)$$

$$D^2g = \frac{1}{h^2}\{\delta^2 - \frac{1}{12}\delta^4 + \frac{1}{90}\delta^6 - \frac{1}{560}\delta^8 + \ldots\}g \qquad (2)$$

$$D^3g = \frac{1}{h^3}\{u\delta^3 - \frac{1}{4}u\delta^5 + \frac{7}{120}u\delta^7 \ldots\}g \qquad (3)$$

$$D^4 g = \frac{1}{h^4} \{\delta^4 - \frac{1}{6}\delta^6 + \frac{7}{240}\delta^8 \ldots\} g \tag{4}$$

$$D^5 g = \frac{1}{h^5} \{u\delta^5 - \frac{1}{3} u\delta^7 + \ldots\} g \tag{5}$$

$$D^6 g = \frac{1}{h^6} \{\delta^6 - \frac{1}{4}\delta^8 + \ldots\} g \tag{6}$$

$$D^7 h = \frac{1}{h^7} \{u\delta^7 \ldots\} g \tag{7}$$

$$D^8 g = \frac{1}{h^8} \{\delta^8 \ldots\} g \tag{8}$$

where D is the linear operator, $D \equiv d/dz$, and h the finite-difference mesh size.

By defining the averaging operator u, and the central difference operator δ, one obtains

$$ug(z) = \frac{1}{2}[g(z + \frac{h}{2}) + g(z - \frac{h}{2})] \tag{9}$$

$$\delta g(z) = g(z + \frac{h}{2}) - g(z - \frac{h}{2}) \tag{10}$$

and

$$\delta^{n+1} g(z) = \delta^n g(z + \frac{h}{2}) - \delta^n g(z - \frac{h}{2}), \quad n=1,2,3,\ldots \tag{11}$$

$$u\delta^{n+1} g(z) = \frac{1}{2} [\delta^{2n+1} g(z + \frac{h}{2}) + \delta^{2n+1} g(z - \frac{h}{2})],$$

$$n = 0, 1, 2 \ldots \qquad (12)$$

In order to reduce the truncation error, Thomas [1] introduced a new variable g relating to the dependent variable, say ϕ, and its derivatives by the expression

$$g = \phi - \frac{1}{6} h^2 D^2 \phi + \frac{1}{90} h^4 D^4 \phi \qquad (13)$$

By substituting this new variable into equations (1) to (8), it can be shown that the truncation errors in ϕ and its derivatives become of higher order [2]. One thus obtains

$$hD\phi = \{u\delta - \frac{1}{6} u\delta^3 + \frac{1}{30} u\delta^5 - \frac{1}{140} u\delta^7 + \ldots\} g$$

$$+ \frac{1}{6} h^3 D^3 \phi - \frac{1}{90} h^5 D^5 \phi \qquad (14)$$

$$h^2 D^2 \phi = \{\delta^2 - \frac{1}{12} \delta^4 + \frac{1}{90} \delta^6 - \frac{1}{560} \delta^8 + \ldots\} g$$

$$+ \frac{1}{6} h^4 D^4 \phi - \frac{1}{90} h^6 D^6 \phi \qquad (15)$$

$$h^3D^3\phi = \{u\delta^3 - \frac{1}{4}u\delta^5 + \frac{7}{120}u\delta^7 \ldots\}g$$

$$+ \frac{1}{6}h^5D^5\phi - \frac{1}{90}h^7D^7\phi \tag{16}$$

$$h^4D^4\phi = \{\delta^4 - \frac{1}{6}\delta^6 + \frac{7}{240}\delta^8 \ldots\}g + \frac{1}{6}h^6D^6\phi - \frac{1}{90}h^8D^8\phi \tag{17}$$

$$h^5D^5\phi = \{u\delta^5 - \frac{1}{3}u\delta^7 + \ldots\}g + \frac{1}{6}h^7D^7\phi - \frac{1}{90}h^9D^9\phi \tag{18}$$

$$h^6D^6\phi = \{\delta^6 - \frac{1}{6}\delta^8 + \ldots\}g + \frac{1}{6}h^8D^8\phi - \frac{1}{90}h^{10}D^{10}\phi \tag{19}$$

$$h^7D^7\phi = \{u\delta^7 \ldots\}g + \frac{1}{6}h^9D^9\phi - \frac{1}{90}h^{11}D^{11}\phi \tag{20}$$

$$h^8D^8\phi = \{\delta^8 + \ldots\}g + \frac{1}{6}h^{10}D^{10}\phi - \frac{1}{90}h^{12}D^{12}\phi \tag{21}$$

For even order, one may approximate equation (21) as

$$h^8D^8\phi = \delta^8 g \tag{22}$$

where the terms of order h^{10} and higher order are neglected.

Substituting equation (22) into equation (19), and successively using these results from equations (17), (15), and (13), one obtains

$$h^6 D^6 \phi = \{\delta^6 - \frac{1}{12}\delta^8\} g \tag{23}$$

$$h^4 D^4 \phi = \{\delta^4 - \frac{1}{240}\delta^8\} g \tag{24}$$

$$h^2 D^2 \phi = \{\delta^2 + \frac{1}{12}\delta^4 - \frac{1}{6048}\delta^8\} g \tag{25}$$

$$\phi = \{1 + \frac{1}{6}\delta^2 + \frac{1}{360}\delta^8 - \frac{67}{907200}\delta^8\} g \tag{26}$$

Similarly, for odd order, equation (20) becomes

$$h^7 D^7 \phi = u\delta^7 g \tag{27}$$

Equations (18), (16), and (14) thus become

$$h^5 D^5 \phi = \{u\delta^5 - \frac{1}{6} u\delta^7\} g \tag{28}$$

$$h^3 D^3 \phi = \{u\delta^3 - \frac{1}{12} u\delta^5 - \frac{11}{360} u\delta^7\} g \tag{29}$$

$$hD\phi = \{u\delta + \frac{3}{40} u\delta^3\} g \tag{30}$$

Since the highest order of the governing differential equation is fourth order, equations (24), (25), (26), (29), and (30) can be written in the form as

$$\begin{bmatrix} \phi \\ hD\phi \\ h^2D^2\phi \\ h^3D^3\phi \\ h^4D^4\phi \end{bmatrix} = \begin{bmatrix} 1 & 0 & \frac{1}{6} & 0 & \frac{1}{360} \\ 0 & 1 & 0 & 0 & 0 \\ 0 & 0 & 1 & 0 & \frac{1}{12} \\ 0 & 0 & 0 & 1 & 0 \\ 0 & 0 & 0 & 0 & 1 \end{bmatrix} \begin{bmatrix} g \\ u\delta g \\ \delta^2 g \\ u\delta^3 g \\ \delta^4 g \end{bmatrix} + \begin{bmatrix} \varepsilon_0 \\ h\varepsilon_1 \\ h^2\varepsilon_2 \\ h^3\varepsilon_3 \\ h^4\varepsilon_4 \end{bmatrix} \quad (31)$$

where $\varepsilon_0 = \frac{-67}{907200} h^8D^8\phi$, $\varepsilon_3 = \frac{-1}{12} h^2D^5\phi$

$$\varepsilon_1 = \frac{1}{120} h^4D^5\phi \;; \quad \varepsilon_4 = \frac{1}{240} h^4D^8\phi \quad (32)$$

$$\varepsilon_2 = \frac{-67}{6048} h^6D^8\phi$$

By using equations (9) to (11), one obtains

$$\begin{bmatrix} g \\ u\delta g \\ \delta^2 g \\ u\delta^3 g \\ \delta^4 g \end{bmatrix} = \begin{bmatrix} 0 & 0 & 1 & 0 & 0 \\ 0 & -\frac{1}{2} & 0 & \frac{1}{2} & 0 \\ 0 & 1 & -2 & 1 & 0 \\ -\frac{1}{2} & 1 & 0 & -1 & \frac{1}{2} \\ 1 & -4 & 6 & -4 & 1 \end{bmatrix} \begin{bmatrix} g(z-2h) \\ g(z-h) \\ g(z) \\ g(z+h) \\ g(z+2h) \end{bmatrix} \tag{33}$$

Substituting equation (33) into (31), one obtains

$$\begin{bmatrix} \phi \\ hD\phi \\ h^2D^2\phi \\ h^3D^3\phi \\ h^4D^4\phi \end{bmatrix} = \begin{bmatrix} \frac{1}{360} & \frac{7}{45} & \frac{41}{60} & \frac{7}{45} & \frac{1}{360} \\ 0 & -\frac{1}{2} & 0 & \frac{1}{2} & 0 \\ \frac{1}{12} & \frac{2}{3} & -\frac{3}{2} & \frac{2}{3} & \frac{1}{12} \\ -\frac{1}{2} & 1 & 0 & -1 & \frac{1}{2} \\ 1 & -4 & 6 & -4 & 1 \end{bmatrix} \begin{bmatrix} g(z-2h) \\ g(z-h) \\ g(z) \\ g(z+h) \\ g(z+2h) \end{bmatrix} + \begin{bmatrix} \varepsilon_0 \\ h\varepsilon_1 \\ h^2\varepsilon_2 \\ h^3\varepsilon_3 \\ h^4\varepsilon_4 \end{bmatrix} \tag{34}$$

which is the resulting matrix for the differential equation of order four.

Similarly, for the differential equation of order two, one can use the following matrix

$$\begin{bmatrix} \phi \\ hD\phi \\ h^2D^2\phi \end{bmatrix} = \begin{bmatrix} \frac{1}{12} & \frac{5}{6} & \frac{1}{12} \\ -\frac{1}{2} & 0 & \frac{1}{2} \\ 1 & -2 & 1 \end{bmatrix} \begin{bmatrix} g(z-h) \\ g(z) \\ g(z+h) \end{bmatrix} + \begin{bmatrix} \varepsilon_0' \\ h\varepsilon_1' \\ h^2\varepsilon_2' \end{bmatrix} \tag{35}$$

where

$$\varepsilon_0' = -\frac{1}{4320} h^6 D^6 \phi,$$

$$\varepsilon_1' = -\frac{1}{12} h^2 D^3 \phi, \tag{36}$$

$$\varepsilon_2' = -\frac{1}{360} h^4 D^6 \phi.$$

APPENDIX 2

ALGORITHMS FOR PENTADIAGONAL AND TRIDIAGONAL MATRICES

1. Algorithm for Pentadiagonal Matrix [3].

$$a_i u_{i-2} + b_i u_{i-1} + c_i u_i + d_i u_{i+1} + e_i u_{i+2} = f_i$$

for $1 \leq i \leq R$ with $a_1 = b_1 = a_2 = e_{R-1} = d_R = e_R = 0$. The algorithm is as follows. First compute

$$\delta_1 = d_1/c_1, \ \lambda_1 = e_1/c_1, \ \gamma_1 = f_1/c_1$$

and

$$\mu_2 = c_2 - b_2\delta_1, \ \delta_2 = (d_2 - b_2\lambda_1)/\mu_2,$$

$$\lambda_2 = e_2/\mu_2, \ \gamma_2 = (f_2 - b_2\gamma_1)/\mu_2$$

Then for $3 \leq i \leq (R-2)$, compute

$$\beta_i = b_i - a_i\delta_{i-2}$$

$$\mu_i = c_i - \beta_i\delta_{i-1} - a_i\lambda_{i-2}$$

$$\delta_i = (d_i - \beta_i\lambda_{i-1})/\mu_i$$

$$\lambda_i = e_i/\mu_i$$

$$\gamma_i = (f_i - \beta_i\gamma_{i-1} - a_i\gamma_{i-2})/\mu_i$$

Next compute

$$\beta_{R-1} = b_{R-1} - a_{R-1}\delta_{R-3}$$

$$\mu_{R-1} = c_{R-1} - \beta_{R-1}\delta_{R-2} - a_{R-1}\lambda_{R-3}$$

$$\delta_{R-1} = (d_{R-1} - \beta_{R-1}\lambda_{R-2})/\mu_{R-1}$$

$$\gamma_{R-1} = (f_{R-1} - \beta_{R-1}\gamma_{R-2} - a_{R-1}\gamma_{R-3})/\mu_{R-1}$$

and

$$\beta_R = b_R - a_R \delta_{R-2}$$

$$\mu_R = c_R - \beta_R \delta_{R-1} - a_R \lambda_{R-2}$$

$$\gamma_R = (f_R - \beta_R \gamma_{R-1} - a_R \gamma_{R-2})/\mu_R$$

The β_i and μ_i are used only to compute δ_i, λ_i and γ_i, and need not be stored after they are computed. The δ_i, λ_i and γ_i must be stored, as they are used in the back solution. This is

$$u_R = \gamma_R$$

$$u_{R-1} = \gamma_{R-1} - \delta_R u_R$$

and $u_i = \gamma_i - \delta_i u_{i+1} - \delta_i u_{i+2}$ for $(R-2) \geq i \geq 1$.

2. Algorithm for Tridiagonal Matrix [4].

$$a_i v_{i-1} + b_i v_i + c_i v_{i+1} = d_i$$

for $1 \leq i \leq N$ with $a_1 = c_N = 0$. The algorithm is as follows. First compute

$$\beta_1 = b_1, \ \gamma_1 = d_1/\beta_1.$$

Then for $2 \leq i \leq N$, compute

$$\beta_i = b_i - a_i c_{i-1}/\beta_{i-1}$$

$$\gamma_i = (d_i - a_i \gamma_{i-1})/\beta_i$$

The β_i and γ_i must be stored, as they are used in the back solution. This is

$$v_N = \gamma_N$$

and $v_i = \gamma_i - c_i v_{i+1}/\beta_i$ for $(N-1) \geq i \geq 1$.

APPENDIX 3

METHOD OF REGRESSION FOR TEMPERATURE EFFECTS ON DENSITY OF WATER BETWEEN 0°C AND 30°C [5]

Consider the relationship,

$$\rho = \rho_{max}[1 - \gamma_1(T - T_{max})^2 - \gamma_2(T - T_{max})^3]$$

and setting $y = \rho$, $x = T - T_{max}$, $c_1 = T_{max}$, and $c_2 = \rho_{max}$, one obtains

$$y = c_2[1 + a_1x^2 + a_2x^3]$$

where $a_1 = -\gamma_1$, and $a_2 = -\gamma_2$.

From Dorsey's Table [6], one obtains 310 pairs of values for the temperature range 0 ~ 30°C as,

$$x_1, x_2, \ldots, x_n,$$

$$y_1, y_2, \ldots, y_n, \quad n = 310$$

The error in the fitting, that is, the residual ε_i, is given by

$$\varepsilon_i = y_i - c_2(1 + a_1 x_i^2 + a_2 x_i^2)$$

The sum of the squares of the residuals is given by

$$P = \sum \varepsilon_i^2$$

Minimizing P, one obtains

$$\frac{\partial P}{\partial a_1} = 0, \quad \frac{\partial P}{\partial a_2} = 0$$

i.e.,

$$\sum a_1 x_i^4 + \sum a_2 x_i^5 = \sum y_i x_i^2 - \sum c_2 x_i^2$$

$$\sum a_1 x_i^5 + \sum a_2 x_i^6 = \sum y_i x_i - \sum c_2 x_i^3$$

Solving the above set of equations, one obtains

$$a_1 = \begin{vmatrix} \sum y_i x_i^2 - \sum c_2 x_i^2 & \sum x_i^5 \\ \sum y_i x_i - \sum c_2 x_i^3 & \sum x_i^6 \end{vmatrix} / D$$

$$a_2 = \begin{vmatrix} \sum x_i^4 & \sum y_i x_i^2 - \sum c_2 x_i^2 \\ \sum x_i^5 & \sum y_i x_i - \sum c_2 x_i^3 \end{vmatrix} / D$$

where $D = \begin{vmatrix} \sum x_i^4 & \sum x_i^5 \\ \sum x_i^5 & \sum x_i^6 \end{vmatrix}$

The numerical results are

$$\gamma_1 = 7.731937895 \times 10^{-6}$$

$$\gamma_2 = -5.182117468 \times 10^{-8}$$

$$\gamma_2/\gamma_1 = -6.70222334 \times 10^{-3}$$

$$\text{standard deviation} = 3.797 \times 10^{-6}$$

In Table A1, Column A represents the values listed in Table 93 of [6], and Column B lists the values calculated by equation (1) using the results of the regression analysis.

APPENDIX 4

PROOF FOR $e_x^+ = e_y^+ = e_z^+ = b_x^+ = 0$

1. From equation (22b) and considering the z-component, one obtains

$$\frac{\partial e_x}{\partial y} = \frac{\partial e_y}{\partial x} .$$

By using the disturbance form $f = f^+(z)e^{iay}$, one obtains

$$iae_x^+ = 0$$

Hence $e_x^+ = 0$ for the whole domain.

2. From equation (21) and the boundary condition (29), one has

$$j_z = ke_z + \phi_u b_y$$

$$j_z = 0, \quad \text{at} \quad z = 0, 1$$

Since $\phi_u = 0$ at $z = 0, 1$, one obtains

$$e_z = 0 \quad \text{at } z = 0, 1$$

This implies that

$$e_z^+ = 0 \quad \text{at } z = 0, 1$$

From the z-component of the electric field equation one obtains

$$(D^2 - a^2)e_z^+ = 0$$

Thus one concludes that $e_z^+ = 0$ for the whole domain.

3. From equation (22d), the z-component gives

$$2Rmj_z = \left(\frac{\partial b_y}{\partial x} - \frac{\partial b_x}{\partial y}\right) = 0, \quad \text{at } z = 0, 1$$

This implies

$$b_x^+ = 0 \quad \text{at } z = 0, 1$$

After the order of magnitude analysis, equation (34) becomes

$$(D^2 - a^2) b_x^+ = 0$$

Hence, one concludes that $b_x^+ = 0$ for the whole domain.

4. The y-component of equation (22d) is

$$2Rm j_y = \left(\frac{\partial b_x}{\partial z} - \frac{\partial b_z}{\partial x}\right)$$

In terms of the amplitude quantities, one obtains

$$2Rm j_y^+ = D b_x^+$$

Since $b_x^+ = 0$ for the whole domain, one concludes that $j_y^+ = 0$ for the whole domain. From equation (21) one has

$$j_y = k e_y - u - \phi_u b_z$$

Since $u = \phi_u = 0$ at $z = 0, 1$, and $j_y^+ = 0$ for the whole domain, one obtains

$$e_y^+ = 0 \text{ at } z = 0, 1$$

From equation (36) one has

$$(D^2 - a^2)e_y^+ = 0$$

Hence one concludes that $e_y^+ = 0$ for the whole domain.

APPENDIX 5

DERIVATION OF STREAM FUNCTION FOR HEXAGONAL CELL [7]

The perturbation equations in dimensionless form are:

$$\frac{\partial u}{\partial x} + \frac{\partial v}{\partial y} + \frac{\partial w}{\partial z} = 0 \qquad (1)$$

$$\frac{\partial u}{\partial t} = - \frac{\partial P}{\partial x} + \nabla^2 u \qquad (2)$$

$$\frac{\partial v}{\partial t} = - \frac{\partial P}{\partial y} + \nabla^2 v \qquad (3)$$

$$\frac{\partial w}{\partial t} = - \frac{\partial P}{\partial z} + \nabla^2 w + Gr(1 + \lambda_1 z + \lambda_2 z^2)\theta \qquad (4)$$

Taking partial derivative of equation (2) with respect to y minus partial derivaties of equation (3) with respect to x, one obtains

$$\left[\frac{\partial}{\partial t} - \nabla^2\right]\left(\frac{\partial u}{\partial x} - \frac{\partial u}{\partial y}\right) = 0 \qquad 95)$$

This equation can be solved by writing

$$u = -\frac{\partial\phi}{\partial x} - \frac{\partial\psi}{\partial y}, \quad v = -\frac{\partial\phi}{\partial y} + \frac{\partial\psi}{\partial x} \tag{6}$$

where ψ is unrestricted and

$$\left[\frac{\partial}{\partial t} - \nu\nabla^2\right]\nabla_1^2\psi = 0 \tag{7}$$

$$\nabla_1^2 = \frac{\partial^2}{\partial x^2} + \frac{\partial^2}{\partial y^2}$$

Then the continuity equation requires that

$$\frac{\partial w}{\partial z} = -\left(\frac{\partial u}{\partial x} + \frac{\partial v}{\partial y}\right) = \nabla_1^2\phi \tag{8}$$

Imposing the condition [9]

$$\nabla_1^2 w + a^2 w = 0, \tag{9}$$

then

$$\phi = -\frac{1}{a^2}\frac{\partial w}{\partial z} + \phi', \tag{10}$$

where ϕ' denotes a plane-harmonic function of x and y.

At the cylindrical boundary, along a plane of symmetry, u and v must satisfy the condition

$$0 = u \cos(x,n) + v \cos(y,n),$$

$$= -\frac{\partial\phi}{\partial n} - \frac{\partial\psi}{\partial s} \quad \text{according to eq. (6)} \tag{11}$$

For steady state, from equation (7), one obtains

$$\nabla^2\nabla_1^2\psi = 0 \tag{12}$$

If ψ is constant and if $\partial\psi/\partial n$ vanishes at every point in the boundary; and when $\partial w/\partial n = 0$ at the boundary, according to equation (10), one obtains ϕ' is constant. Then from equations (6), (8) and (10), one has

$$u = \frac{1}{a^2}\frac{\partial^2 w}{\partial x \partial z}, \quad \text{and} \quad v = \frac{1}{a^2}\frac{\partial^2 w}{\partial y \partial z} \tag{13}$$

The solution for the hexagonal pattern was found by Christopherson [8]. The solution is

$$w = \frac{1}{3} w^+(z)\{2 \cos \frac{2\pi x}{L\sqrt{3}} \cos \frac{2\pi y}{3L} + \cos \frac{4\pi y}{3L}\}, \tag{14}$$

where L measures the sides of the hexagon.

An alternative form of the solution is

$$w = \frac{1}{3} w^+(z)\{\cos \frac{4\pi}{3L} (\frac{\sqrt{3}}{2} x + \frac{1}{2} y)$$

$$+ \cos \frac{4\pi}{3L} (\sqrt{3}\, x - \frac{1}{2} y) + \cos \frac{4\pi y}{3L}\} \qquad (15)$$

One notes that $x = 0$ and $y = 0$ represent the plane of symmetry, and the motion is two-dimensional. Thus for $x = 0$, one obtains

$$u = \frac{1}{a^2} \frac{\partial^2 w}{\partial x \partial z} = 0 \qquad (16)$$

$$v = \frac{1}{a^2} \frac{\partial^2 w}{\partial y \partial z} = -\frac{Dw^+}{3a^2} \frac{4}{3L} (b + 2 \cos \frac{2\pi y}{3L}) \sin \frac{2\pi y}{3L} \qquad (17)$$

$$w = \frac{1}{3} w^+(2 \cos \frac{2\pi y}{3L} + \cos \frac{4\pi y}{3L}) \qquad (18)$$

The equation, $dy/v = dz/w$, gives the streamlines in the (y,z)-plane and can be readily integrated by using equations (17) and (18) to give

$$\left\{\frac{1 + 2\cos\left(\frac{2\pi y}{3L}\right)}{1 + \cos\left(\frac{2\pi y}{3L}\right)} \sin \frac{2\pi y}{3L}\right\}^2 \frac{w^+(z)}{w^+_{max}} = \text{constant} = \psi_v \tag{19}$$

Similarly, for $y = 0$, one obtains

$$u = \frac{1}{a^2} \frac{\partial^2 w}{\partial x \partial z} = - \frac{Dw^+}{3a^2} \frac{4\pi}{L\sqrt{3}} \sin \frac{2\pi x}{L\sqrt{3}} \tag{20}$$

$$v = 0 \tag{21}$$

$$w = \frac{1}{3} w^+\left(2 \cos \frac{2\pi x}{L\sqrt{3}} + 1\right), \tag{22}$$

and the equation for the streamlines in the (x,z)-plane is $dx/u = dz/w$, which gives

$$\left\{\left(1 - \cos \frac{2\pi x}{L\sqrt{3}}\right) \sin \frac{2\pi x}{L\sqrt{3}}\right\}^{2/3} \frac{w^+(z)}{w^+_{max}} = \text{constant} = \psi_u \tag{23}$$

The streamlines of the secondary flow from equations (19) and (23) are plotted in Figs. (11a) and (11b) of Chapter VIII.

References

1. Thomas, L.H., "The Stability of Plane Poiseuille Flow", Physical Review 91, 1953, pp. 780-783.
2. Chen, T.S., "Hydrodynamic Stability of Developing Flow in a Parallel-Plate Channel", Ph.D. Thesis, University of Minnesota, 1966.
3. Conte, S.D., "Elementary Numerical Analysis", McGraw-Hill, 1965, p. 266.
4. Conte, S.D., "Elementary Numerical Analysis", McGraw-Hill, 1965, pp. 183-184.
5. Neville, A.M. and Kennedy, J.B., "Basic Statistical Methods for Engineers and Scientists", International Textbook Company, 1964, Ch. 17, pp. 208-220.
6. Dorsey, N.E., "Properties of Ordinary Water Substance", Hafner Publishing Co., New York, 1967, p. 200.
7. Harries, D.L. and Reid, W.H., "Some Further Results on the Benard Problems", The Physics of Fluid, Vol. 1, No. 2, 1958, pp. 102-110.
8. Christopherson, D.G., "Note on the Vibration of Membranes", Quart. J. of Math. (Oxford Series), 11, 1940, pp. 63-65.
9. Pellow, A. and Southwell, R.V., "On Maintained Convective Motion in a Fluid Heated from Below", Proc. of Roy. Soc., Series A, Vol. 179, 1940, pp. 312-343.

Table A1 Comparison of Water Density with [6]

°C	A	B	°C	A	B
0.0	0.9998676	0.9998730	5.1	0.9999902	0.9999907
0.1	0.9998743	0.9998793	5.2	0.9999884	0.9999890
0.2	0.9998808	0.9998855	5.3	0.9999864	0.9999870
0.3	0.9998871	0.9998915	5.4	0.9999843	0.9999850
0.4	0.9998933	0.9998974	5.5	0.9999820	0.9999828
0.5	0.9998993	0.9999031	5.6	0.9999796	0.9999804
0.6	0.9999051	0.9999086	5.7	0.9999770	0.9999779
0.7	0.9999107	0.9999139	5.8	0.9999742	0.9999753
0.8	0.9999161	0.9999191	5.9	0.9999713	0.9999724
0.9	0.9999214	0.9999242	6.0	0.9999683	0.9999695
1.0	0.9999265	0.9999290	6.1	0.9999651	0.9999664
1.1	0.9999314	0.9999337	6.2	0.9999618	0.9999631
1.2	0.9999362	0.9999382	6.3	0.9999583	0.9999597
1.3	0.9999407	0.9999426	6.4	0.9999546	0.9999562
1.4	0.9999451	0.9999468	6.5	0.9999508	0.9999525
1.5	0.9999493	0.9999509	6.6	0.9999469	0.9999486
1.6	0.9999534	0.9999547	6.7	0.9999428	0.9999447
1.7	0.9999573	0.9999585	6.8	0.9999386	0.9999405
1.8	0.9999610	0.9999620	6.9	0.9999342	0.9999362
1.9	0.9999645	0.9999654	7.0	0.9999297	0.9999318
2.0	0.9999678	0.9999687	7.1	0.9999250	0.9999272
2.1	0.9999710	0.9999717	7.2	0.9999202	0.9999225
2.2	0.9999740	0.9999746	7.3	0.9999153	0.9999177
2.3	0.9999769	0.9999774	7.4	0.9999102	0.9999127
2.4	0.9999796	0.9999800	7.5	0.9999049	0.9999075
2.5	0.9999821	0.9999824	7.6	0.9998995	0.9999022
2.6	0.9999844	0.9999847	7.7	0.9998940	0.9998968
2.7	0.9999866	0.9999868	7.8	0.9998883	0.9998912
2.8	0.9999886	0.9999888	7.9	0.9998825	0.9998855
2.9	0.9999905	0.9999906	8.0	0.9998765	0.9998796
3.0	0.9999922	0.9999922	8.1	0.9998704	0.9998736
3.1	0.9999937	0.9999937	8.2	0.9998642	0.9998674
3.2	0.9999950	0.9999950	8.3	0.9998578	0.9998612
3.3	0.9999962	0.9999962	8.4	0.9998513	0.9998547
3.4	0.9999972	0.9999972	8.5	0.9998446	0.9998482
3.5	0.9999981	0.9999981	8.6	0.9998378	0.9998414
3.6	0.9999988	0.9999988	8.7	0.9998309	0.9998346
3.7	0.9999993	0.9999993	8.8	0.9998238	0.9998276
3.8	0.9999997	0.9999997	8.9	0.9998166	0.9998205
3.9	0.9999999	0.9999999	9.0	0.9998092	0.9998132
4.0	1.0000000	1.0000000	9.1	0.9998017	0.9998058
4.1	0.9999999	0.9999999	9.2	0.9997941	0.9997982
4.2	0.9999996	0.9999997	9.3	0.9997863	0.9997905
4.3	0.9999992	0.9999993	9.4	0.9997784	0.9997827
4.4	0.9999986	0.9999988	9.5	0.9997704	0.9997747
4.5	0.9999979	0.9999981	9.6	0.9997622	0.9997666
4.6	0.9999970	0.9999972	9.7	0.9997539	0.9997584
4.7	0.9999960	0.9999962	9.8	0.9997454	0.9997500
4.8	0.9999948	0.9999951	9.9	0.9997368	0.9997415
4.9	0.9999934	0.9999938	10.0	0.9997281	0.9997328
5.0	0.9999919	0.9999923	10.1	0.9997193	0.9997241

Table A1 Continued

°C	A	B	°C	A	B
10.2	0.9997103	0.9997151	15.4	0.9990674	0.9990719
10.3	0.9997012	0.9997061	15.5	0.9990518	0.9990563
10.4	0.9996919	0.9996969	15.6	0.9990360	0.9990405
10.5	0.9996825	0.9996876	15.7	0.9990202	0.9990246
10.6	0.9996730	0.9996781	15.8	0.9990043	0.9990085
10.7	0.9996634	0.9996685	15.9	0.9989882	0.9989924
10.8	0.9996536	0.9996588	16.0	0.9989721	0.9989761
10.9	0.9996437	0.9996489	16.1	0.9989558	0.9989598
11.0	0.9996336	0.9996389	16.2	0.9989394	0.9989433
11.1	0.9996234	0.9996288	16.3	0.9989229	0.9989267
11.2	0.9996131	0.9996185	16.4	0.9989062	0.9989099
11.3	0.9996027	0.9996081	16.5	0.9988895	0.9988931
11.4	0.9995922	0.9995976	16.6	0.9988726	0.9988761
11.5	0.9995815	0.9995869	16.7	0.9988557	0.9988591
11.6	0.9995706	0.9995762	16.8	0.9988386	0.9988419
11.7	0.9995597	0.9995652	16.9	0.9988214	0.9988246
11.8	0.9995486	0.9995542	17.0	0.9988041	0.9988072
11.9	0.9995374	0.9995430	17.1	0.9987867	0.9987896
12.0	0.9995261	0.9995317	17.2	0.9987691	0.9987720
12.1	0.9995146	0.9995202	17.3	0.9987515	0.9987542
12.2	0.9995030	0.9995087	17.4	0.9987337	0.9987363
12.3	0.9994913	0.9994970	17.5	0.9987158	0.9987184
12.4	0.9994795	0.9994851	17.6	0.9986979	0.9987003
12.5	0.9994675	0.9994732	17.7	0.9986798	0.9986820
12.6	0.9994554	0.9994611	17.8	0.9986616	0.9986637
12.7	0.9994432	0.9994489	17.9	0.9986433	0.9986453
12.8	0.9994309	0.9994366	18.0	0.9986248	0.9986267
12.9	0.9994184	0.9994241	18.1	0.9986063	0.9986081
13.0	0.9994059	0.9994115	18.2	0.9985877	0.9985893
13.1	0.9993932	0.9993988	18.3	0.9985689	0.9985704
13.2	0.9993803	0.9993859	18.4	0.9985501	0.9985514
13.3	0.9993674	0.9993729	18.5	0.9985311	0.9985323
13.4	0.9993543	0.9993598	18.6	0.9985120	0.9985131
13.5	0.9993411	0.9993466	18.7	0.9984928	0.9984938
13.6	0.9993278	0.9993333	18.8	0.9984735	0.9984744
13.7	0.9993143	0.9993198	18.9	0.9984541	0.9984549
13.8	0.9993007	0.9993062	19.0	0.9984346	0.9984352
13.9	0.9992870	0.9992925	19.1	0.9984150	0.9984155
14.0	0.9992732	0.9992786	19.2	0.9983953	0.9983956
14.1	0.9992593	0.9992647	19.3	0.9983754	0.9983756
14.2	0.9992453	0.9992506	19.4	0.9983555	0.9983556
14.3	0.9992311	0.9992363	19.5	0.9983355	0.9983354
14.4	0.9992168	0.9992220	19.6	0.9983153	0.9983151
14.5	0.9992024	0.9992075	19.7	0.9982950	0.9982947
14.6	0.9991879	0.9991930	19.8	0.9982747	0.9982742
14.7	0.9991732	0.9991783	19.9	0.9982542	0.9982536
14.8	0.9991584	0.9991634	20.0	0.9982336	0.9982329
14.9	0.9991436	0.9991485	20.1	0.9982130	0.9982121
15.0	0.9991286	0.9991334	20.2	0.9981922	0.9981911
15.1	0.9991134	0.9991182	20.3	0.9981713	0.9981701
15.2	0.9990982	0.9991029	20.4	0.9981503	0.9981490
15.3	0.9990828	0.9990875	20.5	0.9981292	0.9981278

Table A1 Continued

°C	A	B	°C	A	B
20.6	0.9981080	0.9981064	25.8	0.9968671	0.9968624
20.7	0.9980867	0.9980850	25.9	0.9968406	0.9968360
20.8	0.9980653	0.9980635	26.0	0.9968141	0.9968095
20.9	0.9980438	0.9980418	26.1	0.9967875	0.9967830
21.0	0.9980221	0.9980201	26.2	0.9967608	0.9967564
21.1	0.9980004	0.9979982	26.3	0.9967340	0.9967297
21.2	0.9979786	0.9979763	26.4	0.9967071	0.9967029
21.3	0.9979567	0.9979542	26.5	0.9966801	0.9966760
21.4	0.9979346	0.9979321	26.6	0.9966530	0.9966490
21.5	0.9979125	0.9979098	26.7	0.9966258	0.9966220
21.6	0.9978903	0.9978875	26.8	0.9965986	0.9965948
21.7	0.9978679	0.9978650	26.9	0.9965712	0.9965676
21.8	0.9978455	0.9978425	27.0	0.9965437	0.9965403
21.9	0.9978230	0.9978198	27.1	0.9965162	0.9965129
22.0	0.9978003	0.9977971	27.2	0.9964886	0.9964855
22.1	0.9977776	0.9977742	27.3	0.9964608	0.9964579
22.2	0.9977547	0.9977513	27.4	0.9964330	0.9964303
22.3	0.9977318	0.9977282	27.5	0.9964051	0.9964026
22.4	0.9977088	0.9977051	27.6	0.9963771	0.9963748
22.5	0.9976856	0.9976819	27.7	0.9963490	0.9963469
22.6	0.9976624	0.9976585	27.8	0.9963208	0.9963189
22.7	0.9976390	0.9976351	27.9	0.9962926	0.9962909
22.8	0.9976156	0.9976116	28.0	0.9962642	0.9962628
22.9	0.9975921	0.9975879	28.1	0.9962358	0.9962346
23.0	0.9975684	0.9975642	28.2	0.9962072	0.9962063
23.1	0.9975447	0.9975404	28.3	0.9961786	0.9961779
23.2	0.9975208	0.9975165	28.4	0.9961499	0.9961495
23.3	0.9974969	0.9974925	28.5	0.9961211	0.9961210
23.4	0.9974729	0.9974684	28.6	0.9960922	0.9960924
23.5	0.9974487	0.9974442	28.7	0.9960632	0.9960637
23.6	0.9974245	0.9974199	28.8	0.9960341	0.9960350
23.7	0.9974002	0.9973955	28.9	0.9960049	0.9960061
23.8	0.9973758	0.9973710	29.0	0.9959757	0.9959772
23.9	0.9973512	0.9973465	29.1	0.9959463	0.9959483
24.0	0.9973266	0.9973218	29.2	0.9959169	0.9959192
24.1	0.9973019	0.9972970	29.3	0.9958874	0.9958901
24.2	0.9972771	0.9972722	29.4	0.9958578	0.9958609
24.3	0.9972522	0.9972473	29.5	0.9958281	0.9958316
24.4	0.9972272	0.9972222	29.6	0.9957983	0.9958022
24.5	0.9972021	0.9971971	29.7	0.9957684	0.9957728
24.6	0.9971769	0.9971719	29.8	0.9957384	0.9957433
24.7	0.9971516	0.9971466	29.9	0.9957084	0.9957137
24.8	0.9971262	0.9971212	30.0	0.9956783	0.9956840
24.9	0.9971007	0.9970957	30.1	0.9956480	0.9956543
25.0	0.9970751	0.9970701	30.2	0.9956177	0.9956245
25.1	0.9970494	0.9970445	30.3	0.9955874	0.9955946
25.2	0.9970236	0.9970187	30.4	0.9955569	0.9955646
25.3	0.9969978	0.9969929	30.5	0.9955263	0.9955346
25.4	0.9969718	0.9969669	30.6	0.9954956	0.9955045
25.5	0.9969458	0.9969409	30.7	0.9954649	0.9954744
25.6	0.9969196	0.9969148	30.8	0.9954341	0.9954441
25.7	0.9968934	0.9968886	30.9	0.9954032	0.9954138

APPENDIX 6

COMPUTER PROGRAMS

PROGRAM FOR CHAPTER II

```
C     DECK FOR CALCULATING EIGENVALUES AND EIGENFUNCTION
      IMPLICIT REAL*8 (A-H,O-Z)
      DIMENSION YN(20,201),RN(20,201),FN(20,201)
     1 ,ZN(20,201),DY(20,201),DR(20,201),DF(20,201)
     2 ,DZ(20,201),AL(20),BE(20),EP(20),GA(20),VI(2)
     3 ,EF(201),DE(201),AN(20),BN(20),CN(20),DN(20)
      WRITE (6,5)
      READ (5,6) PE
      WRITE (6,7) PE
    5 FORMAT ('0','INPUT IN FORMAT XXX0.XDX FO PE')
    6 FORMAT (D8.1)
    7 FORMAT ('0','PECLECT NO. =',F5.1)
      KE=201
      N1=20
      READ (5,50) (AL(N),N=1,N1)
      READ (5,50) (BE(N),N=1,N1)
      READ (5,50) (EP(N),N=1,N1)
      READ (5,50) (GA(N),N=1,N1)
      READ (5,50) (CN(N),N=1,N1)
      READ (5,50) (BN(N),N=1,N1)
      READ (5,50) (DN(N),N=1,N1)
      READ (5,50) (AN(N),N=1,N1)
      H=1.D0/(KE-1)
C     CALCULATE AL & YN
      DO 10 N=1,N1
      VI(1)=1.
      VI(2)=0.
      EI=AL(N)
      CALL DRKG(PE,VI,EI,EF,DE,KE,1)
      DO 14 K=1,KE
      YN(N,K)=EF(K)
      DY(N,K)=DE(K)
   14 CONTINUE
      AL(N)=EI
   10 CONTINUE
C     CALCULATE BE & RN
      DO 11 N=1,N1
      VI(1)=1.
      VI(2)=0.
      EI=BE(N)
      CALL DRKG(PE,VI,EI,EF,DE,KE,2)
      DO 15 K=1,KE
      RN(N,K)=EF(K)
      DR(N,K)=DE(K)
   15 CONTINUE
      BE(N)=EI
```

```
 11   CONTINUE
      DO 12 N=1,N1
      VI(1)=0.
      VI(2)=1.
      EI=EP(N)
      CALL DRKG(PE,VI,EI,EF,DE,KE,1)
      DO 16 K=1,KE
      FN(N,K)=EF(K)
      DF(N,K)=DE(K)
 16   CONTINUE
      EP(N)=EI
 12   CONTINUE
      DO 13 N=1,N1
      VI(1)=0.
      VI(2)=1.
      EI=GA(N)
      CALL DRKG(PE,VI,EI,EF,DE,KE,2)
      DO 17 K=1,KE
      ZN(N,K)=EF(K)
      DZ(N,K)=DE(K)
 17   CONTINUE
      GA(N)=EI
 13   CONTINUE
      WRITE (8,71)  (AL(N),N=1,N1)
      WRITE (8,71)  (EP(N),N=1,N1)
      WRITE (8,71)  (BN(N),N=1,N1)
      WRITE (8,71)  (AN(N),N=1,N1)
      WRITE (8,71)  ((YN(N,K),K=1,KE,10),N=1,N1)
      WRITE (8,71)  ((FN(N,K),K=1,KE,10),N=1,N1)
      WRITE (8,71)  ((DY(N,K),K=1,KE,10),N=1,N1)
      WRITE (8,71)  ((DF(N,K),K=1,KE,10),N=1,N1)
      WRITE (10,71)  (BE(N),N=1,N1)
      WRITE (10,71)  (GA(N),N=1,N1)
      WRITE (10,71)  (CN(N),N=1,N1)
      WRITE (10,71)  (DN(N),N=1,N1)
      WRITE (10,71)  ((RN(N,K),K=1,KE,10),N=1,N1)
      WRITE (10,71)  ((ZN(N,K),K=1,KE,10),N=1,N1)
      WRITE (10,71)  ((DR(N,K),K=1,KE,10),N=1,N1)
      WRITE (10,71)  ((DZ(N,K),K=1,KE,10),N=1,N1)
 50   FORMAT (4D20.10)
 60   FORMAT (8D15.6)
 61   FORMAT (6D20.10)
 71   FORMAT (5D16.9)
      STOP
      END
      SUBROUTINE DRKG(PE,VI,EI,EF,DE,KE,IN)
```

```
      IMPLICIT REAL*8 (A-H,O-Z)
      DIMENSION VI(2),EF(201),DE(201)
      SIGN=(-1)**IN
      H=1.D0/(KE-1)
      H2=H*H
      CON=(8./(3.*PE))**2
      T9= 0.5*H2
      EF(1)=VI(1)
      DE(1)=VI(2)
      EPS=0.1D-7
      IMAX=20
      IT=0
10    IT=IT+1
      IF (IT.GT.IMAX) GO TO 14
      EI2=EI*EI
      T10=CON*EI2
      X=0.
      DO 11 K=2,KE
      T1=EF(K-1)
      T2=DE(K-1)*H
      T3=(T9*EI2*(T10+SIGN*(1.-X*X)))*T1
      X=X+0.5*H
      T4=T1+0.5*T2+0.25*T3
      T5=(T9*EI2*(T10+SIGN*(1.-X*X)))*T4
      X=X+0.5*H
      T4=T1+T2+T5
      T6=(T9*EI2*(T10+SIGN*(1.-X*X)))*T4
      T7=(T3+2.*T5)/3.
      T8=(T3+4.*T5+T6)/3.
      EF(K)=T1+T2+T7
      DE(K)=(T2+T8)/H
11    CONTINUE
      ERR=EF(KE)
      IF (IN.EQ.1) ERR=DE(KE)
      IF (DABS(ERR).LE.EPS) GO TO 14
      IF (IT.GE.2) GO TO 12
      ER1=ERR
      EIG=EI
      EI=EI+0.001
      GO TO 10
12    ER2=ERR
      AK=(EI-EIG)/(ER2-ER1)
      EIG=EI
      EI=EI-ER2*AK
      ER1=ER2
      GO TO 10
```

```
14   CONTINUE
     WRITE (6,60) IT,PE,EI
60   FORMAT ('0','NO. OF ITERATION =',I3,5X,'PECLECT NO. =',
    1  D8.1,5X,'EIGENVALUE =',D20.12)
     RETURN
     END
```

```
      IMPLICIT REAL*8 (A-H,O-Z)
      DIMENSION RN(20,201),YN(20,201),FN(20,201)
     1 ,ZN(20,201),AL(20),BE(20),EP(20),GA(20),G(40)
     2 ,DT(20,20),T1(1600),T2(201),E(40,40),P(20,20)
     3 ,Q(20,20),PH(20,201),PY(20,201)
      REAL*8 L1(40),M1(40)
      READ (5,5) PE
      WRITE (6,6) PE
    5 FORMAT (D8.1)
    6 FORMAT ('0','PECLECT NO. =',D10.2)
      N1=20
      N2=N1*2
      KE=201
      THE=1.
      H=0.005D0
C
      READ (15,50) (AL(N),N=1,N1)
      READ (15,50) (BE(N),N=1,N1)
      READ (15,50) (EP(N),N=1,N1)
      READ (15,50) (GA(N),N=1,N1)
      READ (15,51) ((YN(N,K),K=1,KE),N=1,N1)
      READ (15,51) ((RN(N,K),K=1,KE),N=1,N1)
      READ (15,51) ((FN(N,K),K=1,KE),N=1,N1)
      READ (15,51) ((ZN(N,K),K=1,KE),N=1,N1)
   50 FORMAT (1X,4D20.12)
   51 FORMAT (1X,5D16.9)
C
      CALL ORTH(RN,P,PH,N1,KE,H)
      WRITE (6,66)
      WRITE (6,60) ((P(I,J),J=1,N1),I=1,N1)
      CALL ORTH(YN,Q,PY,N1,KE,H)
      WRITE (6,67)
      WRITE (6,60) ((Q(I,J),J=1,N1),I=1,N1)
      CALL EMA(AL,BE,PH,PY,P,Q,N1,KE,H,E)
      DO 10 I=1,N2
   10 G(I)=0.
      DO 12 N=1,N1
      DO 11 K=1,KE
   11 T1(K)=PH(N,K)
      CALL DQSF(H,T1,T2,KE)
   12 G(N)=THE*T2(KE)
C
      K=1
      DO 13 J=1,N2
      DO 13 I=1,N2
      T1(K)=E(I,J)
```

```
 13   K=K+1
C
      WRITE (6,68)
      EPS=0.1D-7
      CALL DGELG(G,T1,N2,1,EPS,IER)
      WRITE (6,61) IER
      WRITE (6,60) (G(I),I=1,N2)
      WRITE (7,71) (G(I),I=1,N2)
C
      CALL ORTH(ZN,P,PH,N1,KE,H)
      WRITE (6,66)
      WRITE (6,60) ((P(I,J),J=1,N1),I=1,N1)
      CALL ORTH(PN,Q,PY,N1,KE,H)
      WRITE (6,67)
      WRITE (6,60) ((Q(I,J),J=1,N1),I=1,N1)
      CALL EMA(EP,GA,PH,PY,P,Q,N1,KE,H,E)
      DO 14 I=1,N2
 14   G(I)=0.
      DO 16 N=1,N1
      DO 15 K=1,KE
      Z=H*(K-1)
 15   T1(K)=Z*PH(N,K)
      CALL DQSF(H,T1,T2,KE)
 16   G(N)=-T2(KE)
      K=1
      DO 17 J=1,N2
      DO 17 I=1,N2
      T1(K)=E(I,J)
 17   K=K+1
      WRITE (6,68)
      CALL DGELG(G,T1,N2,1,EPS,IER)
      WRITE (6,61) IER
      WRITE (6,60) (G(I),I=1,N2)
      WRITE (7,71) (G(I),I=1,N2)
C
 60   FORMAT (8D15.7)
 61   FORMAT ('0','ERROR INDICATOR OF DGELG',I5)
 66   FORMAT ('0','P MATRIX')
 67   FORMAT ('0','Q MATRIX')
 68   FORMAT ('0','THE COEFFICIENTS')
 71   FORMAT (4D20.10)
      STOP
      END
      SUBROUTINE ORTH(RN,P,PH,N1,KE,H)
      IMPLICIT REAL*8 (A-H,O-Z)
      DIMENSION RN(20,201),T1(400),T2(201),D(20)
```

```
     1  ,DT(20,20),A(20,20),P(20,20),PH(20,201)
      REAL*8 L1(20),M1(20)
      DO 12 M=1,N1
      DO 12 N=M,N1
      DO 11 K=1,KE
   11 T1(K)=RN(M,K)*RN(N,K)
      CALL DQSF(H,T1,T2,KE)
      DT(M,N)=T2(KE)
      DT(N,M)=T2(KE)
   12 CONTINUE
C
      D(1)=DSQRT(DABS(DT(1,1)))
      DO 14 N=2,N1
      K=1
      DO 13 J=1,N
      DO 13 I=1,N
      T1(K)=DT(I,J)
   13 K=K+1
      CALL DMINV(T1,N,D1,L1,M1)
      D(N)=DSQRT(DABS(D1))
   14 CONTINUE
C
      DO 15 J=1,N1
      DO 15 I=1,N1
      A(I,J)=0.
   15 P(I,J)=0.
      DO 21 N=3,N1
      IN=N-1
      DO 21 J=1,N
      DO 29 IR=1,N
      IF (IR-J) 16,29,17
   16 K=IR
      GO TO 18
   17 K=IR-1
   18 CONTINUE
      DO 19 IC=1,IN
      A(K,IC)=DT(IR,IC)
   19 CONTINUE
   29 CONTINUE
      K=1
      DO 20 IC=1,IN
      DO 20 IR=1,IN
      T1(K)=A(IR,IC)
   20 K=K+1
      CALL DMINV(T1,IN,D1,L1,M1)
      P(N,J)=D1
```

```
21    CONTINUE
      DO 22 J=1,N1
      DO 22 I=1,N1
22    A(I,J)=0.
      A(1,1)=1./D(1)
      DEN=D(1)*D(2)
      A(2,1)=-DT(2,1)/DEN
      A(2,2)=DT(1,1)/DEN
      DO 23 N=3,N1
      DEN=D(N)*D(N-1)
      DO 23 J=1,N
      I=N+J
      ANM=(-1.)**I*P(N,J)
      A(N,J)=ANM/DEN
23    CONTINUE
      K=1
      DO 24 J=1,N1
      DO 24 I=1,N1
      T1(K)=A(I,J)
24    K=K+1
      CALL DMINV(T1,N1,D1,L1,M1)
      DO 25 J=1,N1
      DO 25 I=1,N1
25    P(I,J)=0.
      K=1
      DO 26 J=1,N1
      DO 26 I=1,N1
      P(I,J)=T1(K)
26    K=K+1
      DO 27 K=1,KE
      DO 27 N=1,N1
27    PH(N,K)=0.
      DO 28 J=1,N1
      DO 28 K=1,KE
      DO 28 N=1,J
28    PH(J,K)=PH(J,K)+A(J,N)*RN(N,K)
      RETURN
      END
      SUBROUTINE EMA(AL,BE,PH,PY,P,Q,N1,KE,H,E)
      IMPLICIT REAL*8 (A-H,O-Z)
      DIMENSION PH(20,201),PY(20,201),P(20,20),Q(20,20)
     1  ,E(40,40),T1(201),T2(201),BE2(20),AL2(20)
     2  ,DT(20,20),AL(20),BE(20)
      N2=N1*2
      DO 10 N=1,N1
      AL2(N)=AL(N)**2
```

```
10    BE2(N)=BE(N)**2
      DO 13 J=1,N1
      DO 13 I=1,N1
13    DT(I,J)=0.
      DO 11 J=1,N2
      DO 11 I=1,N2
11    E(I,J)=0.
      DO 15 M=1,N1
      DO 15 N=1,N1
      DO 14 K=1,KE
14    T1(K)=PH(M,K)*PY(N,K)
      CALL DQSF(H,T1,T2,KE)
      DT(M,N)=T2(KE)
15    CONTINUE
C
      DO 17 M=1,N1
      DO 17 N=M,N1
      E(M,N)=P(N,M)
      E(N1+M,N1+N)=AL2(N)*Q(N,M)
17    CONTINUE
      DO 20 IR=1,N1
      DO 20 IC=1,N1
      C1=0.
      C2=0.
      DO 19 J=1,IC
      C1=C1+Q(IC,J)*DT(IR,J)
      C2=C2+P(IC,J)*DT(J,IR)
19    CONTINUE
      E(IR,N1+IC)=-C1
      E(N1+IR,IC)=BE2(IC)*C2
20    CONTINUE
      RETURN
      END
```

PROGRAM FOR CHAPTER III

```
      IMPLICIT REAL*8(A-H,O-Z)
      DIMENSION DUZ(41),PTX(41),PTZ(41),ZY(30)
     1 ,A3(41),B3(41),C3(41),A5(41),B5(41),C5(41)
     2 ,D5(41),E5(41),G(41),CRA(41),X(30)
     3 ,W(41),WN(41),PU(41),TH(41)
     4 ,BE(20),GA(20),BE2(20),GA2(20),RN(20,21)
     5 ,ZN(20,21),DRN(20,21),DZN(20,21),CN(20),DN(20)
      COMMON /A/M,MI,M1
      COMMON /B/BE2,GA2,CN,DN,RN,ZN,DRN,DZN,N1,K1
      READ (5,5) PE,PR,L1,IN,IE,ID
      READ (5,6) (X(L),L=1,L1)
      WRITE (6,7) PE,PR,L1,IN,IE,ID
    5 FORMAT (2F5.1,4I2)
    6 FORMAT (13F6.3)
    7 FORMAT ('1','PECLECT NO.=',F5.1,5X,'PRANDTL NO.='
     1 ,D9.2,5X,3I3,'INDICATOR=',I2)
      I1=15
      N1=20
      K1=21
      M=40
      EPS=0.1D-5
      MI=M-1
      M1=M+1
      DZ=0.025D0
      DZ2=DZ*DZ
      DZ4=DZ2*DZ2
      PU(1)=0.D0
      PU(M1)=0.D0
      TH(1)=0.D0
      TH(M1)=0.D0
      W(1)=0.0D0
      W(M1)=0.D0
      WN(1)=0.D0
      WN(M1)=0.D0
      THE=1.
      READ (15,50) (BE(N),N=1,N1)
      READ (15,50) (GA(N),N=1,N1)
      READ (15,50) (CN(N),N=1,N1)
      READ (15,50) (DN(N),N=1,N1)
      READ (15,50) ((RN(N,K),K=1,21),N=1,N1)
      READ (15,50) ((ZN(N,K),K=1,21),N=1,N1)
      READ (15,50) ((DRN(N,K),K=1,21),N=1,N1)
      READ (15,50) ((DZN(N,K),K=1,21),N=1,N1)
   50 FORMAT (5D16.9)
      DO 10 N=1,N1
      BE2(N)=BE(N)**2
```

```
      GA2(N)=GA(N)**2
   10 CONTINUE
      DO 41 K=2,M
      DUZ(K)=3.D0*(1.D0-2.D0*DZ*(K-1))
      A1=K
      W(K)=2.*(1.-A1/M)
   41 CONTINUE
C
      DO 100 L=IN,IE
      XA=X(L)
      WRITE (6,163) X(L)
      CALL BTEM(ID,XA,PTX,PTZ)
      WRITE (6,164)
      WRITE (6,160) (PTX(K),K=1,M1)
      WRITE (6,160) (PTZ(K),K=1,M1)
      IRA=1
      IA=1
      RA=1708.0D0
      A=2.50D0
   15 CONTINUE
      X1=(A*DZ)**2/0.6D1
      X2=(A*DZ)**4/0.36D3
      X3=(A*DZ)**2/0.12D2
      B3(1)=-12.D0
      C3(1)=0
      DO 11 K=2,M
      A3(K)=1.D0-X3
      B3(K)=-2.D0-X3*10
      C3(K)=A3(K)
   11 CONTINUE
      B3(M1)=-12.D0
      A3(M1)=0.D0
      C5(1)=264.D0*X1-240.D0
      D5(1)=96.D0*X1-120.D0
      E5(1)=0.D0
      B5(2)=56.D0*X2-8.D0*X1-4.D0
      C5(2)=247.D0*X2+17.D0*X1+7.D0
      D5(2)=B5(2)
      E5(2)=1.D0-X1+X2
      C5(3)=246.D0*X2+18.D0*X1+6.D0
      DO 12 K=3,MI
      A5(K)=E5(2)
      B5(K)=B5(2)
      C5(K)=C5(3)
      D5(K)=B5(2)
      E5(K)=E5(2)
```

```
   12  CONTINUE
       A5(M)=E5(2)
       B5(M)=B5(2)
       C5(M)=C5(2)
       D5(M)=B5(2)
       E5(M)=0.D0
       A5(M1)=0.D0
       B5(M1)=D5(1)
       C5(M1)=C5(1)
       D5(M1)=0.D0
       E5(M1)=0.D0
C START ITERATION
       I=1
  111  DO 60 K=1,M1
   60  G(K)=W(K)*DUZ(K)*DZ2
       CALL TRID(A3,B3,C3,G,PU)
       TEMP4=16.D0/3.D0
       DO 63 K=1,M1
       G(K)=TEMP4*PU(K)/PR*PTX(K)+W(K)*PTZ(K)
   63  G(K)=G(K)*DZ2
       CALL TRID(A3,B3,C3,G,TH)
       DO 67 K=1,M1
   67  G(K)=A*A*RA*TH(K)*DZ4
       CALL PENTAD(A5,B5,C5,D5,E5,G,WN)
       A1=0.0D0
       A2=0.0D0
       DO 70 K=1,M1
       A1=A1+W(K)**2
   70  A2=A2+WN(K)**2
       RAN=RA*DSQRT(A1/A2)
       A1=0.0D0
       A2=0.0D0
       DO 75 K=1,M1
       A1=A1+DABS(WN(K)-W(K))
   75  A2=A2+DABS(WN(K))
       TEMP1=A1/A2
       IF (TEMP1.LE.EPS) GO TO 73
       DO 72 K=1,M1
   72  W(K)=WN(K)*RAN/RA
       RA=RAN
       I=I+1
       IF (I.LE.I1) GO TO 111
   73  CONTINUE
       WRITE (6,161) I,A,RA,TEMP1
       CRA(IA)=RA
       A=A+0.1D0/IPA
```

```
      IA=IA+1
      IF (IA.LE.3) GO TO 15
      SIGN=(CRA(IA-1)-CRA(IA-2))*(CRA(IA-2)-CRA(IA-3))
      IF (SIGN) 13,13,15
   13 CONTINUE
      IF (IRA.GE.100) GO TO 14
      A=A-3*0.1/IRA
      IRA=IRA*10
      CRA(1)=CRA(IA-3)
      IA=2
      A=A+0.1/IRA
      GO TO 15
   14 CONTINUE
  100 CONTINUE
  160 FORMAT (8D15.6)
  161 FORMAT ('0','NO. OF ITERATION=',I4,5X,'WAVE NO.=',
     1 D12.5,5X,'RAYLEIGH NO.=',D15.7,5X,'ERROR=',D15.6)
  163 FORMAT ('0','AXIAL POSITION AT',D12.4)
  164 FORMAT ('0','THE DERIVATIVE OF TEMPERATURE',//)
      STOP
      END
      SUBROUTINE BTEM(ID,X,PTX,PTZ)
      IMPLICIT REAL*8(A-H,O-Z)
      DIMENSION PTX(41),PTZ(41),BE2(20),GA2(20),CN(20)
     1 ,DN(20),RN(20,21),ZN(20,21),DRN(20,21),DZN(20,21)
      COMMON /A/M,MI,M1
      COMMON /B/BE2,GA2,CN,DN,RN,ZN,DRN,DZN,N1,K1
      IF (ID.EQ.1) GO TO 22
      DO 33 K=1,M1
      PTZ(K)=1.
      PTX(K)=0.
      DO 34 N=1,N1
      T1=DEXP(-X*BE2(N))
      T2=DEXP(-X*GA2(N))
      IF (K-K1) 35,35,36
   35 KK=K1-K+1
      PTX(K)=PTX(K)-CN(N)*BE2(N)*RN(N,KK)*T1+DN(N)*GA2(N)
     1 *ZN(N,KK)*T2
      PTZ(K)=PTZ(K)-CN(N)*DRN(N,KK)*T1+DN(N)*DZN(N,KK)*T2
      GO TO 34
   36 KK=K-K1+1
      PTX(K)=PTX(K)-CN(N)*BE2(N)*RN(N,KK)*T1-DN(N)*GA2(N)
     1 *ZN(N,KK)*T2
      PTZ(K)=PTZ(K)+CN(N)*DRN(N,KK)*T1+DN(N)*DZN(N,KK)*T2
   34 CONTINUE
      PTZ(K)=-PTZ(K)
```

17

```
      PTX(K)=-0.5*PTX(K)
   33 CONTINUE
      RETURN
   22 CONTINUE
      DO 23 K=1,M1
      PTZ(K)=0.
      PTX(K)=0.
      DO 24 N=1,N1
      T1=DEXP(-X*BE2(N))
      T2=DEXP(-X*GA2(N))
      IF (K-K1) 25,25,26
   25 KK=K1-K+1
      PTX(K)=PTX(K)+CN(N)*BE2(N)*RN(N,KK)*T1-
     1 DN(N)*GA2(N)*ZN(N,KK)*T2
      PTZ(K)=PTZ(K)-CN(N)*DRN(N,KK)*T1+DN(N)*DZN(N,KK)*T2
      GO TO 24
   26 KK=K-K1+1
      PTX(K)=PTX(K)+CN(N)*BE2(N)*RN(N,KK)*T1+
     1 DN(N)*GA2(N)*ZN(N,KK)*T2
      PTZ(K)=PTZ(K)+CN(N)*DRN(N,KK)*T1+DN(N)*DZN(N,KK)*T2
   24 CONTINUE
      PTX(K)=-0.5*PTX(K)
      PTZ(K)=-PTZ(K)
   23 CONTINUE
      RETURN
      END
      SUBROUTINE TRID(A,B,C,D,PF)
      DOUBLE PRECISION A(51),B(51),C(51),D(51),F(51)
     1 ,BP(51),Q(51),H(51),PF(51)
      COMMON /A/M,MI,M1
      BP(2)=C(2)/B(2)
      Q(2)=D(2)/B(2)
      DO 1 K=3,MI
      H(K)=B(K)-A(K)*BP(K-1)
      BP(K)=C(K)/H(K)
      Q(K)=(D(K)-A(K)*Q(K-1))/H(K)
    1 CONTINUE
      F(M)=(D(M)-A(M)*Q(MI))/(B(M)-A(M)*BP(MI))
      DO 2 KK=2,MI
      K=M1-KK
      F(K)=Q(K)-BP(K)*F(K+1)
    2 CONTINUE
      PF(2)=(10.D0*F(2)+F(3))/12
      DO 3 K=3,MI
      PF(K)=(F(K-1)+10.D0*F(K)+F(K+1))/12
    3 CONTINUE
```

```
      FF(M)=(F(MI)+10*F(M))/12
      RETURN
      END
      SUBROUTINE PENTAD(A,B,C,D,E,F,WN)
      DOUBLE PRECISION A(41),B(41),C(41),D(41),E(41),F(41),
     1 Y(41),WN(41),OMGA(41),BETA(41),GAMM(41),H(41),DELT(41)
      COMMON /A/M,MI,M1
      OMGA(1)=C(1)
      BETA(1)=D(1)/OMGA(1)
      GAMM(1)=E(1)/OMGA(1)
      DELT(2)=B(2)
      OMGA(2)=C(2)-DELT(2)*BETA(1)
      BETA(2)=(D(2)-DELT(2)*GAMM(1))/OMGA(2)
      GAMM(2)=E(2)/OMGA(2)
      DO 10 N=3,M1
      DELT(N)=B(N)-A(N)*BETA(N-2)
      OMGA(N)=C(N)-A(N)*GAMM(N-2)-DELT(N)*BETA(N-1)
      BETA(N)=(D(N)-DELT(N)*GAMM(N-1))/OMGA(N)
   10 GAMM(N)=E(N)/OMGA(N)
      BETA(M1)=0.D0
      GAMM(M1)=0.D0
      GAMM(M)=0.D0
      H(1)=F(1)/OMGA(1)
      H(2)=(F(2)-DELT(2)*H(1))/OMGA(2)
      DO 20 N=3,M1
   20 H(N)=(F(N)-A(N)*H(N-2)-DELT(N)*H(N-1))/OMGA(N)
      Y(M1)=H(M1)
      Y(M)=H(M)-BETA(M)*Y(M1)
      DO 30 KK=1,MI
      I=M-KK
   30 Y(I)=H(I)-BETA(I)*Y(I+1)-GAMM(I)*Y(I+2)
      WN(2)=(56*Y(1)+247*Y(2)+56*Y(3)+Y(4))/360
      DO 40 K=3,MI
      WN(K)=(Y(K-2)+56*Y(K-1)+246*Y(K)+56*Y(K+1)+Y(K+2))/360
   40 CONTINUE
      WN(M)=(Y(M-2)+56*Y(MI)+247*Y(M)+56*Y(M1))/360
      RETURN
      END
```

PROGRAM FOR CHAPTER IV

```
      IMPLICIT REAL*8 (A-H,O-Y)
      DIMENSION BU(41),DBU(41),PTX(41),PTZ(41),PXX(41)
     1 ,PHI(41),A3(41),B3(41),C3(41),A5(41),B5(41)
     3 ,C5(41),D5(41),E5(41),F(41),G(41),CRA(41)
     4 ,W(41),WN(41),PU(41),TH(41),FXX(41),AFX(41)
     2 ,BE(20),GA(20),CN(20),DN(20),RN(20,21)
     5 ,ZN(20,21),DRN(20,21),DZN(20,21),X(30),ZY(30)
      COMMON /A/M,MI,M1
      COMMON /B/BE,GA,CN,DN,RN,ZN,DRN,DZN
      READ (5,8) RAM1,RAM2
      READ (5,5) PE,L1,IN,IE,ID
      READ (5,7) (X(L),L=1,L1)
      WRITE (6,6) PE
    5 FORMAT (F5.1,4I2)
    6 FORMAT ('0','PECTECT NO. =',F5.1,///)
    7 FORMAT (13F6.3)
    8 FORMAT (2F6.3)
      N1=20
      PR=10.
      I1=15
      THE=1.
      EPS=0.1D-5
      M=40
      MI=M-1
      M1=M+1
      K1=M/2+1
      DZ=1.D0/M
      DZ2=DZ*DZ
      DZ4=DZ2*DZ2
      PU(1)=0
      PU(M1)=0.
      W(1)=0.
      W(M1)=0.
      WN(1)=0.
      WN(M1)=0.
      TH(1)=0.
      TH(M1)=0.
C READ IN THE ANALYTIC SOLUTION OF BASIC FLOW
      READ (15,50) (BE(N),N=1,N1)
      READ (15,50) ([illegible](N),N=1,N1)
      READ (15,50) (C[illegible],N=1,N1)
      READ (15,50) (DN(N),N=1,N1)
      READ (15,50) ((RN(N,K),K=1,21),N=1,N1)
      READ (15,5[illegible]) ((Z[illegible],K=1,21),N=1,N1)
      READ (15,50) ((D[illegible],K),K=1,21),N=1,N1)
      READ (15,50) ([illegible](N,K),K=1,21),N=1,N1)
```

```
   50  FORMAT (5D16.9)
C CALCULATE THE VELOCITY FIELD
       DO 30 K=1,M1
       Z=DZ*(K-1)
       BU(K)=3.D0*(Z-Z*Z)
       DBU(K)=3.D0*(1.-2.*Z)
   30  CONTINUE
       WRITE (6,31)
   31  FORMAT (1H0, 'BASIC VELOCITY PROFILE')
       WRITE (6,60) (BU(K),K=1,M1)
       WRITE (6,60) (DBU(K),K=1,M1)
C DEFINE THE INITIAL PERTURBATION VELOCITY
       DO 38 K=2,M
       T3=K
       W(K)=2.*(1.-T3/M)
   38  CONTINUE
       DO 100 L=IN,IE
       WRITE (6,69) X(L)
       XA=X(L)
       CALL TEMP(ID,DZ,XA,PHI,PTX,PTZ,PXX)
       WRITE (6,70)
       WRITE (6,60) (PXX(K),K=1,M1)
       WRITE (6,60) (PTX(K),K=1,M1)
       WRITE (6,60) (PHI(K),K=1,M1)
       WRITE (6,60) (PTZ(K),K=1,M1)
       DO 39 K=1,M1
       F(K)=1-RAM1*PHI(K)+RAM2*PHI(K)**2
       FXX(K)=-RAM1*PXX(K)+2.*RAM2*(PTX(K)**2+PHI(K)*PXX(K))
   39  CONTINUE
       IA=1
       IRA=1
       WA=2.5D0
       RA=1.D5
   15  CONTINUE
       WA2=WA*WA
       X1=WA2*DZ2/6
       X2=WA2*WA2*DZ4/360
       X3=X1/2
C DEFINE THE MATRICES
       B3(2)=-2.D0-10.D0*X3
       C3(2)=1.D0-X3
       DO 11 K=3,M
       A3(K)=C3(2)
       B3(K)=B3(2)
       C3(K)=C3(2)
   11  CONTINUE
```

```
      C5(1)=264.D0*X1-240.D0
      D5(1)=96.D0*X1-120.D0
      E5(1)=0.D0
      B5(2)=56.D0*X2-8.D0*X1-4.D0
      C5(2)=247.D0*X2+17.D0*X1+7.D0
      D5(2)=B5(2)
      E5(2)=1.D0-X1+X2
      C5(3)=246.D0*X2+18.D0*X1+6.D0
      DO 12 K=3,MI
      A5(K)=E5(2)
      B5(K)=B5(2)
      C5(K)=C5(3)
      D5(K)=B5(2)
      E5(K)=E5(2)
   12 CONTINUE
      A5(M)=E5(2)
      B5(M)=B5(2)
      C5(M)=C5(2)
      D5(M)=B5(2)
      E5(M)=0.D0
      A5(M1)=0.D0
      B5(M1)=D5(1)
      C5(M1)=C5(1)
      D5(M1)=0.D0
      E5(M1)=0.D0
      T1=(16.D0/(3*PE))**2
      DO 37 K=1,M1
      AFX(K)=WA2*F(K)-T1*FXX(K)
   37 CONTINUE
C START THE ITERATION
      I=1
1111  DO 80 K=2,M
   80 G(K)=W(K)*DBU(K)*DZ2
      CALL TRID(A3,B3,C3,G,PU)
C CALCULATE THE TH
      T4=16.D0/3.
      DO 81 K=2,M
      G(K)=T4*PU(K)/PR*PTX(K)+W(K)*PTZ(K)
   81 G(K)=G(K)*DZ2
      CALL TRID(A3,B3,C3,G,TH)
C CALCULATE THE NEW W
      DO 82 K=1,M1
   82 G(K)=AFX(K)*RA*TH(K)*DZ4
      CALL PENTAD(A5,B5,C5,D5,E5,G,WN)
C CALCULATE THE NEW RAYLEIGH NUMBER
      T1=0.
```

```
      T2=0.
      DO 83 K=1,M1
      T1=T1+W(K)**2
   83 T2=T2+WN(K)**2
      RAN=RA*DSQRT(T1/T2)
C CHECK THE CONVERGENCE OF W
      T1=0.
      T2=0.
      DO 84 K=1,M1
      T1=T1+DABS(W(K)-WN(K))
   84 T2=T2+DABS(WN(K))
      T3=T1/T2
      IF (T3-EPS) 1000,85,85
C READJUST W
   85 DO 86 K=2,M
   86 W(K)=WN(K)*RAN/RA
      RA=RAN
      I=I+1
      IF (I-I1) 1111,1111,1000
 1000 CONTINUE
      WRITE (6,87) I,WA,RA,T3
C
      CRA(IA)=RA
      WA=WA+0.1/IRA
      IA=IA+1
      IF (IA.LE.3) GO TO 15
      SIGN=(CRA(IA-1)-CRA(IA-2))*(CRA(IA-2)-CRA(IA-3))
      IF (SIGN) 13,13,15
   13 CONTINUE
      IF (IRA.GE.100) GO TO 14
      WA=WA-3*0.1/IRA
      IRA=IRA*10
      CRA(1)=CRA(IA-3)
      IA=2
      WA=WA+0.1/IRA
      GO TO 15
   14 CONTINUE
      WRITE (6,88) X(L),RAM1,RAM2
      ZY(L)=RA
  100 CONTINUE
      WRITE (7,61) (ZY(L),L=IN,IE)
   61 FORMAT (10F8.1)
   60 FORMAT (8D15.6)
   69 FORMAT (1H0, 'X=',D10.3)
   70 FORMAT (1H0, 'TEMPERATURE FIELD')
   88 FORMAT (1H0, 'X=',D10.3,5X,'RAM1=',D10.3,5X,'RAM2=',D10.3)
```

```
87   FORMAT (1HO, 'I=',I3,5X,'WAVE NO.=',D12.5,5X,
    1  'RAYLEIGH NO.=',D20.10,5X,'ERROR=',D16.7)
     STOP
     END
     SUBROUTINE TEMP(ID,DZ,X,PHI,PTX,PTZ,PXX)
     IMPLICIT REAL*8 (A-H,O-Y)
     DIMENSION BE(20),GA(20),BE2(20),GA2(20),BE4(20),GA4(20)
    1  ,RN(20,21),ZN(20,21),DRN(20,21),DZN(20,21),CN(20)
    2  ,DN(20),PTX(41),PTZ(41),PXX(41),PHI(41)
     COMMON /A/M,MI,M1
     COMMON /B/BE,GA,CN,DN,RN,ZN,DRN,DZN
     N1=20
     THE=1.
     K1=21
     DO 10 N=1,N1
     BE2(N)=BE(N)*BE(N)
     GA2(N)=GA(N)*GA(N)
     BE4(N)=BE2(N)*BE2(N)
     GA4(N)=GA2(N)*GA2(N)
10   CONTINUE
     IF (ID.EQ.1) GO TO 22
     DO 33 K=1,M1
     Z=DZ*(K-1)
     Z=Z*2.D0-1.D0
     PHI(K)=1.+Z
     PTZ(K)=1.
     PTX(K)=0.
     PXX(K)=0.
     DO 34 N=1,N1
     T1=DEXP(-X*BE2(N))
     T2=DEXP(-X*GA2(N))
     IF (K-K1) 35,35,36
35   KK=K1-K+1
     PXX(K)=PXX(K)+CN(N)*BE4(N)*RN(N,KK)*T1-DN(N)*GA4(N)
    1  *ZN(N,KK)*T2
     PTX(K)=PTX(K)-CN(N)*BE2(N)*RN(N,KK)*T1+DN(N)*GA2(N)
    1  *ZN(N,KK)*T2
     PHI(K)=PHI(K)+CN(N)*RN(N,KK)*T1-DN(N)*ZN(N,KK)*T2
     PTZ(K)=PTZ(K)-CN(N)*DRN(N,KK)*T1+DN(N)*DZN(N,KK)*T2
     GO TO 34
36   KK=K-K1+1
     PXX(K)=PXX(K)+CN(N)*BE4(N)*RN(N,KK)*T1+DN(N)*GA4(N)
    1  *ZN(N,KK)*T2
     PTX(K)=PTX(K)-CN(N)*BE2(N)*RN(N,KK)*T1-DN(N)*GA2(N)
    1  *ZN(N,KK)*T2
     PHI(K)=PHI(K)+CN(N)*RN(N,KK)*T1+DN(N)*ZN(N,KK)*T2
```

```
      PTZ(K)=PTZ(K)+CN(N)*DRN(N,KK)*T1+DN(N)*DZN(N,KK)*T2
   34 CONTINUE
      PXX(K)=-0.5*PXX(K)
      PHI(K)=-0.5*PHI(K)
      PTZ(K)=-PTZ(K)
      PTX(K)=-0.5*PTX(K)
   33 CONTINUE
      RETURN
   22 CONTINUE
      DO 23 K=1,M1
      PHI(K)=1.+THE
      PTZ(K)=0.
      PTX(K)=0.
      PXX(K)=0.
      DO 24 N=1,N1
      T1=DEXP(-X*BE2(N))
      T2=DEXP(-X*GA2(N))
      IF (K-K1) 25,25,26
   25 KK=K1-K+1
      PTX(K)=PTX(K)+CN(N)*BE2(N)*RN(N,KK)*T1-
     1  DN(N)*GA2(N)*ZN(N,KK)*T2
      PXX(K)=PXX(K)+CN(N)*BE4(N)*RN(N,KK)*T1-
     1  DN(N)*GA4(N)*ZN(N,KK)*T2
      PHI(K)=PHI(K)+CN(N)*RN(N,KK)*T1-DN(N)*ZN(N,KK)*T2
      PTZ(K)=PTZ(K)-CN(N)*DRN(N,KK)*T1+DN(N)*DZN(N,KK)*T2
      GO TO 24
   26 KK=K-K1+1
      PTX(K)=PTX(K)+CN(N)*BE2(N)*RN(N,KK)*T1+
     1  DN(N)*GA2(N)*ZN(N,KK)*T2
      PXX(K)=PXX(K)+CN(N)*BE4(N)*RN(N,KK)*T1+
     1  DN(N)*GA4(N)*ZN(N,KK)*T2
      PHI(K)=PHI(K)+CN(N)*RN(N,KK)*T1+DN(N)*ZN(N,KK)*T2
      PTZ(K)=PTZ(K)+CN(N)*DRN(N,KK)*T1+DN(N)*DZN(N,KK)*T2
   24 CONTINUE
      PTX(K)=-0.5*PTX(K)
      PTZ(K)=-PTZ(K)
      PHI(K)=-0.5*PHI(K)
      PXX(K)=-0.5*PXX(K)
   23 CONTINUE
      RETURN
      END
      SUBROUTINE TRID(A,B,C,D,FF)
      DOUBLE PRECISION A(51),B(51),C(51),D(51),F(51)
     1  ,BP(51),Q(51),H(51),FF(51)
      COMMON /A/M,MI,M1
      BP(2)=C(2)/B(2)
```

```
      Q(2)=D(2)/B(2)
      DO 1 K=3,MI
      H(K)=B(K)-A(K)*BP(K-1)
      BP(K)=C(K)/H(K)
      Q(K)=(D(K)-A(K)*Q(K-1))/H(K)
    1 CONTINUE
      F(M)=(D(M)-A(M)*Q(MI))/(B(M)-A(M)*BP(MI))
      DO 2 KK=2,MI
      K=M1-KK
      F(K)=Q(K)-BP(K)*F(K+1)
    2 CONTINUE
      FF(2)=(10.D0*F(2)+F(3))/12
      DO 3 K=3,MI
      FF(K)=(F(K-1)+10.D0*F(K)+F(K+1))/12
    3 CONTINUE
      FF(M)=(F(MI)+10*F(M))/12
      RETURN
      END
      SUBROUTINE PENTAD(A,B,C,D,E,F,WN)
      DOUBLE PRECISION A(41),B(41),C(41),D(41),E(41),F(41),
     1 Y(41),WN(41),OMGA(41),BETA(41),GAMM(41),H(41),DELT(41)
      COMMON /A/M,MI,M1
      OMGA(1)=C(1)
      BETA(1)=D(1)/OMGA(1)
      GAMM(1)=E(1)/OMGA(1)
      DELT(2)=B(2)
      OMGA(2)=C(2)-DELT(2)*BETA(1)
      BETA(2)=(D(2)-DELT(2)*GAMM(1))/OMGA(2)
      GAMM(2)=E(2)/OMGA(2)
      DO 10 N=3,M1
      DELT(N)=B(N)-A(N)*BETA(N-2)
      OMGA(N)=C(N)-A(N)*GAMM(N-2)-DELT(N)*BETA(N-1)
      BETA(N)=(D(N)-DELT(N)*GAMM(N-1))/OMGA(N)
   10 GAMM(N)=E(N)/OMGA(N)
      BETA(M1)=0.D0
      GAMM(M1)=0.D0
      GAMM(M)=0.D0
      H(1)=F(1)/OMGA(1)
      H(2)=(F(2)-DELT(2)*H(1))/OMGA(2)
      DO 20 N=3,M1
   20 H(N)=(F(N)-A(N)*H(N-2)-DELT(N)*H(N-1))/OMGA(N)
      Y(M1)=H(M1)
      Y(M)=H(M)-BETA(M)*Y(M1)
      DO 30 KK=1,MI
      I=M-KK
   30 Y(I)=H(I)-BETA(I)*Y(I+1)-GAMM(I)*Y(I+2)
```

```
      WN(2)=(56*Y(1)+247*Y(2)+56*Y(3)+Y(4))/360
      DO 40 K=3,MI
      WN(K)=(Y(K-2)+56*Y(K-1)+246*Y(K)+56*Y(K+1)+Y(K+2))/360
   40 CONTINUE
      WN(M)=(Y(M-2)+56*Y(MI)+247*Y(M)+56*Y(M1))/360
      RETURN
      END
```

PROGRAM FOR CHAPTER V

```
C DECK OF ANALYTIC SOLUTION OF VISCOUS DISSIPATION
      IMPLICIT REAL*8 (A-H,O-Z)
      DIMENSION EIGNE(12),EIGNO(12),DZE(12),DZO(12),DRZE(12),
     1  DZRO(12),ZE(12,201),ZO(12,201),CE(12),CO(12),
     2  THL(40,51),TNU(40),BNU(40),BMT(40),X(40),T1(12,40),
     3  TY(201),Z1(201),FZ(10),BR(15)THU(40,51),T2(12,40)
      J1=6
      I1=24
      READ (5,52) (X(I),I=1,I1)
      READ (5,52) (BR(I),I=1,J1)
   52 FORMAT (8D10.3)
      L1=201
      N1=8
      K1=51
      H=1.D0/(K1-1)
      DELT=1.D0
C READ IN DATA
      READ (5,50) (EIGNE(N),N=1,N1)
      READ (5,50) (EIGNO(N),N=1,N1)
      READ (5,50) (DZE(N),N=1,N1)
      READ (5,50) (DZO(N),N=1,N1)
      READ (5,50) (DZRE(N),N=1,N1)
      READ (5,50) (DZRO(N),N=1,N1)
   50 FORMAT (4D20.10)
      DO 55 N=1,N1
   55 READ (5,51) (ZE(N,L),L=1,L1)
      DO 56 N=1,N1
   56 READ (5,51) (ZO(N,L),L=1,L1)
   51 FORMAT (5D16.9)
      WRITE (6,61)
      WRITE (6,71) (EIGNE(N),N=1,N1)
      WRITE (6,62)
      WRITE (6,71) (EIGNO(N),N=1,N1)
      WRITE (6,63)
      WRITE (6,71) (DZE(N),N=1,N1)
      WRITE (6,64)
      WRITE (6,71) (DZO(N),N=1,N1)
      WRITE (6,65)
      WRITE (6,71) (DZRE(N),N=1,N1)
      WRITE (6,66)
      WRITE (6,71) (DZRO(N),N=1,N1)
      WRITE (6,67)
      WRITE (6,71) ((ZE(N,L),L=1,L1),N=1,N1)
      WRITE (6,68)
      WRITE (6,71) ((ZO(N,L),L=1,L1),N=1,N1)
```

```
 61   FORMAT(1H0,'EVEN EIGINVALUE')
 62   FORMAT(1H0, 'ODD EIGENVALUE')
 63   FORMAT(1H0, 'DZE')
 64   FORMAT(1H0, 'DZO')
 65   FORMAT(1H0, 'DZRE')
 66   FORMAT(1H0, 'DZRO')
 67   FORMAT (1H0, 'ZE')
 68   FORMAT (1H0, 'ZO')
 71   FORMAT (1H ,6D20.10)
C CALCULATE CE AND CO
      READ (5,50) (FZ(N),N=1,N1)
      WRITE (6,75)
 75   FORMAT (1H0, 'THE INTEGRAL OF FZ')
      WRITE (6,71) (FZ(N),N=1,N1)
      DO 100 J=1,JI
      WRITE (6,70) BR(J)
 70   FORMAT (1H0, 'BR=',D20.10)
      DO 20 N=1,N1
      T6=BR(J)*EIGNE(N)*FZ(N)/(DZE(N)*DZRE(N))
      CE(N)=-2.D0*DELT/(EIGNE(N)*DZRE(N))-3.D0/2*T6
      CO(N)=2.D0/(EIGNO(N)*DZRO(N))
 20   CONTINUE
      WRITE (7,79) (CE(N),N=1,N1)
      WRITE (7,79) (CO(N),N=1,N1)
 79   FORMAT (4D20.10)
      WRITE (6,69)
 69   FORMAT (1H0, 'THE COEFFICIENTS FO THE SERIES')
      WRITE (6,71) (CE(N),N=1,N1)
      WRITE (6,71) (CO(N),N=1,N1)
C CALCULATE THE TEMPERATURE PROFILE
      DO 21 I=1,I1
      WRITE (6,72) X(I)
      DO 22 K=1,K1
      KI=(K-1)*4+1
      Z=H*(K-1)
      FBZ=BR(J)*(1.D0-Z**4)*3/4
      T5=0.D0
      T6=0.D0
      THU(I,K)=0.D0
      THL(I,K)=0.D0
      DO 23 N=1,N1
      T1(N,I)=-EIGNE(N)**2*X(I)
      T2(N,I)=-EIGNO(N)**2*X(I)
      T3=CE(N)*ZE(N,KI)*DEXP(T1(N,I))
      T4=CO(N)*ZO(N,KI)*DEXP(T2(N,I))
      T5=T5+T3+T4
      T6=T6+T3-T4
 23   CONTINUE
```

```
      THU(I,K)=Z+T5+FBZ
      THL(I,K)=-Z+T6+FBZ
      THU(I,K)=0.5D0*(1.D0-THU(I,K))
      THL(I,K)=0.5D0*(1.D0-THL(I,K))
   22 CONTINUE
      WRITE (6,71) (THU(I,K),K=1,K1)
      WRITE (6,71) (THL(I,K),K=1,K1)
   21 CONTINUE
   72 FORMAT (1H0, 'X=',D11.4,5X,'TEMPERATURE PROFILE')
C CALCULATE THE BULK MEAN TEMP. AND NUSSELT NUMBER
      DO 31 I=1,I1
      T3=0.D0
      T4=0.D0
      T5=0.D0
      DO 32 N=1,N1
      T3=T3+DZE(N)*CE(N)*DEXP(T1(N,I))/EIGNE(N)**2
      T4=T4+CE(N)*DZE(N)*DEXP(T1(N,I))
      T5=T5+CO(N)*DZO(N)*DEXP(T2(N,I))
   32 CONTINUE
      BMT(I)=3.D0/2*(16.D0/35*BR(J)-T3)
      TNU(I)=(1.D0-BR(J)*3+T4+T5)/(1.D0-BMT(I))*4
      BNU(I)=(1.D0+BR(J)*3-T4+T5)/(1.D0+BMT(I))*4
      WRITE (6,73) X(I),BMT(I),TNU(I),BNU(I)
   31 CONTINUE
   73 FORMAT (1H0, 'X=',D12.4,5X,'BMT=',D20.10,5X,'TNU=',
     * D20.10,5X,'BNU'=H,D20.10)
    1 CONTINUE
      CALL EXIT
      END

C     PROGRAM FOR THE CASE OF VISCOUS DISSIPATION EFFECTS
C     IN PARALLEL-PLATE CHANNELS
      IMPLICIT REAL*8 (A-H,O-Z)
      DIMENSION RN(20,21),ZN(20,21),DRN(20,21),DZN(20,21),
     1 CN(20),DN(20),DUZ(41),PTZ(41),PTX(41),A3(41),
     2 A5(41),B5(41),C5(41),D5(41),E5(41),F5(41),D3(41),
     3 W(41),WN(41),PU(41),TH(41),G(41),BETA(20),GAMA(20)
     4  ,B3(41),C3(41),X(50),CRA(41),BR(10),DPU(41),DTH(41)
     5,Y4(41),Z1(41),ANY(41),CRA(20),REU(41),REW(41),RET(41)
      COMMON M,MI,M1
      L1=24
      READ (5,7) (X(I),I=1,L1)
    7 FORMAT (8D10.3)
      J1=1
      J=1
      BR(1)=-100.
      N1=8
      I1=20
```

```
      M=40
      EPS=0.1D-5
      MI=M-1
      M1=M+1
      K1=M/2+1
      DZ=0.025D0
      DZ2=DZ*DZ
      DZ4=DZ2*DZ2
      PU(1)=0.D0
      PU(M1)=0.D0
      TH(1)=0.D0
      TH(M1)=0.D0
      W(1)=0.0D0
      W(M1)=0.D0
      WN(1)=0.D0
      WN(M1)=0.D0
C READ IN THE ANALYTIC SOLUTION OF THE MAIN FLOW
      READ (5,154) (BETA(N),N=1,N1)
      READ (5,154) (GAMA(N),N=1,N1)
  154 FORMAT (4D20.10)
      DO 150 N=1,N1
  150 READ (5,155) (RN(N,I),I=1,K1)
      DO 151 N=1,N1
  151 READ (5,155) (ZN(N,I),I=1,K1)
      DO 152 N=1,N1
  152 READ (5,155) (DRN(N,I),I=1,K1)
      DO 153 N=1,N1
  153 READ (5,155) (DZN(N,I),I=1,K1)
  155 FORMAT (5D16.9)
      DO 9 N=1,N1
      RN(N,21)=0.D0
      DRN(N,1)=0.D0
      DZN(N,1)=1.0D0
    9 CONTINUE
C WRITE ALL DATA OUT
      WRITE (6,161)
  161 FORMAT (1H ,'INPUT DATA')
      WRITE (6,160) (BETA(N),N=1,N1)
      WRITE (6,160) (GAMA(N),N=1,N1)
      WRITE (6,162)
  162 FORMAT (1H ,'RN VALUE')
      WRITE (6,160) ((RN(N,K),K=1,K1),N=1,N1)
  160 FORMAT (1H ,7D17.9)
      WRITE (6,163)
  163 FORMAT (1H ,'ZN VLAUE')
      WRITE (6,160) ((ZN(N,K),K=1,K1),N=1,N1)
      WRITE (6,164)
  164 FORMAT (1H , 'DRN VALUE')
```

```
      WRITE (6,160) ((DRN(N,K),K=1,K1),N=1,N1)
      WRITE (6,165)
  165 FORMAT (1H , 'DZN VLAUE')
      WRITE (6,160) ((DZN(N,K),K=1,K1),N=1,N1)
C CALCULATE THE VELOCITY GRADIENT OF THE MAIN FLOW
      DO 42 K=1,M1
      DUZ(K)=3.D0*(1.D0-2.D0*DZ*(K-1))
   42 CONTINUE
      WRITE (6,160) (DUZ(K),K=1,M1)
      X(31)=0.7
      X(32)=10.
      X(33)=100.
      WRITE (6,21) BR(J)
   21 FORMAT (1H0, 'BR=',D15.5)
      READ (5,154) (CN(I),I=1,N1)
      READ (5,154) (DN(I),I=1,N1)
      WRITE (6,166)
  166 FORMAT (1H ,'CN AND DN VLAUE')
      WRITE (6,160) (CN(N),N=1,N1)
      WRITE (6,160) (DN(N),N=1,N1)
      DO 100 JP=1,3
      PR=X(30+JP)
      DO 100 L=1,L1
      WRITE (6,180) BR(J),X(L)
  180 FORMAT ('0BR=',D11.4,5X,'X=',D11.4)
C CALCULATE THE TEMPERATURE GRADIENT OF THR MAIN FLOW
      DO 43 K=1,M1
      PTX(K)=0.0D0
      Z=DZ*(K-1)
      PTZ(K)=1.D0-3.D0*BR(J)*(2.D0*Z-1.D0)**3
      DO 44 N=1,N1
      A1=-X(L)*(BETA(N)**2)
      A2=-X(L)*(GAMA(N)**2)
      IF (K-K1) 45,45,46
   45 PTX(K)=PTX(K)-CN(N)*BETA(N)**2*RN(N,K1-K+1)*DEXP(A1)
     1 +DN(N)*GAMA(N)**2*ZN(N,K1-K+1)*DEXP(A2)
      PTZ(K)=PTZ(K)-CN(N)*DRN(N,K1-K+1)*DEXP(A1)+DN(N)
     1  *DZN(N,K1-K+1)*DEXP(A2)
      GO TO 44
   46 PTX(K)=PTX(K)-CN(N)*BETA(N)**2*RN(N,K-K1+1)*DEXP(A1)
     1 -DN(N)*GAMA(N)**2*ZN(N,K-K1+1)*DEXP(A2)
      PTZ(K)=PTZ(K)+CN(N)*DRN(N,K-K1+1)*DEXP(A1)+DN(N)
     1  *DZN(N,K-K1+1)*DEXP(A2)
   44 CONTINUE
      PTX(K)=-0.5D0*PTX(K)
      PTZ(K)=-PTZ(K)
   43 CONTINUE
      WRITE (6,167)
```

```
  167 FORMAT (1H .'THE TEMP. GRADIENT OF MAIN FLOW')
      WRITE (6,160) (PTX(K),K=1,M1)
      WRITE (6,160) (PTZ(K),K=1,M1)
C DEFINE THE INITIAL VALUE OF PERTURBATION VELOCITY OFW
      DO 41 K=2,M
      A1=K
   41 W(K)=2.D0*(1.D0-A1/40)
      WRITE (6,160) (W(K),K=1,M1)
      IRA=1
      IA=1
      RA=1708.0D0
      A=2.50D0
   15 CONTINUE
      X1=(A*DZ)**2/0.6D1
      X2=(A*DZ)**4/0.36D3
      X3=(A*DZ)**2/0.12D2
C DEFINE THE GAUSS COEFFICIENT
      B3(1)=-12.D0
      C3(1)=0
      DO 11 K=2,M
      A3(K)=1.D0-X3
      B3(K)=-2.D0-X3*10
      C3(K)=A3(K)
   11 CONTINUE
      B3(M1)=-12.D0
      A3(M1)=0.D0
C DEFINE THE GAUSS5 COEFICIENT
      C5(1)=264.D0*X1-240.D0
      D5(1)=96.D0*X1-120.D0
      E5(1)=0.D0
      B5(2)=56.D0*X2-8.D0*X1-4.D0
      C5(2)=247.D0*X2+17.D0*X1+7.D0
      D5(2)=B5(2)
      E5(2)=1.D0-X1+X2
      C5(3)=246.D0*X2+18.D0*X1+6.D0
      DO 12 K=3,M1
      A5(K)=E5(2)
      B5(K)=B5(2)
      C5(K)=C5(3)
      D5(K)=B5(2)
      E5(K)=E5(2)
   12 CONTINUE
      A5(M)=E5(2)
      B5(M)=B5(2)
      C5(M)=C5(2)
      D5(M)=B5(2)
      E5(M)=0.D0
      A5(M1)=0.D0
```

```
      B5(M1)=D5(1)
      C5(M1)=C5(1)
      D5(M1)=0.D0
      E5(M1)=0.D0
C START ITERATION
      I=1
C CALCULATE PU
1111  DO 60 K=1,M1
   60 G(K)=W(K)*DUZ(K)*DZ2
      CALL TRID(A3,B3,C3,G,DZ,PU,DPU)
C CALCULATE THE THETA
      TEMP4=16.D0/3.D0
      DO 63 K=1,M1
      G(K)=TEMP4*PU(K)/PR*PTX(K)+W(K)*PTZ(K)
     1 +4.D0*BR(J)*DUZ(K)*DPU(K)/PR
   63 G(K)=G(K)*DZ2
      CALL TRIDT(A3,B3,C3,G,TH)
C CALCULATE THE NEW PERTUREATION VELOCITY OF W
      DO 67 K=1,M1
   67 G(K)=A*A*RA*TH(K)*DZ4
      CALL PENTAD(A5,B5,C5,D5,E5,G,WN)
C CALCULATE NEW RAYLEIGH NUMBER
      A1=0.0D0
      A2=0.0D0
      DO 70 K=1,M1
      A1=A1+W(K)**2
   70 A2=A2+WN(K)**2
      RAN=RA*DSQRT(A1/A2)
C CHECK THECONVERGENCE OF W
      A1=0.0D0
      A2=0.0D0
      DO 75 K=1,M1
      A1=A1+DABS(WN(K)-W(K))
   75 A2=A2+DABS(WN(K))
      TEMP1=A1/A2
      IF (TEMP1-EPS) 1000,72,72
C READJUST W
   72 DO 73 K=1,M1
   73 W(K)=WN(K)*RAN/RA
      RA=RAN
      I=I+1
      IF (I-I1) 1111,1111,1000
1000  CONTINUE
      WRITE (6,174) I,PR,A,RA,TEMP1
      CRA(IA)=RA
      A=A+0.1D0/IRA
      IA=IA+1
      IF (IA.LE.3) GO TO 15
```

```
      SIGN=(CRA(IA-1)-CRA(IA-2))*(CRA(IA-2)-CRA(IA-3))
      IF (SIGN) 13,13,15
   13 CONTINUE
      IF (IRA.GE.100) GO TO 14
      A=A-3*0.1/IRA
      IRA=IRA*10
      CRA(1)=CRA(IA-3)
      IA=2
      A=A+0.1/IRA
      GO TO 15
   14 CONTINUE
      WRITE (6,171)
      WRITE (6,160) (WN(K),K=1,M1)
      WRITE  (6,172)
      WRITE (6,160) (PU(K),K=1,M1)
      WRITE (6,173)
      WRITE (6,160) (TH(K),K=1,M1)
  101 CONTINUE
  100 CONTINUE
  171 FORMAT (1H , 'PERTURBATION VELOCITY IN Z DIRECTION')
  172 FORMAT (1H , 'PERTURBATION VELOCITY OF U')
  173 FORMAT (1H , 'PERTURBATION TEMPERATURE')
  174 FORMAT (1H0,'I=',I3,5X,'PRANDTL NO.=',D10.3,5X,'WAVE NO.=',
     1 D12.5,5X,'RAYLEIGH NO=',D15.8,5X,'ERROR=',D15.8)
      STOP
      END
      SUBROUTINE TRID(A,B,C,D,DZ,FF,DFF)
      DOUBLE PRECISION A(41),B(41),C(41),D(41),F(41),BP(41)
     1  ,FF(41),DFF(41),Q(41),H(41),DZ,T1
      COMMON M,MI,M1
      BP(2)=C(2)/B(2)
      Q(2)=D(2)/B(2)
      DO 1 K=3,MI
      H(K)=B(K)-A(K)*BP(K-1)
      BP(K)=C(K)/H(K)
      Q(K)=(D(K)-A(K)*Q(K-1))/H(K)
    1 CONTINUE
      F(M1)=C.DO
      F(M)=(D(M)-A(M)*Q(MI))/(B(M)-A(M)*BP(MI))
      DO 2 KK=2,MI
      K=M1-KK
      F(K)=Q(K)-BP(K)*F(K+1)
    2 CONTINUE
      F(1)=0.D0
      FF(2)=(10.D0*F(2)+F(3))/12
      DO 3 K=3,MI
      FF(K)=(F(K-1)+10.D0*F(K)+F(K+1))/12
    3 CONTINUE
```

```
      FF(M)=(F(MI)+10*F(M))/12
      T1=DZ*2
      DFF(1)=FF(2)/DZ
      DO 4 K=2,M
      DFF(K)=(F(K+1)-F(K-1))/T1
4     CONTINUE
      DFF(M1)=-FF(M)/DZ
      RETURN
      END
      SUBROUTINE TRIDT(A,B,C,D,FF)
      DOUBLE PRECISION A(41),B(41),C(41),D(41),F(41)
     1  ,FF(41),BP(41),Q(41),H(41)
      COMMON M,MI,M1
      BP(1)=C(1)/B(1)
      Q(1)=D(1)/B(1)
      DO 1 K=2,M
      H(K)=B(K)-A(K)*BP(K-1)
      BP(K)=C(K)/H(K)
      Q(K)=(D(K)-A(K)*Q(K-1))/H(K)
1     CONTINUE
      F(M1)=(D(M1)-A(M1)*Q(M))/(B(M1)-A(M1)*BP(M))
      DO 2 KK=1,M
      K=M1-KK
      F(K)=Q(K)-BP(K)*F(K+1)
2     CONTINUE
      DO 3 K=2,M
      FF(K)=(F(K-1)+10.D0*F(K)+F(K+1))/12
3     CONTINUE
      RETURN
      END
      SUBROUTINE PENTAD(A,B,C,D,E,F,WN)
      DOUBLE PRECISION A(41),B(41),C(41),D(41),E(41),F(41),
     1 Y(41),WN(41),OMGA(41),BETA(41),GAMM(41),H(41),DELT(41)
      COMMON M,MI,M1
      OMGA(1)=C(1)
      BETA(1)=D(1)/OMGA(1)
      GAMM(1)=E(1)/OMGA(1)
      DELT(2)=B(2)
      OMGA(2)=C(2)-DELT(2)*BETA(1)
      BETA(2)=(D(2)-DELT(2)*GAMM(1))/OMGA(2)
      GAMM(2)=E(2)/OMGA(2)
      DO 10 N=3,M1
      DELT(N)=B(N)-A(N)*BETA(N-2)
      OMGA(N)=C(N)-A(N)*GAMM(N-2)-DELT(N)*BETA(N-1)
      BETA(N)=(D(N)-DELT(N)*GAMM(N-1))/OMGA(N)
10    GAMM(N)=E(N)/OMGA(N)
      BETA(M1)=0.D0
      GAMM(M1)=0.D0
```

```
      GAMM(M)=0.D0
      H(1)=F(1)/OMGA(1)
      H(2)=(F(2)-DELT(2)*H(1))/OMGA(2)
      DO 20 N=3,M1
   20 H(N)=(F(N)-A(N)*H(N-2)-DELT(N)*H(N-1))/OMGA(N)
      Y(M1)=H(M1)
      Y(M)=H(M)-BETA(M)*Y(M1)
      DO 30 KK=1,MI
      I=M-KK
   30 Y(I)=H(I)-BETA(I)*Y(I+1)-GAMM(I)*Y(I+2)
      WN(2)=(56*Y(1)+247*Y(2)+56*Y(3)+Y(4))/360
      DO 40 K=3,MI
      WN(K)=(Y(K-2)+56*Y(K-1)+246*Y(K)+56*Y(K+1)+Y(K+2))/360
   40 CONTINUE
      WN(M)=(Y(M-2)+56*Y(MI)+247*Y(M)+56*Y(M1))/360
      RETURN
      END
```

```
 15   ER1=ERR
      GU1=BE(N)
      BE(N)=BE(N)+0.002
      GO TO 12
 16   GU2=BE(N)
      BE(N)=BE(N)-ERR*(GU2-GU1)/(ERR-ER1)
      GU1=GU2
      ER1=ERR
      GO TO 12
 17   CONTINUE
      WRITE (6,61) L,BE(N)
      WRITE (6,60) (EN(N,K),K=1,KE)
      WRITE (6,60) (DEN(N,K),K=1,KE)
      WRITE (7,70) (EN(N,K),K=1,KE,10)
      WRITE (7,70) (DEN(N,K),K=1,KE,10)
 14   CONTINUE
      WRITE (7,70) (BE(N),N=1,N1)
 20   CONTINUE
 60   FORMAT (8D16.7)
 61   FORMAT ('0','ITE=',I3,5X,'EIGENVALUE=',D20.12)
 62   FORMAT ('1', 'HARTMANN NO.=',D10.3)
 70   FORMAT (5D16.9)
      STOP
      END

C     PROGRAM FOR CALCULATING ODD  EIGENVALUES
      IMPLICIT REAL*8 (A-H,O-Z)
      DIMENSION ON(16,201),DON(16,201),GA(16),BU(401)
      EPS1=0.1D-6
      IMAX=15
      KE=201
      KE2=401
      DZ=0.005
      DZ2=DZ*DZ*0.5
C
      PE=0.1D+35
      READ (5,50) (GA(N),N=1,N1)
 50   FORMAT (8D10.3)
      WRITE (6,62) HA
      PE2=PE*PE
      T1=HA/(HA*DCOSH(HA)-DSINH(HA))
      DO 10 K=1,KE2
      Z=DZ*0.5*(K-1)
 10   BU(K)=T1*(DCOSH(HA)-DCOSH(HA*Z))
      WRITE (6,60) (BU(K),K=1,KE2,10)
      DO 14 N=1,N1
      L=0
```

```
 12   L=L+1
      IF (L.GT.IMAX) GO TO 17
      T10=GA(N)**2/PE2
      ON(N,1)=0.
      DON(N,1)=1.
      I=1
      DO 13 K=2,KE
      T1=ON(N,K-1)
      T2=DON(N,K-1)*DZ
      T3=-(GA(N)*BU(I)+T10)*T1*DZ2
      I=I+1
      T4=T1+0.5*T2+0.25*T3
      T5=-(GA(N)*BU(I)+T10)*T4*DZ2
      I=I+1
      T4=T1+T2+T5
      T6=-(GA(N)*BU(I)+T10)*T4*DZ2
      T7=(T3+2*T5)/3.
      T8=(T3+4*T5+T6)/3.
      ON(N,K)=T1+T2+T7
      DON(N,K)=(T2+T8)/DZ
 13   CONTINUE
      ERR=ON(N,KE)
      IF (DABS(ERR).LE.EPS1) GO TO 17
      IF (L-2) 15,16,16
 15   ER1=ERR
      GU1=GA(N)
      GA(N)=GA(N)+0.002
      GO TO 12
 16   GU2=GA(N)
      GA(N)=GA(N)-ERR*(GU2-GU1)/(ERR-ER1)
      GU1=GU2
      ER1=ERR
      GO TO 12
 17   CONTINUE
      WRITE (6,61) L,GA(N)
      WRITE (6,60) (ON(N,K),K=1,KE)
      WRITE (6,60) (DON(N,K),K=1,KE)
      WRITE (7,70) (ON(N,K),K=1,KE,10)
      WRITE (7,70) (DON(N,K),K=1,KE,10)
 14   CONTINUE
      WRITE (7,70) (GA(N),N=1,N1)
 20   CONTINUE
 60   FORMAT (8D16.7)
 70   FORMAT (5D16.9)
 61   FORMAT ('0','ITE=',I3,5X,'EIGENVALUE=',D20.12)
 62   FORMAT ('1', 'HARTMANN NO.=',D10.3)
      STOP
      END
```

```
C       PROGRAM FOR CALCULATING THE COEFFICIENTS OF SERIES
        IMPLICIT REAL*8 (A-H,O-W)
        DIMENSION BE(12),GA(12),EN(12,201),ON(12,201)
      1  ,DEN(12,201),DON(12,201),TF(201),BU(401)
      2  ,EO(12,12),A(144),RH(12),X(203),Y(203)
      3  ,THT(20,201),THB(20,201),TNU(20),BNU(20),TBM(20)
      1  ,CE(12),CO(12),AM(201),BM(201),ZT(20,201),AX(20)
C
        CALL PLOTS
        CALL PLOT(2.,2.,-3)
        PE=100.
        N1=6
        HA=0.
        IX1=20
        THE=1.
        EK=1.D0
        N12=N1*2
        KE=201
        KE2=401
        PE2=PE*PE
        DZ=0.005
C
C     N1= NO. OF EIGENVALUES
C     KE= NO. OF MESH POINTS
C     IX1=NO. OF POINTS ALONG THE X-AXIS
C    EK=1  FOR THE CASE OF OPEN CIRCUIT
C
        READ (5,5) (AX(I),I=1,IX1)
    5   FORMAT (8D10.3)
C
C
C    READ IN EIGENVALUES
        READ (5,99) (BE(N),N=1,N1)
        READ (5,99) (GA(N),N=1,N1)
C    CALCULATE THE BASIC VELOCITY PROFILE
        DO 10 K=1,KE2
        AZ=DZ*0.5*(K-1)
   10   BU(K)=1.5*(1.-AZ*AZ)
        WRITE (6,61)
        WRITE (6,60) (BU(K),K=1,KE2,10)
C
C    CALCULATE THE EIGENFUNCTIONS
        DZ2=DZ*DZ*0.5
        DO 11 N=1,N1
        T10=BE(N)**2/PE2
        EN(N,1)=1.
        DEN(N,1)=0.
```

```
      I=1
      DO 11 K=2,KE
      T1=EN(N,K-1)
      T2=DEN(N,K-1)*DZ
      T3=-(BE(N)*BU(I)+T10)*T1*DZ2
      I=I+1
      T4=T1+0.5*T2+0.25*T3
      T5=-(BE(N)*BU(I)+T10)*T4*DZ2
      I=I+1
      T4=T1+T2+T5
      T6=-(BE(N)*BU(I)+T10)*T4*DZ2
      T7=(T3+2*T5)/3.
      T8=(T3+4*T5+T6)/3.
      EN(N,K)=T1+T2+T7
      DEN(N,K)=(T2+T8)/DZ
   11 CONTINUE
      DO 12 N=1,N1
      T10=GA(N)**2/PE2
      ON(N,1)=0.
      DON(N,1)=1.
      I=1
      DO 12 K=2,KE
      T1=ON(N,K-1)
      T2=DON(N,K-1)*DZ
      T3=-(GA(N)*BU(I)+T10)*T1*DZ2
      I=I+1
      T4=T1+0.5*T2+0.25*T3
      T5=-(GA(N)*BU(I)+T10)*T4*DZ2
      I=I+1
      T4=T1+T2+T5
      T6=-(GA(N)*BU(I)+T10)*T4*DZ2
      T7=(T3+2*T5)/3.
      T8=(T3+4*T5+T6)/3.
      ON(N,K)=T1+T2+T7
      DON(N,K)=(T2+T8)/DZ
   12 CONTINUE
C
      WRITE (6,66)
      WRITE (6,60) (BE(N),N=1,N1)
      WRITE (6,60) (GA(N),N=1,N1)
      WRITE (6,68)
      DO 97 N=1,N1
   97 WRITE (6,60) (EN(N,K),K=1,KE,10)
      WRITE (6,69)
      DO 96 N=1,N1
   96 WRITE (6,60) (ON(N,K),K=1,KE,10)
C
C  TF=THETA E-BR*(---)
```

```
      BR=-1.
      WRITE (6,72) BR
      DO 17 L=1,KE
      AZ=DZ*(L-1)
   17 TF(L)=THE-0.75*BR*(1.-AZ**4)
C     CALCULATE THE SERIES COEFFICIENTS
      DO 15 M=1,N1
      N=M-1
   13 N=N+1
      DO 14 L=1,KE
   14 AM(L)=EN(N,L)*EN(M,L)
      CALL DQSF(DZ,AM,BM,KE)
      EO(M,N)=BM(KE)
      EO(N,M)=BM(KE)
      IF (N.LT.N1) GO TO 13
   15 CONTINUE
      L=0
      DO 16 N=1,N1
      DO 16 M=1,N1
      L=L+1
   16 A(L)=EO(M,N)
C
      DO 18 N=1,N1
      DO 19 L=1,KE
   19 AM(L)=TF(L)*EN(N,L)
      CALL DQSF(DZ,AM,BM,KE)
      RH(N)=BM(KE)
   18 CONTINUE
      XEPS=0.1E-5
      CALL DGELG(RH,A,N1,1,XEPS,IER)
      WRITE (6,65) IER
      DO 20 N=1,N1
   20 CE(N)=RH(N)
C
      DO 23 M=1,N1
      N=M-1
   21 N=N+1
      DO 22 L=1,KE
   22 AM(L)=ON(N,L)*ON(M,L)
      CALL DQSF(DZ,AM,BM,KE)
      EO(M,N)=BM(KE)
      EO(N,M)=BM(KE)
      IF (N.LT.N1) GO TO 21
   23 CONTINUE
      L=0
      DO 24 N=1,N1
      DO 24 M=1,N1
      L=L+1
```

```
24    A(L)=EO(M,N)
      DO 25 N=1,N1
      DO 26 L=1,KE
      AZ=DZ*(L-1)
26    AM(L)=-AZ*ON(N,L)
      CALL DQSF(DZ,AM,BM,KE)
      RH(N)=BM(KE)
25    CONTINUE
      CALL DGELG(RH,A,N1,1,XEPS,IER)
      WRITE (6,65) IER
      DO 27 N=1,N1
27    CO(N)=RH(N)
C
      WRITE (7,99) (CE(N),N=1,N1)
      WRITE (7,99) (CO(N),N=1,N1)
      WRITE (6,71)
      WRITE (6,60) (TF(K),K=1,KE,10)
C
      READ (5,99) (CE(N),N=1,N1)
      READ (5,99) (CO(N),N=1,N1)
      WRITE (6,67)
      WRITE (6,60) (CE(N),N=1,N1)
      WRITE (6,60) (CO(N),N=1,N1)
C
C   CALCULATE THE BASIC TEMPERATURE PROFILE
C   CALCULATE THE BULK MEAN TEMPERATURE AND NUSSELT NUMBER
C   T5=THE DERIVATIVE OF FULLY DEVELOPED TEMP. W.R.T. Z AT Z=1
      T5=3.*BR
C
      DO 29 I=1,IX1
      T3=1.-T5
      T4=1.+T5
      DO 28 L=1,KE
      THT(I,L)=0.
      THB(I,L)=0.
      AM(L)=0.
      AZ=DZ*(L-1)
      DO 30 N=1,N1
      T1=CE(N)*EN(N,L)*DEXP(-BE(N)*AX(I))
      T2=CO(N)*ON(N,L)*DEXP(-GA(N)*AX(I))
      THT(I,L)=THT(I,L)+T1+T2
      THB(I,L)=THB(I,L)+T1-T2
      AM(L)=AM(L)+T1
30    CONTINUE
      THT(I,L)=THT(I,L)+THE-TF(L)+AZ
      THB(I,L)=THB(I,L)+THE-TF(L)-AZ
      K=L*2-1
      AM(L)=(AM(L)+THE-TF(L))*BU(K)
```

```
 28   CONTINUE
      CALL DQSF(DZ,AM,BM,KE)
      TBM(I)=BM(KE)
      DO 31  N=1,N1
      T1=CE(N)*DEN(N,KE)*DEXP(-BE(N)*AX(I))
      T2=CO(N)*DON(N,KE)*DEXP(-GA(N)*AX(I))
      T3=T3+T1+T2
      T4=T4-T1+T2
 31   CONTINUE
      TNU(I)=T3/(1.-TBM(I))
      BNU(I)=T4/(1.+TBM(I))
      WRITE (6,64) AX(I),TBM(I),TNU(I),BNU(I)
 29   CONTINUE
      WRITE (7,70) (TBM(I),I=1,IX1)
      WRITE (7,70) (TNU(I),I=1,IX1)
      WRITE (7,70) (BNU(I),I=1,IX1)
 70   FORMAT (7D11.4)
      WRITE (6,63)
      DO 39 I=1,IX1
      WRITE (6,62) AX(I)
      WRITE (6,60) (THT(I,L),L=1,KE,10)
      WRITE (6,60) (THB(I,L),L=1,KE,10)
 39   CONTINUE
C
      DO 40 K=1,201
 40   X(K)=DZ*(K-1)
      X(202)=0.
      X(203)=0.2
      CALL AXIS(0.,0.,'Z',-1,5.,0.,X(202),X(203),20.)
      DO 43 I=1,20,2
      DO 43 K=1,100
      J=(101-K)*2+1
      J1=(K-1)*2+1
      ZT(I,K)=(1.-THB(I,J))*0.5
      ZT(I,K+100)=(1.-THT(I,J1))*0.5
 43   CONTINUE
      Y(202)=0.
      Y(203)=0.2
      CALL AXIS(0.,0.,'TEMPERATURE PROFILE',19,8.
     1 ,90.,Y(202),Y(203),20.)
      DO 42 I=1,20,2
      DO 41 K=1,201
 41   Y(K)=ZT(I,K)
      CALL FLINE(X,Y,-201,1,0,0)
 42   CONTINUE
 202  CONTINUE
      CALL PLOT(0.,0.,999)
C
```

```
60   FORMAT (8D16.6)
61   FORMAT ('0','BASIC VELOCITY PROFILE')
62   FORMAT ('0','AXIAL POSITION AT',D10.3)
63   FORMAT ('0','BASIC TEMPERATURE PROFILE')
64   FORMAT ('0','AX=',D10.3,7X,'TBM=',D14.7,5X,'TNU='
    1   ,D14.6,5X,'BNU=',D14.6)
65   FORMAT ('0','IER=',I3)
66   FORMAT ('0','EIGENVALUES')
67   FORMAT ('0','THE COEFFICIENTS OF SERIES')
68   FORMAT ('0','EVEN EIGENFUNCTIONS')
69   FORMAT ('0','ODD EIGENFUNCTION')
71   FORMAT ('0','THEATER E - BR*(---)')
72   FORMAT ('1','BRINKMAN NO.=',D10.3)
73   FORMAT ('0','HARTMANN NO.=',D10.3)
99   FORMAT (5D16.9)
     STOP
     END
```

COMPUTER PROGRAM FOR CHAPTER VII

```
C       PROGRAM FOR CALCULATING TTHE STABILITY PROBLEM
        IMPLICIT REAL*8 (A-H,O-Y)
        DIMENSION BE(12),GA(12),EN(12,21),ON(12,21),DEN(12,21)
       1 ,CE(12),CO(12),UB(41),DU(41),PTX(41),PTZ(41),CRA(200)
       2 ,A3(41),B3(41),C3(41),A5(41),B5(41),C5(41),D5(41)
       3 ,W(41),WN(41),TH(41),PU(41),PD(41),AU(41),BU(41)
       4 ,DFD(41),YAR(40),DON(12,21),AX(20),E5(41),BX(41),RH(41)
        COMMON M,MI,M1
C
        PE=10.
        HA=10.
        N1=8
        AX(1)=10.
        THE=1.
        EK=1.
        IMAX=25
        EPS=0.1D-5
C
        PE2=PE*PE
        HA2=HA*HA
        M=40
        MI=M-1
        M1=M+1
        DZ=1./M
        DZ2=DZ*DZ
        DZ4=DZ2*DZ2
        KE=21
        W(1)=0.
        WN(1)=0.
        TH(1)=0.
        PU(1)=0.
        PD(1)=0.
        BX(1)=0.
        W(M1)=0.
        WN(M1)=0.
        TH(M1)=0.
        PU(M1)=0.
        PD(M1)=0.
        BX(M1)=0.
C
C READ IN THE BASIC FLOW SOLUTION
        READ (5,99) (BE(N),N=1,N1)
        READ (5,99) (GA(N),N=1,N1)
        DO 10 N=1,N1
```

```
      READ (5,99) (EN(N,K),K=1,KE)
      READ (5,99) (DEN(N,K),K=1,KE)
   10 CONTINUE
      DO 11 N=1,N1
      READ (5,99) (ON(N,K),K=1,KE)
      READ (5,99) (DON(N,K),K=1,KE)
   11 CONTINUE
C  WRITE OUT ALL DATA
      WRITE (6,61)
      WRITE (6,60) (BE(N),N=1,N1)
      WRITE (6,62)
      WRITE (6,60) (GA(N),N=1,N1)
      WRITE (6,65)
      DO 12 N=1,N1
   12 WRITE (6,60) (EN(N,K),K=1,KE)
      WRITE (6,66)
      DO 14 N=1,N1
   14 WRITE (6,60) (ON(N,K),K=1,KE)
      WRITE (6,67)
      DO 13 N=1,N1
   13 WRITE (6,60) (DEN(N,K),K=1,KE)
      WRITE (6,68)
      DO 15 N=1,N1
   15 WRITE (6,60) (DON(N,K),K=1,KE)
C
C
      BR=1.
      DO 101 IBR=1,2
      BR=BR-1.
      WRITE (6,80) BR
      READ (5,99) (CE(N),N=1,N1)
      READ (5,99) (CO(N),N=1,N1)
      WRITE (6,63)
      WRITE (6,60) (CE(N),N=1,N1)
      WRITE (6,64)
      WRITE (6,60) (CO(N),N=1,N1)
      IF (IBR.EQ.1) GO TO 101
C  UB = THE BASIC VELOCITY  PROFILE OF U  X-COMPONENT
C  DU = THE DERIVATIVES OF U
C  DDU = THE SECOND DERIVATIVES OF U
C  DFD = THE DERIVATIVES OF THE FULLY DEVELOPED TEMP. PROFILE
      CU=HA/(HA*DCOSH(HA)-DSINH(HA))
      CU2=CU*CU
      C1=EK-CU*DCOSH(HA)
      C12=C1*C1
      T1=-2.*CU*HA
      DO 16 K=1,M1
      AZ=HA*(2.*DZ*(K-1)-1.)
```

```
      UB(K)=CU*(DCOSH(HA)-DCOSH(AZ))
      DU(K)=T1*DSINH(AZ)
      DFD(K)=1.-BR*HA*(CU2*DSINH(AZ*2)*0.5+2.*CU
     1  *C1*DSIN(AZ)+C12*AZ)
   16 CONTINUE
      WRITE (6,75)
      WRITE (6,60) (UB(K),K=1,M1)
      WRITE (6,69)
      WRITE (6,60) (DU(K),K=1,M1)
      WRITE (6,60) (DFD(K),K=1,M1)
C
C  DEFINE THE INITIAL VALUES OF W
      DO 21 K=2,M
      T1=3.14159*(K-1)/M
      W(K)=DSINH(T1)
   21 CONTINUE
C
      L=1
      WRITE (6,70) AX(L)
C  CALCULATE THE TEMPERATURE GRADIENT OF BASIC FLOW
      DO 20 K=1,M1
      PTX(K)=0.
      PTZ(K)=0.
      DO 19 N=1,N1
      T1=CE(N)*DEXP(-BE(N)*AX(L))
      T2=CO(N)*DEXP(-GA(N)*AX(L))
      IF (K-KE) 17,17,18
   17 KI=KE-K+1
      PTX(K)=PTX(K)-BE(N)*EN(N,KI)*T1+GA(N)*ON(N,KI)*T2
      PTZ(K)=PTZ(K)-DEN(N,KI)*T1+DON(N,KI)*T2
      GO TO 19
   18 KI=K-KE+1
      PTX(K)=PTX(K)-BE(N)*EN(N,KI)*T1-GA(N)*ON(N,KI)*T2
      PTZ(K)=PTZ(K)+DEN(N,KI)*T1+DON(N,KI)*T2
   19 CONTINUE
      PTX(K)=-PTX(K)
      PTZ(K)=-PTZ(K)-DFD(K)
   20 CONTINUE
C
      WRITE (6,71)
      WRITE (6,60) (PTX(K),K=1,M1)
      WRITE (6,78)
      WRITE (6,60) (PTZ(K),K=1,M1)
C
      IPR=0
      PR=0.01
   41 IPR=IPR+1
      IF (IPR.GE.3) GO TO 101
```

```
      EC=BR/PR
      RA=1000.
      WA=1.8
      DO 100 IW=1,20
      WA=WA+0.2
      WA2=WA*WA
C
      X1=DZ2*(WA2+4.*HA2)/12.
      X2=DZ2*WA2/12.
      X3=DZ2*(WA2+2.*HA2)/6.
      X4=DZ4*WA2*WA2/360.
      UC(2)=1.-X1
      BU(2)=-2.-10.*X1
      B3(1)=-12.
      C3(1)=0.
      A3(2)=1.-X2
      B3(2)=-2.-10.*X2
      C3(2)=A3(2)
      T1=1.-X3+X4
      T2=-4.-8.*X3+56.*X4
      T3=6.+18.*X3+246.*X4
      A5(1)=0.
      B5(1)=0.
      C5(1)=-246.*T1+T3
      D5(1)=-112.*T1+2.*T2
      E5(1)=0.
      A5(2)=0.
      B5(2)=T2
      C5(2)=T1+T3
      D5(2)=T2
      E5(2)=T1
      DO 23 K=3,M
      AU(K)=UC(2)
      BU(K)=BU(2)
      UC(K)=UC(2)
      A3(K)=A3(2)
      B3(K)=B3(2)
      C3(K)=A3(2)
      A5(K)=T1
      B5(K)=T2
      C5(K)=T3
      D5(K)=T2
      E5(K)=T1
23    CONTINUE
      UC(M)=0.
      A3(M1)=0.
      B3(M1)=-12.
      C3(M1)=0.
```

```
      C5(M)=C5(M)+E5(M)
      E5(M)=0.
      A5(M1)=0.
      B5(M1)=D5(1)
      C5(M1)=C5(1)
      D5(M1)=0.
      E5(M1)=0.
C
C
      IT=0
C   START ITERATION
   25 IT=IT+1
      IF (IT.GT.IMAX) GO TO 1000
      DO 26 K=2,M
   26 RH(K)=DZ2*2.*DU(K)*W(K)
      CALL TRID(AU,BU,UC,RH,DZ,PU,PD)
C
      DO 27 K=1,M1
   27 RH(K)=DZ2*((PU(K)/PR*PTX(K)+W(K)*PTO(K))*2.+EC
     1  *(DU(K)*PD(K)-4.*HA2*(EK-UB(K))*PU(K)))
      CALL TRIDTB(A3,B3,C3,RH,TH)
C
      DO 28 K=1,M1
   28 RH(K)=4.*DZ4*WA2*RA*TH(K)
      CALL PENTAD(A5,B5,C5,D5,E5,RH,WN)
C
C  CALCULATE THE NEW RA AND CHECK THE CONVERGENCE
      T1=0.
      T2=0.
      DO 24 K=1,M1
      T1=T1+W(K)**2
   24 T2=T2+WN(K)**2
      RAN=RA*DSQRT(T1/T2)
      T1=0.
      T2=0.
      DO 30 K=1,M1
      T1=T1+DABS(WN(K)-W(K))
   30 T2=T2+DABS(WN(K))
      ERR=T1/T2
      IF (ERR.LE.EPS) GO TO 1000
C  ADJUST W AND RA
      DO 31 K=1,M1
   31 W(K)=WN(K)*RAN/RA
      RA=RAN
      GO TO 25
 1000 CONTINUE
      WRITE (6,72) IT,WA,RAN,ERR
      YAR(IW)=RA
```

```
100   CONTINUE
      WRITE (7,99) (YAR(K),K=1,20)
      WRITE (6,74)  PE,HA,BR,PR,THE
      PR=0.7
      GO TO 41
101   CONTINUE
C
 99   FORMAT (5D16.9)
 60   FORMAT (8D16.7)
 61   FORMAT ('0','EVENEIGENVALUES')
 62   FORMAT ('0','ODD EIGENVALUES')
 63   FORMAT ('0','THE COEFF. OF EVEN SERIES')
 64   FORMAT ('0','THE COEFF. OF ODD  SERIES')
 65   FORMAT ('0','EVEN EIGENFUNCTIONS')
 66   FORMAT ('0','ODD  EIGENFUNCTIONS')
 67   FORMAT ('0','DERIVATIVES OF EVEN EIGENFUNCTIONS')
 68   FORMAT ('0','DERIVATIVES OF ODD  EIGENFUNCTIONS')
 69   FORMAT ('0','DERIVATIVES OF VELOCITY PROFILE')
 70   FORMAT ('0','AXIAL POSITION AT',D12.4)
 71   FORMAT ('0','THE PARTIAL DER. OF TEMP. W.R.T. X')
 72   FORMAT ('0','IT=',I3,5X,'WAVE NO.=',D12.5,5X,
     1  'RAYLEIGH NO.',D14.7,5X,'ERROR',D12.5)
 73   FORMAT ('0','THE AMPLITUDE OF DISTURBANCES')
 74   FORMAT ('0','PE=',D10.3,5X,'HA=',D10.3,5X,'BR=',
     1  D10.3,5X,'PR=',D10.3,5X,'THE=',D10.3)
 75   FORMAT ('0','THE BASIC VELOCITY PROFILE OF U')
 76   FORMAT ('0','THE SECOND DERIVATIVES OF U')
 78   FORMAT ('0','THE PARTIAL DER. OF TEMP. W.R.T. Z')
 79   FORMAT ('1','HARTMANN NO.=',D10.3)
 80   FORMAT ('0','BRIBNKMAN NO.=',D10.3)
 81   FORMAT (6E12.5)
      STOP
      END
      SUBROUTINE TRID(A,B,C,D,DZ,FF,PD)
      IMPLICIT REAL*8 (A-H,O-Z)
      DIMENSION A(41),B(41),C(41),D(41),F(41),FF(41),
     1  BP(41),Q(41),H(41),PD(41)
      COMMON M,MI,M1
      BP(2)=C(2)/B(2)
      Q(2)=D(2)/B(2)
      DO 10 K=3,MI
      H(K)=B(K)-A(K)*BP(K-1)
      BP(K)=C(K)/H(K)
 10   Q(K)=(D(K)-A(K)*Q(K-1))/H(K)
      F(M)=(D(M)-A(M)*Q(MI))/(B(M)-A(M)*BP(MI))
      DO 20 KK=2,MI
      K=M1-KK
 20   F(K)=Q(K)-BP(K)*F(K+1)
```

```
      FF(2)=(10*F(2)+F(3))/12.
      DO 30 K=3,MI
30    FF(K)=(F(K-1)+10*F(K)+F(K+1))/12.
      FF(M)=(F(MI)+10*F(M))/12.
      F(1)=0.
      F(M1)=0.
      PD(1)=F(2)/DZ
      DO 40 K=2,M
40    PD(K)=(F(K+1)-F(K-1))/(DZ*2)
      PD(M1)=-F(M)/DZ
      RETURN
      END
      SUBROUTINE TRIDTB(A,B,C,D,FF)
      DOUBLE PRECISION A(41),B(41),C(41),D(41),F(41),
     1  FF(41),BP(41),Q(41),H(41)
      COMMON M,MI,M1
      BP(1)=C(1)/B(1)
      Q(1)=D(1)/B(1)
      DO 1 K=2,M
      H(K)=B(K)-A(K)*BP(K-1)
      BP(K)=C(K)/H(K)
      Q(K)=(D(K)-A(K)*Q(K-1))/H(K)
1     CONTINUE
      F(M1)=(D(M1)-A(M1)*Q(M))/(B(M1)-A(M1)*BP(M))
      DO 2 KK=1,M
      K=M1-KK
      F(K)=Q(K)-BP(K)*F(K+1)
2     CONTINUE
      DO 3 K=2,M
      FF(K)=(F(K-1)+10*F(K)+F(K+1))/12
3     CONTINUE
      RETURN
      END
      SUBROUTINE PENTAD(A,B,C,D,E,F,WN)
      IMPLICIT REAL*8 (A-H,O-Z)
      DIMENSION A(41),B(41),C(41),D(41),E(41),F(41)
     1 ,PDD(41),Y(41),H(41),DELT(41),OMGA(41),GAMM(41)
     2 ,WN(41),PD(41),BETA(41)
      COMMON M,MI,M1
      OMGA(1)=C(1)
      BETA(1)=D(1)/OMGA(1)
      GAMM(1)=E(1)/OMGA(1)
      DELT(2)=B(2)
      OMGA(2)=C(2)-DELT(2)*BETA(1)
      BETA(2)=(D(2)-DELT(2)*GAMM(1))/OMGA(2)
      GAMM(2)=E(2)/OMGA(2)
      DO 10 N=3,M1
      DELT(N)=B(N)-A(N)*BETA(N-2)
```

```
      OMGA(N)=C(N)-A(N)*GAMM(N-2)-DELT(N)*BETA(N-1)
      BETA(N)=(D(N)-DELT(N)*GAMM(N-1))/OMGA(N)
10    GAMM(N)=E(N)/OMGA(N)
      BETA(M1)=0.
      GAMM(M1)=0.
      GAMM(M)=0.
      H(1)=F(1)/OMGA(1)
      H(2)=(F(2)-DELT(2)*H(1))/OMGA(2)
      DO 20 N=3,M1
20    H(N)=(F(N)-A(N)*H(N-2)-DELT(N)*H(N-1))/OMGA(N)
      Y(M1)=H(M1)
      Y(M)=H(M)-BETA(M)*Y(M1)
      DO 30 KK=1,MI
      I=M-KK
30    Y(I)=H(I)-BETA(I)*Y(I+1)-GAMM(I)*Y(I+2)
      WN(2)=(56*Y(1)+247*Y(2)+56*Y(3)+Y(4))/360
      DO 40 K=3,MI
      WN(K)=(Y(K-2)+56*Y(K-1)+246*Y(K)+56*Y(K+1)+Y(K+2))/360
40    CONTINUE
      WN(M)=(Y(M-2)+56*Y(MI)+247*Y(M)+56*Y(M1))/360
      RETURN
      END
```

COMPUTER PROGRAM FOR CHAPTER VIII

```
C      PROGRAM FOR THE CASE OF A HORANZONTAL LAYER LIQUID WITH
C      MAXIMUM DENSITY INDUCED BY SURFACE TENSION & BUOYANCY
C   DECK FOR THE SURFACE TENSION EFFECTS
C   DECK FOR THE CASE OF GIVEN B TO FIND RA
C
      IMPLICIT REAL*8(A-H,C-X)
      DIMENSION AW(101),BW(101),CW(101),DW(101),EW(101)
     1 ,WN(101),AT(101),BT(101),CT(101),TH(101),FZ(101),
     2 RH(101),W(101),CRA(100)
C
C      PARAMETERS RAM1, RAM2,B, ANDAL MUST BE GIVEN
C   AL=BIOT NO. AND B=MARANGONI NO.
      M=50
      M1=M+1
      MI=M-1
      DZ=1.0/M
      DZ2=DZ*DZ
      DZ4=DZ2*DZ2
      IMAX=25
      EPS=0.1D-5
      W(1)=0.
      W(M1)=0.
      WN(1)=0.
      WN(M1)=0.
      TH(1)=0.
C   DEFINE INITIAL W
      DO 10 K=2,M
      A1=K
   10 W(K)=2.*(1.-A1/M)
C
      B=10.
      RAM2=-0.2
      RAM1=-1.5
      DO 11 K=1,M1
      AZ=DZ*(K-1)
   11 FZ(K)=1.0+RAM1*AZ+RAM2*AZ**2
      DO 100 IL=1,5
      READ (5,6) AL,WA,RA
    6 FORMAT (D10.3,D11.4,D12.5)
      CL=DZ*AL/6.0
C
C
      WA2=WA*WA
```

```
      X1=WA2*DZ2/6.0
      X2=(WA2*DZ2)**2/360.0
      X3=X1/2.0
C
      T1=1.0-X1+X2
      T2=-4.0-8.0*X1+56.0*X2
      T3=6.0+18.0*X1+246.0*X2
      T4=1.0-X3
      T5=-2.0-10.0*X3
C
      DO 12 K=2,M
      AW(K)=T1
      BW(K)=T2
      CW(K)=T3
      DW(K)=T2
      EW(K)=T1
      AT(K)=T4
      BT(K)=T5
      CT(K)=T4
   12 CONTINUE
C
      AT(2)=0.
      AT(M1)=2.*T4/(1.0+CL)
      BT(M1)=T5-10.0*CL*T4/(1.0+CL)
      CT(M1)=0.
C
      AW(1)=0.
      BW(1)=0.
      CW(1)=264.*X1-240.
      DW(1)=96.*X1-120.
      EW(1)=0.
      AW(2)=0.
      CW(2)=247.*X2+17.*X1+7.
      CW(M)=T3-T1
      DW(M)=T2-11./2.*T1
      EW(M)=0.
      AW(M1)=0.
      BW(M1)=0.
      CW(M1)=T3-11./2.*T2+62.*T1
      DW(M1)=0.
      EW(M1)=0.
C  START ITERATION
      IT=0
   20 IT=IT+1
      IF (IT.GT.IMAX) GO TO 1000
      DO 21 K=1,M1
```

```
21    RH(K)=-DZ2*W(K)
      CALL TRID(AT,BT,CT,RH,CL,TH,M)
C
      CS=-12.0*DZ2*WA2*B*TH(M1)
C
      DO 22 K=1,M1
22    RH(K)=DZ4*WA2*RA*FZ(K)*TH(K)
      RH(M)=RH(M)+CS*T1/48.0
      RH(M1)=RH(M1)+CS*(T2/48.-7./6.*T1)
      CALL PENTDA(AW,BW,CW,DW,EW,RH,CS,WN,M)
C
      A1=0.0
      A2=0.
      DO 23 K=1,M1
      A1=A1+W(K)**2
23    A2=A2+WN(K)**2
      RAN=RA*DSQRT(A1/A2)
C
      A1=0.
      A2=0.
      DO 24 K=1,M1
      A1=A1+DABS(WN(K)-W(K))
24    A2=A2+DABS(WN(K))
      ERR=A1/A2
C
      IF (ERR-EPS) 1000,25,25
25    CONTINUE
      DO 26 K=1,M1
26    W(K)=WN(K)*RAN/RA
      RA=RAN
      GO TO 20
1000  CONTINUE
      WRITE (6,62) IT,WA,RA,ERR
14    CONTINUE
      WRITE (6,61) B,AL,RAM1,RAM2
      WRITE (6,63)
C
      YMAX=0.
      DO 16 K=1,M1
      T1=DABS(WN(K))
16    IF (T1.GT.YMAX) YMAX=T1
      DO 17 K=1,M1
17    WN(K)=WN(K)/YMAX
      YMAX=0.
      DO 18 K=1,M1
      T1=DABS(TH(K))
```

```
 18   IF (T1.GT.YMAX) YMAX=T1
      DO 19 K=1,M1
 19   TH(K)=TH(K)/YMAX
      WRITE (6,60) (WN(K),K=1,M1)
      WRITE (6,60) (TH(K),K=1,M1)
      WRITE (7,71) (WN(K),K=1,M1)
      WRITE (7,71) (TH(K),K=1,M1)
 71   FORMAT (11F7.4)
C
100   CONTINUE
 65   FORMAT (6E13.6)
 60   FORMAT (8D15.6)
 61   FORMAT ('0','MARANGONI NO.=',D11.4,5X,'AL=',D11.4,5X,
     1 'RAM1=',D10.3,5X,'RAM2=',D10.3)
 62   FORMAT ('0','IT=',I3,5X,'WAVE NO.=',D12.5,5X,
     1 'RAYLEIGH NO.=',D14.7,5X,'ERROR=',D13.6)
 63   FORMAT ('0','**********')
C
      STOP
      END
      SUBROUTINE PENTDA(A,B,C,D,E,F,CS,WN,M)
      IMPLICIT REAL*8 (A-H,O-Z)
      DIMENSION A(101),B(101),C(101),D(101),E(101),F(101),
     1 WN(101),Y(101),H(101),DE(101),OM(101),BE(101),GA(101)
C
      M1=M+1
      MI=M-1
      OM(1)=C(1)
      BE(1)=D(1)/OM(1)
      GA(1)=E(1)/OM(1)
      DE(2)=B(2)
      OM(2)=C(2)-DE(2)*BE(1)
      BE(2)=(D(2)-DE(2)*GA(1))/OM(2)
      GA(2)=E(2)/OM(2)
      DO 10 N=3,M1
      DE(N)=B(N)-A(N)*BE(N-2)
      OM(N)=C(N)-A(N)*GA(N-2)-DE(N)*BE(N-1)
      BE(N)=(D(N)-DE(N)*GA(N-1))/OM(N)
 10   GA(N)=E(N)/OM(N)
      BE(M1)=0.
      GA(M1)=0.
      GA(M)=0.
      H(1)=F(1)/OM(1)
      H(2)=(F(2)-DE(2)*H(1))/OM(2)
      DO 20 N=3,M1
 20   H(N)=(F(N)-A(N)*H(N-2)-DE(N)*H(N-1))/OM(N)
```

```
      Y(M1)=H(M1)
      Y(M)=H(M)-BE(M)*Y(M1)
      DO 30 KK=1,MI
      I=M-KK
   30 Y(I)=H(I)-BE(I)*Y(I+1)-GA(I)*Y(I+2)
      WN(2)=(56.*(Y(1)+Y(3))+247.*Y(2)+Y(4))/360.0
      DO 40 K=3,MI
   40 WN(K)=(Y(K-2)+Y(K+2)+56*(Y(K-1)+Y(K+1))+246*Y(K))/360.
      WN(M)=(Y(M-2)+56.*Y(MI)+245.*Y(M)+50.5*Y(M1)-CS/48.)/360.0
      RETURN
      END
      SUBROUTINE TRID(A,B,C,D,CL,FF,M)
      IMPLICIT REAL*8 (A-H,O-Z)
      DIMENSION A(101),B(101),C(101),D(101),F(101),BP(101)
     1   ,Q(101),H(101),FF(101)
C
      M1=M+1
      MI=M-1
      BP(2)=C(2)/B(2)
      Q(2)=D(2)/B(2)
      DO 10 K=3,M
      H(K)=B(K)-A(K)*BP(K-1)
      BP(K)=C(K)/H(K)
      Q(K)=(D(K)-A(K)*Q(K-1))/H(K)
   10 CONTINUE
      F(M1)=(D(M1)-A(M1)*Q(M))/(B(M1)-A(M1)*BP(M))
      DO 20 KK=2,M
      K=M1-KK+1
      F(K)=Q(K)-BP(K)*F(K+1)
   20 CONTINUE
      F(1)=0.
      DO 30 K=2,M
      FF(K)=(F(K-1)+10.*F(K)+F(K+1))/12.0
   30 CONTINUE
      FF(M1)=(F(M)+5.*F(M1))/(6.*(1.+CL))
      RETURN
      END
C      ***************************************************************
C  DECK FOR THE SURFACE TENSION EFFECTS
C  DECK FOR THE CASE OF GIVEN RA TO FIND THE B
C
      IMPLICIT REAL*8(A-H,O-X)
      DIMENSION AW(101),BW(101),CW(101),DW(101),EW(101)
     1  ,WN(101),AT(101),BT(101),CT(101),TH(101),FZ(101),
     2  RH(101),W(101),CRA(100)
```

```
     2   ,ZY(41)
C
      M=50
      M1=M+1
      MI=M-1
      DZ=1.0/M
      DZ2=DZ*DZ
      DZ4=DZ2*DZ2
      IMAX=15
      EPS=C.1D-4
      W(1)=0.
      W(M1)=0.
      WN(1)=0.
      WN(M1)=0.
      TH(1)=0.
C   DEFINE INITIAL W
      DO 10 K=2,M
      A1=K
   10 W(K)=2.*(1.-A1/M)
C
      RAM1=-2.5
      RAM2=0.4
      DO 11 K=1,M1
      AZ=DZ*(K-1)
   11 FZ(K)=1.0+RAM1*AZ+RAM2*AZ**2
C
      IW1=18
      B=-200.
      AL=0.
      CL=DZ*AL/6.0
C
      DO 101 IR=1,4
      RA=1000.+1000.*IR
      WA=0.6
      DO 100 IW=1,IW1
      WA=WA+0.2
      WA2=WA*WA
      X1=WA2*DZ2/6.0
      X2=(WA2*DZ2)**2/360.0
      X3=X1/2.0
C
      T1=1.0-X1+X2
      T2=-4.0-8.0*X1+56.0*X2
      T3=6.0+18.C*X1+246.0*X2
      T4=1.0-X3
      T5=-2.0-1C.0*X3
```

```
C
      DO 12 K=2,M
      AW(K)=T1
      BW(K)=T2
      CW(K)=T3
      DW(K)=T2
      EW(K)=T1
      AT(K)=T4
      BT(K)=T5
      CT(K)=T4
   12 CONTINUE
C
      AT(2)=0.
      AT(M1)=2.*T4/(1.0+CL)
      BT(M1)=T5-10.0*CL*T4/(1.0+CL)
      CT(M1)=0.
C
      AW(1)=0.
      BW(1)=0.
      CW(1)=264.*X1-240.
      DW(1)=96.*X1-120.
      EW(1)=0.
      AW(2)=0.
      CW(2)=247.*X2+17.*X1+7.
      CW(M)=T3-T1
      DW(M)=T2-11./2.*T1
      EW(M)=0.
      AW(M1)=0.
      BW(M1)=0.
      CW(M1)=T3-11./2.*T2+62.*T1
      DW(M1)=0.
      EW(M1)=0.
C START ITERATION
      IT=0
   20 IT=IT+1
      IF (IT.GT.IMAX) GO TO 1000
      DO 21 K=1,M1
   21 RH(K)=-DZ2*W(K)
      CALL TRID(AT,BT,CT,RH,CL,TH,M)
C
      CS=-12.0*DZ2*WA2*B*TH(M1)
C
      DO 22 K=1,M1
   22 RH(K)=DZ4*WA2*RA*FZ(K)*TH(K)
      RH(M)=RH(M)+CS*T1/48.0
      RH(M1)=RH(M1)+CS*(T2/48.-7./6.*T1)
```

```
      CALL PENTDA(AW,BW,CW,DW,EW,RH,CS,WN,M)
C
      A1=0.0
      A2=0.
      DO 23 K=1,M1
      A1=A1+W(K)**2
   23 A2=A2+WN(K)**2
      BN=B*DSQRT(A1/A2)
C
      A1=0.
      A2=0.
      DO 24 K=1,M1
      A1=A1+DABS(WN(K)-W(K))
   24 A2=A2+DABS(WN(K))
      ERR=A1/A2
C
      IF (ERR-EPS) 1000,25,25
   25 CONTINUE
      DO 26 K=1,M1
   26 W(K)=WN(K)*BN/B
      B=BN
      GO TO 20
 1000 CONTINUE
      WRITE (6,62) IT,WA,BN,ERR
      ZY(IW)=B
  100 CONTINUE
      WRITE (7,65) (ZY(K),K=1,IW1)
      WRITE (6,61) RA,AL,RAM1,RAM2
      WRITE (6,63)
  101 CONTINUE
   65 FORMAT (6E13.6)
   50 FORMAT (8D10.3)
   60 FORMAT (8D15.6)
   61 FORMAT ('0','MARANGONI NO.=',D11.4,5X,'AL=',D11.4,5X,
     1 'RAM1=',D10.3,5X,'RAM2=',D10.3)
   62 FORMAT ('0','IT=',I3,5X,'WAVE NO.=',D12.5,5X,
     1 'RAYLEIGH NO.=',D14.7,5X,'ERROR=',D13.6)
   63 FORMAT ('*****')
C
      STOP
      END
      SUBROUTINE PENTDA(A,B,C,D,E,F,CS,WN,M)
      IMPLICIT REAL*8 (A-H,O-Z)
      DIMENSION A(101),B(101),C(101),D(101),E(101),F(101),
     1 WN(101),Y(101),H(101),DE(101),OM(101),BE(101),GA(101)
C
```

```
      M1=M+1
      MI=M-1
      OM(1)=C(1)
      BE(1)=D(1)/OM(1)
      GA(1)=E(1)/OM(1)
      DE(2)=B(2)
      OM(2)=C(2)-DE(2)*BE(1)
      BE(2)=(D(2)-DE(2)*GA(1))/OM(2)
      GA(2)=E(2)/OM(2)
      DO 10 N=3,M1
      DE(N)=B(N)-A(N)*BE(N-2)
      OM(N)=C(N)-A(N)*GA(N-2)-DE(N)*BE(N-1)
      BE(N)=(D(N)-DE(N)*GA(N-1))/OM(N)
10    GA(N)=E(N)/OM(N)
      BE(M1)=0.
      GA(M1)=0.
      GA(M)=0.
      H(1)=F(1)/OM(1)
      H(2)=(F(2)-DE(2)*H(1))/OM(2)
      DO 20 N=3,M1
20    H(N)=(F(N)-A(N)*H(N-2)-DE(N)*H(N-1))/OM(N)
      Y(M1)=H(M1)
      Y(M)=H(M)-BE(M)*Y(M1)
      DO 30 KK=1,MI
      I=M-KK
30    Y(I)=H(I)-BE(I)*Y(I+1)-GA(I)*Y(I+2)
      WN(2)=(56.*(Y(1)+Y(3))+247.*Y(2)+Y(4))/360.0
      DO 40 K=3,MI
40    WN(K)=(Y(K-2)+Y(K+2)+56*(Y(K-1)+Y(K+1))+246*Y(K))/360.
      WN(M)=(Y(M-2)+56.*Y(MI)+245.*Y(M)+50.5*Y(M1)-CS/48.)/360.0
      RETURN
      END
      SUBROUTINE TRID(A,B,C,D,CL,FF,M)
      IMPLICIT REAL*8 (A-H,O-Z)
      DIMENSION A(101),B(101),C(101),D(101),F(101),
     1  BP(101),Q(101),H(101),FF(101)
C
      M1=M+1
      MI=M-1
      BP(2)=C(2)/B(2)
      Q(2)=D(2)/B(2)
      DO 10 K=3,M
      H(K)=B(K)-A(K)*BP(K-1)
      BP(K)=C(K)/H(K)
      Q(K)=(D(K)-A(K)*Q(K-1))/H(K)
10    CONTINUE
```

```
      F(M1)=(B(M1)-A(M1)*Q(M))/(B(M1)-A(M1)*BP(M))
      DO 20 KK=2,M
      K=M1-KK+1
      F(K)=Q(K)-BP(K)*F(K+1)
20    CONTINUE
      F(1)=0.
      DO 30 K=2,M
      FF(K)=(F(K-1)+10.*F(K)+F(K+1))/12.0
30    CONTINUE
      FF(M1)=(F(M)+5.*F(M1))/(6.*(1.+CL))
      RETURN
      END
```

COMPUTER PROGRAM FOR CHAPTER IX

```
C      PROGRAM FOR THE CASE OF BLAUSIUS FLOW
       IMPLICIT REAL*8 (A-H,O-Y)
       DIMENSION F(6401),FD(6401),FDD(6401),TA(6401),TD(6401),
      1  VF(6401),VFD(6401),TI(6401),ETI(6401),G(1601)
      2  ,AU(1601),BU(1601),CU(1601),AV(1601),BV(1601),CV(1601)
      3  ,DV(1601),EV(1601),AT(1601),BT(1601),CT(1601)
      4  ,PU(1601),PV(1601),TH(1601),VN(1601)
C
       PR=0.01
       M=1600
       ME1=260
       HD=0.04
       IMAX=20
       EPS=0.1D-5
       M1=M+1
       MI=M-1
       M12=M1*2-1
       M14=M1*4-3
C
C CALCULATE THE BASIC FLOW SOLUTION
       H=HD*0.25
       H2=H*H*0.5
       H3=H/6.
       F(1)=0.
       FD(1)=0.
       FDD(1)=0.3320573374D0
       DO 10 K=2,M14
       I=K-1
       YO=F(I)
       V10=FD(I)*H
       V20=FDD(I)*H2
       C1=-YO*V20*H3
       Y=YO+V10*0.5+V20*0.25+C1*0.125
       V2=V20+C1*1.5
       C2=-Y*V2*H3
       V2=V20+C2*1.5
       C3=-Y*V2*H3
       Y=YC+V10+V20+C3
       V2=V20+C3*3
       C4=-Y*V2*H3
       C5=(9*C1+6*(C2+C3)-C4)*0.05
       C6=C1+C2+C3
       C7=0.5*(C1+C4)+C2+C3
```

```
      F(K)=Y0+V10+V20+C5
      FD(K)=(V10+2*V20+C6)/H
      FDD(K)=(V20+C7)/H2
   10 CONTINUE
C
C CALCULATE THE BASIC TEMPERATURE PROFILE
      CALL DQSF(H,F,TI,M14)
C
      DO 11 K=1,M14
      TI(K)=-0.5*PR*TI(K)
      ETI(K)=DEXP(TI(K))
   11 CONTINUE
      CALL DQSF(H,ETI,TI,M14)
      DO 12 K=1,M14
      TA(K)=1-TI(K)/TI(M14)
      TD(K)=-ETI(K)/TI(M14)
      X=H*(K-1)
      VF(K)=0.5*(X*FD(K)-F(K))
      VFD(K)=0.5*X*FDD(K)
   12 CONTINUE
C
      WRITE (6,60) PR
      WRITE (6,61)
      DO 13 K=1,M14,50
      X=H*(K-1)
   13 WRITE (6,62) X,F(K),FD(K),FDD(K),VF(K),VFD(K),TA(K),TD(K)
   60 FORMAT (1H0, 'PRANDTL NO.=',D10.3)
   61 FORMAT (1H0, 4X,'X',10X,'F',15X,'FD',14X,'FDD',13X,'VF',14X,
     1 'VFD',13X,'TA',14X,'TD')
   62 FORMAT (D10.3,7D16.7)
C
C
C CALCULATE THE PERTURBATION SOLUTION
C
      PU(1)=0.
      PU(M1)=0.
      TH(1)=0.
      TH(M1)=0.
      PV(1)=0.
      PV(M1)=0.
      VN(1)=0.
      VN(M1)=0.
C DEFINE THE INITIAL VALUE OF PV
      WRITE (6,64)
      DO 15 K=1,M1
      C5=3.1415926535D0*(K-1)
```

```
      PV(K)=DSIN(C5/M)
   15 CONTINUE
      H=HD
      H2=H*H
      H3=H2*H
      H4=H3*H
      IW1=20
      GR=5000.
      WA=0.
      DO 101 IW=1,IW1
      WA=WA+0.004
      WA2=WA*WA
C
C DEFINE THE MATRICES
      C7=H2*WA2/12
      DO 16 K=1,M1
      I=K*4-3
      C1=H*VF(I)*0.5
      C2=H2*(VFD(I)-WA2)/12
      C3=-H2*(2*WA2+VFD(I))/12
      C4=C1*WA2*H2
      C5=WA2*H4*(WA2+VFD(I))/360
      C6=C1*PR
      AU(K)=1+C1+C2
      BU(K)=-2+10*C2
      CU(K)=1-C1+C2
      AV(K)=1+C1+C3+C5
      BV(K)=-4-C1+8*C3-C4+56*C5
      CV(K)=6-18*C3+246*C5
      DV(K)=-4+C1+8*C3+C4+56*C5
      EV(K)=1-C1+C3+C5
      AT(K)=1+C6-C7
      BT(K)=-2-10*C7
      CT(K)=1-C6-C7
   16 CONTINUE
      AU(2)=0.
      CU(M)=0.
      AT(2)=0.
      CT(M)=0.
      CV(1)=-246*AV(1)+CV(1)
      DV(1)=-112*AV(1)+BV(1)+DV(1)
      AV(1)=0.
      BV(1)=0.
      EV(1)=0.
      CV(2)=AV(2)+CV(2)
      CV(M)=CV(M)+EV(M)
```

```
      EV(M)=0.
      BV(M1)=BV(M1)+DV(M1)-112*EV(M1)
      CV(M1)=CV(M1)-246*EV(M1)
      AV(M1)=0.
      DV(M1)=0.
      EV(M1)=0.
C
C START THE ITERATION
      ITE=0
   20 ITE=ITE+1
      IF (ITE.GT.IMAX) GO TO 100
C CALCULATE THE PU
      DO 21 K=2,ME1
      I=K*4-3
      G(K)=H2*PDD(I)*PV(K)
   21 CONTINUE
      CALL TRID(AU,BU,CU,G,PU,ME1)
      DO 28 K=ME1,M1
   28 PU(K)=0.
C CALCULATE THE TH
      DO 22 K=1,M1
      I=K*4-3
      X=H*(K-1)
      G(K)=H2*TD(I)*PR*(PV(K)-0.5*X*PU(K))
   22 CONTINUE
      CALL TRID(AT,BT,CT,G,TH,M)
C CALCULATE THE VN
      DO 23 K=1,M1
      I=K*4-3
      G(K)=H4*WA2*GR*TH(K)
   23 CONTINUE
      CALL PENTAD(AV,BV,CV,DV,EV,G,VN,M)
C
C CALCULATE THE NEW GRASHOF NUMBER
      C1=0
      C2=0
      DO 24 K=1,M1
      C1=C1+PV(K)*PV(K)
      C2=C2+VN(K)*VN(K)
   24 CONTINUE
      GRN=GR*DSQRT(C1/C2)
C
C CHECK THE CONVERGENCE
      C1=0
      C2=0.
      DO 25 K=1,M1
```

```
      C1=C1+DABS(VN(K)-PV(K))
      C2=C2+DABS(VN(K))
 25   CONTINUE
      ERR=C1/C2
      IF (ERR-EPS) 100,26,26
C READJUST PV
 26   CONTINUE
      DO 27 K=1,M1
      PV(K)=VN(K)*GRN/GR
 27   CONTINUE
      GR=GRN
      GO TO 20
C
 100  CONTINUE
      WRITE (6,73) ITE,PR,WA,GRN,ERR
 101  CONTINUE
C
 64   FORMAT (1H1, 'STABILITY SOLUTION')
 70   FORMAT (8D15.6)
 71   FORMAT (10F8.5)
 73   FORMAT (1H0,'ITE=',I4,3X,'PR=',D10.3,3X,'WAVE NO.=',D12.4,3X,
     1 'EIGENVALUE=',D20.10,3X,'ERROR=',D12.5)
      STOP
      END
      SUBROUTINE TRID(A,B,C,D,FF,M)
      IMPLICIT REAL*8 (A-H,O-Z)
      DIMENSION A(1601),B(1601),C(1601),D(1601),F(1601),BP(1601)
     1 ,Q(1601),H(1601),FF(1601)
      MI=M-1
      M1=M+1
      BP(2)=C(2)/B(2)
      Q(2)=D(2)/B(2)
      DO 1 K=3,MI
      H(K)=B(K)-A(K)*BP(K-1)
      BP(K)=C(K)/H(K)
      Q(K)=(D(K)-A(K)*Q(K-1))/H(K)
   1  CONTINUE
      F(M)=(D(M)-A(M)*Q(MI))/(B(M)-A(M)*BP(MI))
      DO 2 KK=2,MI
      K=M1-KK
      F(K)=Q(K)-BP(K)*F(K+1)
    2 CONTINUE
      FF(2)=(10.D0*F(2)+F(3))/12
      DO 3 K=3,MI
      FF(K)=(F(K-1)+10.D0*F(K)+F(K+1))/12
 3    CONTINUE
```

```
      FF(M)=(F(MI)+10*F(M))/12
      RETURN
      END
      SUBROUTINE PENTAD(A,B,C,D,E,F,WN,M)
      IMPLICIT REAL*8 (A-H,O-Z)
      DIMENSION A(1601),B(1601),C(1601),D(1601),E(1601),F(1601)
     1 ,H(1601),Y(1601),WN(1601),DELT(1601),OMGA(1601),BETA(1601)
     2 ,GAMM(1601)
      MI=M-1
      M1=M+1
      OMGA(1)=C(1)
      BETA(1)=D(1)/OMGA(1)
      GAMM(1)=E(1)/OMGA(1)
      DELT(2)=B(2)
      OMGA(2)=C(2)-DELT(2)*BETA(1)
      BETA(2)=(D(2)-DELT(2)*GAMM(1))/OMGA(2)
      GAMM(2)=E(2)/OMGA(2)
      DO 10 N=3,M1
      DELT(N)=B(N)-A(N)*BETA(N-2)
      OMGA(N)=C(N)-A(N)*GAMM(N-2)-DELT(N)*BETA(N-1)
      BETA(N)=(D(N)-DELT(N)*GAMM(N-1))/OMGA(N)
   10 GAMM(N)=E(N)/OMGA(N)
      BETA(M1)=0.D0
      GAMM(M1)=0.D0
      GAMM(M)=0.D0
      H(1)=F(1)/OMGA(1)
      H(2)=(F(2)-DELT(2)*H(1))/OMGA(2)
      DO 20 N=3,M1
   20 H(N)=(F(N)-A(N)*H(N-2)-DELT(N)*H(N-1))/OMGA(N)
      Y(M1)=H(M1)
      Y(M)=H(M)-BETA(M)*Y(M1)
      DO 30 KK=1,MI
      I=M-KK
   30 Y(I)=H(I)-BETA(I)*Y(I+1)-GAMM(I)*Y(I+2)
      WN(2)=(56*Y(1)+247*Y(2)+56*Y(3)+Y(4))/360
      DO 40 K=3,MI
      WN(K)=(Y(K-2)+56*Y(K-1)+246*Y(K)+56*Y(K+1)+Y(K+2))/360
   40 CONTINUE
      WN(M)=(Y(M-2)+56*Y(MI)+247*Y(M)+56*Y(M1))/360
      RETURN
      END
```

PROGRAM FOR CHAPTER X

```
C     DECK FOR MAXIMUM DENSITY
      IMPLICIT REAL*8 (A-H,O-Z)
      DIMENSION F(1601),FD(1601),FDD(1601),TA(1601),TD(160)
     1  ,VF(1601),VFD(1601),TI(1601),ETI(1601),EV(401)
     3  ,AU(401),BU(401),CU(401),AV(401),BV(401),CV(401)
     4  ,AT(401),BT(401),CT(401),PV(401),PU(401),TH(401)
     2  ,DV(401),G(401)
      COMMON /B/M,M1,MI
C
      PR=10.D0
      HD=0.02
      M=270
      IMAX=15
      EPS=0.1D-4
      M1=M+1
      MI=M-1
      M12=M1*2-1
      M14=M1*4-3
C
C CALCULATE THE BASIC FLOW SOLUTION
      H=HD*0.25
      H2=H*H*0.5
      H3=H/6.
      F(1)=0.
      FD(1)=0.
      FDD(1)=0.332057337400
      DO 10 K=2,M14
      I=K-1
      YO=F(I)
      V10=FD(I)*H
      V20=FDD(I)*H2
      C1=-YO*V20*H3
      Y=YO+V10*0.5+V20*0.25+C1*0.125
      V2=V20+C1*1.5
      C2=-Y*V2*H3
      V2=V20+C2*1.5
      C3=-Y*V2*H3
      Y=YO+V10+V20+C3
      V2=V20+C3*3
      C4=-Y*V2*H3
      C5=(9*C1+6*(C2+C3)-C4)*0.05
      C6=C1+C2+C3
      C7=0.5*(C1+C4)+C2+C3
      F(K)=YO+V10+V20+C5
```

```
      FD(K)=(V10+2*V20+C6)/H
      FDD(K)=(V2 +C7)/H2
   10 CONTINUE
C
C CALCULATE THE BASIC TEMPERATURE PROFILE
      CALL DQSF(H,F,TI,M14)
C
      DO 11 K=1,M14
      TI(K)=-0.5*PR*TI(K)
      ETI(K)=DEXP(TI(K))
   11 CONTINUE
      CALL DQSF(H,ETI,TI,M14)
      DO 12 K=1,M14
      TA(K)=-TI(K)/TI(M14)
      TD(K)=-ETI(K)/TI(M14)
      X=H*(K-1)
      VF(K)=0.5*(X*FD(K)-F(K))
      VFD(K)=0.5*X*FDD(K)
   12 CONTINUE
C
      WRITE (6,60) PR
      WRITE (6,61)
      DO 13 K=1,M14,10
      X=H*(K-1)
   13 WRITE (6,62) X,F(K),FD(K),FDD(K),VF(K),VFD(K),TA(K),TD(K)
   60 FORMAT (1H0, 'PRANDTL NO.=',D10.3)
   62 FORMAT (D10.3,7D16.7)
C
C
C CALCULATE THE PERTURBATICN SOLUTION
C
      PU(1)=0.
      PU(M1)=0.
      TH(1)=0.
      TH(M1)=0.
      PV(1)=0.
      PV(M1)=0.
      VN(1)=0.
      VN(M1)=0.
      H=HD
      H2=H*H
      H3=H2*H
      H4=H3*H
C DEFINE THE INITIAL VALUE OF PV
      DO 15 K=1,M1
      C5=3.14159265350D0*(K-1)
```

```
      PV(K)=DSIN(C5/M)
   15 CONTINUE
    5 FORMAT (3D10.3)
      RA1=-0.5
      RA2=0.8
      WRITE (6,71) RA1,RA2
      IW1=15
      WA=1.46
      DO 101 IW=1,IW1
      WA=WA+0.02
      GR=100.D0
      DO 14 K=1,M1
      I=K*4-3
      TI(K)=1.-RA1*TA(I)+RA2*TA(I)**2
   14 CONTINUE
      WA2=WA*WA
C
C DEFINE THE MATRICES
      C7=H2*WA2/12
      DO 16 K=1,M1
      I=K*4-3
      C1=H*VF(I)*0.5
      C2=H2*(VFD(I)-WA2)/12
      C3=-H2*(2*WA2+VFD(I))/12
      C4=C1*WA2*H2
      C5=WA2*H4*(WA2+VFD(I))/360
      C6=C1*PR
      AU(K)=1+C1+C2
      BU(K)=-2+10*C2
      CU(K)=1-C1+C2
      AV(K)=1+C1+C3+C5
      BV(K)=-4-C1+8*C3-C4+56*C5
      CV(K)=6-18*C3+246*C5
      DV(K)=-4+C1+8*C3+C4+56*C5
      EV(K)=1-C1+C3+C5
      AT(K)=1+C6-C7
      BT(K)=-2-10*C7
      CT(K)=1-C6-C7
   16 CONTINUE
      AU(2)=0.
      CU(M)=0.
      AT(2)=0.
      CT(M)=0.
      CV(1)=-246*AV(1)+CV(1)
      DV(1)=-112*AV(1)+BV(1)+DV(1)
      AV(1)=0.
```

```
      BV(1)=0.
      EV(1)=0.
      CV(2)=AV(2)+CV(2)
      AV(2)=0.
      CV(M)=CV(M)+EV(M)
      EV(M)=0.
      BV(M1)=BV(M1)+DV(M1)-112*EV(M1)
      CV(M1)=CV(M1)-246*EV(M1)
      AV(M1)=0.
      DV(M1)=0.
      EV(M1)=0.
C
C START THE ITERATION
      ITE=0
      ITE=ITE+1
      IF(ITE.GT.IMAX) GO TO 100
C CALCULATE THE PU
      DO 21 K=2,M
      I=K*4-3
      G(K)=H2*FDD(I)*PV(K)
   21 CONTINUE
      CALL TRID(AU,BU,CU,G,PU)
C CALCULATE THE TH
      DO 22 K=1,M1
      I=K*4-3
      X=H*(K-1)
      G(K)=H2*PR*TD(I)*(PV(K)-0.5*X*PU(K))
   22 CONTINUE
      CALL TRID(AT,BT,CT,G,TH)
C CALCULATE THE VN
      DO 23 K=1,M1
      G(K)=-H4*WA2*TI(K)*GR*TH(K)
   23 CONTINUE
      CALL PENTAD(AV,BV,CV,DV,EV,G,VN)
C
C CALCULATE THE NEW GRASHOF NUMBER
      C1=0
      C2=0
      DO 24 K=1,M1
      C1=C1+PV(K)*PV(K)
      C2=C2+VN(K)*VN(K)
   24 CONTINUE
      GRN=GR*DSQRT(C1/C2)
C
C CHECK THE CONVERGENCE
      C1=0
```

```
      C2=0.
      DO 25 K=1,M1
      C1=C1+DABS(VN(K)-PV(K))
      C2=C2+DABS(VN(K))
   25 CONTINUE
      ERR=C1/C2
      IF (ERR-EPS) 100,26,26
      ERR=DABS((GRN-GR)/GRN)
C READJUST PV
   26 CONTINUE
      DO 27 K=1,M1
      PV(K)=VN(K)*GRN/GR
   27 CONTINUE
      GR=GRN
      GO TO 20
C
C
C
  100 CONTINUE
      WRITE (6,73) ITE,PR,WA,GRN,ERR
      WRITE (6,66)
      WRITE (6,70) (PV(K),K=1,M1,5)
      WRITE (6,67)
      WRITE (6,70) (PU(K),K=1,M1,5)
      WRITE (6,68)
      WRITE (6,70) (TH(K),K=1,M1,5)
  101 CONTINUE
   61 FORMAT (1H0, 4X,'X',10X,'F',15X,'FD',14X,'FDD',13X,'VF'
     1 ,14X,'VFD',13X,'TA',14X,'TD')
   66 FORMAT (1H0, 'THE PERTURBED QUANTITIES IN  Y DIRECTION')
   67 FORMAT (1H0, 'THE PERTURBED QUANTITIES IN  X DIRECTION')
   68 FORMAT (1H0, 'THE PERTURBED QUANTITIES IN  TEMPERATURE')
   70 FORMAT (8D15.6)
   71 FORMAT (1H1, 'RAMDA1=',D12.4,[illegible]MD[illegible],D12.4)
   73 FORMAT (1H0,'ITE=',I4,3X,'PR=',D10.3,3X,'WAVE NO.='
     1 ,D12.5,3X,'EIGENVALUES=',D20.10,3X,'ERROR=',D12.5)
      STOP
      END
      SUBROUTINE TRID(A,B,C,D,FF)
      DOUBLE PRECISION A(401),B(401),C(401),D(401),F(401),BP(401)
     1  ,Q(401),H(401),FF(401)
      COMMON /B/M,M1,MI
      BP(2)=C(2)/B(2)
      Q(2)=D(2)/B(2)
      DO 1 K=3,MI
      H(K)=B(K)-A(K)*BP(K-1)
```

```
      BP(K)=C(K)/H(K)
      Q(K)=(D(K)-A(K)*Q(K-1))/H(K)
    1 CONTINUE
      F(M)=(D(M)-A(M)*Q(MI))/(B(M)-A(M)*BP(MI))
      DO 2 KK=2,MI
      K=M1-KK
      F(K)=Q(K)-BP(K)*F(K+1)
    2 CONTINUE
      FF(2)=(10.D0*F(2)+F(3))/12
      DO 3 K=3,MI
      FF(K)=(F(K-1)+10.D0*F(K)+F(K+1))/12
    3 CONTINUE
      FF(M)=(F(MI)+10*F(M))/12
      RETURN
      END
      SUBROUTINE PENTAD(A,B,C,D,E,F,WN)
      DOUBLE PRECISION A(401),B(401),C(401),E(401),F(401)
     1   ,D(401),DELT(401),Y(401),WN(401),OMGA(401)
     1 ,H(401),BETA(401),GAMM(401)
      COMMON /B/M,M1,MI
      OMGA(1)=C(1)
      BETA(1)=D(1)/OMGA(1)
      GAMM(1)=E(1)/OMGA(1)
      DELT(2)=B(2)
      OMGA(2)=C(2)-DELT(2)*BETA(1)
      BETA(2)=(D(2)-DELT(2)*GAMM(1))/OMGA(2)
      GAMM(2)=E(2)/OMGA(2)
      DO 10 N=3,MI
      DELT(N)=B(N)-A(N)*BETA(N-2)
      OMGA(N)=C(N)-A(N)*GAMM(N-2)-DELT(N)*BETA(N-1)
      BETA(N)=(D(N)-DELT(N)*GAMM(N-1))/OMGA(N)
   10 GAMM(N)=E(N)/OMGA(N)
      BETA(M1)=0.D0
      GAMM(M1)=0.D0
      GAMM(M)=0.D0
      H(1)=F(1)/OMGA(1)
      H(2)=(F(2)-DELT(2)*H(1))/OMGA(2)
      DO 20 N=3,M1
   20 H(N)=(F(N)-A(N)*H(N-2)-DELT(N)*H(N-1))/OMGA(N)
      Y(M1)=H(M1)
      Y(M)=H(M)-BETA(M)*Y(M1)
      DO 30 KK=1,MI
      I=M-KK
   30 Y(I)=H(I)-BETA(I)*Y(I+1)-GAMM(I)*Y(I+2)
      WN(2)=(56*Y(1)+247*Y(2)+56*Y(3)+Y(4))/360
      DO 40 K=3,MI
```

```
      WN(K)=(Y(K-2)+56*Y(K-1)+246*Y(K)+56*Y(K+1)+Y(K+2))/360
   40 CONTINUE
      WN(M)=(Y(M-2)+56*Y(MI)+247*Y(M)+56*Y(M1))/360
      RETURN
      END
```